

**The non-destructive evaluation of
Sitka spruce mechanical properties
using acoustic methods**

**Thesis submitted in partial fulfilment of the requirements of
Edinburgh Napier University, for the degree of Doctor of
Philosophy**

Roderick K T Mackenzie, BSc (Hons), AMIOA

Edinburgh Napier University

Edinburgh

June 2009

Declaration

I hereby declare that this thesis is my own work and effort and that it has not been submitted anywhere for any award. Where other sources of information have been used, they have been acknowledged.

Signature: *H. Handman*

Date: *13/06/09*

Table of Contents

Table of Contents.....	3
List of Figures	7
List of Tables.....	10
List of Symbols.....	12
Acknowledgments.....	16
Abstract.....	17
Chapter 1 Introduction	18
1.1 Introduction	18
1.2 Background to topic	18
1.2.1 Forestry in the U.K.	18
1.2.2 Acoustic-timber inter-relation	24
1.2.3 Current state of wood NDT	25
1.3 Research aims	31
1.4 Chapter outline.....	33
1.5 References.....	34
Chapter 2 The nature of the material	38
2.1 Introduction	38
2.1.1 Wood structure and mechanical properties.....	39
2.1.2 Description of key wood properties	41
2.2 Wood characteristics affecting the mechanical properties of timber	44
2.2.1 Age of timber.....	47
2.2.2 Silvicultural effects	48
2.2.3 Grain angle (slope of grain) and spiral grain	50
2.2.4. Density	52
2.2.5. S ₂ layer MFA.....	55
2.2.6. Moisture and temperature	57
2.2.7. Natural defects - knots	59
2.2.8 Natural defects – reaction wood.....	61
2.3. Current strength testing methods.....	62
2.3.1 Visual grading	63
2.3.2. MSG by static bending	64
2.3.2.2 MSG devices currently in use	65
2.4 Summary.....	66
2.5 References.....	67
Chapter 3 Review of wood acoustic NDT literature.....	76
3.1 Acoustic theory	76
3.1.1 Acousto-elastic theory and the one-dimensional equation	77
3.1.3 Issues with the one-dimensional equation	84
3.1.4 Three-dimensional theory	91
3.2 Factors affecting wave propagation in wood	94
3.2.1 Anisotropy and mode conversion.....	95
3.2.2 Grain angle and cross-grain.....	97
3.2.3 Density	98

3.2.4 Fibre structure	99
3.2.5 Microfibril angle	99
3.2.6 Juvenile wood	101
3.2.7 Moisture content and temperature	101
3.2.8 Drying induced defects.....	103
3.2.9 Biological decay	103
3.2.10 Knots and other defects	104
3.2.11 Compression wood	105
3.3 Methods of dynamic MoE determination	107
3.4 Time of Flight (TOF) methods	110
3.4.1 Accuracy of time determination	110
3.4.2 SWT measurement devices	112
3.4.3 Examples of TOF testing.....	113
3.4.3.1 Small Specimens	113
3.4.3.2 Beams.....	114
3.4.3.3 Logs	116
3.4.3.4 Standing trees and poles	118
3.5 Resonance based methods	123
3.5.1 Transverse vibration testing	125
3.5.2 Longitudinal Resonance testing	126
3.5.2.1 Calculation of dynamic MoE by longitudinal resonance	128
3.5.2.2 Factors affecting longitudinal resonance measurements	129
3.6 Acousto-ultrasonic methods.....	132
3.6.1 Damping.....	135
3.6.1.1 Factors controlling damping	136
3.6.1.2 Different measures of damping	138
3.6.1.2.1 Logarithmic decrement.....	138
3.6.1.2.2 Impulse response and reverberation time	139
3.6.1.2.3 Q-Factor	141
3.7 Summary.....	141
3.8 References.....	143
Chapter 4 Test series 1: Velocity variation in Sitka spruce	156
4.1 Introduction	156
4.1.1 Equipment.....	159
4.1.2 Method	159
4.2 TOF velocities	169
4.2.1 200 mm sections	169
4.2.2 400 mm sections.....	173
4.2.3 800 mm sections.....	174
4.2.4 1600 and 2000 mm sections	174
4.3 Timber non-acoustic parameters	177
4.4 Timber parameters: relation to velocity	179
4.5 Discussion of results	185
4.5.1 Test method	185
4.5.2 200 mm sections: velocity variations.....	185
4.5.2.1 Issues with 200 mm velocities.....	186
4.5.3 400 mm and greater section distances	188
4.5.4 Relations between non-acoustic timber properties	192

4.5.5 Relations between velocity and timber properties	193
4.5.6 Differences between low and high frequency velocity	196
4.6 Summary	197
4.7 References	198
Chapter 5 Test series 2: Controlled homogeneity and defect modelling	201
5.1 Introduction	201
5.1.1 Sample preparation	202
5.1.2 Equipment	204
5.1.3 Method	205
5.2 Preliminary results	211
5.2.1 Supports	211
5.2.2 Accelerometer coupling conditions	212
5.2.3 Excitation of the specimen	213
5.3 Beams tested	216
5.4 Damping ratio methods	218
5.5 Velocity, dynamic MoE and damping ratio results	219
5.5.1 Knots at midspan	223
5.5.1.1 Influence on velocity	223
5.5.1.2 Influence on damping ratio and dynamic MoE	224
5.5.1.2.1 Knot orientation	226
5.5.1.2.2 Edge knots	227
5.5.2 Knots at $\frac{1}{4}$ and $\frac{3}{4}$ span	229
5.5.2.1 Influence on velocity	229
5.5.2.2 Influence on damping ratio and dynamic MoE	230
5.5.3 Knots at various positions	232
5.5.3.1 Influence on velocity	233
5.5.3.2 Influence on damping ratio and dynamic MoE	235
5.5.4 Time of flight velocity versus resonance velocity	239
5.6 Static MoE versus dynamic MoE estimations	241
5.7 Discussion of results and issues	242
5.7.1 Experiment methods	242
5.7.2 Velocities, MoE_d and damping ratios	243
5.7.2.1 Influence of varying inhomogeneity	243
5.7.2.2 Influence of defect position on the MoE_d	246
5.7.2.3 Influence of increasing defect size	255
5.7.2.4 Influence of defect orientation	259
5.7.3 Comparison of dynamic and static MoE calculation	260
5.7.4 Measurement technique (TOF <i>versus</i> RF)	264
5.7.5 Comparison with previous research	268
5.7.6 Bifurcation of harmonic peaks	273
5.8 Summary	281
5.9 References	283
6 Test series 3: Industrial-scale testing of logs and battens	288
6.1 Introduction	288
6.2 Series 3a Method: Kershope log testing	289
6.2.1 Sample provenance	289
6.2.2 Log non-acoustic measurements	291

6.2.3 Acoustic testing procedure	292
6.3 Series 3b: Kershope batten testing	301
6.3.1 1 st sub-sample procedure.....	302
6.3.1.1 Equipment.....	302
6.3.1.2 Method	303
6.3.2 Second sub-sample procedure	305
6.3.3 Post-acoustic testing	305
6.4 Kershope sawmill testing: Results	308
6.4.1 Log TOF results	309
6.4.1.1 PUNDIT™ results.....	310
6.4.1.2 PULSE™ TOF peak-to-peak results	311
6.4.2 Log resonance results	316
6.4.3 Log damping ratios.....	321
6.4.4 Acoustic data interrelations	324
6.4.5 Log MoE _d interrelations	335
6.4.6 Log non-acoustic characteristics	340
6.5 Kershope batten testing	342
6.5.1 Batten TOF results.....	345
6.5.2 Batten resonance results	347
6.5.3 Interrelations between acoustic values	351
6.5.4 Batten damping ratio results	356
6.5.5 Batten mechanical properties results	358
6.5.6 Comparison of static and dynamic MoE estimations.....	365
6.5.7 Frequency shift correlations	371
6.5.8 Batten non-mechanical characteristics.....	372
6.5.9 Multi-variance correlations	375
6.6 Kershope log-batten relations	377
6.7 Summary.....	389
6.8 References.....	396
Chapter 7 Conclusions and future recommendations	402
7.1 Introduction	402
7.2 Specific conclusions.....	402
7.3 Conclusions balanced against objectives.....	411
9.4 Summary of future recommendations	414
7.5 References.....	415

Appendix A1 – Journal paper from INSIGHT, July 2005

Appendix A2 – Poster presentation to Royal Society summer exhibition 2007

Appendix B – CD-ROM datasheets from Test series 1 to 4

Appendix C1 – Correlations between MoE and MoR and individual wood parameters

Appendix D1 – Dispersion curves for a wet wooden log of variable parameters

List of Figures

Figure 1.1 Distribution of FC and private forests across Scotland	23
Figure 2.1 The different scales of wood anatomy	43
Figure 3.1 Dispersion curves for a simulated Sitka spruce log.....	88
Figure 3.2 Diagrammatic representation of longitudinal resonance modes	128
Figure 4.1 Test series 1 measurement set-up.....	160
Figure 4.2 Gould oscilloscope and B & K Type 2635 charge amplifier	161
Figure 4.3 Base-to-base measurements on the oscilloscope display	163
Figure 4.4 Operational flowchart and image of transmitting probe application during PUNDIT testing	165
Figure 4.5 Separation of heartwood and softwood content.....	168
Figure 4.6 Side A velocities by 200 mm section.....	170
Figure 4.7 Side B velocities by 200 mm section.....	171
Figure 4.8 All sides' average velocities by 200 mm section	172
Figure 4.9 Comparison of Side A, Side B, average of Sides A and B combined, and PUNDIT™ mean velocities by 200 mm section	172
Figure 4.10 Side A, Side B, Side C, average of Sides A, B and C, and PUNDIT™ mean velocities (ms ⁻¹) by 400 mm section.....	173
Figure 4.11 Side A, Side B, Side C, average of all sides and PUNDIT™ velocities by 800 mm section.....	174
Figure 4.12 Comparison of Sides A, B, and C, all sides combined (T), and PUNDIT™ data for the 1600 mm section.....	175
Figure 4.13 Comparison of the mean velocities for all sides (T) by section for each section spacing	176
Figure 4.14 Comparison of the PUNDIT™ velocities by section for each section spacing.....	177
Figure 4.15 Densities (blue columns) and corresponding mean oscilloscope velocities (red diamonds) averaged from Sides A and B as tested by 200 mm section.....	180
Figure 4.16 Correlations between density and velocity measurement values on 200 mm sections.....	180
Figure 4.17 Correlations between density and corresponding velocity measurement values.....	181
Figure 4.18 Correlations between KAR and velocity measurement values on 200 mm sections.....	181
Figure 4.19 KAR (blue columns) and corresponding mean velocity (red line) from all sides tested per 200 mm section.....	182
Figure 4.20 KAR (blue columns) and corresponding mean velocity (red line) from all sides tested per 400 mm section.....	182
Figure 4.21 Correlations between KAR and corresponding velocity measurement values on all section spacings.....	183
Figure 4.22 Correlations between calculated "true" path length and velocity measurement values on 200 mm sections.....	184
Figure 4.23 Convergence of 200 mm individual test velocities within each section	188
Figure 4.24 Convergence of 400 mm individual test velocities	189
Figure 4.25 Convergence of 800 mm test velocities	190
Figure 4.26 Convergence of 2000 mm test velocities	191
Figure 5.1 Alignment of grain direction in panels	203

Figure 5.2 All L panels	203
Figure 5.3 The 4-4-4 panels.....	203
Figure 5.4 The 3-6-3 panels.....	203
Figure 5.5 PLY panels.....	203
Figure 5.6 Series 2 experimental layout.....	205
Figure 5.7 Load diagram: supports at $\frac{1}{4}$ -span	206
Figure 5.8 Shear force diagram: supports at $\frac{1}{4}$ -span.....	206
Figure 5.9 Bending moment diagram: supports at $\frac{1}{4}$ -span	207
Figure 5.10 Beam mid-span deflection diagram: supports at $\frac{1}{4}$ -span	207
Figure 5.11 Consequences of the support position on the maximum acceleration	212
Figure 5.12 Problems with the calculation of logarithmic decrement	215
Figure 5.13 Correlations between logarithmic decrement, impulse response and reverberation time damping ratios.....	219
Figure 5.14 Images A to E show 6 mm, 10 mm, 16 mm, 25 mm, and 32 mm dowels	222
Figure 5.15 1st, 2nd and 3rd harmonic velocities versus KVR in LVL-L Beam 1 with knots at midspan.....	224
Figure 5.16 Influence of perpendicular knots of increasing diameter (increasing KVR) at midspan on the damping ratio	225
Figure 5.17 Influence of parallel knots of increasing diameter (increasing KVR) at midspan on the damping ratio.....	226
Figure 5.18 Influence of perpendicular edge knots of increasing diameter (increasing KVR) at midspan on the damping ratio.....	227
Figure 5.19 Influence of parallel edge knots of increasing diameter (increasing KVR) at midspan on the damping ratio	229
Figure 5.20 1st, 2nd and 3rd harmonic velocities versus KVR in a (LVL-L Beam 22 with knots at $\frac{1}{4}$ and $\frac{3}{4}$ span)	230
Figure 5.21 Influence of perpendicular knots of increasing diameter (increasing KVR) at $\frac{1}{4}$ and $\frac{3}{4}$ span on the damping ratio	231
Figure 5.22 Beam with holes at the first seven positions drilled along the span ..	232
Figure 5.23 Beam with holes at various positions drilled along the span	233
Figure 5.24 1st, 2nd and 3rd harmonic velocities versus KVR in an LVL-L beam (Beam 33 with 25 mm knots at various positions along the span).	234
Figure 5.25 Influence of perpendicular 25 mm knots inserted at various locations on Beam 33.....	235
Figure 5.26 Influence of increasing KVR (firstly used central knots with a final two knots inserted at the edges) on 1st harmonic damping ratio and MoEd	236
Figure 5.27 Influence of increasing KVR (firstly used knots in a centred location, with a final two knots inserted at the edges) on 1st harmonic damping ratio and MoEd values	237
Figure 5.28 Correlations between KVR (knots initially placed in a centreline location, followed with a final two knots inserted at the edges) and 1st harmonic damping ratio on an LVL.....	238
Figure 5.29 Relationship between KVR and 1st harmonic damping ratios on LVL (blue solid line) and PLY	239
Figure 5.30 Graphical representation of the data presented in Table 6.5	240
Figure 5.31 Vibrational pressure nodes (dark patches) and anti-nodes.....	247

Figure 5.32 Time-amplitude response of a longitudinal impact on a clearwood beam without defect.....	262
Figure 6.1 Progressively increasing scale satellite images(6.1) showing the Kershope 13 site.....	290
Figure 6.2 Production chain of Kershope battens	292
Figure 6.3 Setup of the measurement procedure used in field investigations.....	293
Figure 6.4 Flowchart demonstrating procedure for the acoustic testing (PULSE™) of a single log.....	294
Figure 6.5a, b, and c showing effects of transducer alignment	296
Figure 6.6 FFT frequency-acceleration graph.....	298
Figure 6.7 PULSE image showing the points taken for the deduction of the transit time using the time-acceleration display	299
Figure 6.8 Derivation of the Q-factor by half-power points.....	301
Figure 6.9 Flowchart of specimen preparation, acoustic kit preparation and measurement procedure.....	304
Figure 6.10 Zwick 205D universal testing machine set up for four-point bending test	306
Figure 6.11 Typical force vs. deflection curve from a 4-point bending test	306
Figure 6.12 Schematic diagram for static bending tests.	307
Figure 6.13 TOF Peak-to-peak (R2 only) velocities by progeny.....	312
Figure 6.14 TOF Peak-to-peak individual log velocities in the IN430 progeny.....	314
Figure 6.15 TOF Peak-to-peak individual log velocities in the QCI progeny	314
Figure 6.16 TOF Peak-to-peak individual log velocities in the IN120 progeny.....	315
Figures 6.17a, 6.17b, and 6.17c Comparison of (clockwise from top left) mean TOF P-P R2, 1st harmonic, and PUNDIT™ velocities respectively.....	316
Figure 6.18 Variation in velocities by harmonic, between all three progenies	320
Figure 6.19 Boxplot displaying the 1st harmonic damping ratio variation within each log test for the IN430 progeny.....	323
Figure 6.20 Boxplot displaying the 1st harmonic damping ratio variation within each log test for the QCI progeny	323
Figure 6.21 Boxplot displaying the 1st harmonic damping ratio variation within each log test for the IN120 progeny.....	324
Figure 6.22 Comparison of the various velocity measurements within the IN430 progeny.....	325
Figure 6.23 Comparison of the various velocity measurements within the QCI progeny.....	325
Figure 6.24 Comparison of the various velocity measurements within the IN120 progeny. AR = all 30 responses.....	326
Figure 6.24 Boxplot displaying the percentage deviation (in all tested logs) of harmonics, PUNDIT™, and TOF P-P velocities.....	327
Figure 6.25 Naturally occurring bifurcation in log KR25Y1.....	328
Figure 6.26 A lower 1st harmonic frequency than could be predicted by the division of higher harmonics.	329
Figure 6.27 10% and 25 % of TOF P-P amplitude velocity values.....	333
Figures 6.28a, 6.28b and 6.28c Linear regression correlations between (clockwise from top left) Log PUNDIT™ velocities and TOF P-P velocities.....	334
Figure 6.29 Comparison of acoustically derived MoEd measurements for all logs	336

Figure 6.30 Comparison of acoustically derived MoEd measurements for the IN430 progeny	337
Figure 6.31 PUNDIT™ derived MoEd (x) vs. other acoustically derived MoEd (y) using regressive linear correlations.....	338
Figure 6.32 PULSE™ TOF peak-to-peak (R2 only) derived MoEd (x) vs. 1st and 2nd harmonically derived MoEd (y) using regressive linear correlations	339
Figure 6.33 Comparison of battens tested in first series, second series and in total	343
Figure 6.34 Batten PUNDIT™ velocities by progeny	346
Figure 6.35 Batten PUNDIT™ MoEd by progeny.....	347
Figure 6.36 Batten 1st harmonic velocity (top) by progeny	348
Figure 6.37 Batten 1st harmonic MoEd (bottom) by progeny.....	350
Figure 6.38 Percentage deviations of all tested batten PUNDIT™ velocities from harmonic velocities	353
Figure 6.39 Batten 1st harmonic damping ratio by progeny.....	357
Figure 6.40 Number of battens per each class of MoE.glo.board and MoE.glo.joist	360
Figure 6.41 Number of battens per each class of MoR.board and MoR.joist.....	360
Figure 6.42 MoE.glo.board vs. statically derived MoR measurements	361
Figure 6.43 Boxplot of MoE.glo.board values by progeny.....	363
Figure 6.44 Boxplot of MoE.glo.joist values by progeny	363
Figure 6.45 Boxplot of MoR.board (left) variation by progeny.....	364
Figure 6.46 MoE.glo.board vs. 1 st harmonic (left) and PUNDIT™ (right) MoE _d measurements.	365
Figure 6.47 Frequency distribution of battens as tested by static and dynamic methods	368
Figure 6.48 Batten densities by progeny.....	373
Figure 6.49 Distribution by number of logs per MoE class.....	382
Figure 6.50 Distribution by number of logs per MoE class.....	383
The parameters were then varied to observe the effect of changing these parameters, and the variations has been further analysed in Chapter 6.....	425

List of Tables

Table 2.1 Relationships between MoE and MoR during static bending tests.....	44
Table 2.2 The effects of silvicultural practices on wood quality.....	49
Table 2.3 Strength classes for coniferous species according to BS EN 338.....	64
Table 2.4 principal bending test rigs	66
Table 2.5 Devices capable of MoE estimate based on non-MSG testing	66
Table 3.1 Correlation of dynamic MoE of beams and SCS (TOF and resonance) to static MoE or MoR bending tests	81
Table 3.2 Correlations between velocity or dynamic MoE measurements (TOF and resonance-based) and individual wood parameters.....	106
Table 3.3 The main commercial SWT.....	113
Table 3.4 Correlations between TOF measurements and RF measurements on beams	115
Table 3.5 Correlations between impact TOF MoEd values and RF MoEd values on logs	116

Table 3.6 Correlations between impact TOF MoEd values on logs and TOF-based average MoEd values on the subsequent beams	116
Table 3.7 Correlations between impact TOF MoEd values on logs and RF average MoEd values on the subsequent beams	117
Table 3.8 Correlations between impact TOF velocity values and ultrasonic TOF velocity values measured on standing trees	120
Table 3.9 Correlations between impact TOF velocity values on standing trees and TOF velocity values measured on the subsequent logs and beams	120
Table 3.10 Correlations between impact TOF dynamic MoE values on standing trees and the resonance-based dynamic MoE values measured on the subsequent logs	120
Table 3.11 correlations between impact TOF velocity values on standing trees and the average static MoE of boards cut from the same logs	121
Table 3.12 Correlations between impact TOF velocity values on standing trees and the average static MoE of SCS cut from the same logs	121
Table 3.14 Correlation between static MoE and MoR and dynamic MoE (TOF and RF based) combined with measurements of other wood characteristics	130
Table 3.15 The main commercial resonance-based dynamic modulus devices ..	132
Table 4.1 Images of each side and 200 mm section of the test specimen	158
Table 4.2 Values for non-acoustically measured timber characteristics.....	178
Table 4.3 Values for non-acoustically measured timber characteristics by side ..	178
Table 4.4 R2 value derived between non-acoustical parameters as measured on 200 mm section.....	184
Table 4.5 R2 value derived between non-acoustical parameters as measured on 400 mm sections (five values per parameter)	184
Table 5.1 Laminate beam test series	217
Table 5.2 The comparison of five different measures of damping ratio.....	218
Table 5.3 Velocity (derived from 1st, 2nd, and 3rd harmonics and the average of the three harmonics) averaged over three tests.....	220
Table 5.4 The percentage of cross-sectional area and percentage of beam volume occupied by a single dowel of various diameters	221
Table 5.5 Harmonic and TOF velocity results for initial (A) and final (B) configurations of beams 28 through 35	240
Table 5.6 Comparison between the acoustic MoEd and other measures	241
Table 5.7 Percentage difference between highest velocity and lowest damping ratio	244
Table 5.8 Velocity results (in ms-1) of TOF and resonance tests on beams cut from the same laminated panels	245
Table 5.9 Elam and E2 of LVL-L beam 33 with increasing number of centerline dowels.....	256
Table 5.10 Prediction of central affected section's damping ratio in Beam 33 due to increased knot volume	258
Table 5.11 Percentage difference between PUNDIT™ TOF ultrasonic velocity and low-frequency 1st, 2nd and 3rd harmonic derived velocities.....	264
Table 5.12 Raw frequency data, calculated damping ratios and calculated MoEd values from the bifurcated fundamental frequencies.....	275
Table 6.1 Characteristics of the four families involved in test series 3	291
Table 6.2 Batten test set-up parameters	308
Table 6.3 TOF PUNDIT™ velocities by progeny.....	310

Table 6.4 TOF PULSE™ peak-to-peak (R2 only) velocities by progeny	312
Table 6.5 Amalgamated reproduction from Brüel and Kjær PULSE knowledge library	318
Table 6.6 Velocity data for all logs calculated by individual harmonic	319
Table 6.7 Progeny average damping ratios by harmonic mode	322
Table 6.8 Strength classification from BS EN 338:2003	336
Table 6.9 Summary of correlations (R2) between log velocities (V), MoEd(v), and damping ratios	340
Table 6.10 Summary of correlations (R2) between battens static MoEs, MoRs, visual data, acoustic velocities and damping ratios	344
Table 6.11 Number of battens tested by each method, by progeny and in total ..	347
Table 6.12 Statistical data from both 1st and 2nd batten series acoustic tests ..	349
Table 6.13 Number of battens tested by each MoE or MoR measure in accordance with BS EN 408:2003	358
Table 6.14 Number of battens within each progeny originating from a specific vertical position from the base within each tree	362
Table 6.15 Comparison of statistical data returned from static and dynamic MoE measurements	367
Table 6.16 Statistical data returned from KAR and perpendicular KAR measurement	374
Table 6.17a Multivariate correlations between measures of KAR, or static MoE	376
Table 6.17b Multivariate correlations between measures of static MoR	377
Table 6.18 Summary of correlations (R2) between averaged batten static and acoustic properties and log static and acoustic properties	379
Table 6.19 Statistical data derived from the averaging of individual battens per parent log	384
Figure 6.51 Distribution by number of logs per MoE class	386

List of Symbols

Roman

- a = Distance between two loading points (mm)
- A = Surface area
- A_k = Total surface area occupied by knots
- b = Breadth (mm)
- C_{11} = Stiffness factor in the longitudinal axis (GPa)
- C_n = Bending mode factor
- d = Diameter (mm)
- E = Modulus of elasticity (GPa)
- E_θ = Modulus of elasticity at a given grain angle (GPa)
- E_L = Longitudinal modulus of elasticity (GPa)
- E_{Lam} = Laminate modulus of elasticity (GPa)
- $E_{bending}$ = Flexural modulus of elasticity (GPa)
- E_T = Tangential modulus of elasticity (GPa)
- E_{3pt} = Modulus of elasticity derived from a three-point bending test (GPa)
- E_{4pt} = Modulus of elasticity derived from a three-point bending test (GPa)
- f = Frequency (Hz)

f_c = Peak frequency (Hz)
 f_n = Natural (fundamental) frequency of the bending wave (Hz)
 F = Force (N)
 F_{max} = Maximum force applied
 g = Acceleration due to gravity (ms^{-2})
 G = Shear Modulus (GPa)
 h = Height (mm)
 I_{na} = Moment of Inertia (m^4)
 L = Length (mm)
 m = Central gauge length (mm)
 n = Number
 P = Load at limit of proportionality (N in Newtons)
 Q = Quality factor
 R = Reaction forces
 r = Radius (mm)
 t = Time (s)
 T = Reverberation time (s)
 U = Group velocity (ms^{-1})
 v = Volume (m^3)
 V_0 = Phase velocity (ms^{-1})
 V_L = Longitudinal velocity (ms^{-1})
 w = Specimen width (mm)
 W = Line load self-weight (N)

Greek

θ = Grain angle ($^\circ$)
 α = wave propagation angle ($^\circ$)
 ρ = Density (kgm^{-3})
 μ_{ij} = Poisson's Ratio in the plane of i and j
 ω = Moisture content (%)
 β_v = Coefficient of volumetric symmetry (% swelling / % increase in MC)
 δ = Mid-span deflection at the limit of proportionality (mm)
 λ = Wavelength (m)
 $\tan\zeta$ = Logarithmic decrement
 σ = Decay constant
 ξ = Fraction of critical damping (damping ratio)
 η = Total loss factor
 ε = Strain

Anachronisms

AE: Acoustic emission
 AGM: Above ground mass
 AU: Acousto-ultrasonic
 COV: Coefficient of Variance
 CPB: Constant percentage bandwidth
 CSIRO: Commonwealth Scientific and Industrial Research Organisation
 CT: Computed tomography
 CTE: Centre for Timber Engineering

CW: Compression wood
DD: Drying defects
DEN: Density
DR: Damping ratio
FC: Forestry Commission
FFT: Fast Fourier transform
FPL: Forest Products Laboratory
FSC: Forestry Stewardship Council
FRF: Frequency response function
FR: Forest Research
FSP: Fibre saturation point
GA: Grain angle
GS: General structural
IR: Infrared
JW: Juvenile wood
KAR: Knot area ratio
KDR: Knot diameter ratio
KR: Kershope
KVR: Knot volume ratio
LV: Longitudinal vibration
LVL: Laminated veneer lumber
LVL-L: Laminated veneer lumber (veneer aligned longitudinally)
LVL-T: Laminated veneer lumber (veneer aligned tangentially)
MC: Moisture content
MFA: Microfibril angle
MKAR: Margin KAR
MoE: Modulus of elasticity or Young's modulus
MoE_d: Dynamic modulus of elasticity
MoE_L: Local modulus of elasticity
MoE_G: Global modulus of elasticity
MoR: Modulus of rupture
MRI: Magnetic resonance imaging
MSG: Machine stress grading
MW: Microwaves
NDE: Non-destructive evaluation
NDT: Non-destructive testing
NIR: Near infrared
NMR: Nuclear magnetic resonance
NRS: northern research station
OS: Ordinance survey
PLY: Plywood
P-P: Peak-to-peak
PVA: Polyvinyl acetate
QCI: Queen Charlotte Island
QL: Quasi-longitudinal
QT: Quasi-transverse
RF: Resonance frequency
RW: Ring width
SIRT: Strategic integrated timber research

SCS: Small clear samples
SD: Standard deviation
SNR: Signal to noise ratio
SS: Special structural
SWT: Stress-wave timers
TOF: Time of flight
TOF DEV: Time of flight measured from first deviation from the horizontal
TOF CEN: Time of flight measured from wave centroid peak
TOF NEG: Time of flight measured from nadir of first significant negative trough
T: Transverse
TKAR: Total KAR
TV: Transverse vibration
US: Ultrasonic

Acknowledgments

I wish to express my profound gratitude to all those who have helped with supervisory, technical, and moral support during the creation of this thesis. Firstly, I wish to thank Napier University and The School of the Built Environment for creating the post of Research Student. Its staff has provided endless encouragement and material resources without which this research would not have been possible. In particular, Prof. Charles Fairfield and Prof. R. Sean Smith, my supervisors, who have guided me with constructive advice and patience understanding, whilst ensuring I fulfilled my objectives and developed as an academic. Additionally, SBE and CTE staff past and present who have provided technical support and experimental assistance: Dr. Annie Nyander, Dr. Iain Swan, Dr. John R. Moore, Mr. Andy Lyon, Dr. Franka Bruchert, Mr. Adrian Hapca, Mr. Scott Spence, Mr. Scott Campbell, Ms. Shenzhi Su, Mr. Alan Barber and Mr. Willie Laing; undergraduates Mark and Adam for their assistance during conduct of the test series; and the Staff of RMP Acoustic Consultants for their technical input and encouragement.

Outwith Napier University, I wish to thank Prof. John Walker, Prof. Ken Entwistle, and Mr. Helge Hensen for their warm hospitality, limitless assistance, technical advice, and sound direction during my time at the University of Canterbury. Special mention must also go to Mr. Shaun Mochan and Mr. Barry Gardiner of Forest Research NRS, without their input and provision of specimens this research would never have been possible. Additionally: Mr. Paul Mclean and Prof. Mike Jarvis of Glasgow University; Mr. Barry Longbottom, Mr. Bill Mc Taggart, and Mr. Brian MacMillan of Bruel and Kjaer UK for technical support.

I wish to thank my friends for their love, encouragement and proof-reading, particularly Victoria Swan; Rosie Ferguson; Matthew Yaxley; Andrew Miller, Rowena Prentice; Cherrie Glass, Rob Craig, and Jessica Emed. Finally, I reserve my deepest thanks for my family; Cathy, Robin, Fiona, Roy, Richard and Andrea, Ruarai, Ruby, Geogie and Chico. All of you have kept me going during the last four years; your unconditional love has helped so much during the dark periods and dead ends of this work, whilst your affections and good humour have helped me to enjoy the successes. Finally, finally, my late grandfather Torquil 'togy craic' McIvor.

This thesis is also dedicated to Dr. Fouad Khalaf, lately of Napier University SBE. Fouad's warm conversation, encouragement and genuine interest in my progress were a particular highlight during the dark days of mid-winter testing.

Abstract

The need for improved timber grading is key to improving Scottish forestry: the majority (80%) of the sustainable softwood population in Scotland is Sitka spruce of variable quality. Current visual assessment of strength and stiffness is inaccurate, and machine stress grading in sawmills is little better due to incorrect assumptions regarding consistency within softwood species and between trees of the same stand. The author develops and evaluates non-destructive test (NDT) methods for Scottish Sitka spruce based upon impact-echo testing across a range of scales from plank, to log, to standing tree.

Correlations between harmonic wave propagation velocity and elastic modulus of $0.62 \leq R^2 \leq 0.71$ were possible in Sitka spruce under a range of conditions including: genotype progeny, variable height and radial position in stem, and variable knot content. In achieving this correlation, the research also investigated acoustic parameters such as: time of flight velocity, damping ratio, and resonant peak behaviour with regard to their influence on dynamically derived moduli of elasticity. Examination of variation in wood properties (including static elastic modulus, knot content, simulated decay, density, and grain alignment) on these acoustic parameters was conducted on semi-controlled specimens of differing homogeneities. The consequences of these results should influence the development of timber NDT tools.

In addition to the development of an NDT method, the author has provided the first large-scale derivation of reference values for dynamic stiffness and other acoustic properties for 35 year old logs and beams of Sitka spruce in Scotland.

Chapter 1 Introduction

1.1 Introduction

The research presented in this thesis investigates the use of acoustic non-destructive testing (NDT) for the stiffness and strength assessment of the predominant Scottish softwood species, Sitka spruce (*Picea sitchensis*, Bong. Carr.).

A progressive series of experimental models has been devised to reassess the currently accepted theory behind commercially available acoustic NDT tools and to identify potential limitations. The thesis attempts to identify timber-dependent acoustic parameters not previously used in timber grading assessment, whilst establishing reference values and correlations for the dynamic assessment of Scottish Sitka spruce. Recommendations on future directions for acoustic NDT and its use in timber quality assessment are provided.

1.2 Background to topic

The following three sections set out the nature of the problem of timber quality assessment in terms of U.K. forestry, explain the basic theory behind the proposed solution, and review the current worldwide state of the application of these solutions. It should be noted that timber quality in this instance relates to stiffness, strength, and stability due to industry's focus on maximising the economic returns through maximising higher profit uses such as are found in the construction industry.

1.2.1 Forestry in the U.K.

Approximately 80% of the Scottish timber population is the Sitka spruce species, which is inherently of moderate-to-low quality when grown under the geo-environmental conditions prevalent in the U.K.^(1.1). Sitka spruce, and in particular the Queen Charlotte Island (QCI) provenance, was primarily chosen for planting in Britain due to its ability, amongst other factors, to remain relatively frost resistant

(though this is now questioned^(1.2)) and weevil-resistant; to withstand exposure and grow better on wet uplands and infertile sites than any other exotic species; and to regenerate freely^(1.2-1.4). As such, originally planted following the 1919 creation of the Forestry Commission to improve the UK strategic timber reserve, the majority was planted on the cheapest bulk-purchases of land available, typically the grazing hills of northern England and western Scotland^(1.3). A large increase in planting on private land occurred during the 1950s through to the 1990s, due to favourable tax and grant incentives^(1.3). It currently occupies 24% of all forested land in the UK^(1.4). It is predominantly planted in western areas of Scotland due to the sufficient rainfall required for this species, typically at up to 150 m to 300 m above sea-level (higher in sheltered areas), though it has proved particularly successful on windswept and waterlogged uplands of northern England and southern Scotland (for example, Kielder forest has 42000 ha of 72% Sitka spruce and 12% Norway spruce)^(1.3, 1.4). Petersen *et al.*^(1.3) state that in the UK, it is a reliable, low-risk crop of short rotation period, with high demand and high prices and that it has:

“Proven to be a producer of good quality saw timber, pulp and wood based panels”^(1.3).

The accuracy of this statement could, at best, be questioned. Sitka spruce has major flaws in that it has a relatively high proportion of juvenile wood (before short rotations), a relatively low density, usually requires fertiliser and is unable to compete with heather due to high nutrient requirements^(1.3, 1.4). Indeed, Sitka spruce’s density has a negative correlation to vigorous growth ($R^2 = 0.6$, compared to Norway spruce’s 0.3), leading to many rejections of the most vigorous trees due to low density^(1.3). Due to its relatively fast growth compared to other conifers, when combined with shorter rotations, the yield of good quality timber is rather poor^(1.2).

Additionally, large scale trials on the improvement, genetically and silviculturally, of Sitka spruce have only begun in recent years and it is only now subject to an intensive programme of tree improvement^(1.4). The vast majority of Sitka spruce is planted at 2.5 m by 2.5 m stockings with little pruning or thinning, on a 40 year rotation cycle due to wind-throw damage to heights greater than this in the UK^(1.4, 1.5).

A detailed review of the biology, provenance, history and ecology of Sitka spruce is available from the OECD^(1.6) and its mechanical properties from Brauner *et al.*^(1.7), which also includes a comparison of visual and mechanical grading of Danish Sitka spruce. Incidentally, this article also suggests strong similarity in the mechanical behaviour of Sitka spruce and Norway spruce. Sitka spruce typically shows a high shade tolerance, moderate weight, stiffness, shrinkage, bending and compressive strength^(1.3). It has a relatively low average density (at 12% moisture content) of 450 kgm⁻³^(1.3). Young dense stands exhibit poor self-pruning (due to a slow shedding of branches), therefore generally lacks the knot-free characteristics of other slow-grown spruces^(1.3). Indeed, the development of new branches on previously branch free lower stems (epicormic branching) is a particular characteristic^(1.3). Sitka spruce plantations are not inclined to self-thin either, which can naturally restrict growth characteristics^(1.8). Additionally, it has little inherent resistance to decay whilst its poor permeability makes it resistant to preservative treatments^(1.8).

The environmental growing conditions, such as high exposure, rainfall, and acidic soils in the highlands, prevent higher quality timber such as Norway spruce (*Picea abies*) or the native Scots pine (*Pinus sylvestris*) being grown here. As such, only 10% of timber used in the high profit end-use U.K. construction market comes from Scotland. Of the 9.7 million m³ of coniferous wood consumed in the U.K. in 2006, only 24% was produced in the U.K.^(1.10). In contrast 24% alone is imported from the straighter, denser, and more defect-free Norway spruces of Sweden^(1.1). Sitka spruce sawn timber is currently priced at £150 m³^(1.10).

However, the UK has significant net imports of 7.8 million m³ of sawn timber per annum (as of 2006) at a current value of £1.1 billion per annum^(1.10). Combined with other imported timber products (such as paper, pulp, and wood-based panels) this creates a total net import of £6.6 billion per annum^(1.10). As a result, the forest industry in the U.K., particularly in Scotland, misses out on a significant market share and financial return due to inferior quality timber compared to that produced by foreign competitors.

As will be explained in Section 2.2, this stems primarily from poor straightness (inducing drying distortions) and a high proportion of strength reducing, juvenile wood, compression wood and knots. Attempts to breed-out these factors typically fail, not just due to site specific growth variables, but due to the interdependence of timber characteristics on each other. For example, there is generally a negative correlation between density and vigour, yet results from the Kershope trials (Chapter 6) showed a drop in overall timber performance of progenies selected specifically for improved density or vigour, when compared to the control timber.

A study of four different Sitka spruce provenances in Ireland by Treacy^(1.2) found little differences in the average MFA in the provenances with no significant differences in wood stiffness between samples. However, there was a statistically significant difference between the Washington and Californian provenances with regards to MoR, and with wood density between QCI trees and Oregon provenances^(1.2). Generally though, evidence from this review into Sitka spruce's mechanical properties indicate that it generally follows the pattern of other softwoods in relation to density, growth rate, effects of silviculture, MFA, juvenile wood and their effects on stiffness and strength^(1.2). However, Stirling *et al.*^(1.9) quoted the following statement in regards to the wood quality (presumably stiffness):

“Straightness, which defines log-length was identified as the most important single factor affecting log quality in Sitka spruce (from HGTAC Technical sub-committee).”

A representative survey of Sitka spruce in the UK by Northern Research Station (NRS) found that straightness does not improve with age in the 15 years before typical felling ages, however they did find that increased straightness occurs with thinning and with denser stocking patterns^(1.9). Straightness was found to decrease with wind and altitude^(1.9). Log production in U.K. is set to double from 1996 to 2020, though demand will remain static hence the pallet and packaging market is likely to become oversupplied^(1.9). Additionally, since, on average, the percentage of straight stems available to the sawmill will decline, the construction industry will need even more convincing to accept Sitka spruce^(1.9). However, the issue with

sawmiller uptake may be one of historic perception, coupled with a reluctance to change from strong supply deals with importers who can supply the maximum number of grades.

Figure 1.1 shows the distribution of certified Forestry Commission (FC) woodland areas in Scotland (457,000 hectares), along with those woodlands held in the private sector (618,000 hectares of which 280,000 hectares are certified)^(1.1, 1.10). This certified softwood timber production provides c. £577m of directly related income to the Scottish economy^(1.1).

The problem of attempting to improve timber quality, post-planting, is particularly pertinent at the moment given that the U.K. is approaching, by 2020, the peak of a 50 year plantation cycle predicted to bring 10 million m³ per annum of timber onto the market (see graphs in Figure 1.1), the vast majority being Sitka spruce^(1.1). As a result, the lower economic return on low grade wood is likely to be reduced even further with the increased availability of such wood to the low-grade market (pallets, fence-posts, woodchip, etc.).

Whilst the desire for home-grown timber will increase with predicted rising transportation costs, as well as environmental considerations regarding carbon efficiency, the simple lack of construction grade timber means Scottish forestry is unable to benefit. This initiated research funding from the Scottish Government to seek ways to improve, where possible, the quality of Sitka spruce. As such, in 2004 a Scottish Enterprise commissioned report by Bill Dyck noted that not only was there a lack of knowledge regarding the key stiffness properties such as microfibril angle (MFA), but also in the development of assessment methods for classification of timber quality^(1.11).

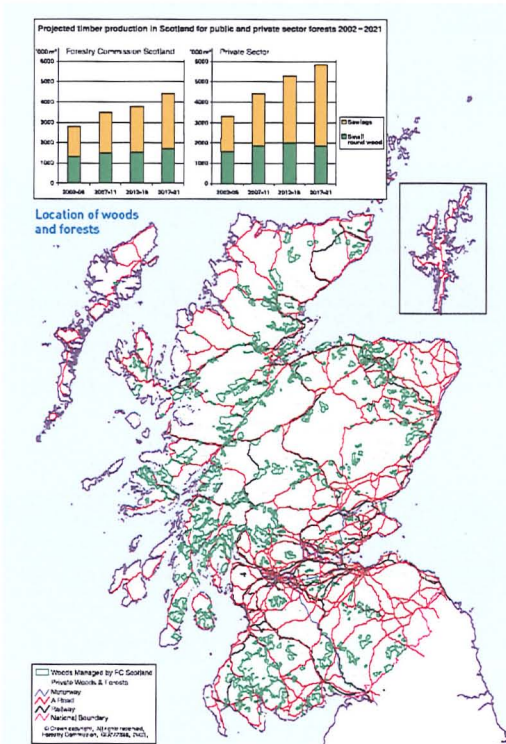


Figure 1.1 Distribution of FC and private forests across Scotland^(1.1). Also shown at the top of the image is the projected timber production in the Scotland 2002 to 2021.

Part of the problem in market penetration and maximising financial returns for U.K. foresters, outside management and silvicultural issues, is a general inability to separate better quality timber from lesser quality stock in the forest itself. As previously noted, unless specified otherwise the author’s “quality” refers to high strength and stiffness.

Temporal inefficiencies are incurred at construction grade sawmills due to a c. 10% rejection rate, with the added economic and environmental cost of subsequent transportation to pallet or wood chipping mills. Additionally, the current grading of timber is done post-harvest, meaning a high lag time in relation to finding out whether the timber planted on a 30 to 40 year turnaround is economically viable.

Further, the sawmilling industry is inherently conservative, often waiting to see the results of extensive trials before implementing new technologies. As such, most sawmills still use visual grading in combination mechanical stress grading (MSG).

On an industrial scale, the process of visual grading has governed forestry and saw milling for centuries. In doing this, for example on traditional assessment of logs or beams, sawmillers can usually assign a grade based on the knot content, straightness, drying defects, ring width and/or presence of reaction wood. However, the results are highly variable and have been shown to have only a moderate correlation to static modulus of elasticity (MoE)^(1,12).

Thus the ability to improve research in post-felling segregation coupled with early identification of low stiffness standing timber are two key issues facing U.K. forestry in the challenge to improve competitiveness. The author has chosen NDT as a potential tool to improve segregation into either above or below C16 grade timber and its subsequent strength and stiffness assessment.

1.2.2 Acoustic-timber inter-relation

Whilst other methods of NDT for timber quality investigation are available, including X-ray tomography, microwave and near infra-red scanning for small sample image analysis, acoustic techniques are assumed by wood scientists to offer the most inexpensive, diverse and portable methods of timber classification. As will be explained further in Chapter 3, classification of timber stiffness using acoustical methods is possible on four scales: small clear specimens (SCS), battens, logs, and standing timber. With increasing scale comes increasing inhomogeneity of the samples and with that, a typically decreasing correlation between acoustic dynamic stiffness in logs and static stiffness in beams (given the lack of static stiffness measurements on logs).

To briefly summarise, the dynamic stiffness is a calculated value of the Young's modulus of a specimen in the longitudinal direction, derived from the measurement of the longitudinal velocity and assuming certain governing conditions are met. Other wave types (flexural and transverse) can also be used and have found favour in much acoustic-timber research. Dynamic modulus (MoE_d) is typically an over-estimate due to the increase in loading rate. The calculation is based on the modelling of wave motion in one or three dimensions, dependent on the

wavelength to specimen diameter ratio, which governs the occurrence of lateral strain. The equations, limitations and applications of this are presented in Chapter 3. The derivation of the equations of motion for a homogenous, anisotropic elastic medium through Christoffel's equations (assuming Hooke's law of linear response and a plane wave motion) is covered in detail in Hearmon^(1.13), Timoshenko and Goodier^(1.14), and Bucur^(1.15). Theoretically, its use should only be applied to the elastic characterisation of homogenous, isotropic materials. Wood itself is typically modelled as orthotropic.

Additionally, because acoustic methods, again explained separately in Chapter 3, are often averages of the whole sample (during resonance testing) or point-to-point specific (time of flight testing, TOF), correlations to mechanically graded smaller samples can often be reduced. The mechanical and visual grading processes are discussed in Chapter 2 and in application of methods in Chapters 5 and 6.

However, due to the encouraging correlations between dynamic and static stiffness in clear specimens of timber at varying scales (typically $R^2 \approx 0.9$ for Sitka spruce dimension timber), which are inherently more homogenous than Sitka spruce (which, in Scotland, generally has more compression wood and a higher knot content), extensive testing has been conducted to assess the varying dynamic stiffnesses of timber worldwide. However, only with the advent of specifically designed devices for timber dynamic stiffness evaluation has any consistent standardisation of methodology been approached.

1.2.3 Current state of wood NDT

This section sets out an overview of the current state of NDT in wood research worldwide, with an emphasis on acoustic research. Specific papers and research are more critically analysed in Chapter 3, and this section is intended to give the reader a broad understanding of the field.

In terms of non-acoustic wood research, it should be noted that much of the research into wood quality (the emphasis of which changes with the end-user

paying for the research) was sporadic before the 1950s. Cown^(1.16) presents a concise overview of the history of general wood research. From the 1960s, research was oriented towards density and tracheid length (at the time believed to be the key influences on timber strength) and factors inducing variation of these parameters, such as species, silviculture, and environmental conditions^(1.16). Indeed, ring width was typically used in visual inspection as the main measure of density and thus strength^(1.16). This produced developments in destructive and NDT techniques to quantify these parameters and hence evaluate strength and stiffness, driven by commercial interests of utility pole owners and end-users of wood products. The additional pressure for development of research came primarily from sawmillers, driven by the financial and quality demands of the end-users, who realised the potential economic benefit of strength-grading their timber.

Focus was initially on manageable samples in which the variable nature of wood's inhomogeneity could be controlled. Cores and SCS from beam sections were favoured. This generally served to accumulate datasets reflecting in-tree patterns of variations, but was essentially destructive and typically reflected systematic sampling rather than whole-stem analysis^(1.16). It did, however, provide us with much of our present knowledge of timber properties. With the advent of MSG, research on whole beam sections became coincident with work on small samples.

It was not until later developments of vibrational and X-ray scanning that research techniques for evaluating whole log sections, in conjunction with SCS and beam analysis, became commonplace in wood research. Additionally, NDT standing tree tools were not readily investigated until the late 1990s^(1.16). Schad *et al.*^(1.17) note that;

“All NDE (non-destructive evaluation) methods use some form of energy propagation through or around a material to infer some important characteristics about the specimen being examined.... (which) may result from static or dynamic loading..... Electromagnetic or elastic waves...characteristics frequently of interest...geometry or orientation, global integrity, strength...defect location and size.”

Bucur^(1.15) noted that acoustical NDT of logs (whilst relatively faster, less invasive and reasonably well correlated to stiffness) is still under-developed in comparison

to other NDT methods, though this may be disputed when compared to methods such as microwave (MW) or magnetic resonant imaging (MRI) testing of timber properties.

For tree NDT testing, the monitoring of tree characteristics has traditionally involved the removal of a sample by an increment borer which takes increment cores (typically at breast-height) and is a relatively rapid process allowing for continual stand development^(1.18). These are considered 'non-destructive,' but do leave the specimen open to biological attack, are problematic to extract intact and ultimately affect the end use of the wood^(1.18-1.20). A poor representation of the whole stem, they have a tendency to over-represent the juvenile wood, which is prevalent in the lowest logs, and are known to underestimate the MoE and modulus of rupture (MoR) of a specimen^(1.18,1.21).

Alternatively, techniques such as resistance drilling (feeling for a loss of resistance thus indicating decay) and Pilodyn™ pin penetration testing have been used for some years as an efficient non-destructive method of testing tree stems. However, other research has shown them to be unrepresentative of the whole stem, with a low repeatability and subject to misleading results on the basis of seasonal temperature and moisture content (MC) variations, in addition to often encountering compression wood^(1.18).

In terms of acoustic investigations, ultrasonic (US) vibrational techniques are favoured in laboratory wood science due to being able to estimate the properties of SCS using resonance (which have a high resonant frequency), but application to whole beam or log comparisons tends to involve low-frequency acoustics. US TOF methods are typically described as scattering techniques due to the scatter-induced variability of velocity and attenuation of the wave, usually between 50 kHz and 200 kHz, as it is impractical to use higher frequencies on anything but very small samples^(1.15,1.22). Other US techniques are typically imaging-based, and use multiple measurements to render a two-dimensional picture of the internal structure based on relative velocities^(1.5, 1.22). This is noted to a greater extent in Chapter 3, but left for now as this thesis is primarily concerned with low-frequency studies.

Further to the elastic characterization of wood through Christoffel's equations^(1.15), Jayne^(1.23) proposed that the properties which control the static behaviour of wood are the same properties that control the behaviour of (acoustical) energy within a material^(1.24). This forms the basis of acoustic and ultrasonic measurements of wood. Further research into individual properties affecting wave transmission was continued by academics such as Gerhards^(1.25-1.28) and Pellerin^(1.29).

Kawamoto and Williams^(1.30) stated that a more co-ordinated approach to non-destructive testing of wood, particularly in the U.S.A., began with the holding of the NDT wood symposium, organised by McDonald and Pellerin, in 1980. This bi-annual conference has seen the majority of key research in wood investigations presented in its proceedings. This has particular benefit in that much of the extensive Japanese research is published in, so the symposium proceedings (in English) allow review of this key contribution.

A review of recent literature reveals that, in general, Scandinavia, North America and Australasia are currently leading the research and development of both techniques and factors that influence wood quality. This is primarily due to increased collaboration between research centres, for example between the Forest Products Laboratory (FPL), Universities of Washington and California in the U.S.A., and between the University of Canterbury, EnsisJV (forest research) and industry in New Zealand. Japanese research should be added to this as a great volume of work is produced, though the majority is published in Japanese-language journals and as such is not always readily available for international review. The same is true of Chinese research. However, much of the more relevant research is published in wood-orientated English-language journals or in the translated Journal of Wood Science from the Japanese Wood Research Society.

Due to the variable nature of timber species grown in each country, availability of measurement techniques and ultimately the desired end-use for the wood products, priorities for research vary substantially between countries.

For example, North American research tends to separate the testing of end-use products (such as battens) and tree biology and genetics, with the majority of research focused on ascribing the variability of timber properties to the effects of forest management^(1.16). Key research centres in North America include the University of British Columbia in Canada, and Washington State University, Oregon State and University of California (Berkeley), and the USDA Forest Products Laboratory in the USA.

European research is more focused towards the effects of timber properties on end-use products and methods of evaluating strength reducing factors which influence longitudinal shrinkage and instability, such as compression wood and spiral grain^(1.16). European centres of timber research include; Sweden's Malmö and Luleå Universities; the French national INRA, CIRAD-Forêt and French Forest Research Center in Nancy; the French-Swiss CBS-CBT collaboration; the Swiss Federal Institute of Technology; in Austria the Vienna Institute of Wood Science and Technology; the University of Freiburg in Germany; and the University of Sopron in Hungary. The Centre for Timber Engineering at Napier University is establishing itself as a further important centre for timber research. There has been productive linkage between many of these universities and industry with several in-line grading systems developed for sawn timber. Timber-based multinational companies such as Weyerhaeuser, or private research institutes funded by the pulp and paper industry such as STFI-Packforsk, also conduct extensive timber testing at various scales, but the majority of this research remains commercial-in-confidence.

Australasian research tends to focus more on the effects of juvenile wood on wood quality (through the collaborative 'Wood Quality Initiative' research) due to the increasing prevalence of juvenile wood in the majority species, *Pinus radiata* (radiata pine)^(1.16). Key research centres are the University of Canterbury (NZ), EnsisJV (NZ) and CSIRO (Australia). Australasia also currently leads the development of tools for wood property measurement, such as Silvascan^{TM(1.31)} (manufactured by CSIRO), HM200^{TM(1.32)} and ST300^{TM(1.33)} (Fibre-gen), A-

Grader™^(1.34) (EnsisJV) and TreeTap™^(1.35) (University of Canterbury). However, many of these devices are as yet not commonly used within the industry, with the HM200™ making the most progress in commercial sales and becoming the industry standard^(1.16). Further discussion of these devices is conducted in Chapter 3.

European devices, such as the IML hammer™^(1.36) tend to be used in wood science as an afterthought to their original design, though the Fakopp 2D™^(1.37) is more timber focused. Their use in academic research is still carried out in conjunction with the more established method of taking increment cores due to its proven ability to predict density and stiffness when combined with pattern-variation models.

It was noted by Carter *et al.*^(1.30) that whilst the relationship between acoustic velocity and properties such as stiffness and MFA has been confirmed experimentally in both laboratory and field tests, this has yet to be exploited effectively in a commercial sense. It is, however, shown in subsequent sections that commercial devices are available for evaluation of these properties with varying degrees of consistency. Cown^(1.16) confirmed the general lack of commercial application of timber property research incorporation into operational tools for timber analysis.

Research in Asia tends to be less commercially, and more academically, orientated than in other regions, and thus more focused towards individual properties of timber and less on silvicultural influences or product development^(1.16). Key research centres include Japan's Forest Tree Breeding Centre and The Forest and Forest Products Research Institute, as well as a variety of forestry and agricultural departments in universities, such as the Chinese Academy of Forestry and Beijing Forestry University.

The FPL *et al.* in North America use mainly Douglas fir (*Pseudotsuga menziesii*), western hemlock (*Tsuga heterophylla*), lodgepole pine (*Pinus contorta*), Sitka spruce and southern pine, whereas Australasian research focuses mainly on

eucalyptus (*Eucalyptus dunnii*) and radiata pine. Northern European research focuses on spruce (Norway and Sitka) and pine derivatives. Asian research focuses on species such as sugi (*Cryptomeria japonica*)^(1.16).

Whilst the development of tools for stiffness assessment of standing trees is still ongoing, resonance-based assessment of felled timber appears to have been accepted, and research now focuses on the combination of this with other techniques to predict factors affecting instability of timber (shrinkage, twist, etc. through spiral grain and internal checking) and strength (knots, pitch pockets and early-latewood ratio)^(1.16). According to Cown^(1.16), Swedish research is leading the field in developing systems to evaluate distortion, whilst the Australian Silvascan™ should help to standardise these methods.

Bucur^(1.15) suggests the development of acoustic techniques such as acoustic microscopy and photo-acoustics, which are outside the remit of this review (particularly due to the sparsity of literature available concerning their use in wood), could be used for the micro-scale elastic characterisation of wood constituents.

1.3 Research aims

The principal objectives of this research programme were largely determined by the case for support under the terms of the Strategic Research Development Grant awarded to The Centre for Timber Engineering (CTE), Napier University, by Scottish Government for research into timber, of which the evaluation of the applicability of current acoustic NDT methods to Scottish Sitka spruce was part. These objectives are:

1. The derivation and comparison of multiple dynamic stiffness estimates for a representative sample of felled timber with the subsequent dynamic, static stiffness and strength measures on battens. In this, establishing the applicability and the best method, if it exists, for the acoustic NDT of

generally low stiffness, high knot content, high compression wood Scottish Sitka spruce.

2. The recording of reference values of velocity for both wet and dry timber from different Sitka spruce progenies for future research comparisons, provided the applicability in terms of accurate strength classification can be achieved.

During the review of current literature and assessment of commercially available devices, it was apparent that the previously rapid development of acoustic NDT techniques for timber had stalled in the last few years, with longitudinal and transverse resonance velocity methods apparently being accepted as a *fait accompli* in terms of dynamic stiffness estimation for battens and logs. Seemingly, all that remained was application to different species. Standing tree investigation was more problematic given the impracticality for longitudinal resonance and the high variability of TOF methods. Additionally, correlations between dynamic log stiffness and static beam stiffness, and the timber grade classifications based thereon, suffered from variability due to species, and in particular were typically reduced with increased age and defectiveness of certain species.

As such, it was decided to progressively recreate the processes of acoustic NDT evolution under controlled conditions, to assess whether additional information could be recovered from these common resonance and TOF methods. Thus the additional aims of this thesis were:

3. To address current inconsistencies regarding the use of acoustic NDT in timber.
4. To evaluate factors influencing both TOF and resonance velocity.
5. To compare TOF and resonance velocities under controlled and field conditions, to observe whether differences can be attributable to mechanical properties, thus potentially providing new methods of timber property quantification.
6. To conduct a similar comparison between harmonics in both controlled conditions and field conditions.

7. To investigate the possibility of using an acoustic measure of the inherent damping of the timber to quantify specific timber characteristics.
8. To improve correlations between dynamic stiffness estimates and static stiffness through the addition of more acoustic information than simply that of velocity alone.

1.4 Chapter outline

Chapter 2 provides a discussion of the nature of timber, its qualities, strengths, and the factors which influence these characteristics. There is a comprehensive critical review of previous research specific to this field, with emphasis on particular Sitka spruce characteristics. Further current non-acoustic timber quality NDT methods are summarised, concluding with an outline of current grading procedures.

Chapter 3 leads the discussion to a critical review of the acoustic NDT of timber, its background and theoretical basis, assumptions and measurement-influencing factors including previous research across the various scales and acoustic methods relevant to this thesis. Debate arising from the findings, highlighted within Chapter 3, influenced the design and objectives of the author's test series.

At the start of each subsequent chapter (Chapters 4 through 7) the equipment, facilities, experimental procedures and objectives of the three laboratory test series and one field test series are presented. Consideration is given, where relevant, to influencing factors on the design of experiments and attempts to show the natural evolution of the research. This is in the form of single Sitka spruce beam investigations, through controlled homogeneity and defect insertion analysis, up to industrial scale acoustic NDT of logs.

Chapter 4 presents the results of initial investigations into the factors influencing longitudinal wave propagation, whilst comparing the relative behaviour and repeatability of low-frequency and ultrasonic waves. Results are discussed in

relation to previous research and recommendations are made regarding the use of TOF studies.

Chapter 5 builds on this work and the research of Chauhan *et al.*^(1.39) through the analysis of variably controlled homogeneity specimens and the resulting differential behaviour of resonance modes, dilatational wave propagation and inherent damping calculations. The effect of artificial defect insertion in relation to these acoustic parameters is evaluated and a new method of defect location and measurement proposed. Best practice advice based on experimental procedure is presented, and the effects of loading rate on dynamic stiffness estimates are examined in relation to previous research. Ultimately the implications of these findings for the prediction of timber quality using acoustic NDT are discussed.

Chapter 6 presents the results, and subsequent discussion, of the first industrial scale acoustic NDT sampling of three improved progeny and a control QCI progeny of British Sitka spruce. Methods devised in the previous chapters under laboratory conditions are examined in relation to field applicability. Six separate dynamic stiffness estimates and three inherent damping characteristics are examined in 150 logs and 650 subsequent battens. These parameters are compared to timber characteristics measured on both the log and batten specimens, and average properties of the logs are created from the battens for analysis of the accuracy of log dynamic estimates.

Finally, Chapter 7 summarises the findings of the earlier experimental chapters and discusses to what extent the thesis has achieved its stated objectives. It concludes with a discussion of how the implications of this study may be followed up with further investigations.

1.5 References

- 1.1 SFIC., *Scotland's forest industries*, 2004, Scottish Forest Industries Cluster, Edinburgh.

- 1.2 Treacy M., *A comparison of mechanical and physical wood properties of a range of Sitka spruce provenances*, 2000, COFORD, ISBN-10: 1902696115, p.35
- 1.3 Petersen, E.B., N.M. Petersen, G.F. Weetman, P.J. Martin, and W. Stanek. *Ecology and Management of Sitka Spruce*, 1997, Univ. of BC Press, Vancouver, BC. 240 pp.
- 1.4 Savill P. S., *The silvaculture of trees used in British forestry*, 1991, CAB International, Wallingford, Oxon, ISBN: 9780851987392
- 1.5 *Wood Handbook: Wood as an engineering material*, 1999, USDA Forest Service, Forest Products Laboratory, General technical report, FPL-GTR-113
- 1.6 'Concensus document on the biology of *Picea sitchensis* (bong.) carr. (*Sitka spruce*),' – ENV/JM/MONO(2002)2, OECD Environmental Directorate, OECD Environmental Health and safety division, 2002
- 1.7 Brauner L, Hoffmeyer P., Poulsson L., 'Mechanical properties of *Picea sitchensis*', Scandinavian Journal of Forest Research, v. 15 n.1, Feb 2000
- 1.8 MacDonald E., Hubert J., *A review of the effects of silviculture on timber quality of Sitka spruce*, 2002, Forestry, 75, 2, pp. 107-138
- 1.9 Stirling G., Gardiner B., Connolly T., Mochan S., Macdonald E., *A survey of Sitka spruce stem straightness in south Scotland*, Project report from August 2000, Northern Research Station, Forest Research
- 1.10 Forestry Commission, *Forestry Facts and Figure 2007*, National Statistics publications.
- 1.11 Dyck B., *Forestry Research in Scotland: A Review*, 2004, Draft 2 Report prepared for Scottish Enterprise.
- 1.12 Green D.W., Gorman T.E., Evans J. W., Murphy J.F, *Mechanical grading of round timber beams*, J. Mat. In Civil Eng., Jan/Feb, 2006, ASCE
- 1.13 Hearmon R.F.S, *An introduction to applied anisotropic elasticity*, 1961, Oxford University Press, Oxford, U.K.
- 1.14 Timoshenko S.P., Goodier J.N., *Theory of Elasticity: 3rd edition*, 1970, McGraw-Hill Publishing Co., New York
- 1.15 Bucur V., *Acoustics of Wood*, 2nd Ed., 2005, CRC Press, London, U.K.
- 1.16 Cown D.J., *Wood quality in the 21st century*, In: Proc. Wood Quality 2004, FIEA Conf., Albury, NSW, August 5-6, 2004.

- 1.17 Schad K.C., Schmoltdt D.L., Ross R.J., *Nondestructive methods for detecting defects in softwood logs*, Research paper, FPL-RP-546, 1996, USDA Forest Service.
- 1.18 Downes G.M., Hudson I.L., Raymond C.A., Dean G.H., Michell A.J., Schimleck L.R., Evans R., Muneri A., *Sampling plantation Eucalypts for wood and fibre properties*, 1997, CSIRO publishing, Australia
- 1.19 TRADA wood information, *Non-destructive testing of timber*, Section 4 Sheet 23, 1995, Department of the Environment, HMSO
- 1.20 Green D.W., Gorman T.E., Evans J. W., Murphy J.F, *Mechanical grading of round timber beams*, 2006, J. Mat. In Civil Eng., Jan/Feb, ASCE
- 1.21 Verkasalo E., Leban J-M., *Predicting modulus of elasticity and modulus of rupture of the major softwoods from Finland and France for the comparison of wood quality*, In: Proc. 13th Int. Symp. NDT wood, Berkley, California, USA, August 19-21 2002, Ed. F. C. Beall, Forest Products Society, Madison, Wisconsin, USA.
- 1.22 Divos F., Szalai L., *Tree evaluation by acoustic tomography*, In: Proc. 13th Int. Symp. NDT wood, Berkley, California, USA, August 19-21 2002, Ed. F. C. Beall, Forest Products Society, Madison, Wisconsin, USA.
- 1.23 Jayne B., *Vibrational properties of wood*, For. Prod. J., November 1959, pp. 413-417.
- 1.24 Ross R.J., Pellerin R., *Non-destructive testing for assessing wood members in structures*, General Technical Report: FPLGTR-70-1994, 1994, FPL, USDA Forestry Service.
- 1.25 Gerhards C.C., *Effect of knots on stress waves in lumber*, Res. Paper FPL-RP-384, 1982, FPL, USDA Forestry Service.
- 1.26 Gerhards C.C., *Effect of cross grain on stress waves in lumber*, Res. paper, FPL-RP-368, 1980, FPL, USDA Forestry Service.
- 1.27 Gerhards C.G., *Effect of earlywood and latewood on stress-wave measurements parallel to the grain*, Wood Sci., v.11, n.2, 1978, pp. 69-72.
- 1.28 Gerhards C.C., *Longitudinal stress waves for lumber stress grading: factors affecting applications: state of the art*, For. Prod. J., v.32, n.2, 1982, pp. 20-25.
- 1.29 Pellerin R.F., Morschauer C.R., *Non-destructive testing of particleboard*, Proc. 7th Int. Particleboard Symposium; March 1973; Pullman, WA. Washington State University.

- 1.30 Kawamoto S., Williams R.S., *Acoustic emission and Acousto-ultrasonic techniques for wood and wood-based composites: A Review*, General Technical Report, FPL-GTR-134, 2002, FPL, USDA Forestry Service.
- 1.31 Silvascan™, CSIRO, Manufacture's Website: <http://www.csiro.au/science/psvs.html>
- 1.32 HM200™, Manufacture's Website: <http://www.fibre-gen.com/hm200.html>
- 1.33 ST300™, Manufacture's Website: <http://www.fibre-gen.com/st300.html>
- 1.34 A-Grader™, Manufacture's Website: <http://www.ensisjv.html>
- 1.35 TreeTap™, Manufacture's Website http://www.canterprixze.ac.nz/docs/treetap_exec.pdf
- 1.36 IML hammer, Manufacture's Website: <http://www.walesch.ch.html>
- 1.37 FAKOPP 2D, Manufacture's Website: <http://www.fakopp.com.html>
- 1.38 Carter P., Wang X., Ross R.J., Briggs D., *NDE of logs and standing trees using new acoustic tools. Technical application and results*, In: Proc. 14th Int. Symp. NDT wood, May 2-4 2005, Hanover, Germany, May 2-4 2005, Ed. F-W Broker, Shaker Verlag, Germany.
- 1.39 Chauhan S.S., Entwistle K.M., Walker J.C.F., 2005, *Differences in acoustic velocity by resonance and transit-time methods in an anisotropic laminated wood medium*, *Holzforschung*, 59, 2005, pp. 428-434

Chapter 2 The nature of the material

2.1 Introduction

In this chapter the nature of the wood, in particular softwoods, is discussed followed by a review of the species that we shall primarily be dealing with in this investigation, namely Sitka spruce. Reference to the non-vibrational methods of NDT which have allowed researchers to come to conclusions concerning the factors affecting wood quality is provided where relevant.

In this investigation wood quality is seen as a function of stiffness and strength rather than appearance or pulp yield. This is because the predicted end-user in this instance is desired to be the construction industry. This industry is particularly concerned with mechanical properties, dimensional stability, durability and appearance to some extent. According to Treacy^(2.1), wood technologists place an increasing emphasis on wood density (though primarily due to historical reasons and the ease of measurement) and fibre length, whilst foresters typically desire higher densities, straightness's and yield volumes.

Ultimately, it is shown that the grain angle, the MFA of the S₂ layer of the cell wall and the density of a specimen controls the axial stiffness to varying degrees dependant on the position of the sample in the tree stem, whilst these factors' influence is reduced in strength testing due to variable macroscopic defects (knots and compression wood) within the timber. As such, in small clear samples, there is a good correlation between stiffness and strength (typically $0.7 > R^2 > 0.8$, dependant on species)^(2.2-2.4), which reduces in larger samples (typically $0.5 > R^2 > 0.7$)^(2.5-2.7). Factors affecting dimensional stability are primarily the reaction of the structural composition to drying through differential shrinkage. Drying induced defects (distortions such as warp, spring, and bow) and checking thus depend on microscopic anisotropies (grain orientation, earlywood to latewood bonding as well as the presence of compression wood, CW).

Bucur^(2.8) noted that anisotropy is characterised by a variation in the material response depending on the direction of applied stress. This is the case in wood at

varying scales (from the cellular structure through to the macroscopic structure) and is responsible for timber's variable response to strain and the inherent variations in stiffness, strength and dimensional stability.

Divos^(2.9) classifies NDT methods to investigate timber characteristics, as outlined below:

Mechanical: proof loading, static bending, Drill resistance, and pin penetration.

Vibrational: acoustic stress-wave TOF, US TOF, acoustic emission (AE), vibrational resonance frequency analysis (longitudinal, transverse and torsional resonances), and acousto-ultrasonics (combination of the previous techniques).

Electromagnetic: moisture meters, MW, near-infrared (NIR) spectroscopy and infrared (IR) thermography.

Nuclear: X-ray and gamma-ray computed tomography (CT), MRI.

Vibrational techniques for timber testing, which are the methods investigated in this thesis, shall be discussed in Chapter 3, though some reference to their use in establishing timber properties is mentioned in this chapter. An excellent review of the variety of techniques available for non-destructive investigation on a variety of materials is given in Halmshaw^(2.10), however a more detailed review specifically focused on wood structures is given in Bucur^(2.11) and from TRADA^(2.12).

2.1.1 Wood structure and mechanical properties

This section shall cover the nature of softwoods, and in particular Sitka spruce, their biology and mechanical properties that affect wood quality.

Unlike other building materials, whose production is quality controlled, natural defects, the influence of species genetics, provenance, and environmental factors affect wood growth and induce inherent variability^(2.13). Wood is an inhomogeneous, anisotropic, multi-layered biological composite material at both the cellular and macroscopic level, where variation in annual ring composition and

the variation of this with age and height in a tree, as well as the type, size and orientation of defects present across the volume add to this inconsistency in structure. Due to this natural anisotropy, strength and stiffness are also influenced by the way it is sawn from a log, and subsequently the direction and duration of loading. Environmental conditions (MC, humidity and temperature) can alter these characteristics or lead to susceptibility to decay^(2.14). The influence of such factors is debated, sometimes strongly, in the literature, for example Feio *et al.*^(2.15) note that;

“Some authors pointed out that wood behaviour in radial compression is strongly dependant on its anatomical features, but others believe that elastic behaviour is more dependant on density than on anatomical characteristics.”

Even this statement is open to question however as density is, of course, an anatomical characteristic. Based on a review of relevant literature^(2.2-2.3, 2.16-2.19), the desirable factors for higher wood quality from a structural engineer's perspective are:

1. A small (shallow) MFA of the S₂ layer of the cell wall with close alignment to the longitudinal axis of the tree stem. A thicker S₂ layer is also suggested by Tang^(2.20), though this is primarily related to density.
2. Higher density (for high quality timber, Tang^(2.20) suggests at least 50% latewood within annual rings).
3. No, or few, large knots or knot clusters (as the size, orientation and distribution affects strength more readily than stiffness)
4. The straightness of grain, as cross-grains such as spiral grain, diagonal grain and interlocked grain invariably affect strength and dimensional stability (including longitudinal shrinkage).
5. A reduction of drying induced defects, which often depend on the fibre alignment and more importantly the nature of sawing and drying.
6. A lack of compression wood, potentially leading to brittle failure.
7. A reduced proportion of juvenile wood (JW), though again this is mainly due to this portion of the stem encompassing negative aspects (lower strength and stiffness) associated therewith.
8. Relatively high tracheid length and cell wall thickness.
9. Low lignin content.
10. A reduction of growth stresses such as shakes, heart checks or cracks, or compression failures.

Many of these factors are interrelated. This list contrasts somewhat with the desired qualities of the forestry and sawmilling industry, which are; vigour, straightness (can begin selecting trees at 6 yrs), and higher wood density (can begin selecting trees at 15 yrs) ^(2.21). Juvenile wood is a principal area of concern for sawmillers, even more so since, due to current silvacultural practices, shorter rotations lead to an increased volume of juvenile wood and thus reduced timber strength and stiffness of timber ^(2.1, 2.19). As shall be seen in subsequent sections, the seedlot families selected for the Kershope study (forming the majority of this research) were done so on this basis, with a control seedlot for comparison.

2.1.2 Description of key wood properties

Wood on the macro-scale is modeled as orthotropic, having three orthogonal lines of symmetry ^(2.22). It is highly anisotropic due to hollow, elongated cells arranged parallel to the stem axis but with radial variation and juxtaposition of cells due to horizontal ray cells and the seasonal induced growth differences ^(2.8, 2.14, 2.16). This is further complicated by lateral and semi-lateral growths, termed defects, interrupting the homogeneously-modeled longitudinal (vertical) axis of the stem.

A tree, and the timber within it, can be modelled on three structural levels: the cell wall itself, the aggregation of these cells to form elongated chains of fibres (forming clear wood), and natural growth defects interrupting the longitudinal orientation of these aggregates ^(2.16). The tree has three physical functions: to support the crown (responsible for food and seed production) at the top of the tree; to conduct minerals from root to crown; and the storage of manufactured food (carbohydrates) ^(2.23). The basic building blocks of wood structure arise from the aggregation of cells in to fibres (tracheids). These fibrous cellulose chains are imbedded in an amorphous hemicellulose and lignin matrix ^(2.15). The variation in the orientation of these aggregates accounts for the majority of the anisotropy of wood as well as inhomogeneity at the micro-scale. An annotated image of the three structural levels of a tree can be seen in Figure 2.1, which covers the basic biology of wood formation. For a more detailed review of wood formation and properties, readers are referred to key subject primers such as Dinwoodie ^(2.23) and

the FPL Wood Handbook^(2.14), or the more detailed wood chemistry presented in Downes^(2.17) or Gibson and Ashby^(2.22).

Figure 2.1 The different scales of wood anatomy

-During growth, tree develops outer protective shell, composed of an outer bark and inner bark, and cambium (c. 30 – 60 μm wide, responsible for growth through radial and periodic tangential cell division)^(2,19). Sapwood (c. 40 mm to 60 mm radial thickness depending on vigour and age) directly behind the cambium is an inner growing region responsible for conduction and storage of sap from roots to leaves (responsible for food production)^(8,15).

-Annual rings, comprised of earlywood and latewood at an approximate ratio of 3:1^(2,2), develop due to seasonal climatic growth conditions. Earlywood is characterised by relatively large cavity cells and thin walls (c.2 μm thick) to support nutrient conduction^(2,8, 2,10, 2,15). Latewood is characterised by smaller cavities and thicker cell walls (c.10% thicker), hence increased wood density, as during this part of the season the primary function is support of the growing stem and crown, hence the need for increased density and structural homogeneity^(2,10, 2,15).

-The trunk grows relative to crown diameter whilst the inner part of the tree, behind the sapwood, gradually changes to become juvenile wood, which is the typically lower strength and stiffness region of the stem containing the pith (the core of the tree from which initial stem and branch growth was initiated) and approximately the first 5 to 20 years of wood growth^(8,9), below the fifth growth ring it comprises the pith area which has its own properties^(2,8, 2,10, 2,15, 2,17,23).

-Cellulosic fibrils aggregate to microfibrils which form the layers of the cell wall: primary wall (random, irregular network^(2,19)) and secondary wall (layers S1, S2 and S3):

-S1 layer: Thin (0.1 μm - 0.2 μm , ~10% cell width) outermost layer, average MFA of 60-70°^(2,17).

-S2 layer: Thickest layer (7 μm - 8 μm , ~80% cell width), significantly affects mechanical properties due to the influence of its density and microfibril orientation^(2,10, 2,17). It transmits most of the longitudinal stresses of the cell (and fibres of the stem) as its MFA is typically shallow, orientated towards the longitudinal axis of the cell. S2 layer is prevented from buckling in compression by the presence of the S1 and S3 layers on each side^(2,17).

-S3 layer: Thinnest layer (~6% of cell width), slightly inclined MFA but no strict order to this orientation^(2,17).

-Central pits of radially varying size between cells allow for cell aspiration, the transfer of fluids and food through actively conducting part of the stem or latently held moisture in other parts^(8,15).

-Daughter cells aggregate into either tracheids or rays; tracheids (or fibres) are close-packed, longitudinally orientated, elongated hexagonal prisms with tapered ends (typical length c. 3 mm – 8 mm), which account for 85-95% by volume of the wood structure^(2,12, 2,15). Tracheid length has been linked to the tensile strength of timber^(2,10). Both tracheid length and cell wall thickness have been negatively correlated with overall fibre angle^(2,10).

-Tracheids are stiffened by higher-density horizontal rays (parenchyma cells transporting and storing food), constraining the lateral spread of adjacent tracheid cells^(2,12). Tracheid longitudinal orientation accounts for anisotropic stiffness in wood. The relative proportions of radially variable thin-walled rays and thicker-walled tracheids play an important part in determining density variations across the stem^(8,15).

-Standard daughter cell created within the cambium consists of; cellulose (c. 40-50% total wood structure), hemicellulose (c. 20-30%), lignin (c. 20-30%), and extractives^(2, 2,15).

-Cellulose: high molecular weight chain polymer of glucose monomers; cellulose macromolecules aggregate during biosynthesis into amorphous crystals (one-third) or into fibrils (two-thirds) - chains of ordered crystalline strands^(2,1-2, 2,8, 2,12, 2,15).

-Fibrils subsequently organised into larger elements constituting the majority of the layers of the cell wall; forms principal cell constituent giving wood inherent mechanical strength and stiffness^(2,2). Hemicellulose (low-molecular-weight polymer of pentose and hexose sugar monomers) acts as cement bonding microfibrils together.

-Lignin occurs throughout the cell wall, mainly as cementing agent between continuous cells in the middle lamella (ML), again as a cell-cementing agent. Also acts to protect other components from water encroachment. The strength of bonding adds much to the strength of the overall timber through the transfer of shear stress from one cell to the next^(2, 2,15).

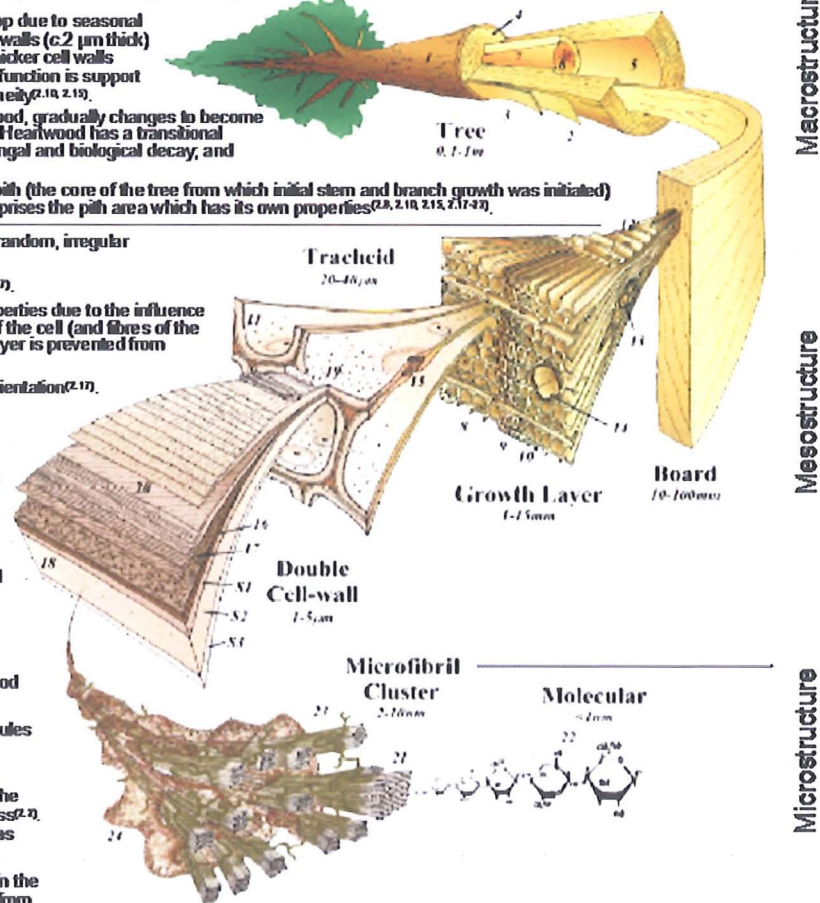


Figure 2.1 The different scales and anatomy of softwoods (from Harrington^(2,14)): [1] stem; [2] cambium; [3] inner bark; [4] outer bark; [5] sapwood; [6] heartwood; [7] juvenile wood; [8] earlywood; [9] latewood; [10] middlewood; [11] tracheid; [12] rays; [13] radial resin canals; [14] axial resin canals; [15] bordered pits; [16] middle lamella; [17] primary wall; [18] secondary wall; [19] warts; [20] cell wall lamella; [21] microfibrils; [22] cellulose molecules; [23] hemicellulose sheath; [24] macromolecular matrix.

2.2 Wood characteristics affecting the mechanical properties of timber

Estimates of the mechanical characteristics (strength and stiffness) are based on wood being an inhomogeneous, anisotropic composite with three mutually perpendicular axes: longitudinally along the stem, radially across the rings and tangentially perpendicular to the rings, as seen in Figure 2.1^(2.8, 2.14, 2.22). Each of these axes has different compressive and tensile stiffnesses but at low strain, deformation is deemed completely recoverable until the yield point where plastic deformation occurs^(2.14). The MoE represents stiffness and MoR represents strength^(2.25). MoR is the maximum load-carrying capacity sustained by the wood in bending before failure, which is proportional to the maximum bending moment in the specimen^(2.14). The determination of both of these parameters is described in subsequent sections; though as noted in the FPL Wood Handbook^(2.14), the measurement of these properties rely on an assumed linear elastic regime, which is not true beyond the yield point. There is a relationship (though species dependent) between MoE and MoR, though this relationship is not due to mutual interdependence but because density is a key parameter in controlling both their values^(2.23). For example, Divos^(2.2) cites an average correlation between MoE and MoR of $0.7 \leq R^2 \leq 0.8$ on SCS. Other examples from recent research papers can be seen in Table 2.1.

Table 2.1 Relationships between MoE and MoR during static bending tests.

Specimen type	species	sample size	Method of Measurement	R ² vs. MoR	Reference
SCS	Red pine	5	static bending	0.78	Deresse <i>et al.</i> ^(2.3)
SCS	Eucalyptus	120	static bending	0.79	Yang and Evans ^(2.4)
Beams	Norway Spruce	62	static bending	0.43	Oja ^(2.26)
Beams	various species	N/A	static bending	0.5 - 0.7	Gaunt and van Wyk ^(2.6)
Beams	Norway spruce	207	static bending	0.68	Johansson and Kliger ^(2.7)
Beams	Norway spruce	404	static bending	0.51	Johansson and Kliger ^(2.7)
Beams	Western hemlock/Douglas fir	98	static bending	0.64	Galligan and McDonald ^(2.27)
Beams	Sitka Spruce	190	static bending	0.56	Brauer <i>et al.</i> ^(2.28)
Beams	Pine	100	static bending	0.72	Hanhijärvi <i>et al.</i> ^(2.29)
Beams	spruce	100	static bending	0.57	Hanhijärvi <i>et al.</i> ^(2.29)
Beams	Eucalyptus	255	static bending	0.81	Piter <i>et al.</i> ^(2.30)
Beams	Eucalyptus	32	static bending	0.88	Ilic ^(2.31)

It can be seen from Table 2.1 that there is a great deal of variability between previous research, and as such within the proposed relationship between MoE and

MoR. MoE, as measured by the deflection under loading, is presumed industrially to reflect MoR and as such static bending machines utilise this relationship for strength prediction through stiffness grading of timber^(2.23). However, as wood is anisotropic, its response to bending stress is different to compressive or tensile stress and depending on the axis under the stress, for example timber is generally 20 to 40 times stiffer in the longitudinal direction than the tangential, due to the alignment of the cellular structure^(2.16). Further, the measurement of these mechanical properties is also reliant on an estimation of Poisson's ratio, which is variable between species (and between individual trees and orthogonal axes), though typically has an average value of 0.3^(2.16). It should also be noted that the comparison of mechanical properties is based on a consistent rate of loading in mechanical strength testing, commonly 5-20 minutes^(2.14). Faster rates of loading result in a higher estimation of the mechanical properties and equally lower rates of loading result in lower mechanical values, the FPL Wood Handbook quotes a 7% to 8% decrease in the stiffness value derived for each decade decrease in the loading rate^(2.14)

In addition to a possible explanation involving the type and method of measuring systems, the timber specimen size (SCS or beams) will influence the relationships^(2.6). Industrially (at full beam scale), the relationship tends to weaken from that found in SCSs: Johansson and Kliger^(2.7) found an $R^2 = 0.51$ (for 404 samples) to $R^2 = 0.68$ (for 207 samples), when full-size beams were tested. Although researchers such as Ilic^(2.31) found a high correlation between MoE and MoR on beams, the tests were conducted on relatively clear beam samples. This would indicate that differing characteristics of timber play a role in determining the MoE and MOR.

The factors controlling stiffness (discussed further in later sub-sections 2.2.1-2.2.8) have often been reported to be the MFA of the S_2 layer, density, and grain angle. However, it can be seen from previous research in Appendix C1, that knot size (though in combination with knot position relative to applied force as a focal point for wood fracture) plays a more important role in determining the MoR and hence strength of timber than in stiffness estimates^(2.32). Green *et al.*^(2.5) quotes MoE

alone as the largest single predictor of MoR ($R^2 = 0.61$), yet the combined MoE and KAR improves the relationship ($R^2 = 0.80$), there is evidence of a large variation in the range of correlation coefficients, more so than using MoE alone as a predictor. Indeed Sandoz^(2.33) states:

“The MoE gives information on the sample’s global (overall) quality (as does the longitudinal velocity), MoR depends more often on a local defect, which does not have a dominating influence on propagation velocity, but rather initiates the rupture mechanism.”

The relationship between MoR and MoE rises (to $R^2 = 0.67$) when the knot content (expressed as maximum knot size, rather than the more common knot area ratio (KAR)) is included as well as reducing the variability of results^(2.5). This was supported in the studies of Johansson and Kliger^(2.7) who found that the largest influence on the MoE was found to be density ($R^2 = 0.75$) and KAR ($R^2 = 0.52$)^(2.7). However, this would be questioned by other researchers based on the correlations between MFA and MoE, as shown in Appendix C1. Despite this, since the 1960s the relationship between MoE and MoR has been the basis of the MSG system and MoR can be predicted from MoE accurately, at the 90% confidence level^(2.8).

The relationship of individual parameters to MoE and MoR, compiled from recent research and including the use of non-destructive estimates of the various parameters, is presented in Appendix C1.

Hanhijärvi *et al.*^(2.29) undertook studies into the influence of various parameters on MoE and MoR, though crucially not MFA, and found that the coefficient of determination (R^2) between MoR and most parameters was ‘remarkably’ higher for pine than spruce (due to an increased variability in the MoE and MoR, but also the grain angle, density and presence of knots), indicating the species dependant nature of these parameters’ influence, which was also the conclusion of Verkalasko and Leban^(2.34). Hanhijärvi *et al.*^(2.29) also concluded that stiffness was the best single indicator of strength. It was also noted that the prediction improves through the combination of other parameters, as is also shown from results of previous research in Appendix C2. Many individual and combined parameters

have been used in correlation to dynamic estimates of MoE and MoR during vibrational testing, these are discussed in Chapter 3.

Standing timber properties are primarily studied by employing an increment borer which takes increment cores (typically at breast-height), which involves the rapid extraction (though samples are prone to damage in extraction and transportation^(2.17)) of a circular sample of the material radially through one side of the tree, which must then be sent for laboratory analysis. As increment cores were not analysed in this thesis, readers are directed to suitable references (TRADA wood information^(2.12); Downes *et al.*^(2.16); Green *et al.*^(2.5); Schad *et al.*^(2.35); and Verkasalo and Leban^(2.34)) on the benefits and limitations of their use, in which the non-destructive nature of their use is debated. Similarly discussions on the use of resistance drilling or Pilodyn testing (neither of which has been employed in this thesis) are also available (resistance drilling: Feio *et al.*^(2.15); Saporiti Machado *et al.*^(2.36); or for Pilodyn testing see Downes *et al.*^(2.17))

Descriptions of the various NDT techniques and their potential application are given in Appendix C3, presenting a summary of the principle wood parameters and their relationship to strength, stiffness, and each other. Appendix C4 displays examples of the use of the different wood property measurement techniques described in Appendix C3, and their relations to either other wood parameters or other methods of calculating the same parameter.

2.2.1 Age of timber

It is accepted that timber quality, its mechanical characteristics and the inherent characteristics contributions to timber quality, generally increases with age^(2.23, 2.37-2.39). There is a pattern in softwoods that young stems have, on average, low density and high MFAs, which together account for low stiffness and, by correlation, low strength^(2.40-2.41). This pattern continues within the juvenile wood, gradually improving until after 15 to 20 years when the wood's cellular structure within annual rings has sufficiently low MFA and higher density to be called mature wood^(2.40). Xu^(2.43) found little difference in log stiffness between the butt and upper

logs, but contrary to historical sawmilling assumptions the butt log typically had less stiffness than the second log in terms of height, with stiffness decreasing vertically thereafter. It is noticeable that more rings, and hence proportionally more mature wood, occur in the lower logs of the tree and as such a general decrease in stiffness in height is expected^(2.40). Additionally Wang *et al.*^(2.43) found evidence that the lowest (butt) log has lower stiffness (through higher MFA and lower density) than the region directly above. It is then found that the decrease in stiffness with height follows the predicted pattern from the second log upwards, indeed Johansson and Kliger^(2.7) noted that, in general, butt and second logs produce stronger timber than other heights.

The current trend of the forestry sector towards shorter rotation periods for timber stands has a detrimental effect on timber quality, as previously stated through the increased proportion of juvenile wood, thus silvicultural efforts attempt to mitigate this loss of quality through thinning, spacing and pruning stands^(2.1, 2.37, 2.41). Since the central section of the stem forms the majority of the end-product (sawn boards), this presents implications for economic returns.

2.2.2 Silvicultural effects

Cown^(2.19) noted that the initial trends in commercial forestry, in Australasia but applicable to most countries, was to deploy environment-specific, fast growing breeds. Later, after one or two rotation cycles, thinning, stocking, fertilising and genetic selection was utilised to improve growth rate, vigour and stem form^(2.18). Bucur^(2.8) states that pruning improves wood quality through the removal of knots and reduction of propensity to longitudinal shrinkage, improves density and the improvement of the straightness of the stem^(2.8). However, Petersen^(2.21) states that thinning improves yield through creating faster growth thus dimensionally larger trees. This creates a point of contention given that increased vigour is coincident with lowering the density through a greater proportion of earlywood and thus the stiffness of timber. This can be shown by research showing that thinning generally decreases the MoE of trees in SCS^(2.1, 2.41, 2.44). Fertiliser improves quality, size and yield growth rate, though with the coincident decrease in density^(2.21). Petersen

also states that spacing and pruning have the largest impact on timber quality^(2.21). Forest managers must ensure sufficient drainage in a site as water stress can lead to decreased latewood and thus decreased density^(2.44).

As result of both silvicultural methods and decreasing rotation period due to improvements in growth rate and vigour, a disproportionate increase in juvenile wood has been observed along with increased stem taper, larger branch sizes and increased variability between trees of the same stand, all of which have negative economic implications for sawmillers^(2.18, 2.45-46). The increase in juvenile wood therefore has the effect of increasing proportional volume of high MFAs, lower densities and low stiffnesses^(2.1, 2.40, 2.47). Laserre *et al.*^(2.48) showed that lower spacing increased whole log stiffness (by 27%) which would seem at odds with the decreased fibre length (by 10%) and MFA (by 18%) found. However, the increased stiffness could be explained by the increase of 17% in latewood percentage and a 28% increase in cell wall thickness and a decrease in ring width (by 61%)^(2.48). Though the basic density was not significantly different between spacings, this would suggest that the outer wood stiffness at least was controlled by factors other than the MFA^(2.48). A summary table of important silvicultural practices is presented below, as adapted from Macdonald^(2.45):

Table 2.2 The effects of silvicultural practices on wood quality^(2.45):

Silvicultural practice	Effects on wood quality
Reduced rotation length	Increased juvenile wood (thus reduced stiffness, strength and dimensional stability)
Wider initial spacing	Increased diameter growth (reduced density through larger earlywood rings), fewer and smaller branches on lower stem, increased taper and compression wood (due to increased wind exposure), possible reduction in stem straightness, increased grain angle
Thinning	Similar to effects of increasing spacings, though in cases of drought or arid conditions the opposite effects are possible
Pruning	Reduces extent and size of knots, reduces taper, accelerates transition from juvenile to mature wood
Fertilisation	Increases growth rate (decreases density), possible uneven growth thus increased dimensional instability or reduced straightness

2.2.3 Grain angle (slope of grain) and spiral grain

Variations in grain angle (θ) arise from the predominant angle of the fibres not being coincident with the longitudinal axis (or edge) of the timber^(2.14). This can occur either due to the cutting process or due to natural variation in grain angle as a response to growth stresses during tree development^(2.14). Note that this is not the same as the MFA which is the orientation of the cell wall layers to the longitudinal axis of the cell, though at times both the MFA and the grain angle may have similar effects on stiffness and strength. The grain angle is expressed as a ratio, derived from a measurement of a tangential variation of 25 mm depth from a starting point at the edge of a sample, and the distance over which this change occurred^(2.14). By deriving this angle, approximations of the mechanical properties (E_θ , representing strength or stiffness at a given grain angle) can be made from a Hankinson-type formula using the theoretical mechanical properties (strength or stiffness) in the longitudinal (E_L) or tangential (E_T) orientation^(2.9, 2.23, 2.49), but note that Bodig and Jayne^(2.49) had an extra E_T in the dividend of the equation, so has been added to this equation:

$$E_\theta = \frac{E_L E_T}{E_L \sin^2 \theta + E_T \cos^2 \theta} \quad \text{Eqn 2.1}$$

Dinwoodie^(2.23), Bucur^(2.8) and Gerhards^(2.50) all present curves showing the effect of a deviated grain angle from the horizontal. From Dinwoodie's curves it can be seen, however, that a grain angle of 60° from the longitudinal axis of stress amounts to a strength reduction of only 10%^(2.23).

However, it should also be noted further studies by Bindzi and Samson^(2.51), supported by Mascia and Lahr^(2.52), suggest an adapted formula (from the Hankinson-type) that claimed represents a more accurate prediction of stiffness when considering to the effect of slope of grain on wood stiffness. It was then further modified by Salikis and Falk^(2.53), who cited the failure of the previous methods to estimate MoE variations of composite panels, primarily because panels (as opposed to solid wood products) have the smallest MoE at 45° (*i.e.* between the longitudinal and tangential) and claimed better calculations of the shear

modulus in axial tests as a result whilst simultaneously removing the need for a derived Poisson's ratio. However, it should be noted that leading wood researchers such as Divos^(2.9) and Bucur^(2.8) still cite the Hankinson-type formula from Bodig and Jayne^(2.49).

Results shown in Appendix C1 would indicate that grain angle does not have a significant influence on stiffness or strength. However, this is most likely due to the small range in grain angle in industrial beams tested, and there is a noticeable improvement in the correlation of KAR to strength when grain angle is incorporated, possibly due to the inducement of spiral grain as a result of branch growth.

Spiral grain, which has a high formational tendency in Sitka spruce, is caused by typically left-handed helical winding of the fibres (or grain) around the tree rather than the traditional vertical (longitudinal) orientation, and occurs primarily in juvenile wood^(2.9). It increases to a peak of 4° before tending to the vertical axis during the transition to mature wood^(2.45). Hence it is less important in older stands but with more short rotation forests, and the corresponding increase in proportions of juvenile wood, it is of increasing importance. The reason for its formation in juvenile wood is believed similar to the explanation of high MFAs in juvenile wood, in that its formation allows increased flexure of the stem in the wind^(2.45, 2.54), and possibly the additional benefit of uniform nutrient distribution within the stem^(2.54). Spiral grain also causes a propensity to twist when over 3-5° from the longitudinal, and is thought to cause the high rates of distortion through longitudinal shrinkage and significant twist in juvenile wood^(2.18) though this is most likely due its co-existence with high MFA rather than the spiral grain itself^(2.5, 2.54). Indeed, Cave and Walker^(2.47) suggested that spiral grain was induced from the S₂ layer of the cellular structure. They found that decreasing prevalence of spiral grain in common with outward distance from the pith means that strength is reduced by a factor of 3 to 5 when compared to the first 30 years of growth^(2.47).

Small changes in grain angle or the occurrence of spiral grain are usually undetectable by visual inspection (unless observation of resin pockets is made). It

can be measured by electrical capacitance testing^(2.14). Traditionally grain angle and spiral grain are detected by mechanical methods based on the geometric angle approximation of dielectrical methods, through resistivity testing^(2.1). More recently, the development of Silviscan[®] has allowed for the measurement of both grain angle and spiral grain through X-ray diffraction^(2.38, 2.4).

2.2.4. Density

Assuming a constant slope of grain, the issue of what controls the strength and stiffness of timber is debated. Historically, density was perceived as having the largest control on stiffness and strength, which also coincided with being an easily (and cheaply) measurable property through 'non-destructive' increment cores in standing timber and ring width observation in sawn timber. According to Cave *et al.*^(2.55) this was also due to;

"A fortuitous correlation between density and cellulose orientation found...in Radiata pine principally because each co-vary with ring number (radially) across the stem...however Evans (1999) has pointed out that these factors are independent and also heritable."

Wood density has been shown to be a function of the cell wall thickness and as such is dependant on the constituents of the cell wall and the relative proportions of high-density cellulose^(2.11). Whole tree density tends to increase with age due to smaller growth rings (reflecting closer packing of early wood and late wood and thus a greater proportion of higher density latewood) with increasing age^(2.16). However, it also may be the result of a thickening of the cellular walls coincident with decreasing MFA. Density is very high at the pith but then decreases in the juvenile zone, typically 8-12 annual rings, and then increases (gradually) by ~50% from this zone to the bark^(2.1, 2.47). McKinley *et al.*^(2.56) observed a relationship between outer wood density and whole tree density of $R^2 = 0.89$. It should be noted that comparisons between investigations concerning density are often difficult due to the different measures of density used (the most commonly used being basic density, alternatives include green density, oven-dried density, and specific gravity, for a review of these measures see the FPL Wood Handbook^(2.14)).

Dinwoodie^(2.23) and Gindl and Teischinger^(2.57) both assert that axial compressional strength properties increase proportionally with density. The dominance of MFA in controlling the axial tensile strength is also acknowledged^(2.57). Density's position as the key controlling factor is more debatable when considering stiffness. In work conducted (using Silviscan[®]) by Evans and Ilic^(2.38), density only accounts for approximately 65% of the variation in stiffness of small clear samples. Other results presented in Appendix C1 indicate this influence is variable depending on the size of sample investigated; however it seems to be the case that density has a significant influence on the stiffness and strength of small samples whilst reducing in larger samples. When the measurement of MFA is added to this prediction, the proportion of the total variation in wood stiffness that is accounted for by a combination of density and stiffness, rises to between 92% and 96%^(2.4, 2.38), as seen in Appendix C2. However, Cown et al. (1999), as quoted in Maclaren^(2.54), suggest that whilst this relationship was true for juvenile wood, the MFA between trees is relatively constant in mature clear wood (*i.e.* not compression wood or wood with high knot contents) and as such density of the cell wall controls the stiffness of mature wood. Density is also subject to the MC of the material. Generally, the influence of MC on density is due to the swelling and shrinkage of the timber altering the volume of the specimen under examination^(2.16). The density of green wood will always be higher than that of dry wood due to the removal of the weight of water^(2.54). However, it should be noted that since the density of the cell wall (*c.*1500 kgm⁻³) is higher than that of water (*c.*1000 kgm⁻³), cell wall thickness and cavity size plays an important role in determining green density^(2.14). Further influences of MC on other factors affecting strength shall be discussed later.)

Overall previous research seems to indicate that the influence of density is greater in correlation to strength (MoR) than to stiffness (MoE), and that whilst its combination with MFA appears to control stiffness (dependant on the radial position of the sample in question), density's controlling influence on strength is also dependant on the influence of knots due to its fracture-inducing nature, as described below in Section 2.2.7.^(2.16, 2.23)

Ring width was used as a historical measure of density, but this relationship is inaccurate as not only will ring width decrease from pith to bark, but increasing growth rate results in increasing the proportions of lower density earlywood (which has approximately half the density of late wood bands), resulting in a contradiction in the proposed relationship^(2.14, 2.16). Brauer *et al.*^(2.28), as shown in Appendix C1, produced a relationship between ring width and density in Sitka spruce of only $0.17 \leq R^2 \leq 0.24$.

Currently density may be measured directly by gravimetric calculation (dimensions and mass measurement) or gravitational immersion techniques (volumetric displacement in water) or indirectly by; NIR spectroscopy (for cellular density^(2.58-2.61), increment core density^(2.62-2.65) and macroscale specimen density variation^(2.66-2.69)); X-ray densitometry^(2.11-2.13, 2.35); or gamma-ray densitometry (which is possible through the linear relationship of radiation absorption and density)^(2.1, 2.35). Examples of the use of these methods are seen in Appendix C4. Commercially available NIR inspection devices include the NIR systems inc. model 5000 and 6500 scanning spectrophotometer^(2.17, 2.67) and the Bruker Matrix-F^(2.66).

The advent of combined optical microscopy, X-ray densitometry, X-ray diffraction and thus X-ray computed tomography (CT) scanning in systems such as Microtec's Goldeneye[®], Newnews Machine Ltd.'s X-ray lumber grader, and CISRO's Silviscan[®] for rapid, non-destructive estimates of radial variations in density through SCS, disks and cores has allowed for more expansive sampling of wood density and its relationship to strength and stiffness. Appendix C4 also lists several studies using X-rays to create density profiles in logs. It has been proposed, by Downes *et al.*^(2.17), that the use of Silviscan[®] could serve to calibrate devices for in-situ detection of increment cores on trees (or even whole tree analysis devices), though subsequent results presented in McKinley *et al.*^(2.46), show that relationships between Silviscan[®] and NIR-derived data on various wood properties from larger specimens were relatively poor, ranging from $R^2 = 0.23$ to 0.67 . Similarly Cown^(2.18) noted that CT-scanning of logs has so far failed to conform to commercial expectations regarding resolution (an inability to detect small resin pockets) or speed. Alternatively, x-ray reflection may be measured

through the 'backscatter technique' which allows for estimates of surface density variations through detection of the reflected rays^(2.12). However this does tend to overestimate the size of surface defects^(2.12).

2.2.5. S₂ layer MFA

The MFA of the S₂ layer, or the inclination to the longitudinal axis of the cell, has been cited by many sources as controlling stiffness, at the fundamental level, and that reduction in the MFA increases the stiffness^(2.17, 2.23, 2.37, 2.47, 2.54, 2.70-2.71). Indeed, Dinwoodie^(2.23) made the assertion that:

“The angle of the microfibrils in the S₂ layer has the most significant effect in determining the strength of wood... (through) a strong negative correlation between tensile strength of the cell wall material and increased MFA, the effect closely parallels that of changing grain angle.”

In the S₂ layer the cellulose content is wrapped around the cell in a steep helix so as to provide support as a structural framework of the cell wall in the longitudinal axis in tension^(2.17, 2.47). The S₁ and S₃ layers, as well as the lignin in the cell wall, act to prevent buckling in compression^(2.23). The orientation of the cells (and thus fibrils) in the cell wall is dependant on the cell's position in the tree, i.e. will take the characteristics necessary to achieve optimal performance in its location^(2.47). Hence, juvenile wood has a high MFA to support the tree in the flexure and bending suffered by young trees due to increased exposure to wind at this age or at the top of the tree^(2.37). The angle shallows with age (by one degree per year) to allow for increased water conduction and support the growing stem (increasing longitudinal stiffness to resist lateral and gravitational forces), as less flexural resistance is required lower down the stem due to the increased size of the tree, though the tops are still subject to flexure and thus have proportionally higher MFA^(2.1, 2.17, 2.37, 2.54, 2.70). Cave and Walker^(2.47), observing the change in stiffness by a factor of 3 to 5 during the first thirty years of growth, and asserted that this could only be due to a shallowing of the MFA (40° down to 10°) during tree growth, as the doubling of density during the same period would only increase the stiffness by a factor of 1.3 to 1.5. Strong correlations between MFA and stiffness can be seen from previous research as displayed in Appendix C1. Thus it is presumed in

young trees, selection for improved stiffness can be conducted due to the repeatable pattern of MFA increase (thus making the early testing by NDT methods on stems considerably more appealing)^(2.47).

It should be noted that even in the outer wood in the stiffest softwoods, the MFA plateaus and is unlikely to fall below 10° ^(2.72). Indeed Evans and Ilic^(2.38) and Yang and Evans^(2.4) found that the reduction in MoE due to increasing microfibril angle has a threshold angle (variable, though approximately 16° in this case) after which little reduction in stiffness occurs. As such it could be hypothesized, that the variation in stiffness of the outer wood (with MFA below this critical angle) is controlled by the variations in density.

The MFA and cell wall thickness has previously been evaluated using techniques such as; Polarised light microscopy^(2.73); confocal scanning electron microscopy (SEM)^(2.74); X-ray diffraction^(2.75); and through the use of combined automated X-ray densitometry, X-ray diffraction and image-analysis devices such as Silviscan-2[®]^(2.17), which also allow for density, grain angle, fibre thickness and tracheid length measurements. The latter device enabled more rapid and hence extensive studies of timber properties, with researchers using the Silviscan-2[®] to make estimates of clear wood MoE of the SCS based primarily on the combination of MFA and density^(2.76), and other examples of its use being shown in the tables in Appendices C1, C2 and C4. However, Silviscan-2[®] is susceptible to overestimating the MFA due to the reorientation of fibres in the longitudinal/tangential plane as a result of spiral grain and drying distortions^(2.17). As such, although this inaccuracy can be dismissed with shallow grain angles, a spiral grain of 10° to 25° can result in an overestimate of MFA by 1.5° to 10° , respectively^(2.17). Further, it was noted by Wang *et al.*^(2.97) that using polarised light methods (and confocal microscopy detecting reflected light) are generally time consuming and prone to error, whilst scanning electron microscope analysis tends to selectively exclude higher MFAs from the measurement in addition to being hard to find and having a small field of vision over the sample. It was also noted by Walker^(2.37) that the use of X-ray diffractometry is unlikely to be possible outside the laboratory or sawmill, due to its dependence on small sample sizes, but devices such as Silviscan[®] can allow

for the benchmarking of NIR or acoustic tools which have increased ruggedness and portability. This is confirmed by Schimleck *et al.*^(2.64) who pointed to its ability to calibrate NIR for detection of MC, density, MFA and other wood property variations. Other indirect methods included time-consuming measurements of the orientation of pit apertures or induced checks which tended to follow the MFA^(2.1).

2.2.6. Moisture and temperature

Moisture exists in wood as a nutrient transportation agent and is present in sapwood cells, and to a lesser extent in heartwood, as either 'free' water (partially or fully filling the cellular cavities or lumen), water vapour in cell cavities or as 'bound' water (held within the cell walls)^(2.8, 2.14, 2.16). In green wood the cell walls are completely saturated, thus the transition from free to bound water being at or above FSP^(2.8). The MC of a material is the weight of water in wood expressed as a fraction of the weight of the oven dry wood, as such it can range from 0% to over 200% (commonly above 60% in living trees)^(2.8, 2.14, 2.16). As such it is typically measured by weighing and properties between species are typically compared at 12% MC^(2.16). Generally speaking, above the FSP most mechanical properties are not affected by free water as the strength is controlled by the cell walls^(2.8). With increasing MC from oven dry to the FSP, the decrease in mechanical properties is due to the swelling of the cell wall resulting in less cellular material for the given volume and water entering the cell walls and weakening the hydrostatic bonds^(2.8, 2.14). Assuming a constant temperature below FSP, the FPL wood handbook states that in general a 1% MC increase leads to a 1.5% change in MoE and a 4% change in MoR, indicating that strength is more affected by MC than stiffness^(2.14, 2.77). Conversely EN384 adjusts MoE by 2% for every 1% change in MC, yet makes no provision for adjusting MoR^(2.7). These relationships vary between species.

Commercial drying of timber after sawing is either by air-drying (seasoning) or kiln drying. Air drying, out in the open or under a cover with separations for air movement, seldom reduces the MC below 16% and can take 2 to 10 years. There is also a risk of fungal or bacterial attack. Kiln drying takes 2 to 5 days (and is thus favoured by sawmillers), where material is placed in a temperature and humidity

controlled room and dehumidifiers and latent heat is used to warm the air which circulates around the timbers. A compromise process involves placing the sawn boards in kiln at 70°C until dried to 18% to 20% MC, and then moved to a conditioning chamber, which takes 2-3 weeks at 20°C/65% relative humidity (RH) to reduce the MC to ~12%, as occurs in this thesis's research.

Longitudinal shrinkage in timber leads to drying defects, essentially occurring due to the inhomogeneous cellular structure and anisotropic nature of timber (earlywood to latewood layers' bonding and MFA variations) inducing differential rates of drying due to uneven exposure, and are thus more prevalent in kiln drying^(2.78). As wood dries, inherent swelling between fibrils is reduced, however due to the anisotropic nature of cellular and fibre alignment, this is far greater in the tangential axis (1 to 2% of cross-section) than in the longitudinal axis (0.1% of length when MFA is less than 35^(2.3), although in juvenile and compression wood longitudinal shrinkage can be as high as 2%^(2.14)), as their swelling (and thus shrinkage) occurs between adjacent fibrils, a situation enhanced by higher MFAs^(2.14, 2.22-2.23). Disproportionate anisotropic shrinkage can occur leading to warping, checking (typically parallel to grain in proximity to rays) or actual splitting of the timber, thus reducing the strength and stiffness properties of the timber^(2.14, 2.19, 2.78).

Most timber moisture content meters are electrical resistivity-based, however capacitance meters can also be used, though the latter only gives surface MC readings rather than providing any indication to internal moisture content^(2.12). In addition to measuring the MC for comparative purposes, they have been used to detect areas at risk of decay, or detect the grain angle through electrical capacitance (as the dielectric content is typically 50% greater along the grain than across the grain^(2.12-2.13, 2.79)). Other methods of MC measurement include microwave^(2.80-2.82), optical and CT scanning^(2.83), NMR^(2.84), MRI^(2.85-2.86), or radar^(2.35) based estimations dependant on relative density variations. These relatively expensive methods are complicated however by inherent density and defect issues due to natural radial density variation, compression wood, and knot content.

Behaving in a similar way to MC, mechanical properties see a proportional linear decrease with increasing temperature above and below freezing point (0°C), which is usually concurrent with decreasing MC^(2.8, 2.14). However studies by Green *et al.*^(2.87) and Bächle and Walker^(2.41) indicate that this is a two-part, segmented linear relationship, as below freezing there is a sharper decrease in stiffness than above it due to the expansion of water in freezing, indicating that green wood is influenced more than dry wood by temperature changes. It was shown in Dinwoodie^(2.23) that at a constant 0% MC, the change in MoE over a temperature range of -20°C to +60°C was only 6%, but for the same range at 20% MC the change in MoE was 40%.

2.2.7. Natural defects - knots

Knots (remnants of branches intergrown with the stem) in wood create interruptions in continuity (dead knots), or deviation (in live and dead knots) of the clear-wood fibres (grain angle), developing localised cross-grain with steeply-inclined slopes, thus deviating the grain angle from the longitudinal axis^(2.14, 2.16, 2.23, 2.88). This deviation is, on a local-scale, similar to the effect of deviations in grain angle on mechanical properties when examined in clear wood and are associated with increased checking in the specimen^(2.23, 2.50, 2.77). Encased knots typically result in less grain deviation than live knots, but may transmit stresses less readily through reducing the cross-sectional area over which stress can be transmitted^(2.14). As such knots reduce the stiffness of a specimen, depending on their size and distribution^(2.42), but over the whole volume of a specimen their influence is less important than those of MFA and density^(2.7). However, knots affect strength (MoR) more readily, accounting for > 50% strength reduction depending on species^(2.29, 2.32), due to creation zones of localised weakness from which fracture and load failure initiates (particularly when comparatively large, formed in clusters, or at the edges of beam specimens). Thus their location and size (relative to the distribution of stresses) is of far more importance than for stiffness^(2.14, 2.17, 2.23, 2.54, 2.77). Due to self-pruning and crown development, knot content typically increases vertically in a stem^(2.29)

The extent of knots is traditionally quantified (due to their visibility on the surface) by the KAR, which is the total area of a knot divided by the cross-sectional area, or the KVR, which is the total volume of knots in a specimen determined by NDT scanning^(2.22-2.23, 2.89). KVR calculation is possible due to the higher density of knots in comparison to clear wood, allowing for visual quantification from CT-scan images. Examples of this are seen in Appendices C1, C2, and C4. KAR and KVR do not take into account knots outwith the beam specimens, *i.e.* those knots whose presence in the log induced grain deviations which may still be present without a visible knot. Additionally, the measures place no emphasis on the orientation of the knots, as longitudinally orientated knots cause less grain deviation. Knot diameter ratio (KDR) can also be used as a calculation method at times but tends to place more emphasis on longitudinally orientated knots (it is not used in this study or common in the literature, for more information see FPL wood Handbook^(2.14)). The shape of the knot is classified optically in several categories; see the FPL wood Handbook^(2.14) or BS EN 14081:2005^(2.90) for further details.

In terms of NDT for knot identification, recent examples include; IR Thermography^(2.91-2.93) based on relative cooling rates between clear wood and the knots; CT scanning^(2.89, 2.92, 2.94-2.95) based on the increased absorption intensity of x-rays by knots; MRI^(2.85-2.86) can identify knots, reaction wood and gum spots based on relative MC differences; and optical recognition devices^(2.95). Pham and Alcock^(2.95) provide a classification guide and review of automated defect detection systems and their operation, focusing primarily on computerised visual recognition systems which recognise surface parameters such as defects (based on grey-scale image analysis). However the paper acknowledges that the system can fail to recognise sound knots (due to their transitional nature and similar grey-level to clear wood) and that the process is still too slow for industrial use, particularly in regards to segmentation of the images^(2.95). Issues such as cost and portability restrict the field NDT potential of most of these methods.

2.2.8 Natural defects – reaction wood

The FPL Wood Handbook describes reaction wood as:

“Abnormally woody tissue frequently associated with leaning boles and crooked limbs formed as natural response to exterior stress (wind and a gravitropic response due to slope instability), and thinning (which possibly makes trees more prone to ‘wind-sway’) to return to a more normal position.”

Due to the nature of its formation, in hardwoods it is termed tension wood and in softwoods termed as compression wood^(2.8). In softwoods it commonly forms in compression on the lower side of inclined branches or stems^(2.14). It has been suggested that it is strongly co-incident with juvenile wood^(2.8). It is fundamentally different in composition from normal wood, though the change is often gradual, in that it typically reflects:

Wider growth rings with a higher proportion of latewood than normal, though the change between early and latewood is more gradational^(2.16).

Increased density (~30 to 40% higher than normal wood^(2.14)) through a greater proportion of latewood, thus adopting a darker colour compared to normal wood. The increased density has also been suggested to be the result of typically thicker cell walls and an increased lignin content^(2.8, 2.96-2.97), which may indicate a requirement for increased bonding strength in compression wood.

Increased MFA ($30^\circ \leq \text{MFA} \leq 45^\circ$)^(2.8, 2.16, 2.46), which may also account for the increased longitudinal shrinkage in compression wood which behaves similar to juvenile wood (~ 10 times that of normal wood^(2.1)). This is coincident with a shortening of tracheid lengths^(2.8). It was suggested by the studies of Donaldson and Turner^(2.96), against accepted theory, that the presence of a high average MFA and compression wood are actually independent of each other (at least for mild compression wood), but are both still related to increased dimensional instability.

A lack of an S₃ layer^(2.46, 2.72), which in normal cells has microfibrils aligned near-tangentially to the longitudinal cell axis and thus strengthens the tissue in standing

trees to mitigate compressional collapse. However studies by Singh *et al.*^(2.97), found an S₃ layer present in mild compression wood.

As a result of the above mentioned characteristics excessive distortion (longitudinal shrinkage and other defects) is typically seen on drying^(2.16). Whilst compression wood has increased relative strength in green wood (compared to normal wood) and in compression^(2.24), when dry, due to a brittle manner and the distortion^(2.14, 2.16), it typically has a reduced MoE compared to normal wood from the same sample. In general there is a lack of literature detailing the relationship between stiffness and compression wood. However, the typical presence of high MFA would indicate reduced stiffness. MacDonald^(2.45) reports the work of Ni Dhubhain *et al.* (1988) in Sitka spruce beam specimens, which found no influence on the MoR but that MoE decreased with increasing compression wood content. No devices currently conduct automated compression wood measurements *per se*, but it can be inferred in Silviscan[®], X-ray and CT scanning due the nature of the wood characteristics within it, similar to juvenile wood. Alternatively compression wood can be determined either through visual observation or automated on the basis of grey-scale recognition via the use of camera images to observe the transmitted light from a thin disk-specimen's surface on a light table (compression wood transmits light less readily than normal wood and therefore shows up as darker regions on wet disk specimens)^(2.98).

2.3. Current strength testing methods

There are several different methods of strength testing available: static bending and compression, impact bending and compression, shear parallel to grain and tensile tests. However, as static bending is the method employed in this research and is the most common test worldwide of timber strength and stiffness, this will be the only one discussed here. Static bending determines the MoE and allowable stresses, and is applicable primarily to timber that will be used structurally. The testing, measuring both MoE and MoR, is based on the relationship between stiffness and strength, as previously discussed.

2.3.1 Visual grading

Traditionally, the various stages of timber production, from trees through logs to sawn timber, are quality-assessed by visual observation by experienced technicians and assigned to strength grades on the basis of observable characteristics. A more detailed summary of the observation of these characteristics is available from the FPL Wood Handbook^(2.14), McKenzie^(2.77) and BS EN 14081:2005^(2.90). The latter describes current regulations for visual grading in the UK. Typical grading criteria include^(2.14, 2.32, 2.77, 2.90):

Knots (limits on size and location, rather than type),

Slope of grain,

Checks and splits,

Shake (visually restricted in parts where shear stresses are highest),

Density (established primarily through rings per unit length and percentage of latewood within a specified range or ring),

Decay,

Heartwood and sapwood (primarily distinguished because heartwood in some species is more decay-resistant)

Pitch pockets,

Wane (lack of clear wood on edge of lumber causing a reduction in cross-section and bearing surface area, primarily appearance problem),

Cupping and twists

In North America, quality strength grading, in general, is still based on visual inspection, though American companies have expanded the use on in-line testers, as discussed in the next section^(2.18, 2.27). However, the adequacy of strength grading by these techniques is questionable, and the majority of observations are only possible on sawn timber^(2.40). The European visual grading method also only results in two strength grades (in addition to those rejected): general structural (GS) and higher quality specialist structural (SS)^(2.90). However, as each species also has its own design value and thus grade, there are over 80 species-specific visual grades, which is far more variable than MSG testing^(2.27). Galligan and McDonald^(2.27) present a review of the history of visual grading criteria.

2.3.2. MSG by static bending

Increased accuracy of grading is achieved by those sawmills employing strength grading machines, which in the UK must conform to regulations set out in BS EN 14081:2005^(2.90). European standards for strength testing are regulated by EN 408 and can be adjusted for smaller dimension timber using the EN 384 standard^(2.7). These allow for the calculation of characteristic values for a population using properties determined from a sample of that population. Static bending, which is a measure of the deflection of the specimen results in the calculation of MoE for the specimen, is then related to its ultimate strength. The relationship between MoE and MoR is based on a lower tolerance limit, and as such the use of MoE calculations through static bending requires the use of safety factors^(2.27). For further examples of the validation of this relationship, see Table 2.1, Ross and Pellerin^(2.99) and the FPL Wood Handbook^(2.14). Classifications for European strength grades are set out in BS EN 338, as seen below in Table 2.3^(2.100).

Table 2.3 Strength classes for coniferous species according to BS EN 338^(2.100).

Strength class	C14	C16	C18	C20	C22	C24	C27	C30	C35	C40	C45	C50
MoR (Mpa)	14	16	18	20	22	24	27	30	35	40	45	50
Mean MoE (GPa)	7	8	9	9.5	10	11	11.5	12	13	14	15	16
Minimum density (kgm ⁻³)	290	310	320	330	340	350	370	380	400	420	440	460
Mean density	350	370	380	390	410	420	450	460	480	500	520	550
5 th percentile values. Results are comparable for testing 150 mm wide beams at 200°C and 65% relative humidity												

However, again this (British Standards) only grades sawn timber, but results in nine strength grades C14 to C50 (strongest) for poplar and coniferous woods^(2.77). Galligan and McDonald^(2.27) again provide a concise review of the history of MSG, though primarily applicable only to standards in North America. It represented an improvement on visual grading's inherent conservatism, thus allowing MSG to be applied to timber that would otherwise be lowly graded but could now achieve higher grades, and thus increased commercial value^(2.27). However, they are still not readily adopted due to the differing economic return and financial margins employed by sawmills, depending on their market-orientation. MSG is favoured amongst end-users however as it proves a less variable predictor of stiffness and strength than visual grading^(2.27).

Additionally, it should also be remembered that determining strength using the MoE is only an indication, as by using elastic theory (*i.e.* Hooke's law) one is assuming certain principles of a uniform and linear visco-elastic relationship between stress and strain under small deformation within an isotropic and homogenous medium. Wood is, of course, subject to both inhomogeneities at varying scales (between cells through to between individual trees and species) and anisotropy between axes and as such has different buckling and deformation regimes between axes, though by ignoring cylindrical anisotropy (the 'continuum theory,' as well as variations with height in the stem) it is often modelled as homogenous (particularly in the case of acoustic modelling of wood, as seen in Chapter 3, though even then this simplified case is not always met, such as the magnitude and strain being uniform across the cross section in terms of vibrational wavefronts)^(2.8, 2.101-2.103). The method and basic theory for MSG testing are presented along with a description of the method used in this thesis in Chapter 4.

Grading machines are typically designed to employ flat-wise bending and to be used 'in-line,' *i.e.* immediately after sawing or drying of the material, though most can be adapted for off-line testing^(2.6). Gaunt and Van Wyk^(2.6) noted, on the basis of previous research, that a better estimate of the ultimate strength of the wood specimen is achieved through the incorporation of a slope of grain calculation, as described in the previous section. However, most static bending testing, for efficiency, does not incorporate this at this time, although most stress grading systems do have visual override capabilities for unacceptable knot quantity or location or drying induced defects^(2.6, 2.27, 2.104).

2.3.2.2 MSG devices currently in use

Gaunt and Van Wyk^(2.27) in their '*Literature review of machine stress grading accuracy check methods*,' provided a review of the most common MSG machines currently employed and correlations for the accuracy of some of the MSG machines. The most commercially common MSG devices for the derivation of flat-wise MoE are (as of 2003) presented in Table 2.4, with non-acoustical MSG

devices or those capable of MoE estimates presented in Table 2.5 (as seen in Appendix C4)^(2.27):

Table 2.4 principal bending test rigs currently used in industrial bending tests (not including devices incorporating acoustical techniques)

MSG device	Company	location	No. in commercial use	grading method
CLT and HCLT	Metriguard Inc.	USA	100+	HCLT incorporates some NDT scanning
Stress-o-matic	Crow Inc.	USA	?	4pt Bending
DART	Eldeco	USA	22	4pt Bending
ESG 240	JEE AB	Sweden	8	bending but incorporates some optical scanning
Micromatic and Computermatic	MPC	UK	153	4pt bending
EuroGrecoMat (702, 704, 706, 904)			6	4pt bending (704) and x-ray radiation (702, 706, 904)
Cook-Bolinder	Techmac	UK	66	4pt bending
Timbergrader	Raute	Finland	19	4pt Bending
E-grader			5	4 pt Bending tests as a flatwise beam or as a joist

Table 2.5 Devices capable of MoE estimate based on non-MSG testing (non-acoustical)

MSG device	Company	location	No. in commercial use	grading method
Goldeneye (MS80/2, MS80/1, 702, 706)	Microtec	?	?	X-ray radiation (702, MS80/2) laser scanning (MS80/1) and vibrational analysis (706) for MoE prediction based on density and knot parameters
Silviscan®	CSIRO	Australia	3	X-ray densitometry and X-ray diffraction on SCS for MoE prediction, not suitable for industrial use
Bintec Oy				MoE prediction from X-ray log scanning
Finscan Oy				MoE prediction from visual scanning
Metsateho Oy				MoE prediction by automated optical scanning of end section annual ring width
SpeedGrader	CSIRO	Australia	?	Microwaves to establish knot content
Finnograder	Innotec Oy			Uses Gamma-ray, microwaves and IR thermography to predict an MoE value based on density, knot content, grain angle and moisture content

2.4 Summary

In this chapter the nature of the material under investigation in this thesis was discussed, both in general characteristics of softwoods and the specific characteristics of Sitka spruce. It was established through the review of previous

research that grain angle, MFA and density control the stiffness of timber. It appears however that (assuming a constant grain angle which is a function of the planning method) the level of control between MFA and density varies depending on the region of wood under investigation. Typically, juvenile wood's stiffness is more dependent on MFA. In mature wood, where the MFA is at its shallowest and the effect on stiffness plateaus, density becomes the controlling factor. These are then further influenced by the environmental conditions of the specimen and the presence of natural or drying induced defects. Wood's strength appears to be controlled more by its density and the presence of fracture inducing weak spots such as knots, compression wood and drying-induced defects such as anisotropic longitudinal shrinkage. Where possible, based on previous research, the correlation of the influencing parameters to stiffness (MoE) and strength (MoR) has been presented. Sitka spruce's tendency towards increasing proportions of juvenile wood, through heritability and silvicultural practices, means that the MFA will play a dominant role in controlling the average stiffness of a stem or log. The varying methods of analyzing these properties have been referred to and, where possible, correlations of their accuracy to traditional methods of observation have been made.

It has also been shown that bending stiffness is an indicator of bending strength, and a concise review of the theory, assumptions and devices available for the monitoring of this relationship has been conducted.

2.5 References

- 2.1 Treacy M., *A comparison of mechanical and physical wood properties of a range of Sitka spruce provenances*, 2000, COFORD, ISBN-10: 1902696115, p.35
- 2.2 *Course in Non-destructive Testing of Wood*, organized by F. Divos, ETSI Montes, ETS Arquitectura – Universidad Politécnica de Madrid, Madrid, June 2005
- 2.3 Deresse T., Shepard R.K., Shaler S.M., *Microfibril angle variation in red pine (Pinus resinosa Ait.) and its relation to the strength and stiffness of early juvenile wood*, 2003, Forest Products Journal, 53, 7/8, pp. 34-40

- 2.4 Yang J.L., Evans R., 'Prediction of MOE of Eucalyptus wood from microfibril angle and density,' 2003, Holz als Roh-und Werkstoff, 61, pg 449-452, 2003
- 2.5 Green D.W., Gorman T.E., Evans J. W., Murphy J.F, (2006), *Mechanical grading of round timber beams*, J. Mat. In Civil Eng., Jan/Feb, ASCE
- 2.6 Gaunt D., Van Wyk L., *Literature review of machine stress grading accuracy check methods*, 2003, Project No. PN02.1905, Australian Government, Forest and Wood Products Development Corporation,
- 2.7 Johansson M., Kliger R., 'Variability in strength and stiffness of structural Norway spruce timber – influence of raw material parameters', Proceedings of WCTE 2000, whistler, Canada, 2000
- 2.8 Bucur V., *Acoustics of Wood*, CRC Press, 2005
- 2.9 *Course in Non-destructive Testing of Wood*, organized by F. Divos, ETSI Montes, ETS Arquitectura – Universidad Politecnica de Madrid, Madrid, June 2005
- 2.10 Halmshaw R., *Non-Destructive Testing, 2nd Edition*, Edward Arnold, 1991
- 2.11 Bucur V., *Nondestructive characterization of wood*, 2003, 1st edition, Springer publishing, 324 pages
- 2.12 TRADA wood information, *Non-destructive testing of timber*, Section 4 Sheet 23, Department of the Environment, 1995
- 2.13 Falk R.H., Patton-Mallory M, McDonald K.A., *Non-destructive testing of wood products and structures: state-of-the-art and research needs*, In: doe Reis, Henrique L.M., ed. Non-destructive testing and evaluation for manufacturing and construction: Proceedings of conference; 1988 August 9-12; Champaign, IL. New York; Hemisphere Publishing Corp.; 1990; 137-147
- 2.14 *Wood Handbook: Wood as an engineering material*, 1999, USDA Forest Service, Forest Products Laboratory, General technical report, FPL-GTR-113
- 2.15 Feio A.O., Machado J. S., Lourenço P. B., *Parallel to the grain behaviour and NDT correlations for chestnut wood (Castanea sativa Mill.)* Found at www.civil.uminho.pt/masonry/Publications/Update_Webpage/2005_CHWS1.pdf
- 2.16 *Timber engineering – STEP 1* – Eurofortech, Edited by Blass H., Aune P., Choo B.S., Gorfacher R., Griffiths D.R, Hilson B.O., Racher P., Steck G., Centrum Hout, Netherlands, 1995

- 2.17 Downes G.M., Hudson I.L., Raymond C.A., Dean G.H., Michell A.J., Schimleck L.R., Evans R., Muneri A., (1997), *Sampling plantation Eucalypts for wood and fibre properties*, 1997, CSIRO publishing, Australia
- 2.18 Cown D., *Wood Quality in the 21st Century*, Australian Wood Quality Conference 2004, Albury, Victoria, Australia.
- 2.19 Moreno J., Walker J.C.F., *Wood Quality in Radiata pine plantations. Why Corewood? Why Microfibril angle? Effects on stiffness, shrinkage and warp.* Australian Wood Quality Conference 2004, Albury, Victoria, Australia.
- 2.20 Tang R.C., *Information on Wood Quality, Properties and Utilization of Southern Pines*, Publications Review paper found at: <http://www.sfws.auburn.edu/sfnmc/class/tangwood.htm>
- 2.21 Petersen, E.B., N.M. Petersen, G.F. Weetman, P.J. Martin, and W. Stanek. *Ecology and Management of Sitka Spruce*, 1997, Univ. of BC Press, Vancouver, BC. 240 pp.
- 2.22 Gibson L., Ashby M., *Cellular solids structural properties*, Pergamon Press, 1998
- 2.23 Dinwoodie J.M., *Timber: its nature and behaviour*, Van Nostrand Reinhold Company, 1981.
- 2.24 Harrington, J.J. 2002. *Hierarchical modelling of softwood hygro-elastic properties*. PhD Thesis, Department of Mechanical Engineering, University of Canterbury, Christchurch, New Zealand. 296 p.
- 2.25 Hayes M.P., Chen J., 'A portable stress wave measurement system for timber inspection' from www.elec.canterbury.ac.nz/research/acoustics/pubs/papers/2003/Hayes_enzcon_2003b.pdf
- 2.26 Oja J., Kallsner B., Grundberg S., *Predicting the strength of sawn wood products: a comparison between x-ray scanning of logs and machine strength grading of lumber*, 2005, Forest Products Journal, 55, 9, pp. 55-60
- 2.27 Galligan W. L., McDonald K. A., *Machine grading of lumber: Practical concerns for lumber producers*, USDA Forest Service, general technical report, FPL-GTR-7, September 2000
- 2.28 Brauner L, Hoffmeyer P., Poulsson L., 'Mechanical properties of *Picea sitchensis*', Scandinavian Journal of Forest Research, v. 15 n.1, Feb 2000
- 2.29 Hanhijärvi A., Ranta-Maunus Alpo., Turk, G., *Potential of strength grading of timber with combined measurement techniques*. Report of the Combigrade-project . phase 1. Espoo 2005. VTT Publications 568. 81 pgs. + app. 6 pgs.

- 2.30 Piter J.C., Zerbino R.L., Blass H.J., *Visual strength grading of Argentinian Eucalyptus grandis*, 2004, Holz als Roh- und Werkstoff, 62, pp. 1-8
- 2.31 Ilic J., *Relationship among dynamic and static elastic properties of air-dried Eucalyptus delgatensis R.Baker*, 2001, Holz als Roh- und Werkstoff, 59, pp. 169-175
- 2.32 Baltrusaitis A., Pranckeviciene V., 'Strength grading of the structural timber,' Materials Science, Vol. 9, No. 3, 2003
- 2.33 Sandoz J.L., Benoit Y., Demay L., 'Wood testing using Acousto-ultrasonic,' In: *Proceedings of the 12th International Symposium on the non-destructive testing of wood*, 13-15 Sept 2000
- 2.34 Verkasalo E., Leban J-M., *Predicting modulus of elasticity and modulus of rupture of the major softwoods from Finland and France for the comparison of wood quality*, 2002, In: *Proceedings of the 13th International symposium on nondestructive testing of wood, Berkley, California, USA, August 19-21 2002*, Ed. F. C. Beall, Forest Products Society, Madison, Wisconsin, USA
- 2.35 Schad K.C., Schmoltdt D.L., Ross R.J., *Nondestructive methods for detecting defects in softwood logs*, 1996, Research paper, USDA forest service, FPL-RP-546
- 2.36 Saporiti Machado J., Doria, C., Cruz, H., *Evaluation of pine timber strength by drilling and ultrasound*, proceedings of International Symposium of NDT in Civil Engineering 2003
- 2.37 Personal communication with inventors of 'TreeTap' John Walker and Michael Hayes, 10th April 2006
- 2.38 Evans R., Ilic J., *Rapid prediction of wood stiffness from microfibril angle and density*, Forest Products Journal 51(3), pg 53-57, 2001
- 2.39 Sandoz J.L., Benoit Y., Demay L., 'Standing tree quality assessments using Acousto-ultrasonic,' internal CBS-CBT report available from www.cbs-cbt.com, 2004
- 2.40 Carter P., Briggs D., Ross R.J., Wang X., *Acoustic testing to enhance western forest values and meet customer wood quality needs*, 2005, In "Productivity of western forests: A forest Products focus Research Paper PNW-GTR-642, USDA forest service, Pacific Northwest station
- 2.41 Bächle H., Walker J.C.F., *The influence of temperature on the velocity of sound in green pine wood*, 2006, Holz als Roh- und Werkstoff, 64 (5), pp 429-430

- 2.42 Xu P., *Estimating the influence of knots on the local longitudinal stiffness in radiata pine structural timber*, Wood Science and Technology, v.36, pg 501-509, 2002
- 2.43 Wang X., Ross R.J., Bradshaw B.K., Punches J., Erickson J.R., Forsman J.W., Pellerin R.E. *Diameter effects on stress-wave evaluation of modulus of elasticity of logs*, Wood and Fibre Science, 36(3), 2004, pp. 368-377
- 2.44 Wang X., Ross R.J., McClellan M., Barbour R.J., Erickson J.R., Forsman J.W., McGinnis G.D., *Strength and stiffness assessment of standing trees using a non-destructive stress wave technique*, 2001, Research Paper FPL-RP-585, USDA forest service, Forest Products Laboratory
- 2.45 MacDonald E., Hubert J., *A review of the effects of silviculture on timber quality of Sitka spruce*, 2002, Forestry, 75, 2, pp. 107-138
- 2.46 Burdon R.D., Kibblewhite R.P., Walker J.C.F., Megraw R.A., Evans R., Cown D.J., *Juvenile versus mature wood: A new concept, orthogonal to corewood versus outerwood, with special reference to Pinus radiata and P. taeda*, 2004, Forest Science, 50 (4), pp. 399-415
- 2.47 Cave I.D, Walker J.F.C., *Stiffness of wood in fast-grown Plantation softwoods: the influence of microfibril angle*, Forest Products Journal, v. 44 n.5, pg 43-45, 1994
- 2.48 Lasserre J.P., Mason E.G., Watt M.S., *Assessing corewood acoustic velocity and modulus of elasticity with two impact based instruments in 11-year-old trees from a clonal-spacing experiment of Pinus radiata D. Don*, 2007, Forest Ecology and Management 239, pp. 217-221
- 2.49 Bodig J. and Jayne B.A. *Mechanics of Wood and Wood Composites*, 1982, Van Nostrand Reinhold Company, NY. pp. 712.
- 2.50 Gerhards C.C., *'Effect of cross grain on stress waves in lumber,'* 1981. FPL-RP-368. USDA Forest Products Laboratory.
- 2.51 Bindzi, I., Samson M., *New Formula for Influence of Spiral Grain on Bending Stiffness of Wooden Beams*, 1995, J. Struct. Engrg., Volume 121, Issue 11, pp. 1541-1546
- 2.52 Mascia N.T., Lahr, F.A.R., *Remarks on orthotropic elastic models applied to wood*, 2006, Materials Research, v.9 n.3, July/Sep. 2006
- 2.53 Saliklis E.P., Falk R.H., *correlating off-axis tension tests to shear modulus of wood-based panels*, 2000, Journal of structural engineering / May 2000 / pp. 621-625

- 2.54 Maclaren P., *Wood Quality of Radiata Pine on farm sites – A review of the issues*, May 2002, Piers Maclaren and Associates, Report no. 80 for Forest & Farm plantation management co-operative
- 2.55 Cave I., Wikaira J., Robinson W., *Measurement of cellulose orientation in wood by x-ray diffraction*, Workshop on high value products from understanding of wood and innovative processing, December 2003, WTRC, University of Canterbury, New Zealand
- 2.56 McKinley R., Ball R., Downes G., Fife D., Gritton D., Ilic J., Koechler A. Pongracic S., Roper J., *Resource Evaluation for future profit: Part A, Wood property survey of the Green Triangle region*, 2004, Project No. PN03.3906, Australian Government, Forest and Wood Products Development Corporation
- 2.57 Gindl W., Teischinger A., *Axial compression strength of Norway spruce related to structural variability and lignin content*, 2002, Composites Part A: applied science and manufacturing, 33, 1623-1628
- 2.58 Pongracic S, Thumm A, Wright J., *Use of near Infrared for determining properties of hardwoods and future applications to softwood operations*, Australian Wood Quality Conference 2004, Albury, Victoria, Australia.
- 2.59 Bailleres H., Davrieaux F., Ham-Pichavant F., *Near infrared analysis as a tool for rapid screening of some major wood characteristics in a eucalyptus breeding program*, 2002, Annals of Forest Science, 59, 479-490
- 2.60 Kelley S.S., Rials T.G., Snell R., Groom L.H., Sluiter A., *Use of near infrared spectroscopy to measure the chemical and mechanical properties of solid wood*, 2004, Wood Science and technology, 38, pp. 257-276
- 2.61 Costa e Silva J., Nielsen B.H., Rodrigues J., Pereira H., Wellwendorf H., *Rapid determination of the lignin content on Sitka spruce wood by Fourier transform infrared spectrometry*, 1999, Holzforschung, 53, pp. 597-602
- 2.62 Schimleck L.R., Mora C., Daniels R.F., *Estimation of physical wood properties of green Pinus taeda radial samples by near-infrared spectroscopy*, 2003, Canadian Journal of Forest Research, 33, 12, pp. 2297-2305
- 2.63 Jones P.D., Schimleck, L.R., Daniels R.F., Clark III A., *Nondestructive estimation of Pinus taeda wood properties for samples from a wide range in Georgia*, 2005, Canadian Journal of Forest Research, 35, 1, pp. 85-92
- 2.64 Schimleck L.R., Evans R., Ilic J., Matheson A.C., *Estimation of wood stiffness of increment cores by near-infrared spectroscopy*, 2002, Canadian Journal of Forest Research, 32, 1, pp. 129-135

- 2.65 Schimleck L.R., Jones P.D., Peter G.F., Daniels R.F., Clark III A., *Nondestructive estimation of tracheid length from sections of radial wood strips by near-infrared spectroscopy*, 2004, *Holzforschung*, vol. 58, pp. 375-381
- 2.66 Thumm A., Meder R., Marston A., *Stiffness prediction of structural lumber performance from green unsawn cants in a sawmill using NIR spectroscopy*. 2002, 13th International symposium on NDT of wood, Berkley, California, 19.21 August 2002, Ed. F Beall, Forest Products Society, Madison, Wisconsin. pp.117-121
- 2.67 Flaete P.O., Haartveit E. Y., *Assessment of natural durability of Scots pine by NIR spectroscopy*, In: *Proceedings of the 13th International symposium on nondestructive testing of wood, Berkley, California, USA, August 19-21 2002*, Ed. F. C. Beall, Forest Products Society, Madison, Wisconsin, USA
- 2.68 Gierlinger N., Jacques D., Schwanninger M., Wimmer R., Hinterstoisser B., Paques L.E., *Rapid prediction of natural durability of larch heartwood using Fourier transform near-infrared spectroscopy*, 2003, *Canadian Journal of Forest Research*, 33, 9, pp. 1727-1736
- 2.69 So C-L., Via B.K., Groom L.H., Schimleck L.R., Shupe T.F., Kelley S.S., Rials T.G., *near infrared spectroscopy in the forest products industry*, 2004, *Forest Products Journal*; Mar 2004; 54, 3; ABI/INFORM Global, pg. 6-16
- 2.70 *Variation of cellulose microfibril angles in Softwoods and Hardwoods – A possible strategy of mechanical optimization’* – H Lichtenegger; A Reiterer; SE Stanzl-Tschegg; P Fratzi, *Journal of Structural Biology*, 128, pg. 257-269, 1999
- 2.71 *‘Forestry Research in Scotland: A Review’* – Bill Dyck, Draft 2 Report prepared for Scottish Enterprise, 2004
- 2.72 Huang C-L., Lindstrom H., Nakada R., Ralston J., *Cell wall structure and wood properties determined by acoustics – a selective review*, 2003, *Holz als Roh- und Werkstoff*, 61, pp. 321-335
- 2.73 Xu P., Walker J.C.F., *Stiffness gradients in radiata pine trees.*, 2004, *Wood Science and Technology*, 38 (1), pp.1-9
- 2.74 Sirvio J., Karenlampi P., *The effects of maturity and growth rate on the properties of spruce wood tracheids*, 2001, *Wood Science and Technology*, 35, pp. 541-554
- 2.75 Wang H.H., Drummond J.G., Reath S.M., Hunt K., Watson P.A., *An improved fibril angle measurement method for wood fibers*, 2001, *Wood Science and Technology*, 34, pp. 493-503.

- 2.76 Ball R.D., McConchie M.S., Cown D.J., *Evidence for associations between Silvascan-measured wood properties intraring checking in a study of twenty-nine 6-year-old Pinus Radiata*, 2005, Canadian Journal of Forest Research, 35, 5, pp. 1156-1172
- 2.77 McKenzie W.M.C., *'Design of Structural Elements'*, Palgrave Mcmillan, 2004
- 2.78 Kawamoto S., Williams R.S., *Acoustic emission and Acousto-ultrasonic techniques for wood and wood-based composites: A Review.*" USDA FS, FPL-GTR-134, 2002.
- 2.79 Benoit Y., Sandoz J-L., *The importance of the nondestructive technologies for wooden pole network assessment management*, In: *Proceedings of the 14th International symposium on nondestructive testing of wood*, Hanover, Germany, May 2-4 2005, Ed. F-W Broker, Shaker Verlag, Germany
- 2.80 James W. L., Yen, Y-H., King R., *A microwave method for measuring moisture content, density, and grain angle of wood*, USDA FS, Research note, FPL-0250, March, 1985
- 2.81 Baradit E., Aedo R., Correa J., *Knots detection in wood using microwaves*, Wood Science and Technology, 40, pp. 118-123
- 2.82 Daian G., Taube A., Birnboim A., Daian M., Sharmkov Y., *Modelling the dielectric properties of wood*, 2006, Wood Science and Technology, 40, pp. 237-246
- 2.83 Johansson J., Hagman O., Oja. *Predicting moisture content and density of Scots pine by microwave scanning of sawn timber*, 2003, Computer and Electronics in Agriculture, 41, pp. 85-90
- 2.84 Johannesson E.H., Hansen E.W., Rosenholm J.B., *Probing structural periodicity (annual ring size) in Scots pine by nmr profiling*, Wood Science and Technology, 2006
- 2.85 Bhandarkar S.M., Faust T.D., Tang M., *Design and prototype development of a computer vision-based lumber production planning system*, 2002, Image and vision computing, 20, pp. 167-189
- 2.86 Contreras I., Guesalaga A., Fernandez M.P., Guarini M., Irarrazaval P., *MRI fast tree log scanning with helical undersampled projection acquisitions*, 2002, Magnetic Resonance Imaging, 20, 781-787
- 2.87 Green D.W., Evans J.W, Logan J.D., Nelson W.J., *Adjusting modulus of elasticity of lumber for changes in temperature*, 1999, Forest Products Journal, 49. 10, Oct 1999, pp 82-94

- 2.88 Kabir M.F., Schmoldt D.L., Schafer M.E., *Ultrasonic detection of knots, cross grain and bark pockets in wooden pallet parts*, Proceedings of the World conference on Timber Engineering 2000, pp. 7.5.2-1
- 2.89 Adjanohoun G., Guillot J., Lanvin R., 'Small roundwood grading by nondestructive X-rays and ultrasonic methods,' www.ndt.net/article/v04n11/adjanoh/adjanoh, v.4 n.11, 1999
- 2.90 BS EN 14081:2005 - Timber structures - Strength graded structural timber with rectangular cross section - Part 1: General requirements, BSI, 2006
- 2.91 Quin F., Steele P.H., Shmulsky R., *Locating knots in wood with an infrared detector system*, 1998, Forest Products Journal, 48, 10, pp. 80-84
- 2.92 Guddanti S., Chang S.J., *Replicating sawmill sawing with TOPSAW using CT images of a full-length hardwood log*, 1998, Forest Products Journal, 48, 1, Jan 1998, pp. 72-75
- 2.93 Jacques D., Marchal M., Curnel Y., Relative efficiency of alternative methods to evaluate wood stiffness in the frame of hybrid larch (*Larix x eurolepis* Henry) clonal selection, 2004, Annals of Forest Science, 61, 35-43
- 2.94 Saravi A.A., Lawrence P.D., Lam F., *Implementation of a mechanics-based system for estimating the strength of lumber*, In: *Proceedings of the 13th International symposium on nondestructive testing of wood*, Berkley, California, USA, August 19-21 2002, Ed. F.
- 2.95 Pham D.T., Alcock R.J., *Automatic grading and defect detection system: a review*, 1998, Forest Products Journal, 48, 4, pp.34-42
- 2.96 Donaldson L.A., Turner J.C.P., *The influence of compression wood and microfibril angle on the occurrence of distortion in window frames from radiata pine*, 2001, Holz als Roh- und Werkstoff, 59, pp. 163-168
- 2.97 Singh A.P., Kim Y.S., Park B.D., Chung G.C., Wong A.H.H., *Presence of a distinct S₃ layer in mild compression wood tracheids of Pinus radiata*, 2003, Holzforschung, 57, 243-247.
- 2.98 Wimmer R., Downes G.M., Evans R., *High-resolution analysis of radial growth and wood density in Eucalyptus nitens, grown under different irrigation regimes*, 2002, Annals of Forest Science, 59, pp. 519-524
- 2.99 Ross R.J., Pellerin R., 'Non-destructive testing for assessing wood members in structures,' USDA General technical report: FPLGTR-70-1994, 1994
- 2.100 BS EN 338:2003 - structural timber – strength classes, BSI, 2003

- 2.101 Brancheriau L. Bailleres H., Guitard D., *Comparison between modulus of elasticity values calculated using 3 and 4 point bending tests on wooden samples*, 2002, *Wood Science and Technology*, 36, pp. 367-383
- 2.102 Hearmon R.F.S, *An introduction to applied anisotropic elasticity*, 1961, Oxford University Press.
- 2.103 Lindsay R.B., *'Mechanical Radiation,'*, Mcgraw-Hill, 1960
- Saren M-P., Serimaa R., Tolonen Y., *Determination of fiber orientation in Norway spruce using X-ray diffraction and laser scattering*, 2006, *Holz als Roh- und Werkstoff*, 64, pp. 183-188

Chapter 3 Review of wood acoustic NDT literature

3.1 Acoustic theory

Initially, before stress-wave timers or frequency analysers, acoustic (low-frequency elastic wave) testing of wood relied on an experienced inspector 'aurally' recognising tonal patterns (indicating the extent of decay or voids) produced from impacts to a specimen, usually utility poles but also logs or tree stems^(3.1, 3.2). By modern standards, this was subjective and could not detect early stages of decay and tonal patterns could be subject to misinterpretation as limited by the experience and range of human hearing^(3.1, 3.2). Experience had also shown it should not be used on *in situ* specimens over 9 cm thick^(3.2). However, until well into the late 20th Century, it remained a favoured method of non-destructive evaluation of logs and trees due to portability and simplicity. As such, it is only recently, with the development of advanced, real-time signal capture and processing equipment that the principles of elastic characterisation could be applied to wood products, through the relationship of acoustic wavespeed, density and stiffness.

This thesis examines the applicability of NDT acoustic testing methods to determine the MoE_d of timber, specifically defect-rich species such as Sitka spruce. As such, the focus of this review is directed to the previous validation and issues arising from the use of timber velocity derivation techniques; the inherent timber characteristics believed to influence returned velocities; and a critique of the recent applications of the techniques. The focus regarding acoustical NDT methods is on the use of point-to-point TOF methods in the time domain and longitudinal resonance frequency (RF, measuring axial deformation behaviour) based methods in the frequency domain, as opposed to flexural transverse vibration (TV) methods (measurement of bending deformations tangential to the longitudinal axis of beams). Previous use of measures of internal absorption, specifically the damping ratio, has also been examined. Other timber acoustic NDT methods, such as acoustic emission (AE) and wavelet analysis are separate subjects outside the scope of this investigation.

3.1.1 Acousto-elastic theory and the one-dimensional equation

For homogenous, isotropic materials exhibiting linear elasticity, the elastic behaviour can be modelled by stiffness and compliance matrices, which contain only two independent elastic constants, a Young's (elastic) modulus and a shear modulus (stiffness moduli C_{11} and C_{12} respectively)^(3.3). It is possible to estimate the values of these stiffness moduli through acoustic and ultrasonic methods. As discussed in Chapter 2, whilst wood composites such as plywood and OSB are often modelled as transversely isotropic (five independent constants and one dependant constant), solid wood is an inhomogenous and anisotropic material. However, most conifers, which we deal with in this investigation, are modelled at the meso-scale as orthotropic (producing nine independent elastic constants), the elastic behaviour of which can be analysed in albeit more complex stiffness and compliance matrices^(3.3). Young's modulus (C_{11}) is one of the nine independent constants in the corresponding stiffness matrix and, assuming that wave propagation is purely axial along the specimen, can be calculated from wave velocity in the same manner as for isotropic materials.

When elastically characterising wood structures, the three main types of vibrational waves used are non-dispersive fundamental bulk waves (planar longitudinal and transverse waves), non-dispersive surface waves (primarily Rayleigh waves), or dispersive waves (Lamb, rod or flexural waves). Common characteristics of these waves are that they all travel with distinct measurable wavespeeds (varying with frequency in the case of dispersive waves), wavelengths, frequencies, phases, periods, and amplitudes that can be subject to intrinsic and extrinsic attenuation; spreading, reflection and scattering depending on the dimensions and nature of the material through which they are propagating^(3.4). This thesis focuses on the wavespeed and attenuation of longitudinal waveforms. The elastic characterisation of a wood specimen is possible through a calculation of the wavespeed, derived via methods described later in this chapter, though sufficient at this point to state that velocity measurements are conducted, using sonic (usually through impact excitation) or ultrasonic frequencies (via transmitting transducers), to produce TOF or spectral RF measurements.

3.1.2 Validation of the one-dimensional theory

The validation of the applicability of the dynamic stiffness equation (plane stress solution, Equation 3.1) to timber specimens stems from over 50 years of research in comparing the static and dynamic values of elastic stiffness in wood specimens. This forms the general expression for the longitudinal (compression) rod wavespeed of an axially propagating wave in a notionally thin rod of material (compared to the wavelengths used) when treated as an expression of one-dimensional theory, assuming no shear (or torsion-flexure) coupling. It also assumes, according to Lindsay^(3.5), that the lateral dimensions are of a lesser order of magnitude than the wavelength of the longitudinal rod wave (or, as stated by Brown^(3.6), less than one-fifth the wavelength of the rod wave) and hence subject to deformation at both lateral sides of the specimen as the specimen expands and contracts to relieve stress imposed by the propagating wave. It can be modeled by the one-dimensional rod wave equation, often cited as the “pure longitudinal” one-dimensional equation^(3.3, 3.7-3.8):

$$V_0 = \sqrt{\frac{MoE_d}{\rho}}$$

Eqn. 3.1

Where:

V_0 = phase velocity of a rod wave

ρ = density (kgm^{-3})

Due to the longitudinal rod wave's purely axial propagation path, this has often been incorrectly confused with the measurement of pure longitudinal bulk plane waves which is a different wave type calculated using the three-dimensional equation (as discussed in Section 3.1.4.). Fundamental body waves, such as planar longitudinal and transverse waves, travel only within the body of a material with assumedly infinite lateral dimensions. This confusion does not in itself invalidate the relation of measured axial wave velocity to the static stiffness of timber specimens, but should prompt concern over the knowledge base of many researchers utilizing the method. Bucur^(3.3) stated that previous experiments had validated the orthotropic modelling of wood and use of global elastic characterisation of anisotropic media, through longitudinal velocity measurements conducted on small specimens in the symmetrical and off-diagonal components and corresponding stiffness components. Indeed, it is commonly accepted by most wood-acoustic researchers that MoE_d can be used to estimate the static MoE ^(3.9).

Following on from the theories of Timoshenko^(3.8) and Hearmon^(3.10), Jayne^(3.11) was among the first to show that static MoE could be predicted by MoE_d . Jayne^(3.11) proposed that the properties which control the static behaviour of wood are the same properties that control the behaviour of (acoustical) energy within a material. As such it has been hypothesized, and validated to some extent, that the external work input/internal energy dissipation balance, is independent of rate effects thereby enabling static MoE prediction from calibrated dynamic tests^(3.11). These two theories form the basis of current acoustic and ultrasonic measurements of wood.

A review of research papers investigating the correlation between static and dynamic MoE and MoR is presented in Ross and Pellerin^(3.12), as well as

summarising the work of other acoustic investigations of wood. Ross and Pellerin^(3.12) generally cite examples from the sixties and seventies to indicate that the square of the longitudinal velocity of sound in SCS timber has a correlation to wood MoE of between $R = 0.95$ to 0.99 , providing validation of the one-dimensional theory. Good correlations are also shown in small clear specimens to compressive and tensile strength^(3.1, 3.3, 3.12).

Bucur^(3.3) gives reference to a large proportion of acoustical investigations of timber and experiments to validate the use of dynamic and static correlations. For example, she states that Musgrave (1961) was first to calculate all the terms of the stiffness matrix of spruce, followed by Hearmon (1965) comparing dynamic (via ultrasonic tests) and static determination of elastic coefficients of the matrix^(3.3). In the same year, Bertolf (1965) used stress waves to predict the dynamic strain in small clear specimens and Galligan and Courteau (1965) first applied the stress wave TOF technique to structural lumber^(3.1). This work was then expanded from clear wood to larger sawn timbers, and the research of Pellerin and Galligan (1973) showed good correlations between dynamic and static measurements ($R^2 = 0.96$)^(3.12). Gerhards^(3.13), whilst agreeing with this for clear timber battens ($R^2 = 0.96$), found that the correlation between static and dynamic stiffness was slightly less in wood with a high knot content ($R^2 = 0.87$)^(3.13). Bucur^(3.3) cites her work of Bucur and Archer (1984) using ultrasonic TOF velocity, “determined the elastic compliance matrix for various species of wood.” *i.e.* in all directions and Poisson’s ratio. Other examples from more recent investigations (most of which are referred to in greater detail in subsequent sections) are presented in Table 3.1:

Table 3.1 Correlation of dynamic MoE of beams and SCS (TOF and resonance) to static MoE or MoR bending tests (* = coefficient of correlation R used instead of R²).

Reference (Ref.)	Method	Excitation (Ext.)	Device used	Velocity or MoE _d	Specimen	Sample no.	Age of samples (yrs)	Orientation (Ort.)	Species	R ²
Wang and Ko ^(3.14)	TOF	impact	oscilloscope	velocity	beams (dry)	200	41	transverse nail insertion (longitudinal measurement)	Japanese cedar	0.46 *
Wang and Ko ^(3.14)	TOF	impact	oscilloscope	velocity	beams (dry)	200	41	longitudinal nail insertion (longitudinal measurement)	Japanese cedar	0.65 *
Wang and Ko ^(3.14)	TOF	impact	oscilloscope	dynamic MoE	beams (dry)	200	41	transverse nail insertion (longitudinal measurement)	Japanese cedar	0.7 *
Wang and Ko ^(3.14)	TOF	impact	oscilloscope	dynamic MoE	beams (dry)	200	41	longitudinal nail insertion (longitudinal measurement)	Japanese cedar	0.79 *
Dickson <i>et al.</i> ^(3.15)	TOF	impact	FAKOPP™	velocity	beams (green)	35	9	longitudinal	eucalyptus dunnii	0.85
Dickson <i>et al.</i> ^(3.15)	TOF	impact	FAKOPP™	velocity	beams (green)	35	25	longitudinal	eucalyptus dunnii	0.89
Dickson <i>et al.</i> ^(3.15)	TOF	impact	FAKOPP™	velocity	beams (dry)	35	9	longitudinal	eucalyptus dunnii	0.75
Dickson <i>et al.</i> ^(3.15)	TOF	impact	FAKOPP™	velocity	beams (dry)	35	25	longitudinal	eucalyptus dunnii	0.75
Green and Kretschmann ^(3.16)	TOF	impact	oscilloscope	dynamic MoE	beams (dry)	99	?	longitudinal	southern pine	0.71
Green and Kretschmann ^(3.16)	TOF	impact	oscilloscope	dynamic MoE	beams (dry)	99	?	longitudinal	southern pine	0.71
Green and Kretschmann ^(3.16)	TOF	impact	oscilloscope	dynamic MoE	beams (dry)	102	?	longitudinal	southern pine	(MoR) 0.30
Cai <i>et al.</i> ^(3.17)	TOF	impact	oscilloscope	dynamic MoE	Joists (dry)	15	?	longitudinal	southern pine	0.63
Cai <i>et al.</i> ^(3.17)	TOF	impact	oscilloscope	dynamic MoE	Joists (green)	15	?	longitudinal	southern pine	0.75
Cai <i>et al.</i> ^(3.17)	TOF	impact	oscilloscope	dynamic MoE	Joists (green)	9	?	longitudinal	southern pine	0.96
Jang ^(3.18)	TOF	impact	Metriguard 239A	dynamic MoE	beams (dry)	20	20 to 25	longitudinal	larch	0.84
De Oliveira <i>et al.</i> ^(3.19)	TOF	US	Sylvatest®	dynamic MoE	beams (dry)	33	n/s	longitudinal	Pinus taeda	0.8
Castellanos <i>et al.</i> ^(3.20)	TOF	US	PUNDIT™	dynamic MoE	beams	24	n/s	longitudinal	Japanese Sugi	0.53 to 0.83
Castellanos <i>et al.</i> ^(3.20)	TOF	impact	oscilloscope	dynamic MoE	beams	24	n/s	longitudinal	Japanese Sugi	0.66 to 0.83
Hanhijarvi <i>et al.</i> ^(3.22)	TOF	impact	Sylvatest®	dynamic MoE	beams	100	n/a	longitudinal	Norway spruce	0.57
Hanhijarvi <i>et al.</i> ^(3.22)	TOF	impact	Sylvatest®	dynamic MoE	beams	100	n/a	longitudinal	Norway spruce	0.48 (MoR)
Hanhijarvi <i>et al.</i> ^(3.22)	TOF	impact	Sylvatest®	dynamic MoE	beams	100	n/a	longitudinal	Scotch pine	0.75
Hanhijarvi <i>et al.</i> ^(3.22)	TOF	impact	Sylvatest®	dynamic MoE	beams	100	n/a	longitudinal	Scotch pine	0.79 (MoR)
Wang <i>et al.</i> ^(3.21)	TOF	impact	oscilloscope	dynamic MoE	SCS	168	38 to 70	longitudinal	Sitka spruce and western Hemlock	0.91
Wang <i>et al.</i> ^(3.21)	TOF	impact	oscilloscope	dynamic MoE	SCS	168	38 to 70	longitudinal	Sitka spruce and western Hemlock	0.69 (MoR)
Sonderegger and Niemz ^(3.23)	TOF	impact	oscilloscope	dynamic MoE	SCS	125	n/a	longitudinal	Norway spruce	0.75
Sonderegger and Niemz ^(3.23)	TOF	impact	oscilloscope	dynamic MoE	SCS	125	n/a	longitudinal	Norway spruce	0.08
Cai <i>et al.</i> ^(3.17)	TV	impact	oscilloscope	dynamic MoE	Joists (green)	9	?	transverse	southern pine	0.82
Cai <i>et al.</i> ^(3.17)	TV	impact	oscilloscope	dynamic MoE	Joists (dry)	9	?	transverse	southern pine	0.91
Cai <i>et al.</i> ^(3.17)	TV	impact	oscilloscope	dynamic MoE	Joists (salavaged)	9	?	transverse	southern pine	0.98
Ilic ^(3.24)	RF	impact	FFT-based software	velocity	65 cm beams	70	?	longitudinal	eucalytus	0.78

Reference (Ref.)	Method	Excitation (Ext.)	Device used	Velocity or MoE _d	Specimen	Sample no.	Age of samples (yrs)	Orientation (Ort.)	Species	R ²
Ilic (3.24)	RF	impact	FFT-based software	dynamic MoE	65 cm beams	70	?	longitudinal	eucalytus	0.95
Jang (3.18)	TV	impact	oscilloscope	dynamic MoE	beams (dry)	20	20 to 25	transverse	larch	0.75
Piter <i>et al.</i> (3.25)	RF	impact	Fluke 123 scopemeter	dynamic MoE	beams (dry)	142	?	longitudinal	eucalyptus	0.85
Piter <i>et al.</i> (3.25)	TV	impact	Fluke 123 scopemeter	dynamic MoE	beams (dry)	142	?	transverse	eucalyptus	0.92
Green <i>et al.</i> (3.26)	TV	impact	DynaMOE	dynamic MoE	beams (dry)	550	70-90	transverse	Douglas fir	0.82
Ayarkwa <i>et al.</i> (3.27)	RF	impact	oscilloscope	dynamic MoE	beams (dry)	276	?	longitudinal	African Hardwoods	0.92
Ayarkwa <i>et al.</i> (3.27)	RF	impact	oscilloscope	dynamic MoE	beams (dry)	276	?	longitudinal	African Hardwoods	0.88 (MoR)
Ayarkwa <i>et al.</i> (3.27)	RF	impact	oscilloscope	dynamic MoE	finger jointed beams (dry)	100	?	longitudinal	African Hardwoods	0.98
Ayarkwa <i>et al.</i> (3.27)	RF	impact	oscilloscope	dynamic MoE	finger jointed beams (dry)	100	?	longitudinal	African Hardwoods	0.81 (MoR)
Nzokou <i>et al.</i> (3.28)	TV	impact	Metriguard 340 E	dynamic MoE	wood-plastic composites	12	?	longitudinal	WPC	0.04 to 0.52
Brancheriau and Bailleres (3.29)	RF	impact	BING tester	dynamic MoE	beams (high defect content)	80	?	longitudinal	larch	0.76
Brancheriau and Bailleres (3.29)	RF	impact	BING tester	dynamic MoE	beams (high defect content)	82	?	longitudinal	larch	0.54 (MoR)
Brancheriau and Bailleres (3.29)	TV	impact	BING tester	dynamic MoE	beams (high defect content)	80	?	transverse	larch	0.73
Brancheriau and Bailleres (3.29)	TV	impact	BING tester	dynamic MoE	beams (high defect content)	82	?	transverse	larch	0.53 (MoR)
Brancheriau and Bailleres (3.30)	TV	impact	n/s	dynamic MoE	beams	n/s	n/s	transverse	n/s	0.83
Brancheriau and Bailleres (3.30)	TV	impact	n/s	dynamic MoE	SCS	n/s	n/s	transverse	n/s	1
Johansson and Kiger (3.31)	RF	impact	n/s (but low freq res.)	dynamic MoE	beams	401	60-135	longitudinal	Norway spruce	0.87
Johansson and Kiger (3.31)	RF	impact	n/s (but low freq res.)	dynamic MoE	beams	401	60-135	longitudinal	Norway spruce	0.7 (MoR)
Castellanos <i>et al.</i> (3.20)	RF	impact	oscilloscope	dynamic MoE	beams	24	n/s	longitudinal	Japanese Sugi	0.9 to 0.95
Ilic (3.32)	RF	impact	oscilloscope	dynamic MoE	SCS	104	n/s	longitudinal	eucalyptus	0.95
Ilic (3.32)	RF	impact	oscilloscope	dynamic MoE	SCS	104	n/s	longitudinal	eucalyptus	0.83 (MoR)
Ilic (3.32)	TV	impact	oscilloscope	dynamic MoE	SCS	104	n/s	flexural	eucalyptus	0.99
Ilic (3.32)	TV	impact	oscilloscope	dynamic MoE	SCS	104	n/s	flexural	eucalyptus	0.90 (MoR)
Ilic (3.32)	RF	impact	oscilloscope	velocity	SCS	104	n/s	longitudinal	eucalyptus	0.78
Ilic (3.32)	RF	impact	oscilloscope	velocity	SCS	104	n/s	longitudinal	eucalyptus	0.63 (MoR)
Hanhijarvi <i>et al.</i> (3.22)	RF	impact	Rion SA77 GP analyser	dynamic MoE (default density)	beams	100	n/a	longitudinal	Scotch Pine	0.79
Hanhijarvi <i>et al.</i> (3.22)	RF	impact	Rion SA77 GP analyser	dynamic MoE (global density)	beams	100	n/a	longitudinal	Scotch Pine	0.92
Hanhijarvi <i>et al.</i> (3.22)	RF	impact	Rion SA77 GP analyser	dynamic MoE (global density)	beams	100	n/a	longitudinal	Scotch Pine	0.69 (MoR)
Hanhijarvi <i>et al.</i> (3.22)	RF	impact	Rion SA77 GP analyser	dynamic MoE (default density)	beams	100	n/a	longitudinal	Norway spruce	0.67
Hanhijarvi <i>et al.</i> (3.22)	RF	impact	Rion SA77 GP analyser	dynamic MoE (global density)	beams	100	n/a	longitudinal	Norway spruce	0.89
Hanhijarvi <i>et al.</i> (3.22)	RF	impact	Rion SA77 GP analyser	dynamic MoE (global density)	beams	100	n/a	longitudinal	Norway spruce	0.60 (MoR)
Shmulsky <i>et al.</i> (3.33)	RF	impact	HM200™	dynamic MoE	small diameter dry dowels	69	n/a	longitudinal	lobolly pine	0.45
Shmulsky <i>et al.</i> (3.33)	RF	impact	HM200™	dynamic MoE	small dia. green dowels	69	n/a	longitudinal	lobolly pine	0.51

However, whilst the linear correlations shown may often have been very strong, it does not mean that the predicted dynamic modulus is accurate. Wang^(3.9) found that using this one-dimensional equation to calculate a dynamic stiffness overestimated the static MoE by 19% to 37%. De Olivera *et al.*^(3.19) found that dynamic tests on beam specimens (using the 22 kHz Sylvatest[®]) provided a MoE_d 20% higher than those provided by the static bending tests ($R^2 = 0.80$), with no correction made for Poisson's ratio. Similar examples of this overestimation are presented throughout this chapter.

This over-estimation of static MoE by acoustically-derived MoE_d could be attributed to factors such as the rate of loading (as discussed later in Chapter 5). For example, the difference can be attributed, according to Bucur^(3.3), to wood being viscoelastic, in that when a transient force is applied the material is essentially solid, but when the force is applied over a longer duration (as in static bending) then it behaves more like a viscous liquid. As such, the modulus of the transient impact will obviously appear higher, whilst an US MoE_d should theoretically (negating dimensional and environmental effects) be higher than sonic-derived MoE_d due to a fast rate of loading.

Harris *et al.*^(3.34) observed that the static and dynamic MoE would naturally differ as the grain distortions due to knots can be at least five times the width of the knot (thus inducing a zone of severe stress concentration compared to clear wood). Harris *et al.*^(3.34) noted that in principle, the MoE_d calculated by standing wave RF testing will only be affected by the proportion of knots relative to the whole sample and not the location of these defects. However as shown in Chapter 5, MoE_d calculated by RF testing from lower-order harmonic modes will be less susceptible to the influence of a specific knot concentration than higher order modes, unless the knots are locally coincident with standing wave antinodes (in which case the lower-order derived MoE_d will be significantly reduced in comparison to the higher order derived MoE_d). Higher-order modes have a greater number and spread of stress node and antinodes and are thus more likely to have stress antinodes coincident with knot concentrations, resulting in a typically lower RF-derived MoE_d value than lower-order derived MoE_d values.

Static MoE will be dictated by the location and quantity of the defects, thus naturally having a lower MoE value than the lower-order RF tested MoE_d value, particularly in knot-prone softwoods^(3.34). Falk *et al.*^(3.1) similarly noted that dynamic prediction of MoR is complicated by the MoR's increased dependence on knot content and location.

Concerning non-solid wood products relation to stiffness, Sandoz *et al.*^(3.35) found strong correlations ($R^2 = 0.93$) between ultrasonic TOF velocity and the static MoE of laminated timber beams. Strong correlations between MoR and wavespeed squared were found in similarly oriented particleboard ($R^2 = 0.87$ to 0.93), suggesting the greater anisotropy of natural timber and wave path is the complicating factor in this relationship^(3.36).

3.1.3 Issues with the one-dimensional equation

The one-dimensional equation neglects entirely any lateral strain (Poisson's contraction) associated with longitudinal strain which, while justified for low frequency rod and near-axial longitudinal waves (with a large wavelength which are not bounded by lateral movement) at higher frequencies the corresponding wavelengths are of a similar order of magnitude to the lateral dimensions of a infinite specimen (for example for a beam of wood ≈ 250 kHz, in a log ≈ 25 kHz)^(3.4). In such a situation, frequency-related dispersion occurs, called "configurational dispersion"^(3.4), "wave dispersion"^(3.153), or "velocity dispersion"^(3.154) to avoid confusion with dispersion from the internal damping of the material. Both attenuation through intrinsic damping and dispersion lead to a spreading of the wavefront, though whilst attenuation leads to a rounding of the wavefront, dispersion results in a broadening of the wave packet signal (both in front and behind the main wavefront).

This internal dispersion is induced not only by the geometry of the specimen but also by the nature of the material through the scattering (diffraction and reflection) produced by inhomogeneities which interact with the higher frequencies more

readily than lower frequencies (in the case of traveling waves measured by TOF testing, as opposed to standing waves measured by RF testing), as well the internal absorption of energy by the material^(3.3).

Velocity dispersion, the separation of phase and group velocities, occurs due to the imposition of boundary conditions. Longitudinal and shear waves which exist in theoretically infinite structures (as often assumed for cases using the one-dimensional equation) are subject to mode conversion in situations where the originally generated longitudinal or transverse waves within the material interact with specimen boundaries. In such a situation, plane bulk waves are essentially guided by the boundaries (becoming guided waves) and upon surface interaction undergo elements of reflection (governed by Snell's Law) but also mode conversion; where Rayleigh, Lamb (in the case of plate specimens) or rod waves (in the case of rod specimens) are generated^(3.154). Rayleigh waves present (at depths up to five times the wavelength) are non-dispersive and will travel with a constant velocity below that of the shear wave. The longitudinal and shear waves are also non-dispersive, and as such their velocities will not vary with frequency^(3.154).

However Lamb, rod or flexural waves generated within waveguides are dispersive and their velocity dependent on the additional factors of material thickness and measured frequency^(3.153). These waves may exist as symmetric modes, where the vibrational character waves within the structure form a series of longitudinal compressions and rarefactions (*i.e.* rod waves), or antisymmetric modes, which may be interpreted as flexural wave modes^(3.42, 3.154). The imposition of boundary conditions causes a frequency-dependant separation between the velocity of the wavefront (phase velocity) and the velocity at which the vibrational energy propagates (group velocity). The group velocity ' U ' in a rectangular beam specimen is determined by the "Rayleigh Correction"^(3.4):

$$U = V_0 - \lambda \left(\frac{dV}{d\lambda} \right)_0 \quad \text{Eqn. 3.2}$$

Where:

V_0 = phase velocity for mean λ of the pulse (ms^{-1})

λ = wavelength (m) determined by the frequency under investigation

d = diameter of the specimen

It has been shown in anisotropic specimens, in Halmshaw^(3.4) and Craik^(3.7), that whilst for long wavelengths (i.e. low frequencies) $U \approx V_0$, as the frequency increases the longitudinal rod velocity decreases steadily from the value given by the one-dimensional theory, until it ultimately approaches and plateaus near the value of a non-dispersive Rayleigh wave^(3.4). This is important because, as stated in Lindsay^(3.5), in the case of experimentally-measured velocity derivation (via frequency and distance) from spectral resonance; it will be the group velocity that results unless the wavefront of the pulse is very narrow compared with the lateral dimensions of the specimen^(3.5). Lindsay's assertion of deriving group velocity from spectral resonance may be questioned however, as extracting a velocity from a wave pulse's resonant peak in the frequency domain, based on a relatively instant measurement, will be the product of the phase velocity and not the group velocity. In contrast, a measurement of transit time (TOF) of a wave pulse in the time domain will produce a group velocity.

Dispersion curves are used to show the relationship in these instances between the frequencies, wave modes, phase and group velocities^(3.42). As such, at any chosen frequency there will be a finite number of discrete sinusoidal wave modes (symmetric and asymmetric motion around the midplane of the specimen), each traveling with a separate group and phase velocity. Wave resonances that may exist in a structure must come from exact points (neither below nor above) on the curves for a given structure and below certain cut-off frequencies (nascent frequencies) these waves are unable to propagate^(3.42, 3.43). As the longitudinal, transverse and Rayleigh wave modes are non-dispersive, their velocities remain on a horizontal line, unchanging with increasing frequency.

Figure 3.1 shows a series of phase and group velocity dispersion curves for a simulated rod (i.e. log without any taper) of Scottish Sitka spruce using typical mechanical characteristics and dimensions. These were derived from a MATLAB

routine called PCDISP, a program designed for creating dispersion curves for pipes and cylinders but used in this setting despite being unable to handle material with internal damping, as would be the case in wood^(3,43). As can be seen from Figure 3.1, for zero-order symmetrical rod modes at low-frequencies ($L0,n$, where n is the wavenumber), these rod wave phase and group velocities are finite and will be approximately equal, as dictated by the one-dimensional equation. As the frequency increases the rod wave phase velocity gradually decreases to the Rayleigh wave velocity asymptotically, dependent on the specimen's thickness. The group velocity decrease will be at a faster rate with increasing frequency, falling below that of the Rayleigh wave velocity until rising again for both to plateau near the Rayleigh wave velocity.

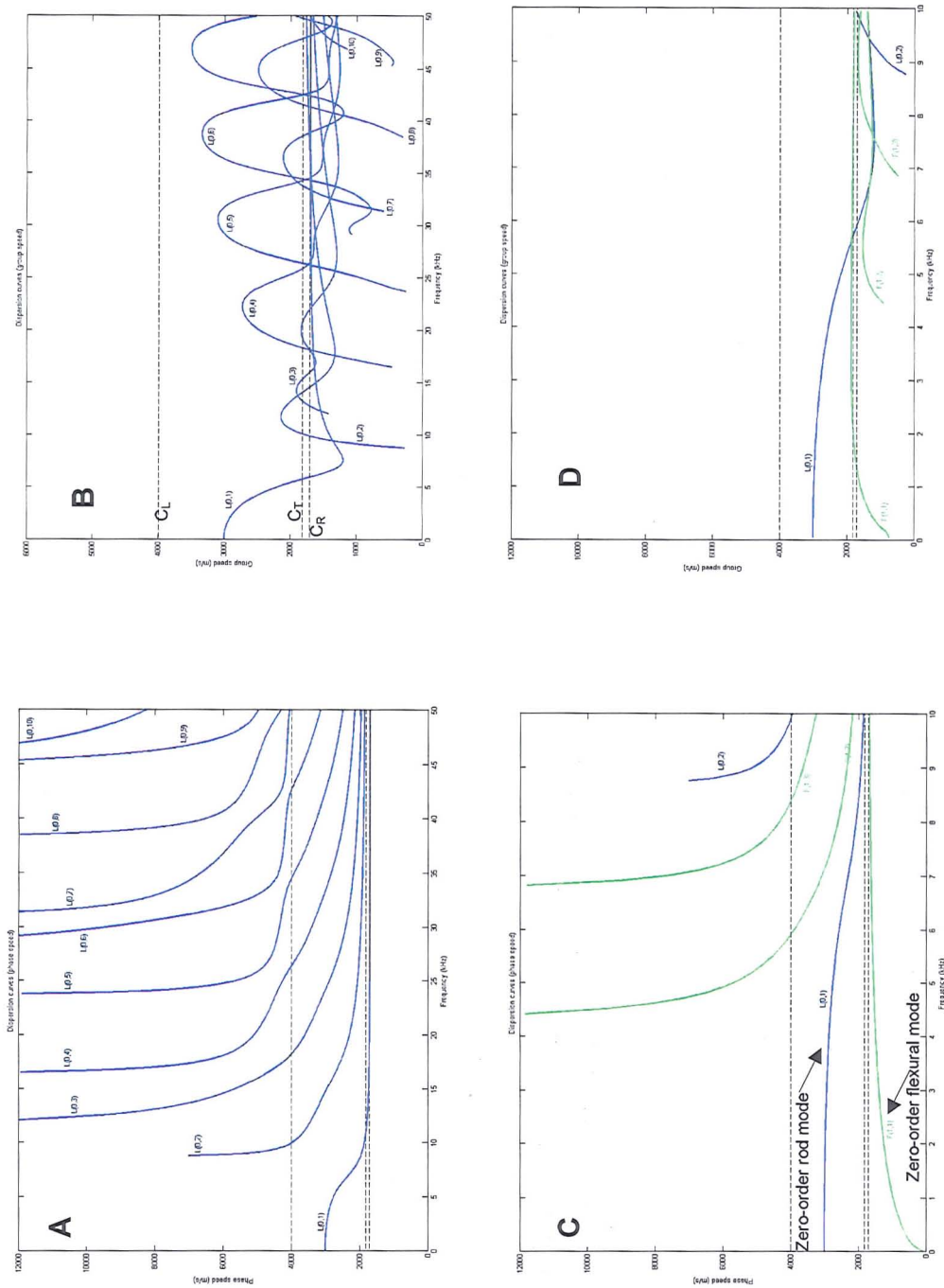


Figure 3.1 Dispersion curves for a simulated Sitka spruce rod created on MATLAB using PCDISP software^(3,154). Graphs on the bottom show phase velocities and on the top show group velocities. Graphs A and B show the possible wave modes present up to 50 kHz for the longitudinal rod wave modes, whereas graphs C and D show the same information for both the longitudinal and flexural modes restricted to below 10 kHz. The parameters of the rod model were: An initial rod speed of 3000

ms^{-1} ; Poisson's ratio = 0.37, density = 450 kgm^{-3} ; radius of the rod 0.125 m and cut-off frequency tolerance of 0.1 Hz. Dashed horizontal lines C_L , C_T , and C_R represent longitudinal, transverse and Rayleigh wavespeeds respectively, that appear in descending order of wavespeed. The mode names displayed in graphs A and B represent the type of wave; (L) Longitudinal (rod wave) and (F) Flexural whilst the numbers in brackets (n, m) denotes; (n) the order of symmetry around the longitudinal axis (NOTE: $n = 0$ denotes symmetrical modes), whilst (m) denotes the number of the wave of a particular family in ascending order of wavespeed. Torsional wave modes have been omitted for clarity.

Appendix D1 displays a parametric series of model retests run on the same PCDISP routine, for ranges typically encountered within this thesis's experiments, with any changes to those benchmark results in Figure 3.1 are analysed where relevant in Chapters 4 through 6.

Coincident with the increase in frequency are the formation of a finite number of propagating symmetrical and asymmetrical modes (rod and/or flexural) existing at any given frequency and their respective velocities at that frequency. Higher order modes have cut-off frequencies from which the phase velocities tend towards the Rayleigh velocity from an initial infinite velocity, and conversely the group velocities tend to increase in velocity, converging towards the same final velocity.

The phase and group velocity of the fundamental rod modes (blue line) tends towards the Rayleigh wave velocity, albeit with the group velocity tending towards the constant Rayleigh velocity at a faster rate than the phase velocity. By contrast, the zero-order (fundamental) flexural (green line) wave group and phase velocity will increase with frequency until it tends towards the value of the Rayleigh wave. Notice here that the flexural group velocity crosses-over the Rayleigh wave velocity at considerably lower frequency than the phase velocity's cross-over.

The question remains however of why researchers such as Bucur and Wang find that longitudinal velocity appears to change with either increasing frequency or decreasing length-to-width ratio. Bucur^(3.3) noted that the velocity is nearly constant when the ratio of length-to-width is above 20:1, but decreases below when the dimensions are below this ratio, citing a reduction in velocity of 12%. However, as

reported in Wang *et al.*^(3.21), the effects of a changing length of specimen was observed experimentally by Porter (1972) who noted that as the beam section under examination was progressively shortened (from 12ft to 6ft to 3ft) with no change in diameter, there was a continuous increase in wavespeed. The difference between these two opposing views may be the result of misusing the rod and fundamental wave equations by incorrectly applying the equations to measurements conducted using ultrasonic and low frequency waves.

Bucur^(3.3) suggests that the reasoning behind this reduction in velocity is the mode conversion as a result of the changing dimensional nature of the specimen. It is the author's opinion however that the discrepancy of changing wavespeed is actually the result of an inappropriate usage of the wave equations for the frequencies and material dimensions involved. In such cases involving anisotropic, orthotropic material, Hearmon asserted that two-dimensional theory needs to be applied^(3.10). If the material were a plywood plate for example it would be assumed that the plate could be replaced with an "equivalent solid plate of uniform thickness and suitably modified elastic properties as to represent the plywood itself^(3.10)". It should also be noted that whilst the inducement to mode conversion may complicate or cause errors in the calculation of velocities, there is opportunity in detailed analysis of the signal for possible quantification of the scatter (and hence mode conversion) inducing parameters^(3.3).

Ouis^(3.44) suggests that the observance of an increasing MoE_d value with frequency (due to an apparent increasing velocity, which is debated) is a consequence of applying non-linear mathematical concepts to linear systems. This is attempting to ascribe non-linear characteristics to what in the author's view is a linear system relationship, and that the discrepancies of velocity increases seen by Ouis, Bucur and others is the result of misinterpretation of the applicable geometry-related measurement techniques for dispersive and non-dispersive waves.

3.1.4 Three-dimensional theory

In situations where the wavelength is of a lower order of magnitude than the diameter of both dimensions (i.e. typically higher frequency waves), it becomes necessary to use a three-dimensional equation^(3.5). This corresponds to a bulk longitudinal wave propagating in an unbounded medium. Surface waves (or the mode conversion to) will not be present in this situation as the material is deemed infinite in three dimensions. As such, and shown from Timoshenko^(3.8), the general expression for bulk plane longitudinal (compression) wave in an (initially stress-free) isotropic, unbounded medium^(3.8) is:

$$V = \sqrt{\left(\frac{(\psi + 2\gamma)}{\rho}\right)} \quad \text{Eqn. 3.3}$$

Where:

V = Velocity of a propagating wave (ms^{-1})

γ = Lamé constant described by: $\gamma = E/(2 \cdot (1 + \nu))$

ψ = Lamé constant described by: $\psi = (E \cdot \mu) \cdot (1 - 2\mu) \cdot (1 + \mu)$

μ = Poisson's ratio

ρ = Density (kgm^{-3})

Expanding on this by substituting in the equations for Lamé's Constants, it is possible to describe a "pure longitudinal" (a.k.a. dilatational or compressional) wave velocity propagating in a bounded homogenous anisotropic medium, by three-dimensional theory by the equation^(3.4, 3.5, 3.7, 3.8):

$$V = \sqrt{\left(\frac{MoE_d}{\rho}\right)} \cdot \sqrt{\left\{\frac{(1 - \mu)}{[(1 + \mu) \cdot (1 - 2\mu)]}\right\}} \quad \text{Eqn. 3.4}$$

Where:

V = Velocity (ms^{-1})

μ = Poisson's ratio (assumed equal in all directions as in a homogenous solid)

ρ = Density (kgm^{-3})

Note that the three-dimensional equation will give a higher value for the three-dimensional longitudinal velocity than the one-dimensional rod wave propagation phase velocity (V_0) equation, the ratio given by^(3.8):

$$\frac{V_0}{V} = \sqrt{\left\{ \frac{(1-\mu)}{[(1+\mu) \cdot (1-2\mu)]} \right\}} \quad \text{Eqn. 3.5}$$

As such for an average Poisson's ratio for Sitka spruce of 0.37, this ratio would be 1:1.329 or a 33% underestimate by the simplified one-dimensional equation^(3.8). However, if one was to take the general value of Poisson's ratio for wood of 0.3, then there would be only a 16% difference. Similarly, a Poisson's ratio of 0.4 would result in a 46% discrepancy between measured velocities.

Therefore, rather than a changing longitudinal velocity with frequency (which cannot be the case given a longitudinal wave is non-dispersive), the discrepancy between high- and low-frequency measured velocity results are often a function frequency-related dispersion (as shown in the dispersion curves in Figure 3.1) in the case of rod wave measurements, or comparing the measured rod wave phase or group velocities with the measurement of bulk longitudinal waves.

Indeed Andrews^(3.40) states that the velocity derived from resonance testing is controlled by the three-dimensional equation. However, he notes that the use of the one-dimensional equation in low-frequency longitudinal resonance testing is sufficient as the resultant speed measured is the combination of multiple reflections from the boundary conditions and thus results in multiple interferences of the waves. This results in an approximation to a plane wave in a long slender rod and thus the speed is reflective of the whole volume of material in the specimen^(3.34). However, Andrews^(3.40) also notes that an amount of wave energy (whose decay is inversely proportional to the square of the distance traveled) will still reach the end of the specimen without interference and reflection, which will be the dilatational wave. It is suggested that this wave is the "frontrunner," which is controlled by the grain angle and is first detected by TOF stress-wave timers (SWT), as opposed to the greater wave packet velocity produced by the resonance^(3.40). The evidence for this was produced from measuring the RF, 10 cm incremental TOF velocity and the TOF velocity along a log as a whole^(3.40). Nine logs 6.12 m long were tested and it was found that the incremental speed was the

fastest^(3.40) thus concluding that highest velocities are found in measurements where the wave cannot begin to approximate a long, slender rod^(3.40). TOF velocity appears to increase with decreasing length-to-diameter ratio ($L:d$) due to potentially decreased scattering and wall reflections. Thus butt logs (which have the lowest $L:d$ ratio) will appear to be faster than they actually are^(3.40).

It was therefore suggested that two speeds exist: a dilatational speed (longitudinal wave measured by the TOF measurement) and the resonance speed (group velocity derived from the behaviour of the rod velocity as shown in Figure 3.1). The incremental dilatational speed was c. 30% faster than the rod speed, whilst the incremental speed was c. 5% faster than the end-to-end TOF speed (most likely due to a slower rise time than the incremental signals due to increased attenuation of the signal)^(3.40).

Thus whilst measurements of resonance are suitably characterized by the one-dimensional equation, TOF measurements over short distances (such as on tree stems) will not approximate plane waves in a rod, therefore are subject to the three-dimensional longitudinal wave equation. It was also noted from the end to end TOF measurements that the only radial variation in velocities was due to the slope of the grain angle and not, as argued by other researchers such as Jang^(3.18), due to spreading and taking the fastest path along the outerwood^(3.40). This also indicated the non-planar nature of dilatational waves, as opposed to the planar waves measured by resonance^(3.40).

Thus, as a result of wave propagation through an anisotropic inhomogeneous medium, different values of velocity may result when calculating velocity via a RF method (which measures the group velocity) and a TOF method, which typically measures the phase velocity. Since the velocity is squared when characterized by the equation for dynamic modulus, any change in velocity becomes increasingly significant. The phase velocity and group velocity can be estimated through a visual inspection of the time trace signal (the group velocity being detectable from the wave centroid packet^(3.153)), but automated TOF devices for the velocity calculation will tend to identify the velocity from the time of passing a threshold

level, thus usually measuring the phase velocity unless it is sufficiently damped. Hence it will not be reflective of the specimen volume as a whole.

Lindsay^(3.5) implies that the group velocity of a pulse measured in cylindrical rods, where there is dispersion potential analogous to a wooden log or tree, does not represent the whole cross-section of the rod if the wavefront of the pulse is very narrow when compared with the lateral dimensions of the rod. Hence when using ultrasonic waves the resultant velocity may not be representative of the cross-section as a whole.

Generally, it has been reported that longitudinal velocities in timber can range from 6000 ms^{-1} for a longitudinal wave propagating along the fibers (though this seems unrealistically high and values of $\sim 4000 \text{ ms}^{-1}$ are considered more appropriate for dry specimens), down to 400 ms^{-1} for longitudinal waves propagating tangentially across an undecayed specimen^(3.3).

3.2 Factors affecting wave propagation in wood

The use of the one- and three-dimensional equations relies on wood essentially reacting to induced wave propagation as an isotropic solid, through the longitudinal orientation of the fibers. However, wood is not an idealized orthotropic solid, often having arbitrary orientation and at higher frequencies is subject to wood's characteristic scattering mechanisms (due to density variations resulting in acoustic impedance variations) through inhomogeneity in the structure (cellular structure variation in fiber angles, ring-width and density variations with age and height in a stem, early/latewood and sap/heartwood boundaries) as well as defects (knots, compression wood, etc.) all causing a deviation from the idealized homogenous isotropic model on which the Euler-Bernoulli equations are based. It is commonly assumed (Feeney *et al.*^(3.43)) that inhomogeneities are neglected provided they are significantly smaller than the wavelength used. It must also be considered that the wave must have achieved a planar wavefront (with wave intensity varying inversely with distance squared) to be truly valid^(3.6), as TOF

measurements taken within the Fresnel region (near-field) will be based on the more variable dilatational velocity.

Additionally, since wood is not homogenous and the propagation is much faster along the grain than across it, the wavefront would not remain normal to the longitudinal axis, especially in the case of sloping grain^(3.44). However, in specimens with a low diameter to length ratio, the interactions from boundary conditions may help to create an essentially planar wavefront earlier than in an unbounded medium, similarly resonance techniques become valid estimations as they measure multiple reflections along the length of a specimen to create a frequency spectrum, over which length a plane wave will have been created^(3.38).

3.2.1 Anisotropy and mode conversion

Due to wood's anisotropic nature, bulk waves will be subject to off-axis propagation and coupling to other wave modes, the degree to which being governed by Snell's laws of refraction and reflection, called "mode conversion"^(3.4, 3.8). It should also be noted that the reflection of the waves can also lead to phase changes^(3.4). In this case, the velocity will depend on the angle of propagation (α , or propagation vector) out of the principle axis of symmetry. This can be evaluated experimentally by cutting the specimen at convenient angles to the orientation of the specimen^(3.3). Experiments outlined in Bucur^(3.3) indicated that at angle of 45° to the longitudinal axis, an error of 3% in the calculation of the angle can result in a velocity error of 100%. Additionally, in spruce the transition between early and late wood is very sharp, inducing refraction of the wave adding to the propensity to mode conversion, particularly at high frequencies^(3.3).

It is unclear, or not currently investigated, from the literature whether or not the refraction of a wave between different densities, e.g. between green sapwood and heartwood on a macro-scale or within micro-scale annual ring variations, contributes to the enhancement of velocity. For example, it is possible that by striking the wood at the centre of the pith, a wave subject to beam-spreading through the lower density heartwood into the higher density (and faster

transmitting) sapwood, which may therefore be refracted into the direction of general wave propagation, thus producing a faster velocity in the refracted portion than would otherwise occur if sapwood alone were tested. Similarly it is possible that due to this behaviour at a quasi-impedance boundary, an amount of energy would be reflected back into the heartwood, potentially causing interference with the unreflected dilatational wave already present.

The propagating pure longitudinal and pure shear waves described above will (in three-dimensional theory) propagate as 'Quasi-longitudinal (QL) and Quasi-transverse (QT)' bulk waves, for which the slower transverse bulk will effectively model a pure transverse wave and therefore has the notation (T)^(3.3, 3.8). The QL velocity will always be the fastest^(3.3, 3.5), most likely due to the elongated tubular array of tracheid cells (the bulk of which are axially orientated) acting as a primary conduit. Typical values for velocity in Sitka spruce at 12% MC, as given by Bucur^(3.3), are a QL velocity of 5500 ms⁻¹, QT velocity of 2250 ms⁻¹ and T velocity of 1850 ms⁻¹. For further discussion on slowness sheets (as they are not used in these investigations), see Bucur^(3.3) or Hearmon^(3.8).

As a result the majority of dissipation of the energy in this QL wave type most likely takes place at the end of the tracheids^(3.3) or upon mode conversion to other wave modes which are more readily attenuated by the radial anisotropy. However, Bucur^(3.45) noted that there is continual conversion between the mode types. The different propagation velocities for the two shear waves may be induced by the annual ring structure's alternation of late and early wood (which is ignored in the elastic theory of Christoffel's equations)^(3.3), particularly at high frequencies (100 kHz to 2 MHz) where the annual ring structure induced frequency stop-bands (due to the sharp impedance between early and latewood layers providing a strong scattering) in radial propagation^(3.43). This level of anisotropy may be neglected during this thesis as the wavelengths under investigation are considerably longer, with no frequencies greater than 54 kHz investigated.

On the subject of anisotropy, Chauhan *et al.*^(3.46) investigated the influence of varying degrees of inhomogeneity of a wood member specimen by progressively

increasing the degree of macro-inhomogeneity in laminated beams. It should be noted at this point that the same beams (or rather similar beams cut from the same original laminated plate specimens) were used in the investigations of energy loss and damping presented later in this thesis. Chauhan *et al.*^(3.46) found that velocity (as measured by both resonance and TOF methods) progressively decreased with increasing degrees of macro-scale inhomogeneity, however differences between the resonance and TOF velocities were observed, which will be discussed later in this chapter.

3.2.2 Grain angle and cross-grain

This is particularly important when dealing with specimens with an inclined slope of grain, spiral grain or high defect content inducing a change in grain direction. Gerhards conducted much of the key research into the nature of stress-wave propagation across changing grain angle (and the related effects of knots, as discussed below)^(3.11, 3.44). He was amongst the first to note that cross-grain or a changing grain angle will cause the wavefront or contour to be skewed in the direction of grain angle, rather than to advance with a front normal to the longitudinal axis, with velocity reportedly varying by 1% per degree of grain up to a grain angle of 30°^(3.44) (which we remember from the previous section being similar to the effect of grain angle on the static MoE). Gerhards' subsequent work on the effects of knots on velocity confirmed that stress-waves propagate fastest in the direction of grain angle^(3.11).

As an aside in regards to experimental procedure, Gerhards also showed that averaging smaller distance measurements along the specimen where produced better correlations to the actual MoE than longer measurements along the whole length of the sample, though the relative error was reduced when testing over longer distances^(3.44). It was also noted that with significant grain angle change, the choice of end at which to strike could affect the result^(3.44). However, Gerhards'^(3.44) study was conducted on only five samples with significant variations in density and growth rate, it did not account for the effect of knots and changing grain angle separately and it is possible that the starting accelerometers were within the near-

field area of propagation. The samples were also relatively short with no mention of the way in which the SWT calculated its propagation time. It also failed to establish whether, given subsequent propagation over a distance with no change in grain angle, the wave would return to a planar nature, though experiments by Divos have indicated it would not^(3.47-3.48).

It was established by Gerhards^(3.44) and others such as Kabir^(3.49) and Divos^(3.47) that, whilst the change in angle due to knots are a specific case, if there is a constant or a calculable average angle of deviation from the symmetrical axis, a derivation of Hankinson's formula based on the laws of refraction, which can be related to static or dynamic loading at a given grain angle, allows for the accurate prediction of velocity at this angle in conjunction with the static modulus^(3.47-3.49). However, it was generally noted in this literature that the accuracy of the velocity calculations is far more important in establishing grain angle than in dynamic elastic modulus prediction. The majority of this research was conducted using ultrasonics on small samples and it is unclear from the literature, though inferred as such, as to whether this holds for low-frequency investigations of larger timber samples.

3.2.3 Density

Bucur^(3.3) cites the research of Barducci and Pasqualini (1948) who examined the resonance of multiple species to determine that the contribution of density to the velocity of stress-wave propagation, as determined by resonance methods, was statistically poor ($R^2 = 0.05$)^(3.3). Schad *et al.*^(3.50), on small clear specimens from railroad switch-ties found a better, but still weak, negative correlation ($R^2 = 0.44$) of stress-wave velocity to density.

However, Kumar *et al.*^(3.51) noted relationships between density and velocity in both felled and standing timber. Chauhan and Walker^(3.52) explained this by noting that the correlation between velocity and density will increase (despite being unrelated) due to the coincidental increase in MFA with age, and thus good correlations may be observed particularly in older specimens with a distinct variation in both density

and stiffness. Wang *et al.*^(3.53) found a linear correlation of $R^2 = 0.27$ between velocity and bulk density. Regarding standing tree measurements of TOF velocity, Hayes and Chen^(3.54) and Andrews^(3.38) observed that density only has little variation across a site as the green density of a material is so dominated by water that regardless of the basic density the wet density is always close to 1000 kgm^{-3} ^(3.54). As such the TOF velocity alone is often used, particularly in standing tree devices such as FAKOPP™ 2D and ST300™, as the sole indicator of MoE_d ^(3.35).

3.2.4 Fibre structure

Due to the typical pattern of both density and MFA variance radially between juvenile and mature wood and the described variation with height due to increasing juvenility, it was described in Chapter 2 that the stiffest part of the wood occurs on outer portion of the second log up the tree^(3.29). As such, several studies have indicated that the velocity is highest in this portion of the tree^(3.13, 3.55-3.60). Feeney *et al.*^(3.43) noted that the curvature of rings only have an effect on the radial US velocities, through increased mode conversion with increasing curvature in zones such as juvenile wood, and not longitudinal ones. Wang *et al.*^(3.61), found a good correlation between stress-wave (using an impact-based Metriguard 239A test) and ultrasonic wave times parallel to grain in veneer sheets ($R^2 = 0.82$), but the correlation was reduced perpendicular to grain ($R^2 = 0.66$). This was assumed to be the effect of increased inhomogeneity between the longitudinal to tangential planes. Huang *et al.*^(3.62) stated that the velocity of sound in wood relates specifically to "the intrinsic wood quality and the ultrastructure of the tracheid wall"^(3.62).

3.2.5 Microfibril angle

As such, in clear wood samples (that are free from defects such as knots, resin pockets and spiral grain), the acoustic energy's path will be controlled by the orientation of the cellular structure and the bonds between the cells^(3.10). In softwoods such as Sitka spruce these cells are arranged in long tracheids (fibres) ideally orientated axially to the stem of the tree and ultimately the variation in this orientation is believed to control the strength of the wood, assuming similar

densities between samples^(3.63-66). Therefore the fastest path of propagation is assumed to be axially in the direction of these fibres^(3.65). It should be remembered that at a cellular level, the S₂ layer's microfibril angle will control structural cell strength and thus potentially that of each tracheid. Since this is the largest layer in the cell wall (approximately 85%), the bulk of vibrational energy could be hypothesised to propagate within this structure. The more axially aligned microfibril angle also potentially indicates the fastest path of propagation.

Thus the MFA, which is reflective of the ultrastructure through its relations to both cell wall thickness and tracheid length (though it has not been proven conclusively that these factors are dependently linked to the MFA, as seen in Chapter 2) has enabled a correlation to be drawn between MFA of the S₂ layer and the stiffness of wood. Huang *et al.*^(3.62) then noted that the velocity of sound is largely determined by the microfibrils. Evans^(3.65-3.66), based on Silvascan™ analysis, infer the conclusion that acoustic velocity is strongly related to the MFA through its control on stiffness. However, MFA determination is only possible in laboratory settings on small samples due to its macro-variability.

The stiffness dependence on microfibril angle is believed to hold at the microscopic and small sample level but with increasing scale the high occurrence of inherent defects in Sitka spruce and its tendency to produce spiral grain during the formation of new wood during the growing season causes particular problems in the assessment of the acoustic behaviour within the timber, particularly in standing trees. Bucur suggests that it is the variation in the slope of grain around knots, in small specimens, that is the principle reason for their strength reducing properties^(3.67). The MoE gives information on the sample's global (overall) quality (as does the longitudinal velocity), MoR depends more often on a local defect, which does not have a dominating influence on propagation velocity, but rather initiates the rupture mechanism^(3.33). It is the shift in scale that separates the high correlations found between both static MoE and MoR with longitudinal velocity (in both cases $R^2 \approx 0.90$) from lower linear correlations between MoR and longitudinal velocity seen in beam samples ($R^2 \approx 0.25$)^(3.33, 3.68-3.69) compared to the static MoE of the same beam samples ($R^2 \approx 0.6$ to 0.9) (see Table 3.1).

3.2.6 Juvenile wood

Although not a variable in itself that affects velocity, the difference in this area when compared to normal mature wood concerning annual ring variations, higher MFA, lower density and shorter tracheids, means that it often will behave in a similar manner to compression wood (indeed they share many of the same characteristics). As will be shown, compression wood shows a decrease in longitudinal velocity, compared to normal wood, when measure by TOF methods. A similar decrease in velocity from outer mature wood to inner juvenile wood was observed by several researchers^(3.52, 3.57-3.58, 3.63, 3.70-3.71), although, as with static stiffness profiles radially across timber samples, the increase in velocity towards the outer wood tends to plateau outwith the juvenile zone of influence.

3.2.7 Moisture content and temperature

Above the FSP it is often assumed that there is no noticeable change in velocity, due to the correlation between velocity and stiffness, since there is no change in static stiffness above FSP. Bucur^(3.3) notes that the static stiffness does remains constant due to the addition to the mass of the free water, thus increasing the density and maintaining the apparent stiffness whilst the increased moisture weakens the bonding between cells. Booker^(3.72) points out that increased moisture above FSP does not affect the cell bonding strength as the additional moisture increase only affects the cell lumen and not the walls. He also noted, on SCS, an 86 to 222 MPa decrease in MoE_d (54 kHz PUNDIT™ SWT) *per* percentage increase in MC up to FSP, followed by a slow rise in MoE_d above FSP. This has been attributed, in a the later paper by Kang and Booker^(3.73), to a combination of increasing density due to moisture content above FSP and to the rate of loading of the vibration, in that the water does not have time to move between cells (as is the case in static bending) and thus adds to the resistance and stiffness of the material.

Simpson and Wang^(3.74) confirmed these results by observing a linear increase in TOF velocity with decreasing MC above FSP ($R^2 \approx 0.98$). However, no mention

was made of the change in this overall linearity below the FSP, which was clearly visible from the presented graphs. It should be noted however that this observation was for relatively high temperatures (as the study was related to the monitoring of velocity and MC during kiln drying) and as such the applicability of the last statement would be irrelevant to standard field testing of wood velocity. It was observed, by combining the PUNDIT™ signal with a Fast Fourier Transform (FFT) display, that in longer boards, the high-frequency content was removed due to attenuation and a lower frequency was dominant (at 2 kHz instead of the transducer resonance of 54 kHz, which was attributed to the overtones of the repetition rate of the pulser, though this was only 10 Hz and would seem far too low to contribute substantial energy at this frequency, it is possible that this frequency was the result of a surface wave created by the initial signal).

Several researchers^(3.38, 3.54) have noted that density above FSP is practically constant at 1000 kgm^{-3} due to the mass of the water (free and bound) being added to the mass of the wood and as such the stiffness of wood can be determined solely by the velocity-squared. It should be noted however that if testing is conducted after the log has had time to dry (even in part, i.e. either at the ends or due to removal of surface bark) then higher velocities may result, thus overestimating the stiffness relative to other logs in the test series. Wang *et al.*^(3.53) also noted the segmented (above ($R^2 = 0.57$) and below ($R^2 = 0.31$) FSP) increase in ultrasonic velocity with decreasing MC on SCS (from 0 to 240% MC, $R^2 = 0.76$), but added observations that US velocity (determined by a 54 kHz PUNDIT™ device) decreased with increasing bulk density (though the R^2 for this was only 0.27, but significant at the 1% level). By combining the two parameters, MC and bulk density, in a polynomial regression model to account for the variation in velocity, they observed that MoE_d remained constant above FSP, thus mirroring the behaviour of static MoE above FSP.

Bächle and Walker^(3.76), Carter *et al.*^(3.35), Green *et al.*^(3.77) and Bucur^(3.3) all noted that increasing temperature decreases the RF (based on average velocity) and TOF velocities. Van Dyk and Rice^(3.78) noted a correlation of $R^2 = 0.98$ between temperature and ultrasonic velocity tangentially propagating across small beams.

This would be expected as we have already established in Chapter 2 that stiffness decreases with temperature.

Ultimately it would appear that below the FSP, the changing moisture content has a larger influence on velocity, but above the FSP temperature plays an increasing role in velocity^(3.3). As noted earlier, they also provide conditions favourable to decay, whose effect on velocity is seen in the next section.

3.2.8 Drying induced defects

It was noted by Gerhards^(3.44), during his study of the effects of grain angle on wave velocity, that cupping of the specimen can influence the TOF-derived velocity. With no cupping, the wavefront is nearly uniform in nature, but with positive cupping (i.e. the bark side is concaved) the stress-wave leads along the centre of the specimen and lags at the edges; negative cupping (bark side convex) shows lagging at centre and leading from the edges^(3.44). Thus velocity derived by TOF methods will see an induced variability between specimens where drying defects are present.

3.2.9 Biological decay

The effect of biological decay on the propagation of waves depends upon the method, frequency and direction of the waves used to investigate the specimen, and the extent and orientation of the decay itself.

Several research papers^(3.79-83) dealing with decay (and its detection by acoustic techniques) are discussed in section 3.4.4.3 and 3.4.4.3. The general conclusion, though methods of evaluation differ, is that biological decay increases TOF transit times and wave attenuation (through increased path deviation and scattering), and decreases resonance frequencies (primarily through removal of mass rather than reduction of stiffness). It is also clear that attenuation and shifting lowering resonances, where tests can be conducted, are more sensitive to decay than transit time reduction. As will be shown later in this thesis (Chapter 6), this general conclusion is based on a general misunderstanding of specific areas of the sample which are measured by resonance methods.

3.2.10 Knots and other defects

It has been known for some time, from the work of Gerhards^(3.11), that TOF velocities are susceptible to influence from knots, particularly at high frequencies where the effect of scatter is much greater. As a result of wood fibres being distorted around knots, leading to the development of cross grain, Gerhards^(3.11), and Kabir *et al.*^(3.84-3.85), found that the velocity was reduced (shown through longer TOF transit times) when propagating through a region containing knots or adjacent to it. Gerhards noted that localised changes in grain angle had a greater effect on velocity than the overall presence of spiral grain^(3.44). There is no significant variation of this effect based on whether the knot is intergrown or loose, but the size and orientation of the knots, and their presence in clusters do have a varying effect^(3.11).

Both this work and the work of Divos^(3.47-3.48) have shown that a wave, which has developed a planar wavefront within a specimen, will lose this planar wavefront as parts of the cross-section transmit the wave quickly through clear wood and other parts are subject to slower transmission due to the induced grain deviation. In short specimens a low-frequency wavefront would not have enough space to spread out to re-establish a planar wavefront, and may be subject to additional knot influences. The work of Divos also showed the increasing attenuation of wave energy due to knots^(3.47). However, Divos noted that velocity is incapable of indicating defects if the sensor is next to the defect^(3.48).

Resonance testing is assumed to be less affected by the presence of knots than TOF, through averaging the whole volume of the specimen rather than one part. Previous literature, such as Huang *et al.*^(3.62), noted that in resonance testing knots are so small compared to the wavelength examined that the stiffness measured is reflective of the intrinsic quality of the clear wood in the specimen. Again the results of Chapter 5 may offer a dispute to this assumption.

Work by Divos^(3.48) and Sandoz^(3.33, 3.68) examined the propagation of acousto-ultrasonic waves around artificially induced notches (designed to simulate knots and decay). Similar experiments, though with different techniques, on the artificial

replacement of wood with other material to simulate knots were conducted by Ouis^(3.86). The general conclusion of all these studies, which are referred to in greater detail in subsequent sections, is that whilst the presence of both knots and decay will affect the derived velocity (depending on the cross-sectional location), and the affect of the discontinuities on the amplitude of the wave is significantly greater compared TOF velocity studies where the 'fastest path' round the discontinuity was still available. For example, Sandoz^(3.87) noted that if over 50% clear wood exists across the cross-section, then there will be no discernable effect on the velocity measurement. Divos^(3.48) also noted the change to the nature of the spherical waveform as a direct result of the presence of knots. However, Schad *et al.*^(3.88) asserted that increased knots simply lead to a greater variability in the measured wavespeeds with no clear correlation between number of defects and transmission times.

Unless the entire cross section contains a knot, the stress-wave will still have areas of the cross section through which it can propagate without deviation, and as such both TOF methods, and particularly resonance methods which develop a planar wavefront over longer distances due to reflections and average the whole cross-section of a specimen (as opposed to most TOF methods), are less influenced by the presence of knots than a measure of the damping.

3.2.11 Compression wood

However, it is also suggested by Bucur^(3.3) (with reference to compression wood in spruce) that since the velocity of a wave is controlled by the density (which increases in compression wood due to a decrease in earlywood) and the stiffness (which decreases in compression wood) there will be little change in the velocity between compression wood and normal wood^(3.3). Bucur^(3.3) also quoted her work from Bucur (1991); using 45 kHz longitudinal waves showed that the compression wood had a slightly lower velocity than normal wood. From this she suggested that since:

“a fibre is the basic anatomic element for ultrasonic wave propagation... the fact that in compression wood the tracheids are shorter than in normal wood, and have a higher lignin content and a flatter microfibril angle^(3.3).”

This would suggest that tracheid length is linked to ultrasonic velocity. The same study indicated that the highest velocities were found in the tension wood of hardwood species, due to the longer fibres and higher cellulose content^(3.3). Whilst this latter point is not debated and the author of this thesis agrees that longer, continuous fibres allow for the fastest transmission of a compressional wave (MFAs being equal), the former point regarding the lack of variation in velocity between normal and compression wood should be subject to the caveat that this will be the case in outerwood, where there is little variation in MFA between normal and compression wood (particularly when studying SCS) in juvenile wood with a more variable MFA, which was shown in Chapter 2 based on Cave and Walker^(3.64), to exert far greater influence over the stiffness than the density. However, Reynolds^(3.89) examined full-size structural specimens of Sitka spruce and found little correlation between both dynamic and static MoE values and the presence of compression wood ($R^2 = 0.24$).

Examples from recent studies of the correlations of individual wood characteristics to dynamic MoE values are given in the Table 3.2:

Table 3.2 Correlations between velocity or dynamic MoE measurements (TOF and resonance-based) and individual wood parameters (Ort. = orientation of the specimen relative to the compressional wave).

Ref.	Method	Excitation	Measurement device	Velocity or dynamic MoE	Specimen size	Sample no.	Specimen age	Ort.	Species	Wood property	R ²
Ilic ^(3.22)	RF	impact	FFT-based software	dynamic MoE	beams	70	?	L	eucalytus	moisture content	0.45
Ilic ^(3.22)	RF	impact	FFT-based software	dynamic MoE	beams	70	?	L	eucalytus	moisture content	0.53
Ilic ^(3.22)	RF	impact	FFT-based software	velocity	beams (dry)	70	?	L	eucalytus	density	0.44
Ilic ^(3.22)	RF	impact	FFT-based software	dynamic MoE	beams (dry)	70	?	L	eucalytus	density	0.45
Ilic ^(3.22)	RF	impact	FFT-based software	velocity	beams (green)	70	?	L	eucalytus	density	0.4
Ilic ^(3.22)	RF	impact	FFT-based software	dynamic MoE	beams (green)	70	?	L	eucalytus	density	0.13

Ref.	Method	Excitation	Measurement device	Velocity or dynamic MoE	Specimen size	Sample no.	Specimen age	Ort.	Species	Wood property	R ²
Ilic ^(3.30)	RF	impact	FFT-based software	velocity	SCS	104	n/s	L	eucalytus	density	0.39
Johansson and Kliger ^(3.29)	RF	impact	n/s	dynamic MoE	beams	401	60-135	L	Norway spruce	density	0.79
Johansson and Kliger ^(3.29)	RF	impact	n/s	dynamic MoE	beams	401	60-135	L	Norway spruce	KAR	-0.51
Johansson and Kliger ^(3.29)	RF	impact	n/s	dynamic MoE	beams	401	60-135	L	Norway spruce	ring width	-0.42
Johansson and Kliger ^(3.29)	RF	impact	n/s	dynamic MoE	beams	401	60-135	L	Norway spruce	grain angle	-0.29
Evans and Ilic ^(3.65)	RF	impact	n/s	dynamic MoE	SCS	20	n/s	L	eucalytus	MFA	0.83
Evans and Ilic ^(3.65)	RF	impact	n/s	dynamic MoE	SCS	20	n/s	L	eucalytus	density	0.7
Evans and Ilic ^(3.65)	RF	impact	n/s	dynamic MoE	SCS	20	n/s	L	eucalytus	MFA and density	0.94
Chauhan <i>et al.</i> ^(3.52)	RF	impact	HM200™	velocity	logs	50	8	L	Radiata pine	density	0.22
Chauhan <i>et al.</i> ^(3.52)	RF	impact	HM200™	velocity	logs	50	25	L	Radiata pine	density	0.49
Hanhijärvi <i>et al.</i> ^(3.20)	RF	impact	Rion SA77 GP analyser	dynamic MoE	boards	100	n/a	L	Norway spruce	density	0.19
Hanhijärvi <i>et al.</i> ^(3.20)	RF	impact	Rion SA77 GP analyser	dynamic MoE	boards	100	n/a	L	Scotch pine	density	0.5
Knowles <i>et al.</i> ^(3.90)	TOF	impact	IML Hammer™	velocity	standing trees	180	18	L	douglas fir	density (cores)	0.52
van Dyk and Rice ^(3.78)	TOF	ultrasonic (100 kHz)	HP 500 oscilloscope	velocity	SCS	10	-	T	spruce	Moisture content	0.97
van Dyk and Rice ^(3.78)	TOF	ultrasonic (100 kHz)	HP 500 oscilloscope	velocity	SCS	10	-	T	spruce	Temperature	0.98
Dickson ^(3.13)	TOF	impact	FAKOPP™	velocity	logs	35	9	L	eucalyptus dunnii	density (cores)	0.67
Dickson ^(3.13)	TOF	impact	FAKOPP™	velocity	logs	35	25	L	eucalyptus dunnii	density (cores)	0.71
Hanhijärvi <i>et al.</i> ^(3.20)	TOF	impact	Sylvatest®	velocity	boards	100	n/a	L	Norway spruce	global density	0.23
Hanhijärvi <i>et al.</i> ^(3.20)	TOF	impact	Sylvatest®	velocity	boards	100	n/a	L	Scotch pine	global density	0.54

3.3 Methods of dynamic MoE determination

Generally, there are four types of non-destructive acoustic investigation that can evaluate dynamic stiffness, though these can be subsequently subdivided into further categories. These are:

- a) TOF measurements
 - i. Sonic measurements
 - ii. Ultrasonic measurements
- b) RF measurements
 - iii. Sonic longitudinal measurements
 - iv. Ultrasonic longitudinal measurements
 - v. Transverse vibration measurements
- c) Acousto-ultrasonic measurements
 - vi. Damping and energy loss in sonic measurements
 - vii. Damping and energy loss in ultrasonic measurements
- d) AE measurements

This section is divided between the TOF (3.4) and RF (3.5) methods and evaluates potential issues with each method as raised by previous research, as well as providing examples of their application to recent timber research. Particular focus is given to previous research which is closely related to the methods, scales of investigation, and objectives employed in later chapters of this thesis. AE studies have no overlap with this investigation and are not discussed. Elements of acousto-ultrasonic measurement techniques do overlap however (particularly damping measurements), and at the end of this section discussion is made of recent research within applicability to this thesis.

Typically, the standard measurement of velocity in timber research is based either on the TOF between two transducers of a known distance or the flexural or longitudinal (or in some cases, torsional) resonance of rods and bars measured via one transducer^(3.54). The measurement of the velocities has its own inherent errors dependent upon the measurement method used. Propagation off-axis (of symmetry) when the other coefficients are not equal to zero does not overly concern this investigation, for a fuller review of this see Bucur^(3.3), Chapters 4 and 5.

The RF and TOF methods are the only NDT techniques with the ability to relate a direct wood characteristic (i.e. velocity) to stiffness, all other relying on proxy

indicators, such as MFA or tracheid length. The simple yet key advantages of both these methods, when conducted properly, are that they allow for repeatability and reproducibility of a true non-destructive test of wood's stiffness, in addition to being relatively rapid and portable in terms of NDT techniques. Both methods were discussed in Hearmon^(3.8).

Returning to the applicability of the use of dynamic stiffness theory, Divos^(3.47) noted that whilst the one-dimensional equation is sufficient for the modeling of wave propagation and velocity in beams or rods (either by RF or low-frequency TOF), a velocity calculated on the outer wood of a standing tree (only possible through TOF measurements) requires the 3D model as the free dilatation and compression of waves is not fully possible (which it is in elongated beams and rods). It is noted that, for standing trees, the Poisson's ratio is reduced by half to accommodate this partial dilatation and compression^(3.47). Thus a typical Poisson's ratio (in the Longitudinal-Radial direction) of 0.39 for timber will reduce to 0.195. If this result (from the three-dimensional theory) was then correlated to a RF test (one-dimensional theory) on the subsequent log specimen, it would thus have an error of c. 5% between the two results^(3.47).

Specimen scale selected for stiffness evaluation (tree; log; beam or batten; SCS) greatly affects the correlations between dynamic and static MoE, as is seen later in this section. The vast majority of investigations into wood quality centre on the effects of the natural variability of each species, and thus inherent characteristics' affects on the final wood quality. Typically, the use of acoustic techniques in wood investigations is in finding an early indication of stiffness of the specimens. As such, only a minority of acoustical NDT investigations focus on the effect of these characteristics (density, grain angle, cellular structure and macro-scale defects) on velocity and attenuation. The choice of both method and frequency is dictated by the property under investigation.

Bucur^(3.3) gives a detailed review of other factors to consider when using (primarily high frequency) vibration to calculate the velocity in a particular axis including; probe diameter and maximum pulse width relative to the specimen dimensions; the

need for wavelengths of sufficient size so as to assume planar wave propagation (thus the minimum size of wavelength should be less than half the minimum dimension of the specimen); differing attenuation across the three axes and increasing attenuation with increasing frequency; separation time of the QL and QT waves; off-axis deviation of the energy flux vectors where more than the three modes of wave propagation can occur simultaneously^(3.3). As her focus is based primarily on her own extensive ultrasonic investigations and related works, little attention is paid to the practically encountered issues of variability of low-frequency TOF measurements based on the point at which a start stop signal is taken by a SWT, and what part of a compressional wave a SWT is actually measuring. These issues are discussed shortly.

3.4 Time of Flight (TOF) methods

The TOF (or transit-time) method involves a calculation of the velocity between two points (accelerometers), of a known distance apart, and determining a transit time via the location of the two leading edges of the waveforms on the time-signal trace returned from each position.

3.4.1 Accuracy of time determination

However, there exists an initial problem with TOF measurements through the establishment of where best to measure the wave velocity: at the deviation from the horizontal trace of the background vibration? At a percentage of the wave's amplitude peak? At the peak itself?

Misidentification of the arrival time will lead to a significant error in the estimate of MoE_d (since it is the square of the velocity that is used)^(3.38). Andrews^(3.38) noted that the detection of the arrival time is more difficult than that of the fast-rising start time due to small oscillations in the arrival signal which begin immediately upon impact at the start transducer (which are not explained by electrical faults). No explanation was offered, though possibilities exist for the excitation of faster surface waves contributing to the signal, as is the favoured explanation of this thesis's author, or physical displacement of the specimen.

Andrews^(3.38) did note that to correctly identify the correct rise-time at the receiver requires a temporal resolution of less than 15 μ s (thus requiring a channel bandwidth of 60 kHz, which most accelerometers don't possess). A solution presented was the use of higher frequencies which have sharper leading edges, but this is discounted from use on wet logs due to the greater attenuation of these frequencies (as is proven in Chapter 7 of this thesis).

Berndt *et al.*^(3.92) studied the use of TOF velocity calculation by means of threshold crossing (a.k.a. "First-break" determination) and peak-to-peak energy calculation, but noted that both methods are error-prone due to changes in the pulse shape due to wood anisotropy. It was suggested that a more accurate velocity calculation can be obtained from the use of short-time Fourier transforms for ultrasonic signals, though as the experiments were conducted using a 5 MHz transducer its applicability to sample lengths larger than 1 cm is questionable. The advantage of this technique is that it determines the velocity from the phase slope, which is not influenced by attenuation of interference effects^(3.92). The method involves converting the time signal to a frequency signal and observing the time shift (seen as the slope of the linear difference) between two pulses, through the comparison of the phase curves^(3.92). However the method has further complications outside the scale of applicability in requiring a constant phase slope and the use of a single ultrasonic wave packet (as more than one will interfere with each other's phase information).

Traditionally, a regression back from the peak is taken to a percentage of the total amplitude of the signal to approximate the base of the rise times^(3.19). More often, the start and stop points are not specified, making method comparisons difficult. However, the slopes of the two signals vary, especially if the first slope is the result of a signal trace from a force transducer hammer or an accelerometer close to the impact. The second accelerometer will have a more gradual slope due to the dissipation of the wavefront.

3.4.2 SWT measurement devices

However, due to reasons previously discussed, the wavefront usually has not been propagated over a long enough distance to form a planar wavefront, unlike a resonance method. This may in itself not be a problem with low frequencies in long specimen but if the measurement points are close together or near the source then the three-dimensional elastic equation may need to be used. Typically however, only one-dimensional theory is applied, creating a possible source of error. Commercial SWT devices for standing trees, such as the TreeTap™, ST300™, IML Hammer™ and FAKOPP 2D™, are also strongly dependant on the nature of the hammer hit and the subsequent wave front induced, though this can be compensated for by increasing the distance between sensors^(3.54).

However, this increasing distance will also serve to increase the variability of the result. Harris *et al.*^(3.32) also pointed out other failings in TOF devices in that they lack repeatability, accuracy (as they are grain, defect and cross-sectional area dependant) and cables are safety risk on site. Wang *et al.*^(3.41) observed that the MoE_d returned by SWTs typically over estimated the static MoE of logs by 19 to 27%, attributed to TOF taking the fastest path along the outside of the log rather than through the whole cross-section. Bodig^(3.93) noted that TOF methods only measure the fastest sound wave thus bypassing the weakest areas (not strictly true, as it has been shown to depend on the distance-travelled and attenuation), and requires a knowledge of the density below FSP (as does the resonance method). Additionally Rus *et al.*^(3.94) note that the main disadvantage of US SWT such as the PUNDIT™ device is the large measurement faces, which induce signal distortions and near-field (aperture) effects, *i.e.* aperture effects consist of vanishing signals due to the cancellation of the waves when the contact area is coincident with the wavelength^(3.94). Note that in this thesis however sample length is far greater than the Fresnel region coincident with PUNDIT™ operation.

Table 3.3 shows commercially available SWT devices, additionally numerous oscilloscopes and transducers can be used for the same purpose. Similarly, an extensive report by Crews^(3.96), reviewed multiple devices capable of measuring transit time.

Table 3.3 The main commercial SWT and their scale of application in timber research (SS = small samples, B = beam samples, L = log samples, T = tree samples).

Device	Manufacture	Start/stop transducers	Probe type	Scale of use
PUNDIT™ (James V meter)	CNS Farnell (UK)	Transmitter and receiver	US flat-faced transducers (37kHz to 220 kHz)	SS, B, L
Metriguard 239A	Metriguard (USA)	Force transducer Hammer and accelerometer	Uniaxial accelerometer	B, L
Sylvatest® and Sylvatest® Duo	CBS-CBT technologies (Franco-Swiss)	Transmitter and receiver	Spiked insertion, US wave (22-25 kHz)	B, L,
FAKOPP™ and FAKOPP 2D™	FAKOPP™ enterprises (Hungary)	Hammer impact onto lower start transducer and multiple receivers	Spiked insertion	B, L, T
IML Hammer™	Walesch Electronic GmbH (Germany)	Force transducer hammer and receiver	Spiked insertion	B, L, T
TreeTap™	University of Canterbury (NZ)	Two receivers detecting hammer impact	Spiked insertion	T
ST300™	Fibre-gen (NZ)	Hammer impact onto lower start transducer and one receiver	Spiked insertion	T

3.4.3 Examples of TOF testing

Presented in this section are examples of recent literature citing usage of the TOF method across increasing scales.

3.4.3.1 Small Specimens

SCSs are not tested within the scope of this thesis, however due to extensive NDT of SCS in the field of timber research, it is important to mention them. Typically, SCSs are taken from increment cores or sections cut from battens and converted to 1x1x16 inch clear wood samples without knots or compression wood^(3.55). These are commonly tested to avoid the increased inhomogeneities of larger specimens, allowing for a degree of control over the variables, However this represents a fundamental flaw therefore exists in their use as NDT wood quality indicators in that they do not take account of important strength reducing defects. Ross and Pellerin^(3.10) provide a review of research using this technique from the 1950's to early 1990's, showing generally good correlation of $R = 0.87$ to 0.99 . Due to their size and thus predisposition to physical displacement, TOF US testing is primarily

favoured for SCS (although light impacts allow for flexural or longitudinal resonance testing).

Recent examples of the use of SCS for TOF NDT investigation include: Koponen *et al.*^(3.100) (velocity variation in radial or tangential velocities within annual rings as a function of distance from the pith); Bengtsson^(3.101) and Booker *et al.*^(3.72) (velocity variation with moisture content and specimen age).

3.4.3.2 Beams

As beam specimens typically allow for RF testing due to reflective ends, the majority of NDT on timber beams is conducted using in this manner. However, some recent examples of TOF of beam specimens include Wang and Ko^(3.12), who generated stress-waves in boards of Japanese cedar using nails as impact couplants between the specimen and the hammer. One test series had the nail inserted into the end of the specimen at 90° (thus running parallel to the longitudinal axis of the board) with a sensor at the opposite face along the length of the board (210 cm), and a start-stop time calculated via an oscilloscope^(3.12). The other series with the nail inserted at 90° to the specimen's top-face, thus perpendicular to the longitudinal axis, with accelerometers on the top surface a set distance (100 cm) apart^(3.12). It was found that there was a correlation ($R = 0.68$) between the two velocities. Further anecdotal accounts stated that there was "no significant effect on the propagation velocities of stress waves" due to either the differing nail angle or the distance between the nails and the sensors^(3.12). However, despite the average velocities per type of board tested being similar, the moderate correlation observed between the two velocities would suggest that the testing method does have an influence. In particular, it is this author's conclusion that the lack of correlation was less a function of the two methods but more likely the two different distances of separation used.

It was also seen that the top-surface method was inferior to the end tests when the velocity-squared was correlated to the static MoE ($R = 0.46$ and $R = 0.65$ respectively) and MoR ($R = 0.5$ and $r = 0.38$ respectively)^(3.12). This is important as

the first test series of this thesis examines the use of surface-mounted accelerometers using the TOF method. When the velocity-squared was multiplied by the density (to predict a MoE_d) these showed improved correlations ($R = 0.79$ for the end-tests and $R = 0.70$ for the top-surface tests)^(3.12).

Wang and Ko^(3.12) also noted that their results for MoE_d were 20-30% higher using TOF than results reported for a similar study, this was attributed to the previous results using transverse vibration and/or higher width-to-height ratios. Additionally it was noted, though results were not presented, that using the nail as a couplant produced significantly sharper first arrival crests on oscilloscope displays than by hitting the surface alone and that the results were more reproducible (reducing the coefficient of variation) by the nail method. It was further indicated, based on previous results that whilst the propagation velocity was affected by the force of the hammer impact (presumably through the slope of the arriving wave), support conditions (such as concrete, foam or stackings) had no effect on stress-wave velocities. It would be this thesis author's conclusion that the force does not influence the returned longitudinal velocity, but rather by increasing the force of the impact the surface accelerometers detected a faster surface wave, which is imputed-force dependant (due to frequency dependence of surface waves). As such, this would also account for the higher variability in velocities observed in the surface mounted accelerometers.

Relationships observed between TOF measurements on beams and RF tests on the same beams in selected other recent literature are presented in Table 3.4:

Table 3.4 Correlations between TOF measurements and RF measurements on beams specimens

Reference	TOF device used	velocity or dynamic MoE	Specimen	Sample no.	Age of samples (years)	Orientation	Species	RF device used	R ²
Grabianowski et al ^(3.98)	FAKOPP™	velocity	beams	43	8 to 11	longitudinal	radiata pine (green)	WoodSpec™	0.64
Grabianowski et al ^(3.98)	FAKOPP™	velocity	beams	43	8 to 11	longitudinal	radiata pine (dry)	WoodSpec™	0.62
Cai et al ^(3.15)	oscilloscope	dynamic MoE	Joists (dry)	15	?	longitudinal	southern pine	LVDT (Lucas/scaevitz)	0.72
Cai et al ^(3.15)	oscilloscope	dynamic MoE	Joists (salvaged)	15	?	longitudinal	southern pine	LVDT (Lucas/scaevitz)	0.92

3.4.3.3 Logs

Much of the testing of wood quality using acoustics in the mid to late 1990s until the early 2000s was conducted by single accelerometers and hammer impacts measuring the TOF between ends. Since the development of resonance-based tools and portable frequency analysers for determining log MoE_d, very little TOF testing has been conducted on logs. Of those MoE_d tests conducted on logs in the recent literature, correlations between TOF MoE_d values from tests on logs and corresponding measured RF MoE_d values on logs are presented in Table 3.5. Also presented are the correlations between the TOF MoE_d values taken from log specimens in recent studies, and the average MoE_d values derived from averaging the TOF MoE_d values (Table 3.6) or RF MoE_d values (Table 3.7) of the logs' subsequently cut beams.

Table 3.5 Correlations between impact TOF MoE_d values and RF MoE_d values on logs. * denotes R rather than R² used for correlation.

Reference	Device used	Specimen	Sample no.	Age of samples (years)	Orientation	Species	RF device used	R ²	notes
Dickson ^(3.97)	FAKOPP™	logs	316	30	longitudinal	radiata pine	HM200™	0.94	probes place in centre of boards
Dickson ^(3.97)	FAKOPP™	logs	316	30	longitudinal	radiata pine	HP3560A	0.9	probes place in centre of boards
Matheson ^(3.98)	FAKOPP™	logs	144	c.30	longitudinal	radiata pine	HM200™	0.91	phenotypic correlation
Grabianowski et al. ^(3.58)	FAKOPP™	logs	43	8 to 11	longitudinal	radiata pine	WoodSpec™	0.92	average both sides
Grabianowski et al. ^(3.58)	FAKOPP™	logs	43	8 to 11	longitudinal	radiata pine	WoodSpec™	0.77*	beams from logs (corewood)
Grabianowski et al. ^(3.58)	FAKOPP™	logs	43	8 to 11	longitudinal	radiata pine	WoodSpec™	0.79*	beams from logs (outerwood)
Bachle and Walker ^(3.76)	TreeTap™	logs	NA	NA	longitudinal	radiata pine	WoodSpec™	0.91	small logs, probes on end
Bachle and Walker ^(3.76)	Sylvatest®	logs	NA	NA	longitudinal	radiata pine	WoodSpec™	0.86	small logs, probes on end

Table 3.6 Correlations between impact TOF MoE_d values on logs and TOF-based average MoE_d values on the subsequent beams. * denotes R rather than R² used for correlation.

Reference	Device used	Value derived	Sample no.	Age of samples (years)	Orientation	Species	TOF device used	R ²	notes
Grabianowski et al. ^(3.58)	FAKOPP™	velocity	43	8 to 11	longitudinal	radiata pine	FAKOPP™	0.86*	corewood
Grabianowski et al. ^(3.58)	FAKOPP™	velocity	43	8 to 11	longitudinal	radiata pine	FAKOPP™	0.94*	outerwood
Jang ^(3.10)	Metriguard 239A	dynamic MoE	20	20 to 25	longitudinal	larch	Metriguard 239A	0.55	sonic
Jang ^(3.10)	Metriguard 239A	dynamic MoE	20	20 to 25	longitudinal	larch	PUNDIT™ 37 kHz	0.46	ultrasonic
Ross et al. ^(3.102)	oscilloscope	dynamic MoE	111	?	longitudinal	douglas fir	oscilloscope	0.83	

Table 3.7 Correlations between impact TOF MoEd values on logs and RF average MoEd values on the subsequent beams.

Reference	Excitation	Device used	Sample no.	Age of samples (years)	Orientation	Species	RF device used	R ²
Jang ^(3.19)	impact	Metriguard 239A	20	20 to 25	longitudinal	larch	TV via load cells	0.55
Ross <i>et al.</i> ^(3.102)	impact	oscilloscope	111	?	longitudinal	douglas fir	TV via load cells	0.9
Green and Ross ^(3.103)	impact	oscilloscope	98	n/s	longitudinal	eastern Spruce	TV via load cells	0.82
Green and Ross ^(3.103)	impact	oscilloscope	95	n/s	longitudinal	Balsam fir	TV via load cells	0.33
Green and Ross ^(3.103)	impact	oscilloscope	98	n/s	longitudinal	Southern pine	TV via load cells	0.63
Green and Ross ^(3.103)	impact	oscilloscope	100	n/s	longitudinal	douglas -fir	TV via load cells	0.5
Green and Ross ^(3.103)	impact	oscilloscope	100	n/s	longitudinal	Western Hemlock	TV via load cells	0.34

It can be seen by comparing the results from Ross *et al.* ^(3.102) that typically the TOF MoE_d values obtained in logs have a weaker correlation to average MoE_d values returned from the averaging of subsequent beam TOF MoE_d values, than to the averaged beam RF MoE_d values. It should be noted that in this instance, the log TOF MoE_d values also had less of a relation to the static MoE of beams than the log RF MoE_d values. Further studies by Ross also showed the influence of species type on the correlation between dynamic and static MoE. Ross *et al.* ^(3.104) found a correlation of R² = 0.82 between Eastern spruce log MoE_d by TOF methods and the average board MoE_d deduced by transverse vibration. However, the same parameters correlated for balsam fir logs and boards were significantly weaker however (R² = 0.33) and the correlation to individual boards showed reductions in both species (R² = 0.50 and R² = 0.17 for spruce and fir respectively).

Hanhijärvi *et al.* ^(3.20) coordinated a study of different measures of wood quality evaluation using 100 pieces spruce and 100 pines logs and the resulting boards. Results showed that the average RF MoE_d of the logs correlated reasonably to the average boards' static MoE with a correlation of R² = 0.60 ^(3.20). Despite a good correlation for spruce between TOF MoE_d and average board static MoE, correlations were always weaker for spruce than for pines (note that no TOF measurements were conducted on the pine logs due to device failure) ^(3.20). Note however that the sample size was rather small (particularly for the TOF measurements), and different tests were conducted under different conditions varying from the laboratory to the sawmill with associated issues of environmental conditions, coupling and signal noise concerning the acoustic measurements. Green *et al.* ^(3.105) having dynamically evaluated 60 small diameter logs, confirmed

that TV MoE_d was better correlated to static MoE than TOF MoE_d, with the root mean square error of the TV results being 2.5 times less than the TOF MoE_d^(3.105).

In regards to the correlations of TOF MOE_d values relation to the static values obtained from boards, Yin *et al.*^(3.106) compared sonic TOF (by FAKOPP™), US TOF (PUNDIT™) and RF (FFT analyser) dynamic MoE measurements on sixty 36 year old Chinese fir logs with the static MoE of small specimens cut from the logs. It was found that RF MoE_d in green logs compared best to the dry MoE and MoR of SCS, with correlations of $R^2 = 0.77$ and 0.76 respectively^(3.106). Sonic TOF MoE_d and US TOF MoE_d had significantly lesser correlations to static MoE ($R^2 = 0.57$ and 0.45 respectively).

3.4.3.4 Standing trees and poles

Before the use of TOF methods on standing trees, assessment of their quality was based primarily on increment cores or visual grading^(3.66). TOF velocity measurements on standing trees can be conducted either vertically through the outer stem (and relating measurements by inference to the inner stem) or horizontally across the radial section of the tree (focusing on the internal biological quality)^(3.87). The latter is often used as a basis for acoustic tomographic imaging of a tree's internal structure. This is not used in this investigation, but has been extensively used for to evaluate the effect of decay (Yamamoto *et al.*^(3.108), Axmon *et al.*^(3.109), Lawday and Hodges^(3.110), Socco *et al.*^(3.111), Sandoz^(3.87), Bucur^(3.112)) or with higher-frequency ultrasonics to evaluate the relative proportions of early and latewood through the inducement of frequency stop-bands^(3.43). A review of current understanding of radial acoustic tomography on standing trees for decay detection is presented in Wang *et al.*^(3.79), whilst Divos and Szalai^(3.113) provided baseline reference velocities for different species for tree evaluation which can be used to evaluate presence of decay.

TOF measurements vertically along the stem of a standing trunk are the only possible method of directly relating the velocity derived to the stiffness, due to the inability to use resonance as previously stated. The method has developed from

previous work on utility poles^(3.9). The FPL began using vertical TOF measurements on standing trees in 1998^(3.19). To overcome the variable external boundary conditions of tree stems, and thus produce a longitudinal wave, conical penetrating metal probes attached to transducers are inserted at a 45° angle to the stem, as is the case in the major commercial devices, to allow the excitation and reception of the wave. Divos *et al.*^(3.48) noted that 45° represents a compromise between greater coupling forces required at steeper angles and the benefit of increased amplitude of the received signal, whilst also noting that waves excited that are not travelling parallel to the grain will degenerate quickly (due to higher damping in the radial and tangential planes). However this was for tests on dry beam samples using 48 kHz transducers, which have a higher damping than transient impact frequencies. It was also noted that increasing the angle of insertion also increases the coupling area, thus requiring greater coupling forces^(3.48).

The majority of devices use low-frequency stress wave, primarily due to the ease of application and the attenuation of high-frequencies (particularly in the high moisture content outer sapwood). However, some studies involving the longitudinal ultrasonic testing of stems have been conducted, for example Bucur^(3.112), though these are still in the development process and no subsequent work has been published.

In one of the earliest examples of the recent interest in this method, Wang *et al.*^(3.19) found a correlation of $R^2 = 0.83$ between TOF velocity measured on standing trees and the TOF velocity of small batten samples cut from the trees. The correlations were reduced however (to $R^2 = 0.75$) when density estimates were incorporated to both measurements to produce MoE_d estimates^(3.19). This further reduced when the MoE_d estimates of the standing trees were correlated against static MoE tests on the small clear samples ($R^2 = 0.66$) and static MoR tests ($R^2 = 0.56$), despite the dynamic MoE of small clears having a good relationship to the static MoE values ($R^2 = 0.91$)^(3.19).

Presented below are tables showing the correlation between impact TOF velocity (or TOF-based MoE_d values) on trees and: (Table 3.8) ultrasonic TOF measurements on trees: (Table 3.9) TOF measurements on logs and subsequent beams: (Table 3.10) resonance-based MoE_d measurements on logs: (Table 3.11) static MoE measurements on the subsequent boards: and (Table 3.12) static MoE measurements of SCS from increment cores, billets or boards taken from the trees:

Table 3.8 Correlations between impact TOF velocity values and ultrasonic TOF velocity values measured on standing trees.

Ref.	Method	Excitation	Device used	Specimen	Sample no.	Age of samples (years)	Orientation	Species	Ultrasonic device used	R ²
Chuang and Wang (3.117)	TOF	hammer	oscilloscope	standing trees	c.1000	47	longitudinal	Japanese cedar	Sylvatest®	0.6
Chuang and Wang (3.117)	TOF	hammer	oscilloscope	standing trees	c.1000	47	radial	Japanese cedar	Sylvatest®	0.51

Table 3.9 Correlations between impact TOF velocity values on standing trees and TOF velocity values measured on the subsequent logs and beams.

Ref.	Method	Ext.	Device used	Specimen	Sample no.	Age of sample (years)	Ort.	Species	Device used on logs	R ²
Dickson (3.97)	TOF	impact	FAKOPP™	standing trees	316	30	diagonal	radiata pine	FAKOPP™	0.62
Matheson (3.98)	TOF	impact	FAKOPP™	standing trees	144	c.30	diagonal	radiata pine	FAKOPP™	0.54
Dickson (3.13)	TOF	impact	FAKOPP™	standing trees	35	9	diagonal	eucalyptus dunnii	FAKOPP™	0.62
Dickson (3.13)	TOF	impact	FAKOPP™	standing trees	35	2	diagonal	eucalyptus dunnii	FAKOPP™	0.41
Wang et al. (3.19)	TOF	impact	oscilloscope	standing trees	168	38 to 70	longitudinal	Sitka spruce and western Hemlock	oscilloscope	0.83
Wang et al. (3.19)	TOF	impact	oscilloscope	standing trees	168	38 to 70	longitudinal	Sitka spruce and western Hemlock	oscilloscope	0.75

Table 3.10 Correlations between impact TOF dynamic MoE values on standing trees and the resonance-based dynamic MoE values measured on the subsequent logs.

Ref.	Method	Excitation	Device used	velocity (three sides) derived	50 Sample no.	Age of samples (years)	Orientation	radiata pine Species	HM200™ device used	R ²
Carter et al (3.35) Reference	TOF	impact	ST300™	velocity (three sides) derived	50	n/s	longitudinal	radiata pine	HM200™	0.67
Dickson (3.97)	TOF	impact	FAKOPP™	dynamic MoE	316	30	diagonal	radiata pine	HM200™	0.66
Dickson (3.97)	TOF	impact	FAKOPP™	dynamic MoE	316	30	diagonal	radiata pine	HP 3560A	0.64
Matheson (3.98)	TOF	impact	FAKOPP™	dynamic MoE	144	c.30	diagonal	radiata pine	HM200™	0.61
Kumar (3.51)	TOF	impact	IML Hammer™	dynamic MoE	72	13-14	longitudinal and diagonal	radiata pine	HM200™	0.6
Kumar (3.116)	TOF	impact	FAKOPP™	dynamic MoE	72	12	longitudinal	radiata pine	HM200™	-0.39
Carter et al (3.35)	TOF	impact	ST300™	velocity (one side)	50	n/s	longitudinal	radiata pine	HM200™	0.45-0.50
Carter et al (3.35)	TOF	impact	ST300™	velocity (2 sides)	50	n/s	longitudinal	radiata pine	HM200™	0.61

Table 3.11 correlations between impact TOF velocity values on standing trees and the average static MoE of boards cut from the same logs.

Reference	method	excitation	Device used	specimen	sample no.	age of samples (years)	orientation	speices	R ²
Dickson (3.97)	TOF	impact	FAKOPP™	standing trees	316	c.30	diagonal	radiata pine	0.23
Matheson (3.98)	TOF	impact	FAKOPP™	standing trees	144	c.30	diagonal	radiata pine	0.01-0.33
Dickson (3.13)	TOF	impact	FAKOPP™	standing trees	35	9	diagonal	eucalyptus dunnii	0.4
Dickson (3.13)	TOF	impact	FAKOPP™	standing trees	35	25	diagonal	eucalyptus dunnii	0.43

Table 3.12 Correlations between impact TOF velocity values on standing trees and the average static MoE of SCS cut from the same logs.

Reference	Method	Excitation	Device used	TOF parameter	Sample no.	Age of samples (years)	Orientation	Species	R ²
Knowles et al (3.99)	TOF	impact	IML Hammer™	velocity	180	18	diagonal	douglas fir	0.37
Kumar (3.118)	TOF	impact	FAKOPP™	velocity	72	12	longitudinal	radiata pine	-0.69
Kumar (3.118)	TOF	impact	FAKOPP™	velocity	72	12	longitudinal	radiata pine	(MoR) -0.68
Dickson (3.13)	TOF	impact	FAKOPP™	velocity	35	9	diagonal	eucalyptus dunnii	0.64
Dickson (3.13)	TOF	impact	FAKOPP™	velocity	35	25	diagonal	eucalyptus dunnii	0.07
Dickson (3.13)	TOF	impact	FAKOPP™	velocity	35	9	diagonal	eucalyptus dunnii	(MoR) 0.61
Dickson (3.13)	TOF	impact	FAKOPP™	velocity	35	25	diagonal	eucalyptus dunnii	(MoR) 0.09
Lindstrom et al. (3.82)	TOF	Impact	FAKOPP™	velocity	7	4	longitudinal	radiata pine	0.96
Wang et al. (3.19)	TOF	impact	oscilloscope	dynamic MoE	168	38 to 70	longitudinal	Sitka spruce and western Hemlock	0.66
Wang et al. (3.19)	TOF	impact	oscilloscope	dynamic MoE	168	38 to 70	longitudinal	Sitka spruce and western Hemlock	(MoR) 0.63

Typical assumptions made in the use of TOF devices to segregate trees and green logs included: assuming constant density (as based on Hayes's assertion of the domination of density by water^(3.54)); minimal seasonal temperature effects; and relatively no change in velocity above FSP^(3.41, 3.55). Hu *et al.*^(3.119) examined the factors affecting the reliability of TOF-based standing tree methods and found the main factors involved were the repeatability of the signals and the accuracy of the density measurements. It was suggested that correlations could be improved through the standardisation of the measurement setup to create a repeatable impact force and sensor attachment (the variation in which was deemed to be the primary cause of variation in the TOF velocities tests on individual trees). Additionally, a more accurate measure of whole tree density was stipulated as a

requirement. However, unlike other researchers as outlined below, he found poor correlations between standing tree TOF MoE_d values and RF MOE_d values on the corresponding logs.

Despite Carter *et al.*^(3.55) showed a strong correlation ($R^2 = 0.92$) between ST300™ derived velocities on standing trees and resonance-based velocities on logs from HM200™ tests, it was noted in a subsequent paper, Carter *et al.*^(3.35), that the correlations between standing tree ST300™ TOF velocities and HM200™ resonance velocities decreases with age and diameter in a tree, with young trees showing an $R^2 = 0.90$ correlation for 10-year old trees, which explains the previous good correlation due to the increased uniformity of the cross-section. Results from Dickson *et al.*^(3.13) also confirmed this decrease in linear correlation with age. Thus this may explain the poor correlations observed in Hu *et al.*^(3.119).

Additionally, it was shown that correlations could be improved by testing on two sides of the tree plus another random test ($R^2 = 0.67$) rather than one ($R^2 = 0.44-0.50$)^(3.35). Bascunan *et al.*^(3.56), using TreeTap™ velocities to derive stiffnesses, found that outerwood stiffness decreased away from stand edges, which validated predictions based on the coincident increase in tree height and the reduction of taper, though a predicted reduction in stiffness with increased spacing did not occur. It was also found that averaged results were necessary from two sides, due to increased variability in stiffness with age and lean of trees^(3.56). This need for more than one measurement was confirmed by Grabianowski *et al.*^(3.58), whose testing on logs evaluated the FAKOPP™ 2D longitudinally as a SWT (which it has now been modified to be) and found an increasing difference between sides with increasing age of specimen. They also found no influence on velocity from specimen diameter, vertical height of specimen from the tree, or stocking patterns^(3.58).

Grabianowski *et al.*^(3.58) found excellent correlations between the average TOF MoE_d for each log and the RF MoE_d results on each log from Woodspec™. Lasserre *et al.*^(3.59) also noted a strong correlation between TOF-measured MoE (by TreeTap™) and the average of the whole log MoE via HM200™

measurements ($R^2 = 0.94$). However, unlike Grabianowski *et al.*^(3.58), they noted that stand spacing had a significantly positive influence on TOF derived MOE and that tree diameter exhibited a negative correlation ($R^2 = 0.50$) to TOF MOE^(3.59). This would be expected due to the reduction of outer wood stiffness with increased growth rate and increase in stiffness as discussed earlier. It was found that the dynamic modulus had significant correlations to MFA, cell wall thickness and fibre length, as well as ring width^(3.59).

Chauhan and Walker^(3.52) compared velocities measured by the FAKOPP™ 2D in trees and HM200™ in logs, observing that the velocities using the TOF device were generally higher than the resonance-based HM200™, with the difference tending to increase with age from 8 years (8.74%) through 16 years (8.95%) to 25 years (17.55%). This was attributed to the older stands (widest diameter) having a larger difference between stiffnesses. It was also noted that a “mass loading effect” of gross bark volume in radiata pine can be 15-17% of the total under-bark volume, and, since bark has little stiffness, a high proportion of bark will pull down the resonance based stiffness whilst not affecting the TOF velocity. This was also noted by Grabianowski *et al.*^(3.58) with a modest ($R^2 = 0.86$) correlation between RF (via WoodSpec™) and TOF on outerwood. Since radial variation in stiffness follows (at least in Radiata pine) a stiffness gradient, it has been advocated by Walker^(3.120), that using TOF MoE_d on standing trees not only allows for the early segregation of stems and prediction of future stiffnesses, but also for the selection of superior genetic clones, which can only be done on using live trees.

3.5 Resonance based methods

Resonance-based methods are derived from the creation of standing wave patterns produced between two parallel faces of a specimen. They are divided into forced (constant driven excitation) or free (transient source) vibration methods^(3.3, 3.9). The measurement of the subsequent vibrational in torsion, flexural or longitudinal modes can further subdivide the procedures^(3.2).

Following excitation, a series of compressions and rarefactions are stimulated as a waveform with the specimen (as discussed previously). Upon reaching a reflective surface, with a face parallel to the face of excitation, reflections of waves of the same frequency create a resonance. With a constant excitation source, this is the result of constructive interference in wave propagation of two reflected waves (of fixed frequency and wavelength) in the same plane that are in phase with each other^(3.4, 3.5). This will progressively increase the amplitude (energy content) of the wave until the dynamic equilibrium of energy input equalling that lost to damping (internal friction)^(3.5). If the source for this wave is transient, e.g. a hammer blow, the vibration will naturally die away due to internal friction, however the standing wave at resonance will take longer to decline due to this higher energy content^(3.4). Eventually, all the energy will be lost to intrinsic or extrinsic damping, which is directly proportional to the frequency^(3.5).

Provided certain assumptions are met, the resonant frequency will reflect the characteristic nature of the whole of the material specimen. These assumptions will be discussed as we discuss the review of investigations techniques. This investigation focuses on the characteristics of transient frequency responses. Transient excitation can also be a swept sine wave, as demonstrated in the operation of the 'WoodSpec™' resonance tester^(3.32). However both swept sine waves and transient impacts have a tendency towards mode conversion to flexural waves, with the resulting wave packet being a combination of these wave types.

In standing trees resonance is only possible radially or tangentially (or through natural sway flexure) across the tree (between two exactly opposite points on the stem rather than across the stem as a whole) as there is no reflective surface in the longitudinal axis. In logs, sawn timber beams or small clear specimens, resonance is possible in all three planes of symmetry, and occurs as dynamic longitudinal, dynamic torsional or dynamic flexural (transverse vibration) resonance^(3.5). These correspond to static tension, static torsion and dynamic bending respectively, allowing for the direct calculation of young's moduli, shear moduli and Poisson's ratios^(3.3). Additional resonant measurements can be taken on circular cross sectioned rods, rectangular cross sectioned beams and plates,

with minor adjustments to the theories presented here. For a more detailed review see Craik^(3.5) or Bucur^(3.3).

3.5.1 Transverse vibration testing

Initially, the majority of wood testing was done by flexural resonance testing through transverse vibration, particularly on SCS. Whilst this is not used in this thesis, other than in Chapter 8 for flexural resonance of standing trees, it shall briefly be discussed due to its importance to wood research. Additionally a review of frequency and modes shall be discussed in the more applicable longitudinal resonance section. Transverse vibration measurements for beam and small specimens involves impacting vertically down onto the specimen at the centre of the maximum amplitude of the frequency under investigation, which is typically the fundamental and thus in the centre of the beam^(3.47). This sets the beam into flexural vibration which is measured by an accelerometer or microphone, which is placed at the side of the specimen towards the nodal points of the second harmonic, to ensure that it is relatively weak in comparison to the fundamental so as to aid automated detection.

However, when a beam is excited into vibration either flexurally or longitudinally, these will not be the only modes of vibration as all other modes of vibration (flexural and other surface waves as well as torsional in this plane as well as in the other planes and across other faces)^(3.122). Thus the flexural mode has a more varied frequency spectrum (as opposed to the sharper, clearer resonances of the longitudinal spectrum) care must be taken when interpreting signals. However, it was noted by Wang *et al.*^(3.7) that transverse vibration measurements, tested on small clear specimens, provided a better correlation to MoE ($R^2 = 0.91$) than longitudinal resonance or stress-wave techniques, explaining this as transverse vibration's decreased sensitivity to geometrical imperfections^(3.19). The formula for calculation of flexural MoE_d can be found in Ross and Pellerin^(3.10) along a review of pre-1990 research validating the use of transverse vibration testing. Murphy^(1.123) provides a synopsis of factors which can influence the measurement procedure.

Jayne^(3.9) was one of first studies of wood using transverse vibration (flexural MoE_d) for wood strength evaluation. The measurements involved excitation by a speaker source. He was successful in demonstrating a relationship between energy storage and dissipation properties using 46 clear and straight grained 400 mm specimens of Sitka spruce, as shown by a correlation between dynamic and static MoE (R = 0.95). It was also observed that the MoE_d was consistently higher than the static value. Haines *et al.*^(3.124) and Haines and Leban^(3.150) both found that mean flexural MoE_d (by transverse vibration) on SCS correlated near-perfectly to mean static MoE, with a variation in results of less than 1%. This near perfect correlation at the SCS scale was confirmed by Brancheriau and Balleries^(3.28), with a lower correlation in full scale timber samples (R² = 0.83). Haines and Leban^(3.125) found longitudinal RF tests on SCS, whilst being well correlated to static MoE and dynamic MoE_d (by flexural and longitudinal resonance testing), consistently overestimated the flexural MoE_d by 4.7% (Haines *et al.*^(3.124) saw similar results of a 6.2% overestimation). Ultrasonic TOF MoE_d tests (though the frequency was not mentioned) were found to overestimate the flexural MoE_d by 13.6%^(3.150). Haines *et al.*^(3.124) saw a 16.7% overestimation. They concluded that the variations were the result of frequency-dependant viscoelastic effects (with flexural resonances being lower in frequency than longitudinal resonances and both being lower than US frequencies).

3.5.2 Longitudinal Resonance testing

Due to the limitations of TV methods (see Murphy^(1.123)), including the influence of shape and supporting positions, particularly on larger beam and log specimens, it has increasingly been recognised that longitudinal vibration (LV) testing offers more potential in efficient laboratory and field experiments^(3.2).

The advantage of LV testing is that it averages the radial properties of the specimen (through the law of mixtures) and provides a single repeatable velocity at each harmonic under investigation (due to the formation of plane waves, being less influenced by local inhomogeneities and spatial variations), thus improving accuracy over TOF measurements due to less variability in the data^(3.54, 3.76).

Whether the specimen as a whole is averaged is debated further in Chapter 6. The conduction of resonance testing is also less complicated and more efficient than most TOF measurements in requiring only one operator and one accelerometer, with no force transducer hammer. Additionally, the temporal resolution constraints which affect TOF SWT systems are spread over a longer interval in LV testing, thus increasing the accuracy of the measurement^(3.54). This also means that smaller samples can be tested than would typically be possible using conventional SWT due to a less relevant temporal resolution. A further advantage is it allows for the subsequent measurement of inherent damping of a signal by the wood structure (assuming negligible coupling via extrinsic factors) through the methods described in the next section, where as TOF damping studies rely solely on the input/output energy loss ratio.

LV and TV MoE_d testing are the two most commonly used methods in timber NDT, with TV MoE_d seemingly more accurate in its correlation to static MoE. TV MoE_d in particular seems to be favoured in the NDT of SCS worldwide (most likely due to less physical displacement of the specimen as can occur with longitudinal impact) and larger specimens in North America, whilst LV MoE_d seems favoured in Australasia and northern Europe for larger specimens including beams and logs. TV MoE_d also has the benefit of having a typically lower fundamental frequency and thus lower harmonic frequencies which, due to increased damping at higher frequencies, potentially allows for more stiffness calculations. The majority of RF testing (for the derivation of a dynamic stiffness) is conducted through the fundamental or 1st harmonic frequency (as it represents the greatest proportion of the wave energy)^(3.54). Bucur^(3.3) states that typically stiffness values from TV MoE_d will be a few percentage points (2%) lower than those calculated by LV MoE_d. However, flexural resonance is more sensitive than longitudinal resonance to small changes in grain angle and the deviation between flexural results increased dramatically as the induced grain angle tended towards 60° and upwards^(3.3).

3.5.2.1 Calculation of dynamic MoE by longitudinal resonance

The fundamental (1st harmonic mode) frequency of the longitudinal resonance corresponds to wavelength which matches twice the specimen dimensions in a given axial plane. In addition to the fundamental resonances, harmonics of the fundamental are created which correspond to other wavelengths, which are exact fractions of the total dimension, thus the wavelength corresponding to the full length of the dimension will be the 2nd mode. It then follows that the n^{th} mode will have a frequency and wave number^(3.5):

$$f_n = \left(\frac{V}{2}\right) \cdot \left(\frac{n}{L}\right) \quad \text{Eqn. 3.8}$$

Where:

f_n = frequency of the n^{th} mode

V = velocity (ms^{-1})

n = (wave or mode) number

L = length of the dimension

A more detailed explanation of the methods of resonance testing is discussed in Chapter 4. Presented in Figure 3.2 is an illustration of the pattern of longitudinal modal resonances:

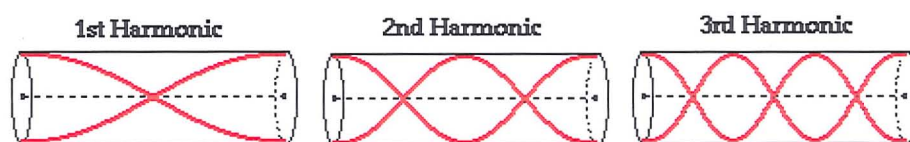


Figure 3.2 Diagrammatic representation(3.127) of longitudinal resonance modes for free-free vibration showing the fundamental mode (1st harmonic), 2nd and 3rd harmonics. Note the positions of zero vibrational amplitude (nodal points) and maximum amplitude (anti-nodal points) created by constructive interference due to reflectance of the waves, and how the number of these positions increases with increasing harmonic number (and thus subsequent halving of the wavelength).

3.5.2.2 Factors affecting longitudinal resonance measurements

Disadvantages of the technique are mostly self explanatory, for example the shape of the specimen has specific requirements for parallelism and can affect the method of calculation of stiffness. The demands of shape may place constraints on the type of resonance available (for example a long rod sample in the axial plane allows for only one young's modulus and one shear modulus calculation, out of the nine required for full elastic characterisation) and also dictates the support conditions, which must meet criteria for coupling and thus extrinsic damping to be neglected. Additionally, the calculation of the moment of inertia required for flexural resonance is difficult for complicated specimen geometries, thus providing another reason for the use of longitudinal testing.

Certain factors affecting the use of the one-dimensional equation should be discussed now however as by not accounting for these factors, inaccurate estimations can be made. In particular, the geometry of the specimen can affect the accuracy of the dynamic MoE calculation. Deviation from the conditions for the one-dimensional equation previously presented, i.e. not long and laterally infinite, result in velocity dispersion between the phase and group velocities. It should be sufficient at this point to note that with small-length specimens (i.e. a radius to wavelength (r/λ) ratio greater than 0.3), a Rayleigh correction to the one-dimensional theory is required^(3.128). Above a radius/wavelength ratio of 0.3, the wavelength under investigation increasingly approaches the lateral dimensions of the specimen and as such there is increased velocity dispersion between the group and phase velocities. Specimens with greater ratios find that the harmonics will cease to be exact multiples of the fundamental (due to the diameter effects on the fundamental rather than the harmonics), and as such are termed overtones^(3.32, 3.38).

The use of longitudinal resonance was spurred from the advances of the flexural resonance method via transverse vibration^(3.2). It should be noted that until the development of advanced computer processors able to conduct instantaneous FFT measurements, the process of resonance frequency evaluation was done through

cycling through individual frequencies. It is widely accepted^(3.9, 3.3) that longitudinal resonance-based MoE_d correlates well to static MoE, depending on the scale and species under investigation (see table 3.1). It is also noted in the literature that MoE_d by this RF method tends to overestimate the static MoE by c.10%^(3.3, 3.7, 3.17, 3.22, 3.38, 3.75, 3.124-3.125)

Examples of the recent papers regarding the combined linear correlations of both TOF and RF MoE_d values (taken on various scales) in multi-parameter combination with a further characteristic, to static measures are set out in Table 3.14 below:

Table 3.14 Correlation between static MoE and MoR and dynamic MoE (TOF and RF based) combined with measurements of other wood characteristics.

Ref.	Method	Ext.	Device used	Scale	No.	Age (yrs)	Species	MoE _d incorporated with other parameter	Measured by	R ² correlation to static MoE or MoR
Knowles <i>et al.</i> ^(3.90)	TOF	impact	IML Hammer™	standing trees	180	18	douglas fir	density (cores)	grav.	0.42
Kumar ^(3.51)	TOF	impact	IML Hammer™	standing trees	72	13-14	radiata pine	density (cores)	grav.	0.38
Kumar ^(3.118)	TOF	impact	FAKOPP™	standing trees	72	12	radiata pine	density (SCS)	grav.	-0.26
Wang <i>et al.</i> ^(3.12)	TOF	US	PUNDIT™	SCS	n/a	n/a	Tawania	density (SCS)	grav.	0.27
Wang <i>et al.</i> ^(3.12)	TOF	US	PUNDIT™	SCS	n/a	n/a	Tawania	MC (SCS)	oven-dry method	0.76
Kumar ^(3.118)	RF	impact	HM200™	logs	72	12	radiata pine	density (SCS)	grav.	0.48
Kumar ^(3.118)	RF	impact	HM200™	logs	72	12	radiata pine	density (SCS)	grav.	0.84
Hanhijärvi <i>et al.</i> ^(3.20)	RF	impact	Rion SA77 GP analyser	logs	100	n/a	Scotch Pine	knot content	X-ray	0.7
Hanhijärvi <i>et al.</i> ^(3.20)	RF	impact	Rion SA77 GP analyser	logs	100	n/a	Scotch Pine	knot content	X-ray	0.92
Hanhijärvi <i>et al.</i> ^(3.20)	RF	impact	Rion SA77 GP analyser	logs	100	n/a	Scotch Pine	knot content	X-ray NDT	0.78 (MoR)
Hanhijärvi <i>et al.</i> ^(3.20)	RF	impact	Rion SA77 GP analyser	logs	100	n/a	Norway spruce	knot content	X-ray NDT	0.48
Hanhijärvi <i>et al.</i> ^(3.20)	RF	impact	Rion SA77 GP analyser	logs	100	n/a	Norway spruce	knot content	X-ray NDT	0.9
Ref.	Method	Ext.	Device used	Scale	No.	Age (yrs)	Species	MoE _d incorporated with other parameter	Measured by	R ² correlation to static MoE or MoR
Hanhijärvi <i>et al.</i> ^(3.20)	RF	impact	Rion SA77 GP analyser	logs	100	n/a	Norway spruce	knot content	X-ray NDT	0.62 (MoR)
Hanhijärvi <i>et al.</i> ^(3.20)	RF	impact	Rion SA77 GP analyser	logs	100	n/a	Scotch Pine	ring width	image analysis	0.64
Hanhijärvi <i>et al.</i> ^(3.20)	RF	impact	Rion SA77 GP analyser	boards	100	n/a	Scotch Pine	KAR	optical NDT	0.79

Hanhijärvi <i>et al.</i> ^(3.20)	RF	impact	Rion SA77 GP analyser	boards	100	n/a	Scotch Pine	KAR	optical NDT	0.92
Hanhijärvi <i>et al.</i> ^(3.20)	RF	impact	Rion SA77 GP analyser	boards	100	n/a	Scotch Pine	KAR	optical NDT	0.77 (MoR)
Hanhijärvi <i>et al.</i> ^(3.20)	RF	impact	Rion SA77 GP analyser	boards	100	n/a	Norway spruce	KAR	optical NDT	0.71
Hanhijärvi <i>et al.</i> ^(3.20)	RF	impact	Rion SA77 GP analyser	boards	100	n/a	Norway spruce	KAR	optical NDT	0.9
Hanhijärvi <i>et al.</i> ^(3.20)	RF	impact	Rion SA77 GP analyser	boards	100	n/a	Norway spruce	KAR	optical NDT	0.65

The commercial use of both longitudinal TOF and RF NDT to identify logs of different stiffnesses is not based on the specific identification of exact characteristics (for example the prediction of individual board stiffnesses, or strength by knot identification). Rather, acoustics is used to segregate the lowest quality (stiffness) wood through the average stiffness of a log, because 90% of all problems in the production of good timber are attributed to 10% of the logs (*i.e.* the ones with the lowest stiffness)^(3.62). This is not just due to poor average stiffness of the logs (which may have passable stiffnesses in the outerwood, but the majority of beams cut will take in some form of inner juvenile wood) but also due to the high correlation between longitudinal shrinkage (and other drying-induced defects) and average log stiffness below 7 GPa (in *Radiata* pine, see Huang *et al.*^(3.62)). By segregating out the poorest logs, the higher stiffness logs can be processed more efficiently at the sawmill (in addition to the forester demanding a higher price for the timber).

The reasonably good correlations seen in small and beam samples LV MoE_d and static MoE, but more importantly the low rejection rate of higher class segregated logs, lead to the development of commercial resonance-based stiffness evaluation devices, seen in Table 3.15.

Additionally, timber producers such as Weyerhaeuser Ltd. have filed several United States patent applications relating to acoustic testing of timber, but as devices are kept in-house then their operation and accuracy is unknown^(3.120, 3.138).

Table 3.15 The main commercial resonance-based dynamic modulus devices and their scale of application in timber research (SS = small samples, B = beams, SL = small logs, LL = large logs).

Device	Manufacturer	Type of vibration	Excitation	Receiver	Scale of use	Used in
Grademaster	Dimter	?	?	?	?	?
WoodSpec™	Industrial Research Ltd. (NZ)	Longitudinal	Hammer or speaker	Accelerometer or microphone	SS, B, SL	Lab
Metriguard E-computer	Metriguard (USA)	Transverse	hammer			Sawmill
Dynagrade	Dynalyse (AB, Sweden)	longitudinal	hammer	microphone	B	Sawmill
Bing 2000	CIRAD (France)	Longitudinal or transverse	hammer	Microphone or accelerometer	SS, B, SL	Lab, Sawmill
A-Grader™	Falcon Engineering/EnsisJV	longitudinal	impactor	microphone	B	Sawmill
HM200™	Fibre-gen (NZ)	Longitudinal	hammer	accelerometer	B, L	Lab, sawmill, forest
SWAT (defunct)	Fletcher Challenge (NZ)	?	?	?	B, L	forest
Portable Lumber Grader	FAKOPP™ enterprises (Hungary)	Longitudinal	hammer	accelerometer	B, L	Lab, sawmill, forest
Grindosonic™	Lemmens (Belgium)	Longitudinal or transverse	hammer	Accelerometer or microphone	SS, B	Lab
Buzz-o-sonic	Buzzmac Int. (USA)	Longitudinal or transverse	hammer	microphone	SS, B	Lab
ViScan	Microtec (Germany)	longitudinal	impactor	Laser vibrometer	B	Lab, sawmill
HP3560a	CSIRO (Australia)	?	?	?	?	Lab

3.6 Acousto-ultrasonic methods

Acousto-ultrasonic (AU) methods are derived from AE methods of non-destructive characterisation. AU methods are not used in this investigation but some overlap between recent research using AU and low-frequency experiments presented in later chapters does occur. Reviews of the subject and in particular its application to wood products can be found in Bucur^(3.3, 3.141) and Kawamoto and Williams^(3.142), or as recent case studies of individual papers relating to its use in wood^(3.143-3.145). A review of acousto-ultrasonic literature was conducted during this thesis however due to its use in NDT defect detection. Whilst the acousto-ultrasonic techniques have been useful in metal and polymer beams for detecting defects, Bucur^(3.3) stated that acousto-ultrasonics could not be used for defect location in wood.

In contrast, Kawamoto and Williams^(3.142) showed that it can be used both as an estimated measure of the overall strength and bonding characteristics of a wooden beam and provide defect location if the material is systematically scanned tangentially across its length^(3.142). They also evaluated any differences due to

density and Microfibril angle, and found that lower amplitudes correspond to higher MFA and lower densities, which therefore will correspond to lower stiffness as well as indicating an area with propensity to drying-induced internal checking or splitting^(3.142). Indeed they proposed that wave propagation was dominated by the latewood bands due to the lower microfibril angle in these layers^(3.142). They also noted however that variation in amplitude was induced by grain or growth ring angle, moisture content and natural defects^(3.142).

Typically procedures involve using ultrasonic stress-waves (typically in the range of 20 kHz to 300 kHz with a narrow bandwidth, which allows for an increased and controlled energy content and initial waveform) either through the specimen or to a reflecting surface, the received signal may be analysed by the same acoustic parameters used in AE analysis^(3.1, 3.3, 3.142). Upon reception after propagation, the received waveform information is related to temporal field characteristics such as velocity and relative energy loss (from a known transmission level) through the observation of maximum peak signal energy at reception (via the integrated signal energy over a defined time base) and/or the attenuation of the reflected signals within the structure (via logarithmic decrement or Q-factor). A higher attenuation of the wave's energy will generally indicate a decrease in strength in a localised area^(3.142). Its sensitivity to the microstructure of wood through the high-frequencies used is the principle advantage of the technique, but also limits its application to field measurements on standing trees except when used radially to indicate decay, as shown by Sandoz^(3.87).

A problem however to its application to standing trees is that it requires calibration, before each test series, on a control specimen due to seasonal variations in propagation characteristics^(3.87). Additionally, comparisons between researchers use of this technique is limited due to the influence of experimental conditions, in addition to the inherent variability of the species and individual specimens used means that the repeatability of the technique is poor^(3.3).

Of relevance to the discussion of experiments in Chapter 5, investigations by Sandoz *et al.*^(3.33, 3.68, and 3.91) looked at using the AU technique longitudinally in

timber beams (using Sylvatest[®], and later Sylvatest[®] Duo) to observe the effect of artificially induced defects on TOF velocity and energy loss. Results showed relatively low correlations of velocity to static MoE ($R^2 = 0.58$) and MoR ($R^2 = 0.25$)^(3.33). Sandoz had previously shown good correlations of TOF velocity to MoR ($R^2 = 0.79$) in Sandoz *et al.*^(3.68), but this was on SCS with no significant knots or grain deviation. Although the weak correlation to MoR would be expected, the relatively low correlation to static MoE, for small samples, indicates that there may have been errors in the measurement setup, possibly due to the use of conical transducers penetrating longitudinally into the wood. Additionally, the start timer seems to measure from the peak of the start impact, but the stop timer measures from a percentage of the first arrival peak, rather than corresponding levels^(3.91). It was also noted that whilst progressive increases in the depth of the artificial discontinuity had little effect on velocity (a 50% depth of saw-cut saw a 3.3% reduction in velocity, 75% cut saw a 5.65% reduction in velocity), the affect on RMS energy content was more dramatic (25% and 35.4% reduction for 50% and 75% depth cuts respectively)^(3.33).

The effect of artificial sawn notches (progressively increasing in depth) in the wood on velocity and amplitude was also evaluated by Divos *et al.*^(3.48), similar in manner to the experiment of Sandoz^(3.33). It was found that on dry, clear Norway spruce specimens that ultrasonic signal amplitude decreases proportionally with the remaining cross-section^(3.48). Conversely, TOF velocity does not decrease significantly (with no decrease in shallow cuts) until a majority of the cut has occurred. It was also established that slope of grain deviations could significantly influence the amplitude result. Divos *et al.*^(3.48) used the maximum amplitude of the first received signal (thought to be primarily composed of the fundamental wave) and established that it was far more sensitive to defects in the samples than amplitude ratio or velocity^(3.48). However, using the decrease of received signal amplitude from a known initial amplitude was limited to small clear beams (with a cross section not larger than 100 mm²) due to the varying influence of defects altering the received amplitude^(3.48). A similar impact on transmitted US signal energy content, but not US TOF velocity, in response to defects was noted by Kabir and Araman^(3.84) and Kabir *et al.*^(3.84). It should be noted however that bark

pockets within the specimens were found to have the same effect as knots on the energy loss, possibly due to the weak internal bonding surrounding them^(3.85).

Sandoz *et al.*^(3.87) and Divos^(3.48) are the only researchers known to have attempted acousto-ultrasonic measurements on standing trees; however this was in the radial orientation and is essentially related to decay detection as an improved form of acoustic tomography. To the author's knowledge no papers have been published relating to energy loss vertically within a tree specimen, though researchers at the University of Canterbury are working along these lines of investigation.

3.6.1 Damping

Chapters 5 and 6 devote time to the measurement and analysis of inherent damping (energy loss) values and its variations within timber specimens. Sandoz and Benoit^(3.33) noted that the Sylvatest[®] Duo improved on the TOF SWT Sylvatest[®] by incorporating energy level measurements, and that whilst the MoE dictates the speed of longitudinal wave propagation, received energy content is a reflection of the damping of the wave energy, which is directly dependant on local singularities. This damping in wood is both intrinsic and extrinsic^(3.5). Extrinsic damping concerns all the energy lost in a system (or structure) that is not intrinsic, this essentially covers radiated energy into the air as sound and heat, or energy lost through coupling to other structures such as the beam supports^(3.5). In freely supported situations, the loss to the supports should be negligible. Internal dissipation of vibrational energy in a wood specimen is, as stated by Lindsay^(3.40), the irreversible attenuation in which wave energy is transformed into heat, that is, random energy of the constituent atoms and molecules of the solid^(3.40). As such, intrinsic damping is a measure of the internal friction or resistance of the material to this change. It should be noted at this point that it is impossible to separate intrinsic and extrinsic damping outside statistical energy analysis (see Craik^(3.5)). Thus to attempt to physically measure internal damping, the extrinsic energy losses must be as small as possible.

3.6.1.1 Factors controlling damping

At the fundamental level, the internal friction in wood is controlled by the bonding properties between the cells^(3.63). Indeed, Ross and Pellerin^(3.10) cite their own experiments in Ross (1984) and Ross and Pellerin (1988) as showing that wave attenuation is sensitive to bonding characteristics, thus providing an ability to predict the tensile and flexural behaviour in wood composites^(3.10). However, the absorption of this wave energy is itself dependent on not only this anatomical structure but also on the frequency of wave propagation, as these controls the wavelengths in the structure. Due to the principles of reflection and refraction, the smaller wavelengths (and thus higher frequencies) are subject to increasing scatter from any inhomogeneities in the wood structure, not just macro-defects such as knots but the annual ring variance and cellular juxtaposition.

Particularly concerning ultrasonic frequencies, the geometry and dimensions of the specimen controls the level of beams spread possible, thus influencing the macro-scale level of the stochastic scattering regime (wave diffraction, reflection, and refraction) and hence energy conservation and loss for a given wavelength^(3.3).

It has been suggested that if the structure of wood is modelled (ultrasonically) as an array of finite-length, elongated hollow tubes in a amorphous lignin matrix (allowing for faster, easier propagation along these tubes as opposed to radially across them), then longitudinally the majority of dissipation of acoustical energy will take place at the ends of these tubes, due to dispersion when moving from one tube to the next across the lignin between the cells^(3.3). There is little damping within the 'tubes' due to the low damping of the crystalline cellulose microfibrils^(3.3). As such damping may potentially reflect the average MFA of a specimen, due to the negative correlation observed (see Chapter 2) between MFA and tracheid length, with increased damping occurring with higher MFAs^(3.120). Therefore damping could potentially be related to the tracheid length, MFA, and lignin content of a specimen^(3.120). Feeney *et al.*^(3.43) noted that species with a higher amount of "scatterers" (*i.e.* the level of variation in anatomical elements of different densities) were subject to increasing attenuation^(3.42). This would suggest that species with a greater degree of density variation in the annual ring structure are subject to

increasing damping at higher frequencies. The example of spruce was cited as having greater attenuation coefficients than maple, due to increased density differences^(3.3). As such, this means that the grain angle relative to propagation has an increasing role in damping. On a larger scale it is clear from previous research presented in this chapter, that there will be greater energy loss tangentially or radial across a sample than longitudinally along it.

The damping of transient excitation vibrations is rarely examined in timber research due to the inhomogeneous variability of multiple timber properties potentially corrupting returned results. In an one example, Hori *et al.*^(3.147) calculated the loss tangent from free-free vibrations (though whether this was by the Q-factor or logarithmic decrement was not stated) in Sitka spruce and found it to have a negative correlation to the velocity-squared ($R^2 = -0.42$). It should be noted that Gerhards^(3.148), often cited, found no evidence of velocity or amplitude variations as a result of measurements being conducted on either early or late wood, though the accelerometers used in this study overlaid both the early and latewood layers and thus put the conclusion into question.

Additionally, like their affects on velocity, temperature and MC play an important role in damping in wood as internal friction is a complex function of the two parameters, with damping significantly increasing as a result of increasing MC up to the FSP, above which, like velocity, the damping is relative constant^(3.3, 3.149). The FPL Wood Handbook^(3.149) notes that there is an arbitrary value for the moisture content, which varies with temperature, at which the damping is at a minimum and increases either above or below this moisture, content^(3.149). It cited examples of minimums at 6% moisture content at room temperature, and at higher temperature the value for minimum damping decreases, and similarly the temperature of minimum damping increases with decreasing moisture content^(3.149).

3.6.1.2 Different measures of damping

A number of different methods exist for the measurement of damping, primarily due to different branches of science developing their own techniques, though these can roughly be divided into three groups^(3.150):

1. Vibration decay measurements: Logarithmic decrement ($\tan\beta$), Impulse Response via the decay constant (σ), Reverberation time (T).
2. Bandwidth determination of measured modal resonances: Quality-factor (Q), fraction of critical damping (ζ), decay constant (σ).
3. Steady-state measurements of inputted and stored energy: loss factor (η).

The majority of these methods (reverberation time, Q-factor, impulse response function, logarithmic decrement), whilst accurately reflecting the internal damping of a structure, can be applied only to specimens set into resonance. As such their application is limited to felled and subsequently processed timber specimens and not standing trees. From each of these measures a damping ratio may be derived. For standing trees, attenuation coefficients would have to be calculated, it therefore may only ever be possible to make relative comparisons of attenuation between species for a fixed distance of separation, due to the inherent variability of timber.

It is important to note that, whilst they have similar behaviour, damping and attenuation is not the same thing. The damping ratio describes the percentage loss of energy due to one cycle through the material for a given frequency. The attenuation coefficient is the decay rate of a wave through a material, reflects the energy intensity loss with distance, which is a function of dispersion and absorption. The focus of this thesis is on the behaviour of damping ratios rather than attenuation coefficients. For further reference on attenuation coefficients in wood, see Bucur^(3.3) or Ouis^(3.39).

3.6.1.2.1 Logarithmic decrement

Bucur^(3.3) cites Haines (1979) as having conducted the most complete analysis of logarithmic decrement measurements between species in both the longitudinal and

radial orientations, showing that typically longitudinal decrement is far less than radial. Typically, the logarithmic decrement for the fundamental frequency of wood is of the range 0.1 (for warm, moist wood) to 0.02 (for warm, dry wood) which therefore translates to a subsequent damping correction of less than 0.2%, which is relatively small^(3.47, 3.149). The fundamental frequency's logarithmic decay is typically favoured in material analysis as the broadband signal returned are an amalgamation of various frequencies subject to increasing scattering with increasing frequency. As such, the time-trace signal will not remain a uniformly-decaying sinusoidal curve due to different arrival times of the peak energy at different frequencies. Where individual frequency separation is not possible, it is perhaps better to calculate the logarithmic decrement from peaks of larger separation after the first five to ten peaks, as the higher harmonics will tend to die away quickly in inhomogeneous materials such as wood. Cai *et al.*^(3.151) cites a variation between logarithmic decrement measurements of 50% when using different amplitude peaks for the calculation. Lindsay^(3.40) noted that in general, material which has a large dielectric constant tend to have a comparatively lower logarithmic decrement. Bucur^(3.3) noted that attenuation measurements were particularly sensitive to delaminations in wood structures.

However, it was noted by Ross and Pellerin^(3.10) that due to the different methods of excitation used in calculating the logarithmic decrement, comparisons between researchers' investigations are often impossible. Additionally, obtaining accurate amplitudes is dependant on the sampling rate of the analyser used, with faster sampling rates providing amplitudes closer to the true amplitude of the decaying signal^(3.151). It was also noted by Cai *et al.*^(3.151) that the nature of the couplant, support conditions, material geometric non-uniformity and background noise also affect the derived amplitudes, though specific examples were not given.

3.6.1.2.2 Impulse response and reverberation time

The calculations involved when using these methods are discussed in Chapter 5. Ouis^(3.82) was the first (and only, to the author's knowledge) researcher to use measurements of reverberation time in logs (resulting from induced flexural

vibrations at the centre point) to evaluate the level of decay in a log. His method, rather than the typical building acoustic software, was to use impulse response functions to evaluate the decay time in frequency bands, thus compiling reverberation times. It was found that increasing levels of decay shortened the reverberation time of the specimen. It was also noted however that the used of RT measurements in logs is complicated by more than one wave type propagating within the material.

Additionally, whilst a pistol shot is sufficient for RT measurements in a room; theoretically the sound field within a room or specimen should reach an equilibrium condition before the sound source is turned off^(3.82). It was observed that the decay had a greater influence on the MoE than on the RT and that using early RT provides a greater indication of decay than the full T_{60} ^(3.82). It was also observed that a 'beating' phenomenon (periodic amplitude modulation with time) occurs in the sound specimen's impulse response, which is not present in decayed specimens^(3.82). This was attributed to a bifurcation of the fundamental peak of the major bending mode into two smaller peaks; the analogy of vibrational energy flowing alternately from one energy reservoir to another during the decay is presented^(3.82).

Though the conclusions of this research are not disputed (it is accepted that decay does increase damping and reduce MoE), certain problems arise in this research, specifically: the location and proportion of the decay within the log was not specified, the logs were modeled as homogenous cylindrical beams making no regard for specimen taper or potential of increased KVR and compression wood in one or other logs, the use of flexural vibration with the impact point close to the measurement accelerometer (i.e. near-field interference), and the calculation of MoE was not explained (was it dynamic or static?).

Ouis^(3.122) again used the early RT method to evaluate rot in a single wooden beam through simulation by the replacement of clear wood with multiple holes filled with sand, and observing the effect on the RT and MoE_d (longitudinal resonance technique). It was shown that the MoE_d decreased, RT decreased and thus loss

factor increased (though at a slower rate than the MoE decrease) as a result of increasing the number of the holes^(3.122).

In this study longitudinal vibration was used with an acknowledgement that the previous method of using bending vibrations (as in Ouis^(3.82)) may have been subject to a coupling of wave types and that bending vibrations are subject to increased loss of energy through external radiation^(3.122). It was also noted, though not investigated, that the position of the holes relative to the nodal points of the longitudinal waves would have an affect on the results, in that holes at or near the nodal points of vibration would have less of an affect on the calculated damping than holes positioned elsewhere. However, there appears to be some confusion in language used, as it was stated that the antinodal stress point of the fundamental frequency would be at the centre of the bar. In free-free vibrations, the central point would be the nodal point for vibrations (but would indeed be an 'antinodal' or point of maximum stress concentration). Ultimately it does appear that it is recognized that holes at the centre of the beam will have a greater effect on the damping of the fundamental frequency than elsewhere.

3.6.1.2.3 Q-Factor

The Quality factor, or Q-factor, is one of the most commonly used measures of damping, particularly in electronics and material analysis. It is typically used in forced vibrations but may also be applied to transient ones provided the response is captured early enough. It is a relative, dimensionless quantity^(3.177). It was first applied to wood measurements by Jayne^(3.9). Other examples of application to wood include the previously discussed Ouis^(3.134). The operational use of the Q-factor is discussed in Chapter 4.

3.7 Summary

In summation of this Chapter, the methods of determination of a dynamic MoE value for an inhomogeneous, anisotropic wood specimen have been described. This is possible through making assumptions regarding the combination of the

equation of motion of a plane wave and traditional beam theory, which is then expanded to separate components of Christoffel's stiffness and compliance matrices. It has been shown that a one-dimensional equation is adequate for the calculation of MoE_d , provided certain assumptions are met regarding, in particular, the wavelength and boundary conditions used. Examples of correlations between one-dimensional MoE_d and static MoE were presented. Other issues concerning the use of the one-dimensional equation were reviewed, and generally speaking, it has been shown that testing specimens by resonance testing (*i.e.* deriving the velocity through the frequency) satisfies the one-dimensional equation. Issues concerning the velocity dispersion present with changing frequency were also discussed. In situations which do not meet this equation (such as the non-creation of a planar wavefront), it was shown that a three-dimensional stiffness equation, incorporating a measure of Poisson's ratio, should be used. This applies to most TOF measurements over relatively short distances.

Regarding the measurement of TOF velocity, certain issues regarding the measurement, such as the determination of actual transit time or which waveform is measured, was discussed. Similarly, the use of resonance was debated in terms of factors which can affect the measurement (such as taper, specimen diameter in relation to length, *et al.*). Following discussion of the condition of measurement, the intrinsic characteristics of wood were discussed in relation to their influence on wave propagation in wood. It was determined that grain angle, MFA and knot content within the specific path of propagation dictate TOF-measured velocity, whilst the resonance-based velocity is the result of the law of mixtures of the various stiffnesses concerning the multi-layered anisotropy of a specimen (including variation in the MFA and juvenile wood content throughout the volume of the specimen). Both methods are also subject to the environmental conditions (moisture content and temperature) of the specimen.

In a review of key previous research into both TOF and resonance techniques in wood, their uses in relation to the various scales of testing (small specimens, beams, logs and trees) have been discussed, particularly in relation to the use of scale-specific devices for the establishment of dynamic MoE. Following on from

this is a discussion and review of the use of acousto-ultrasonics, involving the measurement of both velocity and waveform characteristics, in particular damping measurements. This chapter should serve to provide a knowledge base for the reader during explanation of the methods and the later discussions (Chapters 4 through 6) of the test series undertaken during the creation of this thesis.

3.8 References

- 3.1 Falk R.H., Patton-Mallory M, McDonald K.A., *Non-destructive testing of wood products and structures: state-of-the-art and research needs*, In: Proc. NDT & E for Manf. and Const 1988 August 9-12; Champaign, IL, USA; Ed. doe Reis H.L.M., 1990; pp.137-147, Hemisphere Publishing Corp., Mcgraw-Hill, New York
- 3.2 Kaiserlik J., *Stress wave timing non-destructive evaluation tools for inspecting historic structures: A guide for use and interpretation*, General Technical Report, FPL-GTR-119, 1978, FPL, USDA Forest Service.
- 3.3 Bucur V., *Acoustics of Wood*, 2nd Ed., 2005, CRC Press, London, U.K.,
- 3.4 Halmshaw R., *Non-Destructive Testing; 2nd Edition*, 1991, Edward Arnold publishing, London, U.K.
- 3.5 Craik, R.J., *Sound Transmission Through Buildings: Using Statistical Energy Analysis*, 1996, Gower Publishing Company, Aldershot, U.K.
- 3.6 Timoshenko S.P., Goodier J.N., *Theory of Elasticity: 3rd edition*, 1970, McGraw-Hill Publishing Co., New York, USA.
- 3.7 Wang X., Ross R.J., Mattson J.A., Erickson J.R., Forsman J.W., Geske E.A., Wehr M.A., *Non-destructive evaluation techniques for assessing modulus of elasticity and stiffness of small diameter logs*. For. Prod. J., v.52. n.2, 2002, pp. 79-85.
- 3.8 Hearmon R.F.S, *An introduction to applied anisotropic elasticity*, 1961, Oxford University Press, Oxford, U.K.
- 3.9 Jayne B., *Vibrational properties of wood*, 1959, For. Prod. J., November 1959, pp. 413-417.

- 3.10 Ross R.J., Pellerin R., *Non-destructive testing for assessing wood members in structures*, General Technical Report: FPL-GTR-70-1994, 1994, FPL, USDA Forestry Service.
- 3.11 Gerhards C.C., *Effect of knots on stress waves in lumber*, Res. Paper FPL-RP-384, 1982, FPL, USDA Forestry Service.
- 3.12 Wang S-Y., Ko C-Y., *Dynamic modulus of elasticity and bending properties of large beams of Taiwan-grown Japanese cedar from different plantation spacing sites*, J. Wood Sci., 44, 1998, pp. 62-68.
- 3.13 Dickson R.L., Raymond C.A., Joe W., Wilkinson C.A., *Segregation of Eucalyptus dunnii logs using acoustics*, For. Eco. Management, 179, 2003, pp. 243-251.
- 3.14 Green D.W., Kretschmann D.E., *Properties and grading of southern pine timbers*, For. Prod. J., v.47, n.8, 1997, pp. 78-85.
- 3.15 Cai Z., Hunt M.O., Ross R.J., Soltis L.A., *Static and vibration moduli of salvaged and new joists*, For. Prod. J., v.50, n.2, 2000, pp. 35-40.
- 3.16 Jang S.S., *Evaluation of Lumber Properties by applying stress waves to larch logs grown in Korea*, For. Prod. J., v.50, n.3, 2000, pp. 44-48.
- 3.17 de Olivera, F.G.R., de Campos J.A.O., Pletz E., Sales A., *Assessment of mechanical properties of wood using an ultrasonic technique*, In: Proc. 13th Int. Symp. NDT wood, Berkley, California, USA, August 19-21 2002, Ed. F. C. Beall, Forest Products Society, Madison, Wisconsin, USA.
- 3.18 Castellanos J.R.S., Nagao H., Ido H., Kato H., Onishi Y., *NDE methods applied to the study of a wood beam's discontinuity*, In: Proc. 13th Int. Symp. NDT wood, Hanover, Germany, May 2-4 2005, Ed. Broker F.W, Shaker Verlag, Germany.
- 3.19 Wang X., Ross R.J., McCellan M., Barbour R.J., Erickson J.R., Forsman J.W., McGinnis G.D., *Strength and stiffness assessment of standing trees using a non-destructive stress wave technique*, Res. Paper, FPL-RP-585, 2001, FPL, USDA Forest Service.
- 3.20 Hanhijärvi A., Ranta-Maunus Alpo., Turk, G., *Potential of strength grading of timber with combined measurement techniques*. Rep. of the Combigrade-project: phase 1, 2005, VTT Publications 568. 81 pgs. + app. 6 pgs.
- 3.21 Sonderegger W., Niemz P., *The influence of compression failure on the bending, impact bending and tensile strength of spruce wood and the evaluation of non-destructive methods for early detection*, Holz als Roh und Werkstoff, 62, 2004, pp. 335-342.

- 3.22 Ilic J. *Variation of the dynamic elastic modulus and wave velocity in the fiber direction with other properties during the drying of Eucalyptus regnans Muell F.*, Wood Sci. Tech., 35, 2001, pp. 157-166.
- 3.23 Piter J.C., Zerbino R.L., Blass H.J., *Effectiveness of fundamental resonant frequency for determining the elastic properties of Argentinian Eucalyptus grandis in structural sizes*, Holz als Roh und Werkstoff, 62, 2004, pp. 88-92.
- 3.24 Green D.W., Lowell E.C., Hernandez R., *Structural lumber from dense stands of small-diameter Douglas-fir trees*, For. Prod. J., v.55, n.7/8, 2005, pp. 42-50.
- 3.25 Ayarkwa J., Hirashima Y., Sasaki Y., *Predicting modulus of rupture of solid and finger-jointed tropical African hardwoods using longitudinal vibration*, For. Prod. J., v.51, n.1, 2001, pp. 85-92.
- 3.26 Nzokou P., Freed J., Kamdem P.D., *Relationship between non-destructive and static modulus of elasticity of commercial wood plastic composites*, Holz als Roh und Werkstoff, 64, 2006, pp. 90-93.
- 3.27 Brancheriau L., Bailleres H. *Use of partial least squares method with acoustic vibration spectra as a new grading technique for structural timber*, Holzforschung, 57, 2003, pp. 644-652.
- 3.28 Brancheriau L., Bailleres H., *Natural vibration analysis of clear wooden beams: a theoretical review*, Wood Sci. Tech., 36, 2002, pp. 347-365.
- 3.29 Johansson M., Kliger R., *Variability in strength and stiffness of structural Norway spruce timber – influence of raw material parameters*, Proc. World Conf. Timber Eng. 2000, Whistler, Canada, 2000.
- 3.30 Ilic J., *Relationship among the dynamic and static elastic properties of air-dry Eucalyptus delegatensis*, R. Baker, Holz als Roh und Werkstoff, 2001, pp. 169-175.
- 3.31 Shmulsky R., Seale R.D., Snow R.D., *Analysis of acoustic velocity as a predictor of stiffness and strength in 5-inch-diameter pine dowels*, For. Prod. J., v.56, n.9, 2006, pp. 53-55
- 3.32 Harris P., Petherick R, Andrews M, *Acoustic Resonance tools*, In: Proc. 13th Int. Symp. NDT wood, Berkley, California, USA, August 19-21 2002, Ed. F. C. Beall, Forest Products Society, Madison, Wisconsin, USA.

- 3.33 Sandoz J.L., Benoit Y., Demay L., *Wood testing using Acousto-ultrasonic*, In: Proc. 12th Int. Symp. NDT wood, University of West Hungary, Sopron, Hungary, September 13-15 2000, Ed. Divos F.
- 3.34 Pellerin R.F., Morschauer C.R., *Non-destructive testing of particleboard*, Proc. 7th Int. Particleboard Symposium; March 1973; Pullman, WA. Washington State University.
- 3.35 Carter P., Wang X., Ross R.J., Briggs D., *NDE of logs and standing trees using new acoustic tools. Technical application and results*, In: Proc. 14th Int. Symp. NDT wood, May 2-4 2005, Hanover, Germany, May 2-4 2005, Ed. F-W Broker, Shaker Verlag, Germany.
- 3.36 Consultation with Dr. Charlie Fairfield and Dr. Sean Smith, 9th February, 2005.
- 3.37 Tucker B.J., Bender D.A., Pollock D.G., Wolcott M.P., *Ultrasonic plate wave evaluation of natural fiber composite panels*, In: Proc. 13th Int. Symp. NDT wood, Berkley, California, USA, August 19-21 2002, Ed. F. C. Beall, Forest Products Society, Madison, Wisconsin, USA.
- 3.38 Andrews M., *Which Acoustic Speed?*, In: Proc. 13th Int. Symp. NDT wood, Berkley, California, USA, August 19-21 2002, Ed. F. C. Beall, Forest Products Society, Madison, Wisconsin, USA.
- 3.39 Ouis D., *On the frequency dependence of the modulus of elasticity of wood*, Wood Sci. Tech., 36, 2002, pp. 335-346.
- 3.40 Lindsay R.B., *Mechanical Radiation*, 1960, Mcgraw-Hill, New York, USA.
- 3.41 Wang X., Ross R.J., Bradshaw B.K., Panches J., Erickson J.R., Forsman J.W., Pellerin R.E. *Diameter effects on stress-wave evaluation of modulus of elasticity of logs*, Wood and Fibre Sci., v. 36, n.3, 2004, pp. 368-377.
- 3.42 Bartholomeu A., Gonclaves R., Bucur V., *Dispersion of ultrasonic waves in Eucalyptus lumber as a function of the geometry of boards*, Scientia Forestalis, v.63, 2003, pp. 235-240.
- 3.43 Feeney F.E, Chivers R.C., Evertsen J.A., Keating J., *The influence of inhomogeneity on the propagation of ultrasound in wood*, Ultrasonics, v.36, 1998, pp. 449-453.
- 3.44 Gerhards C.C., *Effect of cross grain on stress waves in lumber*, Res. paper, FPL 368, May 1980, USDA Forest Service

- 3.45 Bucur V., Lancelleur P., Roge B., *Acoustic properties of wood in tri-dimensional representation of slowness surfaces*, Ultrasonics, v.40, 2002, pp. 537-541,
- 3.46 Chauhan S.S., Entwistle K.M., Walker J.C.F., 2005, *Differences in acoustic velocity by resonance and transit-time methods in an anisotropic laminated wood medium*, Holzforschung, 59, 2005, pp. 428-434.
- 3.47 *Course in Non-destructive Testing of Wood*, organized by F. Divos, ETSI Montes, ETS Arquitectura – Universidad Politecnica de Madrid, Madrid, June 2005.
- 3.48 Divos F., Daniel I., Bejo L., *Defect detection in timber by stress wave time and amplitude*, E-J. of NDT, Vol. 6 no.3, 2001.
- 3.49 Kabir M.F., *Prediction of ultrasonic properties from grain angle*, J. Inst. Wood Sci., 15, 5, 2001, pp. 235-246.
- 3.50 Schad K.C., Kretschmann D.E., McDonald K.A., Ross R.J., Green D. W., *Stress wave techniques for determining quality of dimensional lumber from switch ties*, Research Note, FPL-RN-0265, 1995, USDA Forest Service.
- 3.51 Kumar S., *Genetic parameter estimates for wood stiffness, strength, internal checking, and resin bleeding in radiata pine*, Can. J. of For. Res., v.34, n.12, 2004, pp. 2601-2610.
- 3.52 Chauchan S.S., Walker J.C.F., *Variations in acoustic velocity and density with age, and their interrelationship in radiata pine*, For. and Eco. Man., 229, 2006, pp. 388-394.
- 3.53 Wang S-Y, Lin C-J., Chiu C-M, *The adjusted modulus of elasticity above the fiber saturation point in Tawania plantation wood by ultrasonic-wave measurement*, Holzforschung, 57, 2003, pp. 547-552.
- 3.54 Hayes M.P., Chen J., *A portable stress wave measurement system for timber inspection*, Internal University of Canterbury publication, 2003.
- 3.55 Carter P., Briggs D., Ross R.J., Wang X., *Acoustic testing to enhance western forest values and meet customer wood quality needs*, In: Productivity of western forests, Res. Paper, PNW-GTR-642, 2005, USDA Forest Service.
- 3.56 Bascunan A, Moore J.R., Walker J.C.F., *Impacts of silviculture on wood quality: Variations in the dynamic modulus of elasticity with*

- proximity to the stand edge in radiata pine stands on the Canterbury Plains, New Zealand, NZ J. For., v.51, n.3, 2006, Pages: 4–8.*
- 3.57 Xu P., Walker J.C.F., *Stiffness gradients in radiata pine trees*, Wood Sci. and Tech., v.38, n.1, 2004, pp.1-9.
- 3.58 Grabianowski M., Manley B., Walker J.C.F., *Acoustic measurements on standing trees, logs and green lumber*, Wood Sci. and Tech., v.40, 2006, pp. 205–216.
- 3.59 Lasserre J.P., Mason E.G., Watt M.S., *Assessing corewood acoustic velocity and modulus of elasticity with two impact based instruments in 11-year-old trees from a clonal-spacing experiment of Pinus radiata Don D*, For. and Eco. Man., 239, 2007, pp. 217–221.
- 3.60 Lindstrom H., Harris P., Nakada R., *Methods for measuring stiffness of young trees*, Holz als Roh und werkstoff, 60, 2002, pp. 165-174.
- 3.61 Wang J., Biernacki J.M., Lam F., *non-destructive evaluation of veneer quality using acoustic wave measurements*, Wood Sci. and Tech., 34, 2001, pp. 505-516.
- 3.62 Huang C-L., Lindstrom H., Nakada R., Ralston J., *Cell wall structure and wood properties by acoustics – a selective review*, Holz als Roh und werkstoff, 61, 2003, pp321-335.
- 3.63 Dinwoodie J.M., *Timber: its nature and behaviour*, 1981, Van Nostrand Reinhold Company, New York, USA.
- 3.64 Cave I.D., Walker J.C.F., *Stiffness of wood in fast-grown Plantation softwoods: the influence of microfibril angle*, For. Prod. J., v. 44, n.5, 1994, pp. 43-45,.
- 3.65 Evans, R., Ilic J., *Rapid prediction of wood stiffness from microfibril angle and density*, For. Prod. J., v.51, n.3, 2001, pg 53-57.
- 3.66 Yang J.L., Evans R., *Prediction of MOE of Eucalyptus wood from microfibril angle and density*, Holz als Rohund Werkstoff, v.61, 2003, pg 449-452.
- 3.67 Bucur V., *Acoustics as a tool for the non-destructive testing of wood*, Proc. Int. Symp. NDT contribution to Infrastructure safety systems, Nov 22-26,1999.
- 3.68 Sandoz J.L., *Non-destructive evaluation of building timber by ultrasound*, 8th Int. NDT of Wood Symposium, Vancouver, Sept 23-25, 1991.

- 3.69 Adjanohoun G., Gulliot J., Lanvin R., *Small roundwood grading by non-destructive X-rays and ultrasonic methods*, E-J. NDT, v.4 n.11, 1999.
- 3.70 Tsehaye A., Buchanan A.H., Walker J.C.F., *Sorting of logs using acoustics*, Wood Sci. Tech., 34, 2000, pp. 337-344.
- 3.71 Carter P., Chauchan S., Walker J., *Sorting logs and lumber for stiffness using Director HM200*, Wood and Fibre Sci., 38, 1, 2006, pp. 49-54.
- 3.72 Booker R.E., Froneberg J., Collins F., *Variation of sound velocity and dynamic Young's modulus with moisture content in three principal directions*, In: Proc. 10th Int. Symp. NDT wood, Swiss Federal Institute of Technology, Lausanne, Switzerland, August 26-28 1996, Ed. Sandoz J.L., Presses Polytechniques et Universitaires Romandes.
- 3.73 Kang H., Booker R.E., *Variation of stress-wave velocity with MC and temperature*, Wood Sci. Tech., v.36, 2002, pp. 41-54.
- 3.74 Simpson W.T., Wang X., *Relationship between longitudinal stress wave transit time and moisture content of lumber during kiln-drying*, For. Prod. J., v.51, n.10, 2001, pp. 51-54.
- 3.75 Machek L., Militz H., Sierra-Alvarez R., *The influence of wood moisture content on dynamic modulus of elasticity measurements in durability testing*, Forschung Verwertung, 5, 2001, pp. 97-100.
- 3.76 Bächle H., Walker J.C.F., *The influence of temperature on the velocity of sound in green pine wood*, Holz als Roh und Werkstoff, v.64, n.5, 2006, pp 429-430.
- 3.77 Green D.W., Evans J.W, Logan J.D., Nelson W.J., *Adjusting modulus of elasticity of lumber for changes in temperature*, For. Prod. J., v.49. n.10, 1999, pp 82-94.
- 3.78 van Dyk H., Rice R.W., *Ultrasonic wave velocity as a moisture indicator in frozen and unfrozen lumber*, For. Prod. J., v.55, n.6, 2005, pp. 68-72.
- 3.79 Wang X., Divos F., Pilon C., Brashaw B.K., Ross R.J., Pellerin R.F., *Assessment of Decay in Standing timber using stress wave timing non-destructive evaluation tools: A guide for use and interpretation*, General technical report, FPL-GTR-147, 2004, USDA Forestry Service.

- 3.80 Socco L.V., Sambuelli L., Nicolotti G., *Feasibility of ultrasonic tomography for non-destructive testing of decay on living trees*. Res. in NDE, v.15 n.1, 2004, pp. 31-54.
- 3.81 Ross R.J., DeGroot R.C., Nelson W.J., *Non-destructive evaluation of biologically degraded wood*, In Proc. 6th Int. Conf. Non-dest. Charact. of Mat., Ed. Green R.E., Plenum Press, New York.
- 3.82 Ouis D., *Detection of decay in logs through measuring the dampening of bending vibrations by means of a room acoustical technique*, Wood Sci. and Tech., 34, 2000, pp. 221-236.
- 3.83 Axmon J., Hansson M., Sornmo L., *Experimental study on the possibility of detecting internal decay in standing Picea abies by blind impact response analysis*, Forestry, 77, 3, 2004, pp. 179-192.
- 3.84 Kabir M.F., Schmoldt D.L., Schafer M.E., *Ultrasonic detection of knots, cross grain and bark pockets in wooden pallet parts*, Proc. World Conf. Timber Eng. 2000, pp. 7.5.2-1.
- 3.85 Kabir M.F., Schmoldt D.L., Schafer M.E., *Time domain ultrasonic signal characterization for defects in thin un-surfaced hardwood lumber*, Wood and Fiber Sci., v.34, n.1, 2002, pp.165-182.
- 3.86 Ouis D., *Frequency dependence of strength and damping properties of wood and their influence by structural defects and rot*, In: Proc. 14th Int. Symp. NDT wood, May 2-4 2005, Hanover, Germany, May 2-4 2005, Ed. F-W Broker, Shaker Verlag, Germany.
- 3.87 Sandoz J.L., Benoit Y., Demay L., *Standing tree quality assessments using Acousto-ultrasonic*, 2004, internal CBS-CBT report available from www.cbs-cbt.com.
- 3.88 Schad K., Schmoldt D., Ross R.J., *Non-destructive methods for detecting defects in softwood logs*, Research Paper, FPL-RP546, 1996, FPL, USDA Foresty Service.
- 3.89 Reynolds T.N., *Compression wood project – Final Report*, BRE Client Report No., 218-309, 2004, Building Research Establishment Ltd.
- 3.90 Knowles R.L., Hansen L.W., Wedding A., Downes G., *Evaluation of non-destructive methods for assessing stiffness of Douglas fir trees*, NZ J. For. Sci., v.34, n.1, 2004, pp. 87-101.
- 3.91 Sandoz J.L., *Ultrasonic solid wood evaluation in industrial applications*, In: Proc. 10th Int. Symp. NDT wood, Swiss Federal Institute of Technology, Lausanne, Switzerland, August 26-28 1996, Ed. Sandoz J.L., Presses Polytechniques et Universitaires Romandes.

- 3.92 Berndt H., Johnson G.C., Schiewind A.P., *Using phase slope for arrival time determination*, In: Proc. 14th Int. Symp. NDT wood, May 2-4 2005, Hanover, Germany, May 2-4 2005, Ed. F-W Broker, Shaker Verlag, Germany.
- 3.93 Bodig J., *The process of NDE research for wood and wood composites*, In: Proc. 12th Int. Symp. NDT wood, University of West Hungary, Sopron, Hungary, September 13-15 2000, Ed. Divos F.
- 3.94 Rus G., Wooh S-C., Gallego R., *Design of ultrasonic wedge transducer*, Ultrasonics, 43, 2005, pp. 391-395.
- 3.95 Bradshaw B.K., Vatalaro R.J., Wacker J.P., Ross R.J., *Condition assessment of timber bridges: 2. Evaluation of several stress wave tools*, FPL-GTR-160, 2005, USDA Forest Service.
- 3.96 Crews K., *Development of data bases for the NDE systems for timber poles in service*, commercial report, 2001, University of Technology – Sydney.
- 3.97 Dickson R.L., Matheson A.C., Joe B., Ilic J., Owen J.V., *Acoustic segregation of Pinus radiata logs for sawmilling*, NZ J. of For. Sci., 34, 2, 2004, pp. 175-189.
- 3.98 Matheson A.C., Dickson R.L., Spencer D.J., Joe B., Ilic J., *Acoustic segregation of Pinus radiata logs according to stiffness*, Ann. For. Sci., 59, 2002, pp. 471-477.
- 3.99 Gerhards C.C., *Longitudinal stress waves for lumber stress grading: factors affecting applications: state of the art*, For. Prod. J., 32, 2, 1982 pp. 20-25.
- 3.100 Koponen T., Karppinen T., Haeggstrom E., Saranpaa P., Serimaa R., *The stiffness modulus in Norway spruce as a function of year ring*, Holzforschung, 59, 2005, pp. 451-455.
- 3.101 Bengtsson C., *Stiffness of spruce wood – Influence of moisture conditions*, Holz als Roh und Werkstoff, 58, 2000, pp. 344-352.
- 3.102 Ross R.J., Zebre J.I., Wang X., Green D.W., Pellerin R.F., *Stress wave non-destructive evaluation of Douglas-fir peeler cores*, For. Prod. J., 55, 3, 2005, pp. 90-94.
- 3.103 Green D.W., Ross R.J., *Linking Log Quality with Produce Performance; in role of wood production in ecosystem management*, General Technical Report, FPL-GTR-100, 1997, FPL, USDA Forestry Service.

- 3.104 Ross R.J., McDonald K.A., Green D.W., Schad K.C., *Relationship between log and lumber modulus of elasticity*, For. Prod. J., v. 47 n. 2, Feb 1997.
- 3.105 Green D.W., Gorman T.E., Evans J. W., Murphy J.F, *Improved grading system for structural logs for log homes*, For. Prod. J., 54, 9, 2004, pp. 52-62.
- 3.106 Yin Y., Nagao H., Liu X., Nakai T., *Evaluating bending properties of Chinese fir plantation wood with three different methods*, In: Proc. 14th Int. Symp. NDT wood, May 2-4 2005, Hanover, Germany, May 2-4 2005, Ed. F-W Broker, Shaker Verlag, Germany.
- 3.107 Wang X., Ross R.J., Green D.W., Bradshaw B., Englund k., Wolcott M., *Stress wave sorting of red maple logs for structural quality*, Wood Sci. Tech., 37, 2004, pp. 531-537.
- 3.108 Yamamoto K., Sulaiman O., Hashim R., *Non-destructive detection of heart rot in Acacia mangium trees in Malaysia*, For. Prod. J., 48 (3), 1998, pp. 83-86.
- 3.109 Axmon J., Hansson M., Sornmo L., *Modal analysis of living spruce using a combined proxy and DFT multi-channel method for detection of internal decay*, Mech. Sys. and Sig. processing, 16, 4, 2002, pp. 561-584.
- 3.110 Lawday G., Hodges P.A., *The analytical use of stress waves for the detection of decay in standing trees*, Forestry, 73, 5, 2000, pp. 447-456.
- 3.111 Socco L.V., Sambuelli L., Martinis R., Comino E., Nicolotti G., *Feasibility of ultrasonic tomography for non-destructive testing of decay on living trees*, Res. in NDE, 15, 2004, pp. 31-54.
- 3.112 Bucur V., *Ultrasonic techniques for non-destructive testing of standing trees*, Ultrasonics, v.43, 2005, pp. 237-239.
- 3.113 Divos F., Szalai L., *Tree evaluation by acoustic tomography*, In: Proc. 13th Int. Symp. NDT wood, Berkley, California, USA, August 19-21 2002, Ed. F. C. Beall, Forest Products Society, Madison, Wisconsin, USA.
- 3.114 Harris W. T., *Pole testing apparatus*, 1962, US patent 3,066,525.
- 3.115 Wagner F.G., Gorman T.M., Wu S-Y., *Assessment of intensive stress-wave scanning of Douglas-fir trees for predicting lumber MOE*, For. Prod. J., v.53 n.3, Mar 2003.

- 3.116 Personal communication with Mike Jarvis, University of Glasgow, 21st January 2005.
- 3.117 Chuang S-T., Wang S.Y., *Evaluation of standing tree quality of Japanese cedar grown with different spacing using stress-wave and ultrasonic-wave methods*, J. of Wood Sci., 47, 2001, pp. 245-253.
- 3.118 Kumar S., Jayawickrama K.J.S., Lee J., Lausberg M., *Direct and indirect measures of stiffness and strength show high heritability in a wind-pollinated radiata pine progeny test in New Zealand*, Silva Genetica, 51, 5-6, 2002, pp. 256-261.
- 3.119 Hu L.J., Zhang S.Y., Saal U., *Factors affecting reliability of longitudinal vibration technique to non-destructively determining modulus elasticity (MOE) of standing trees*, In: Proc. 14th Int. Symp. NDT wood, May 2-4 2005, Hanover, Germany, May 2-4 2005, Ed. F-W Broker, Shaker Verlag, Germany.
- 3.120 Personal communication with John Walker, March 2006
- 3.121 Lindstrom H., Harris P., Sorensson C.T., Evans R., *Stiffness and wood variation of 3-year old Pinus radiata clones*, Wood Sci. Tech., 38, 2004, pp. 579-597.
- 3.122 Ouis D., *Effect of structural defects on the strength and damping properties of a solid material*, Euro. J. of Mech. and Solids, 22, 2003, pp. 47-54.
- 3.123 Murphy J.F. *Commentary on factors affecting transverse vibration using an idealised theoretical equation*, Research Note, FPL-RN-0276, 2000, USDA Forest Service.
- 3.124 Haines D.W., Leban J.M., Herb C., *Determination of Young's modulus for spruce, fir and isotropic materials by the resonance flexure method with comparisons to static flexure and other dynamic methods*, Wood Sci. Tech., 30, 1996, pp. 253-263.
- 3.125 Haines D.W., Leban J-M., *Evaluation of the MOE of Norway spruce by the resonance flexure method*, For. Prod. J., 47, 10, 1997, pp. 91-93.
- 3.126 Divos F., Divos P., *Resolution of stress wave based acoustic tomography*, In: Proc. 14th Int. Symp. NDT wood, May 2-4 2005, Hanover, Germany, May 2-4 2005, Ed. F-W Broker, Shaker Verlag, Germany.
- 3.127 Harmonics diagram from www.glenbrook.k12.il.us.

- 3.128 Mason W.P., *Physical acoustics and the properties of solids*, 1958, D. Van Nostrand Co., pp. 402.
- 3.129 Solodov I., Pfeleiderer K., Busse G., *Nondestructive characterization of wood by monitoring of local elastic anisotropy and dynamic non-linearity*, *Holzforschung*, 58, 2004, pp. 504-510.
- 3.130 Divos F., Denes L., Iniguez G., *Effect of cross-sectional change of a board specimen on stress-wave velocity determination*, *Holzforschung*, 59, 2005, pp. 230-231.
- 3.131 Brancheriau L., Bailleres H., Sales C., *Acoustic resonance of xylophone bars: experimental and analytic approaches of frequency shift phenomenon during the tuning operation of xylophone bars*, *Wood Sci. Tech.*, 40, 2006, pp. 94-106
- 3.132 Narkis Y., *Identification of crack location in vibrating simply supported beams*, *J. Sound Vib.*, 172, 4, 1994, pp. 549-558.
- 3.133 Douka E., Bamnios G., Trochidis A., *A method for determining the location and depth of cracks in double-cracked beams*, *App. Acous.*, 65, 2004, pp. 997-1008.
- 3.134 Ouis D., *Assessment of severity and localization of a transversal crack in a wood beam through a study of its natural mode of vibration*, *Holz als Roh und Werkstoff*, 62, 2004, pp. 17-22.
- 3.135 Ouis D., *Vibrational and acoustical experiments on logs of spruce*, *Wood Sci. Tech.*, 33, 1999, pp. 151-184.
- 3.136 Ilic J., *Dynamic MOE of 55 species using small wooden beams*, *Holz als Roh und Werkstoff*, 61, 2003, pp. 167-172.
- 3.137 Edlund j., Lindstrom H., Nilsson F., Reale M., *Modulus of elasticity of Norway spruce saw logs vs. structural lumber grade*, *Holz als Roh und Werkstoff*, 64, 4, 2006, pp. 273-279.
- 3.138 Gaunt D., Van Wyk L., *Literature review of machine stress grading accuracy check methods*, Project No. PN02.1905, 2003, Australian Government, Forest and Wood Products Development Corporation.
- 3.139 Watt M.S., Moore J.R., Facon J-P., Downes G.M., Clinton P.W., Coker G., Davis M.R., Simcock R., Parfitt R.L., Dando J., Mason E.G., Bown H.E., *Modeling the influence of stand structural, edaphic and climatic influences of juvenile Pinus radiata dynamic modulus of elasticity*, *For. Eco. Management*, 2006, pp. 136-144.

- 3.140 Xu P., *Estimating the influence of knots on the local longitudinal stiffness in radiata pine structural timber*, Wood Sci. Tech., v.36, 2002, pp. 501-509.
- 3.141 Bucur V., *'Non-destructive characterization of wood,'* 2003, 1st edition, Springer publishing, Berlin, Germany, 324 pgs
- 3.142 Kawamoto S., Williams R.S., *Acoustic emission and Acousto-ultrasonic techniques for wood and wood-based composites: A Review*, General Technical Report, FPL-GTR-134, USDA Forestry Service, 2002.
- 3.143 Raczlowski J., Lutomski K., Molinski W., Wos R., *Detection of early stages of wood decay by acoustic emission technique*, Wood Sci. Tech., 33, 1999, pp. 353-358.
- 3.144 Aicher S., Hofflin L., Dill-Langer G., *Damage evolution and acoustic emission of wood at tension perpendicular to fiber*, Holz als Roh und werkstoff, 59, 2001,, pp 104-116.
- 3.145 Cyra G., Tanaka C., *The effect of wood fiber directions on acoustic emission in routing*, Wood Sci. Tech., 34, 2000, pp. 237-252.
- 3.146 Seeling U., Ballarin A. W., Beall F.C., *Process and analysis of signals through dimension wood using acousto-ultrasonics*, In: Proc. 13th Int. Symp. NDT wood, Berkley, California, USA, August 19-21 2002, Ed. F. C. Beall, Forest Products Society, Madison, Wisconsin, USA.
- 3.147 Hori R., Muller M., Watanabe U., Lichtenegger H.C., Fratzi P., Sugiyama J., *The importance of seasonal differences in the cellulose microfibril angle in softwood in determining acoustic properties*, J. Mat. Sci., 37, 2002, pp. 4279-4284.
- 3.148 Gerhards C.G., *Effect of earlywood and latewood on stress-wave measurements parallel to the grain*, Wood Sci., 11, 2, 1978, pp. 69-72.
- 3.149 *Wood Handbook: Wood as an engineering material*, General technical report, FPL-GTR-113, 1999, FPL, USDA Forest Service,
- 3.150 Beall F.C., *Overview of the use of ultrasonic technologies in research on wood properties*, Wood Sci. Tech., 36, 2002, pp. 197-212.
- 3.151 Cai Z., Hunt M.O., Fridley K.J., Rosowky D.V., *New technique for evaluating damping of longitudinal free vibration in wood based materials*, J. Testing and Ev., 25, 4, 1997, pp.456-460.

- 3.152 Gade S., Herlufsen H., *Digital filtering techniques vs. FFT techniques for damping measurements (damping part 1)*, Bruel and Kjaer Technical Review Paper No.1 – 1994, Bruel and Kjaer A/S, Denmark.
- 3.153 Alleyne D.N., *The non-destructive testing of plates using ultrasonic lamb waves*, Doctoral Thesis, Imperial College London, Feb. 1991
- 3.154 Rose J.L., *Dispersion curves in guided wave testing*, Materials Evaluation, Jan., 2003, pp.20-23
- 3.155 Seco F., Martin J.M., Jimenez A., Pons J.L., Calderon L., Ceres R., *PCDISP: A tool for the simulation of propagation in cylindrical waveguides*, 9th Int. Cong. Sound and Vib., Orlando, Florida, 2002.

Chapter 4 Test series 1: Velocity variation in Sitka spruce

4.1 Introduction

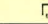


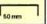



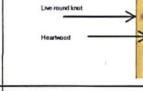
















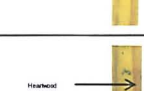
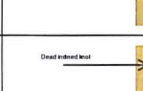



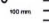
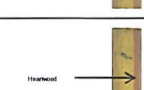
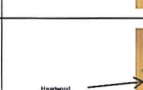




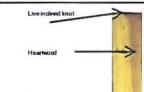
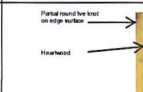




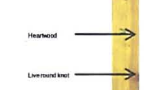
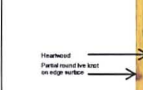





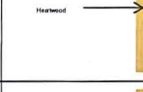


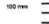


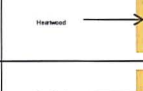















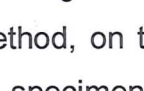
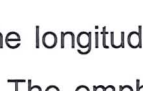


Low-frequency (hammer impact) stress wave and ultrasonic TOF tests were conducted on a single, 2110 mm beam of C16 Sitka spruce. In the low-frequency oscilloscope tests, using longitudinal vibrations induced by hammer impact at the end of beam Section 1, 30 TOF tests were conducted every 200 mm tests along Sides A and B (encompassing 200 mm beam sections 2 to 11, see Table 4.1). The tests were then repeated at 400 mm, 800 mm, 1000 mm, 1600 mm and finally 2000 mm increments. Side C was also tested at every incremental level except 200 mm. The whole batten was then tested by the 54 kHz PUNDIT™ tester. The battens were then progressively shortened by sections relative to the increments tested (and tested by PUNDIT™), until each Section was reduced to a 200 mm section. Measurements of the beam's timber characteristics by section (density, KAR, heartwood content, ring width, and grain angle) were also made.

Thesis Section 4.2 presents the results of both types of TOF velocity calculations, and is sub-divided by the various section lengths. Section 4.3 presents the results of the non-acoustical measures of timber properties. Section 4.4 presents the potential correlations between the velocities and timber properties. Section 4.5

discusses the difference in the TOF velocities, in relation to method, section size and timber parameters. A summary of this test series is presented in Section 4.6.

Table 4.1 displays each 200 mm beam Section of the sample by Sides A to D, and notes the presence of heartwood, type of knots or significant grain deviation. Only one sample was tested in this investigation due to the time taken to derive results and the requirement to begin test series 3 (Chapter 6). Upon reflection, more samples would have benefited the investigation of timber properties influence on longitudinal wave propagation; however the primary focus of this series was to determine the accuracy of TOF methods in preparation for field testing. The results of TOF tests on this single beam were sufficient to draw conclusions on this applicability, as discussed later in this chapter.

Table 4.1 Images of each side and 200 mm section of the test specimen.

	Side A 	Side C 	Side B 	Side D 
Section 1  				
Section 2  				
Section 3  				
Section 4  				
Section 5  				
Section 6  				
Section 7  				
Section 8  				
Section 9  				
Section 10  				
Section 11  				
Section 12 				

These tests investigated the effect of Sitka spruce wood properties, using the stress-wave method, on the longitudinal propagation velocity and hence Young's modulus of the specimen. The emphasis of the tests was also on establishing a repeatable and reproducible series of experiments^(4.1) to minimise effects of

experimental error during tests on an inherently anisotropic, inhomogeneous material. The object of these experiments, the first TOF measurements to be conducted in this research, was to establish the effect of several inherent mechanical properties on the longitudinal TOF velocity (whilst establishing the accuracy of this method). The primary hypothesis here is that the wavespeed will not remain constant due to internal factors distorting the nature of the wave front and altering the propagation velocity, as seen in the experiments of Gerhards^(4.2) and Divos *et al.*^(4.3)

4.1.1 Equipment

- 1 x Brüel & Kjær (B & K) PULSE™ Platform (Type 3760-B) with Type 3109 four channel input-output module and Type 7533 LAN interface module and software (Type 7705 time capture facility and Type 7770 FFT analyser)^(4.4)
- 1 x Dell™ laptop (Latitude™ D600) and dongle^(4.5)
- 2 x 3 m AO-0463-F 10–32 UNF to 10–32 UNF cables and pin connectors^(4.6)
- 2 x Type 4308-B uniaxial accelerometers (denoted x & y in Fig. 5.1)^(4.7)
- 1 x Type 4294 calibration exciter^(4.8)
- 1 x Endevco™ Type 2302 impact hammer^(4.9)
- 1 x sample of C16-grade Sitka spruce
- 1 x hanging frame to isolate sample from background vibrations
- 1 x dual-channel Gould™ 20 MHz digital storage oscilloscope Type OS300^(4.10)
- 2 x B & K Type 2635 charge amplifiers (denoted x' & y' in Fig. 5.1)^(4.11)
- PUNDIT™ 54 kHz concrete tester^(4.12)
- 1 x Mitutoyo™ standard Digimatic calipers^(4.13)

4.1.2 Method

Firstly, a set of experiments was devised to minimise the potential for measurement error. Following fabrication of the test rig, measures were taken to isolate the timber beam from background vibrations and coupling to adjacent surfaces (see Figure 4.1).

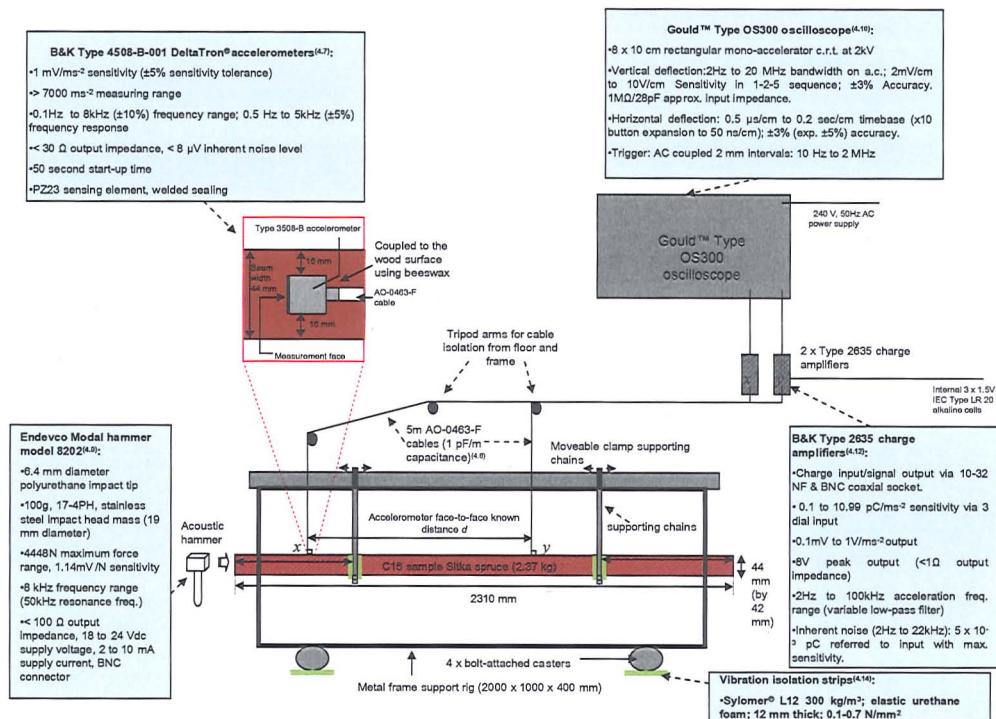


Figure 4.1 Test series 1 measurement set-up, test rig and equipment specifications. The red box on the right shows an enlarged schematic of the accelerometer placement on the beam's top surface. It can be seen that the beam is supported by hanging from 6 mm link chains, which are isolated from the beam and the rig frame by green rubber-foam padding. Figure is not to scale.

This consisted of supporting the beam on two chain cradles coated in 12 mm thick 'Sylomer'^(4.14) to add an extra layer of acoustic impedance to the system. The chains were separated from their shackles by the same foam, and a twin layer inserted between the base of the rig and the rigid laboratory strong floor. Overall, the resulting background vibration levels transmitted to the beam were reduced to less than 0.005 ms⁻². As such any longitudinal wave excited by a hammer blow was easily distinguishable. More problematic was the background vibration entering the accelerometer cables. This was overcome by hanging the cables from string lines between tripods above the rig, but resulted in a natural oscillation, and subsequent oscillating response on the oscilloscope, due to any airflow (which was therefore controlled) and the recovery time between tests was extended beyond the time it took the beam to stop oscillating. This served to create practically free oscillation conditions.

Initially it was expected that the B & K PULSE™ system would be used for these experiments, but following a series of tests and discussions with B & K technicians it was established that this was unfeasible due to insufficient resolution of the response time. A dual-channel Gould 20 MHz digital storage oscilloscope (Type 1421) was therefore used. This was connected to two B & K Type 2645 charge amplifiers, which were themselves connected by 5 m long cables to the accelerometers, one of which was battery powered and was regularly monitored for any power loss. This equipment is shown in Figure 4.2.

The two piezoelectric Type 5308-B accelerometers were calibrated each morning before testing began, using a Type 4294 calibration exciter and the PULSE™ system's auto-calibration function for Type 5308-B accelerometers, calibrated for an acceleration of 10 ms^{-2} at a frequency of 159.2 Hz (in this case the PULSE™ was used simply for convenience over the oscilloscope). The accelerometers were then reattached to the charge amplifiers, which were set to a sensitivity of 0.499 pC/ms^{-2} , with a lower frequency limit of 2 Hz and an upper frequency limit of 10 kHz.



Gould Dual channel oscilloscope



B & K Type 2635 charge amplifier

Figure 4.2 Gould oscilloscope and B & K Type 2635 charge amplifier.

The oscilloscope was set to capture and record any signal where the amplitude of the acceleration exceeded a set trigger level (75% pre-roll trigger) on Channel 1 (the first accelerometer) thus when the stress wave generated by a hammer blow passed the accelerometer it would be recorded. The trigger level was adjusted

before testing and was kept constant throughout. The time division on the display function's x-axis was set to 0.1 ms and a 10 times magnification used to distinguish any deviations from background vibration. The y-axis displayed the amplitude response.

It was originally envisaged that at least two samples would be examined, however time constraints did not permit this. Therefore the experiments described here centre on one 2310 mm x 44 mm x 42 mm C16 Sitka spruce timber beam – specimen W1. The sample was deemed to have sufficient variety, such as live and dead knots, heartwood and sapwood, *etc.* to potentially influence propagation velocity. The measurement of these characteristics is described later in this section. However, this will obviously limit the validity of any conclusions that may be drawn from these experiments but proved useful for further study. Care was taken to ensure that from the beginning of the experiments to the sectioning of the beam for subsequent density measurements, the sample was not subject to any external forces or environments (particularly temperature and humidity which, as stated in Chapter 3, can have a significant effect on the speed of longitudinal wave propagation) that would affect its structure or alter its mechanical properties.

Each side of the beam is labelled, 'A' through 'D', and every 200 mm from the impact end of the beam represents a separate section to be examined, 'A1' through 'A12' and so on from B1 to B12 and so on, as Shown in Table 5.1

Each side of the beam was to be examined in turn at a variety of spacings between the accelerometers. The two accelerometers (x and y , x always being the closest to the impact end) were calibrated and then placed 200 mm apart. They were coupled to the top surface of the wood by beeswax (density at 15°C \approx 0.958 to 0.970 g/cm³, elastic modulus *c.* 0.2 GPa)^(4.15-16), a minimum of 200 mm from the impact face to avoid near-field effects (*i.e.* testing begins at Section 2 on each face). The beam was then excited by an instrumented hammer on the end face of the beam and the resulting impulse waves propagated through the wood at velocities depending on the axis in question. The accelerometers were placed with their face axially aligned towards the impact^(4.17) (see Figure 4.1).

At this point an experiment was undertaken to observe the effect of the two accelerometers being aligned in different orientations and at different sides of the beam, this consisted of ten repeated impacts. Testing was also conducted to assess whether the striking force or its point of impact affected the response.

The time difference was then measured between the wave reaching the first accelerometer and the second.

The time t is divided by the distance d to derive the longitudinal velocity V_L :

$$V_L = \frac{d}{t} \quad \text{Eqn 4.1}$$

This is achieved by observing, on the oscilloscope, the deviation from the resting horizontal response induced by the longitudinal wave towards the first peak of the free vibration response ('base-of-peak to base-of-peak' as in Figure 4.3).

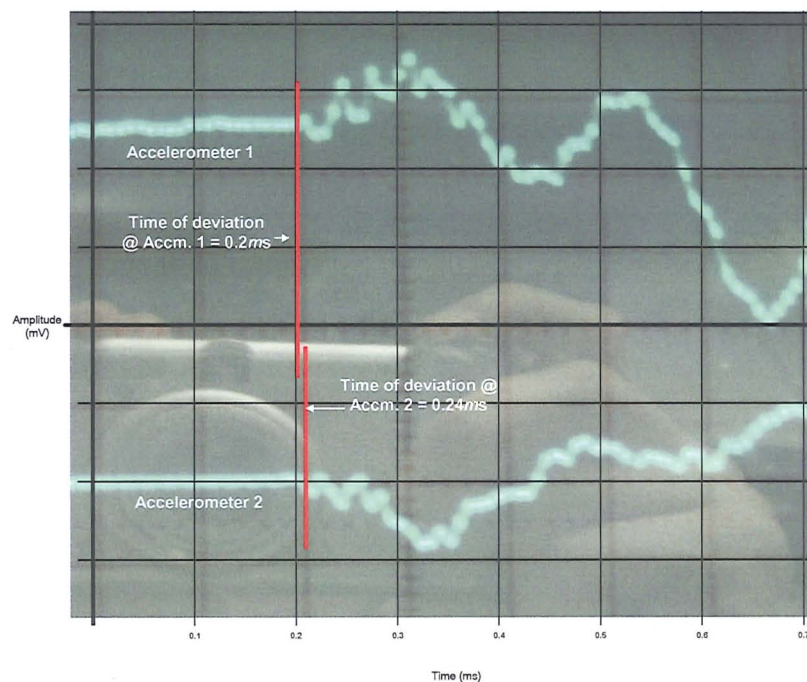


Figure 4.3 Base-to-base measurements on the oscilloscope display. The grid system is 0.1 ms per square using the x10 magnification.

The example has shown in Figure 4.3 display values for the time of deviation of 0.2 ms and 0.24 ms for accelerometers 1 and 2 respectively. In this instance

accelerometers were positioned in-line 200 mm apart on Section A:2. As such the time difference between the longitudinal wave reaching each accelerometer is very small compared to later tests. Using Eqn 4.1, with a time difference (t) of 0.04 ms and a separation (d) of 200 mm, the returned velocity in this instance was 5000 ms⁻¹.

Thirty, nominally identical, measurements in the longitudinal axis for the first accelerometer separation were undertaken. Following this the accelerometers were moved 200 mm along to position A:3 (with the 200 mm separation kept constant). This was repeated along side A until the end of Section A:10.

The separation between accelerometers was then doubled to 400 mm and a further 30 tests conducted, this time between 200 and 600 mm from the impact, *i.e.* Section A:2-3. Similarly, the accelerometers are then moved 400 mm along the beam as before until the final test covering Section A:9 through A:10. This continues along the beam at separations of 200, 400, 800, 1000, 1600 and 2000 mm until all tests on one side have been completed. The beam is then turned to side B and repeat measurements are taken. Sides A and B were measured completely, Side C was measured from separations of 400 mm upwards.

The 54 kHz PUNDIT™ concrete tester^(4.12) was then applied to the ends of the beam to determine the macroscopic compression wave velocity along the whole beam. It was assumed that the PUNDIT™ wavespeeds would represent the actual longitudinal wavespeed along the entire cross-section using the shortest pathway and hence not be affected by surface features unless they were present across the whole section.

The beamspread angle, θ , of the 54 kHz PUNDIT transducer in a timber specimen can be calculated using Equation 4.2^(4.18):

$$\sin \frac{\theta}{2} = \frac{0.514V_L}{2rf} \quad \text{Eqn 4.2}$$

Where:

θ = Beamspread angle (degrees)

r = radius (of transducer head) (cm)

f = frequency of transducer (Hz)

V_L = velocity of the longitudinal wave in the specimen (cms^{-1})

Using a typical longitudinal velocity for a dry, spruce timber beam of 500000 cms^{-1} , the PUNDIT frequency of 54000 Hz and transducer radius of 2.5 cm , the equation becomes:

$$\sin \frac{\theta}{2} = \frac{0.514 \times 500000 \text{ cms}^{-1}}{2 \times 2.5 \text{ cm} \times 54000 \text{ Hz}} = 0.9519 \quad \text{Eqn 4.3}$$

Thus the beamspread half-angle $\theta/2 \approx 72^\circ$ and $\theta \approx 144^\circ$, thus the shadow zone in each half of the beam will be approximately 18° from the edge of the transducer. However, since the PUNDIT™ transducer emits the ultrasonic pulse across the whole of its surface (50 mm), there would be no shadow zone in a specimen with cross-sectional dimensions less than 50 mm (as in Test Series 1 and 2). In Test series 3, with beam specimens of dimensions $3100 \times 98 \times 45 \text{ mm}$ ($L \times b \times h$), this would equate to a shadow zone along the length of the specimen (provided the transducer is at the centre of one end's cross-section) of 15.9 mm . The procedure for the PUNDIT™ tests and an image showing the application of the transducer to the specimens in Test Series 3 is shown in Figure 4.4.

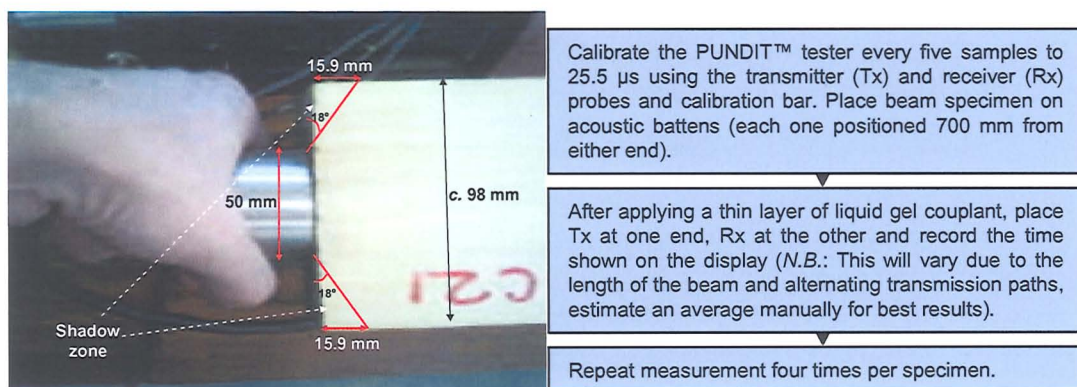


Figure 4.4 Operational flowchart and image of transmitting probe application during PUNDIT testing of Sitka spruce beams in test series 3.

It can clearly be seen that $\sin\theta/2$ must be less than or equal to 1. As such if we set this part of the equation to its maximum value of 1, we can determine the maximum velocity for which this equation is applicable:

$$v_{\max} = \frac{2\alpha f}{0.514} = 5253.\text{ms}^{-1} \quad \text{Eqn 4.4}$$

Therefore any velocity returned by the PUNDIT greater than this velocity would be questionable. However, this can clearly not be the case as the beamspread angle will not limit the velocity of a wave in a specimen, thus the equation is only useful in determining the maximum extent of the shadow zone within the rectangular beam specimen, which will not be sensed by the ultrasonic wave. This discrepancy can be explained by the equation only being applicable to frequencies between 0.4 MHz to 10 MHz. If Equation 5.2 was used for a wet log (with a lower longitudinal velocity of c. 3000 ms^{-1}) with a diameter of, on average 200 mm, as in Test Series 3 described in Chapter 6, then the beamspread angle would equate to a total of 70° or a 35° half-angle. As such, this equates to a shadow zone in a wet log of 286 mm, far less than the total log length of 3100 mm.

Following the measurement of TOF velocity, density measurements were conducted. The beam was then subdivided into the smaller sections (2000 mm, then subsequently through 1000, 800, 400, and finally 200 mm sections), and PUNDIT™ and density measurements retaken. This allowed for PUNDIT™ to measure the same specimen size as the surface mounted accelerometers. It should be noted that due to cutting up to 5 mm were lost from each section with a cut end, though the lengths were all recorded and individually used to calculate the PUNDIT™ wavespeeds, which should therefore be similar as the wavespeed should not change over a few millimetres. This process of cutting, weighing and measuring was repeated following the removal of the 400 mm Section 10 from the end of the beam to create the 1600 mm Sections A:2 through A:9, then measured using the accelerometers. This was then itself measured and halved, re-measured and so on until each individual 200 mm section (as seen in Table 4.1) had had its density and PUNDIT™ wavespeed calculated for later analysis.

All results were then subjected to analysis establishing the mean, median, maximum, minimum, standard deviation and acceptability at the 95% confidence level for assessment of accuracy. Measured parameters were then compared against each other and with factors believed to influence the speed of wave propagation in the timber.

The density was calculated by using a calibrated electronic balance to determine its mass (to ± 0.0005 kg) and the dimensions taken with a tape measure (length to ± 0.5 mm) and electronic calipers (cross-sectional dimensions to 0.005 mm) under procedures set out in BS EN 384:2004^(4.19).

The size and shape of knots on the surface of each face were observed and recorded as stated in BS EN 1310:1997^(4.20) in the form of KAR measurements (though KAR normally refers to the transverse face only). This wood characteristic, described in Chapter 2, was recorded using a ruler to measure the approximate rectangular surface area of the knot, as well as the type and shape of the knot and its position on the beam. The total knot area of each section was then calculated, as was the KAR;

$$KAR = \frac{A_k}{A} \times 100\% \quad \text{Eqn 4.5}$$

Where:

A = Surface area of the beam side

A_k = total area occupied by knots on the same side

A correlation between this result and the mean velocities for each side and in total for each section was then calculated.

As can be seen from the Figure 4.5, sides A and C whose edges were closest to the pith of the log from which the beam was cut, have a significant (typically 20% to 45% on Side A and 42% to 55% on Side C, though certain sections do have an

anomalously high heartwood content) heartwood content (determined by surface area content).

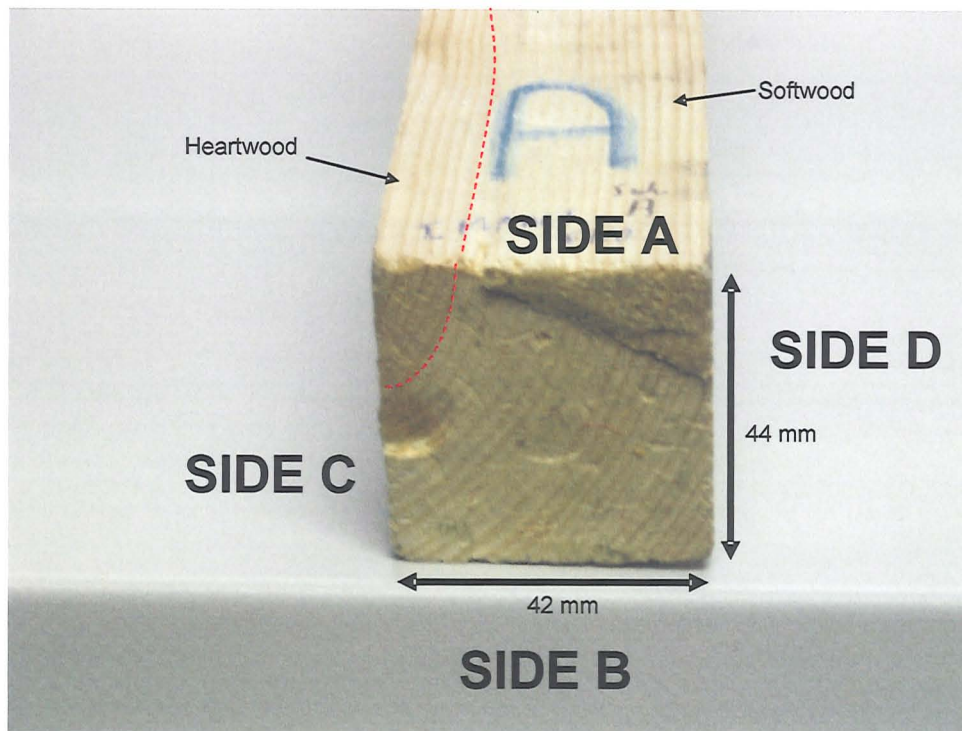


Figure 4.5 Separation of heartwood and softwood content.

The area of the heartwood *per* section was measured using a ruler and converted to a percentage of total area. This was then compared with measured velocity results. The average, maximum and minimum annual growth ring width was also measured using electronic calipers^(4.13). Sides C and D were cut close to perpendicular to the growth ring (as seen from Figure 4.5) and as such the rings they displayed were not true representations of ring width, and hence were not measured. The mean ring width was derived from measurements on sides A and B. The slope of grain or grain angle was assessed under the methodology suggested in BS EN 1310:1997^(4.20). The method consists of measuring the deviation from the axial alignment of the two accelerometers and using Pythagoras's theorem. This is often required in two phases when deviations around knots are involved and not just change in slope of grain. This enables approximation to the true length of longitudinal transmission. The actual

transmission path when the grain deviates from the horizontal will then encompass elements of transverse and tangential components in addition to longitudinal. Any correlations will be observed between the increases or decreases in actual path length and the variable longitudinal wavespeed as measured by the accelerometers.

4.2 TOF velocities

This section presents the results of the velocity tests conducted on the specimen by each section size investigated. Each side's results are presented, followed by and averaging of the velocity results for comparison with the PUNDIT™ velocity.

4.2.1 200 mm sections

Figures 4.6 to 4.8 show the mean (black diamonds), median (black lines within box), inter-quartile ranges (yellow boxes) and overall range (error bars) of the 30 longitudinal velocity tests on each 200 mm section of Sides A and B. Tabulated results that produced these graphs are shown in Appendix B. The same pattern is repeated during subsequent sections. Figure 4.6 shows the velocity data from the 30 tests on side A at 200 mm spacings.

The mean section velocity and standard deviation of the 30 TOF velocity tests in each section was calculated by Eqns 4.6 and 4.7 respectively:

$$\bar{x} = \frac{\sum x}{n} \quad \text{Eqn 4.6}$$

$$SD = \sqrt{\frac{(x - \bar{x})^2}{(n - 1)}} \quad \text{Eqn 4.7}$$

As seen in Figure 4.6, Section A:7 had the highest mean velocity (6711 ms^{-1}), as well as the largest range of velocities (4444 ms^{-1}). Section A:11 had the lowest mean velocity (5183 ms^{-1}). The standard deviations ranged from 531 ms^{-1} (A:3) to 849 ms^{-1} (A:7).

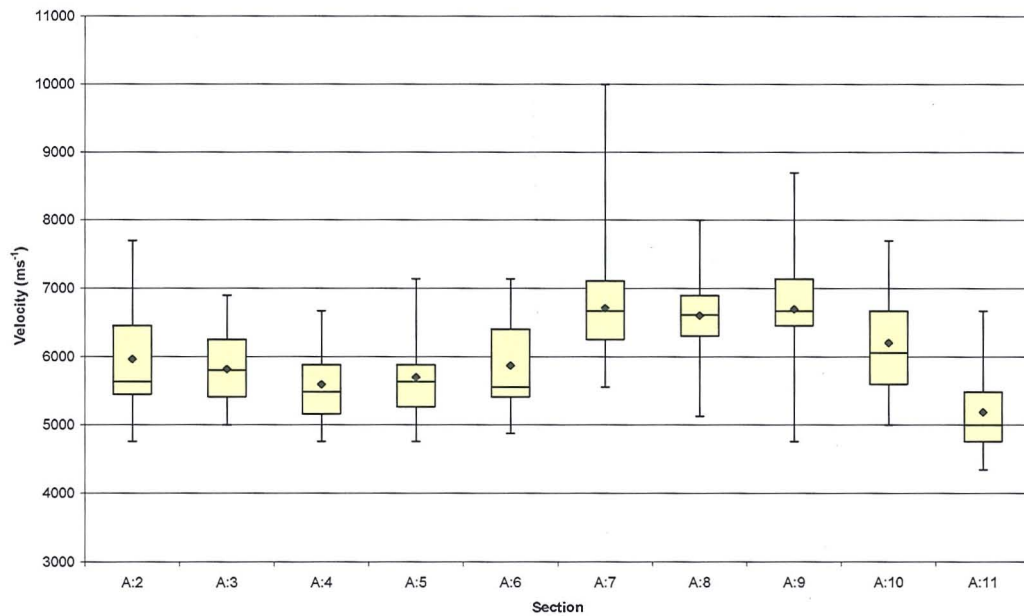


Figure 4.6 Side A velocities by 200 mm section

Figure 4.7 shows the velocity data from the 30 tests on Side B. It can be seen from this graph that Section A:9 had the highest mean velocity (6118 ms^{-1}). Section B:3 had the lowest mean velocity (4016 ms^{-1}). The standard deviations ranged from 285 ms^{-1} (B:7) to 484 ms^{-1} (B:11).

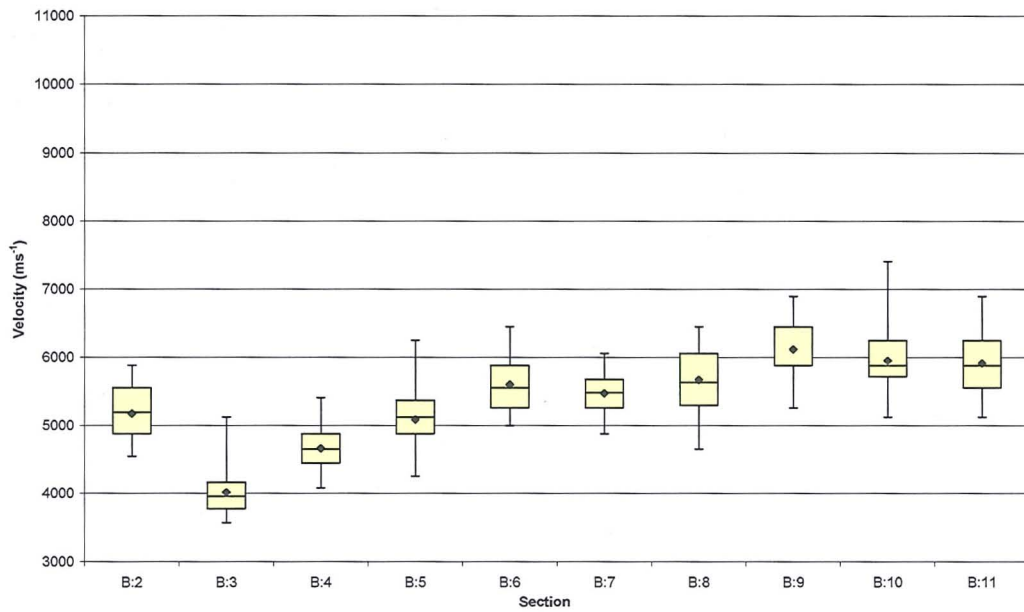


Figure 4.7 Side B velocities by 200 mm section.

Figure 4.8 shows the velocity data from the 60 tests on Side A and Side B combined at 200 mm spacings. The combination of Side A and Side B Sections, and where stated Side C sections (*i.e.* ≥ 400 mm sections), are presented as T Sections. Therefore, the combination of Section A:2 and B:2 is presented as Section T:2. It can be seen from this graph that Section T:9 had the highest mean velocity (6405 ms^{-1}). Section B:3 has the lowest mean velocity (4915 ms^{-1}). The standard deviations ranged from 611 ms^{-1} (B:10) to 1010 ms^{-1} (B:3).

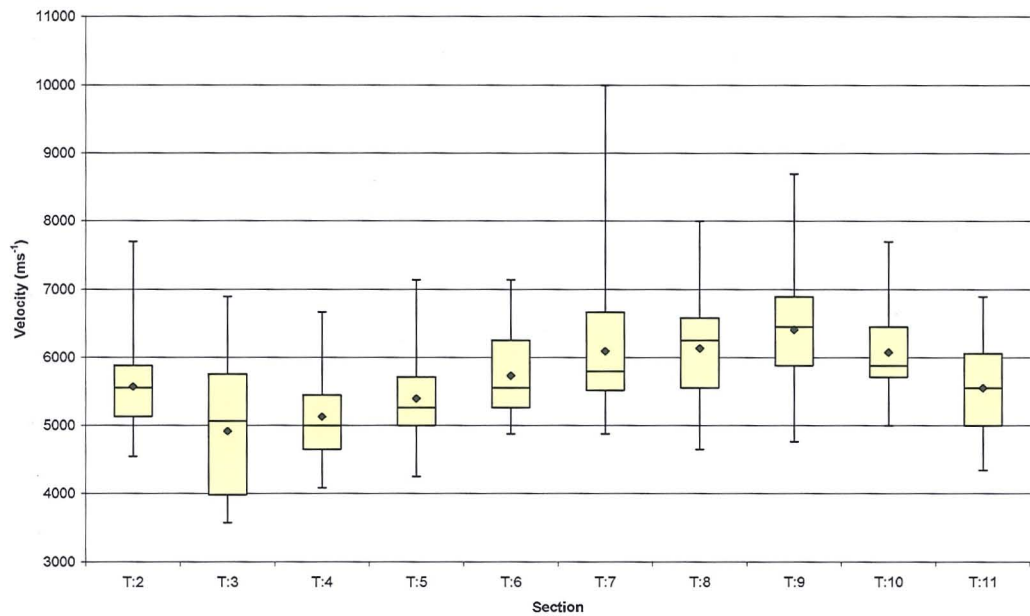


Figure 4.8 All sides' average velocities by 200 mm section.

Figure 4.9 uses a line graph to display a comparison of the mean velocities by 200 mm section shown in Figures 4.6 and 4.7. Also displayed is the mean velocity of Side A and Side B combined (as shown in Figure 4.8), as well as the PUNDIT™ derived longitudinal velocity for each section.

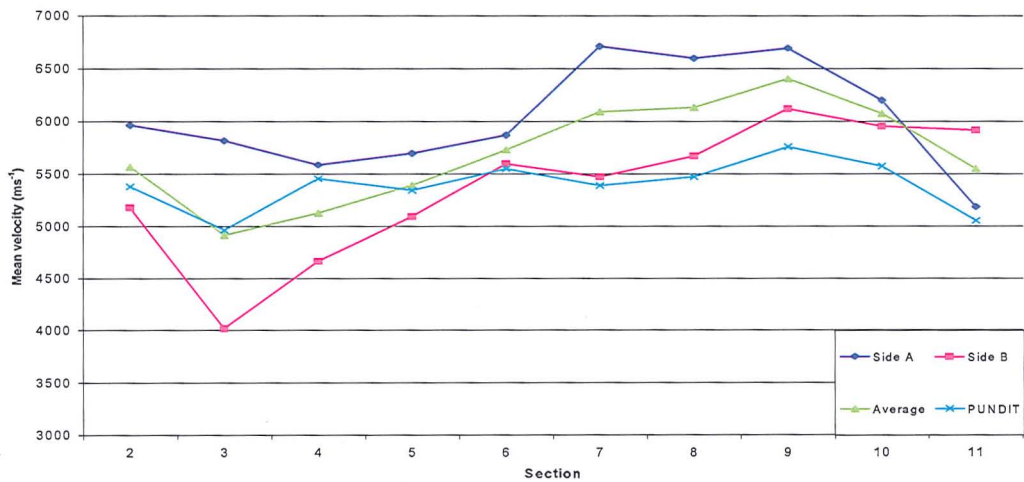


Figure 4.9 Comparison of Side A, Side B, average of Sides A and B combined, and PUNDIT™ mean velocities by 200 mm section.

4.2.2 400 mm sections

Figure 4.10 uses a line graph to display a comparison of the mean velocities by 400 mm section. Also displayed is the average mean velocity of Side A, Side B and Side C combined, as well as the PUNDIT™ derived longitudinal velocity for each section.

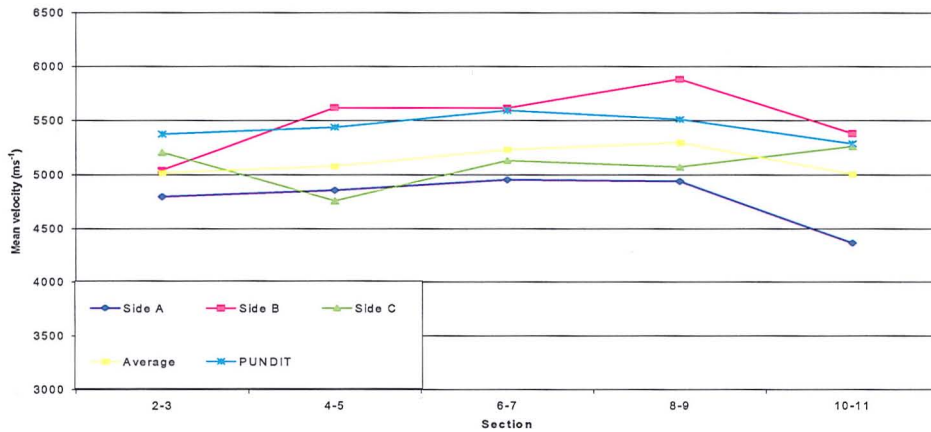


Figure 4.10 Side A, Side B, Side C, average of Sides A, B and C, and PUNDIT™ mean velocities (ms⁻¹) by 400 mm section.

It can be seen that Section A:8-9 had the highest mean velocity (4938 ms⁻¹) for Side A. Section A:10-11 had the lowest mean velocity (4363 ms⁻¹) for Side A. The standard deviations ranged from 131 ms⁻¹ (A:4-5) to 263 ms⁻¹ (A:8-9). Section B:8-9 has the highest mean velocity (5882 ms⁻¹) on Side B. Section B:2-3 had the lowest mean velocity (5040 ms⁻¹). The standard deviations ranged between 198 (B:2-3) and 291 (B:10-11). Section C:10-11 had the highest mean velocity (5264 ms⁻¹) on Side C. Section C:4-5 had the lowest mean velocity (4757 ms⁻¹). The standard deviations ranged between 96 (C:4-5) and 307 (C:2-3).

When looking at the average velocity of all 3 sides tested by the oscilloscope method, Section T:8-9 has the highest mean velocity (5296 ms⁻¹). Section T:10-11 has the lowest mean velocity (5003 ms⁻¹). The standard deviations ranged between 294 (T:2-3) and 506 (T:10-11).

4.2.3 800 mm sections

Figure 4.11 uses a line graph to display a comparison of the mean velocities *per* 800 mm sections for each side. Also displayed is the average mean velocity of Side A, Side B and Side C combined, as well as the PUNDIT™ derived longitudinal velocity for each section.

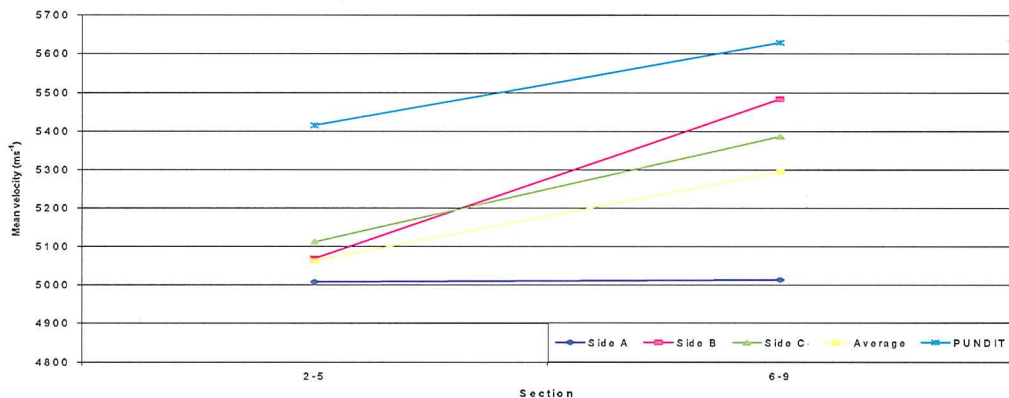


Figure 4.11 Side A, Side B, Side C, average of all sides and PUNDIT™ velocities by 800 mm section.

It can be seen from this graph that Section A:6-9 had the highest mean velocity (5013 ms^{-1}), but this is only 6 ms^{-1} higher than Section A:2-5. The standard deviations ranged from 141 ms^{-1} (A:2-5) to 189 ms^{-1} (A:6-9).

Section B:6-9 had the highest mean velocity (5484 ms^{-1}) on Side B, whilst Section B:2-5 had a mean velocity of 5068 ms^{-1} . The standard deviations ranged between 168 (B:6-9) and 194 (B:2-5). Section C:6-9 had the highest mean velocity (5387 ms^{-1}) for Side C, whilst Section C:2-5 had a mean velocity of 5112 ms^{-1} . The standard deviations ranged between 107 (C:2-5) and 114 (C:6-9). When all sides' velocities are averaged, Section T:6-9 had the highest mean velocity (5295 ms^{-1}), whilst Section T:2-5 had a mean velocity of 5065 ms^{-1} . The standard deviations ranged between 156 (T:2-5) and 259 (T:6-9).

4.2.4 1600 and 2000 mm sections

Since the 1600 mm spacing involved the testing of only one section in each case, Figures 4.12 displays a boxplot comparison of the two spacings as tested on each

of Sides A, B, and C, the average of all sides, and the PUNDIT™ derived velocities. Since the PUNDIT™ velocities were based on only one test *per* section (after a consistent transit time was displayed), there was no range of velocities for each test. It can be seen from Figure 4.12 that PUNDIT™ returned the highest velocity (5637 ms⁻¹), whilst the range between sides A, B and C was 69 ms⁻¹, the average of the combined sides being 390 ms⁻¹ below the PUNDIT™ velocity. The standard deviation for the three sides ranged between 97 ms⁻¹ (Side C) and 195 ms⁻¹ (Side B). The same pattern in velocity and ranges was seen for the 2000 mm sections, though the velocities were consistently lower at 5055 ms⁻¹ for Side A, 5169 ms⁻¹ for Side B, 5172 ms⁻¹ for Side C, a mean velocity averaged from all tested sides of 5132 ms⁻¹. The PUNDIT™ velocity was also lower than in the 1600 mm section, at 5433 ms⁻¹.

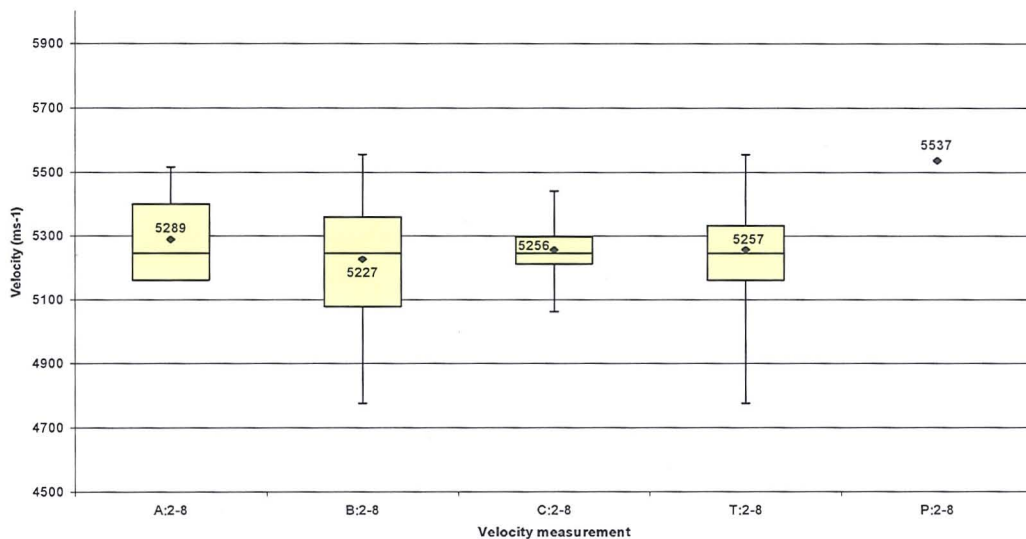


Figure 4.12 Comparison of Sides A, B, and C, all sides combined (T), and PUNDIT™ data for the 1600 mm section.

Using Eqn 4.8 for one-dimensional wave propagation, a MoE_d value for the 2000 mm section can be calculated:

$$MoE_d = V^2 \cdot \rho \quad \text{Eqn 4.8}$$

Where:

MoE_d = Young's modulus (GPa)

V = measured velocity (ms⁻¹)

ρ = density (kgm^{-3})

The mean velocity averaged from all tested sides along the 2000 mm section, combined with the measured density, equated to a MoE_d value of 14.5 GPa. The same calculation using the PUNDIT™ derived velocity equates to a MoE_d of 16.3 GPa, thus producing a difference between the hammer impact and ultrasonic derived MoE_d values of 1.8 GPa.

Figure 4.13 shows a line-graph comparison of the mean velocity average of all sides *per* section corresponding to the size of section tested, *i.e.* for the 200 mm Section 2 each individual mean velocity from the 200 mm test was used (*i.e.* T:2), whilst at the 400 mm section spacing the mean velocity for all sides from T:2-3 was used, and so on. Figure 4.14 uses the same type of display, but instead shows the PUNDIT™ velocities by section for each test.

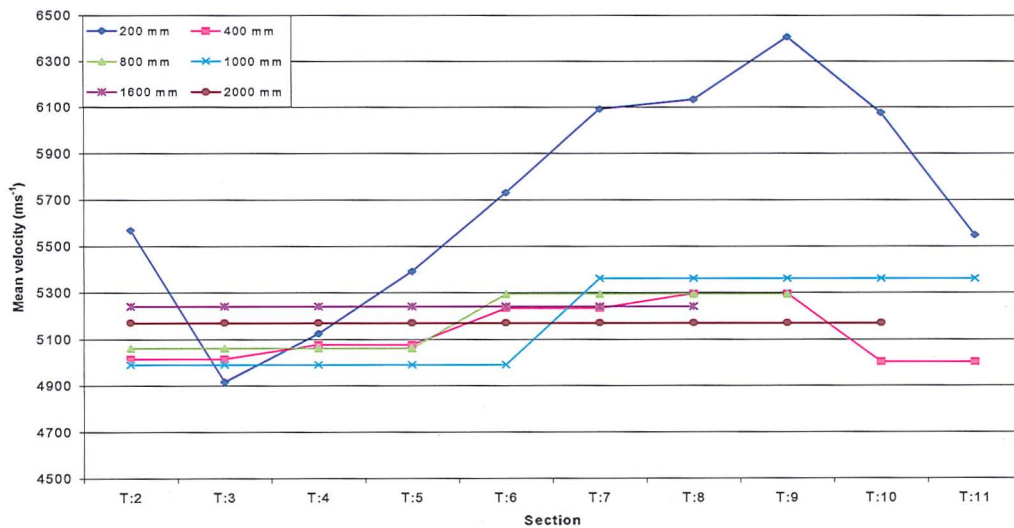


Figure 4.13 Comparison of the mean velocities for all sides (T) by section for each section spacing.

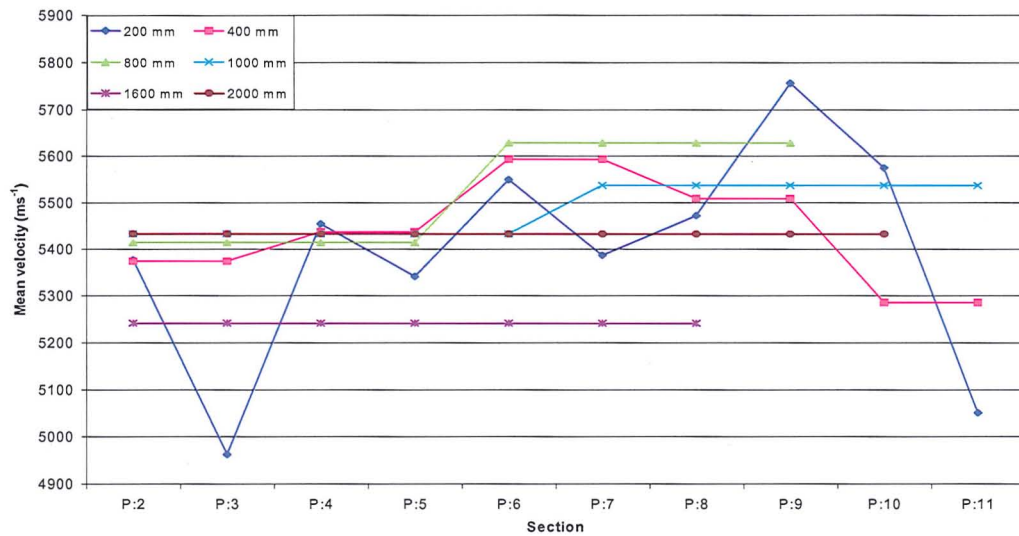


Figure 4.14 Comparison of the PUNDIT™ velocities by section for each section spacing.

4.3 Timber non-acoustic parameters

Table 4.2 presents the average non-acoustically measured timber parameters by 200, 400, 800, 1600 and 2000 mm sections for all four longitudinal sides (A to D) combined. The density and ring width will be the same regardless of timber side, as they are cross-sectional quantities. Table 4.3 displays (for later comparison with side-specific velocities); the KAR calculated for each side of the beam tested by acoustical methods (A to C); the heartwood percentage calculated for sides A and C, sides B and D having no surface heartwood content; the increase in path length (in mm) for an acoustic wave calculated by deviations in grain angle from the longitudinal for each side of the beam tested by acoustical methods (A to C). Blank cells for KAR columns indicate no knots in that section, as can be seen in Table 4.1. Blank cells in path length columns indicate no deviation in grain angle, thus no change in path length from the longitudinal section length.

Table 4.2 Values for non-acoustically measured timber characteristics: density (ρ); KAR; mean ring width (RW); heartwood (HW); and the average path length increase *per section*.

Section	Section length (mm)	ρ (kgm ⁻³)	KAR (%)	RW (mm)	HW (%)	Path length increase (mm)
T:2	200	502	0.00	2.40	19	0.00
T:3	200	612	2.02	2.60	23	0.11
T:4	200	515	0.00	2.43	19	0.00
T:5	200	542	1.61	2.80	20	0.13
T:6	200	546	0.34	2.98	19	0.36
T:7	200	545	1.06	2.70	22	0.12
T:8	200	591	0.70	2.80	22	0.07
T:9	200	551	0.00	2.50	21	0.00
T:10	200	558	0.79	2.84	27	0.12
T:11	200	558	0.64	2.73	19	0.57
T:2-3	400	557	1.01	2.50	21	0.12
T:4-5	400	527	0.80	2.61	20	0.13
T:6-7	400	545	0.70	2.84	20	0.48
T:8-9	400	570	0.35	2.80	21	0.07
T:10-11	400	560	0.72	2.86	23	0.69
T:2-5	800	541	0.91	2.79	21	0.25
T:6-9	800	558	0.52	2.87	21	0.55
T:2-9	1600	550	0.72	2.83	21	0.79
T:2-11	2000	552	0.72	2.85	21	1.48

Table 4.3 Values for non-acoustically measured timber characteristics by side: KAR; heartwood (HW); and the path length increase for that side *per section*.

Section	Section length (mm)	Side A KAR (%)	Side B KAR (%)	Side C KAR (%)	Side A Heartwood (%)	Side C Heartwood (%)	Side A path length increase (mm)	Side B path length increase (mm)	Side C path length increase (mm)
2	200				27	50	0.01		
3	200	1.43	1.64	2.95	45	48		0.22	0.34
4	200				32	44			
5	200		3.18	3.25	27	55	0.01	0.25	
6	200	1.25			32	42	0.32	0.40	0.17
7	200	3.50		0.73	42	47	0.08	0.16	0.03
8	200	0.41		0.91	32	56		0.13	0.05
9	200				32	50			
10	200		1.43	1.73	30	77	0.04	0.20	0.81
11	200		1.03	1.55	20	55	0.12	1.01	0.16
2:3	400	0.72	0.82	1.48	36	49	0.01	0.22	0.34
4:5	400		1.59	1.63	30	49	0.01	0.25	
6:7	400	2.38		0.36	37	44	0.40	0.56	0.20
8:9	400	0.20		0.45	32	53		0.13	0.05
10:11	400		1.23	1.64	25	66	0.16	1.21	0.97
2:5	800	0.36	1.20	1.55	33	49	0.02	0.47	0.34
6:9	800	1.29		0.41	34	49	0.40	0.69	0.26

2:9	1600	0.82	0.60	0.98	34	49	0.42	1.17	0.59
2:11	2000	0.66	0.73	1.11	32	52	0.58	2.38	1.57

4.4 Timber parameters: relation to velocity

Figure 4.15 displays the density, corresponding oscilloscope velocity and PUNDIT™ velocity for each 200 mm section, the velocity being the average of all sides tested at that spacing. The data used in the generation of each graph are displayed in the grid immediately below each section.

The square of the Pearson product moment correlation coefficient, r , was used in this chapter to provide the degree of colinearity between two separate sets of known parameter values (x and y). The equation used is provided in Eqn 4.9:

$$r = \frac{\sum (x - \bar{x})(y - \bar{y})}{\sqrt{\sum (x - \bar{x})^2 \sum (y - \bar{y})^2}} \quad \text{Eqn 4.9}$$

Figure 4.16 shows two scatter plots displaying the linear correlation between the calculated density and corresponding velocity for each of the ten 200 mm sections. It can be seen that whilst the PUNDIT™ velocities displayed a weak correlation to density, no correlation between either Side A, Side B or the average velocity of the two sides combined existed.

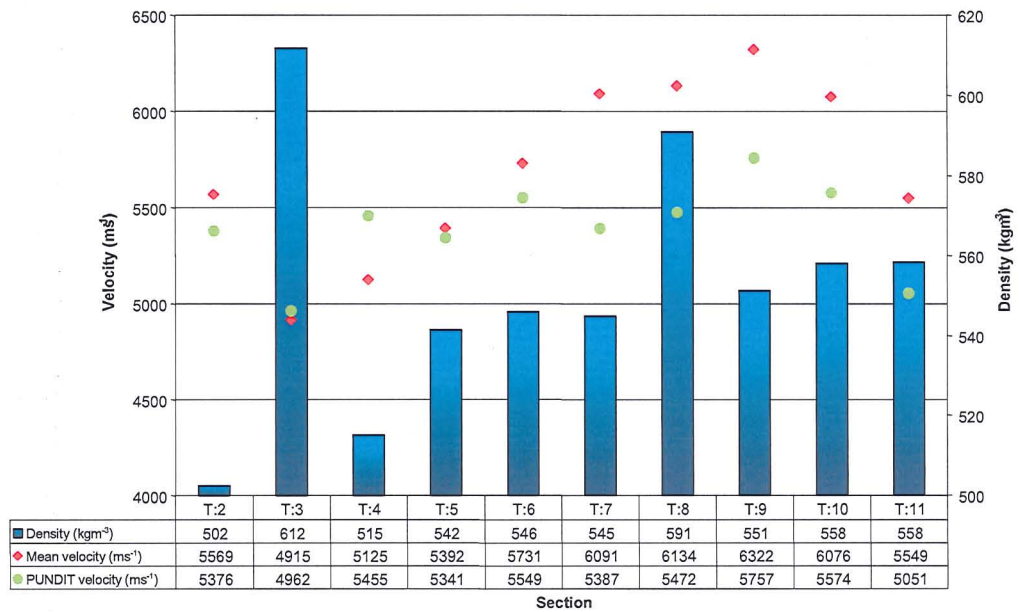


Figure 4.15 Densities (blue columns) and corresponding mean oscilloscope velocities (red diamonds) averaged from Sides A and B as tested by 200 mm section. PUNDIT™ velocities by section are displayed as green circles.

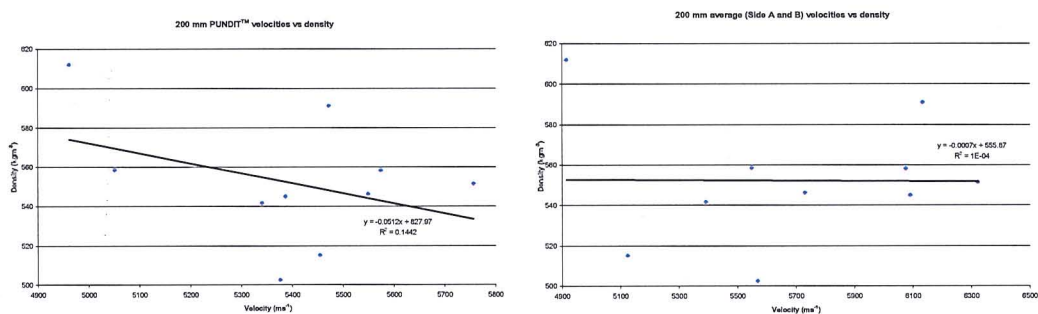


Figure 4.16 Correlations between density and velocity measurement values on 200 mm sections.

There were only five density values and velocities for the 400 mm sections, and no more than two for each subsequent increase in section length, thus correlations by section were not possible. Figure 4.17 shows a scatter plot displaying the complete lack of a linear correlation between the calculated densities and corresponding velocity for all spacing measures, in total 19 velocity and corresponding density measures.

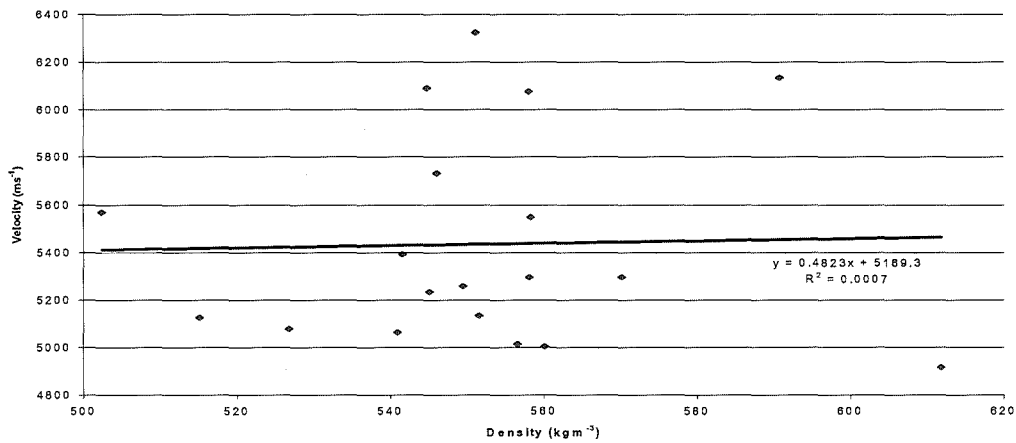


Figure 4.17 Correlations between density and corresponding velocity measurement values (averaged from all measured sides) on all section spacings (total 19 measures).

Figure 4.18 shows four scatter plots displaying the linear correlation between the calculated KAR and corresponding velocity for each of the ten 200 mm sections, for sections where KAR \neq 0. It can be seen that the combined oscilloscope velocities displayed the highest correlation ($R^2 = 0.51$) and PUNDIT™ displayed a weaker correlation ($R^2 = 0.35$).

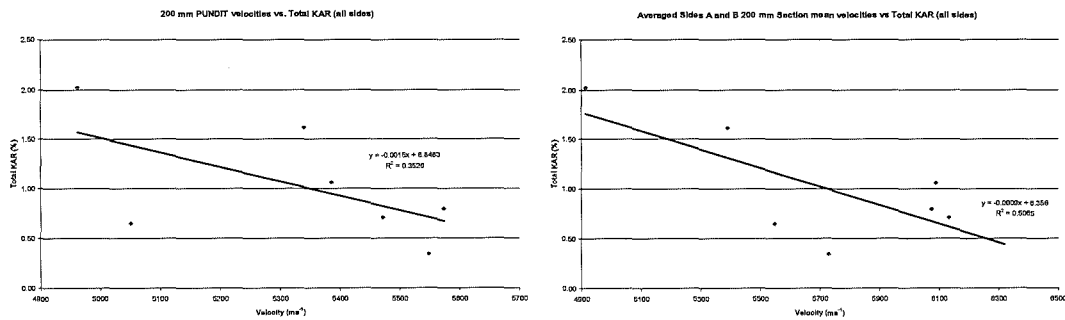


Figure 4.18 Correlations between KAR and velocity measurement values on 200 mm sections. Note that non-zero KAR values have been removed.

Figure 4.19 graphically displays the KAR (blue columns) and corresponding velocity (red line) for each 200 mm section, the velocity being the average of all sides tested at that spacing. The data used in the generation of each graph are displayed in the grid immediately below each section. Figure 4.20 uses the same display to show the KAR and velocities by 400 mm section.

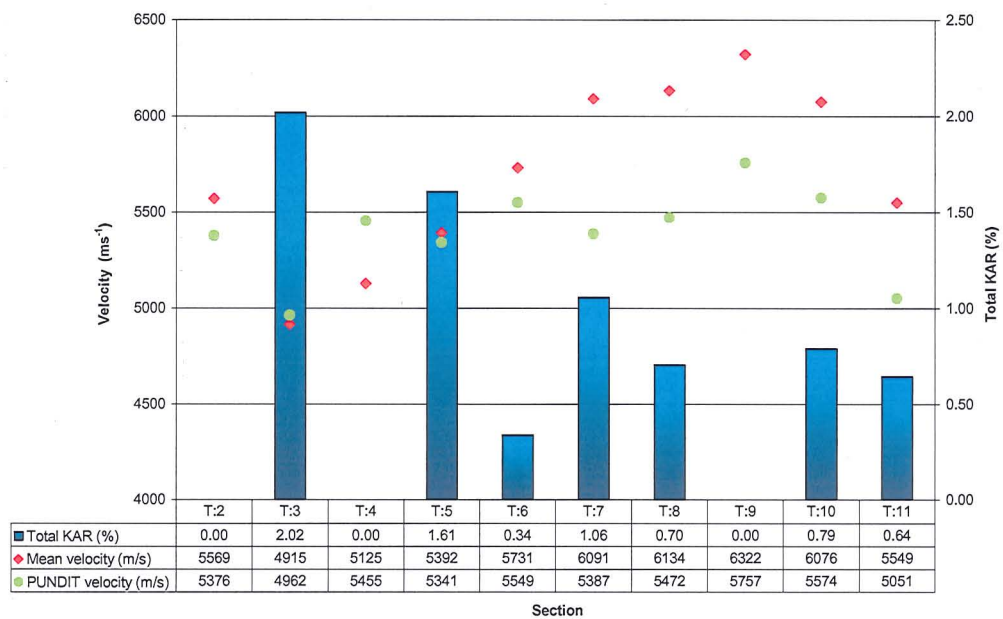


Figure 4.19 KAR (blue columns) and corresponding mean velocity (red line) from all sides tested per 200 mm section.

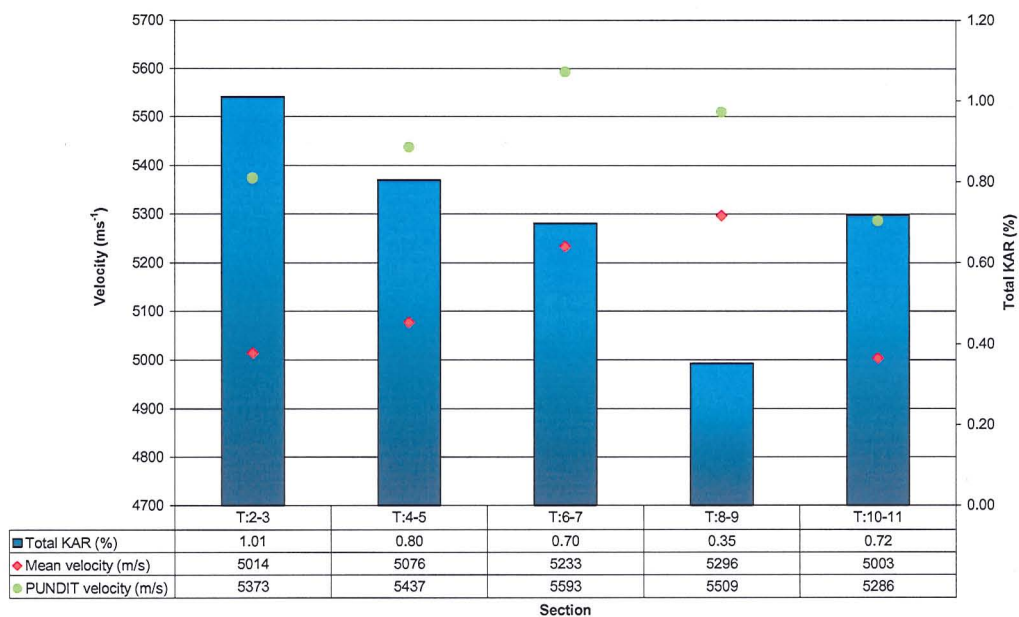


Figure 4.20 KAR (blue columns) and corresponding mean velocity (red line) from all sides tested per 400 mm section.

With regards to measurements made on the two 800 mm sections, the KAR was seen to drop from 0.9% to 0.52% KAR. Conversely, the average velocities rose between subsequent sections from 5062 ms^{-1} to 5295 ms^{-1} and from 5414 ms^{-1} to

5628 ms^{-1} for the oscilloscope derived, and PUNDIT™ derived, velocities respectively.

Figure 4.21 shows a scatter plot displaying the linear correlation between the calculated KAR and corresponding velocity for all spacing measures, in total 19 velocity and corresponding KAR measures (for measures of KAR not equal to zero).

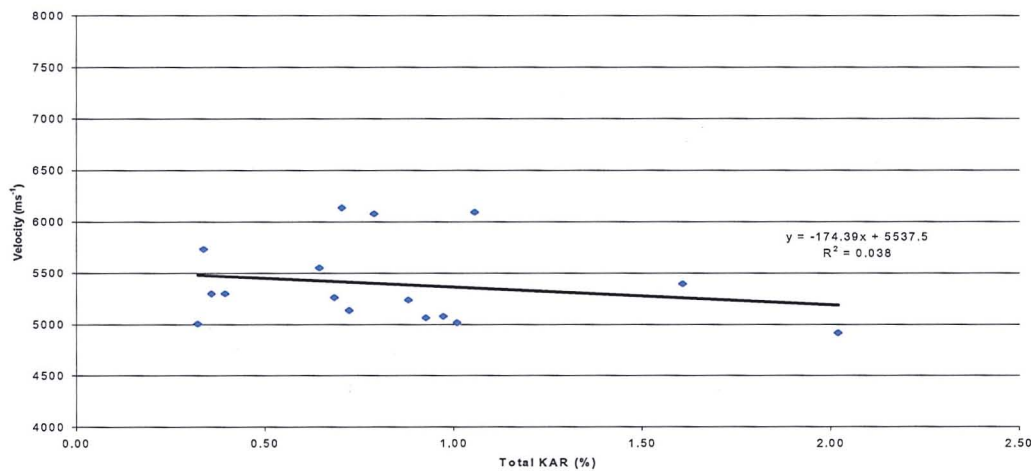


Figure 4.21 Correlations between KAR and corresponding velocity measurement values on all section spacings (total 19 measures).

There was no correlation between measures of heartwood or ring width on the 200 mm, 400 mm or 800 mm sections and any measure of velocity.

As can be seen from Figure 4.22, PUNDIT™ velocities showed a very weak correlation ($R^2 = 0.18$) to path length for the 200 mm sections, whilst no significant correlation was observed between measured oscilloscope velocities by side or when averaged.

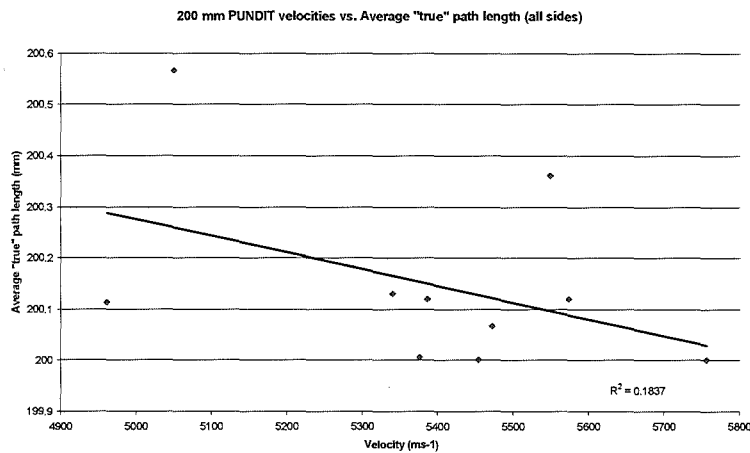


Figure 4.22 Correlations between calculated "true" path length and velocity measurement values on 200 mm sections.

Table 4.4 shows the correlations (R^2) between the non-acoustically measured parameters (density, total KAR, mean heartwood content, mean ring width, and mean "true" path length) for the 200 mm sections based on 10 corresponding sectional values. Table 4.5 presents the 400 mm datasets for the same categories, based on five values for each category.

Table 4.4 R^2 value derived between non-acoustical parameters as measured on 200 mm sections (ten values per parameter).

200 mm sections	Density (kgm ⁻³)	Total KAR (%)	Mean heartwood content (%)	Mean ring width (mm)	Mean path length (mm)
Density	X	0.43	0.24	0.16	0.03
Total KAR	X	X	0.21	0.12	0.01
Mean heartwood content	X	X	X	0.06	0.09
Mean ring width	X	X	X	X	0.31
Mean path length	X	X	X	X	X

Table 4.5 R^2 value derived between non-acoustical parameters as measured on 400 mm sections (five values per parameter).

400 mm sections	Basic density	Total KAR (%)	Mean heartwood content (%)	Mean ring width (mm)	Mean path length (mm)
Density	X	0.22	0.55	0.11	0.00
Total KAR	X	X	0.01	0.49	0.00
Mean heartwood content	X	X	X	0.12	0.28
Mean ring width	X	X	X	X	0.44
Mean path length	X	X	X	X	X

4.5 Discussion of results

Issues arising from the results of this test series are discussed in the following sub-chapters.

4.5.1 Test method

Certain issues arose during testing concerning the test method. The determination of the deviation from the background level was subject to the author's ability to distinguish between unforced background vibrations caused by the free suspension of the cables, all other sources having been isolated by the foam mounts, which often triggered the stop function on the oscilloscope. As the beam was freely suspended, following impact excitation it took considerable time for the beam to come to rest where the motion of the beam did not trigger the stop function. To compensate, the trigger level was increased, though this meant a forceful hammer blow was required, which occasionally created problems in dislodging accelerometers. As such, future recommendations would be to not use free suspension of the sample. Additionally, with the lack of a cursor function on the oscilloscope and the need for manual measurement of the deviation time, an automated system for wave arrival time recognition is highly recommended.

It should be noted that whilst the environmental condition of the sample and test environment were consistent, other stiffness influencing factors such as the MFA could not be determined for the beam or its variation between sections.

4.5.2 200 mm sections: velocity variations

Section A:2 begins at just under 6000 ms^{-1} and 5174 ms^{-1} for B:2 (see Figures 4.6 and 4.7) using oscilloscope-derived velocities. On progression to Section 3, there was a clear drop in velocity on both sides, though more drastic on Side B on which it forms the floor of a general trough in velocity until Section 6 (*i.e.* recorded mean velocities for sections until Section 6 were lower than Section 2). Side A had the floor of this trough in Section 4, from where it rises to a velocity just below that of Section 2. Upon reaching Section 6, the velocity of the two Sides diverges (despite

being within one standard deviation of each other, with Side A rising steeply to its whole beam peak of 6711 ms^{-1} , whilst Side B falls slightly by 124 ms^{-1} . Side A then maintains a high velocity ($> 6500 \text{ ms}^{-1}$) until Section 10, whilst Side B rises sharply through Sections 8 and 9 before falling in Section 10. Both sides continue this fall into Section 11, but the Side A decrease (of 1017 ms^{-1}) was more dramatic compared to a fall of just 40 ms^{-1} on Side B.

When averaging the response of the two sides, the pattern clearly showed a large decrease in velocity from Sections 2 to 3 to a trough floor of 4915 ms^{-1} , followed by a continual rise in velocity, past the initial velocity of Section 2 in Section 6, to a peak mean velocity of 6405 ms^{-1} in Section 9. This is then followed by a sharp, near linear decline in the mean velocity, heavily affected by the dramatic reduction in Side A velocity. Overall, apart from a slight decrease during Section 7 for Side B alone, the mean velocity pattern of rises and falls is identical to the Side B pattern.

4.5.2.1 Issues with 200 mm velocities

In the 200 mm sections, Side A had a consistently higher velocity than in Side B (See Figure 4.9). However, in sections of 400 mm and greater, Side B consistently had a higher velocity than Side A (though by the 2000 mm section the velocities were roughly equal). Side A also had a consistently higher standard error and standard deviation than Side B. This standard deviation can be seen to reduce with increasing section size. There was the potential that the ability of the tester to accurately recognise the deviation from the horizontal increased with increasing number of tests (Side B having been tested after Side A).

If predictions of the average velocities were made combining the 200 mm sections to form 400 mm sections, Side A would have been consistently higher than Side B. Whilst the general pattern of velocity behaviour by section would be consistent, the significantly lower velocity levels of the 400 mm sections (generally *c.* 1500 ms^{-1} lower) would suggest a problem with the 200 mm measurements. Most noticeably, not one 400 mm velocity measure on either side is above 6000 ms^{-1} , compared to five measures on the 200 mm sections, including one on Side B. Previous studies,

as noted in Chapter 3, would suggest that a longitudinal velocity of this level is unrealistic for any timber specimen. When comparing the convergence to the mean result of Sides A and B, as shown in Figure 4.23, it may be the case that Side A is subject to a greater error than Side B, most likely the result of this being the first test series conducted.

However, whilst Side A velocities were clearly overestimated, in most cases the 30 tests conducted ensured an adequate convergence. Tests on Side B can clearly be seen to converge sooner in number of tests (to within 1 standard deviation) than Side A. Indeed the clearest evidence for this apparent overestimation of the actual velocity comes from the PUNDIT™ tests, which in every other section size can be seen (as is discussed later) to be of a reasonably consistent percentage higher than the oscilloscope-derived velocity averages. In the 200 mm sections, the difference between PUNDIT™ and average oscilloscope velocities ranged from +6% for Section 4 to -13% for Section 7. Sections 7 to 11 oscilloscope average velocities were consistently > 10% higher than PUNDIT™ velocities. It should be noted that the accelerometer on the Section 6 to 7 boundary on Side A intersected with the occurrence of a large knot (as seen in Figure 4.6), which may have unduly influenced the measured velocity.

However, it should be noted that the PUNDIT™ does reflect the same sections of peak (Section 9) and basal (Section 3) velocities, whilst also reflecting the average oscilloscope pattern or prominent rises and falls (particularly in the early and later sections), though maintaining an undulating plateau of velocity within the middle sections.

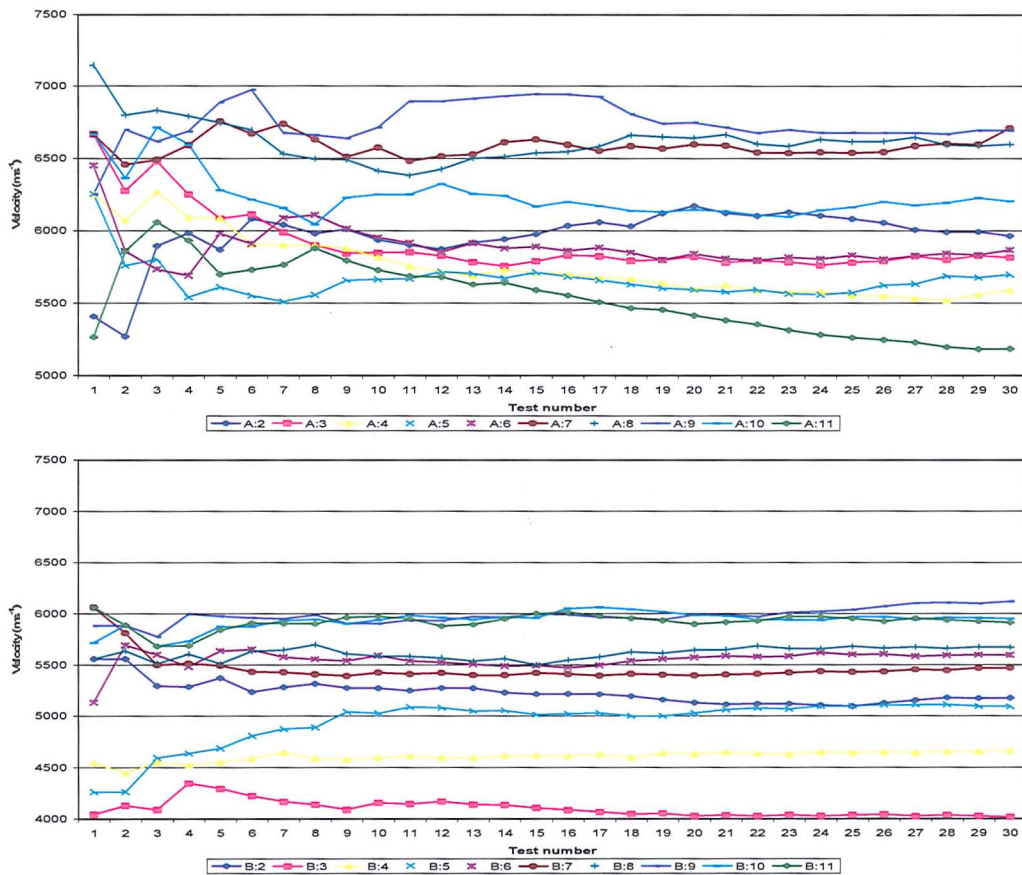


Figure 4.23 Convergence of 200 mm individual test velocities within each section (Side A top graph, and Side B bottom graph).

4.5.3 400 mm and greater section distances

As a result of the general overestimation of the velocities on both sides, predicted values for 400 mm section velocities were also overestimated. However, the combined average of Sides A, B, and C 400 mm section velocities in general, seen in Figure 4.11, follow a consistent trend of rises and falls set by the combined average 200 mm velocities. In terms of specific sides, the pattern of low velocities predicted by the combination of sections 2 and 3 (the latter being shown in have a low individual velocity on all sides) and Section 10 and 11, were reflected in the 400 mm sections 2:3 and 10:11. Similarly, all sides for the 400 mm sections attain a peak velocity in Section 8:9, comparing favourably with the same pattern in Section 9 alone on all sides.

However whilst its inclusion in the averaged velocity by section of all measured sides does not affect the overall pattern, Side C (not measured by 200 mm section) diverts from the overall agreement between 200 and 400 mm section velocities by dropping during Section 4:5, whilst Sides A and B, as expect, rise. Additionally, C10:11 can be seen from Figure 4.11 to have a peak velocity for the beam. However, the overall range in Side C section velocities was smaller than for both Sides A and B. Side A was seen to have a shallower pattern of rises and falls to and from the middle sections, than Side B.

In comparison with the PUNDIT™ derived velocities, the average of all three measured sides appears consistently less than the PUNDIT™ velocities. The greater PUNDIT™ velocities ranged between +4% and +7%, with an average of +6%. Interestingly, the lowest difference was in Section 8:9, which had the highest mean velocity for all sides combined. Figure 4.24 displays the convergence to the mean velocity by Section for oscilloscope tests on Sides A, B, and C.

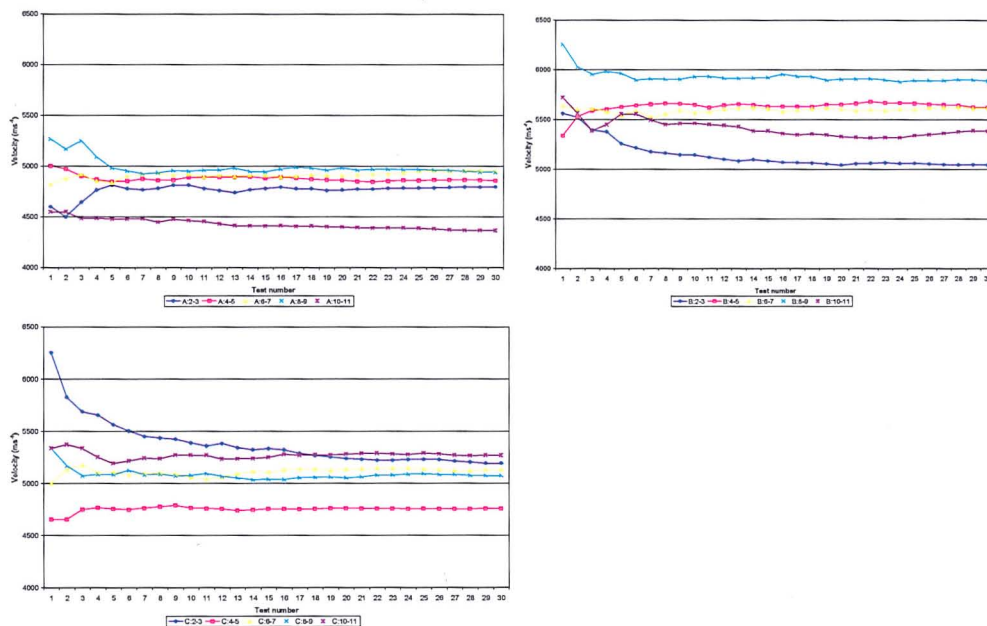


Figure 4.24 Convergence of 400 mm individual test velocities (Clockwise from top-left: Side A, Side B, and Side C).

Looking at the graph of 800 mm sections, Figure 4.13, with a finer resolution on the y-scale, it was clear that there was a rise in wave velocity, between Sections 2:5 and 6:9, of similar proportions on sides B and C, taking the combined average of all sides with them. Side A, however, had mean velocities rising by only 6 ms⁻¹

between the subsequent sections. The PUNDIT™ tests mirror this rise, with a 7% and 6% greater velocity than the oscilloscope average. The convergence to the mean at 800 mm can be seen, in Figure 4.25, to be far sharper than at previous scales, converging to within 1% of the 30-test mean velocity within 5 tests on all sides.

This pattern of rapid convergence continues with increasing length of accelerometer separation. A similar convergence to within 1% of the 30-test mean velocity on each side can be seen in Figure 4.26, showing the 2000 mm sections. Again convergence was within 5 tests. Contrasting Figures 4.26 and 4.25 with Figure 4.24 for 400 mm sections, increasing the distance of separation can be seen to decrease the number of tests required to acquire a repeatable and stable value for mean velocity.

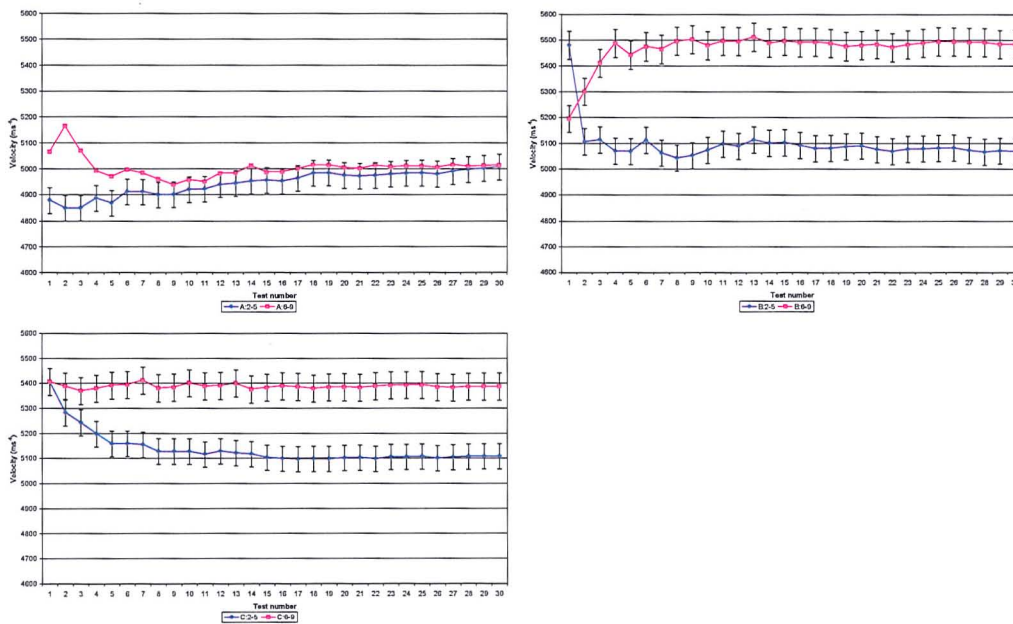


Figure 4.25 Convergence of 800 mm test velocities (Clockwise from top-left: Side A, Side B, and Side C). Error bars denote 1% of measured velocity.

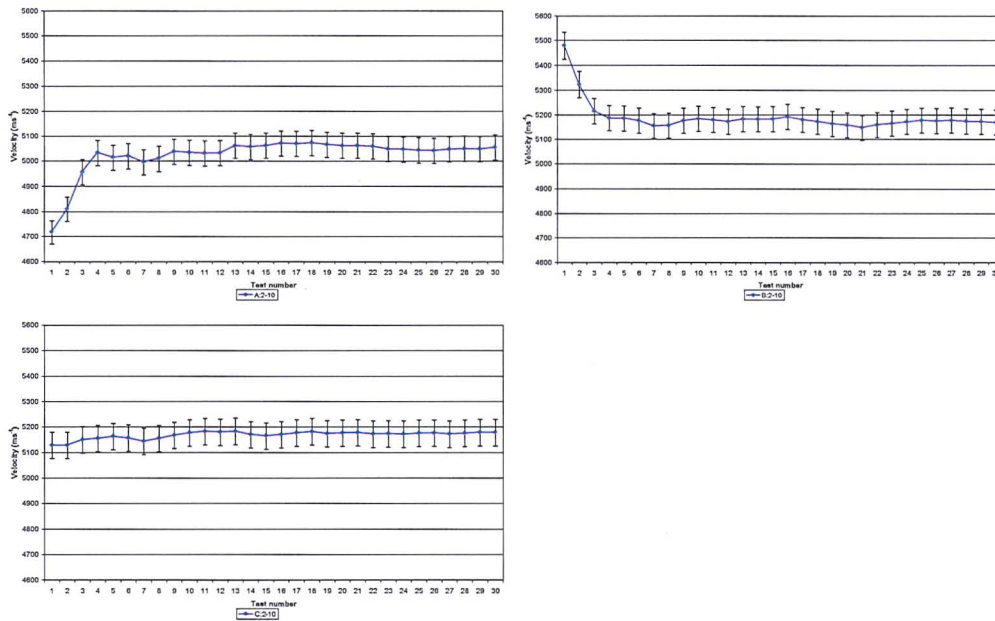


Figure 4.26 Convergence of 2000 mm test velocities (Clockwise from top-left: Side A, Side B, and Side C). Error bars denote 1% of measured velocity.

Similarly, it can be seen by observing the velocity values for each side at 1600 mm and 2000 mm separation that each velocity returned from oscilloscope measurements on each side have converged to individual velocity values $\pm 1\%$ of the average velocity of all sides. The exception being the 2000 mm oscilloscope test for Side A, which was within $\pm 2\%$ of the mean velocity from all sides combined. For the 1600 mm tests the range between sides was 62 ms^{-1} , the 2000 mm sections had a range across the sides of 117 ms^{-1} , but only 3 ms^{-1} between Sides B and C. In comparison to the ranges of the 800 mm, 400 mm, and in particular the 200 mm sections, that the side measured to determine the longitudinal wavespeed becomes increasingly irrelevant with increasing distance of separation. This could be explained by the tendency for low-frequency waves to form a planar wavefront (and thus consistent velocity across the cross-section) at larger distances than ultrasonic testing. This was consistent with previous research by Gerhards^(4.20), who observed a reduction in relative error with increasing distance of transducer separation. Based on the work of Divos *et al.*^(4.21), this can be attributed this to the achievement, by the longitudinal wave, of a planar wavefront with increasing transmission distance.

When comparing the mean velocities of the all sides in the 1600 mm and 2000 mm sections (5257 ms^{-1} and 5132 ms^{-1} respectively), it was clear that there was a velocity reducing factor in Section 10:11, as was indicated even in the 200 mm section sizes.

The PUNDIT™ velocities for the 1600 mm and 2000 mm can be seen from Figure 4.14, to take account of this area of velocity reduction, by maintaining a consistent 5% overestimation of the average velocity from all sides tested by oscilloscope. The causes of this overestimation shall be discussed in Section 4.5.6.

4.5.4 Relations between non-acoustic timber properties

In terms of the relations between non-acoustical timber parameters, the limited number of data samples makes conclusions about their relation somewhat tentative, particularly in the case of the 400 mm sections with a maximum of only five data points available for correlation. In general the 400 mm correlations do serve to indicate potential correlations, though these tend to reduce by doubling the data points. However, in relation to the 200 mm sections: the highest correlation was seen between density and total KAR ($R^2 = 0.43$). This positive linear correlation was not surprising given the increased density of knots, and compares favourably with other correlations from Chapter 2. The density values calculated for this specimen were of the order of c. $100\text{-}150 \text{ kgm}^{-3}$ higher than the average value for at Sitka spruce specimen at 12% moisture content.

The weak yet positive linear correlation of density to heartwood was somewhat surprising, given the latter's typically lower density. However, as the calculation of heartwood by surface area included indeterminate areas which intersected with knots, this potentially influenced the result. Similarly this may explain the correlation of KAR to heartwood content, in addition to knots generally being more frequent in juvenile wood^(4.22-4.23). The positive correlation between ring width and path length ($R^2 = 0.31$ in 200 mm) can be explained by the increase in ring width in areas of high knot content, and relation of path length to KAR as previously mentioned.

4.5.5 Relations between velocity and timber properties

In comparison with previous literature outlined in Section 3.2, the lack of a significant correlation between velocity and density or ring width was surprising, with previous correlations being of the order of $R^2 = 0.4$ to 0.5 ^(4.24-4.28). This was most likely due to the samples used in the previous research being generally having significantly less knot content than the sample used here. Similarly the lack of any significant correlation between velocity and heartwood, despite previous research indicating the lower velocity within such juvenile regions^(4.27, 4.29-4.30), can be explained by the existence of a faster path of transmission through the more mature majority of softwood present across the cross-section of the specimen in all sections.

A correlation between the increases in path length per section, calculated from the combination of any increase in grain angle or grain deviation due the presence of knots, would have been expected given the research cited in both chapters 2 and 3 in relation to both its control on both stiffness and tracheids acting as the primary pathway of propagation. The lack of significant correlations of velocities, with the exception of a weak correlation of the PUNDIT™ velocities, to path length was most likely the result of a lack of real deviation compared to the length of the specimen (only an average 1.5 mm deviation per side for the whole 2000 mm section), coupled with the dominating influence of the knot content. The minor correlation of PUNDIT™ velocities to path length ($R^2 = 0.18$, for instances where a change in path length occurred) may due to its smaller wavelength of operation being more susceptible to these minor changes in path length. More likely, the largest increases in path length can be seen to be in sections with large knot content, thus the correlation was most likely a by-product of the greater correlation between velocities and KAR.

It can be seen from Table E3 in Appedix E, and Figure 4.19, that Section 3 had the highest KAR (over all sides) across throughout the beam. It should be noted that this does not mean that Section 3 had the highest knot volume per section, simply the highest knot surface area, a proxy indication.

Figure 4.18 shows the negative linear correlations between both measures of velocity for 200 and 400 mm sections (the latter having a reduced number of data points from which to provide correlations and thus was questionable). A significant negative correlation exists between KAR and longitudinal velocity ($R^2 = 0.51$ and 0.35 for oscilloscope mean and PUNDIT™ velocities respectively). This negative correlation compares well with the previous results of Johansson and Kliger ($R^2 = 0.42$)^(4.31). Traditional theory would dictate that the higher frequency pulse would be subject to increased diversion of its wave path, *i.e.* the higher scattering and reflection of the waveform due to its wavelength in comparison to the size of the defects. Traditional theory would also dictate however that a low-frequency wave is unlikely to see a defect due to the greater wavelength involved.

However, the greater correlation of the low-frequency wave velocity to the KAR, compared to the PUNDIT™, would contradict this traditional theory. It can be seen that from Figure 4.19, that Section 3 was coincident with a drop in all measures of velocity when moving from the clear (knot-free) Section 2. Similarly there is a rise in mean oscilloscope and PUNDIT™ velocity through the knot-free Section 4. However, although Section 5 had the second highest prevalence of knots in the 200 mm sections, the mean oscilloscope velocity (from all sides) through this section was continuously rising at the same rate (possibly increasing slightly) since the low point in Section 3 and it will continue to do so until Section 7. The PUNDIT™ velocity immediately rises to a velocity in Section 4 above that of Section 2, before falling again in section 5, though not as much as in Section 3.

This would indicate that not only was the PUNDIT™ velocity more reflective of the presence of knots, a relative causing a proportional drop in velocity with increasing KAR, but that the recovery to initial velocity levels (from knot-free sections) was more gradual than with the PUNDIT™. The PUNDIT™ velocity per section, for both the 200 and 400 mm sections, maintains an opposite pattern of rises and falls in velocity when compared to the pattern of rises and falls in the KAR. This may be explained however as the PUNDIT™ 200 mm sections were measured individually as sawn 200 mm sections, whilst the oscilloscope based velocities were dependent

on the previous sections setting the initial level of velocity from which it may rise or fall.

If the level had been set particularly low from the preceding section, for example from Section 3, then the velocity can be seen to still be increasing through Section 5 despite a higher knot content, as the influence (or amount) of the knots was still less than it was in Section 3. Thus rather than a cumulative effect of subsequent knots continually lowering the velocity between sections, the effect would seem to be that upon reaching a section with the greatest KAR, the velocity will begin to recover its original (clear-section) speed through subsequent sections provided a section does not exceed this previously set maximum in KAR. Thus continued presence of knots, as in Section 7 and 8, could be said to cause a reduction in the rate of velocity recovery. However, whilst the drop from the maximum velocity in Sections 10 and 11 was consistent with the appearance of knots, this previous theory would indicate that due to the reduced knot content from Section 10 through to 11, the velocity should begin to rise again, which was not the case for both the PUNDIT™ and oscilloscope velocities.

Thus whilst the influence of knots on the velocity was apparent, it was less clear as to the differing effect on low and high frequency wave velocities. It may be the case that live and dead knots, not separated by KAR, do indeed vary in the intensity of the effect of their presence on velocity, but as the same knot appears live on one beam side and dead on another, it was difficult to see a pattern in this relationship.

With increasing section size, 400 mm and 800 mm sections, it becomes apparent that the sections with the higher KAR have a reduced velocity compared to clear sections. With hindsight, the testing of clearer specimens of timber, which may rule out Sitka spruce due to typically high defect content, may have been more appropriate for examining differences in other timber properties due to the perceived dominance of the knot influence.

4.5.6 Differences between low and high frequency velocity

It could be argued that as the PUNDIT™ sends and receives the electrostatic pulse through the wood across the whole specimen cross section, it therefore finds the path of least resistance through each section or sections, thus being less susceptible to defects in a beam unless the defects occur across the entire cross-section. This would be in contrast to the surface mounted accelerometers, for which a wave must travel around a defect to reach the surface. As such, one would expect individual defects to have less influence on the measured PUNDIT™ wavespeed. However, if this were the case, the pattern of the PUNDIT™ velocities would be unlikely to mirror the particular undulations of the average oscilloscope velocities. Additionally the difference between the low and high frequency velocities would be expected to increase, but in this case the difference appears to have stabilised at c. 5% with increasing distance of transducer separation. This consistently higher high-frequency velocity was consistent with values from previous studies^(4.32).

Pure longitudinal velocity should not vary with frequency however. A change in strain rate, according to Divos and Tanaka^(4.33), by one order of magnitude would cause a 1.7% increase in velocity, less than the consistent overestimation observed. In Section 4.2.2, it was noted that the difference in the returned MoE_d values by the oscilloscope and PUNDIT™ methods was 1.8 GPa, using the one-dimensional rod or bar wave equation consistently used to estimate beam longitudinal dynamic stiffness in the literature.

If an estimated value for the Poisson's ratio of Sitka spruce (0.37) was used in relation to the three-dimensional equation for longitudinal wave propagation as shown in Equation 4.10^(4.33-4.35):

$$V_L = \sqrt{\left(\frac{E}{\rho}\right)} \cdot \sqrt{\left\{\frac{(1-\mu)}{[(1+\mu)(1-2\mu)]}\right\}} \quad \text{Eqn 4.10}$$

Where:

V_L = predicted pure longitudinal bulk velocity (ms^{-1})
 MoE_d = Young's modulus (GPa)
 μ = Poisson's ratio (assumed equal in all directions as in a homogenous solid)
 ρ = density (kgm^{-3})

If the MoE_d value from the one-dimensional equation (14.5 GPa) is imputed as the MoE , and the equation is solved for V_L , then the velocity becomes 5410 ms^{-1} , compared to the oscilloscope mean velocity of 5433 ms^{-1} . Rearranging the equation to find a value for Poisson's ratio where the velocities match exactly, the Poisson's ratio becomes 0.334. Thus the difference in velocities could be attributable to the high-frequency wave taking account of lateral strain in the specimen due to its shorter wavelength. This would indicate that for this specimen, the PUNDIT™ was measuring the bulk longitudinal velocity and that the oscilloscope was measuring the group velocity (given the TOF method) of a dispersive compression bar wave.

4.6 Summary

The primary aims of this test series was: i) to evaluate the use of TOF methods in distinguishing between areas of different inhomogeneity of a single Sitka spruce beam, and ii) to evaluate the influence of timber characteristics on longitudinal velocity. It had been found that longitudinal velocity had a significantly negative linear correlation to KAR ($R^2 = 0.35$ to 0.51 for ultrasonic and impact testing respectively). No other significant correlations were observed. As previous literature, namely Cave and Walker^(4,37), had asserted that the majority control (92% to 96%) of stiffness relies on the microfibril angle and density, this would indicate that the velocity was to an extent controlled by the proportion of defects, within a stiffness range set by these two factors.

It had been shown that whilst both methods (low frequency impact and ultrasonic) can determine differences in 200 mm sections within 30 tests, the repeatability of the low-frequency method increases with increasing distance of separation. This is most likely attributable to difficulty in the manual time separation measurement

using an oscilloscope. 200 mm tests were also subject to a far larger standard error and deviation, whilst producing relative velocities that were unrealistic for a timber specimen. It would therefore be recommended that low-frequency impact TOF testing on samples less than 400 mm be subjected to between 20 and 30 repeatable impacts, and their velocities used only in relative comparisons rather than as a true estimation of MoE_d . Additionally an automated time recognition system is desirable to reduce variability in shorter sections. Samples larger than this will see a faster rate of convergence to a stable mean, generally five tests should be sufficient on a dry beam specimen.

It had also been observed that the side to which the accelerometers were attached during impact testing becomes less relevant with increasing distance of separation. This was attributed to the formation of planar wavefronts with increasing section distance. As a result, an averaging of two or more sides is recommended on distances of accelerometer separation less than 800 mm.

Further, it had been confirmed that ultrasonic testing will consistently overestimate the impact-derived velocity by c. 5%, provided the length of sample is a minimum of 400 mm. This overestimation had been shown to be the consequence of the high-frequency waves being subject to lateral strain and the resulting measurement being a measure of longitudinal bulk velocity, whilst the low-frequency impact oscilloscope measurements are dispersive longitudinal bar waves. The difference between the two velocities on large sections had the potential to determine the Poisson's ratio of a specimen.

4.7 References

- 4.1 BS ISO 5725-1:1994 – *Accuracy (trueness and precision) of measurement methods and results – Part 1: General principles and definitions*, 1994, BSI, U.K..
- 4.2 Gerhards C.C., *Effect of knots on stress waves in lumber*, Res. Paper FPL–RP–384, 1982, FPL, USDA Forest Service.

- 4.3 Divos F., Daniel I., Bejo L., *Defect detection in timber by stress wave time and amplitude*, E-J. of NDT, Vol. 6 no.3, 2001.
- 4.4 Brüel & Kjær, PULSE 12 Product data sheet no. BU-0229-27, 2007-09, www.bskv.com B & K, Noerum, Denmark.
- 4.5 Dell™ Latitude™ D600 Systems User's Guide, Nov. 2004, P/N 6T524, www.dell.com
- 4.6 Brüel & Kjær, Accelerometers and conditioning: Product catalogue February 2005, pp. 51-54 www.bskv.com, B & K, Noerum, Denmark.
- 4.7 Brüel & Kjær, Type 3508-B accelerometer Product data sheet no. BP-1841-14, 04/06, www.bskv.com, B & K, Noerum, Denmark.
- 4.8 Brüel & Kjær, Type 4294 calibrator Product data sheet no. BP-2101-11, 05/06, www.bskv.com, B & K, Noerum, Denmark.
- 4.9 Brüel & Kjær, Endevco Model 8202 Modal hammer Product data sheet, 0805, www.bskv.com, B & K, Noerum, Denmark.
- 4.10 OS300 20MHz Dual trace oscilloscope Instruction manual, Gould, Hainault, Essex, England
- 4.11 Brüel & Kjær, Type 2635 Charge amplifier Product data sheet no. BP-0099-15, 97/08, www.bskv.com, B & K, Noerum, Denmark.
- 4.12 PUNDIT 6, 54 kHz concrete tester instruction manual, CNS Farnell Ltd, Borehamwood, Herts.
- 4.13 Absolute digimatic caliper Manual no. 2074M, Series no. 500, Mitutoyo (UK), Andover, U.K.
- 4.14 Sylomer R-12 Product data sheet, Soundown Corp., 17 Lime street, Marblehead, MA 01945, USA, www.soundown.com
- 4.15 Beeswax density: <http://en.wikipedia.org/wiki/Beeswax>
- 4.16 Beeswax MoE: <http://invsee.asu.edu/nmodules/engmod/propym.html>
- 4.17 Smith, R.S., *Sound transmission through lightweight parallel plates*, PhD Thesis, Heriot-Watt University, 1997
- 4.18 Beamspread angle equation: <http://www.ndt-ed.org/EducationResources/CommunityCollege/Ultrasonics/EquipmentTrans/beamspread.htm>
- 4.19 BS EN 384:2004 – *Structural Timber – Determination of characteristic values of mechanical properties and density* – 2004, BSI, U.K.

- 4.20 BS EN 1310:1997 – *Round and sawn timber – Method of measurement of features* – 1997, BSI, U.K.
- 4.21 Gerhards C.C., *Effect of knots on stress waves in lumber*, Res. Paper FPL–RP–384, 1982, FPL, USDA Forestry Service.
- 4.22 Divos F., Daniel I., Bejo L., *Defect detection in timber by stress wave time and amplitude*, E-J. of NDT, Vol. 6 no.3, 2001.
- 4.23 Carter P., Briggs D., Ross R.J., Wang X., *Acoustic testing to enhance western forest values and meet customer wood quality needs*, In: Productivity of western forests, Res. Paper, PNW-GTR-642, 2005, USDA Forest Service.
- 4.24 Bächle H., Walker J.C.F., *The influence of temperature on the velocity of sound in green pine wood*, Holz als Roh- und Werkstoff, v.64, n.5, 2006, pp 429-430
- 4.25 Hanhijärvi A., Ranta-Maunus Alpo., Turk, G., *Potential of strength grading of timber with combined measurement techniques*. Report of the Combigrade-project . phase 1. Espoo 2005. VTT Publications 568. 81 pgs. + app. 6 pgs.
- 4.26 Ilic J. *Variation of the dynamic elastic modulus and wave velocity in the fiber direction with other properties during the drying of Eucalyptus regnans F. Muell*, Wood Sci. Tech., 35, 2001, pp. 157-166
- 4.27 Chauchan S.S., Walker J.C.F., *Variations in acoustic velocity and density with age, and their interrelationship in radiata pine*, For. Eco. Management, 229, 2006, pp. 388-394
- 4.28 Knowles R.L., Hansen L.W., Wedding A., Downes G., *Evaluation of non-destructive methods for assessing stiffness of Douglas fir trees*, NZ J. For. Sci., 34, 1, 2004, pp. 87-101
- 4.29 Xu P., Walker J.C.F., *Stiffness gradients in radiata pine trees.*, 2004, Wood Sci. Tech., v.38, n.1, pp.1-9
- 4.30 Dinwoodie J.M., *Timber: its nature and behaviour*, 1981, Van Nostrand Reinhold Company, New York, USA.
- 4.31 Johansson M., Kliger R., *Variability in strength and stiffness of structural Norway spruce timber – influence of raw material parameters*, Proc. World Conf. Timber Eng. 2000, Whistler, Canada, 2000.
- 4.32 Bucur V., *Acoustics of wood*, 2nd Ed., 2005, CRC Press, London.

- 4.33 Divos F., Tanaka T., *Effect of creep on modulus of elasticity determination of wood*, J. Vib. and Acous., V.122, 1, 2000, pp.90-92
- 4.34 Hearmon R.F.S, *An introduction to applied anisotropic elasticity*, 1961, Oxford University Press
- 4.35 Timoshenko S.P., Goodier J.N., *Theory of Elasticity: 3rd edition*, 1970, McGraw-Hill Publishing Co., NY.
- 4.36 Halmshaw R., *Non-Destructive Testing; Second Edition*, 1991, Edward Arnold publishing
- 4.37 Cave I.D, Walker J.F.C., *Stiffness of wood in fast-grown Plantation softwoods: the influence of microfibril angle*, Forest Products Journal, v. 44 n.5, pg 43-45, 1994

Chapter 5 Test series 2: Controlled homogeneity and defect modelling

5.1 Introduction

This chapter presents an investigation into the effects of increasing wood inhomogeneity on calculated MoE_d and harmonic damping ratio values. Glue-laminated panels with different configurations of laminations (longitudinal or transverse) were assessed following on from previous work by Chauhan *et al.*^(5.1). Chauhan *et al.*^(5.1) compared the effects of increasing inhomogeneity of laminated panels and beams on the TOF and resonance velocity of the specimens. Further to this investigation, artificial defects (originally envisaged to simulate the presence of knots) were inserted at specific points within the beams to assess their effect on the MoE_d and damping ratio. This chapter first considers the results of preliminary tests designed to find the optimum repeatable conditions for the NDT. Following this, the results of velocity, MoE_d and damping ratio tests are presented. These are then discussed in relation to the variables considered during the tests, concluding with a summary of the investigation. In Series 2, the damping ratio and the propagation speed of longitudinal stress waves in engineered wooden beams (*Pinus radiata*) cut from four laminated panels, each of them having a different

orientation of the 12 individual layers, were investigated using various acoustic parameters.

The advantage of testing laminated beams is that defects such as knots or areas of variable properties (early and latewood, heart and sapwood or compression wood) are redistributed by peeling logs and gluing these individual sheets together. The result is a reconstituted panel of improved quality compared to the raw wood material (enhanced strength for laminated veneer lumber, LVL, and reduced shrinkage and create more homogeneous strength properties along the length and across the width of the panel for plywood). Of course, perpendicular to the laminations, the anisotropy and inhomogeneity of the specimens will be far greater than in solid wood specimens, however since all four types of panels have the same glue content, then comparisons can be based on the differing homogeneity due to the orientations of individual laminations. Additionally, the primary focus of this study is longitudinal transmission of stress-waves, rather than across the beams. Thus by altering the orientation of the individual layers it is possible to control the inhomogeneity of the panel. This provides ideal conditions to investigate the impact of longitudinal inhomogeneity on acoustic properties of wood. Three beam specimens of solid radiata pine were also examined in this study for comparison.

5.1.1 Sample preparation

The beams were cut from four laminated panels (2.40 m x 1.20 m x 40 mm), each of which had a different orientation of the 12 individual layers (each 3 mm thick). The panels were cold pressed for 20 hours using a commercial adhesive, Sylvic S3 as hardener and Resin 4260 with 69.9% formaldehyde^(5.1). The configurations of the panels, adapted from Chauchan *et al.*^(5.1), were as follows (Figures 5.1 to 5.5):

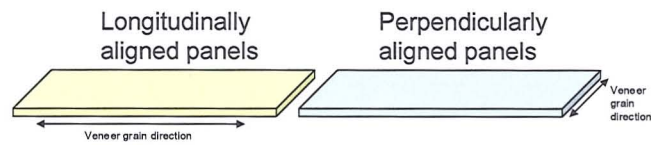


Figure 5.1 Alignment of grain direction in panels

Panel 1: All plies laid up with the grain direction parallel (as in LVL, designated: 'All L')

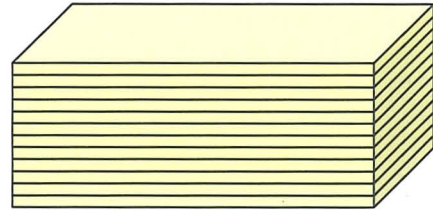


Figure 5.2 All L panels

Panel 2: Four plies laid up with their grain direction perpendicular to the panel's length and sandwiched between four-face plies laid up with their grain direction parallel to the length (four longitudinal-four transverse-four longitudinal, designated: '4-4-4').

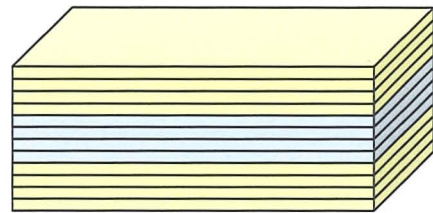


Figure 5.3 The 4-4-4 panels

Panel 3: Six plies laid up with their grain direction perpendicular to the panel's length and sandwiched between three face plies laid up with their grain direction parallel to the length (three longitudinal-six transverse-three longitudinal, designated: '3-6-3').

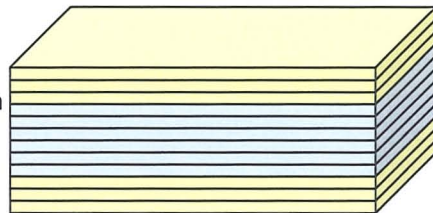


Figure 5.4 The 3-6-3 panels

Panel 4: Conventional plywood with alternate veneers lying parallel or perpendicular to the panel's length, respectively (alternately longitudinal and transverse, designated: 'PLY'). To maintain symmetry with respect to the neutral axis, both the core plies were laid up with their grain direction parallel to the panel's length.

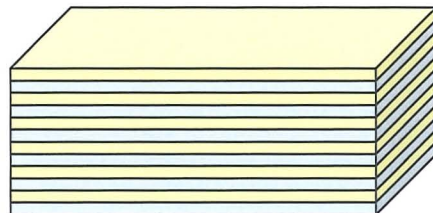


Figure 5.5 PLY panels

Beams can be either cut along the longest side of the panel or perpendicular to it. Therefore it is possible to cut eight different configurations, each of them having a different degree of anisotropy. Moreover, the beams can be measured when they are supported such that individual layers are aligned horizontally or vertically. For this study, 1960 mm long beams were cut along the length of each panel, resulting in; twelve All L; eight PLY; six 4-4-4; and five 3-6-3 beams. Furthermore, two beams were cut across the grain (width direction) from the all longitudinal-aligned

panel, so the grain direction of all plies in these two beams was perpendicular to its longitudinal axis (*i.e.* all transverse). The cross-section of all beams was consistently 40 mm x 40 mm to have the same depth and width whether the beams were aligned with the individual layers lying horizontal or vertical. The beams were cut to a length of 1960 mm, which was the length of the shortest panel. The same panels had been used for acoustic testing before this study^(5.1). Three clearwood beams of radiata pine of the same dimensions were also cut.

The principal aim of this test series was to verify the velocity calculations from Chauhan *et al.*^(5.1) by observing the change in velocity, and investigate the effects on damping ratios and different methods of velocity calculation due to both the increase in inhomogeneity of LVL panels and the insertion of artificial defects (holes) to simulate the occurrence of knots in a specimen.

5.1.2 Equipment

- 1 x B & K PULSE™ Platform (Type 3760-B) with Type 3109 four channel input-output module and Type 7533 LAN interface module and software (Type 7705 time capture facility and Type 7770 FFT analyser)^(5.2)
- 1× laptop and dongle^(5.3)
- 1 x 5 m AO-0463-F cables and pin connectors^(5.4)
- 1 x Type 4308-B uniaxial accelerometer^(5.5)
- 1 x Type 4294 calibration exciter^(5.6)
- 1 x Impact hammer^(5.7) and BNC connection cable
- PUNDIT™ 54 kHz concrete void tester^(5.8)
- Hot glue gun (to attach the accelerometers to the beams)
- 2× foam triangles (for support and vibration isolation)
- 1× drilling machine + borers (6, 10, 16, 20, 25, 32 mm diameters)
- Dowels (6, 10, 16, 20, 25, 32 mm)
- PVA wood glue (to glue the dowels into the beam)
- Electronic balance (accuracy ± 0.05 g) to weigh the beams
- Moisture meter (accuracy ± 0.5 % volumetric moisture content)

5.1.3 Method

The procedure of the test series was designed to be similar to the experiments of Ouis^(5.9), Sandoz *et al.*^(5.10) and Divos *et al.*^(5.11) in evaluating the effects of artificial discontinuities. The experimental configuration was also designed to be near-identical to the configuration used in Series 3b, and follows the same procedure for Test Series 3b as set out in the flowchart presented in Figure 6.3. Figure 5.6 shows the layout of the experimental procedure used.

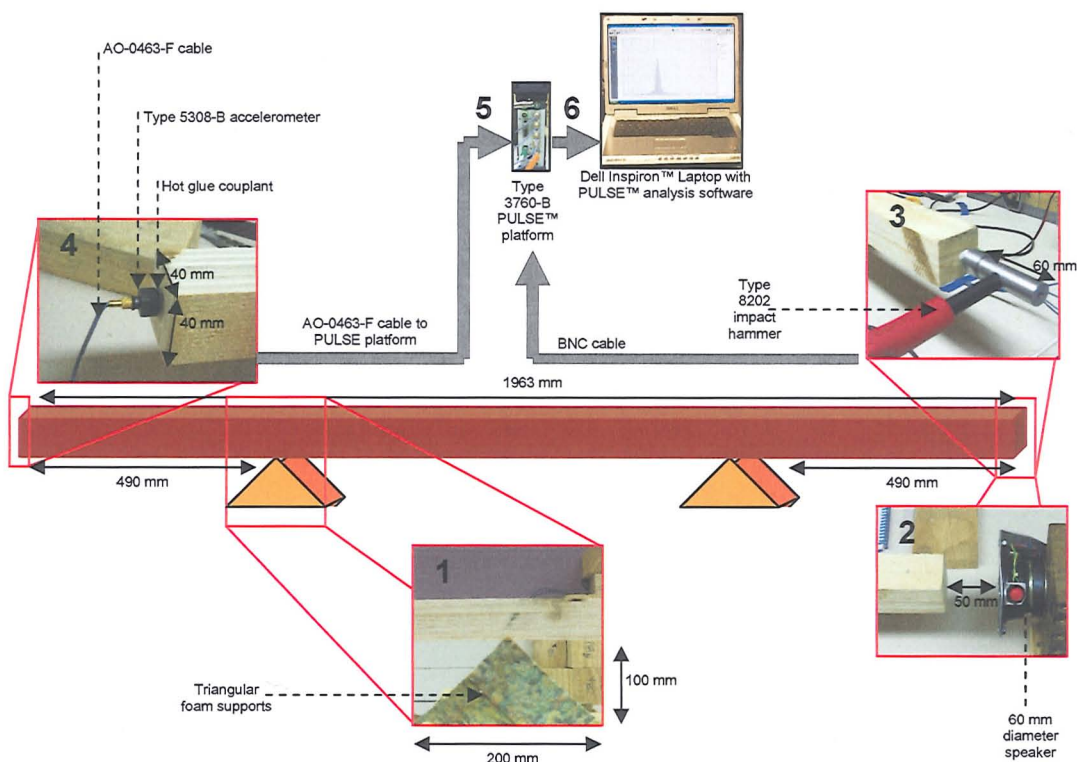


Figure 5.6 Series 2 experimental layout. The glued panels were supported on two foam triangles at $\frac{1}{4}$ span for vibration isolation (1). During the initial experimental design, the use of both transient and continuous non-contact speaker excitation (2) and impact hammer excitation (3) was investigated. Ultimately impact hammer excitation was used for the main test series, the longitudinal wave travelling along the length of the specimen. The waveform was detected by a Type 5308-B accelerometer coupled with hot glue (4). The accelerometer was connected to a Type 3760-B PULSE™ platform through 5 m AO-0463-F cables.

As shown in Figure 5.6, beams were supported on foam triangles at quarter-span with a foam density of 150 kgm^{-3} and a low stiffness of 4.93 Nmm , which equates to a compression of the foam support apexes of 0.5 mm . This means rather than a

knife-edge point support, the actual width of support is c. 1 mm. Before continuing, it must be established that the self-weight of the beam on the supports will not alter the minimum bending moment, such that the material is differentially stressed leading to an increase in wave speeds at the centre of the beam. The self weight mid-span deflection of the laminated beams and the solid specimens can be calculated using the load diagram seen in Figure 5.7:

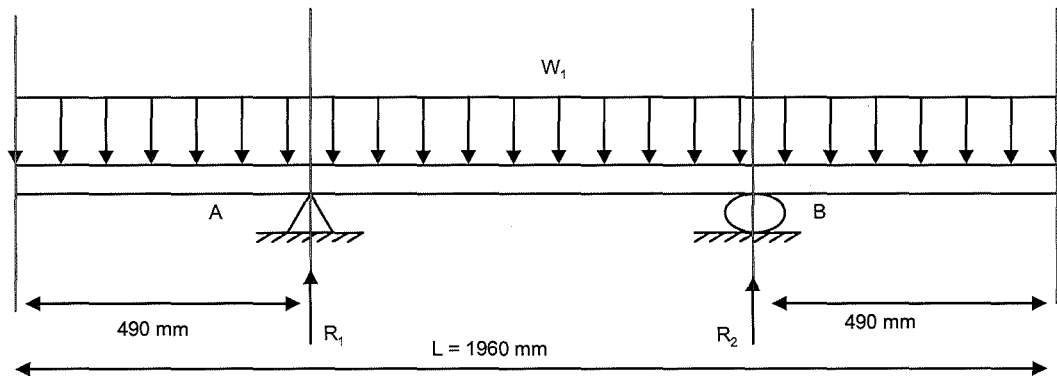


Figure 5.7 Load diagram: supports at $\frac{1}{4}$ -span

To find W_1 , The mass of the sample beam is 1.4112 kg and dimensions of 1.96 m x 0.04 m x 0.04 m equates to a volume of 0.0031 m^3 . Therefore the weight of the beam (mass x gravity) is 13.84 N, which, when divided by the length of the beam, equates to an average line load self-weight (W_1) of 7.1 Nm^{-1} . Thus the reaction forces R_1 and R_2 equate to 6.96 N. This produces a shear force diagram seen in Figure 5.8, which in turn allows production of a bending moment diagram as seen in Figure 5.9:

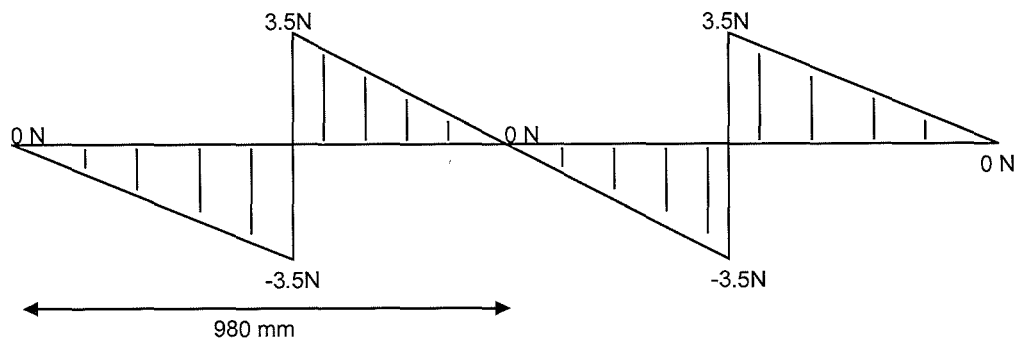


Figure 5.8 Shear force diagram: supports at $\frac{1}{4}$ -span

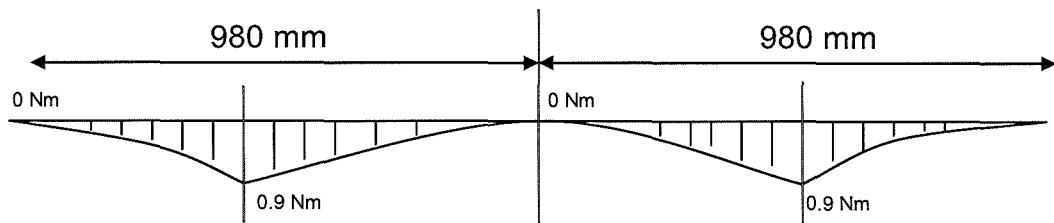


Figure 5.9 Bending moment diagram: supports at 1/4-span

The moment of inertia (I_{na}) of the beam is calculated as:

$$I_{na} = \frac{bd^3}{12} = \frac{0.04 \times (0.04)^3}{12} = 2.1333 \times 10^{-7} m^4 \quad \text{Eqn 5.1}$$

Using an average static MoE of softwood of c. 8 GPa, the mid-span deflection of the sample beam can be calculated and produces a beam mid-span deflection diagram as shown in Figure 5.10.

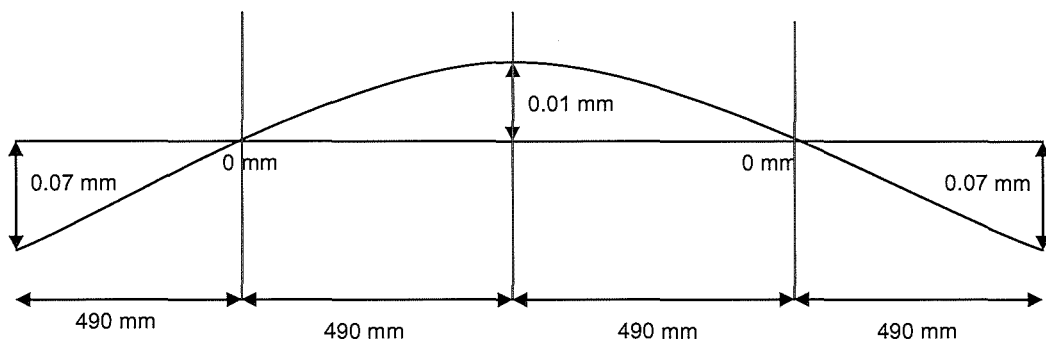


Figure 5.10 Beam mid-span deflection diagram: supports at 1/4-span

Thus it can be seen that the mid-span deflection of the beams will be 0.01 mm, which can be assumed to have negligible impact on the stress distribution of the beam and hence not affect the velocity. Additionally, as the supports have been shown to have a support area of 4 mm² (1 mm x 4 mm), then the self-weight effects will be reduced, theoretically reducing the midspan deflection and bending moment peaks slightly.

A hammer impact on one end of the specimen was used to induce a longitudinal wave, which was then detected by a glue-coupled single accelerometer in the longitudinal orientation on the receiving end. The impact and receiver signals were

recorded on the PULSE™ analyser. Each beam was acoustically tested before any holes were drilled. It was decided to use holes of increasing diameter instead of progressive saw cuts to mimic defects in timber. Pre-test experiments with progressive saw cuts indicated that this method was not suitable when using the resonance technique as a progressively larger peak, at approximately half the frequency of the fundamental, was evident with increasing depth of cut.

There were advantages to drilling holes to introduce artificial defects. Not only was the hole closer to the shape of an idealised knot type, it could also be placed at the centre of the cross-section (centreline knots) or at the edge of the cross-section (edge knots) with a more consistent profile than by a combined drilling and sawing practice. Moreover, the waves hitting the hole are reflected in various directions, and will be attenuated quickly. Filling the holes with dowels of corresponding size kept the mass of the beam constant (assuming that the dowels had a near identical density to that of the laminated beams). Glue was used to hold the dowel in place: this was necessary because when the hole needed to be enlarged the ring-saw (drill) tool tip had to be accurately located at the centre of dowel plugging the hole. Dowels were either fitted perpendicular or parallel to the individual layers of the beams.

At this point it should be noted that whilst the size of drill bits used and dowels inserted will be of the same diameter, in practice the holes will not be perfectly cylindrical due to the process of hand-drilling. As such it is likely (and was later observed as such) that a degree of eccentricity will exist in the hole diameters, typically increasing with increasing hole size. Thus with increasing diameter, an element of repeatability between tests will be lost.

To ensure repeatability of the measurements, each test was repeated twice before the knot size was increased. The test series occurred as follows:

1. The first test series was conducted on the beams without introducing any artificial defects. Recorded are the fundamental frequency and subsequent harmonics (to the 3rd), TOF time trace, harmonic distortion, auto-damping

ratio by PULSE™, damping ratio as calculated manually based on the Q-factor, damping ratio calculated from the logarithmic decrement (between peak 5 and 20), damping ratio according to the impulse response function, damping ratio according to the reverberation time and the velocity of the signal between the 3rd and fourth arrival peak).

2. A second test series (one long beam from each panel) was conducted in which wooden dowels (*Pinus radiata*) of increasing diameter (6, 10, 16, 20, 25, 32 mm) were drilled through the centre at mid-span and perpendicular to the individual layers. The dowels were fixed using polyvinyl acetate (PVA) wood glue within a standard room environment (21°C, 45% RH). Following a three minute settling period for the glue to dry, the acoustic measurements were started. Note at this point that with increasing diameter of holes, the closeness of fit of the dowels decreased. The acoustic measurement itself took c. 5 minutes *per* beam. Note: The beams were always supported in a way that the dowel(s), where present, were aligned vertically.
3. A third test series was conducted where the holes were drilled at mid-span but parallel to the individual layers of the beam.
4. A fourth test series was conducted where the holes were drilled at mid-span, but instead of drilling through the centre they were now drilled along one side perpendicular to the individual layers. The tip of the drill was placed at the edge of the beam. Thus a semi-cylindrical hole was drilled across the surface of the beam. This hole was then filled with a dowel of corresponding size, which has been split in two halves along its grain. First, the holes with increasing diameters were drilled only from one side. Once the 32 mm hole was drilled the same procedure was repeated at the opposite side of the beam.
5. A fifth test series was conducted repeating series four, but with the holes now oriented along the individual layers. Note: only 3-6-3 and 4-4-4 beams were tested in this series.

6. A sixth test series was conducted with knots placed at firstly $\frac{1}{4}$ - and then $\frac{3}{4}$ -span. $\frac{3}{4}$ -span indicated that the knots were introduced at the quarter that is closer to the accelerometer, whereas $\frac{1}{4}$ -span is closer to the impact end of the beam. The holes were drilled perpendicular to the orientation of the individual layers (or the rings in clearwood) of the beam.
7. A seventh test series was conducted on a single LVL beam by introducing knots perpendicular to the layers firstly at $\frac{3}{8}$ - and then at $\frac{5}{8}$ -span.
8. An eighth test series was conducted, where holes of 20 mm and 25 mm were introduced perpendicular to the orientation of the individual layers (or annual rings in clearwood) at specified positions along the beam. The beam (LVL Beam 33) was firstly tested without any insertions (Stage A) The series was then tested at the end of each stage (B to J) in the following sequence:
 - A. No insertions
 - B. 25 mm dowels inserted at $\frac{1}{4}$ -, $\frac{1}{2}$ - and $\frac{3}{4}$ -span
 - C. B plus 20 mm dowels at $\frac{3}{8}$ + $\frac{5}{8}$ span
 - D. C plus 20 mm dowels at $\frac{1}{8}$ + $\frac{7}{8}$ span
 - E. D plus 20 mm dowels at $\frac{7}{16}$ + $\frac{9}{16}$ span
 - F. E plus 20 mm dowels at $\frac{5}{16}$ + $\frac{11}{16}$ span
 - G. F plus 20 mm dowels at $\frac{3}{16}$ + $\frac{13}{16}$ span
 - H. G plus 25 mm dowels at $\frac{1}{16}$ + $\frac{15}{16}$ span
 - I. H plus 20 mm dowels at $\frac{15}{32}$ + $\frac{17}{32}$ span parallel layers/rings
 - J. I plus 20 mm dowels at $\frac{7}{32}$ + $\frac{25}{32}$ span parallel layers/rings
9. A ninth test was done on short beams to compare the LVL configuration with the "All Transverse (All-T)."

Beams were numbered according to their configuration; in all 36 beams were tested. The configurations of each beam are presented in Table 5.1, Section 5.3. Beams 1 to 25 were tested between 22 Mar. and 28 Mar. 2006 at the University of

Canterbury, Christchurch, New Zealand. Beams 26 to 36 were tested between 11 Sept. and 15 Sept. 2006 at Napier University, Edinburgh and were also subject to PUNDIT™ testing using the procedure set out in Figure 5.4. Following the conclusion of these test series, five different methods of calculating the damping ratio of a laminated beam were compared with each other: logarithmic decrement, impulse response function, manual Q-factor estimation, PULSE™ auto-damping function, and reverberation time. The calculation of these parameters is shown in Section 5.4 as they are post-processing procedures. MoE_d values were calculated from the velocities, deduced by resonance (using the method shown in Section 4.1) and PUNDIT™ TOF measurements (Eqn 4.1).

5.2 Preliminary results

Before the main test series, preliminary investigations were conducted to derive the optimum experimental conditions to satisfy the objectives. These investigations concerned: specimen support positions, accelerometer coupling conditions, excitation of the specimen, and the damping ratio calculation to be used. A summary and discussion of these investigations is presented in Sections 5.2.1 to 5.2.3.

5.2.1 Supports

Two triangular foam supports were positioned at both ends of all-longitudinal (LVL-L) beams and subsequently each support was moved to each one-twelfth, one-tenth, one-eighth, one-fifth, one-quarter, and one-third span point. The beam was excited by hammer and the FRF measured by accelerometer. No change in the fundamental or harmonic frequencies was observed during the variation of support positions. This would be expected as the self-weight deflection was less than 0.7 mm when supported at $\frac{1}{4}$ spans, therefore there is little additional stress (which would increase the measured frequency) placed on the specimen regardless of support position. The maximum acceleration amplitude (ms^{-2}) of each harmonic (1st to 5th) was also measured for each support position. The acceleration of the 1st

harmonic was taken as 100% and the subsequent harmonics' acceleration expressed as a percentage of the 1st harmonic's acceleration, known as the harmonic distortion. This is graphically displayed in Figure 5.11, which shows that the effect on the energy content of each harmonic through moving the position of support when measuring longitudinal resonance was negligible. The first harmonic was always the greatest value in terms of acceleration. It can also be seen however that the strongest contribution of subsequent harmonics, when compared to the 1st harmonic, occurred when supporting the beam at both ends. The test was repeated and showed similar results when the specimen was supported freely using two thin-wire slings instead of foam supports.

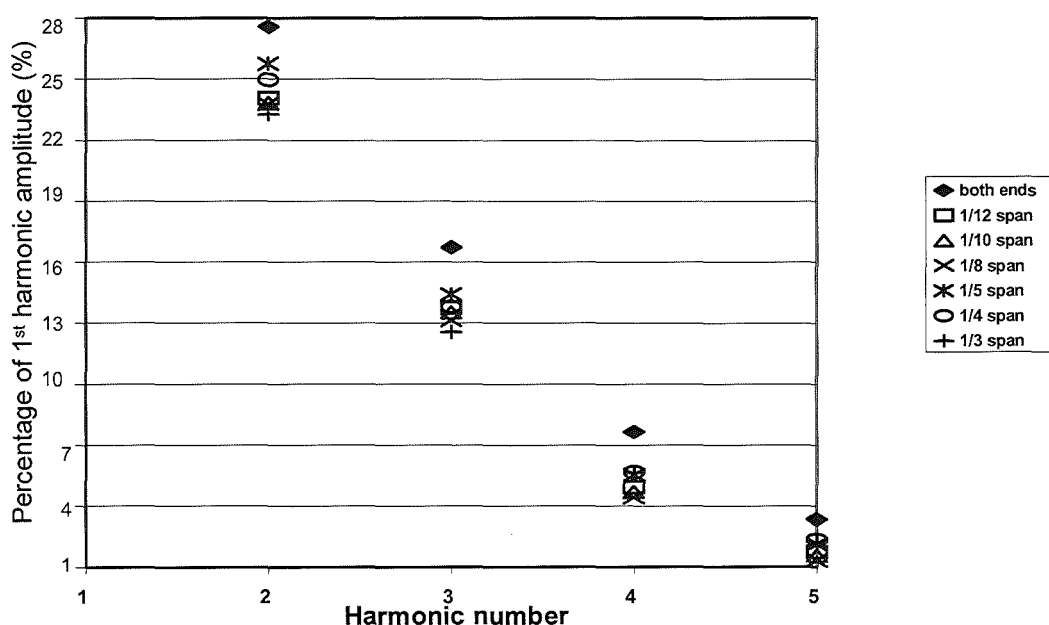


Figure 5.11 Consequences of the support position on the maximum acceleration of the harmonics, *i.e.* harmonic distortion. The 1st harmonic is taken as the reference value of 100% and the harmonics presented as the percentage of the 1st harmonic.

5.2.2 Accelerometer coupling conditions

Whilst the ideal method of coupling would have been to use a steel stud screwed into both the vibrating surface and the base of the accelerometer^(5.12), the accelerometers used were not equipped with such a mechanism. Additionally, such a use could be considered partially destructive and have initiated further ruptures

along the panel glue lines. As such, three coupling agents were considered: beeswax, Vaseline™ and thermoplastic glue (Loctite™ glue sticks) spread with a hot glue gun. All three methods gave repeatable resonance frequencies and maximum acceleration values when testing the same LVL-L beam. However, the main disadvantage of beeswax, and in particular Vaseline™, is that the bond between accelerometer and specimen was relatively fragile. This would be unacceptable during the experiments as drilling holes into the beams would inevitably result in vibration of the beam that may loosen or break the weaker bonds, compromising the repeatability of the experiment. Therefore, the thermosetting glue was chosen.

5.2.3 Excitation of the specimen

Four different excitation methods were used to launch compression waves into the sample. These were a broadband hammer impact and three loudspeaker-based methods: a sinusoidal pulse corresponding to the frequency of the harmonic under investigation; a swept tone over a set frequency range (100 Hz to 10 kHz); and a broadband pink-noise signal. A Brüel & Kjær Type 3508-B-001 piezoelectric accelerometer was fixed with thermoplastic adhesive in the centre of the opposite end to acquire the structural axial response of the beam.

- Problematic issues with loudspeaker excitation

It was noted that the distance between loudspeaker and specimen influenced the harmonic distortion (*i.e.* percentage of each harmonic's velocity from the 1st harmonic as seen previously in Figure 5.11), which shifted depending on the distance of the loudspeaker from the specimen. As such, a sinusoidal pulse of the 1st harmonic frequency (previously derived by hammer impact and measured by accelerometer using the PULSE™ system) was generated by a loudspeaker, and the test was repeated over the following distances between the speaker and the end of the specimen: 2 mm, 10 mm, 20 mm, 30 mm, 40 mm, 50 mm, 100 mm, and 150 mm. The energy (5 mVrms) of the signal was kept constant. At a distance of 2 mm the response showed a strong 1st harmonic, a 3rd harmonic with *c.* 20% energy of the 1st harmonic and a weak 5th harmonic with *c.* 1.5% energy respectively. By

increasing the distance between speaker and specimen (from 2 mm to 100 mm) a change in transmitted energy content was evident. However, there was no uniform pattern which could be related to the change of distance between the speaker and the specimen. It appeared that higher frequencies got relatively stronger with increasing distance as the maximum relative amount of the response for the 5th harmonic was observed at 100 mm distance. This might be because sound at the higher frequencies was emitted in a focused, narrower beam and did not spread so widely with distance in comparison to the lower harmonics. The fact that there was no uniform pattern in change of energy when changing the distance between speaker and specimen might be due to resonance or near-field interaction occurring within the air gap between speaker and specimen. Moreover, the various harmonics will have an optimum distance at which they penetrate the specimen at a maximum level. When keeping the distance between speaker and specimen constant at 50 mm and decreasing the energy of the generated pure tone (1st harmonic frequency) stepwise by 5 mVrms, 4.5 mVrms, 4 mVrms, 3.5 mVrms, 3 mVrms and 2.5 mVrms, the energy content of the 1st harmonic and subsequent harmonics decreased proportionately. At an energy level of 2.5 mVrms the subsequent harmonics' acceleration levels were indistinguishable from background vibration levels.

- Problematic issues with hammer excitation

Tests using hammer excitation highlighted difficulties in getting a clear decay curve from which to calculate logarithmic decrement. The first few peaks of the decay curve do not usually show a logarithmic decay pattern, as shown in Figure 5.12.

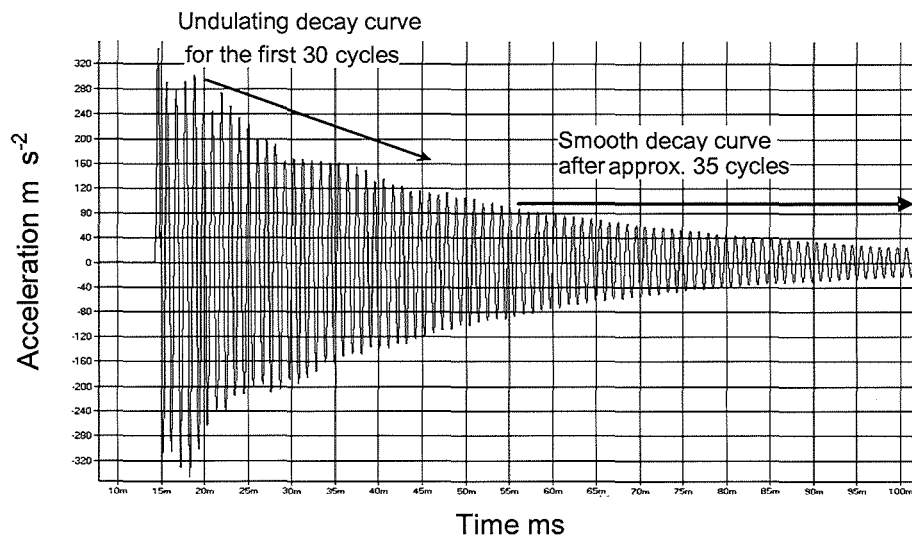


Figure 5.12 Problems with the calculation of logarithmic decrement. Displayed is a typical amplitude-time display (from the PULSE™ system) measured by accelerometer on a 4L-4T-4L beam when excited by hammer excitation.

This was most likely due to the broadband impact generating non-harmonic frequencies of significant acceleration, the interaction of both longitudinal resonance harmonics with each other when generated by a broadband impact, and the minor contributions to the longitudinal signal of other vibrational modes. However, it can be seen that frequencies other than the 1st harmonic and its subsequent harmonics decay quickly (probably during the first 10 cycles) and the higher harmonics decay relatively quickly as higher frequencies are more greatly damped than lower harmonic frequencies. Therefore, after c. 20 to c. 40 cycles the 1st harmonic should be by far the strongest frequency within the remaining signal, and reliable measurements should be obtainable when calculating from around the c. 35th cycle onwards (as seen in Figure 5.12). It was observed that when the number of cycles (n) between peaks, from which the readings of maximum amplitude used in the calculation of the logarithmic decrement are taken, was chosen to be 15 rather than 5, the spread of the damping ratio calculated from the logarithmic decrement was seen to decrease by c. 15% when averaged over five tests. Thus the accuracy of the logarithmic decrement measure was deemed to increase as n is increased.

Ultimately it was decided that the use of a broadband impact was favorable as it combines many advantages, not least in efficiency, that can not be realized when the specimen is excited by a loudspeaker source, particularly when using a pure tone. It allows for various modes to be identified in the frequency domain by a single hammer tap, and the modal hammer that was used to excite the specimen was able to connect to the PULSE™ unit which then allowed for calculating an FRF and the rise time of the impact. Additionally, a hammer hit seems a more feasible excitation method in terms of potential relation to future field work, especially when large timber specimens and standing trees are investigated, given the low levels of energy inputted using speaker excitation.

5.3 Beams tested

Table 5.1 displays the beams tested during this test series by beam number, beam laminate configuration (or radiata pine clearwood) and the type of simulated knot inserted into the beams.

Several configurations were repeated to check the validity of earlier beam results, typically having been prompted by supposed anomalies in previous beams. This included: LVL and PLY beams tested perpendicularly with central knots at midspan (Beams 1 and 28, and 4 and 6 for LVL and PLY respectively), PLY and 3L-6T-3L beams tested parallel with central knots at midspan (Beams 13 and 29, and 7 and 32 for LVL and PLY respectively), PLY beams tested perpendicularly with central knots at $\frac{1}{4}$ and $\frac{3}{4}$ span (Beams 20 and 30), and LVL beams tested perpendicularly using multiple 25 mm holes at various positions (Beams 27 and 33). Results of the first beams tested began to influence the initial test plan.

This led to a testing of $\frac{3}{8}$ - and $\frac{5}{8}$ -span holes on an LVL beam and PLY beam as well as multiple holes testing and clearwood testing, this limited the number of beam types available for testing from the final panels, which coupled with time constraints (Beams 9, 15 and 16, though 15 and 16 were identical in configuration to Beams 10 and 34 respectively), meaning no test was conducted on $\frac{1}{4}$ -span

knots other than perpendicular central $\frac{1}{4}$ - and $\frac{3}{4}$ - span knots. Lack of availability also meant a 3L-6T-3L beam was not tested at this configuration. However, whilst it would have been desirable, the effect of differing inhomogeneity could be seen in the no-knot and midspan knot tests, meant that testing of edge knots and parallel laminations at $\frac{1}{4}$ and $\frac{3}{4}$ span was not of paramount importance to the series.

Table 5.1 Laminate beam test series. Beams 1 through 27 were tested at the University of Canterbury, Christchurch, NZ. Beams 28 through 36 were tested at Napier University, Edinburgh, UK.

Beam no.	Beam configuration	Type of knots (sizes, position, location, orientation)
1	LVL-L	> 32 mm, central, $\frac{1}{2}$ span, perpendicular
2	LVL-L	> 32 mm, 2x edges, $\frac{1}{2}$ span, perpendicular
3	LVL-L	> 32 mm, central, $\frac{1}{2}$ span, parallel
4	PLY	> 32 mm, central, $\frac{1}{2}$ span, perpendicular
5	PLY	> 32 mm, 2x edges, $\frac{1}{2}$ span, perpendicular
6	PLY	> 32 mm, central, $\frac{1}{2}$ span, perpendicular
7	3-6-3	> 10 mm, central, $\frac{1}{2}$ span, parallel (TEST INCOMPLETE)
8	3-6-3	> 32 mm, central, $\frac{1}{2}$ span, perpendicular
9	3-6-3	> 32 mm, 2x edges, $\frac{1}{2}$ span, perpendicular (NOT TESTED)
10	4-4-4	> 32 mm, 2x edges, $\frac{1}{2}$ span, perpendicular
11	4-4-4	> 32 mm, 2x edges, $\frac{1}{2}$ span, parallel
12	4-4-4	> 32 mm, central, $\frac{1}{2}$ span, parallel
13	PLY	> 32 mm, central, $\frac{1}{2}$ span, parallel
14	3-6-3	> 32 mm, 2x edges, $\frac{1}{2}$ span, parallel
15	4-4-4	> 32 mm, 2x edges, $\frac{1}{2}$ span, perpendicular (NOT TESTED)
16	LVL-L	> 32 mm, 2x edges, $\frac{1}{2}$ span, parallel (NOT TESTED)
17	LVL-L	none, short length (0.98 m)
18	All transverse	none, short length (0.98 m)
19	LVL-L	25 mm filling and glue test
20	PLY	> 32 mm, central, $\frac{1}{4}$ & $\frac{3}{4}$ span, perpendicular
21	PLY	> 32 mm, central, $\frac{3}{8}$ & $\frac{5}{8}$ span, perpendicular
22	LVL-L	> 32 mm, central, $\frac{1}{4}$ & $\frac{3}{4}$ span, perpendicular
23	LVL-L	> 32 mm, central, $\frac{3}{8}$ & $\frac{5}{8}$ span, perpendicular
24	Clearwood	> 32 mm, central, $\frac{1}{2}$ span, perpendicular
25	Clearwood	> 32 mm, central, $\frac{1}{4}$ & $\frac{3}{4}$ span, perpendicular
26	Clearwood	> 25 mm multiple positions
27	LVL-L	> 25 mm multiple positions, perpendicular
28	LVL-L	> 32 mm, central, $\frac{1}{2}$ span, perpendicular
29	PLY	> 32 mm, central, $\frac{1}{2}$ span, parallel
30	PLY	> 32 mm, central, $\frac{1}{4}$ & $\frac{3}{4}$ span, perpendicular
31	4-4-4	> 32 mm, central, $\frac{1}{2}$ span, perpendicular
32	3-6-3	> 32 mm, central, $\frac{1}{2}$ span, parallel
33	LVL-L	> 25 mm multiple positions, perpendicular
34	LVL-L	> 32 mm, 2x edges, $\frac{1}{2}$ span, parallel
35	4-4-4	> 32 mm, central, $\frac{1}{4}$ & $\frac{3}{4}$ span, perpendicular
36	All transverse	none, short length (0.94 m)

5.4 Damping ratio methods

The five different methods of calculating the damping ratio of a beam were compared to identify the most consistent measure. These were: logarithmic decrement, impulse response function, manual Q-factor estimation, PULSE™ auto-damping function, and reverberation time. Table 5.2 shows the damping ratio results of repeatable impact testing on an LVL, PLY and 4L-4T-4L beams. Although more than these three beams were tested, this summary table accurately reflects trends seen across the specimens (Beams 1 to 12) evaluated. It can be seen that using the logarithmic decrement resulted in a significantly higher standard deviation and coefficient of variation. Both the reverberation time and logarithmic decrement damping ratios were seen to be inconsistent with the other auto-damping, Q-factor and Impulse response measures (which were relatively consistent with each other).

Table 5.2 The comparison of five different measures of damping ratio (%) on unaltered laminated Beams 1, 4, and 10. The mean value is the average of all tests on each beam, also shown is the standard deviation (SD) and coefficient of variation (COV).

Beam no.	Configuration	Test no.	Log. dec. damping ratio (%)	Auto-damping ratio (%)	Q-factor damping ratio (%)	Impulse response damping ratio (%)	Rev. time damping ratio (%)
1	LVL-L	1	0.512	0.450	0.447	0.453	0.451
1	LVL-L	2	0.463	0.452	0.451	0.454	0.449
1	LVL-L	3	0.511	0.447	0.453	0.451	0.453
1	LVL-L	4	0.510	0.450	0.447	0.453	0.451
1	LVL-L	5	0.426	0.452	0.451	0.454	0.449
	Mean		0.484	0.450	0.450	0.453	0.450
	SD		0.039	0.002	0.003	0.001	0.002
	COV		8.008	0.455	0.605	0.293	0.385
Beam no.	Configuration	Test no.	Log. dec. damping ratio (%)	Auto-damping ratio (%)	Q-factor damping ratio (%)	Impulse response damping ratio (%)	Rev. time damping ratio (%)
10	4-4-4	1	0.400	0.429	0.426	0.430	0.483
10	4-4-4	2	0.608	0.425	0.423	0.426	0.485
10	4-4-4	3	0.551	0.424	0.426	0.425	0.491
	Mean		0.520	0.426	0.425	0.427	0.486
	SD		0.107	0.003	0.002	0.002	0.004
	COV		20.678	0.621	0.404	0.560	0.907
Beam no.	Configuration	Test no.	Log. dec. damping ratio (%)	Auto-damping ratio (%)	Q-factor damping ratio (%)	Impulse response damping ratio (%)	Rev. time damping ratio (%)
4	PLY	1	0.582	0.512	0.507	0.514	0.458
4	PLY	2	0.424	0.508	0.502	0.511	0.453
4	PLY	3	0.524	0.512	0.507	0.509	0.453
	Mean		0.510	0.511	0.505	0.512	0.455
	SD		0.080	0.002	0.003	0.002	0.003
	COV		15.591	0.452	0.637	0.471	0.683

It was found that the PULSE™ auto-damping function was derived automatically from the Q-factor, hence a near-identical result to the manually calculated Q-factor ($R^2 = 0.994$), and hence reduced the number of damping ratio calculation measures to four, with the auto-damping used instead of manually calculating the Q-factor on the basis of efficiency. Figure 5.13 shows three scatter plots highlighting the correlation between impulse response, logarithmic decrement and reverberation time derived damping ratio values.

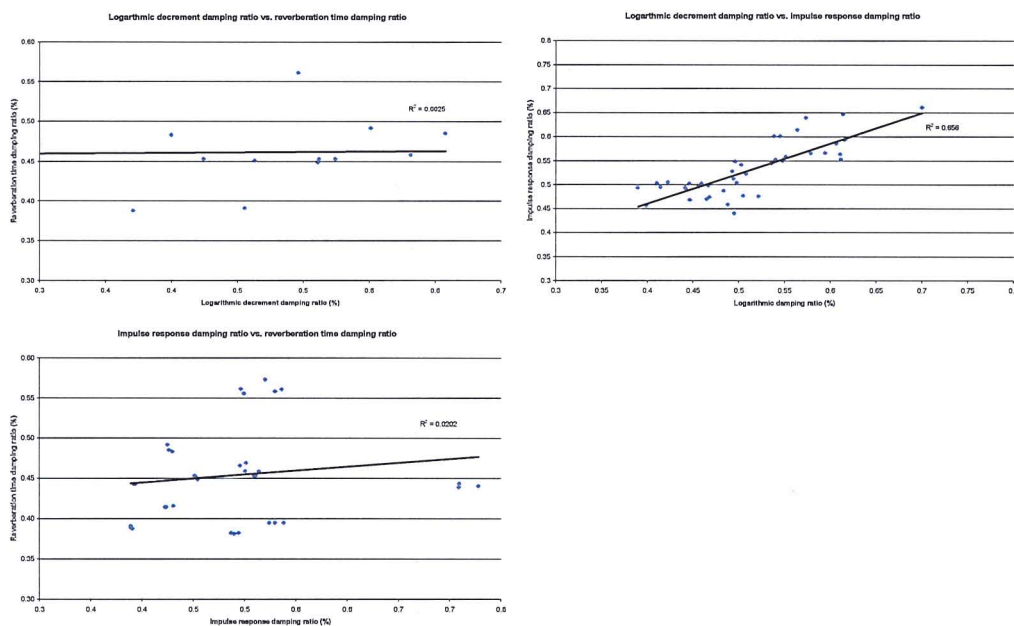


Figure 5.13 Correlations between logarithmic decrement, impulse response and reverberation time damping ratios. The reverberation time damping ratios and their corresponding data are based on beams 1 to 12 whilst the logarithmic decrement vs impulse response correlation is based on results from Beams 27 through Beam 36. It should be noted that Beam 1-12 results showed similar lack of correlation between logarithmic decrement and impulse response ($R^2 = 0.02$).

5.5 Velocity, dynamic MoE and damping ratio results

Table 5.3 summarises the results of the first part of the test series, where three beams of each configuration (Beams 1 through 12 as in Table 5.1) were tested before artificial knot insertion. As expected, the average velocity of sound (calculated from the 1st, 2nd, and 3rd harmonic frequencies) in the LVL-L beams was

the highest at 4799 ms⁻¹ (100%) and lowest in the beam with all laminates orientated transversely (LVL-T) at 989 ms⁻¹ (20.6%). The average velocities for the plywood and 3L-6T-3L beams, which both have six longitudinal and six transverse oriented layers were 3487 ms⁻¹ (72.7%) and 3251 ms⁻¹ (67.8%), respectively. The average velocity of sound in the 4L-4T-4L beams, where the proportion of longitudinal to transverse layers is 2 to 1, was 3863 ms⁻¹ (80.5%). In the clearwood beams (Beams 24 to 26) the velocity was 4868 ms⁻¹, slightly higher than the velocity of the LVL-L beams: the clear, solid Radiata pine beams had narrow, flat rings and came from stiff outerwood of trees, whereas the LVL-L was a mixture of veneer from most likely (though not a certainty) the outer parts of peeled radiata logs.

Table 5.3 Velocity (derived from 1st, 2nd, and 3rd harmonics and the average of the three harmonics) averaged over three tests on each of the three beams of each type before artificial knot insertion. Also presented is the damping ratio (auto-damping function).

	Velocity 1 st (ms ⁻¹)	Velocity 2 nd (ms ⁻¹)	Velocity 3 rd (ms ⁻¹)	Velocity average (ms ⁻¹)	Damping ratio (%)
LVL-L	4749	4816	4831	4799	0.389
Ply	3460	3515	3488	3487	0.511
4L-4T-4L	3865	3890	3852	3863	0.447
3L-6T-3L	3286	3282	3185	3251	0.505
LVL-T	983	992	993	989	1.55
Clearwood	4848	4885	4871	4868	0.374

The damping ratio was lowest for the LVL-L beams at 0.389% (25.1% of the highest value) and was highest at 1.55% (taken as 100%) for the LVL-T beam. The values for the plywood and the 3L-6T-3L beams were 0.511% (33%) and 0.505% (32.5%) and the damping ratio for the 4L-4T-4L beams was 0.447% (28.9%). The damping ratio of the clearwood beams was 0.374% which was similar to the LVL-L beams. The MoE_d values presented later in this section are calculated from the actual whole density of each beam (through division of the beam's mass by its volume). The density of the laminate beams was consistently c. 530 kgm⁻³, whilst the density of the clearwood beams was c. 440 kgm⁻³.

Following the testing of the first 12 beams in their unaltered state, holes were drilled at specified locations along the beam and filled with dowels of increasing diameter, to simulate knots. The subsequent changes (or lack thereof) in 1st, 2nd and 3rd harmonic frequency (and thus velocity and dynamic MoE) and damping ratio of the 1st harmonic were recorded. Table 6.4 presents the diameters of the artificial knots (dowels), the percentage area of the beam cross-section occupied by each size of dowel, and the percentage of the beam volume occupied by a single dowel. When there are one or more knots in a beam, this is expressed as the knot volume ratio (KVR).

Table 5.4 The percentage of cross-sectional area and percentage of beam volume occupied by a single dowel of various diameters.

Diameter of dowel (mm)	Percentage area of beam cross section (%)	Total knot volume (KVR) as percentage of whole beam (%)
6	15	0.036
10	25	0.100
14	35	0.256
20	50	0.400
25	63	0.625
32	80	1.024

Figure 5.14 shows photographs of these variously sized dowels (knots) inserted perpendicular to the laminate layers in Beam 1 (Images A through E). Also shown is an example (Beam 13) of a dowel (knot) having been inserted parallel to the laminate layers, as well as two examples of parallel edge knot insertions (Beams 5 and 15).

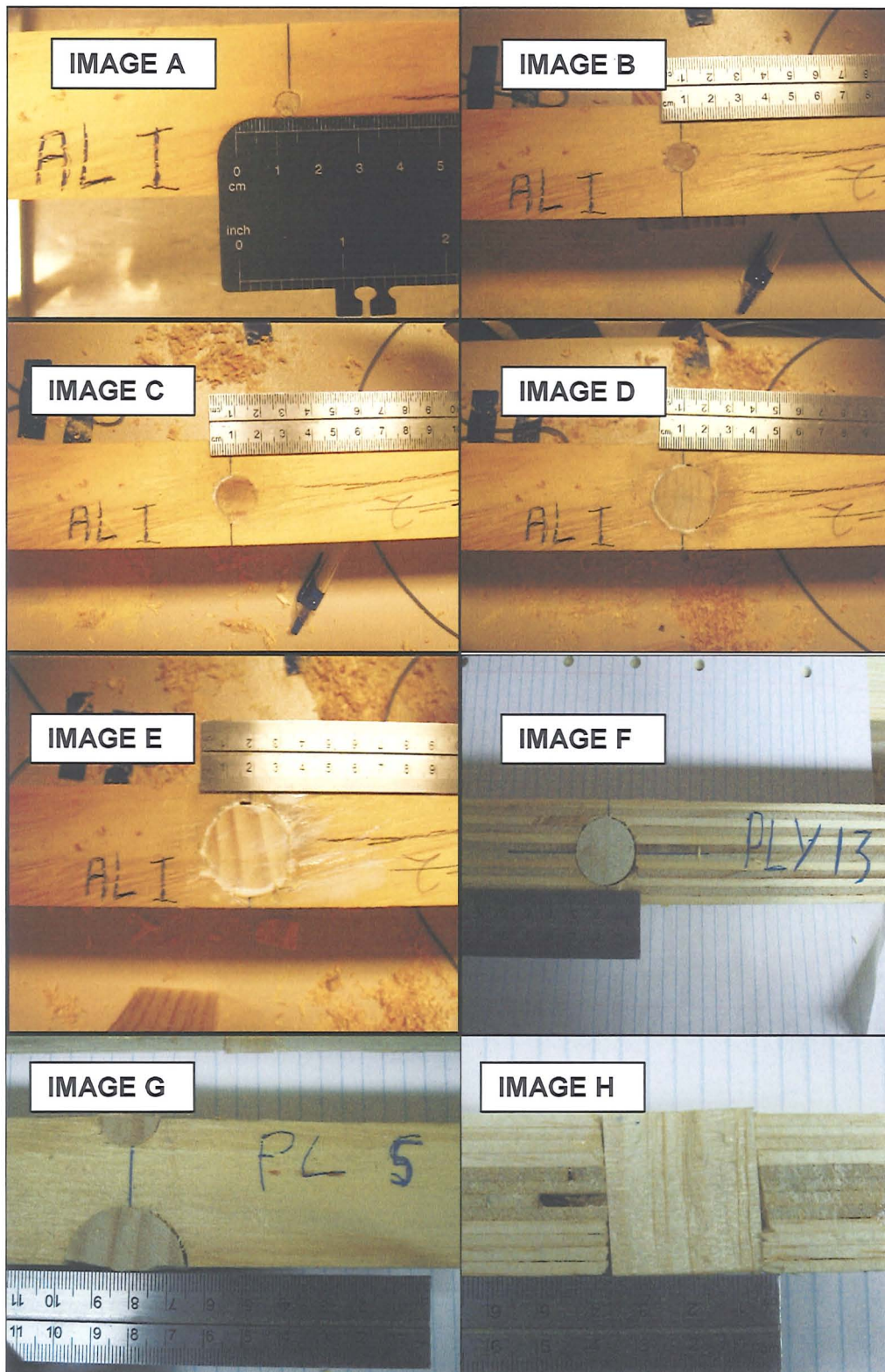


Figure 5.14 Images A to E show 6 mm, 10 mm, 16 mm, 25 mm, and 32 mm dowels inserted perpendicularly in Beam 1 (LVL-L). Image F shows a 25 mm dowel inserted perpendicularly in Beam 13 (PLY). Image G shows 32 mm and 16 mm dowels inserted perpendicularly in Beam 5 (PLY). Image H shows a 32 mm dowel perpendicularly across Beam 15 (4L-4T-4L).

During the test series, the frequency of the 1st harmonics and both subsequent harmonics did not always drop uniformly with each subsequent knot insertion. The relationship between the frequency of the harmonics changed where the knots were drilled at different positions, e.g. at midspan or at $\frac{1}{4}$ and $\frac{3}{4}$ span.

5.5.1 Knots at midspan

5.5.1.1 Influence on velocity

To illustrate this phenomenon, the velocity as based on the first three harmonics was plotted against the KVR of the beam in Figure 5.15. This shows that the velocities calculated on Beam 1 (LVL-L) from the 1st and 3rd harmonics dropped almost linearly when the KVR increased (R^2 correlation to KVR of 0.95 and 0.98 respectively, based on seven data points). Significantly, the velocity based on the 2nd harmonic only reduced by 0.21%. This can be seen to significantly affect the derived MoE_d depending on the harmonic used, *i.e.* if the MoE_d is calculated from the 1st harmonic after the 32 mm dowel insertion, a value of 9.93 GPa is derived as opposed to 12.23 GPa from the second harmonic, a difference of 19%. This pattern, of a relatively stable 2nd harmonic and reducing 1st and 3rd harmonics, is seen not only in Beams 28 (which repeated the test configuration) and 34 (edge-inserted knots at midspan), but across all five types of specimen when holes were solely inserted at midspan. This is discussed further in Sub-Section 5.7.2.2.

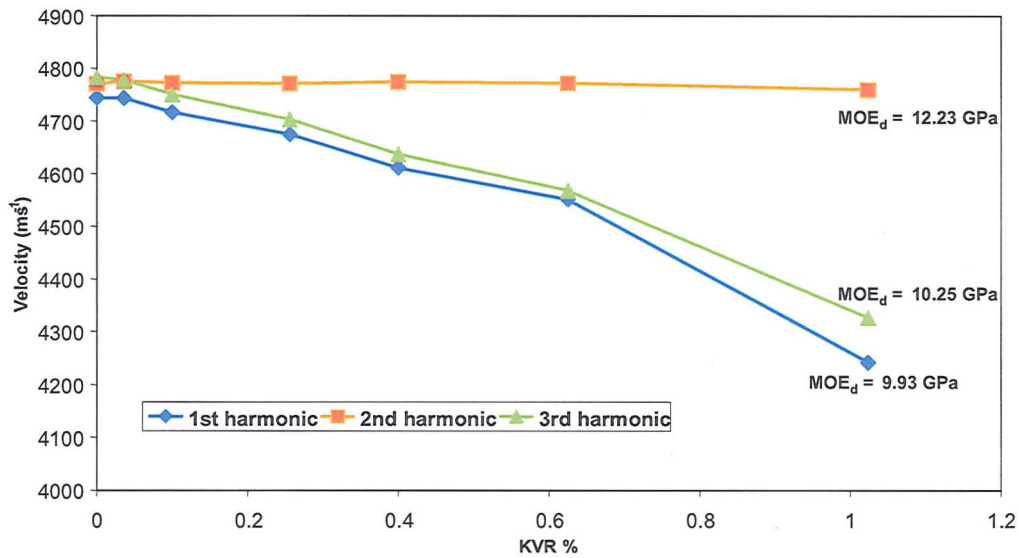


Figure 5.15 1st, 2nd and 3rd harmonic velocities versus KVR in LVL-L Beam 1 with knots at midspan. Also displayed are the equivalently calculated MOE_d values.

5.5.1.2 Influence on damping ratio and dynamic MoE

Figure 5.16 shows the effect on the damping ratio and the MOE (based on the 1st harmonic) of stepwise increases in the diameter of the perpendicular knots (shown as KVR) at midspan. In the case of the clearwood beam, the holes were drilled perpendicular to the annual rings. Note that in Figure 5.16 and subsequent Figures, the damping ratio is on the left-hand y-axis and the MOE_d on the right and that both have different scales.

The clearly anomalous increase of the PLY (Beam 4) damping ratio when the 25 mm dowel is introduced at midspan (shown within a red-dashed circle); can be explained by bifurcation of the frequency peak in this range. A second PLY beam (Beam 6) was tested to confirm this unusual pattern and gave similar results. The LVL test is based on Beam 1 whilst Beam 28 (same configuration on an LVL beam) also showed consistent results. The effects of bifurcation on the calculation of the velocity, elastic and damping properties are discussed in Sub-Chapter 5.7.6. This bifurcation was an unexpected, but recurring feature of this and subsequent test series and shall be highlighted throughout.

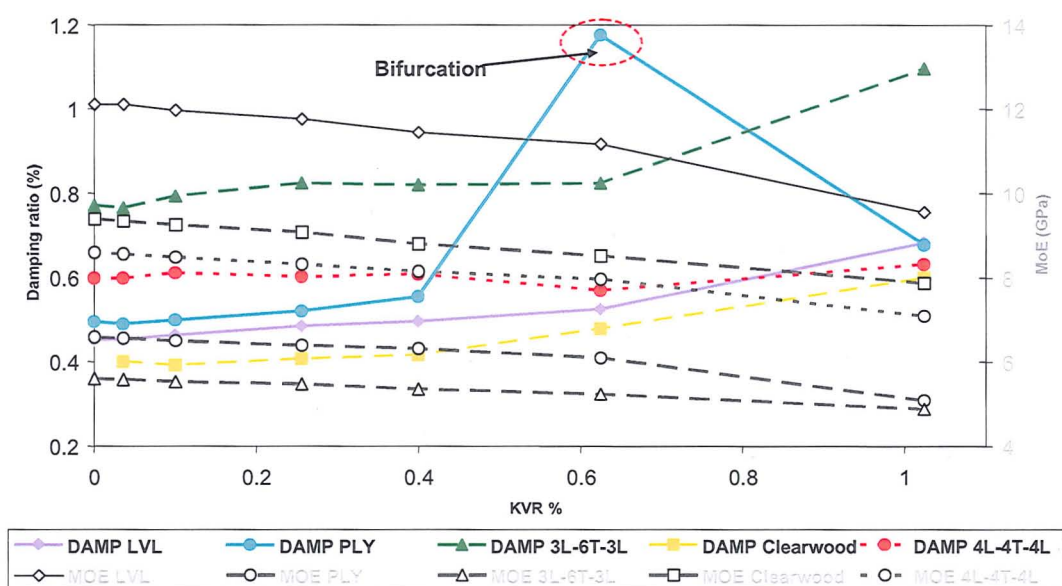


Figure 5.16 Influence of perpendicular knots of increasing diameter (increasing KVR) at midspan on the damping ratio (coloured lines) and MOE (grey lines). The red-dashed circle indicates an area of peak bifurcation.

It can be seen from Figure 5.16 that the damping ratio increased by c. 40% by the time that the largest 32 mm dowel had been introduced. In all beams, the damping ratio increased up to the 20 mm or 25 mm dowel. When introducing the 32 mm dowel, which takes up c. 80% of the cross-section at midspan, or 1.024 % of the total beam volume, the damping ratio increased at a significantly higher rate in all cases. However, the 4L-4T-4L beam actually dropped upon the introduction of the 25 mm dowel, though also rose significantly again on the introduction of the 32 mm dowel. This may have also been the result of bifurcation of the 1st harmonic at the 25 mm dowel size (an example of bifurcative behaviour is shown in Figure 6.22, bifurcative behaviour is discussed further in Section 6.7.6). Note however that the clearwood and LVL beams were not affected in the same way and continued with a near linear increase. The damping ratio of the Radiata clearwood beam (without artificial knots) was the lowest at 0.4% and remained the lowest throughout the insertion, ending the test with a damping ratio of 0.59%. A similar damping ratio (0.2% to 0.6%) was reported by Cai *et al.*^(6,13) for Douglas fir.

The bifurcation of the 1st harmonic in the PLY and 4L-4T-4L beams did not seem to have as much of an impact on the MoE_d as it had on the damping ratio. With increasing knot size, the MoE_d (displayed in grey lines) of all beams decreased

almost linearly. It can be seen that the LVL beam, despite maintaining a position as the beam with the highest MoE_d value, suffered the greatest reduction in MoE_d , falling by c. 20% from its initial value for the largest dowel (32 mm).

5.5.1.2.1 Knot orientation

The differing response of the various beams, as a result of their differing level of inhomogeneity, to the insertion of differently orientated discontinuities is discussed in Section 5.7.2.4. It is sufficient to say at this point that the orientation of the insertion into a laminated beam affects the response, due to the layers that are affected by the discontinuity.

Artificial knots were also inserted parallel to the centre of the laminate layers. It can be seen from Figure 5.17, that the LVL-L beam showed the same increase in damping ratio and the same near linear decrease of MoE_d (by c. 20%) as in the test where the holes were drilled perpendicular to the layers (Figure 5.16).

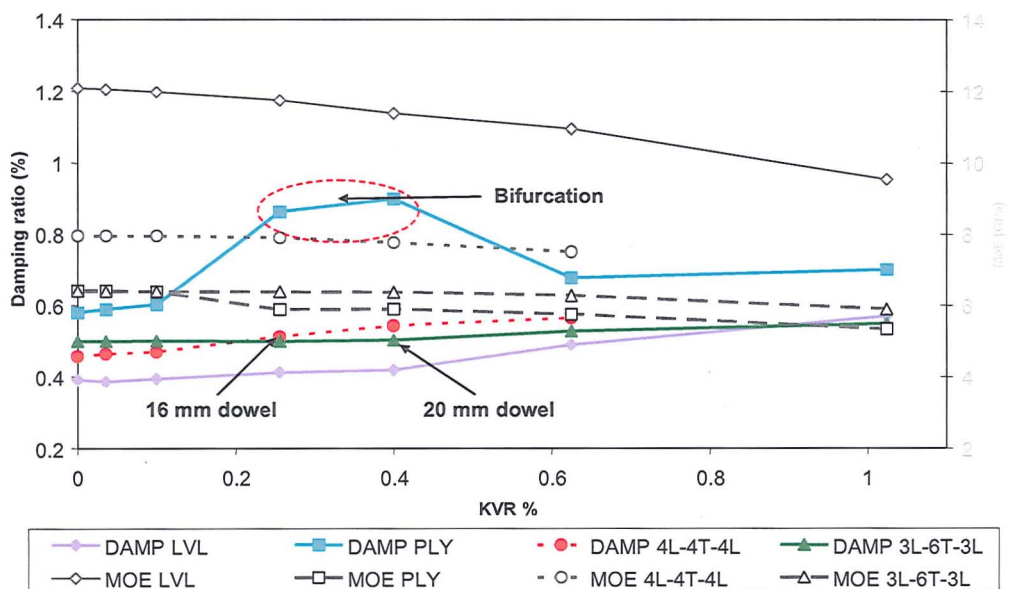


Figure 5.17 Influence of parallel knots of increasing diameter (increasing KVR) at midspan on the damping ratio (colored lines) and MOE (grey lines). The red-dashed circle indicates an area of potential bifurcation.

As expected the sandwiched beams showed different results. The 4L-4T-4L and the 3L-6T-3L beams showed only a slight increase in damping ratio (and relatively

little decrease in MoE_d) until the diameter of the dowel became bigger than the sandwiched transverse layers, *i.e.* a 16 mm dowel and a 20 mm dowel respectively. Until then, the damping ratio of both sandwiched beams only increased by less than 10% and likewise the MoE_d dropped less than 10%. Once those dowels were fitted both the damping ratio and the MoE_d were affected. The test for the 4L-4T-4L beam was stopped after the 25 mm dowel was fitted as the beam started to delaminate while drilling the 32 mm hole. It can be seen that the pattern of behaviour for the LVL beam's damping ratio and MoE_d tended to follow a clearly symmetrical pattern of increase and decrease.

5.5.1.2.2 Edge knots

Figure 5.18 shows the results of two hemispherical holes (edge knots) drilled perpendicular to the layers at midspan. The situation was similar where the holes were drilled perpendicular to the layers but through the centre at midspan (Figure 5.16) as in both cases all of the layers (longitudinal and transverse were applicable) were cut. As a result of the stepped increase in one edge followed by the other, there are more data points to consider. Beam 9 (3L-6T-3L) remained untested due to time constraints.

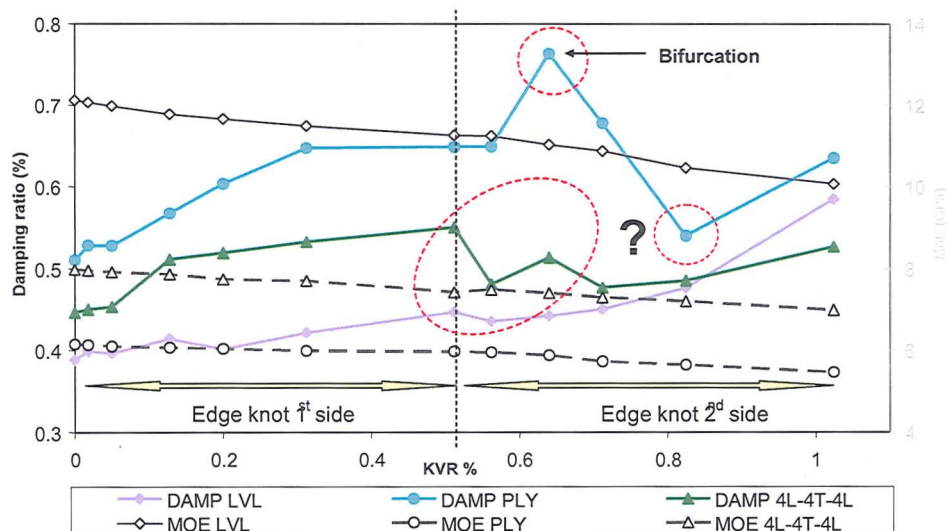


Figure 5.18 Influence of perpendicular edge knots of increasing diameter (increasing KVR) at midspan on the damping ratio (colored lines) and MOE (grey lines). The red-dashed circle indicates an area of potential

bifurcation. The question mark next to the red-dashed oval and small red circle indicate areas of uncertain behaviour.

In these tests, the LVL-L beam showed a systematic increase in damping ratio from 0.39% to 0.59%, whereas the PLY beam again showed the highest damping ratio before knot introduction. As in previous tests on perpendicular central knots, both the PLY and 4L-4T-4L means were affected by a bifurcation causing an anomalous spike in the damping ratios (though in the perpendicular central knot 4L-4T-4L beam this was shown by a distinct drop in the damping ratio, another result of bifurcation as explained in Section 5.7.6) when the beam reaches c. 0.6% KVR.

The damping ratio of the plywood beam and the LVL showed no consistent response to an increasing knot volume of the beam particularly during the 2nd edge knot insertion). In contrast, the MoE_d of all three beams investigated in this test showed an almost linear decrease with increasing knot volume of the beam.

When the holes were drilled parallel to the individual layers of the beams (Figure 5.19), the 4L-4T-4L beam showed significantly higher damping ratios (c. 1.7%) compared to the perpendicular test for the same hole configuration (Figure 5.18). The points at which the outer longitudinal layers were completely cut at midspan correspond to the steepest damping ratio slopes in the 1st and 2nd edge knots respectively, as shown in Figure 5.19. This represents when the three longitudinal outer layers of one side of the 3L-6T-3L have been cut after the 20 mm dowel was inserted. Thus the 3L-6T-3L and the 4L-4T-4L curves for the damping ratio are slightly out of phase which was probably caused by the additional longitudinal outer layer of the 4L-4T-4L beam, requiring larger holes to cut through this extra longitudinal layer of veneer on either side. Unfortunately, it was not possible to finish the tests for the two sandwiched beams as the central portions of each beam fractured during the drilling process.

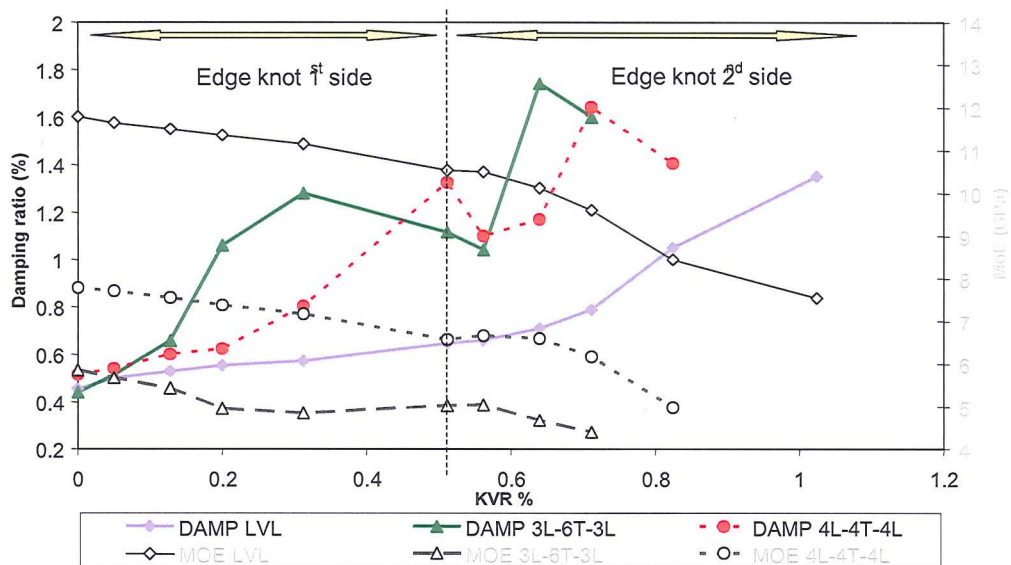


Figure 5.19 Influence of parallel edge knots of increasing diameter (increasing KVR) at midspan on the damping ratio (colored lines) and MOE (grey lines). No PLY test beam was inspected due to beam availability.

Whilst the behaviour of the damping ratios in the 3L-6T-3L and 4L-4T-4L beams depended on the layers cut, their MoE_d values showed a more consistent reduction. The LVL beam, by contrast, showed both a steady decrease and a steady increase in MoE_d and damping ratio indicating a very similar reaction to increased KVR at the edges at midspan.

5.5.2 Knots at $\frac{1}{4}$ and $\frac{3}{4}$ span

Following on from the results of the midspan insertion, where clear patterns in harmonic behaviour were observed, it was hypothesized that the 2nd harmonic would respond in a similar fashion (to the 1st harmonic for defects at midspan), if defects were inserted at $\frac{1}{4}$ and $\frac{3}{4}$ span.

5.5.2.1 Influence on velocity

When the artificial knots are inserted firstly (up to 32 mm dowels) at the $\frac{1}{4}$ of the span length from the impact end and repeated at $\frac{3}{4}$ of the span length, the velocity based on the 2nd harmonic velocity decreased sharply with KVR (Figure 6.10). The 3rd harmonic velocity was least affected and the 1st harmonic velocity lay

somewhere in between the 2nd and 3rd harmonic velocities. The linear correlation for all three velocities to KVR remained extremely high ($R^2 = 0.96$ to 0.97) based on the eleven separate KVR increases. Once again, this pattern was repeated across the types of specimen where these test configurations were repeated. Note that 6 mm dowels were not inserted at either quarter-point due to their lack of influence seen in previous tests.

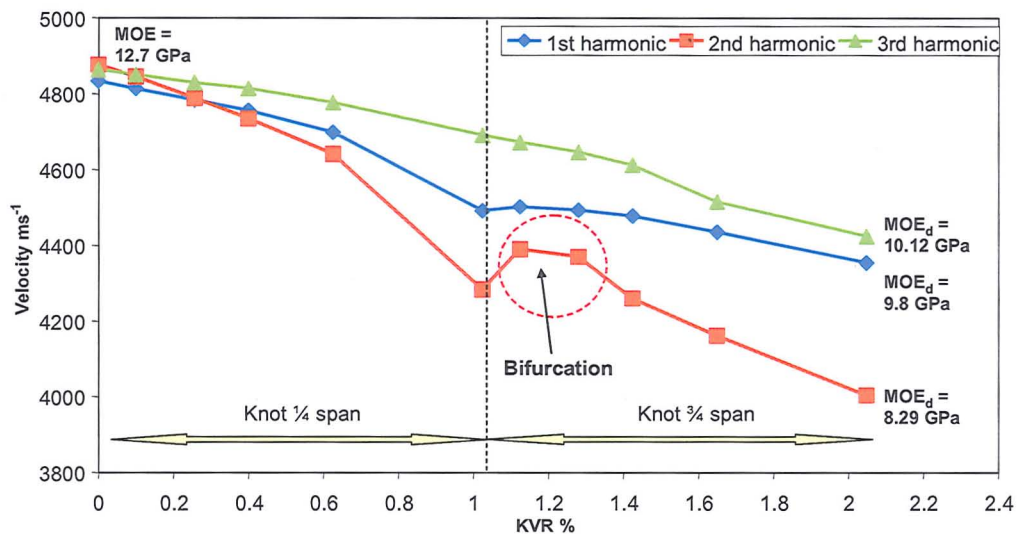


Figure 5.20 1st, 2nd and 3rd harmonic velocities versus KVR in a (LVL-L Beam 22 with knots at ¼ and ¾ span). Also displayed are the equivalently calculated MoE_d values. The red-dashed circle indicates an area of potential bifurcation.

The increase of velocity of the 2nd harmonic, when a second dowel is introduced at ¾ of the span (shown within a red-dashed circle), can be explained by bifurcation red-dashed of the frequency spectrum in this range. The effects of bifurcation on the calculation of the elastic and damping properties are discussed in Section 5.7.6.

5.5.2.2 Influence on damping ratio and dynamic MoE

Figure 5.21 shows the impact of knots at ¼- and ¾-span on the damping ratio and MoE_d . Since the 2nd harmonic had its vibrational displacement nodes at the quarters of the beam span, the velocity (and hence MoE_d) and damping ratio for these tests were calculated from the 2nd harmonic. As such, the damping ratio

should theoretically start from a higher percentage for the 2nd harmonic due to increased internal friction at this wavelength, results shown in Figure 5.21, when compared with Figure 5.16, would indicate that this is not the case, with both the LVL and clearwood beams having lower initial damping ratios for the 2nd harmonic. Figure 6.11 shows that the 2nd harmonic damping ratio and the MoE_d of the LVL-L beam was affected in a similar manner to that of the 1st harmonic when the knots were introduced at midspan only, particularly when first introducing the knots at 1/4-span.

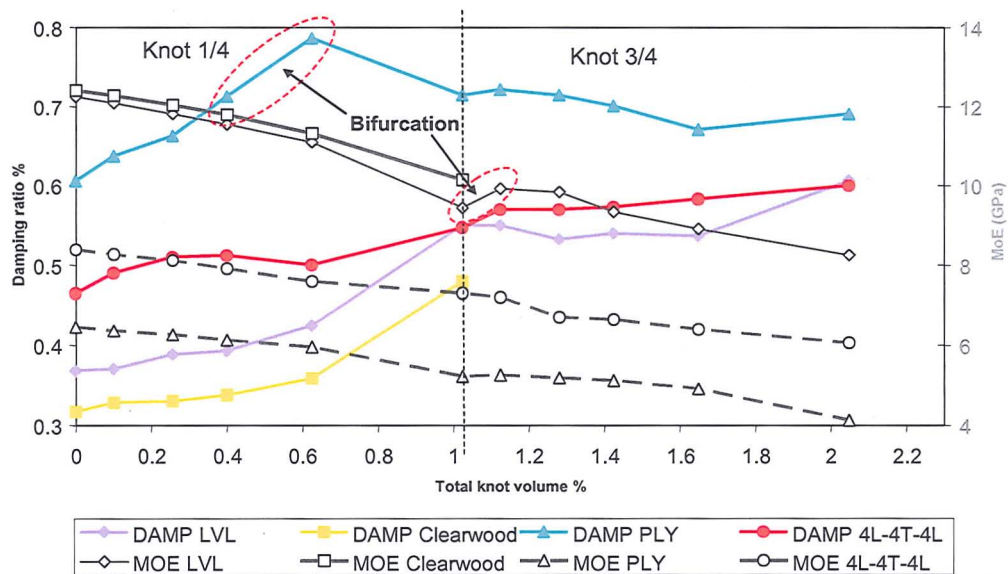


Figure 5.21 Influence of perpendicular knots of increasing diameter (increasing KVR) at 1/4 and 3/4 span on the damping ratio (colored lines) and MOE (grey lines). The red-dashed circle indicates an area of potential bifurcation. No 3L-6T-3L test beam was inspected due to beam availability.

However, when a second knot was added at the 3/4 span, the damping ratio did not change significantly until the final and largest, 32 mm, knot was inserted. The 32 mm knot at 1/4 span increased the damping ratio by about 45%, whereas the second 32 mm knot at 3/4 increased the damping ratio by only an additional 15%. Again the graphed MoE_d and damping ratio of the LVL-L beam (based on the 2nd harmonic) follow a close linear symmetry *i.e.* when knots at 3/4 span were introduced the damping ratio dropped and the MoE_d increased. In this case however there was added complexity to the issue as a bifurcation of the 2nd harmonic occurred between the 1/4 span 25 mm knot and the insertion of the 6 mm

$\frac{3}{4}$ span knot. A second peak arose close to the peak taken as the 2nd harmonic and, with increased KVR, became bigger than the original causing a shift to a higher resonance frequency for the second harmonic. This explains the rise in the 2nd harmonic MoE_d value. This is discussed in more detail in Section 5.7.6. As in Figure 5.16, and for the same reasons, the damping ratio of the plywood beam again showed a peak at c. 0.6% KVR, while the MoE_d decreased linearly. The 4L-4T-4L beam showed a reasonably linear pattern for both damping ratio and MoE_d.

5.5.3 Knots at various positions

Following observation of the results of the previous tests, further tests were conducted to evaluate whether the damping ratio and the MoE_d are affected at approximately the same rate if the KVR of the beam is progressively increased to c.10%. Additionally it was hypothesized that if the 2nd harmonic could be “protected” from frequency reduction through the specific placement of defects, then the same could be done for higher level harmonics. In Beams 27 and 33 (LVL-L) and Beam 26 (clearwood), various perpendicular 25 mm central holes were introduced at specific positions along the span. The first knots were introduced at locations where the 8th harmonic has its anti-nodes for vibrational displacement, as shown in Figure 5.22. This was to keep stable the 8th harmonic’s frequency and to show that other harmonics which have nodes (points of maximum stress concentration) at these positions drop in frequency.

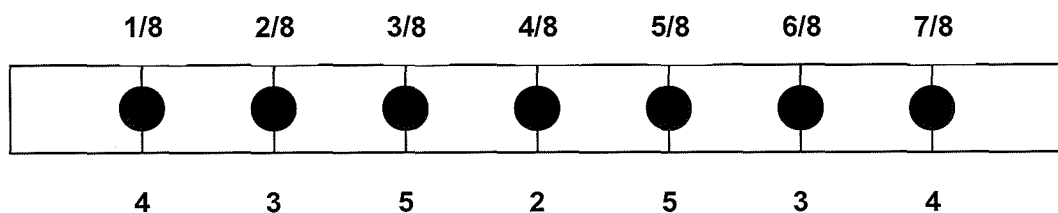


Figure 5.22 Beam with holes at the first seven positions drilled along the span. The numbers on the top mark the eighths of the span from the left side impact end (vibrational pressure nodes for the 8th harmonic) and the numbers on the bottom refer to the steps of the experiment. Step 1 was without holes.

The first 25 mm defect (step 2) was drilled at midspan (an anti-nodal point for all even harmonics) followed by two defects (step 3) at $\frac{2}{8}$ and $\frac{6}{8}$ (anti-nodal points for the 4th and 8th harmonic), the next two defects (step 4) were put at $\frac{1}{8}$ and $\frac{7}{8}$ (anti-nodes for 8th harmonic) and then the last anti-nodal positions for the 8th harmonic at $\frac{3}{8}$ and $\frac{5}{8}$ span were filled with dowels (step 5). After this, knots were introduced at places where the 8th harmonic has nodes, as shown in Figure 5.23.

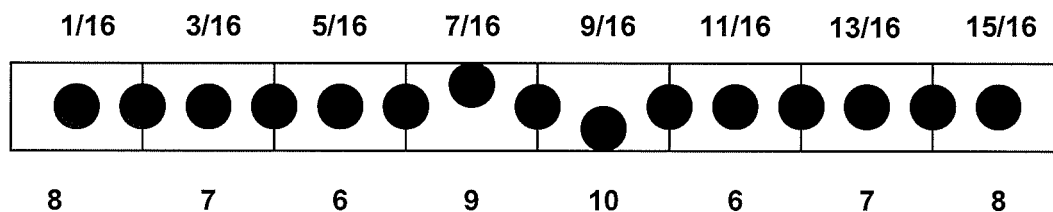


Figure 5.23 Beam with holes at various positions drilled along the span. The numbers on the top mark the odd 16th of the span from the left side impact end (vibrational pressure nodes for the 8th harmonic) and the numbers on the bottom refer to the steps of the experiment. Step 1 was without holes.

In step 6, defects were placed at $\frac{5}{16}$ and $\frac{11}{16}$ span, which corresponded to anti-nodes for the 3rd harmonic. As such, the hypothesis was that the 8th harmonic should start to drop while the 3rd harmonic should not be affected. Knots at $\frac{1}{16}$ and $\frac{15}{16}$ followed in step 7. Up to this point all the defects would have been drilled in one straight line (centre line) perpendicular to the individual layers of the beam. As such there is still a 7.5 mm × 40 mm wide clear passage for a wave on either side of the dowels (c. 40% of the cross-section). As such, in step 9, a defect was inserted into one of these ‘fast passes’ on one side of the beam at $\frac{7}{16}$ span. Finally, the last fast pass obstructed by a defect on the opposite site at $\frac{9}{16}$ span (step 10).

5.5.3.1 Influence on velocity

Figure 5.24 shows the response of the first three harmonics (on LVL Beam 33) with increasing KVR through steps 1 to 10 in this test series. It was observed that the velocities based on the first three harmonics were affected more equally with increasing number of defects (after c. 6% KVR). The 2nd harmonic velocity was initially unaffected as the first defect was introduced at midspan, the next insertion

took place simultaneously at $\frac{1}{4}$ and $\frac{3}{4}$ span, thus accounting for the observed reduction in 2nd harmonic velocity below the 1st and 3rd MoE_d values. The correlations to the total beam KVR for all three harmonic velocities on the basis of the 10 data points shown in Figure 5.24 were significant ($R^2 = 0.95$ to 0.97). The same pattern of reductions occurred in the clearwood specimen under the same test configuration (Beam 26).

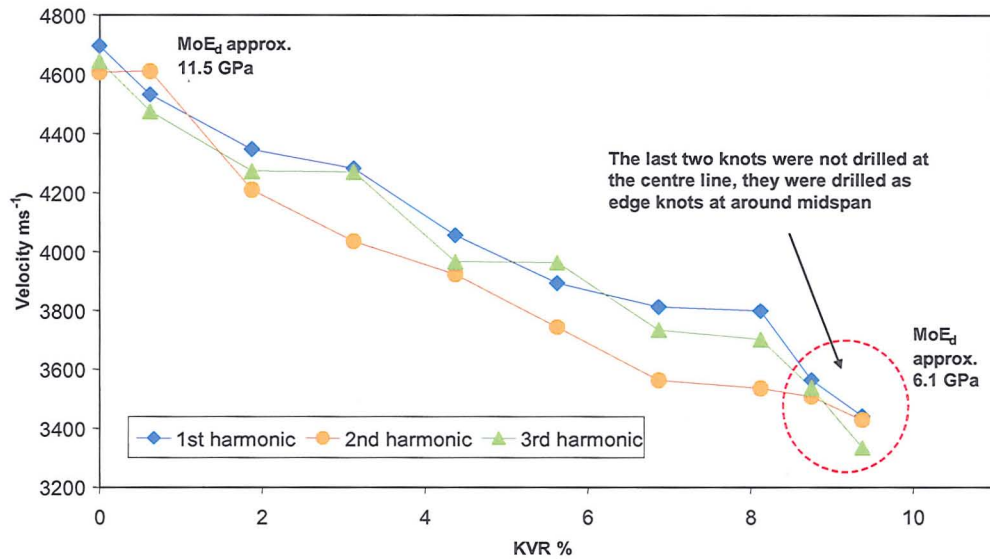


Figure 5.24 1st, 2nd and 3rd harmonic velocities versus KVR in an LVL-L beam (Beam 33 with 25 mm knots at various positions along the span). Also displayed are the approximate MoE_d values.

Figure 5.25 shows the response of the first eight harmonics to the ten steps of the test series. It can be seen that before the holes were drilled, the velocities derived from the first eight harmonics were spread over a small range (114 ms⁻¹). There was no tendency for higher harmonics to produce higher velocities.

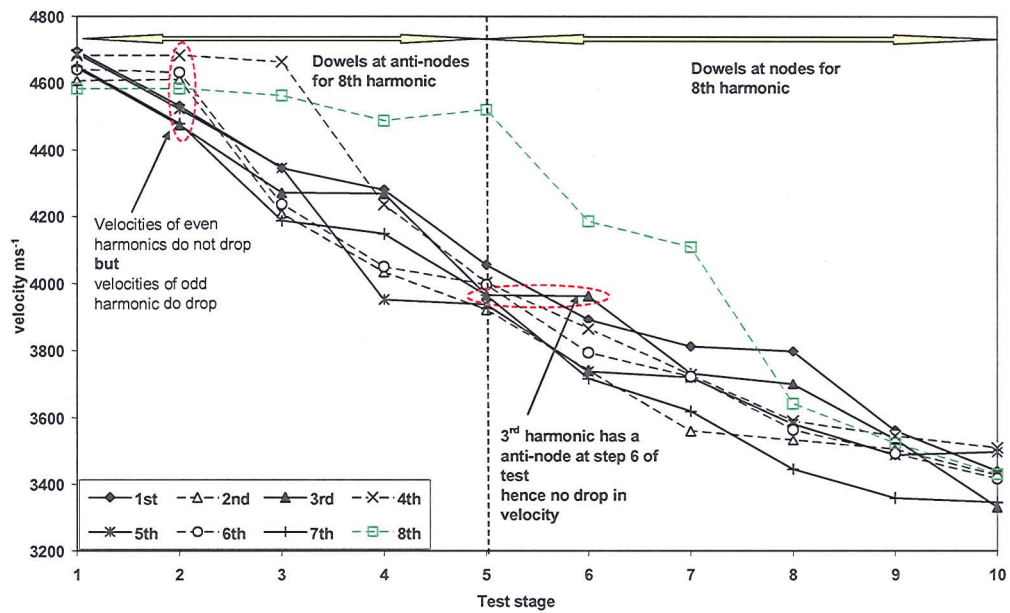


Figure 5.25 Influence of perpendicular 25 mm knots inserted at various locations on Beam 33 (LVL). The x-axis shows the stages of the test (Stages 1 to 10 corresponding to Stages A to J as described in Section 4.3.3: Test series 8). The y-axis shows the velocity recovered from the specific harmonic frequency. Red dashed circles display areas of specific interest.

Figure 5.25 shows that the dowels fitted at specific positions along the span of a LVL-L beam had a significant impact on the velocity of the first eight harmonics. When the first dowel was placed at midspan only the odd harmonics which have a node at midspan showed a drop in velocity. It was possible to protect the 8th harmonic by introducing knots at position where the 8th harmonic has its nodes. This situation is discussed further in Section 5.7.2.2.

5.5.3.2 Influence on damping ratio and dynamic MoE

Figure 5.26 shows the damping ratio of the 1st harmonic and the MoE_d of Beam 33 (LVL-L) plotted against increasing KVR, as based on the multiple position test series. On this graph, the MoE_d was either calculated from the average of the first eight harmonic velocities, from the 1st harmonic velocity, or from the harmonic which had the lowest velocity at each step (For example, at the 2nd step, when the

dowel at midspan was fitted, the 3rd harmonic showed the lowest velocity, at the 3rd step it was the 7th and so on).

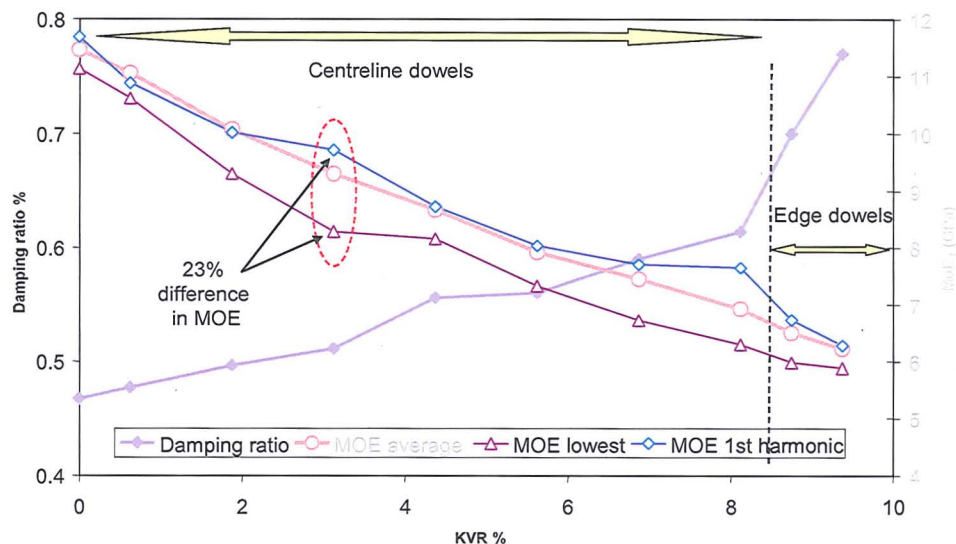


Figure 5.26 Influence of increasing KVR (firstly used central knots with a final two knots inserted at the edges) on 1st harmonic damping ratio and MoEd values. Results displayed are from LVL Beam 33.

From Figure 5.26, it can be seen that the 1st harmonic damping ratio increased almost linearly until the two edge knots were introduced. The linear correlation between the damping ratio and KVR was $R^2 = 0.985$ if the edge dowel insertions were discounted. Only within the last two steps did the damping ratio increase at a much higher level (a 25% increase in the damping ratio solely due to the insertion of the two edge dowels). Thus, cutting of the remaining 'fast passes' had a bigger impact on the 1st harmonic damping ratio than putting more dowels in line with the already fitted dowels. The MoE_d as calculated from the average of the first eight harmonics dropped systematically with increasing knot volume ($R^2 = 0.997$), even with the final two steps included.

Similar correlations were seen with the other two measures of MoE_d. However, the difference in MoE_d between the different calculations was as high as 23%. In all cases a negative exponential function brought the strongest correlation between MoE_d and KVR. That indicates that the impact of knots gets weaker the knottier the

wood gets. It should be noted however that despite a negative exponential function providing the closest correlation, a negative linear correlation still provides an extremely significant correlation between MoE_d and KVR ($R^2 > 0.95$). As can be seen from Figure 5.27, the situation is similar in the case of a clearwood beam (Beam 26) tested under the same knot configurations.

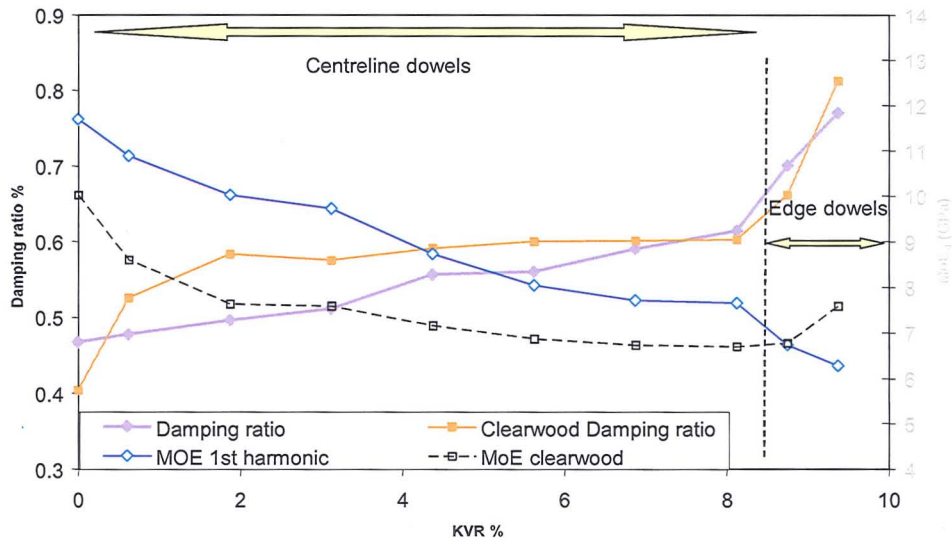


Figure 5.27 Influence of increasing KVR (firstly used knots in a centred location, with a final two knots inserted at the edges) on 1st harmonic damping ratio and MoE_d values. Results displayed are from LVL Beam 33 and clearwood Beam 26.

Figure 5.28 shows a positive linear correlation between KVR and damping ratio for both LVL and clearwood beams. However it can be seen that this correlation is improved by using a positive exponential regression, indicating that the impact of knots on the damping ratio increases with increasing knot content. It can also be seen that the correlations were higher for the LVL beam than the clearwood beam.

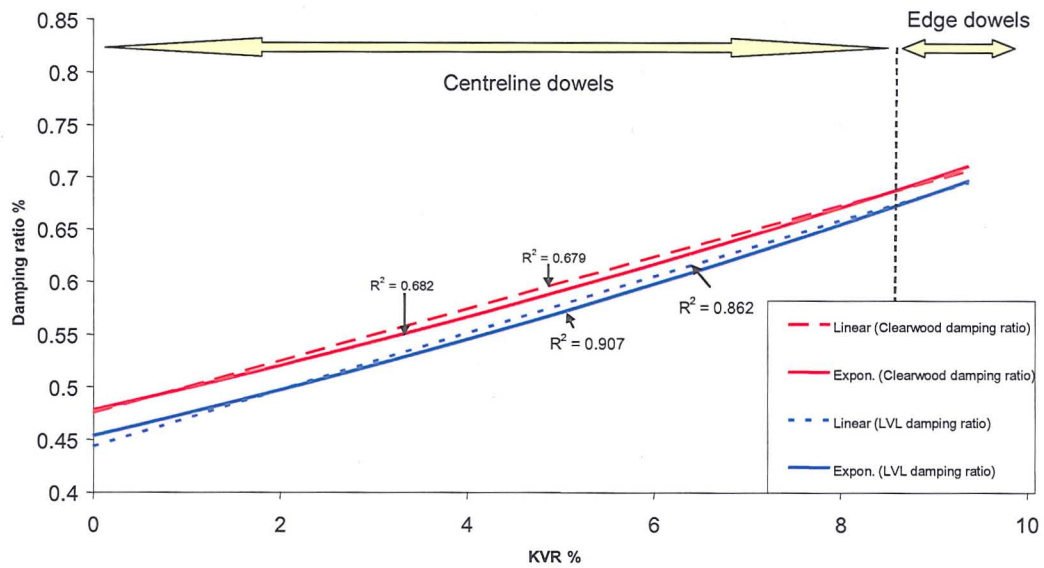


Figure 5.28 Correlations between KVR (knots initially placed in a centreline location, followed with a final two knots inserted at the edges) and 1st harmonic damping ratio on an LVL (blue) beam and a clearwood (red) beam. Linear correlations displayed are from LVL Beam 33 (solid line) and clearwood Beam 26 (solid line). Positive exponential correlations are displayed as a small-dashed and a medium dashed line respectively.

The same improvement in correlation through the use of an exponential regression (in place of a linear regression) can be seen in Figure 5.29, which shows the correlations between KVR and 1st harmonic damping ratio on beams (LVL Beam 23 and PLY Beam 21) with knots inserted perpendicularly at $\frac{3}{8}$ and $\frac{5}{8}$ of span. It can be seen, however, that whilst the correlation of an LVL beam's damping ratio to its KVR remains significantly high ($R^2 > 0.91$), any meaningful correlation between the same two parameters is absent for a PLY beam ($R^2 < 0.2$).

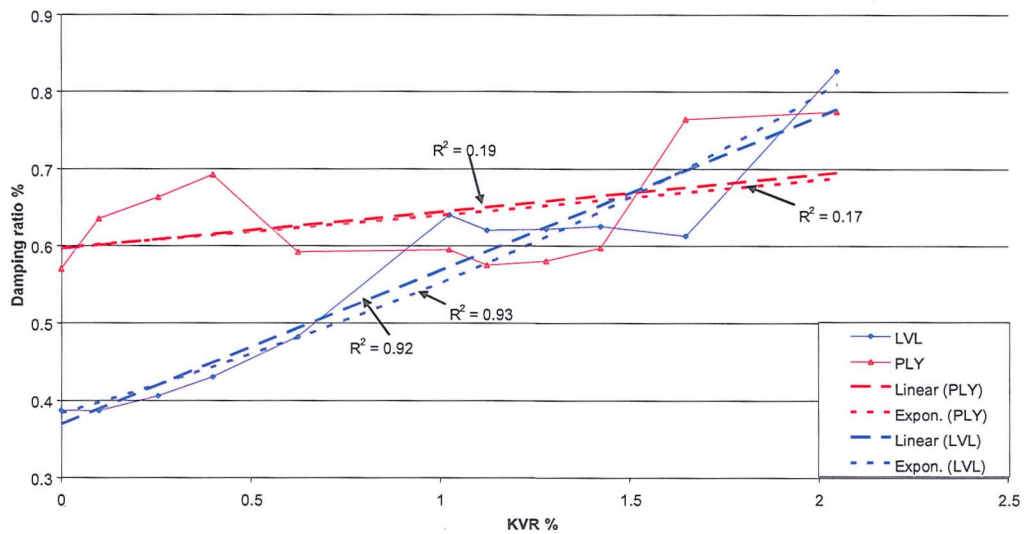


Figure 5.29 Relationship between KVR and 1st harmonic damping ratios on LVL (blue solid line) and PLY (red solid line) beams with artificial knots of increasing size inserted at $\frac{3}{8}$ and $\frac{5}{8}$ span. Linear correlations displayed are from LVL beam 23 (blue medium dashed line) and PLY beam 21 (red medium dashed line). Exponential correlations are displayed as small-dashed lines.

5.5.4 Time of flight velocity versus resonance velocity

Beams 28 through 35 were also tested using the PUNDIT™ 54 kHz TOF system. Table 5.5 shows the PUNDIT™ TOF velocities from each of the beams tested before any knots were inserted (designated configuration type A) and after the maximum number of knots for each configuration had been inserted (designated configuration type B). The corresponding harmonic velocities are also displayed. Figure 5.30 graphically represents these results. A discussion of the implication of the results is given in Section 5.7.4.

Table 5.5 Harmonic and TOF velocity results for initial (A) and final (B) configurations of beams 28 through 35. Beam 35 had no knots.

Beam	configuration	Chart label (Figure 6.20)	PUNDIT™ vel. (ms ⁻¹)	Resonance method		
				Vel. 1 st (ms ⁻¹)	Vel. 2 nd (ms ⁻¹)	Vel. 3 rd (ms ⁻¹)
28 (LVL)	No knot	A	4996	4717	4684	4757
	Knot 32mm perpendicular midspan	B	4971	4372	4656	4353
29 (PLY)	No knot	A	3957	3487	3451	3507
	Knot 32mm parallel midspan	B	3866	3184	3451	3183
30 (PLY)	No knot	A	4083	3564	3616	3620
	Knots 32mm perpendicular 1/4+3/4	B	3944	3306	3164	3397
31 (4L-4T-4L)	No knot	A	4876	4026	3977	3994
	Knot 32mm perpendicular midspan	B	4900	3659	3981	3615
32 (3L-6T-3L)	No knot	A	4075	3484	3410	3369
	Knot 32mm parallel midspan	B	4242	3347	3412	3243
33 (LVL)	No knot	A	4975	4695	4605	4643
	Various 25mm holes	B	4506	3440	3427	3332
34 (4L-4T-4L)	No knot	A	5026	4060	3989	3981
	Knots 32mm perpendicular 1/4+3/4	B	4612	3742	3392	3740
35 (LVL - transverse)	No knot	A	1090	925	957	947

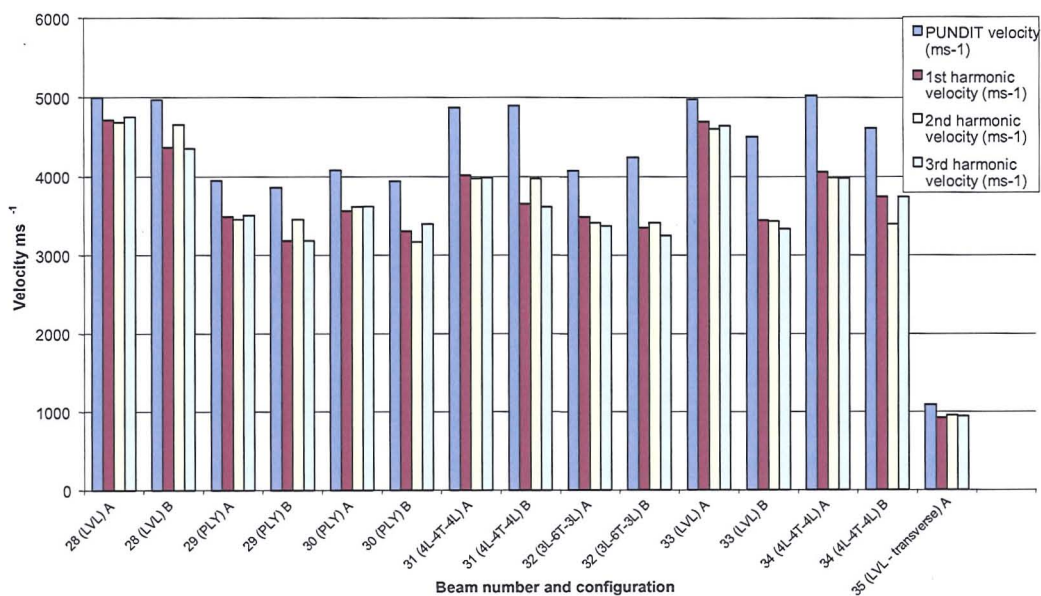


Figure 5.30 Graphical representation of the data presented in Table 6.5.

5.6 Static MoE versus dynamic MoE estimations

Table 5.6 compares the unaltered (*i.e.* dowel-free) acoustic MoE_d values (calculated by the average of the first three harmonics so as to not just estimate the midspan MoE_d) and the static MoE (derived from static 3 or 4-point bending tests). When the shear correction factor was applied to the static MoE for 3 or 4-point bending, the static MoE increased by approximately 3.5%. Each beam configuration was represented by three specimens, thus producing an average MoE_d from the average of the three harmonics on each of the three beams of each type.

Table 5.6 Comparison between the acoustic MoE_d and other measures: i) static apparent MOE measured when layers are oriented perpendicular (90°) to the applied load; ii) static apparent MoE measured when layers are oriented parallel (||) to the applied load; and iii) the average of i) and ii). E-modulus in GPa. Note that static MoE values are not corrected for shear. Also shown are the ratios of the static MoE values to the average MoE_d values.

Beam type	Acoustic MoE _d (GPa)	Static MoE Layers 90° (GPa)	Static MoE Layers (GPa)	Static MoE Average (GPa)	Stat. MoE 90° divided by Acoustic MoE _d	Stat. MoE divided by Acoustic MOE _d	Stat. MoE average divided by Acoustic MOE _d
LVL-L	12.37	10.37	10.08	10.23	0.84	0.82	0.83
PLY	6.4	5.39	5.308	5.35	0.844	0.83	0.84
3L-6T-3L	5.49	2.96	4.638	3.79	0.54	0.84	0.69
4L-4T-4L	8.03	4.48	6.738	5.60	0.56	0.84	0.7
LVL-T	0.50	0.41	0.41	0.41	0.81	0.80	0.81
Clearwood	9.48	8.51	8.1	8.30	0.9	0.85	0.88

It can be seen that the MoE_d values are always significantly higher than all measures of static MoE. The LVL beams showed the highest MoE_d (12.4 GPa), whereas the LVL-T beam (all transverse) had the lowest MoE_d (0.505 GPa). The same trend is seen in the static MoE values (10.23 GPa and 0.41 GPa respectively). The clearwood beam shows the closest relation of dynamic to static values with a 12% higher MoE_d value than the static MoE. The largest difference between static and dynamic values is a c. 30% difference in the case of 3L-6T-3L and 4L-4T-4L beams. It is also evident that the beams having four or six transverse layers sandwiched between the longitudinal layers displayed a higher MoE where the load was applied parallel to the layers rather than perpendicular (showing a 50% and 57% increased for the 4L-4T-4L beams and the 3L-6T-3L beams

respectively). There was relatively little difference in static MoE in other beam types due to orientation.

5.7 Discussion of results and issues

In this study, it has been observed that artificial defects inserted into both laminated and clear wood beams have a significant and predictable influence on a beam's dynamic elastic and damping properties as determined by acoustic NDT. The degree of predictability is determined by the level of inhomogeneity of the sample.

5.7.1 Experiment methods

Preliminary testing showed that support conditions for longitudinal resonance testing was not important, provided that the samples are suitably isolated from external coupling. It was also found that hot-glue was the most efficient method of semi-permanent attachment of the accelerometers. Impact excitation was shown to be the most reliable method of inputting a longitudinal stress-wave into the specimen with sufficient strength to observe multiple harmonics. Using a modal hammer was deemed favourable as it allowed for an FRF to be created and the auto-damping calculated. Further, five different methods of calculating the damping ratios were assessed, and it was found that using the auto-damping function of the PULSE system was the most repeatable and consistent with the manual estimation of the Q-factor. Reverberation time and logarithmic decrement were found to be too variable, and the calculation of impulse response too time-consuming, despite promising initial results. The calculated value for the fundamental frequency damping ratio of wood are consistent with previous estimations of 0.2% to 0.7%^(5.13-5.16).

5.7.2 Velocities, MoE_d and damping ratios

During the following sub-chapters 5.7.2.1 to 5.7.2.4, the effects of variables considered during these test series shall be discussed in relation to the results from previous sub-chapters.

5.7.2.1 Influence of varying inhomogeneity

The results presented in Table 5.3 demonstrate the effects of increasing inhomogeneity on acoustic velocity. In all cases the difference between averaged 1st, 2nd and 3rd harmonic velocities from 3 tests each on three different beams of the same composition was less than 100 ms^{-1} in all cases. Thus conclusions can be drawn from the average harmonic velocities. It is clear that the average velocity was highest within solid clearwood beams, followed by engineered LVL beams. These two beam types have similar acoustic velocities just under 5000 ms^{-1} . There is a much greater jump to the 3rd highest velocities, the 4L-4T-4L beams (at 3863 ms^{-1}), though its position as the third highest velocity is not unexpected as it has 8 layers orientated longitudinally. Similarly the PLY beams have a higher average velocity (3487 ms^{-1}) than the 3L-3T-3L beams (3251 ms^{-1}), though not by much, despite having equal numbers of longitudinal and transverse orientated layers. This may be due to having the longitudinal layers spread more evenly throughout the material, increasing the dynamic stiffness as opposed to having the six layers distributed on the outer portions of the beam. As expected, the All-T beams have a velocity 80% of that of the All-L beams, confirming the velocity differences based on orientation as discussed in Chapter 3.

Similarly, it can be seen from the damping ratio column of Table 5.3, that the effect of increasing inhomogeneity had an approximate proportionality between the decrease in velocity and increase in specimen damping ratio.

Table 5.7 Percentage difference between highest velocity and lowest damping ratio (Clearwood = 100%) and other beams with higher or lower values respectively.

Beam type	Velocity: percentage of highest velocity (%)	Damping ratio: percentage of the lowest damping ratio (%)
Clearwood	100	100
LVL-L	99	104
4L-4T-4L	79	120
PLY	72	137
3L-6T-3L	67	135
LVL-T	20	414

It can be seen from Table 5.7 that the percentage decrease in velocity from the highest velocity (*i.e.* clearwood) is reflected as a percentage increase in the damping ratio. For example, for 4L-4T-4L beams, a 21% reduction in velocity compared to the clearwood beams is mirrored by a 20% increase in the damping ratio. Similarly, a 33% reduction in the 3L-6T-3L velocity is mirrored by a 35% increase in the damping ratio. The slightly greater increase in damping ratio for the PLY beams (37%) compared to the 3L-6T-3L, whilst having a lesser velocity reduction (28%), may indicate that the damping ratio is increased by having to have the 1st harmonic longitudinal wave pass between alternating single layers across the cross-section of the beam as opposed blocks of three, then six, the three across the whole beam. Since the damping ratio for the All-T beams has increased by 4.1 times, as opposed to a fivefold velocity reduction, may indicate a tendency for the damping ratio to plateau with increasing inhomogeneity. This may also be seen in Figure 5.27, where the damping ratio is seen to plateau in solid clearwood after progressive increases in artificial defect insertions.

In comparison to the previous results of Chauhan *et al.*^(5.1), Table 5.8 displays the velocity results from this test series against those cited.

Table 5.8 Velocity results (in ms⁻¹) of TOF and resonance tests on beams cut from the same laminated panels. Resonance results are displayed as (a) PULSE™ 1st harmonic-derived velocities and (b) 1st harmonic velocities measured by WoodSpec™ in Chauhan *et al.*^(5.1). TOF results are displayed as (a) PUNDIT™ 54 kHz ultrasonic velocities and (b) TOF velocities measured by Fakopp 2D™ in Chauhan *et al.*^(5.1). The percentage difference of (b) to (a) and (d) to (c) are also displayed.

Beam type	(a) Velocity 1 st PULSE (ms ⁻¹)	(b) 1 st WoodSpec ™ (ms ⁻¹)	% difference (a to b)	(c) PUNDIT ™ (ms ⁻¹)	(d) Fakopp 2D™ (ms ⁻¹)	% difference (c to d)
LVL-L	4749	4660	-1.9	4996	4770	-4.5
PLY	3460	3380	-2.3	3957	3660	-7.5
4L-4T-4L	3865	3880	0.4	4876	4370	-10
3L-6T-3L	3286	3370	2.6	4075	4270	4.8
LVL-T	983	1030	4.8	1090	1060	-2.8
Clearwood	4848	-		-	-	

Whilst there is some variation between the results found in this study and that of Chauhan *et al.*^(5.1), it can be seen that the ranking order of the decreasing velocity by both resonance and TOF methods has not changed. The reason for an increased discrepancy between resonance and TOF results was explained by Chauhan *et al.*^(5.1). They asserted that resonant velocities are the result of obeying the law of mixtures, whilst TOF results measure the leading edge of the dilatational wave. By reducing the separation between probes in LVL-L panels, it was found that the dilatational energy increasingly dominated (due to less beamspread of the wave), and was given as proof of the TOF devices measuring the fastest path.

Thus TOF results are measuring the phase velocity rather than the group velocity. If this were the case, the TOF results should be subjected to the Rayleigh correction. However, in the case of using PUNDIT™, it is more likely that the discrepancy is the consequence of assuming a one-dimensional equation for the calculation, whereas since the wavelength for the 54 kHz signal is much less than twice the diameter of the specimens, the MoE_d should be calculated from the three-dimensional equation with the incorporation of Poisson's ratio to reduce the overestimation. This is shown by Craik^(5.17), that for a Poisson's ratio of 0.3, the one-dimensional equation will underestimate the three-dimensional equation by 16%. Wang *et al.*^(5.18) noted that this overestimation of the static MoE could be as large as 19% to 37%.

The difference may also be contributed to by a difference in strain rate between the low-frequency resonance measurements and the 54 kHz ultrasonic impulse (the effects of strain rate are discussed in Section 5.7.3). However, other factors such as the detection by the PUNDIT™ ultrasonic probes of the phase velocity rather than the group velocity, due to the smaller beams spread of the ultrasonic wave having a greater percentage of unreflected wave energy as a leading edge through the centre of the beam, cannot be discounted.

It is noticeable that the greatest variation in resonant velocities occurs with the all transverse panels, whilst this set has the lowest variation in TOF measurements. Further, the 7.5% and 10% discrepancy (in the PLY and 4L-4T-4L beams respectively) between PUNDIT™ and Chauhan *et al.*'s FAKOPP 2D™ results is of concern^(5.1). However, this is most likely the result of using a low-frequency TOF tool (with angled spike insertion) against an ultrasonic tool, with the associated overestimation of the later due to differing strain rates, as discussed in Section 5.7.4. However, it may also be due to the measurement technique. The FAKOPP™ uses a conical insertion probe, whilst the PUNDIT™'s transducers cover the end of the beam's cross-section. Thus it is possible that whilst both find the fastest path along the beam, the FAKOPP™ may have started from a position within a transversely orientated layer. However, it is noticeable that the LVL beams had a 4.5% difference, thus it may be the case that not all longitudinally orientated layers have the same stiffness, or some contain discontinuities in that layer. Since the PUNDIT™ covers the end of the cross-section; it will seek the fastest of these layers whereas the FAKOPP™ may have to start within a slower layer. Regardless, the results confirm the progressive velocity decrease with increasing inhomogeneity of the panels.

5.7.2.2 Influence of defect position on the MoE_d

It is clear from Figures 5.15, 5.20 and 5.25 that different harmonics clearly can produce different results in MoE_d due to even small inserted defects at critical positions. For example, in Figure 5.15, when MoE_d calculated for hole taking up 80% cross-section at midspan; MoE_d of the 2nd harmonic did not change from the

initial but the 1st and 3rd harmonics showed a 20-25% decrease in calculated MoE (with the 1st harmonic most affected). Similarly it was shown from Figures 5.25 that the 8th harmonic frequency can be 'protected' (*i.e.* maintain a consistent frequency and hence calculated velocity and MoE_d) by not inserting defects in its nodal positions. Similarly Figure 5.20 shows that the 2nd harmonic can be dramatically reduced (compared to the 1st and 3rd harmonics) by defect insertion at its nodal positions. This proves that the calculation of the MoE_d is significantly weighted to the localised stiffness at the anti-nodal positions.

Effectively this means that the calculation of the MoE_d on the basis of solely one harmonic can result in a MoE_d value well below the static MoE value of the beam, should defects exist at a harmonic node. This effect is most pronounced should the defect be located at the centre of the node. However, results from Figure 5.20, showing the effect of holes away from the 1st harmonic's node, show that decreases in 1st harmonic MoE_d will occur, though not to the extent of harmonics with nodes at this position. Thus it can be surmised that the influence of defects, whilst still present, reduces with distance from a node. This can be seen in the diagram presented in Figure 5.31.

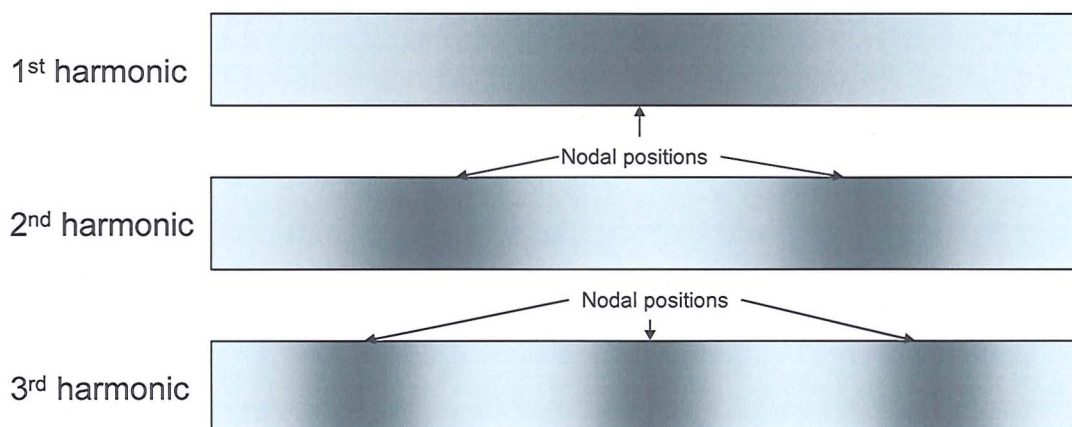


Figure 5.31 Vibrational pressure nodes (dark patches) and anti-nodes (light patches) positions of the first three harmonics. The dark patches reflect the areas with the greatest influence on the returned harmonic velocity.

It can be seen that the 1st, 2nd, and subsequent harmonics measure the MoE_d not as an average of the entire longitudinal MoE, but weighted towards specific points

dependant on where their nodes are centered. If the ends of the beam will always be vibrational amplitude antinodes with the nodal points shifting location depending on the frequency mode under investigation, then these nodal points, whilst having zero amplitude, will be positions of maximum stress concentration due to equally alternating tensional and compressional forces on either side (and consequently the antinodes will have theoretically zero stress concentration)^(5.19).

Therefore a reduction in the cross-sectional area will result in a decrease in the ability of said area to transmit stress, thus lowering the stiffness and hence the measured frequency. Thus for the fundamental frequency, with only one nodal point located at the centre, the frequency will be dictated by the ability of the material to resist this stress solely within the nodal point's immediate area of influence. For a second harmonic, with two nodal points, the maximum stress concentration will be split between the nodal regions and so on for higher harmonics. Thus the dynamic MoE calculation is not an average of the beam as a whole but rather of the average of the MoE at specific locations depending on the mode investigated. It will however be an average of the cross-section of the specimen due to the planar waveform which has developed, as opposed to TOF investigations which typically do not average the cross-section.

For example the 2nd harmonic will not take account of lower stiffness areas located at midspan of a sample, with the stiffness of the areas around the ¼- and ¾-span controlling the derived MoE_d. As such, it can be proposed that the higher harmonics, though more difficult to measure due to the decreased energy content imparted by a hammer blow and being subject to increased internal damping, would be more representative of the sample as a whole than the 1st or 2nd harmonic. If possible, the best measurement would include an average of at least one odd and one even harmonic (as in lower harmonics their nodal areas will not intersect). Potentially therefore an average of the 3rd and 4th harmonic could give a better representation of the sample's true MoE, as the higher harmonics take account of the stiffness along a greater percentage of the beams' length as there are more nodes to contribute to the average of the beam's dynamic stiffness. This may explain why there is typically a reduction in dynamic stiffness with increasing

harmonic as typically it would be more likely that an inhomogeneity would be included in this average.

Kaiserlik^(5.20) reported Reneker *et al.* (1978) as carrying out NDT involving the simulation of cracks, mass defects and temperature changes on the modulus of elasticity of small polymethacrylate and Lucite bars, as established by longitudinal resonance testing. They reported frequency shifts, amplitude modification and the appearance of new modes (most likely through unstated bifurcation). They also suggested, as confirmed by this study, that higher order modes could be used for defect location. However, the presence of large stiffness variations between two or more nodal points (in higher harmonics) may result in bifurcation of the resonance spectrum (which is discussed further in Section 5.7.6). This would suggest that defects in the nodal region would significantly reduce the dynamic stiffness at this point and thus reduce the frequency of the investigated mode.

However, due to the requirement for a detectable signal for correct evaluation, and to take account of the importance to MoR (and to a much lesser extent MoE) of defects at the centre as focal points of rupture, it may be the case that an average of the 1st and 2nd harmonics will produce a better correlation to the actual static MoE of the specimen than using either one alone. Similarly, there is the potential for defect location, should the 1st harmonic be significantly lower than that predicted by halving the 2nd harmonic (or similar predictions from higher harmonics), or *vice versa*. This would allow automated devices to identify those samples with an increased tendency towards a low MoR. A similar proposal for unspecified solid beams was made by Narkis^(5.21), who conducted experiments on simply supported, free-free condition beams in which a crack was finite-element modelled as a linear spring between two separate beams. He presented linear equations demonstrating that a crack's position in a beam could be located on the basis of the relative variation in the first and second modal frequencies.

This however means knowledge of the original uncracked beam frequencies is required. It is also suspected that the beam was a homogenous isotropic

specimen, as no account was made for the 2nd harmonic not being a direct multiple of the fundamental frequency, which has been shown to not be the case in wood specimens with overtones replacing harmonics due to anisotropy. It also was shown that his model was correct up to crack depth to beam depth ratios of 0.3, after which the model was invalidated by the occurrence of additional resonance modes^(5.21). Alternative reasons for any reduction in stiffness may be the presence of compression wood, but no evidence of a reduction in MoE_d due to compression wood has been presented in the recent literature.

Brancheriau *et al.*^(5.22) cites Bork's PhD thesis (1983, in German) as having observed that the removal of material from different positions on a xylophone bar affects certain frequency modes more than others (allowing for the tuning of the bars), though this is one of the few papers dealing with the dynamic behaviour of bars with irregularities. Brancheriau *et al.*^(5.22), examined eleven 20 x 20 x 400 mm long xylophone bars (straight grained and defect-free), and observed that there is a gradual deviation in both longitudinal and transverse resonance frequencies (induced through hammer impact and detected by microphone) relative to the original frequency as a result of a 'weak element' gradually decreasing the MoE_d, though there was a greater shift observed in the transverse frequencies. It was also observed that the reduction in frequency is dependant on the frequency mode examined relative to the weak element position, *i.e.* by placing the weak element at the centre of the beam; the greatest reduction is in the fundamental frequency and the third harmonic. These results are comparable with the results seen in this Chapter's test series. Also comparable is the assertion by Brancheriau *et al.*^(5.22) that, contrary to popular opinion (as described in Chapter 3 regarding Divos, Bucur, *etc.*), that whilst a defect must be of a comparable dimension to the wavelength used in US TOF testing to have an effect, this is not the case in resonance testing. This was attributed to the reduction in rigidity of the specimen by even very small irregularities, though the author would attribute it to the reduction in elastic modulus rather than the modulus of rigidity.

Further, it can be seen from both these experiments and the Brancheriau *et al.*^(5.22) study that the proportional reduction of a harmonic (when interacting with a nodal

point) is related to the number of nodes for the particular mode of vibration. In essence, the third harmonic will be less affected by a weak element at the centre (despite having an anti-nodal position in the same position as the fundamental) because it also has two other anti-nodes that are not located over a weakened position. Thus one would expect a third of the relative shift in frequency that is seen in the first harmonic. This however is not seen in the results shown in Figure 6.5, where the third harmonic is reduced by 84% of the total reduction in the 1st harmonic, rather than the expected 67% (or two-thirds). Thus in Figure 5.15, the third harmonic was reduced by more than would have been expected.

It should be noted at this point that there is an error in Brancheriau *et al.*^(5.22) in that testing was conducted on 400 mm beams, thus the fundamental wavelength would be 800 mm rather than the stated 600 mm. Whilst the author of this thesis favours the conclusions of Brancheriau *et al.*^(5.22), the test method employed may amplify the deviation as, rather than the removal and replacement of material as in Ouis^(5.23), the beam was physically separated, a 20 mm³ section removed and rotated such that the transverse axis was aligned to the longitudinal axis of the entire beam. The beam was then glued back together. As this separation is across the whole cross-section of the beam, the transmission of the wave types will be affected by the amount of glue and any air gaps present. This may serve to create sub-resonances between the end of the specimen and the glued face of the cube thus, for example, contributing to the resonance of the second harmonic in the case of a weak element being placed at the centre of the beam.

However, results of previous experiments by Hansen, and presented in his MPhil thesis^(5.24), have led to the conclusion that introducing holes, whilst simulating the effect of checks, splits or decay in a specimen, will not mirror the effect of knots.

In Chapter 4 of his thesis, Hansen took Radiata pine logs and progressively shortened the logs so that branch nodes and nodal swirls (knots) appeared at nodal positions.

In contrast to the results of the laminated beam tests, with artificially introduced dowels to simulate knots, it was stated in Hansen's thesis that harmonics have a diametrically opposite response to holes when compared to real knots, when both are located at specific positions. For example, logs cut so that knots existed at midspan had the 1st and 3rd harmonics giving the highest MoE_d, whilst in the laminated beam tests with artificial insertions the 2nd harmonic gave the highest MoE_d (as shown in Figure 5.15). Of course the key difference here is that in logs real knots distort the grain so as to locally stiffen the area, whilst removing a section and replacing with a dowel has no effect on the grain of the beam, except perhaps a minor relaxation of the tangential stiffness.

Hansen's assessment of these responses can be summarized: Actual knots (branch or nodal whorls) reacting differently to inserted holes due to two different implications for stiffness, *i.e.* a hole simply reduces the cross section at the point, inserting a dowel allows for a maintenance of mass but not the continuity of wave transmission, which through which the dynamic stiffness is evaluated. Thus inserted dowels do not contribute to the mechanical properties of the beam and are thus more comparable to a loose knot. However a loose knot will still have a degree of fiber deflection (though far less than intergrown or live knots), and thus drilled holes are more comparable to rot. Further distinctions were made regarding the differing shape of beams (evenly shaped rectangles) and logs (tapered and crooked with oval cross-sections).

Two arguments could be presented for this apparent discrepancy between artificial defects and real knots.

Firstly, the laminated beam series was measured using accelerometers, whilst the logs in Hansen's earlier study were measured using a microphone connected to the Woodspec™ system. Brancheriau *et al.*^(5.22) clearly state that at the nodes of vibration, the corresponding modal frequencies are unaltered by the presence of a weak element. As such, since it was observed that placing a weak element at the centre of the beam does not affect the second harmonic, one can assume that the second harmonic has a nodal point at this position (despite the specimens being in

free-free suspension). Whilst this would be true in fixed end or room acoustics (*i.e.* nodal points at the ends or walls of a specimen) the majority of timber researchers (Ross, Bucur, Walker, Andrews *etc.*) believe that beams in free-free conditions have anti-nodal points at the ends and thus the second harmonic would have an anti-node (one of three) at the centre, which would see it being highly susceptible to frequency shift.

This was not seen in the case of Brancheriau *et al.*^(5.22). The microphone NDT is based on changes to exterior sound pressure displacement (which would “see” the log as being set into free-free longitudinal vibration, whereas when testing using an accelerometer one measures the acceleration of the beam. It may therefore be the case that the appearance of the wave will be diametrically opposite with the nodal and anti-nodal positions reversed in each case. Whilst in a defect-free specimen there would be no difference in the measured harmonics, when defects are inserted (knots or holes) at specific nodal points the harmonics will vary. Since, in previous studies, the various harmonics have not been observed in the case of progressive artificial defection insertion (or for that matter in published work outside the University of Canterbury for knot location) this has not previously been noticed. This discrepancy between measurement of anti-nodes for displacement (using accelerometers) and nodes for sound pressure (using a microphone) is acknowledged by Hansen, but is not taken into account when the contrasting effect of holes in beams and real knots in logs was discussed. As such, the contention in this case would be that if the log experiments of Hansen were to be repeated using an accelerometer, a pattern similar to that of the hole insertions experiments would be found. However, this is against the conventional wisdom of wave transmission in timber beams, where free-free wave patterns are considered to be normal^(5.15, 5.17, 5.25).

The second argument for the differing harmonic response (favoured by Hansen and the author) was that branch nodes and whorls cause nodal swelling, which is an increase in the diameter and hence cross-section of the corresponding region of the log compared to knot-free regions. This in turn increases the volume and mass, in addition branch nodes and whorls being of typically higher density compression

wood than its surrounds. Conversely, a drilled hole serves to reduce the cross section (and even with a dowel the mass at most remains the same). Whereas a hole at certain points may cause a reduction of the specific harmonic frequency, real knots will serve to increase the frequency due to a bigger cross-section increasing the spring constant and thus producing higher MoE_d . This would be the case if the log is modeled as a one-degree-of-freedom mass-spring system in free-free conditions with the nodal position (*i.e.* spring) at midspan.

Under this argument, holes reduce the cross-section, reduce the spring constant and thus result in a lower MoE_d . As such, under this argument, the 2nd harmonic with an anti-node at midspan, will not detect the higher mass from the knots at midspan of logs, thus not changing the 2nd harmonic MoE_d whilst raising the MoE_d of the 1st and 3rd harmonics. A hole filled with a dowel at midspan will see no reduction in the 2nd harmonic due to its location away from a nodal position. On this basis, if the 2nd harmonic is significantly lower than that which could be predicted by doubling the 1st harmonic, there is a possibility of knots at midspan (with none at the quarter-spans). Due to the increased dependency of the MoR on the location and size of knots, this should mean that the 2nd harmonic should have an increased correlation to the MoR. Low 1st harmonic frequencies (when compared to that predicted by halving the 2nd harmonic) would indicate rot.

This would mean that high knot concentrations can lead to a significant overestimation of the MoE_d , particularly as knots cause a focal point of rupture. Further investigation is required into the effect of real knots at nodal positions on the MoE_d and damping ratio in timber beams as opposed to in logs. In this case, there would be no increase in cross-section, mass or volume resulting from swelling (if anything swelling would reduce the apparent mass in knotty areas, which may trade-off against a higher density knot cluster). As such, it is more likely that the interruption of the clearwood may after all reflect the same pattern as has been seen with hole insertions during the laminated beam series.

5.7.2.3 Influence of increasing defect size

Regardless of which theory is chosen to explain the effect of a defect at a certain position on differing harmonics, and ignoring the misleading effects of bifurcation, it is clear from Figure 5.26 that:

- Harmonic velocity decreases linearly with increasing simulated KVR (or perhaps more realistically local density and stiffness changes). Similarly, it can be seen from Figure 5.26 that the MoE_d (calculated from the average of the first 8 harmonics) decreases linearly ($R^2 = 0.997$) with increasing KVR. Though again it should be noted that using a single harmonic instead of an average of harmonics can result in a difference in calculated MoE_d of 23%.
- In Figure 5.26, damping ratio on an LVL beam is seen to increase linearly ($R^2 = 0.98$) with various 25 mm holes until edge knots are inserted on the last two steps, at which point the DR increases dramatically.
- As previously mentioned, the damping ratio may tend towards plateauing with both increasing inhomogeneity (Table 5.6) and defect insertion along the same central line (Figure 5.21). This effect can also be seen in clearwood Beam 26 (Figure 5.27), which shows a plateauing damping ratio with multiple 25 mm dowel insertions, but rises significantly on the insertion of two off-axis edge dowels.

This tendency for a plateauing of the not only the increasing damping ratio, but also the decreasing MoE_d , has a degree of predictability. Firstly, based on the results discussed earlier, it is clear that there is an inverse relationship between velocity (hence MoE_d) and damping ratio. Secondly, it is possible to predict the MoE_d of the individual laminations affected by increasing knot insertion through the law of mixtures presented in Chauhan *et al.*^(5.1). This can be seen Beam 33, with multiple 25 mm centerline dowels inserted up until the insertion of the edge knots.

Under the method shown by Chauhan *et al.*^(5.1), the all longitudinally laminated beam can be separated into three sections tangentially: with two outer layers 12.5 mm wide and a single central layer 25 mm wide which the inserted dowels intersect. These form two sections of differing MoE_d . Using the equation from the law of mixtures:

$$E_{lam} = E_1 \frac{v_1}{v_0} + E_2 \frac{v_2}{v_0} \quad \text{Eqn. 5.2}$$

Where:

E_{lam} = MoE of the total laminate, E_1 = MoE of unaltered longitudinal plies, E_2 = MoE of the plies where the dowels are drilled in, v_0 = total volume of the beam, v_1 = volume of unaffected longitudinal plies and v_2 = volume of the knotty plies.

Since the MoE of the overall laminate can be taken as the average MoE_d calculated from the average of the first eight harmonics as shown in Figure 5.26, E_1 can be taken as the original MoE_d calculated from the pre-insertion test (LVL $MoE_d = 11.68$ GPa), and the volumes of the sections can be calculated and remain unchanged, E_2 remains as the only unknown in the equation. E_2 can therefore be calculated during the process of increasing dowel content or simulated KVR, and the results are shown in Table 5.9.

Table 5.9 E_{lam} and E_2 of LVL-L beam 33 with increasing number of centerline dowels perpendicular to individual layers as calculated from the 1st harmonic, from the harmonic with the lowest value and from the average of the first 8 harmonics (as shown in Figure 5.26). The percentage change is the change in E_2 due to a 2% change in knot volume.

E2 %knot volume	1 st harmonic				Harmonic with lowest value				Average of first 8 harmonics			
	E_1	E_{lam}	E_2	E_2 %Change	E_1	E_{lam}	E_2	E_2 %Change	E_1	E_{lam}	E_2	E_2 %Change
0	11.68	11.68	11.68		11.12	11.12	11.12		11.45	11.45	11.45	
1	11.68	10.88	10.39	-11.04%	11.12	10.60	10.29	-7.43%	11.45	11.04	10.79	-5.74%
3	11.68	10.01	9.01	-7.63%	11.12	9.29	8.20	-8.77%	11.45	10.05	9.22	-6.49%
5	11.68	9.71	8.53	-5.39%	11.12	8.28	6.57	-8.18%	11.45	9.28	7.98	-6.05%
7	11.68	8.72	6.94	-5.80%	11.12	8.15	6.37	-6.10%	11.45	8.69	7.04	-5.50%
9	11.68	8.03	5.84	-5.56%	11.12	7.32	5.05	-6.07%	11.45	7.92	5.80	-5.48%
11	11.68	7.70	5.31	-4.95%	11.12	6.72	4.08	-5.76%	11.45	7.47	5.08	-5.06%
13	11.68	7.64	5.22	-4.25%	11.12	6.29	3.40	-5.34%	11.45	6.90	4.17	-4.89%

It can be seen from Table 5.9 that the percentage knot volume is taken from the E_2 section only, thus is ultimately higher than that shown in Figures 5.26 and 5.27. Two points become clear:

Firstly, whilst an increase of just 1% knot volume causes an 11.04% reduction in MoE_d calculated from the first harmonic per 1% increase in knot volume, a 13% increase in knot volume only causes a 4.25% reduction in MoE_d calculated from the first harmonic per 1% increase in knot volume. This shows both the tendency for the diminishing impact of increased KVR when the knots are located in the same

longitudinal line, as well as the best fit regression between MoE_d and KVR being a negative exponential function, when calculated from a single harmonic.

Secondly, however, when the MoE_d is calculated from an average of the first eight harmonics, the decrease is more linear (though still negatively exponential) and consistent. This is the effect of the first dowel being inserted at midspan, which has the greatest effect on the 1st harmonic, and since subsequent dowels are inserted away from the impact-weighted 1st harmonic nodal position, an average of the first eight harmonics shows a greater overall reduction in the MoE_d of the central section. Thus proving that an average of the first eight harmonics is better than using a single harmonic for MoE_d calculation to reflect the static MoE . However in all methods of calculation, a linear regression shows a significantly high correlation ($R^2 > 0.97$) with a negative exponential regression showing the best correlations between KVR and MoE_d ($R^2 > 0.99$).

If the holes are modeled as rot, rather than knots as originally predicted, these results confirm observations presented Ross and Pellerin^(5.25), and Ouis^(5.23), that velocity decreases linearly with advancing real (or simulated in the latter case) decay. However, Ross and Pellerin^(5.25) asserted that higher frequencies are particularly sensitive to early stages of decay, was not observed in this study. Indeed it was shown that higher frequencies (> 8 kHz) could be 'protected' from observing the effects of decay compared to lower frequencies, provided the decay did not occur at their nodal positions.

Ross's assertions are correct in that if the rot was randomly located, there would be a greater probability of it intersecting with a higher harmonic's nodal position (though the effect would be lesser than if a single area of rot intersects lower harmonic's node). Ross and Pellerin^(5.25) also noted the reduction in signal amplitude with increasing decay, which was not evaluated in this study, but could be construed as an increase in energy loss and thus damping, which is reflected here. Ouis^(5.23) noted that the resonance frequency decreased proportionally to the number of induced defects (holes or cracks), though this was attributed to a removal of mass causing the frequency reduction. This study has shown that the

removal of mass is not the cause of this frequency reduction as dowels were inserted in the defects place. Additionally Ouis^(5.23, 5.26) demonstrated the damping properties were inversely related to increasing defects, and that a splitting (bifurcation), of the resonance frequencies occurred during testing, though this was not discussed.

Divos^(5.27) and Sandoz^(5.28-29) both examined the effects of artificially induced notches (designed to simulate knots and decay) on acousto-ultrasonic waves. The general conclusion of both was that presence of knots and decay will affect the derived velocity depending on the severity (or size) of the induced defect, but that discontinuities affect the amplitude of the wave far more (these studies are discussed further in Section 5.7.2.3). This study confirms their conclusions that TOF velocity is not as affected as a measure of the inherent damping, and that TOF will find the fastest available path around the inclusion. However, it is clear that increasing defect size does affect the resonant velocity in a similar manner to the damping ratio.

The damping ratio for the altered middle layers can also be calculated based on the law of mixtures. Table 5.10 shows the effect of increasing knot volume in Beam 33 on the damping ratio of unaffected outer layers, the overall beam, and thus the calculated damping ratio if the affected central layers. Also shown is the percentage change in damping ratio for affected layers per 2% increase in knot volume. The pattern of increasing damping ratio is best described by a linear regression ($R^2 = 0.98$), as opposed to the negative exponential shown in the MoE_d results.

Table 5.10 Prediction of central affected section's damping ratio in Beam 33 due to increased knot volume (simulated by perpendicularly drilled centerline dowels).

E2 % knot volume	Damping ratio % unaffected plies	Overall damping ratio %	Damping ratio % knotty plies	% Change E2
0	0.467	0.467	0.467	
1	0.467	0.477	0.483	3.43%
3	0.467	0.496	0.513	3.31%
5	0.467	0.511	0.537	3.01%
7	0.467	0.556	0.609	4.36%
9	0.467	0.560	0.616	3.54%
11	0.467	0.590	0.664	3.83%
13	0.467	0.614	0.702	3.87%

It can be seen that the average increase in the 1st harmonic damping ratio is 3.4% per 1% increase in knot volume. As such, this is a more consistent reflection of the increasing knot content, as opposed to the weighted effects observed for the 1st harmonic's calculation of MoE_d . The standard deviation was 0.44% and COV was 12% indicating a slightly greater than low variance if 10% COV is regarded as low).

5.7.2.4 Influence of defect orientation

LVL Beams 2 and 34 both had two edge defects at midspan, however on Beam 34 the defects were inserted perpendicular, rather than parallel as in Beam 2, to the laminations. It was observed that edge knots drilled parallel to the layers of an LVL beam had a greater effect on the MoE_d (c. 35% decrease in MoE at maximum knot size) than edge knots drilled perpendicular (c. 15% decrease in MoE_d at maximum knot size) to the individual layers. Additionally, damping ratio doubled with maximum sized edge knots inserted perpendicular to the layers and damping ratio tripled when they were inserted parallel to the layers. There was no difference, however, between the MoE_d of the LVL beams to centerline defects being inserted either perpendicular or parallel to the layers (Beams 1 and 3 respectively). This increase in energy loss can be explained by Gerhards's^(5.30) assertion that upon passing a knot, a longitudinal wave returns to a planar wavefront, though the distance at which this takes place is not specified. Divos *et al.*^(5.27) agree, though their results indicate that there will be a leading edge to this wavefront skewed to one side of the beam (though this is based on a non-centreline knot). To achieve this post-knot planar nature, the energy from the leading edge of the wave which has passed round the inclusion must spread out. As such, in the case of perpendicularly inserted dowels, waves are forced round the inclusion, but within the same 12 individual laminations, to reform on the other side still within these laminations. However for defects inserted parallel to the laminations, the pathway within individual laminations is broken and thus the wave must cross to the outer glue-laminated layers, through the glue lines, and back again post-inclusion. Therefore there is greater potential for increased internal friction, as reflected in the increased damping ratio. Similarly, it was asserted by Gerhards^(5.30) that the

increase in grain deviation around a knot would be the primary reason for reductions in velocity.

5.7.3 Comparison of dynamic and static MoE calculation

It can be seen from Table 6.6, that the average static MoE (derived from the average of beams tested with laminations orientated parallel and perpendicularly tested) bending tests is, on average, lower than the average MoE_d derived by resonance testing by an average of c. 21%. The clearwood showed the closest dynamic MoE calculation to the static MoE (overestimating by 12%) with the sandwich beams (3L-6T-3L and 4L-4T-4L) having the greatest difference (c. 30%). In Chauhan *et al.*^(5.1), no static bending tests were conducted so comparisons on that scale cannot be made.

However, in comparison with other previous research, as presented in Chapter 3, Wang^(5.18) found that resonance velocities, and hence MoE_d based on the one-dimensional wave equation, overestimated static MoE by 19% to 37%. Jayne^(5.31) found a 5% overestimation, based on flexural resonance testing. De Olivera^(5.32) found a 20% overestimate by dynamic methods. Ilic^(5.33) found a 29% overestimation by dynamic methods on SCS. All three studies found high linear correlations ($R^2 > 0.8$) between dynamic and static values of MoE (though Ilic's correlation reduced for larger samples). Machek *et al.*^(5.34) found dynamic overestimations of static MoE by 5-15%. A further study by Wang *et al.*^(5.35) noted a 19 to 27% overestimation, though this was for log averages and their respective beams (this is discussed further in Chapter 6). Divos and Tanaka asserted that there was generally a 10% overestimation of static MoE by resonance methods. Ouis^(5.23) noted that all his previous research had indicated a general rise in predicted MoE with increased frequency of operation from bending tests through ultrasonics.

The reasons for the variability of this overestimation are that whilst the static method of calculation maintains roughly the same procedure, the calculation of velocities differs between researchers, not simply in choosing TOF or RF methods,

but also inherent variability within the methods themselves. Many of the reasons for these variations were discussed in Chapter 3, however it can be said definitively that dynamic methods do overestimate the static MoE.

The reason for this overestimate by the use of dynamic methods compared to static is most likely due to the loading rate (or strain rate) of the measurement technique. As reported in Section 4.5.6, Divos and Tanaka^(5.36) looked at the differences in loading rates by static and dynamic methods. They used 3-point bending tests with different velocities of crosshead loading, and noted that shorter characteristic MoE determination times (characteristic times) resulted in higher values of MoE. Indeed, they suggested that for each order of magnitude increase in the loading rate, there was a 1.7% increase in the derived MoE. This phenomenon was attributed to the reaction of creep processes in the wood (creep is possible even on short time-scales), in that the standards for determining static MoE sets controls on the strain rate to account for the creep deflection of a tested beam, producing a consistent creep deflection and thus the resultant static MoE is reflective of the elastic deflection. Hence the effects of creep are not accounted for during higher loading rates (in either static or dynamic testing). Similar explanations have been proposed by other researchers who state that wood is a viscoelastic material which responds differently to different loading rates^(5.37-5.38). Divos and Tanaka provided a formula to take account of the loading rate during bending tests:

$$E_{t_1} = E_{t_2} \left(1 + 0.017 \log \left(\frac{t_2}{t_1} \right) \right) \quad \text{Eqn 5.3}$$

Where: t_1 is the characteristic time of E_{t_1} determination and t_2 is the characteristic time of E_{t_2} determination.

Applying this theory to the results shown in these experiments, the characteristic time of static loading was 0.03 mms^{-1} (crosshead speed of 2mm/min) whilst the dynamic characteristic time can be calculated as such:

$$\frac{\partial \varepsilon}{\partial t} = \left(\frac{F/A}{E} \right) \frac{1}{t}$$

Eqn. 5.4

Where:

ε = Strain

F = Applied Force (from hammer impact) (N)

A = Area (of application with impact hammer-head, *i.e.* 0.01 m²)

E = Elastic modulus of specimen (Pa)

t = time taken for maximum force to be applied from rest position (s), note that the temporal resolution of the PULSE™ system is 0.03 ms

In this example to show a typical rate of strain resulting from a hammer impact onto a wooden specimen, Figure 5.22 displays a typical response time-amplitude response. A compatibility error between the Endevco Type 8202 modal hammer and the PULSE™ measurement software caused the force to use Giga-Newtons rather than Newtons in the resulting FFT displays.

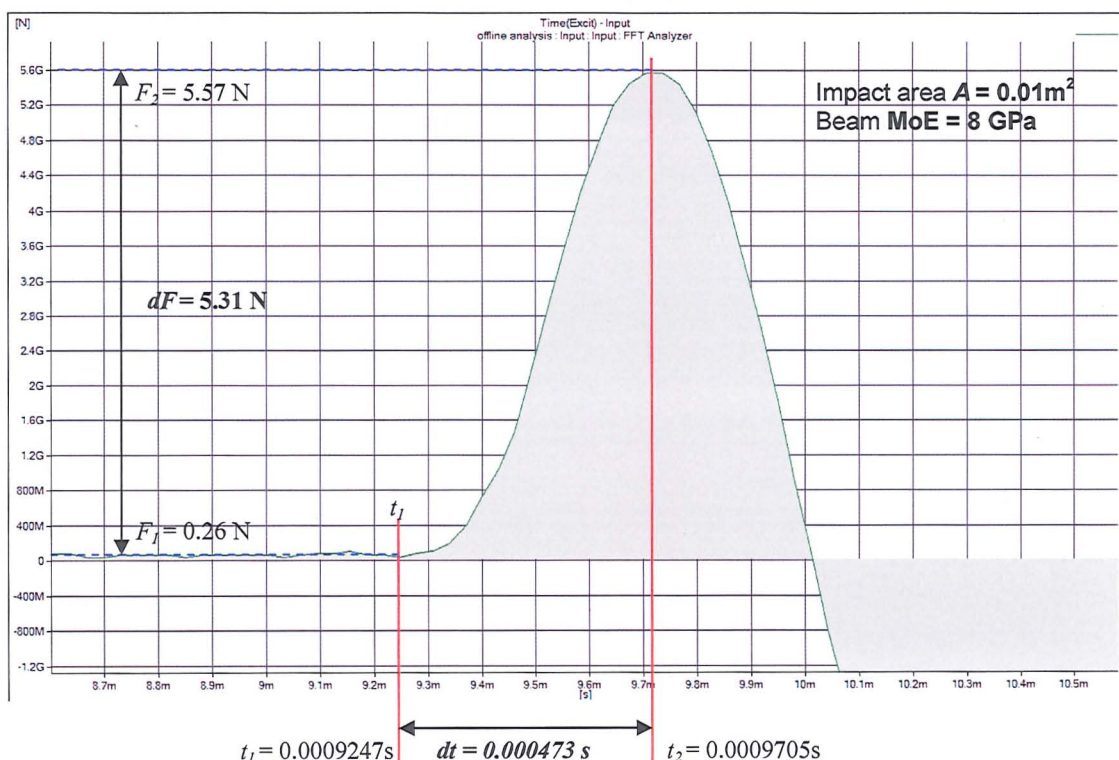


Figure 5.32 Time-amplitude response of a longitudinal impact on a clearwood beam without defects (Beam 26). Time is displayed in seconds on the x-axis and inputted force is displayed on the y-axis. Red lines denote start (t_1) and end (t_2) of input force.

Thus the equation for strain rate becomes:

$$\frac{\partial \varepsilon}{\partial t} = \frac{\left(\frac{5.31/0.01}{8} \right)}{0.000473} \quad \text{Eqn 5.5}$$

Thus the calculated strain rate is $\frac{\partial \varepsilon}{\partial t} = 140327.7 \text{ mm}^{-1} \text{ s}^{-1}$

If this strain rate, and the static strain rate, is inputted into Divos and Tanaka's model (Eqn 5.4), using the calculated average static MoE of 8.3 GPa (MoE_{t2}), it would be expected that the resulting calculated dynamic MoE (MoE_{t1}) would be close to the average dynamic MoE of 9.48 GPa. However, when this is calculated as such:

$$\text{MoE}_{t1} = 8.3 \left(1 + 0.017 \log \left(\frac{140327.7}{0.03} \right) \right) \quad \text{Eqn 5.6}$$

The resulting dynamic MoE prediction (MOE_{t1}) would be 7.36 GPa. Similarly if the static and dynamic inputs were reversed, the prediction of the static MoE from the dynamic would be 10.55 GPa. As such it is clear that this cannot hold true since the static is predicted to be higher than the dynamic and *vice versa* in the alternate case. If however, a minor amendment to Divos and Tanaka's equation is made (by dividing t_1 by t_2), in that instead of Eqn 5.3, the equation takes the form of Eqn 5.7:

$$E_{t1} = E_{t2} \left(1 + 0.017 \log \left(\frac{t_1}{t_2} \right) \right) \quad \text{Eqn 5.7}$$

The resulting dynamic MoE prediction based on the static value (of 8.3 GPa) is 9.24 GPa, both higher than the static value and closer to the observed MoE_d value of 9.48 GPa. If, instead of the 0.017 value representing the percentage difference of dynamic to static MoE, 0.021 is used (representing 10% of the average overestimation of static values by dynamic methods across all types of beams tested), the predicted value becomes 9.46 GPa. However, if the percentage difference for clearwood alone is used (12%), then the prediction of dynamic MoE

is lower than the calculated dynamic MoE of 9.48 GPa, at 8.96 GPa. It should be noted however that rather than the gradual increase in velocity with order of magnitude in the loading rate, both Andrews and Walker^(5.19, 5.39) favour an abrupt change from static to dynamic modulus.

5.7.4 Measurement technique (TOF versus RF)

It has already been shown, in Figure 5.30 and Tables 5.3 and 5.8, that the rankings of unaltered beam types in terms of dynamic stiffness remains the same, regardless of which method is used. However, as shown from Table 5.5 and Figure 5.30 there is considerable variation between the two methods' velocities with both increasing inhomogeneity of laminations and once defects are inserted. Table 5.11 displays the percentage difference between PUNDIT™ TOF and PULSE™ RF harmonic calculations of velocity based on transit-time and harmonic frequencies respectively. Also shown is the average harmonic difference from the TOF velocity and the range of harmonic velocities in each instance. Beams were evaluated before any insertions and after the maximum knot insertions. For example, In Table 5.11, where the percentage difference (for the LVL beam 28 with no knots inserted) between the first harmonic and TOF is 5.6%, this means that the TOF velocity was 5.6% higher than the 1st harmonic velocity.

The observation by Chauhan *et al.*^(5.1), that TOF velocities in the laminated panels were always higher than resonance velocities by 14% to 26% is confirmed. Andrews^(5.40), put the difference between TOF and resonance velocities at 8% to 21%, with Haines and Leban^(5.41) noting a 8.9% difference in solid beams. Further experiments (on solid beam specimens) by Chauhan and Walker^(5.42) confirms a 10% discrepancy.

Table 5.11 Percentage difference between PUNDIT™ TOF ultrasonic velocity and low-frequency 1st, 2nd and 3rd harmonic derived velocities within different beams.

Beam	Config.	Chart label (figure 6. XXX)	% diff. between TOF and harmonic velocity				
			1 st harmonic	2 nd harmonic	3 rd harmonic	Average harmonic	Range of harmonic difference (%)
28 (LVL)	no knot	A	5.6	6.2	4.8	5.5	1.5
	knot 32mm perpendicular midspan	B	12.0	6.3	12.4	10.3	6.1
29 (PLY)	no knot	A	11.9	12.8	11.4	12.0	1.4
	knot 32mm parallel midspan	B	17.6	10.7	17.7	15.3	6.9
30 (PLY)	no knot	A	12.7	11.4	11.3	11.8	1.4
	knots 32mm perpendicular 1/4+3/4	B	16.2	19.8	13.9	16.6	5.9
31 (4L-4T-4L)	no knot	A	17.4	18.4	18.1	18.0	1.0
	knot 32mm perpendicular midspan	B	25.3	18.8	26.2	23.4	7.5
32 (3L-6T-3L)	no knot	A	14.5	16.3	17.3	16.0	2.8
	knot 32mm parallel midspan	B	21.1	19.6	23.6	21.4	4.0
33 (LVL)	no knot	A	5.6	7.4	6.7	6.6	1.8
	Various 25mm holes	B	23.7	23.9	26.1	24.6	2.4
34 (4L-4T-4L)	no knot	A	19.2	20.6	20.8	20.2	1.6
	knots 32mm perpendicular 1/4+3/4	B	18.9	26.5	18.9	21.4	7.6
35 (LVL - transverse)	no knot	A	15.1	12.2	13.1	13.5	2.9

The results presented here appear to confirm the assertions of Castellanos *et al.*^(5.43), in that the resonance frequency has a better linear relation to increasing number of artificial defects than TOF methods. The author would add to this however that it is dependent on the location of the defect if this relationship is to be sustained.

LVL beams had the lowest difference in velocity with and average of c. 6%, though when comparing the two LVL beams tested, no harmonic was seen to be consistently closer to the TOF than another. PLY beams had the 2nd lowest difference from TOF velocities (on average 11.9%), followed by All-T (13.5%), followed by 3L-6T-3L (16%) and finally 4L-4T-4L beams (c.19.1%). Apart from the PLY beams (which are presumed to be the most inhomogeneous of the beams),

these results are as would be expected due to the increasing degree of inhomogeneity.

4T-4L-4T beams also had the greatest range (c. 15%) between the average harmonic differences of two measured beams (though 3L-6T-3L and All-T had only one beam measured). Generally, without knot insertion, the percentage difference range between the harmonic's difference to TOF velocity is less than 2% (lowest for PLY at 1.4%), except for the 3L-6T-3L beam (at 2.8%) and All-T beam (2.9%). This seems to confirm reports from Wang *et al.*^(5,44), who noted a good linear correlation between stress-wave and ultrasonic velocities in veneer sheets ($R^2 = 0.82$), but the correlation was reduced perpendicular to the grain ($R^2 = 0.66$).

Generally, it can be seen that the TOF method is far less affected by dowel insertion than the RF method. In beams which have undergone insertions at certain positions which are then measured by both methods, Beam 28 (LVL with single midspan insertion) shows, overall, the least average increase in the difference from TOF, with the 2nd harmonic remaining relatively unchanged (increasing by 0.1%). Overall, when knots are inserted at midspan (on beams LVL 28, PLY 29, and 3L-6T-3L beam 32), this increases the average harmonic difference by 3-6%. For a single 32 mm centerline hole at midspan, 1st harmonic velocity decreased by c. 10%, but TOF velocity dropped by only c. 1-2% on average. For knots at both midspan and quarter spans, the 4L-4T-4L beams had the highest range of harmonic differences from TOF velocity following these insertions.

In beam 30 (PLY) with knots at quarter-spans, the average harmonic velocity difference from TOF velocity increases by 5.2%, with the greatest increase in the 2nd harmonic difference of 8.4%, the 1st by 3.5% and the 3rd by 2.6%. In beam 33, with various 25 mm holes, the range of harmonic difference barely increases from 1.8% to 2.4%, but the actual difference from the TOF velocity at full insertion has increased on average by 18%. In real terms, the RF velocity has decreased by 25%, but TOF velocity has dropped by only 9%. A decrease in TOF velocity of 9% is significantly higher than may be expected (since there is a x10 to x5 increase in

the difference between TOF and RF velocities for one 32 mm centerline dowel, so would expect TOF to be around 2.5% to 5%) but consider that by the end of the test (after edge knot insertion) no straight path to the other end existed, thus inducing the wave to bend round the insertions. This also explains the reason for the lack of reduction in TOF velocity when only one or two centerline dowels are inserted, in that a fast path along the outer of the laminations of the beam remains.

This is perhaps one of the most important results of the study. It indicates that whilst the difference between RF and TOF is relatively consistent in unaltered beams for any harmonic used (c. 5-6%), if a beam has defects along its entire length then whilst the range in harmonic velocities may be low, the difference between harmonic and TOF velocities, which are apparently less susceptible to defects, increases. This shows that local defects have a significantly lower impact on the TOF velocity compared to the RF velocity, even when a straight path between the ends is interrupted. This is in contrast to the results of Gerhards^(5.30) and Kabir *et al.*^(5.45-5.46), who noted that TOF velocities (especially at high frequencies) are particularly susceptible to influence from knots due to increased scatter and development of cross-grain. This different conclusion can be explained by the fact that knots induce grain distortions in the surrounding area, whereas the artificial defects here have no such effect on the outer layers. Thus the results here are more akin to rot or cracks in a solid wood sample, which confirms the advice of previous research in being wary of using TOF in samples with voids, cuts or cracks^(5.27-5.28,5.47) due to the lack of reflection by TOF velocity of the reduction in strength.

Overall it can be seen that the biggest discrepancy between RF and TOF results is seen in sandwiched beams. This indicates that the PUNDIT™ finds the fastest path through the longitudinal layers, whilst RF averages the whole system of beams. This is in agreement with unpublished tests by Carter, Chauhan and Walker (2006) (reported by Jarvis^(5.48) and in personal communication with Walker) in which they tested firstly logs, and then subsequently cut and tested cants and boards from the 24 year old radiata pine using the HM200™. The resonant

velocities of the volume-weighted cants and the source logs were in close agreement.

5.7.5 Comparison with previous research

Ouis^(5.49), who drilled increasing number of 10 mm holes through single Norway spruce wooden beam (700 x 70 x 70 mm). The most comparable test in this instance would be the insertion of multiple 25 mm holes in beams 26, 27, and 33 (with this series calculating the damping ratio, which is twice the loss factor). Ouis used longitudinal vibration to calculate MoE_d and the reverberation time this vibration to calculate a loss factor. Ouis's results showed a clear decrease in MoE_d with increasing number of holes. However, during insertion of first 50 holes the MoE_d response was undulating with an increase in MoE_d from the initial starting point, following the pattern: decrease: increase: decrease: increase: final decrease. His loss factor calculations also showed overall increase, however the final result after 300 holes was not much above the starting loss factor. The loss factor was also seen to decrease initially, before starting to increase with overall far more undulation than in the MoE_d tests.

This test series initially highlighted the erratic nature of reverberation time calculation as a measure of the damping ratio in Section 5.4. The problems in Ouis's results were most likely compounded by using a filtered impulse response at $1/4$ octave (hence potential problem of leakage over wide band). Additionally, it was not clear whether Ouis adjusted the central frequency of the impulse response calculation as the harmonic reduced, or if the results were based on the starting frequency. If this was not adjusted, the loss factor based on the first harmonic and with increasing holes would have the second harmonic leaking into the calculation (which potentially may not have been as affected as the first).

The erratic nature of the initial MoE_d calculations may have been caused by the location of inserted holes. For example, it was observed as a footnote to this study that upon testing the beams with a single hole at midspan using the 1st harmonic, the harmonic frequency can be seen to drop. However, if the beam is then retested

20 minutes later, the frequency can be seen to increase slightly. At an hour later, the frequency can have increased by several hertz. This could be attributed to a relaxation of the stress at these positions increasing the apparent stiffness. Ouis suggested that the behaviour of the curve at the lowest number of defects to the periodical pattern of the holes in the wood bar setting more resonances into vibration.

It was also noted, though not investigated, that the position of the holes relative to the nodal points of the longitudinal waves would have an affect on the results, in that holes at or near the nodal points of vibration would have less of an affect on the calculated damping than holes positioned elsewhere. However, there appears to be some confusion in language used, as it was stated that the antinodal stress point of the fundamental frequency would be at the centre of the bar. In free-free vibrations, the central point would be the nodal point for vibrations (but would indeed be an antinodal or point of maximum stress concentration). Ultimately it does appear that it is recognized that holes at the centre of the beam will have a greater effect on the damping of the fundamental frequency than elsewhere.

In the tests most comparable to Ouis^(5.50), Beam 33 showed a more linear increase in damping ratio than in Ouis's study, though Test Series 2 was conducted using larger inhomogeneities for the stepped increases: hence possibly if smaller insertions had been used a smaller scale undulation, as in the case of earlier LVL beams, may have resulted. This undulation could be attributed to bifurcation, as discussed in Section 5.7.6. However, the damping ratio of the PLY, 3-6-3, and 4-4-4 beams showed a more erratic pattern with knot volume increase, meaning the non-linear response of the damping ratio may be associated in both cases with increasing material inhomogeneity *i.e.* with the solid beams being more susceptible to variation. However, in tests for damping ratio and MoE_d behaviour in response to artificial defects, the LVL and solid clearwood beams displayed the most similar responses. Hence solid wood is less likely to display the initial erratic patterns.

However, Ouis does state that one should distinguish between different types of damping when waves propagate in beams, in that material damping is the most

important: most energy loss (at frequencies in the kHz) is due to viscous friction. In LVL beams, however, energy is also dissipated (scattered/reflected) at the various beam boundaries e.g. sound radiation at outer edges as well as acting upon internal inhomogeneities. In an LVL beam these may be the boundaries between layers themselves, real knots with each layer, early/late wood, gaps in the longitudinal structure of each layer, glue bonds, and particularly cracks in the laminations, or indeed the result of the inserted dowels. Typically, the results of this study indicate that the damping ratio and MoEd calculations are more inconsistent with increasing inhomogeneity of the PLY and sandwich beams, and more consistent for LVL and solid timber specimens.

Ouis's study generally proved that the dynamic MoE decreased, RT decreased and thus loss factor increased (though at a slower rate than the MoE decrease) as a result of increasing the number of the holes.

Concerning non-solid wood products relation to stiffness, Sandoz *et al.*^(5.28) found strong correlations ($R^2 = 0.93$) between ultrasonic TOF velocity and the static MoE of laminated timber beams. It should also be noted that very strong correlations between MoR and wavespeed squared are found in similarly oriented particleboard ($R^2 = 0.87$ to 0.93), suggesting the complete anisotropy of natural timber and wave path is the complicating factor in this relationship^(5.51).

A similar set of investigations by Sandoz *et al.*^(5.29, 5.48) looked at using the TOF acousto-ultrasonic technique longitudinally in solid beams (using Sylvatest®, and later Sylvatest® Duo) to observe the effect of artificially induced defects on velocity and energy loss. Results showed relatively low correlations of static MoE to velocity ($R^2 = 0.58$) and MoR ($R^2 = 0.25$)^(5.28). It was also noted that whilst progressive increases in the depth of the artificial discontinuity had little effect on TOF velocity (a 50% depth of saw-cut caused a 3.3% reduction in velocity, 75% cut saw a 5.65% reduction in velocity), the affect on RMS energy content was more dramatic (25% and 35.4% reduction for 50% and 75% depth cuts respectively)^(5.28). The effect of artificial sawn notches (progressively increasing in depth) in the wood on TOF velocity and amplitude was also evaluated by Divos *et al.*^(5.27) similar to the

experiment of Sandoz^(5.28). It was found that on dry, clear Norway spruce specimens, using a 48 kHz transducer, 60 cm separation and sampling frequency of 5 MHz, that amplitude decreases proportionally with the remaining cross-section^(5.27). Conversely, velocity does not decrease significantly (with no decrease in shallow cuts) until a majority of the cut has occurred.

These results would concur with the results of this test series, in that damping is far more affected by the insertion of defects than TOF velocity while a clear path from one transducer to another still exists. This study has gone further however in evaluating the effect of defects, and particularly their location, on two measures of velocity and a measure of the inherent damping capacity. Van Dyk and Rice^(5.50), testing tangentially across spruce wood with artificially induced holes of varying diameter (presumably one enlarging hole *per* specimen, though this was not explained) using 100 kHz transducers, also found that TOF velocity showed little variation in respect to the increasing diameter of the holes. They also noted a decrease in wave amplitude with increasing size of defect, but ruled this out as method of defect detection due to the high COV returned.

It was suggested by Van Dyk and Rice^(5.50) that perhaps the most consistent measure of the presence of defects (due to a low standard deviation between tests) was from the changing ratios of amplitudes of the three main peaks (60, 80 and 110 kHz): with increasing hole diameter, there was a constant decrease in the peak magnitude ratio 60/80 kHz and a constant increase in the peak magnitude ratio 110/80 kHz^(5.50). Interestingly, the increase in diameter of the holes saw an increase in the fundamental resonance frequency, which is the opposite of expectations due to the reduction of stiffness and velocity and the results presented in this chapter. No mention of this apparent anomaly was made. It is possible that the placement of the hole (presumably in the centre of the specimen though not explained) resulted in a increasing bifurcation of the resonance peak and misinterpretation as a rising resonance frequency with increasing hole diameter (as discussed in Section 5.7.6). This then confuses the observation of peak magnitude ratios as outlined above: *i.e.* was the ratio calculated from the

observed level at that specific frequency (*i.e.* for clear wood) or from the maximum peak frequency as it shifted with increasing hole diameter?

If the latter, then it would explain the trend as the maximum peak frequency shifted towards 110 kHz and away from 60 kHz. Van Dyk and Rice's explanation was that the decreases were due to increased scattering with increased hole diameters^(5.50). Additionally, sound intensity measurements (with a reference intensity level derived from tests on Plexiglas[®]) were conducted, which showed a reduction in intensity due to the presence of defects, though extensive refinement was suggested for any future application^(5.50).

In this chapter, it was also established that damping was increased by the increased presence of non-axially aligned fibres (*i.e.* increasing inhomogeneity), which was also found by Divos^(5.27) as increasing slope of grain significantly influencing the amplitude result. However it was also seen that maximum amplitude decrease was also a function of cross-section, despite exponential amplitude decays with distance in varying cross sections. The rate of amplitude decrease increasing with increasing board width, presumably due to beams spread. It was also noted that the application amplitude investigation was limited to small clear beams (with a cross-section not larger than 100 cm²) due to the varying influence of defects altering the received amplitude^(5.27). It should be noted however that it was found that bark pockets within the specimens have the same effect as knots on the energy loss, possibly due to the weak internal bonding surrounding them^(5.45).

Finally, it was noted by Harris *et al.*^(5.52) that the static and dynamic MoE would naturally differ as the grain distortions due to knots can be at least five times the width of the knot (thus inducing a zone of severe stress concentration compared to clear wood). As such, the dynamic MoE calculated by resonance testing will only be affected by the proportion of knots relative to the whole sample and not the location of these defects. Static MoE will instead be dictated by the location and quantity of the defects, thus naturally having a lower MoE, particularly in knot-prone softwoods^(5.52). However, the results of Test Series 2 have clearly shown that

the dynamic MoE is highly dependant on both the proportion of the defects but also their location, particularly if they should intersect the nodal positions of the harmonic used in velocity calculation.

5.7.6 Bifurcation of harmonic peaks

In terms of a resonant peak on a frequency-amplitude display, bifurcation is where the harmonic resonance peak splits into two distinctive peaks with a central trough, whilst maintaining approximately the same energy content as an unbifurcated peak. Similarly, the occurrence of trifurcations can occasionally be observed.

In Chapter 6, it becomes apparent that bifurcated peaks appear naturally in wood samples of both beams and logs, which will be discussed later. The emergence of bifurcation during the controlled-homogeneity test series in this chapter appears to be a gradated process resulting from of knot insertion at specific points, in which pattern to the occurrence of bifurcated peaks emerges. We have already discussed the reduction in MoE_d which occurs when knots are inserted at midspan of a beam and the reasons for this. This reduction is not simply a case of the single peak maintaining its initial form and reducing in frequency (corresponding to a reduction in velocity and hence MoE_d).

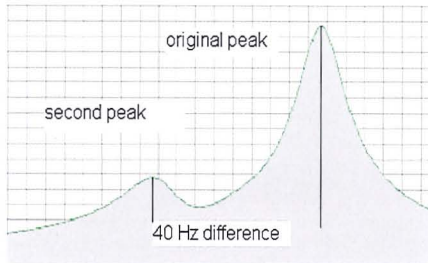
For example, in the case of an LVL beam, measured harmonic frequency (i.e. from the highest amplitude peak in the harmonic area) reduction occurs through a progressive rise and fall of dominant peaks of decreasing frequency. The occurrence of two distinct peaks is preceded by the appearance of a small sub-peak on the lower-frequency limb of a main resonant peak. With increasing interference with the midspan of the beam, the small blip will start to grow in amplitude until two distinct peaks emerge, typically less that 20 Hz apart. This occurrence at this stage is important due its problematic affect on calculation of the damping ratio, which will be discussed shortly.

Following this and with increasing knot volume at midspan, the lower-frequency peak will rise in amplitude, whilst the upper-frequency peak will reduce. During this

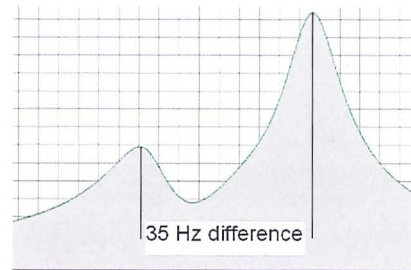
the separation distance may or may not increase. A consistent trend is that with increasing insertion, both peaks will reduce in frequency, but not necessarily by the same amount and in some cases the reduction is minimal (typically the lower-frequency peak at this stage). With increasing knot insertion, the lower-frequency peak will continue to grow in amplitude, and the upper peak reduce, until the upper peak has effectively disappeared into the background noise, and what was the lower peak is left as a single harmonic peak.

With a further increase in knot size, the process begins again with a second, lower-frequency peak developing. In some cases the occurrence of trifurcation may indicate the creation of the lowest-frequency peak before the upper-frequency peak has vanished, in this case typically the central peak will be the highest. As such, a clear pattern of rises and falls in peaks develops, with increasing distance of separation between peaks, possibly as the result of increasing the difference in volume of each subsequent dowel (*i.e.* a change from a 6 mm to 10 mm dowel is only 4 mm, less than the 7 mm change from a 25 mm to 32 mm dowel at the latter stages of each test). As such it can be observed that when lower peaks develop in the latter stages of the tests, they are no longer growing out of the original upper peaks but clearly separated by tens of hertz. It should be remembered that this only occurs on harmonic peaks whose nodal points intersect with the position of the inserted defects.

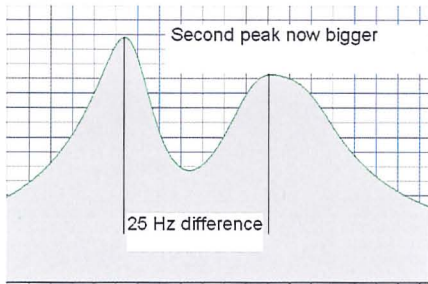
For example, Figure 5.32 shows the progressive rise of a lower-frequency peak caused by the gradational increase in size of a centerline dowel at $\frac{3}{8}$ span within a PLY beam (Beam 21), which seem to be most susceptible to the bifurcation process. Indeed an element of bifurcation is already present before the insertion of defects. When compared to a LVL beam which shows no such initial bifurcation, it becomes clear that bifurcation must be a result of either the increased inhomogeneity. However, this initial bifurcation did not occur in all PLY beams, therefore in the case of Beam 21 there may have been an unnoticed delamination of the layers (which can cause the same effect), or an as yet undetermined factor. Table 5.12 presents the raw frequencies from each of the graphs A-D in Figure 5.32, along with the derived MoE_d values.



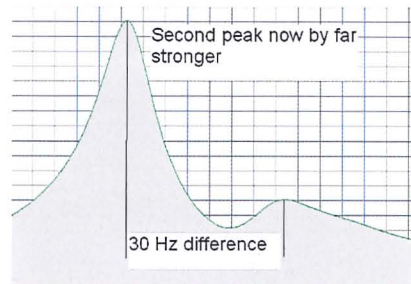
A: No hole test; a small second peak 40 Hz below the 1st harmonic



B: 10mm dowel test; second peak grows bigger and peaks come closer together



C: 20mm dowel test; second peak is now bigger, peaks only 25 Hz apart



D: 25mm dowel test; second peak predominant and sharper than before

Figure 5.32 Bifurcation process of the 1st harmonic of PLY Beam 21 due to the gradational increase in the size of a centreline dowel inserted at $\frac{3}{8}$ span. Graph A displays the frequency spectrum without any insertion, where it can be seen that a lower peak has already developed before any alteration. Graphs B, C, and D display the effect of inserting dowels of 10, 20 and 25 mm diameter respectively. Frequency (Hz) is displayed on the x-axis and acceleration amplitude (ms^{-2}) is displayed on the y-axis.

Table 5.12 Raw frequency data, calculated damping ratios and calculated MoEd values from the bifurcated fundamental frequencies. Values in brackets indicate the lower acceleration-amplitude peak.

Size of dowel	Fundamental frequency (Hz)		Damping ratio (%)	MOE (GPa)	
	Original peak	Second peak		Original peak	Second peak
Test A 0mm	923	(886)	0.57	6.95	(6.41)
Test B 10mm	918	(883)	0.64	6.89	(6.37)
Test C 20mm	(904)	878	0.69	(6.68)	6.29
Test D 25mm	(896)	868	0.59	(6.56)	6.16

It can be seen from Figure 5.32 that the process of bifurcation can cause an apparent over-proportional shift in the reduction of the measured frequency (taken as the highest amplitude in the harmonic range to reflect the processes of commercial resonance devices such as the Woodspec™, HM200™ or Grindosonic™). Since the MoE_d is determined by the square of the velocity (determined from the frequency), that apparent jump has a significant impact on the derived MoE_d by causing a greater reduction in MoE than would be expected (from the linear nature of the MoE_d -KVR relationship highlighted in Section 5.5.3.2)

It can also be seen from Table 5.12 that the damping ratio, as calculated from the fundamental frequency's half power points using the PULSE™ auto-damping function (*i.e.* the Q-factor method), is affected due to an apparent broadening and contraction of the width of the measured peak. The damping ratio appears to rise with increasing size of dowel insertion with a broadening (and amplitude-reduction) of the upper-frequency peak due to the development of 'shoulder' peaks on the lower-frequency limb of the original harmonic peak (*i.e.* occurs within a few hertz of the original). Thus the calculation of the damping ratio encompasses both peaks.

However, as two distinct peaks emerge with a greater distance of separation (*c.* 30-40Hz), an automated harmonic peak recognition system (as simulated in these tests) is forced to continue to take its measurement from the higher of these two peaks, as was done in these experiments, then the peaks have developed such individuality that instead of the half-power points from the larger peak encompassing both peaks (as was the case in the initial 'shoulder' peak stages, showing an increase in damping ratio), there is a greater than 3 dB drop each side of the individual peaks. As such the damping ratio may appear to rise upon the insertion of a small knot, and then fall due to the sharper peaks of the bifurcated harmonic. This is the case as seen in Figures 5.16, 5.17, 5.18 and 5.21 for PLY beams. Indeed PLY beams seem to be particularly affected by bifurcated resonant peaks. However, with increasing knot insertion bifurcation can appear on even LVL beams (particularly seen during the various holes test).

Further, with increasing size of insertion, and as the harmonic frequency falls further, the transfer of vibrational energy away from the upper peak to the lower peak will amplify the lower-frequency peak acceleration level, narrowing the width of the dominant, single, lower-frequency peak. The lower-frequency peak of the bifurcation will then be recognized as dominant one, causing not just a potentially overestimated jump in reduction of MoE, but the lower-frequency peak will likely also have a different, typically lower, damping ratio to the higher-frequency peak of the bifurcation. With increased insertion, this lower peak will totally dominate and the upper peak will effectively disappear, leaving a single harmonic peak, typically with a slightly higher damping ratio than the original, unbifurcated harmonic peak (but of a lower damping ratio than that of a peak with a small secondary peak developing on its lower limb). With further insertion a lower-frequency peak will develop on the now dominant peak of what was the lower part of the previous bifurcated peak, and the process begins again, akin to a wave motion of peaks traveling towards the low frequency end of the spectrum.

The matter of bifurcation is further complicated however by the occasional appearance of a 2nd peak at a higher frequency to the original peak which may also build up and become of larger amplitude than the original. This causes the apparent increase in MoE_d seen in Figure 5.10. This situation was rare, and may be a consequence of inserting a second defect at the remaining nodal point.

Ultimately it can be seen that the issue of bifurcation, due to defects or rot (or due to delamination in the case of engineered wood products, presents a problem for automated recognition systems such as the HM200™ (which identify the 2nd harmonic) or Woodspec™ and Grindosonic™ (1st harmonic) through respectively observing the 2nd or 1st highest amplitude peak on an FFT display. In the case of using the 2nd harmonic, even with a failsafe designed not to allow 2nd highest peaks in close proximity to the 1st harmonic (should it have be bifurcated), there is still the potential for the 2nd harmonic (or 1st for Woodspec™), should it be bifurcated, to therefore be misidentified by tens of Hertz. As shown in Test A of Table 5.12, this can lead to a miscalculation of the MoE_d by up to 0.54 GPa.

The question is therefore raised: in the case of bifurcation (or trifurcation), what is the true harmonic frequency value? The answer may be the mid-way frequency between the two peaks, but this would then require a value at which point one peak becomes so insignificant that it no longer counts, with the value then reverting to the lower peak. Whilst for the purposes of experimental calculation this seems a plausible solution, it is unrealistic in that since it is dependant on setting arbitrary cut-off amplitudes for a peak, it cannot reflect the true harmonic frequency in all cases. As such, the simple answer appears to be that in the case of bifurcated peaks, there is a potential range, or margin of error to be incorporated with the estimate of dynamic MoE.

The question remains of why bifurcation occurs, particularly in beams of increased inhomogeneity (sandwich and PLY beams). Presented in the following few paragraphs are a discussion of some theories:

As previously stated, different harmonics 'see' different parts of the specimen and their fundamental or harmonic frequency is a reflection of the stiffness at specific points, with an evaluated weighting towards the points of maximum pressure amplitude (*i.e.* measures the stiffness at the anti-nodes, hence the greater reduction in the fundamental frequency MoE_d , as opposed to the 3rd harmonic, seen from midspan knot insertion). Thus it may be hypothesized that, because not all of the stiffness-controlled resonance is made up from the portion of the beam affected by the knot insertion, though the majority is, there is a competition between the reduced resonant frequency of the altered portion (which has increased weighting in the average stiffness estimate due to the anti-nodal positions) and the unaffected regions which maintain the original stiffness of the beam. Thus when using higher harmonics (2nd or higher) it may be possible to see a greater difference between altered and unaltered portions of the beam where nodal points occur (for example when a knot is at $\frac{1}{4}$ span but not yet at $\frac{3}{4}$ span). As such, there is the potential for an increased range in terms of frequency between bifurcated peaks ($> 100\text{Hz.}$). Previous research (Feeney *et al.*^(5.53), Carter *et al.*^(5.54), and Huang *et al.*^(5.55)) theorised that low-frequency waves cannot "see" defects due to their longer wavelengths effectively skipping passed the inclusion,

based on the principles of diffraction. If this was the case however, then why are certain waves of a specific length affected by the inclusion of a relatively small defect at certain locations, as has been observed in this study?

Assuming that there can be no change in wavelength, another explanation could be that on reaching the defect, the part of the wave undergoes a phase shift or velocity reduction whilst passing, and potentially after, the inclusion. This would cause the wave to have two fronts of different velocities and hence a slightly lower frequency which might become visible as a second peak in the same range of the frequency spectrum where the original peak can be found. However, the problem with this theory is that the wavespeed will constantly be changing within a timber specimen due to micro-inhomogeneities, for example the changes in velocity between earlywood and latewood. However, that study used high-frequency waves, and this may not be the case when using longer wavelengths which effectively skip passed the change in homogeneity. Further, Walker and Carter (reported by Walker^(5.19) and Jarvis^(5.48)) stated that when beams of different velocities are taped together, the resulting resonance is that of the average of the beams (as dictated by the law of mixtures and shown in Chauhan *et al.*^(5.1)) and that individual resonances of each beam are not detectable, since all components behave as one system. Thus, only in the case of de-coupling (delamination) would it be possible. It may be the case that whilst this is true of transverse inhomogeneity, longitudinal variations in velocity may result in separate peaks being developed. For example, Gerhards^(5.30) and Divos^(5.15) have both noted that a longitudinal wave loses its planar nature whilst traveling around a defect, only for it to return to its planar nature some distance after it has passed.

Alternatively, the bifurcation is a result of the splitting of energy upon interaction with the inclusion. Tests conducted without the dowel in place showed that, despite the loss of mass when no dowel is present, there is no change in the harmonic frequencies or bifurcational behaviour with or without the dowel present. Thus any energy change as a result of passing through the inclusion can be discounted and the primary wave pathways are around the unaltered areas outwith the inclusion. Since the typical response of an LVL and clearwood beam tends not to bifurcate on

smaller inclusions, as opposed to PLY and sandwich beams, it could be argued that distinct velocity differences on either side of the inclusion arise in these beams. If, as stated by Divos^(5.15), the wave reforms a planar nature after interaction with a centreline inclusion, then upon each interaction the longitudinal wave is likely to evenly split its energy content to either side of the inclusion. Thus if one side is of less stiffness (hence lower frequency) two peaks may develop. However, if one side of the inclusion sees a velocity reduction then two wave fronts would develop. Therefore upon reflection from the end and the return interaction with the inclusion, four wave fronts would develop, and so on (making this theory impractical).

However, it may well be the case that there are not two close but separate resonances at all. Rather the bifurcated peaks are purely due to a splitting of the energy content either side of the actual resonance, which is contained within the trough between the peaks and slowly falls to once again become the single peak before the next bifurcation starts. In which case perhaps the principle gradients of outer limbs/slopes of the two peaks should be continued upwards until they reach an imaginary central peak and the frequency and damping ratio taken from there.

Ouis^(5.49) also observed that a 'beating' phenomenon (periodic amplitude modulation with time) occurs in the sound specimen's impulse response, which is not present in decayed specimens. This is attributed to a bifurcation of the fundamental peak of the major bending mode into two smaller peaks; the analogy of vibrational energy flowing alternately from one energy reservoir to another during the decay is presented^(6.39).

Finally a further alternative, favoured by the author, is that the bifurcation phenomena is simply the result of a flexural wave harmonics occurring at the same frequency as the longitudinal, with mode conversion shifting energy content from the longitudinal wave into a flexural wave.

5.8 Summary

Acoustic NDT experiments were conducted on increasingly inhomogeneous glue-laminated timber beams. Variations in TOF velocity, harmonic resonance velocity from multiple harmonics, their subsequent MoE_d , harmonic damping ratios and static MoE values have been observed. As a result, certain conclusions can be drawn.

It has been shown that the longitudinal velocity in the longitudinal axis of laminations is five times higher than in the transverse direction (equivalent to a 25-fold increase in dynamic stiffness along the grain compared to across it). Conversely, it has been shown that the damping ratio of the fundamental harmonic is four times lower than in the transverse direction. Typical damping ratios for unaltered LVL beams were similar to solid clearwood beam specimens, ranging between 0.35% to 0.45%, whilst PLY beams were typically 0.45% to 0.6%. Beams of higher inhomogeneity, 3L-6T-3L and 4L-4T-4L beams were shown to be highly susceptible to bifurcation of the resonance peaks, inducing errors in both the MoE_d and, more dramatically, in the damping ratio calculation. This was found to be the main limitation of an otherwise efficient application of the Q-factor method of damping determination. Excluding the more inhomogeneous engineering wood products, there is potential for the automated damping ratio to be used to identify the existence of strength-reducing defects such as rot, checks and cracks (and potentially knots) at specific points of a beam, provided that a consistent average value can be established. The values presented above would be a good starting indication. Further investigation into the effects and causes of bifurcation is required, particularly the reasons for its natural occurrences (as seen in Chapter 6). This could be simply done, in retrospect, by investigating the flexural and longitudinal harmonics simultaneously.

As expected, TOF MoE_d predictions overestimated resonance predictions, which in turn overestimated static predictions. Calculations have been presented to account for these overestimations as a result of increasing orders of magnitude of the strain rate.

It has been shown that TOF methods will take the fastest path available to them, and as such may not reflect either the inhomogeneities or defects present within a beam. This is in addition to a general overestimation due to the propagation of dilatational waves. Further, whilst it is not currently debated that resonance methods do average the entire cross-section of a specimen, it has been shown that individual harmonics reflect the longitudinal stress concentration and stiffness of specific areas of the beams corresponding to their nodal positions. If a defect was located at the anti-node of a harmonic, it would have no influence on the returned velocity, as opposed to a noticeable effect at nodal positions. In this case, it has been shown that two harmonics can return MoE_d estimates with as much as 30% difference in their value. This is not an issue in homogenous material or even relatively defect free wood, such as NZ North Island radiata pine, but presents a serious issue to the NDE of highly defect prone timber such as Scottish Sitka spruce.

As such, it is recommended that a minimum average of two harmonics, one even and one odd, be used to establish a beam's dynamic stiffness. Better still would be the use of four harmonics. This study has shown accuracy of dynamic stiffness predictions can be improved by this method. Higher harmonics will take less account of singular defects, but are more susceptible to increased damping and thus less likely to appear on conventional frequency spectrums without adequate signal-to-noise filtering. A further enhancement to automated systems would come from the observations of large discrepancies between the two-way predicted values of the 1st and 2nd harmonics, either in beams or logs (the latter being subject to further testing), which may indicate a high midspan knot concentration. Whilst this may not be picked up by conventional timber NDT equipment, it could seriously affect the MoR of a beam.

It has been shown that damping ratio can be increased ($> 1.7\%$) through the insertion of progressively larger artificial defects. LVL and clearwood beams were found to have an exponential relationship between defect volume (simulated KVR) and MoE_d when multiple defects are placed at various positions along a beam. The damping ratio generally behaves linearly, but does plateau eventually with

increasing volume, unless defects are inserted either at different orientations or off-axis. The orientation of these defects is of a consequence in laminated beams, particularly with edge defects, but it is unlikely to affect solid wood specimens. Instead the location and size, relative to the harmonic used for velocity determination, is far more important in influencing the return MoE_d prediction.

It cannot be confirmed that these defects mirror the effects of knots in beams, with previous studies suggesting an opposite effect in relation to MoE_d predicted from harmonics whose nodal points interact with the defects. However, it is most probable that the effect on the damping ratio would be similar as both interrupt the normal path of transmission of a longitudinal wave. It has been shown that even small defects, correctly located, will affect the return harmonic velocity. There is no evidence to suggest that the size of a wavelength must be comparable to the size of the defect to reflect its presence. Further study is required, but whilst it is accepted that log specimens with nodally located knots may have an opposite effect to holes, in beam specimens it is predicted that they will have a similar effect.

5.9 References

- 5.1 Chauhan S.S., Entwistle K.M., Walker J.C.F., 2005, *Differences in acoustic velocity by resonance and transit-time methods in an anisotropic laminated wood medium*, *Holzforschung*, 59, 2005, pp. 428-434.
- 5.2 Brüel & Kjær, PULSE 12 Product data sheet no. BU-0229-27, 2007-09, www.bskv.com B & K, Noerum, Denmark.
- 5.3 Dell™ Latitude™ D600 Systems User's Guide, Nov. 2004, P/N 6T524, www.dell.com
- 5.4 Brüel & Kjær, Accelerometers and conditioning: Product catalogue February 2005, pp. 51-54 www.bskv.com, B & K, Noerum, Denmark.
- 5.5 Brüel & Kjær, Type 3508-B accelerometer Product data sheet no. BP-1841-14, 04/06, www.bskv.com, B & K, Noerum, Denmark.
- 5.6 Brüel & Kjær, Type 4294 calibrator Product data sheet no. BP-2101-11, 05/06, www.bskv.com, B & K, Noerum, Denmark.

- 5.7 Brüel & Kjær, Endevco Model 8202 Modal hammer Product data sheet, 0805, www.bskv.com, B & K, Noerum, Denmark.
- 5.8 PUNDIT 6, 54 kHz concrete tester instruction manual, CNS Farnell Ltd, Borehamwood, Herts.
- 5.9 Ouis D., *Frequency dependence of strength and damping properties of wood and their influence by structural defects and rot*, In: Proc. 14th Int. Symp. NDT wood, May 2-4 2005, Hanover, Germany, May 2-4 2005, Ed. F-W Broker, Shaker Verlag, Germany.
- 5.10 Sandoz J.L., Benoit Y., Demay L., *Wood testing using Acousto-ultrasonic*, In: Proc. 12th Int. Symp. NDT wood, University of West Hungary, Sopron, Hungary, September 13-15, 2000, Ed. Divos F.
- 5.11 Divos F., Daniel I., Bejo L., *Defect detection in timber by stress wave time and amplitude*, E-J. of NDT, Vol. 6 no.3, 2001.
- 5.12 Smith, R.S., *Sound transmission through lightweight parallel plates*, PhD Thesis, Heriot-Watt University, 1997
- 5.13 Cai Z., Hunt M.O., Fridley K.J., Rosowky D.V., *New technique for evaluating damping of longitudinal free vibration in wood based materials*, J. Testing and Ev., 25, 4, 1997, pp.456-460.
- 5.14 Hori R., Muller M., Watanabe U., Lichtenegger H.C., Fratzi P., Sugiyama J., *The importance of seasonal differences in the cellulose microfibril angle in softwood in determining acoustic properties*, J. Mat. Sci., 37, 2002, pp. 4279-4284.
- 5.15 *Course in Non-destructive Testing of Wood*, organized by F. Divos, ETS Arquitectura – Universidad Politecnica de Madrid, Madrid, June 2005
- 5.16 *Wood Handbook: Wood as an engineering material*, General technical report, FPL-GTR-113, 1999, FPL, USDA Forest Service.
- 5.17 Craik, R.J., *Sound Transmission Through Buildings: Using Statistical Energy Analysis*, 1996, Gower Publishing Company, Aldershot, U.K.
- 5.18 Wang X., Ross R.J., Mattson J.A., Erickson J.R., Forsman J.W., Geske E.A., Wehr M.A., *Non-destructive evaluation techniques for assessing modulus of elasticity and stiffness of small diameter logs*. For. Prod. J., v.52. n.2, 2002, pp. 79-85.
- 5.19 Personal communication with John Walker, March 2006
- 5.20 Kaiserlik J., *Stress wave timing non-destructive evaluation tools for inspecting historic structures: A guide for use and interpretation*, General Technical Report, FPL-GTR-119, 1978, FPL, USDA Forest Service.
- 5.21 Narkis Y., *Identification of crack location in vibrating simply supported beams*, J. Sound Vib., 172, 4, 1994, pp. 549-558.

- 5.22 Brancheriau L., Bailleres H., Sales C., *Acoustic resonance of xylophone bars: experimental and analytic approaches of frequency shift phenomenon during the tuning operation of xylophone bars*, Wood Sci. Tech., 40, 2006, pp. 94-106
- 5.23 Ouis D., *Frequency dependence of strength and damping properties of wood and their influence by structural defects and rot*, In: Proc. 14th Int. Symp. NDT wood, May 2-4 2005, Hanover, Germany, May 2-4 2005, Ed. F-W Broker, Shaker Verlag, Germany.
- 5.24 Hensen H., *Acoustic Studies on Wood*, MFS Thesis, 2006, New Zealand school of Forestry, University of Canterbury
- 5.25 Ross R.J., Pellerin R., *Non-destructive testing for assessing wood members in structures*, General Technical Report: FPL-GTR-70-1994, 1994, FPL, USDA Forestry Service.
- 5.26 Ouis D., *Assessment of severity and localization of a transversal crack in a wood beam through a study of its natural mode of vibration*, Holz als Roh und Werkstoff, 62, 2004, pp. 17-22.
- 5.27 Divos F., Daniel I., Bejo L., *Defect detection in timber by stress wave time and amplitude*, E-J. of NDT, Vol. 6 no.3, 2001.
- 5.28 Sandoz J.L., Benoit Y., Demay L., *Wood testing using Acousto-ultrasonic*, In: Proc. 12th Int. Symp. NDT wood, University of West Hungary, Sopron, Hungary, September 13-15, 2000, Ed. Divos F.
- 5.29 Sandoz J.L., *Non-destructive evaluation of building timber by ultrasound*, 8th Int. NDT of Wood Symposium, Vancouver, Sept 23-25, 1991.
- 5.30 Gerhards C.C., *Effect of knots on stress waves in lumber*, Res. Paper FPL-RP-384, 1982, FPL, USDA Forestry Service.
- 5.31 Jayne B., *Vibrational properties of wood*, 1959, For. Prod. J., November 1959, pp. 413-417.
- 5.32 de Olivera, F.G.R., de Campos J.A.O., Pletz E., Sales A., *Assessment of mechanical properties of wood using an ultrasonic technique*, In: Proc. 13th Int. Symp. NDT wood, Berkley, California, USA, August 19-21 2002, Ed. F. C. Beall, Forest Products Society, Madison, Wisconsin, USA.
- 5.33 Ilic J. *Variation of the dynamic elastic modulus and wave velocity in the fiber direction with other properties during the drying of Eucalyptus regnans Muell F.*, Wood Sci. Tech., 35, 2001, pp. 157-166.
- 5.34 Machek L., Militz H., Sierra-Alvarez R., *The influence of wood moisture content on dynamic modulus of elasticity measurements in durability testing*, Forschung Verwertung, 5, 2001, pp. 97-100.
- 5.35 Wang X., Ross R.J., Bradshaw B.K., Panches J., Erickson J.R., Forsman J.W., Pellerin R.E. *Diameter effects on stress-wave evaluation of modulus of elasticity of logs*, Wood and Fibre Sci., v. 36, n.3, 2004, pp. 368-377.

- 5.36 Divos F., Tanaka T., *Effect of creep on modulus of elasticity determination of wood*, J. Vib. and Acous., 2000, V.122, 1, pp.90-92
- 5.37 Tucker B.J., Bender D.A., Pollock D.G., Wolcott M.P., *Ultrasonic plate wave evaluation of natural fiber composite panels*, In: Proc. 13th Int. Symp. NDT wood, Berkley, California, USA, August 19-21 2002, Ed. F. C. Beall, Forest Products Society, Madison, Wisconsin, USA.
- 5.38 Bucur V., *Acoustics of wood*, 2nd Ed., 2005, CRC Press
- 5.39 Personal conversation with Mike Andrews at IRL, Wednesday 26th April, 2006
- 5.40 Andrews M., *Which Acoustic Speed?*, In: Proc. 13th Int. Symp. NDT wood, Berkley, California, USA, August 19-21 2002, Ed. F. C. Beall, Forest Products Society, Madison, Wisconsin, USA.
- 5.41 Haines D.W., Leban J-M., *Evaluation of the MoE of Norway spruce by the resonance flexure method*, 1997, For. Prod. J., 47, 10, pp. 91-93
- 5.42 Chauhan S.S., Walker J.C.F., *Variations in acoustic velocity and density with age, and their interrelationship in radiata pine*, 2006, For. and Eco. Management, 229, pp. 388-394
- 5.43 Castellanos J.R.S., Nagao H., Ido H., Kato H., Onishi Y., *NDE methods applied to the study of a wood beam's discontinuity*, In: *Proceedings of the 14th International symposium on nondestructive testing of wood, Hanover, Germany, May 2-4 2005*, Ed. F-W Broker, Shaker Verlag, Germany
- 5.44 Wang J., Biernacki J.M., Lam F., *nondestructive evaluation of veneer quality using acoustic wave measurements*, 2001, Wood Sci. tech., 34, pp. 505-516
- 5.45 Kabir M.F., Schmoltdt D.L., Schafer M.E., *Ultrasonic detection of knots, cross grain and bark pockets in wooden pallet parts*, Proc. World conf. Timber Eng. 2000, pp. 7.5.2-1
- 5.46 Kabir M.F., Schmoltdt D.L., Schafer M.E., *Time domain ultrasonic signal characterization for defects in thin unsurfaced hardwood lumber*, 2002, Wood and Fiber Sci., 34 (1), pp.165-182
- 5.47 Sandoz J.L., *Ultrasonic solid wood evaluation in industrial applications'*, 1996, In *Proceedings of the 10th International symposium on nondestructive testing of wood, Swiss Federal Institute of technology, Lausanne, Switzerland, August 26-28 1996*, Ed. Sandoz J.L., Presses Polytechniques et Universitaires Romandes
- 5.48 Personal communication with Mike Jarvis, University of Glasgow, 21st January 2005
- 5.49 Ouis D., *Detection of decay in logs through measuring the dampening of bending vibrations by means of a room acoustical technique*, 2000, Wood sci. tech., 34, pp. 221-236
- 5.50 Van Dyk H., Rice R.W., *An assessment of the feasibility of ultrasound as a defect detector in lumber*, Holzforschung, 2005, 59, pp. 441-445

- 5.51 Pellerin R.F., Morschauer C.R., *Non-destructive testing of particleboard*, Proc. 7th Int. Particleboard Symposium; March 1973; Pullman, WA. Washington State University.
- 5.52 Harris P., Petherick R, Andrews M, *Acoustic Resonance tools*, In: Proc. 13th Int. Symp. NDT wood, Berkley, California, USA, August 19-21 2002, Ed. F. C. Beall, Forest Products Society, Madison, Wisconsin, USA.
- 5.53 Feeney F.E, Chivers R.C., Evertsen J.A., Keating J., *The influence of inhomogeneity on the propagation of ultrasound in wood*, 1998, Ultrasonics, 36, 449-453.
- 5.54 Carter P., Wang X., Ross R.J., Briggs D., *NDE of logs and standing trees using new acoustic tools. Technical application and results*, In: Proc. 14th Int. Symp. NDT wood, May 2-4 2005, Hanover, Germany, May 2-4 2005, Ed. F-W Broker, Shaker Verlag, Germany.
- 5.55 Huang C-L., Lindstrom H., Nakada R., Ralston J., *Cell wall structure and wood properties by acoustics – a selective review*, 2003, Holz als Roh und werkstoff, 61, pp321-335.

6 Test series 3: Industrial-scale testing of logs and battens

6.1 Introduction

This chapter presents and discusses the results of acoustic NDT on the logs and battens of four separate Sitka spruce progenies. Following the presentation of the methods employed, a review of the history and silviculture of the progenies. Secondly, is a review of the results of the NDT tests on logs, discussing comparability between methods and progenies where relevant. The relationship between the calculated MoE_d and harmonic damping coefficients using a variety of methods and progenies is then discussed.

The chapter moves on to the batten acoustic NDT results and includes the static mechanical testing (MoE and MoR), drawing similar comparisons between acoustic measures and discussing where appropriate. Comparisons follow of dynamic and static measures in addition to comparisons between batten characteristics by progeny and in relation to MoE_d . Ability to increase the correlations between acoustic MoE_d and static measures, with emphasis on MoR prediction, through multi-variant combination is then investigated. Finally, a comparison of log MoE_d results and the average properties of their subsequent battens (to establish the accuracy of acoustic NDT on logs) is conducted. The conclusions of the discussions are summarised.

The samples used in this investigation are sourced from Stand 13 of Kershope Forest, Cumbria. Open-pollinated seed from the four progenies (see Table 6.1) were planted 1968 by the Forestry Commission, and were 35 years old at the time of felling in September 2004. The Kershope 13 forest, formerly grazing land with a peaty-clay soil, had a mean elevation of 190 m. Average annual rainfall was c. 1400 mm. All progenies were planted at 1.83 m spacings, in a mixture of plot sizes and shapes under a randomised complete block design. The progenies were not subject to thinning at any point before felling.

The principle aim of the FC study was to evaluate any differences in the tree and log characteristics, recoverable yield, and properties of the progenies of Sitka

spruce. It was assumed that selecting trees for relatively improved straightness or vigour would increase the low proportions of C16 recovered in unimproved Scottish Sitka spruce. QCI seeded timber is used as a control in the investigation.

A study conducted before felling the Kershope 13 trees found some evidence of differences in DBH amongst the progenies, but this did not produce statistically significant differences in stem volume of individual trees.

6.2 Series 3a Method: Kershope log testing

Preparation for field-testing of logs began in September 2004 with assistance in test planning from Shaun Mochan at Forest Research NRS who outlined the Kershope progeny trials. This was an ongoing timber quality and breeding research project headed by Mochan that was part of the Strategic Integrated Timber Research in tree breeding (SIRT) project. Its objective was to see if selecting for growth and form leads to improvements in outturn and timber performance. The principal aim of this acoustic test series was to conduct the first large scale trial of acoustic NDT on Sitka spruce logs and observe if the correlations to static beam MoE, found in previous studies of other spruces, were similar to our more defect-prone species. Additionally, a further aim was to see if the pattern of acoustic behaviour of the laminated and solid specimens seen in Chapter 5 (Test series 2), was repeated in relation to the effects of defects.

6.2.1 Sample provenance

The specimens under investigation were three families of Sitka spruce and a bulk QCI seedlot planted in 1968 (age at felling was 36 years) at the progeny trial in compartment 13 of Kershope forest (Ordnance Survey, OS, grid ref: NY 47297734, Lat 55° 05'N, Long 2° 50'W), Kershope forest, Cumbria, England (see Figure 6.1).

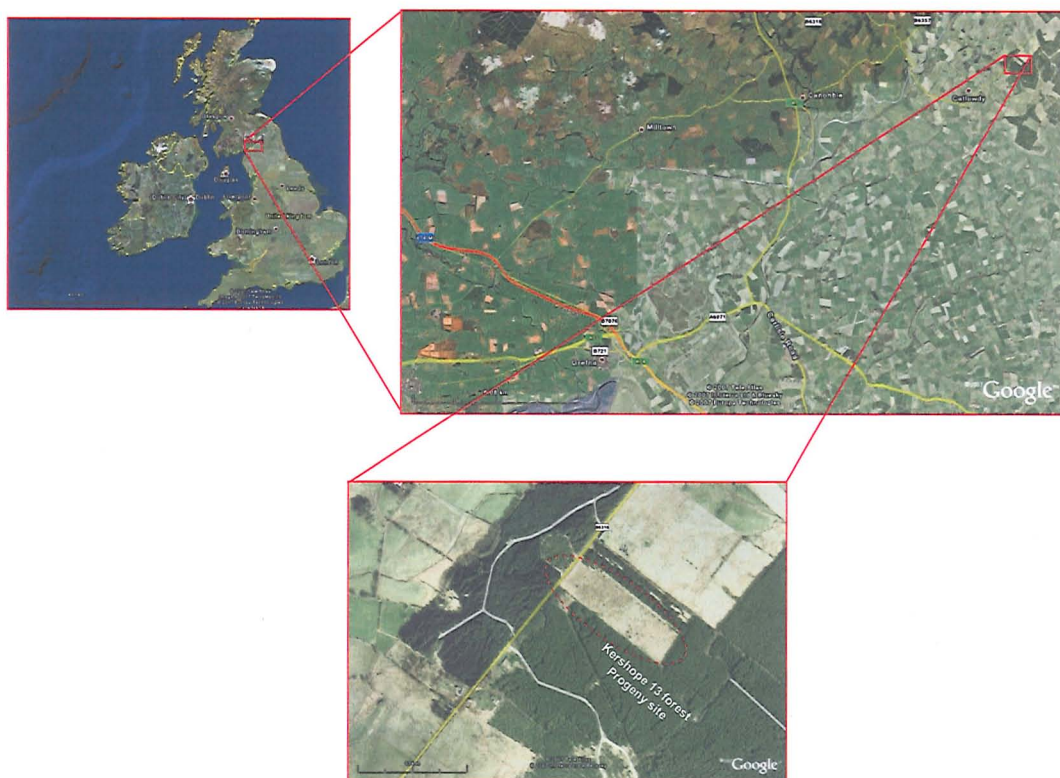


Figure 6.1 Progressively increasing scale satellite images(6.1) showing the Kershope 13 site, at Kershope Forest, Dumfries and Galloway, Scotland.

The trees were planted at regular spacings in a mix of plot sizes (2 m x 2 m to 6 m x 6 m) and stand sizes (single plots through to 12 tree row plots). No thinning occurred during growth. The three selected families were progenies of “plus trees”, that is trees which have been specifically selected for superior growth and form relative to the general population, through open-pollenated progeny selection (each family being numerically coded with the prefix IN specifying the NRS “industrial” experiment code). The characteristics of the three families^(6.2) are shown in Table 6.1.

Table 6.1 Characteristics of the four families involved in test series 3.

Progeny	Colour code	Original progeny seed source	NRS code	Comparison to QCI	Breeding enhancement
QCI	White and yellow	QCI, Canada	QCI	-	Control specimen
Family 2	Orange and red	(SS140) Glenbranter, Scotland	IN120	Less dense, more vigorous	Straightest treatment
Family 3	Green and blue	(SS430) Glenbranter, Scotland	IN420	Less dense, slightly straighter, more vigorous	Most vigorous treatment
Family 4	Cerise, pink, and black	(SS445) Glenbranter, Scotland	IN430	More dense, less vigorous	Most dense treatment

6.2.2 Log non-acoustic measurements

Measurements of DBH, stem straightness, spiral grain, northwards orientation, and Pilodyn testing were made by Forest Research before felling as part of a wider investigation by Napier University CTE/Forest Research into Sitka spruce properties^(6.2). A total of 144 “industrial” and 48 “scientific” sample trees were felled in the autumn of 2004. This thesis’s experiments concern only the industrial trees, which were sawn into 3100 mm log sections and transported to the sawmill.

Here the logs were subject to further spiral grain, bark depth and dimensional (length, cross-sections and taper) measurements by the author and his co-workers. In total 270 logs were cut from the trees (56 QCI, 84 Family 2, 66 Family 3, and 64 Family 4). The logs’ ends were colour coded (by family as outlined), with the tree number and log number sprayed and stencilled on respectively. The record system took the form: KR (Kershope Industrial batten), then tree number, then colour code, and finally log number (1 to 5). For example: KR15.C.2 would be Tree 15, from Family 4 (cerise colour) and Log 2 (from the butt log upwards) of that tree. This same system was later applied to the identification of the sawn battens. Discs were cut from the top and bottom of each log for compression wood assessment. This procedure is shown below in Figure 6.2.

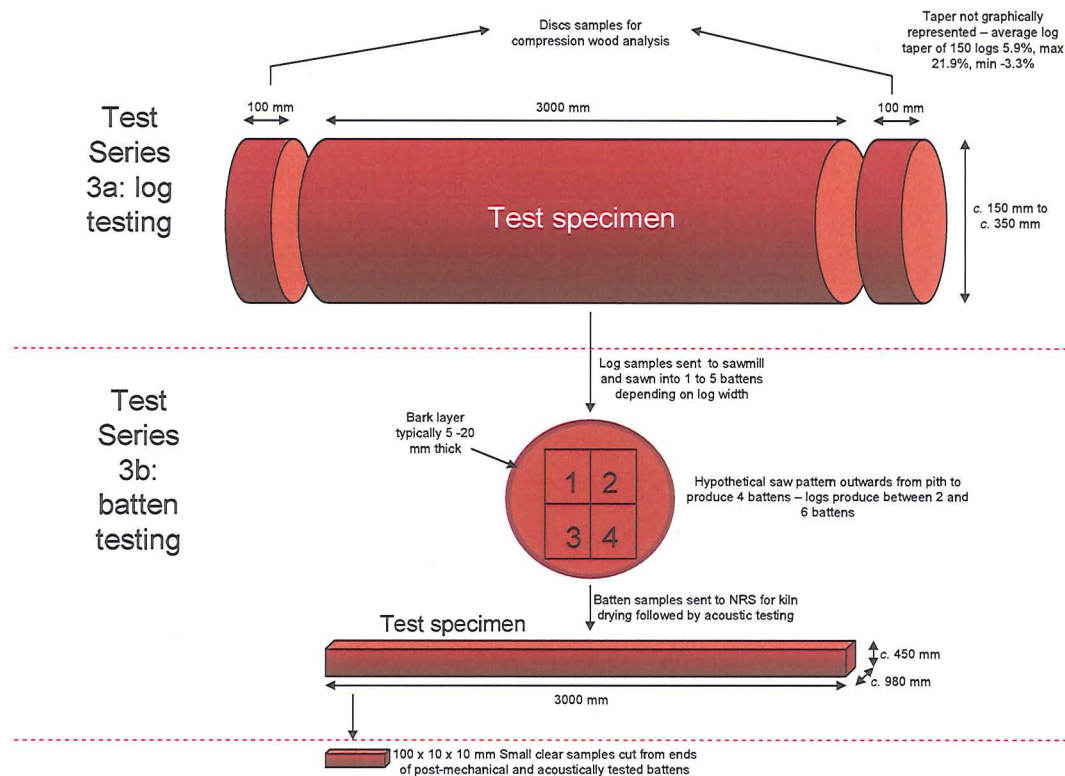


Figure 6.2 Production chain of Kershope battens

The logs and disc sections were assessed by the author and co-workers according to visual grading criteria set out in DD ENV 1927-1:1999^(6.3), essentially for the separation of red (poor quality) and green (higher quality) wood. This criterion assesses, amongst other parameters; visual knots (branches), grain angle, checks, splits, and compression wood. Additional measurements included the rate of growth, pith eccentricity, and ovality of the logs.

6.2.3 Acoustic testing procedure

The logs were acoustically tested outdoors at Howie's sawmill in Dalbeattie between 24 Nov. and 2 Dec. 2004. Unlike the initial laboratory tests on beams (Test series 1), the temporal resolution of the PULSE™ system was not as important an issue, because of the increased length of test specimen, thus the velocity resolution was reduced to c. 50 ms⁻¹. This was deemed acceptable when compared to the error involved in human estimation of oscilloscope displays from

the laboratory tests. The equipment set-up of these experiments is shown in Figure 6.3.

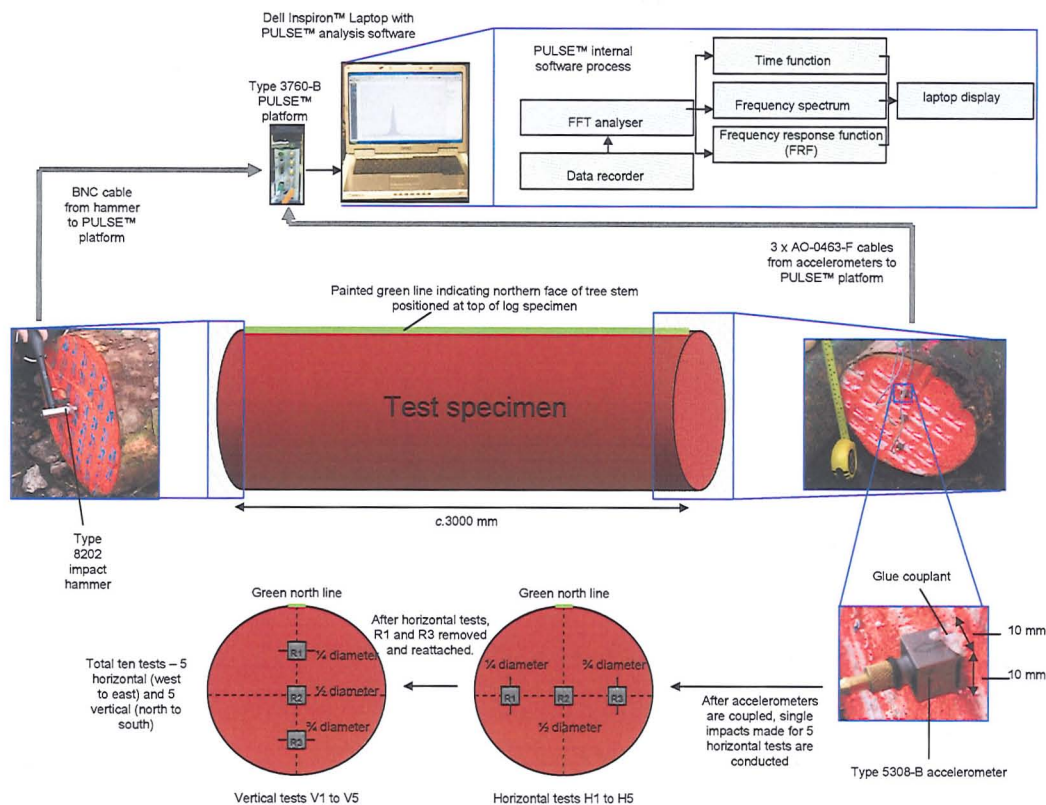


Figure 6.3 Setup of the measurement procedure used in field investigations.

The equipment used was the PULSE™ 3703-B 4-channel platform with the fast Fourier transform (FFT) available^(6.4). The FFT used a uniform window rather than a transient window (used for short time length impulses) as it allows an observation of the background signal, essential for TOF calculations based on deviations from the background, as well as not requiring time lengths to be inputted for each measurement. Further a uniform window avoids leakage outwith each frequency bandwidth so as to better isolate resonant peaks. The transform was set to display the peak level values in the frequency response functions (FRF) so time-weighting became irrelevant (as occurs with Hanning, exponential or Kaiser-Bessel time-weighting windows^(6.4)). In addition to the time display and frequency spectrum, a constant percentage bandwidth (CPB), and data recorder modules were activated. The FFT and CPB analysers determine the frequency, additional harmonics,

energy content, and FRF between the input hammer response and the accelerometers. The time function allows for measurement of the wave generation by the impact hammer and its arrival time at each accelerometer, thus allowing velocity determination. It also allows for any measurement of amplitude and internal damping coefficients to be determined. The recorder function allows the measurement to be replayed to allow time-slice study of the waveforms recorded. The test procedure used in the test Series 3a is set out in Figure 6.4.

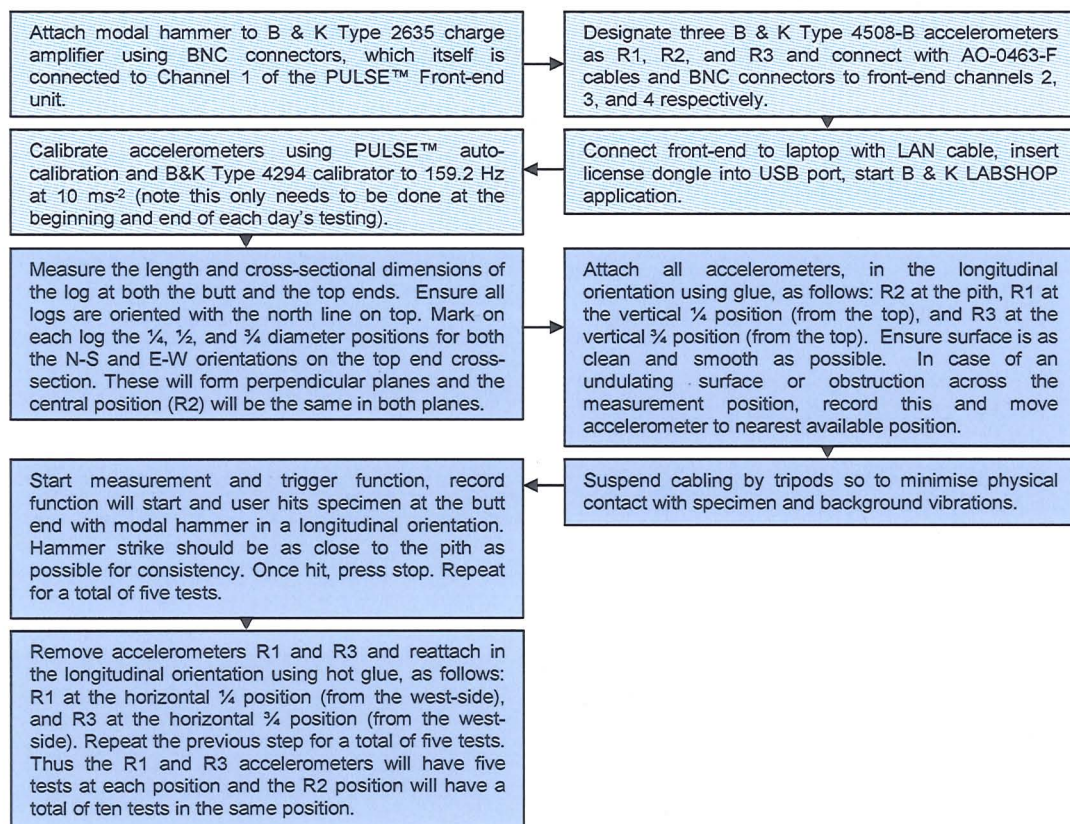


Figure 6.4 Flowchart demonstrating procedure for the acoustic testing (PULSE™) of a single log.

Testing at the sawmill gave rise to certain issues in the test protocol. Firstly, beeswax could not be used as a couplant due to the temperature consistently being below 5°C, therefore hot glue was preferred. Secondly, since the test series was conducted in the logyard, it was necessary to source power from a portable generator, which was placed 20 m away to avoid unwanted vibration. Background vibration levels were monitored before and after each test to ensure that they were

less than an arbitrary c. 1% (c. 150 mm s^{-2}) of a typical impact event's minimum peak amplitude (c. 15 m s^{-2}).

As noted in Figure 6.4, convention dictates that the surface should be as clean and smooth as possible to ensure no air gaps in arise in the couplant and that the couplant is of a consistent thickness. Whilst the ends of the beams in Test Series 1 and 2 were planed, the ends of the logs and beams in Test Series 3 were not, due to the logs being cut by chainsaw producing a somewhat irregular profile, as seen in Figure 6.3. As a result, the log's surface, tested at the logyard of the sawmill, has irregularly extruding fibres, creating a variation in the amount of couplant across the transducer face (both accelerometers and PUNDIT™ transducers). This may also affect the uniaxial alignment of the transducer face in being truly perpendicular to the longitudinal axis of the specimen. Dirt must also be removed from the logs at the logyard to ensure direct contact with the transducers.

Figure 6.5a, b, and c displays three sketches of the effect of surface roughness on wave transmission angle. Figure 6.5a shows a perpendicularly aligned transducer head, attached with hot glue. Whilst this removes irregularity by filling in the troughs of the contact area, it means that some of the contact area has more couplant than others. In this instance, the specimen will be subject to normal beamsread and full reception of the arriving energy content of the longitudinal wave.

Figures 6.5b and 6.5c show the effects on the transmission angle of the PUNDIT™ transducer if the signal reception transducers of the PUNDIT™ and PULSE™ accelerometers are not axially aligned, for a 1° to 2° and a 10° misalignment respectively. In this instance, the energy content received by the transducer will have a greater than 4% contribution of other wave modes' energy (which is the maximum in the case of uniaxial alignment) or the amount of longitudinal wave energy received may be reduced. In the latter case, this may create discrepancies in derived velocities, particularly in log specimens with a greater area of cross-section. This is because with uniaxial alignment, and applicable to TOF calculations by PUNDIT™ or PULSE™, the receiving transducer may detect

elements of the unreflected dilatational wave approaching before the main body, which may have been significantly weakened due to the increased energy loss due to beamspread with distance and the greater inherent damping. This could mean that in some cases that the threshold level of the detection system is triggered in cases of axial alignment but not in non-axial alignment of the transducers. This possibility is discussed later in this chapter, in relation to potential errors in the results.

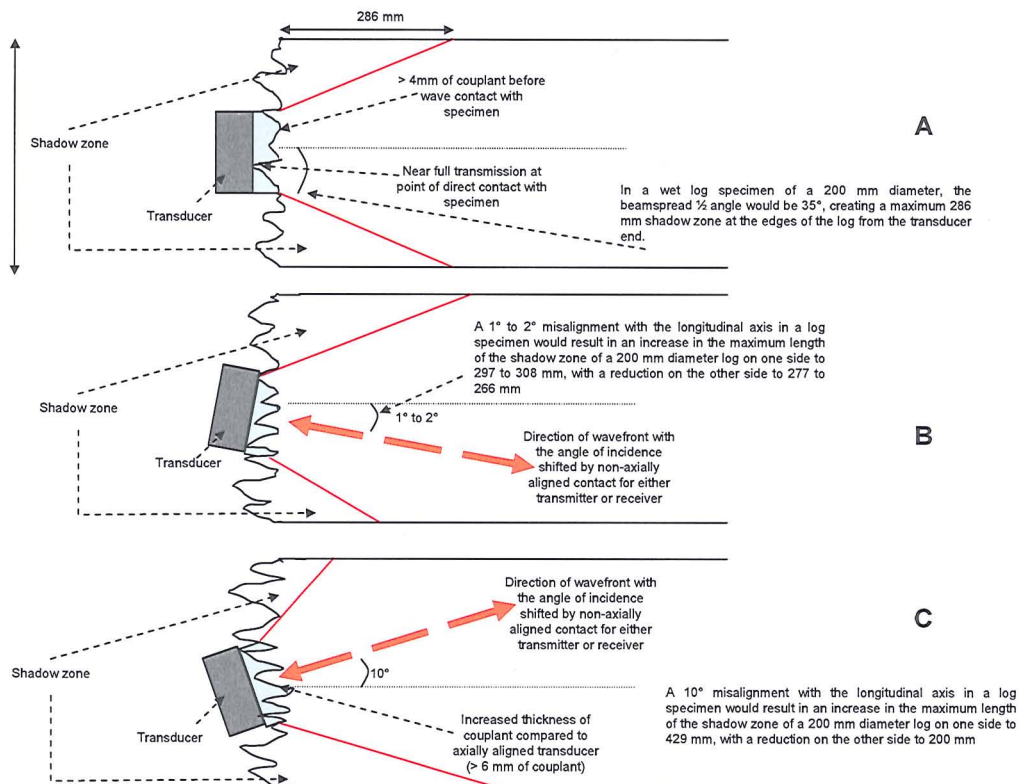


Figure 6.5a, b, and c showing effects of transducer alignment. Figure 6.5a shows the case of axially aligned accelerometers, demonstrating the potential maximum shadow zone of PUNDIT wave transmission. Figure 6.5b demonstrates the change due to a small change in axial alignment, whilst Figure 6.5c shows the effect of a large change in alignment angle. In all figures illustrations are not to scale.

The use of thermoplastic glue for attaching the accelerometers reduces the potential for air gaps to arise. A liberal application combined with a strong force of application forces the glue to either fill the gaps in the rough surface whilst excess glue is forced out with the sensing area. The fast setting of the glue ensures no couplant drains away during the test, whilst proving a more stable adhesive at low

temperatures on rough surfaces than beeswax. Sufficient force of application and the larger surface area of the PUNDIT™ transducer should ensure transmission despite a less viscous couplant (Vaseline™).

In total, 150 logs out of 270 were tested from the four families using the PULSE™ system. This includes all 84 logs from IN120 progeny (improved straightness) and all 56 logs from the QCI progeny. However, due to time constraints only 10 logs from the IN430 progeny were tested and no logs from the IN420 progeny could be tested (though the progeny was subject to testing as battens). Sixty of these were also tested using the PUNDIT™ system, including all 56 QCI progeny logs, 30 IN120 progeny logs and five IN430 progeny logs. The PUNDIT™ test procedure followed that of Test Series 1, with the PUNDIT™ transducers placed at the centre-point of the log end. However, due to the combined effects of a small wavelength (c. 55 mm), large distance (3100 mm) and high moisture content (between 60% and 300%), certain logs either did not display a result or the result was anomalously low. As such these results were discounted from the results displayed later in this chapter.

The post-processing of the results involved the calculation of three PULSE™-based TOF velocity estimates (to complement the PUNDIT™ five-test-averaged TOF velocity), four resonance-based velocities, and a damping ratio for both the 1st and 2nd harmonic modes of vibration.

Resonance-based velocity is calculated using the FFT frequency-acceleration display, which has a frequency span of 0 Hz to 12.8 kHz using 6400 spectral lines, equating to a frequency resolution of 2 Hz. This was deemed an acceptable resolution as it allowed for the simultaneous display of the time-amplitude graph for TOF calculations. The procedure consists of identifying the largest amplitude peak (1st harmonic) and activating the harmonic sideband function (shows theoretical harmonics of the 1st harmonic, as seen in Figure 6.6); near to these theoretical values will be frequency overtones (harmonics), now finally record the frequencies of the 1st to 4th harmonics. The length of the specimen is then used to calculate velocity using Eqn 6.1

$$V_c = \frac{2f_n l}{n}$$

Eqn 6.1

Where:

f_n = frequency of the n^{th} mode

V_c = velocity

n = (wave or mode) number

l = length of the specimen

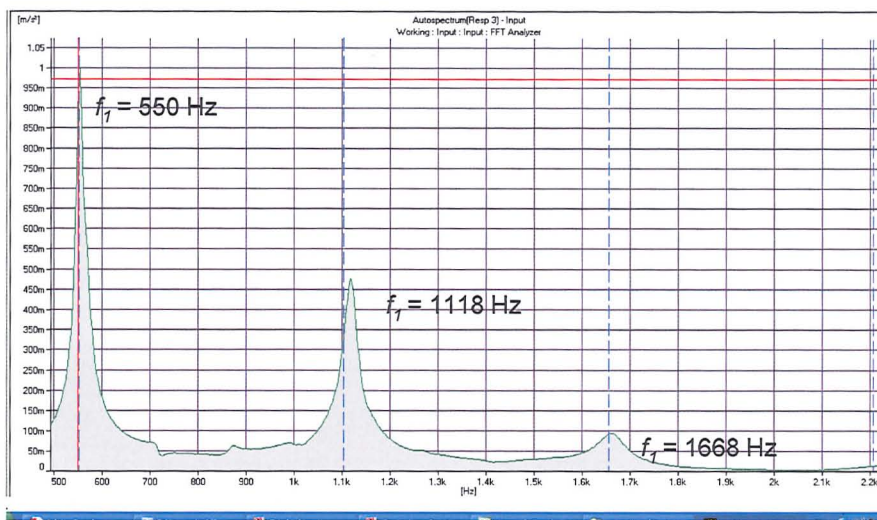


Figure 6.6 FFT frequency-acceleration graph showing the 1st harmonic (left) and subsequent 2nd and 3rd harmonics. Note the theoretical harmonic frequency derived from the fundamental predicted by the dashed blue line.

TOF-based velocity is calculated using the FFT time-acceleration display, which has a frequency span of 0 Hz to 12.8 kHz using 6400 spectral lines, equating to a temporal resolution of 30 μs . This equated to a velocity resolution of approximately 100 ms^{-1} on a 3 m batten sample. For an average density of Sitka spruce of 450 kgm^{-3} and average velocity in dry spruce of 5000 ms^{-1} , This 100 ms^{-1} error range equates to a potential MoE_d error of 0.9 GPa or approximately 8% of the mean value. It should be noted that in the log calculations, where the velocity is on average 3000 ms^{-1} and the bulk density 850 to 1000 kgm^{-3} due to the water content, this dynamic range will reduce to 0.54 GPa or c. 13% of the mean value. Due to the difficulty in accurately determining the first deviation from the horizontal

(caused by small background vibrations), comparable points on the exciting and receiving signal trace are used. A fault occurred with the compatibility of the Endevco 8202 modal hammer with the B and K PULSE™ platform, which was not noticed during the test series. In this, the excitation display repeatedly produced clearly incorrect impact forces between 500 GN and 1 TN. Subsequent testing after this series revealed the compatibility issue to be the result of the PULSE™ FFT analyser multiplying the received signal content by a factor of $\times 10^9$. Thus when the axis displays 800 GN, in actuality the force input was 8 N. The procedure consists of three stages:

1. Peak to peak: after identifying and recording the time of the peak (lowest point on the inverted signal) of the impact on the hammer signal trace (see Figure 6.7), the time of the first peak on the receiving signal is also recorded. The difference between the two times is taken giving the transit time of the wave which is then used with Eqn 5.1 to produce the velocity.

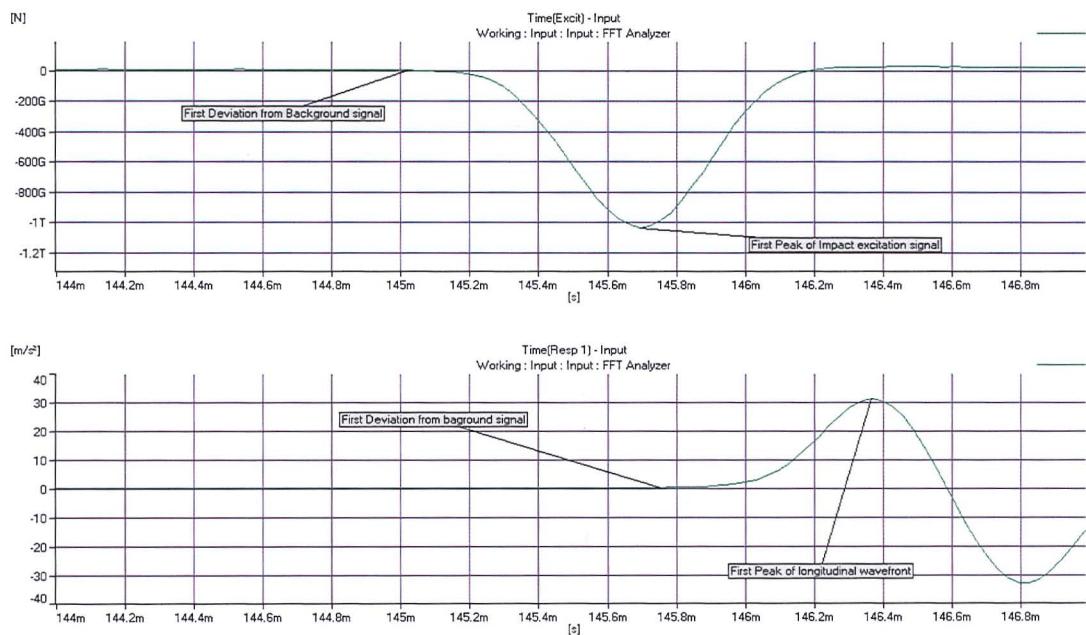


Figure 6.7 PULSE image showing the points taken for the deduction of the transit time using the time-acceleration display.

2. 25% to 25%: the peak amplitude's acceleration from Stage 1 is recorded for both the excitation and reception signal and divided by 4

to give acceleration amplitude of 25%. The time corresponding to these two amplitudes is deduced from the signal trace.

3. 10% to 10%: to give a transit time closer to the actual deviation from the horizontal, the same procedure as in Stage 2 is repeated but acceleration amplitude of 10% of the peak is used instead. These 3 stages are repeated for all 10 tests at position R2 and five tests at the other four positions.

The velocities are then converted to MoE_d values using the one-dimensional equation set out in Equation 3.1, by assuming a constant density of 1000 kgm⁻³ (due to the moisture content being above the FSP^(6.5)).

The damping ratio of the 1st, 2nd, and 3rd harmonics was calculated using the FRF function of the PULSE™ system with the excitation signal being used as the reference signal. The integrated resonance function allows for the automated calculation of the Q-factor, which is then automatically converted to a damping ratio, by placing the cursor over the desired peak. The equations used in this process are presented in Eqns 6.2 and 6.3.

$$Q = \frac{f_c}{f_2 - f_1} \quad \text{Eqn 6.2}$$

$$\xi = \frac{1}{2Q_1} \quad \text{Eqn 6.3}$$

Where:

Q = Q-factor

f_c = peak frequency of the 1st, 2nd, or 3rd harmonic (Hz)

f_1 and f_2 = lower and upper half-power frequency, respectively, of the corresponding harmonic (Hz)

ξ = damping ratio

A simplified frequency *versus* decibels (dB) graph is presented in Figure 6.8 to illustrate the derivation of the central peak and half-power (*i.e.* -3 dB) frequencies of the n^{th} harmonic.

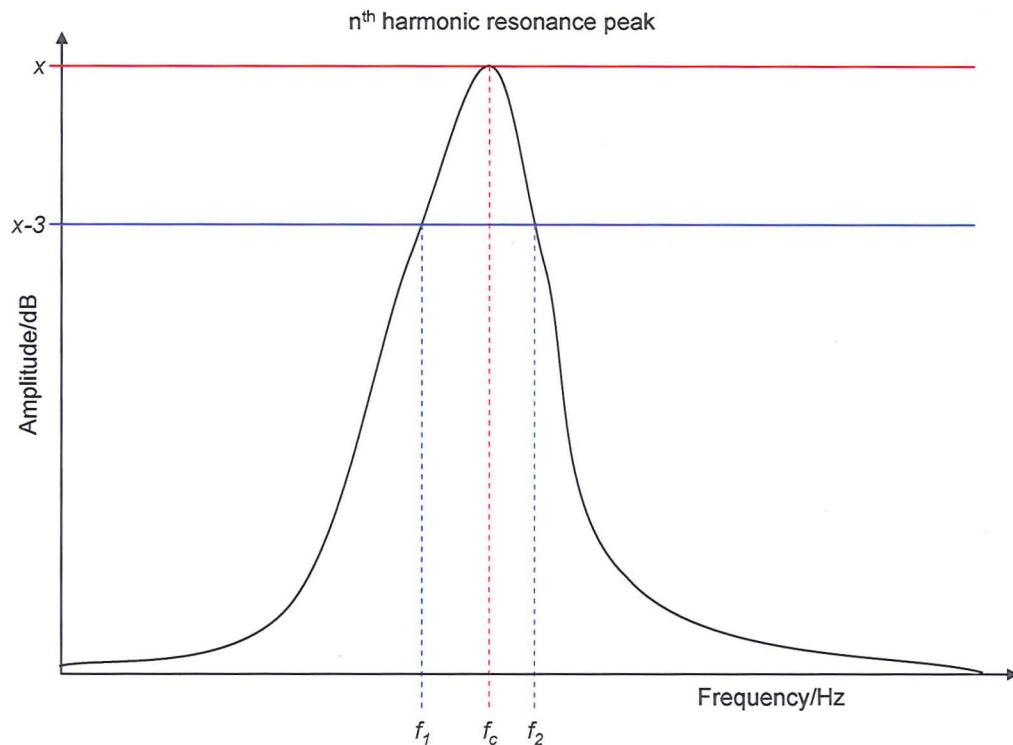


Figure 6.8 Derivation of the Q-factor by half-power points, this is done automatically by the PULSE system and converted to a damping ratio.

6.3 Series 3b: Kershope batten testing

Following the acoustic testing the 270 logs were sawn into 600 industrial sized (typical size: 98 x 45 x 3000 mm) battens. The logs then underwent conventional kiln drying at Howies at 60°C (relative humidity was 77%) to 20% MC^(6.2). The battens were then transported to Napier University where they were conditioned in an environmental chamber, at 21°C and 65% relative humidity, until they achieved a consistent mass^(6.2), *i.e.* no reading outwith 0.05% of the previous MC reading. This typically reduced the batten MC to between 10% and 14%.

The battens were divided into sub-samples. The first sub-sample was acoustically tested by the author; the second sub-sample was acoustically tested by Moore and Lyon under instruction from the author. Before acoustic testing, the battens were assessed by the author, with assistance from Nyander, for dimensions (using a tape measure for length and digital calipers at the ends, though no closer than 150

mm from the ends, and mid-span for the cross-section calculation), mass (using a digital balance), moisture content (using a Protimeter™ MC meter at the ¼- and ½-spans^(6.2)) and temperature (using an infrared sensitive thermometer at the ¼- and ½-spans). Each batten in sub-sample 1 was measured for KAR, slope of grain (grain angle), growth rate, boxed pith, compression wood, distortional characteristics, annual ring structure and ultimately visual grading assessment in accordance with BS EN 518^(6.6), prEN 14081-1^(6.7) and BS EN 4978^(6.8). Sub-sample 2 was only subject to destructive bending test assessment.

Acoustic tests using the Grindosonic™^(6.9) were abandoned due to the low repeatability of results, attributed to the Grindosonic™ being designed for smaller samples. This conclusion was drawn following the high repeatability observed when testing of 100 x 10 x 10 mm small samples for longitudinal and flexural resonance, but its failure replicate this with larger batten samples.

6.3.1 1st sub-sample procedure

The principal objectives of this study were to determine the MoE_d from TOF and resonance-based velocities. The results of the velocities from the different harmonics and TOF measurements (PULSE™ and PUNDIT™) would then be compared against each other and the static MoE values. Further, the damping ratio for each beam at the 1st, 2nd and 3rd harmonics was calculated, estimates of which could then be correlated to the other acoustic and wood parameters measured.

6.3.1.1 Equipment

- 1 x B & K PULSE™ Platform (Type 3760-B) with Type 3109 four channel input-output module and Type 7533 LAN interface module and software (Type 7705 time capture facility and Type 7770 FFT analyser)^(6.10)
- 1x Dell™ laptop (Latitude™ D600) and dongle^(6.11)
- 1 x 5 m AO-0463-F cables and pin connectors^(6.12)
- 3 x Type 4308-B uniaxial accelerometers^(6.13)

- 1 x Type 4294 calibration exciter^(6.14)
- 1 x Type 8202 Impact hammer^(6.15) and BNC connection cable
- PUNDIT™ 54 kHz concrete void tester^(6.16)
- 1 x PUNDIT™ couplant (Vaseline® or washing-up liquid)
- Hot glue gun (to attach the accelerometers to the beams) and Locite glue sticks
- 1× tape measure (read to ± 0.5 mm)
- 2× acoustic battens^(4.35) (for support and vibration isolation)
- Electronic balance (accuracy ± 0.05 g) to weigh the beams
- Moisture meter (accuracy $\pm 0.5\%$ volumetric moisture content)
- 1 x electronic calipers
- 1 x remote temperature monitor

6.3.1.2 Method

The method used in deducing the MoE_d and damping ratios of the battens cut from the Kershope logs is outlined in the flowchart in Figure 6.9.

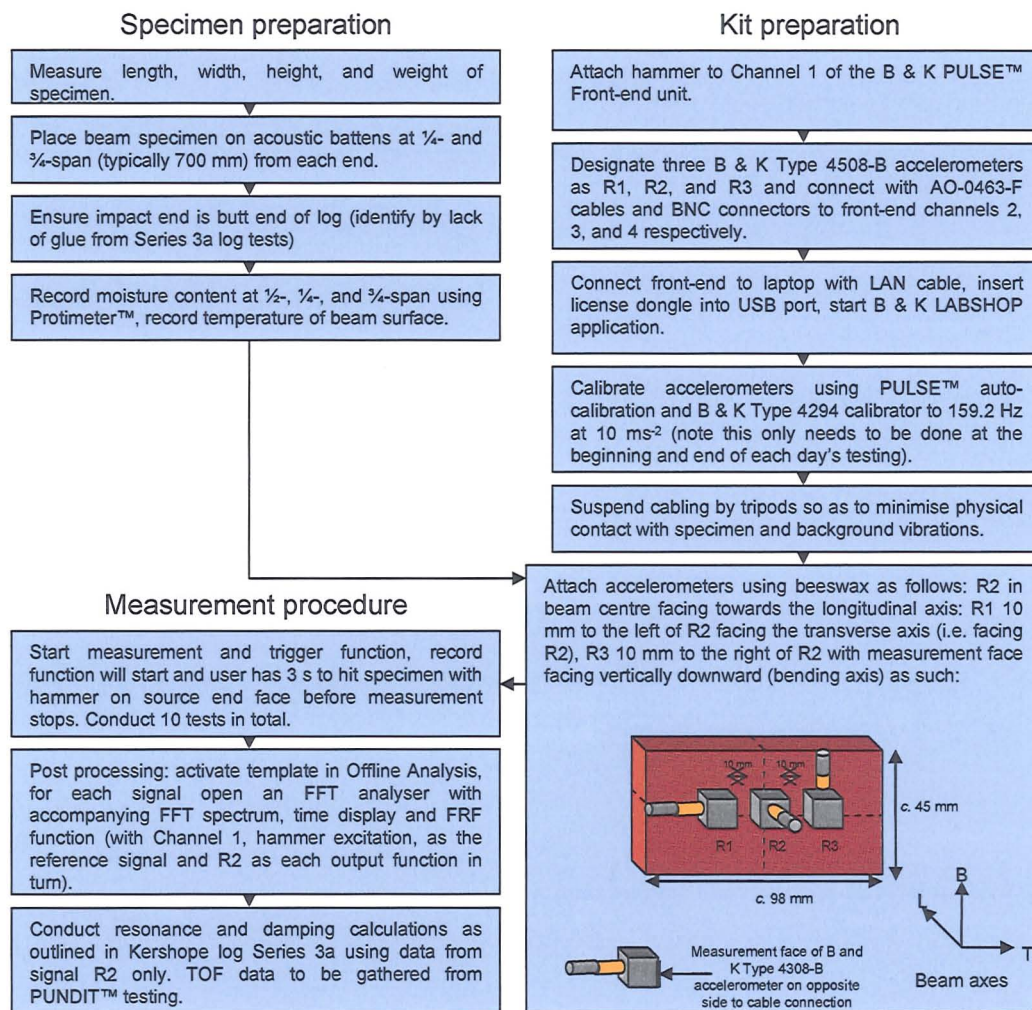


Figure 6.9 Flowchart of specimen preparation, acoustic kit preparation and measurement procedure

The measurement set-up was the same as that used for the LVL beam testing as shown in Figure 5.6, with the exception of the use and arrangement of three accelerometers as shown in Figure 6.9, and the supports being Proctor dynamic battens^{®(6.18)}, designed for vibration isolation in timber flooring.

The PULSE™ velocities were then calculated and converted to MoE_d values in the same manner as in the Kershope log test Series 3a. TOF transit time and hence velocity was also calculated in a repeatable manner by the 54 kHz PUNDIT™ tester. The procedure for this exactly follows that set out for Test Series 1, as shown in Figure 4.4. The PUNDIT™ velocities were then calculated in the same manner as in the Kershope log test series. The MoE_d values were then calculated

using the same procedure as in the Kershope log tests; however the density values were calculated using the actual density as derived from the batten mass divided by the batten volume.

6.3.2 Second sub-sample procedure

The acoustic test procedure for the second subset was the same as in the first subset. However, only the second sub-sample was subject to testing by the HM200™^(6.18) due to equipment availability.

6.3.3 Post-acoustic testing

Following acoustic testing of both sub-samples, the battens were subject to 3 and 4-point bending testing to destruction by CTE staff using a Zwick Z050 stress-grading machine^(6.19) (as shown in Figure 6.10, test recorded deflection continually using a crosshead displacement rates shown in Table 6.2). In a static bending test, the load is slowly applied (typically at a standard rate of 2.5 mm per minute) by a further one or two roller-bearing on the opposite side (*i.e.* from above over a 5-20 minute periods, depending of the nature of the timber) and the deflection (δ) is measured. A graph measuring the load *versus* deflection is then produced, such as the sample graph as seen in Figure 6.11.



Figure 6.10 Zwick 205D universal testing machine set up for four-point bending test

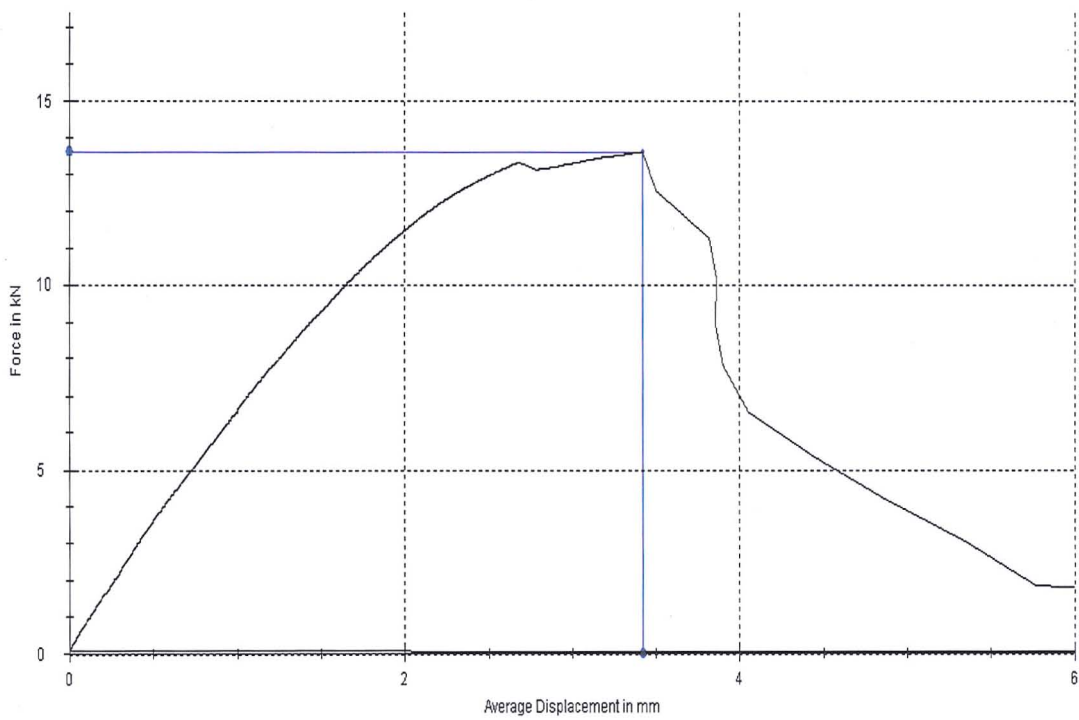


Figure 6.11 Typical force vs. deflection curve from a 4-point bending test

It should be noted that in the 3-point bending test, shear deflection will typically account for up to c.10% to 11% of the overall measured deflection whilst indentation effects of the loading head accounts for an 8%^(6.20, 6.21). This will therefore lead to a combined underestimate in three-point bending tests of on average 18% to 19% (which varies based on the density of the specimen) and as such the calculated MoE value will not represent the 'true' MoE of the specimen^(6.20, 6.21). That said, the correlation between the three and four-point bending tests in $R^2 = 0.99$ ^(6.21).

Bending tests were conducted in accordance with BS EN 408:2003^(6.22). Sub-sample 1 battens were tested flat-wise as boards, whilst sub-sample 2 battens were tested as boards and edge-wise as joists. This determined both the MoE and MoR of the specimens (see Figure 6.12). Table 6.2 shows the batten bending test set-up parameters, whilst Eqns 6.4 to 6.6 show the calculation of the local MoE (MOE_L), global MoE (MOE_G) and MoR respectively. The deflection used to calculate MOE_L and MOE_G is the deflection of point B relative to points A and C.

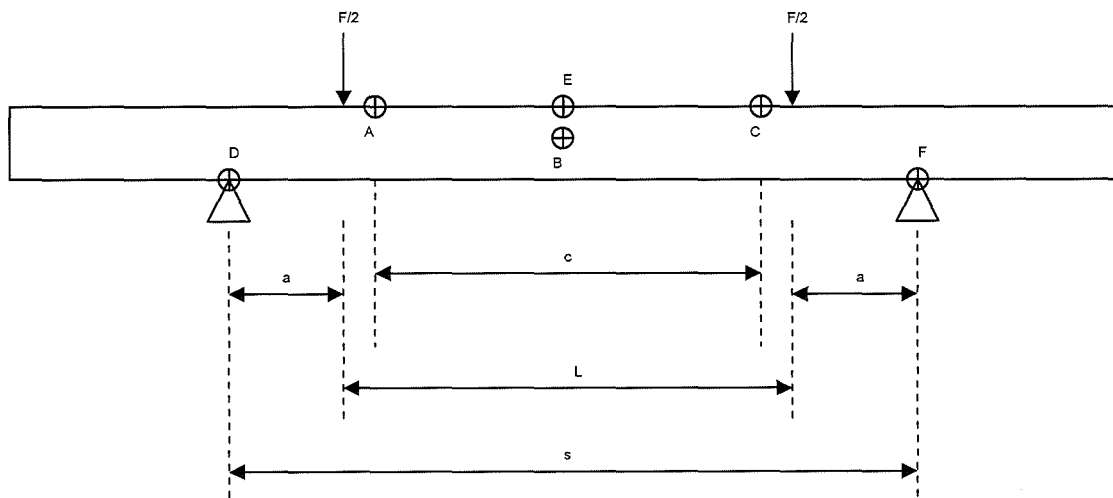


Figure 6.12 Schematic diagram for static bending tests.

$$MOE_L = \frac{ac^2(F_2 - F_1)}{16I(w_{c2} - w_{c1})} \quad \text{Eqn. 6.4}$$

$$MOE_G = \frac{a(3s^2 - 4a^2)(F_2 - F_1)}{48I(w_{s2} - w_{s1})} \quad \text{Eqn. 6.5}$$

$$MOR = \frac{3aF_{max}}{bh^2}$$

Eqn. 6.6

Where:

$F_2 - F_1$ = an increment of load in the linear region of the load-deflection curve

$w_{c2} - w_{c1}$ = an increment of deflection corresponding to $F_2 - F_1$

$w_{s2} - w_{s1}$ = an increment of deflection corresponding to $F_2 - F_1$

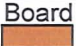


I = second moment of area about the batten's neutral axis ($I = bd^3/12$)

a & c = span distances shown in Figure 4.18 and Table 4.1.

s = span between supports

F_{max} = maximum force applied to the batten

Table 6.2 Batten test set-up parameters.

Nominal dimension/ mm	Orientation	Test set-up dimensions/ mm				Displacement rate/ mms ⁻¹
		s	a	L	c	
100 x 50	Board 	900	300	300	250	0.15
100 x 50	Joist 	1800	600	600	500	0.30
150 x 50	Joist 	2700	900	900	750	0.45

Each batten in sub-sample 2 was tested as both a board and a joist. All battens need their board MoE measured first and were then tested as joists. The load applied to measure MoE as a board was not large enough to cause likely plastic deformation of the batten and affect the results when the sample was tested as a joist. The maximum deflection permissible when testing battens as boards was determined from previous force-displacement curves such as those displayed in Section 5.1, and the average 3.1 m batten supported at quarter spans, with a 9 GPa MoE, had minimal midspan deflection of 4×10^{-3} mm.

6.4 Kershope sawmill testing: Results

In total, 144 Sitka spruce trees were felled by Forest Research and cut into 270 logs. Of these logs, 150 were tested using the PULSE™ system, encompassing the TOF, resonance and damping ratio measurements; 80 of these 150 logs were

tested using the PUNDIT™ system. This excludes 10 logs through which no signal could be transmitted.

Difficulties with individual log results, regarding wet logs, were encountered during the operation of the PUNDIT™ system are discussed in Section 6.4.1.1. Crucially, the PULSE™ and PUNDIT™ acoustic NDT tools are designed primarily for laboratory use, and as such were found to be unsuitable for sustained, efficient field investigations. However, PULSE™ velocities were recovered in all tested logs, unlike PUNDIT™. The PUNDIT™ required two operators and the constant reapplication of couplant. Battery operation at least allowed for a greater degree of portability with the PUNDIT™ compared to the PULSE™ platform, which required external power generation, extensive cabling isolation, and weather-proofing (through the use of a portable greenhouse). The result being that PULSE™ operation was time-consuming in terms of set-up for an individual test, allowing for the testing of approximately 15 to 30 logs *per* day, weather dependant.

A further PULSE™ issue was the requirement for accelerometer mounting. This needed time for the hot glue couplant to set (plus external power). Beeswax was found to be ineffective as a couplant to rough-sawn log ends in damp, low temperature conditions. In terms of the subsequent analysis of recovered FFT spectra and time displays, the harmonic derivation was considerably quicker, due to repeatability and the calculation from four, rapidly identifiable frequencies captured instantaneously during signal reception. The TOF calculation took significantly longer however, owing to manual calculation of transit times from the time of peak amplitudes of each excitation and reception signal. In retrospect, an automated system of time derivation would have been preferable, as the frequency velocity calculations took two days, whilst the TOF calculations from the time spectrum took over two months.

6.4.1 Log TOF results

This section displays the velocities derived by the PUNDIT™ tester, PULSE™ TOF peak-to-peak (P-P) velocities, and the 10 tests of the IN430 progeny, which

evaluated the difference between using 25% and 10% of the P-P amplitude for calculation of the velocity.

6.4.1.1 PUNDIT™ results

Table 6.3 displays the results of the PUNDIT™ velocities by progeny. Transmission of the PUNDIT™ 54 kHz wave was found to be inconsistent: transit times for wave velocity along the 3100 mm length of the green logs was only possible when the probes were placed at the central pith region of the cross-sections.

The inability to transmit a signal outside the central pith region was most likely attributable to higher moisture content in the outer wood. The MFA of the outer wood being more axially aligned should suggest good transmission (discussed in Chapter 3). Therefore, no radial variation in PUNDIT™ velocity could be determined. Additionally, ten logs did not return transit times even for the central region. The QCI progeny shows the highest mean velocity, as well as the largest range of velocities. The IN430 shows the greatest range in the inter-quartile velocities, although since this series only had five tests, this would be expected and this progeny also has double the standard deviation of the other two progenies. The progeny's mean velocity is only slightly lower than the QCI progeny, but the median velocity is significantly higher. The IN120 progeny has the lowest mean velocity, median velocity and smallest inter-quartile range of the three progenies tested. The mean velocity for all 80 logs tested by PUNDIT™ is 2518 ms⁻¹, and the range between progeny means is only 41 ms⁻¹, which represents 1.62% of the overall log mean PUNDIT™ velocity. Ultimately, on the basis of PUNDIT™ results there appears to be far greater variation within progenies than between them. The PUNDIT™ results are discussed further in respect to the other acoustic methods, as well as previous studies, in Section 6.4.4.

Table 6.3 TOF PUNDIT™ velocities by progeny. Results are in ms⁻¹, apart from the number of samples.

	IN430 Progeny	QCI Progeny	IN120 Progeny
Mean	2524	2536	2495
SD	228	157	134
Median	2625	2531	2506
Minimum	2261	2233	2237

Maximum	2745	2809	2765
No. of samples	5	48	27

6.4.1.2 PULSE™ TOF peak-to-peak results

As expected, following Kang and Booker^(6.23), there was no variation radially between low-frequency TOF velocities derived at the pith (accelerometer R2) or those at the ¼ and ¾ of the diameter of the receiving end (as shown in Figure 6.2). In relation to the observed results of Kang and Booker, who noted a radial variation in PUNDIT™ TOF velocities, their work was conducted on shorter specimens through which radial measurement was possible, unlike this study. The velocities calculated at each accelerometer position for an individual test were always the same, however this may be the result of a poor maximum temporal sampling resolution of the PULSE™ (sampling every 15 µs), which over a 3100 mm log equates to an error range of c. 300 ms⁻¹. A lack of radial variation is not without precedent, Wang *et al.* ^(6.24) noted a lack of variation radially in logs, attributed to a spreading of the wave into the faster TOF velocity outer wood and then across the cross-section at the measurement end of the log. However Jang^(6.25) in a similar experiment to this series, noted pith TOF velocities typically 4.4% lower than at the perimeter.

The range in mean velocities and standard deviations between the averaging of the ten tests at R2 and the 30 tests from all accelerometer responses (5 tests at each of the four other accelerometer positions, see Figure 6.2) varied by only ± 25 ms⁻¹ (for each of the progenies). This indicated that ten tests were sufficient for the conditions of repeatability and to establish a consistent mean velocity value for each log. As such, and due to the lack of radial variation, the results presented in this section only use the R2-derived data.

Figure 6.13 shows a boxplot of the range of PULSE™ TOF P-P velocities by progeny for the central R2 accelerometer only (ten tests *per* log). In contrast with the PUNDIT™ results, overall mean velocity of all 150 logs is 4655 ms⁻¹, with a range of 341 ms⁻¹ representing 7.34% of the mean velocity. Table 6.4 shows the statistical data for the TOF P-P velocities by progeny. It can be seen from Figure

6.13 that the IN120 progeny had the highest mean and median velocity, with the QCI progeny second highest and the IN430 progeny with the lowest. Also in contrast to the PUNDIT™ velocity results, the IN430 progeny had both the lowest range and inter-quartile range of the three progenies. The overall mean velocity for all 150 logs tested based on all 30 tests for each log was 4650 ms⁻¹. This was a decrease of only 5 ms⁻¹ between the average of 10 tests, and the average of 30 tests.

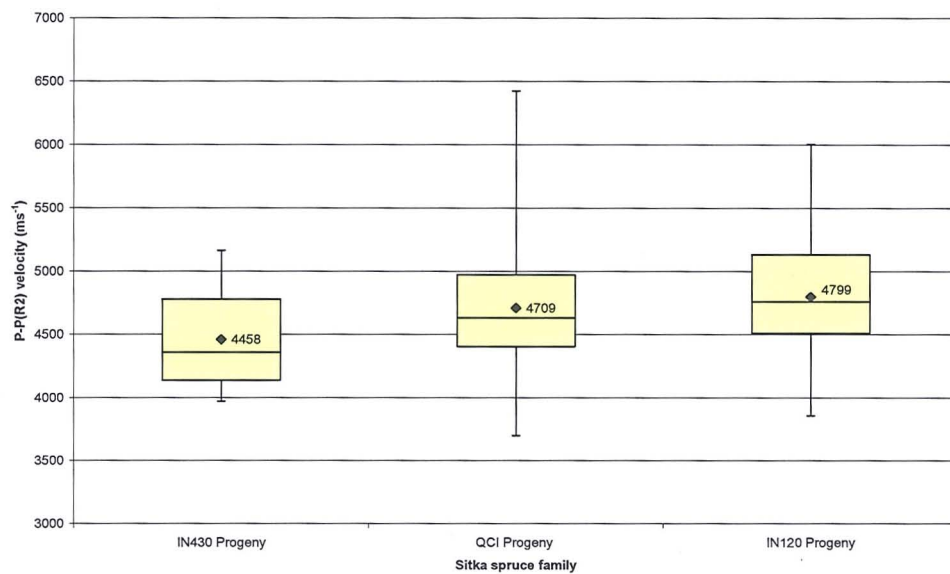


Figure 6.13 TOF Peak-to-peak (R2 only) velocities by progeny. Graphs show the maximum, minimum, inter-quartile ranges (yellow boxes), median (black line within boxes) and mean (diamonds) velocities for the specific progeny, based on the number of logs tested as specified in Fig 7.1.

Table 6.4 TOF PULSE™ peak-to-peak (R2 only) velocities by progeny. Results are in ms⁻¹, apart from the number of samples.

	IN430 Progeny	QCI Progeny	IN120 Progeny
Mean	4458	4709	4799
SD	405	458	428
Median	4359	4633	4761
Minimum	3970	3700	3859
Maximum	5165	6424	6006
No. of samples	10	56	84

Based on the TOF P-P velocities, and assuming a constant density above FSP of 1000 kgm^{-3(7.4)}, the IN430 progeny appears to have a lower mean stiffness than the QCI or IN120 progenies (which were only 90 ms⁻¹ apart). However, only ten logs of

the IN430 progeny were tested, but the standard deviation of each progeny was very similar. Whilst the minimum velocities for each progeny were similar (within 200 ms^{-1} of each other), the maximum values of the QCI and IN120 progenies were 1300 ms^{-1} and 900 ms^{-1} greater, respectively, than the IN430 progeny.

Although ten tests at the R2 position were sufficient to establish a stable mean value, it should be noted that there was, in certain logs, a wide variation of velocities. For example, log KR25Y1 has inter-quartile ranges for the ten tests across a 1500 ms^{-1} spread, with minimum to maximum values differing by 2500 ms^{-1} . There were no observable trends to explain such wide variations within the ten results either through mean velocities, impact force amplitude, log type or any measured timber characteristic. Table 6.4 and Figures 6.14 to 6.16, showed that many individual results produced velocities that were unfeasibly high ($> 8000 \text{ ms}^{-1}$), even for dry timber samples (the fibres of the samples used were fully saturated). This is discussed further in relation to US TOF and RF derived velocities in Section 6.4.4.

Figures 6.14 to 6.16 show the individual variation of the ten R2 tests for each log in the IN430, QCI and IN120 progenies respectively. This information is presented in boxplot form. The vertical red lines denote the change from logs of the lowest section of the tree (for example log ID code KRXXX01) to the next log vertically in the tree (for example log ID code KRXXX02). Not all logs tested had samples within that progeny corresponding to their respective upper or lower logs. Two sets of logs were tested for the IN430 progeny, three sets for the QCI progeny and four vertical log classes were displayed for the IN120 progeny. The horizontal green line between the y-axis and vertical red lines represents the mean P-P velocity for each log height.

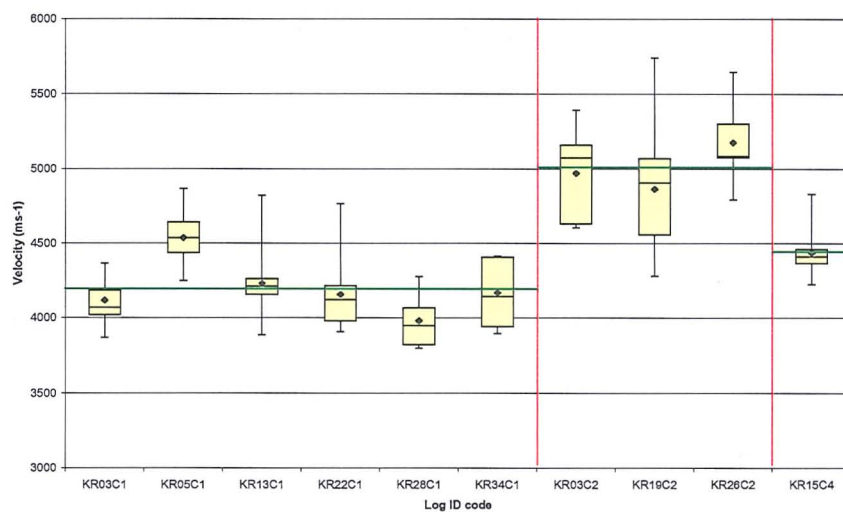


Figure 6.14 TOF Peak-to-peak individual log velocities in the IN430 progeny. Graphs show the maximum, minimum, inter-quartile ranges (yellow boxes), median (black line within boxes) and mean (diamonds) of ten tests on each of the ten individual logs in the IN430 progeny. The vertical red line separates logs by position in the tree from which they are cut (1st log, 2nd log and 4th log), whilst the mean velocity for each log position is shown by the horizontal green line. The raw data used in the production of this graph can be seen in Appendix B.

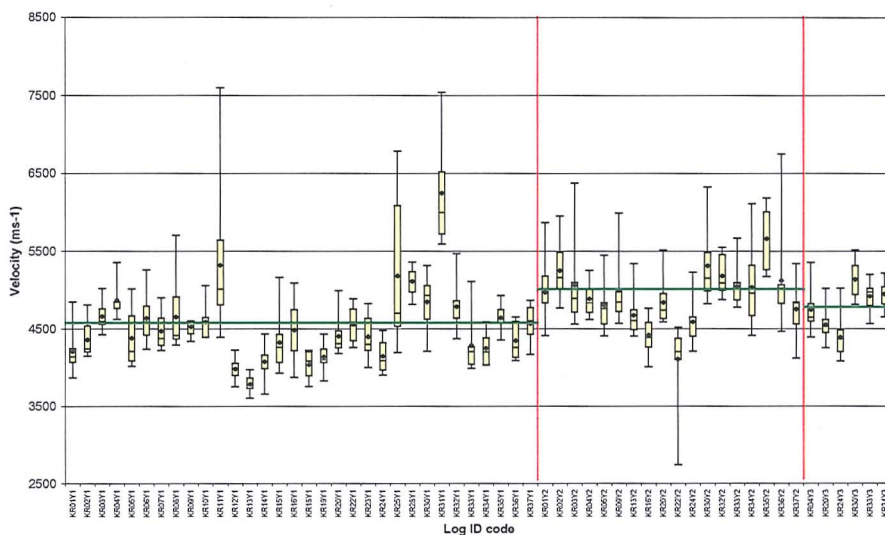


Figure 6.15 TOF Peak-to-peak individual log velocities in the QCI progeny. Graphs show the maximum, minimum, inter-quartile ranges (yellow boxes), median (black line within boxes) and mean (diamonds) of ten tests on each of the ten individual logs in the QCI progeny.

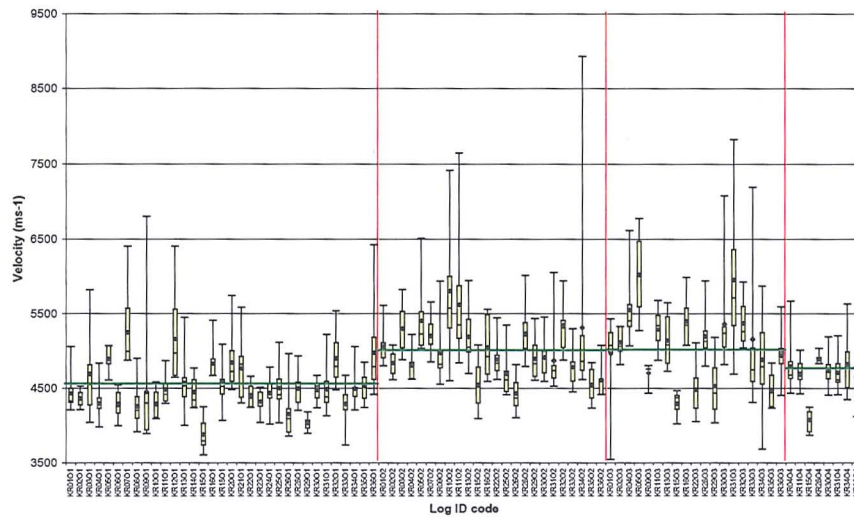
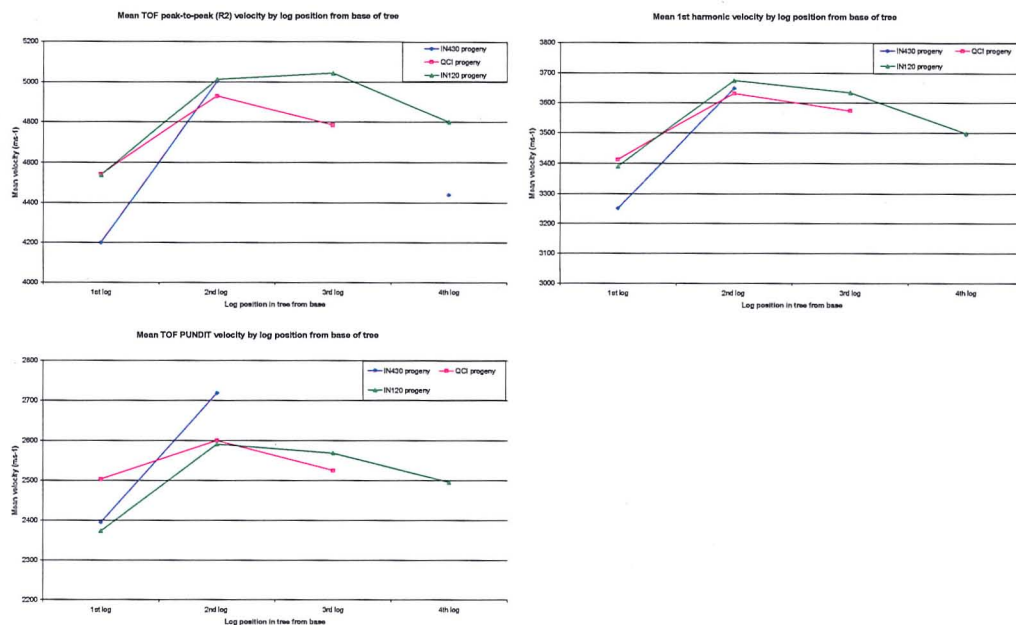


Figure 6.16 TOF Peak-to-peak individual log velocities in the IN120 progeny. Graphs show the maximum, minimum, inter-quartile ranges (yellow boxes), median (black line within boxes) and mean (diamonds) of ten tests on each of the ten individual logs in the IN120 progeny.

An increase in mean velocity was observed, in all progenies, from the first log (lowest) in any tree to the second. A general trend showed a decrease in velocity through the third and fourth logs, although their velocities are of a higher value than those of the first logs.

Figures 6.17a, b, and c show the variations in mean TOF P-P, PUNDIT™ and 1st harmonic mean velocities, respectively, through the corresponding height of each log in the tree. Only the 1st harmonic behaviour is shown as all four harmonics exhibited the same pattern of behaviour. The trends of all three graphs showed a general increase in velocity from the first to second log regardless of the number of logs in each category. There followed a decrease through subsequent logs, except for a small increase in the P-P R2 velocity in the IN120 progeny, although no 3rd logs were tested for the IN430 progeny.



Figures 6.17a, 6.17b, and 6.17c Comparison of (clockwise from top left) mean TOF P-P R2, 1st harmonic, and PUNDIT™ velocities respectively, by progeny from the 1st vertical log position to the 4th, where applicable.

This is consistent with the results of Xu and Walker^(6.27), who found the second log of the tree to be the stiffest, reportedly due to the higher proportion of juvenile wood (with high MFA and low stiffness) in the lowest (first) log. This indicates that segregation or rejection of lower stiffness 1st logs should occur at an earlier stage so as to avoid unnecessary costs of transportation to structural grade sawmills. A similar conclusion was reached by Mclean^(6.28) for Sitka spruce.

The velocity results presented here are discussed in relation to other methods of velocity determination in Section 6.4.4. Also addressed are the potential reasons for the anomalously high velocity values. Ultimately, it is the author's opinion that the use of TOF P-P is valid for relative comparisons between logs, but certainly should not be taken as representing plausible velocities for wood.

6.4.2 Log resonance results

The Brüel and Kjær noise and vibration analysis engine Type 7700 enabled real-time observation of the signal content to ensure impacts were successfully received by the accelerometers. The Type 7701 data recorder function was used to

playback the signals through the Type 7707 FFT analyser in the spectrum averaging function (as opposed to the signal enhancement function used in the calculation of the TOF P-P velocities: both signal enhancement and spectrum averaging are not possible simultaneously using the same FFT analyser). The track length of each recording was 3 seconds, within which a trigger function (set at 20 mms^{-2} , twice the typical background level) captured both signal generation (through the Type 8202 impact hammer transducer) and signal reception at each of the three Type 4508-B-001 accelerometers. Cross-correlation of the excitation and reception signals - through the spectrum averaging function - enabled the production of coherence and signal-to-noise ratio (SNR) spectra to monitor the signal content.

The PULSE™ system has six different types of time-weighting: uniform; Hanning; transient; exponential; flat-top; and Kaiser-Bessel^(6.4). Before analysis and velocity derivation by harmonic frequency observation, it was established that a uniform window auto-spectrum function was the most efficient for rapid assessment of the harmonic frequencies. Ideally a transient windowing function would have been most appropriate for impact NDT of the logs (to ensure only the actual impact is recorded and analysed), however the requirement of this method to input the time shift, taper and length of the impact or reception duration made the transient window impractical for field testing of multiple test specimens with variable wave transit times.

Table 7.3 is an amalgamated reproduction of information given by the PULSE™ system^(6.4). The Hanning, Kaiser-Bessel, and flat-top time windows are generally applied to continuous signals, thus were deemed ineffective for impact testing. Hanning windows can be useful for long transient signals however, the high acoustic damping within wet logs further made this an inappropriate window. The exponential window had similar issues to the transient time-window regarding the time taken for measurement set-up, as well as being more appropriate to lightly damped systems^(7.6).

Table 6.5 Amalgamated reproduction from Brüel and Kjær PULSE knowledge library^(6.4) showing the potential applicability, bandwidths, and weighting parameters for various time windows.

Time window	Continuous signals	Noise bandwidth (Hz)	Ripple (dB)	Highest side lobe (dB)	Side lobe fall-off rate per decade (dB)	Transient signals
Uniform	Order analysis and system analysis using pseudo-random noise	1.0	3.92	- 13.3	20	General purpose
Hanning	General purpose	1.5	1.42	- 31.3	60	
Kaiser-Bessel	For two-tone separation of signals with widely different levels	1.8	1.02	- 66.6	20	
Flat-top	Calibration	3.77	0.01	- 93.6	0	
Exponential	(FFT analyser only)					Decaying signals longer than the analyser's record length
Transient	(FFT analyser only)					Short transients – improves signal-to-noise ratio

In actuality, the uniform window is not really a weighting, as it is the direct representation of the signal content. An additional benefit of this weighting is reduced leakage from the central frequency to nearby frequencies, essential for accurate damping ratio determination.

No acoustic weighting function was required for either TOF P-P or harmonic velocity analysis. Time records were kept deliberately short (3 s) for rapid measurement, whilst being long enough to exceed the impact signal length which is essential for using uniform windowing. 6400 lines were used over a frequency span of 0 Hz to 6.3 kHz, producing a frequency resolution of 1 Hz (for an average log length of 3100 mm, this is equivalent to an error range of $\pm 3 \text{ ms}^{-1}$). A peak averaging mode was preferred over a linear mode to produce the least-damped harmonic frequencies, compensating for the reduced SNR compared with using a transient window. Approximately 2000 averages were taken during the 3 s recording. A maximum (99.9%) overlap was selected between averages to improve amplitude accuracy through improving the SNR, and avoiding data loss.

Resonance velocities, based on the 1st to 4th harmonic frequencies, were calculated for each of the 150 logs. The repeatable nature of longitudinal resonance testing (*i.e.* no discernible variation within the accelerometers' position or between any of the ten tests) meant there was no individual variation in log results as shown in the PULSE™ TOF tests in Section 6.4.1. Variation was present between the velocities dependent on the harmonic used to calculate the velocity. Table 6.6 shows the harmonic statistical data from all 150 logs where available.

Table 6.6 Velocity data for all logs calculated by individual harmonic. Results are in ms⁻¹, apart from the number of samples.

	1 st harmonic velocity	2 nd harmonic velocity	3 rd harmonic velocity	4 th harmonic velocity
Mean	3514	3509	3475	3403
SD	203	196	191	200
Median	3520	3521	3481	3426
Minimum	3056	3040	3007	2852
Maximum	3976	3976	3964	3843
No. of samples	150	150	150	128

Due to the decreasing amplitude of harmonics with increasing harmonic mode number, 22 logs were unable to produce a 4th harmonic for calculation in any of the ten tests on those logs. It can be seen that the difference between the mean velocities of the 1st and 2nd harmonic was only 5 ms⁻¹, whilst the mean velocity tended to reduce in the 3rd and 4th harmonics (with the range and standard deviation increasing slightly).

In terms of the deviation in mean velocity from the 1st harmonic: the 2nd harmonic decreased by only 0.14%; the 3rd harmonic decreased by 1.09%; and the 4th harmonic decreased by 2.7%. The mean and ranges of these percentage deviations can be seen later in Section 6.4.4. This is predicted by Timoshenko beam theory^(7.7), in that cases where the radius/wavelength ratio is greater than 0.3 (as in low-frequency resonance testing) the wavelength increasingly approaches the specimen's lateral dimensions, causing an increase in velocity dispersion between the group and phase velocities, including a reduction in velocity with increasing frequency, as seen in Appendix D1. The small percentage decrease seen in this investigation would be expected, at least in the case of the 1st to 2nd harmonic, owing to the relatively low mean taper of the logs (0.95). Comparing

percentage variations for the deviation between the 1st and 2nd harmonic, as provided by Walker^(7.8) for a 0.9 taper value, this should equate to a 0.08% difference. The small, but greater percentage decrease of 0.14% (for a smaller taper value) seen here is most likely the result of either increased attenuation of higher frequency waves due to the moisture content of the author's logs, or the method measuring a dispersive rod wave rather than a bulk longitudinal wave.

Most likely, the decrease in velocities would be the result of measuring the dispersive rod velocity, as opposed to bulk longitudinal velocity, with an inherent decrease in velocity with increasing frequency.

A comparison of resonance velocities between progenies, as shown in Figure 6.18 for the 1st harmonic, shows that IN120 had the highest mean velocity, followed by the QCI and then IN430 progenies. The pattern was consistent for all four harmonics, with the range in harmonic velocities between progenies in derived velocities decreasing with increasing harmonic mode (from 127 ms⁻¹ or 3.64% of the total mean velocity for all logs for the 1st harmonic, to 105 ms⁻¹ or 3.11% of the mean velocity for the 4th harmonic).

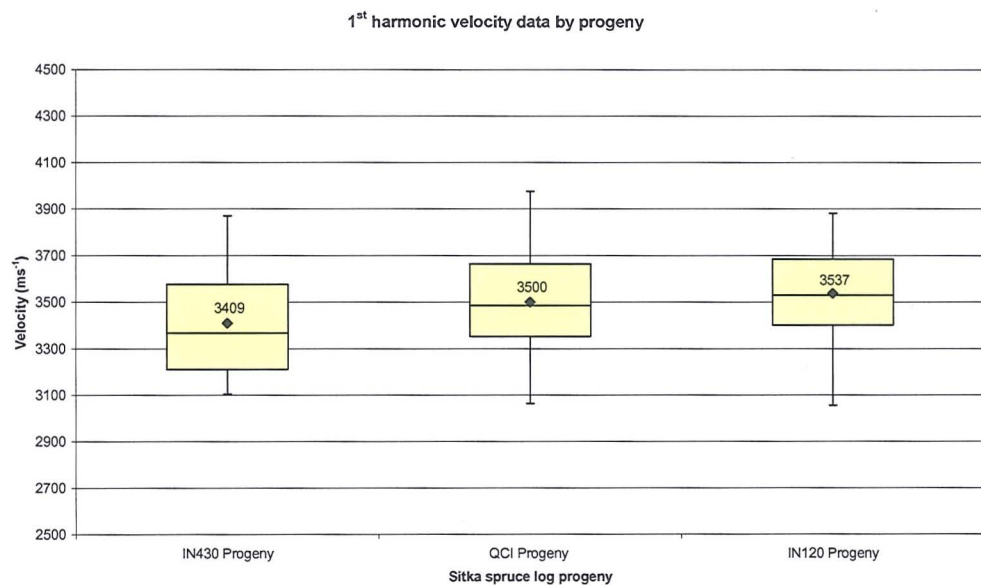


Figure 6.18 Variation in velocities by harmonic, between all three progenies. Graphs show the maximum, minimum, inter-quartile ranges (yellow boxes), median (black line within boxes) and mean (diamonds)

velocities of progenies by harmonic. The mean value is displayed as a number directly below the black diamonds. The raw data used are seen in Appendix B.

6.4.3 Log damping ratios

For every R2 accelerometer test on each log, the auto-damping function was used to calculate a damping ratio for 1st, 2nd and 3rd harmonics (the 4th harmonic typically having insufficient signal amplitude for accurate calculation). A maximum total of 10 damping ratios *per* harmonic *per* log and thus a potential maximum of 30 damping ratios *per* log were calculated. A naturally occurring bifurcation of the resonant peaks leading to weakened signal amplitudes, as discussed in Section 5.7.6, meant measurement of the damping ratio was not always possible for each test. No measurement recording was available for damping ratio analysis using the FRF display on the 1st or 2nd harmonic for KR34Y2 (QCI progeny) and KR14O1 (IN120 progeny), whilst KR36O4 (IN120 progeny) was severely bifurcated and damping ratios could not be calculated. For the 3rd harmonic damping ratios, KR14O1, KR31O3, KR36O4, KR34O3, KR16O2 and KR10O2 were removed from analysis as no damping ratio calculation was possible owing to insufficient signal amplitude.

As seen from Table 6.7 for the 1st harmonic damping ratios, the mean damping ratio of the IN430 progeny (1.07%) is noticeably lower than those for QCI (1.23%) and IN120 (1.24%) progenies. The IN430 progeny also has a lower mean standard deviation, maximum standard deviation and range (0.01%, 0.02%, and 0.64% respectively) compared to the QCI (0.02%, 0.44%, and 1.69% respectively) and IN120 (0.04%, 0.56%, and 2.60% respectively) progenies. This pattern is also seen in the 2nd and 3rd harmonic damping ratios. It should be remembered however that the IN430 statistics are based on a reduced number of tests.

Table 6.7 Progeny average damping ratios by harmonic mode. The raw data used in the production of this table can be seen in Appendix B.

	1st harmonic			2nd harmonic				3rd harmonic			
Progeny	IN430	QCI	IN120	Progeny	IN430	QCI	IN120	Progeny	IN430	QCI	IN120
Mean	1.07	1.23	1.24	Mean	1.26	1.6	1.6	Mean	1.59	2.08	2.06
Mean SD	0.01	0.02	0.04	Mean SD	0.01	0.03	0.07	Mean SD	0.06	0.09	0.14
Max. SD	0.02	0.44	0.56	Max. SD	0.04	0.16	0.32	Max. SD	0.28	0.37	0.6
Median	1.03	1.19	1.16	Median	1.24	1.5	1.52	Median	1.51	1.96	2.02
Minimum	0.86	0.73	0.74	Minimum	0.9	1	0.78	Minimum	1.08	1.03	1.1
Maximum	1.49	2.42	3.34	Maximum	1.62	3.59	3.15	Maximum	3.37	3.56	3.89
Range	0.64	1.69	2.6	Range	0.72	2.59	2.37	Range	2.29	2.53	2.79
Count	10	55	82	Count	10	54	81	Count	10	55	78

Figure 6.19 to Figure 6.21 shows the boxplot variations for the 1st harmonic damping ratios on the basis of the R2 tests for the IN430, QCI and IN120 progenies respectively. These three figures are deemed sufficient to indicate the variation between damping ratios tests on individual logs, with similar patterns, albeit with generally higher damping ratios, occurring in the 2nd and 3rd harmonic tests. The majority of logs (61%) had a damping ratio range from their R2 results of 0.05%. 32% of logs had a range in damping ratio results less than 0.02%, whilst 10% and 4% of the 147 logs tested had damping ratio ranges greater than 0.1% and 0.2% respectively. Logs with high variability are shown in the figures, they tend to be higher than the average mean damping ratio. The mean damping ratio across all 147 logs tested is 1.23%.

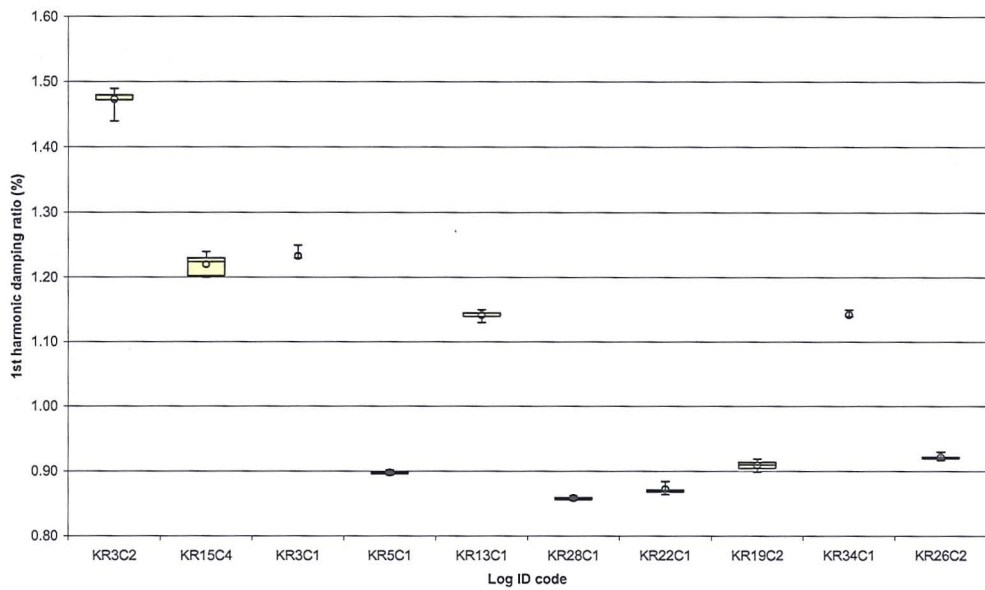


Figure 6.19 Boxplot displaying the 1st harmonic damping ratio variation within each log test for the IN430 progeny. Graphs show the maximum, minimum, inter-quartile ranges (yellow boxes), median (black line within boxes) and mean (hollow diamonds) damping ratios of each log. The raw data used in the production of this graph are seen in Appendix B.

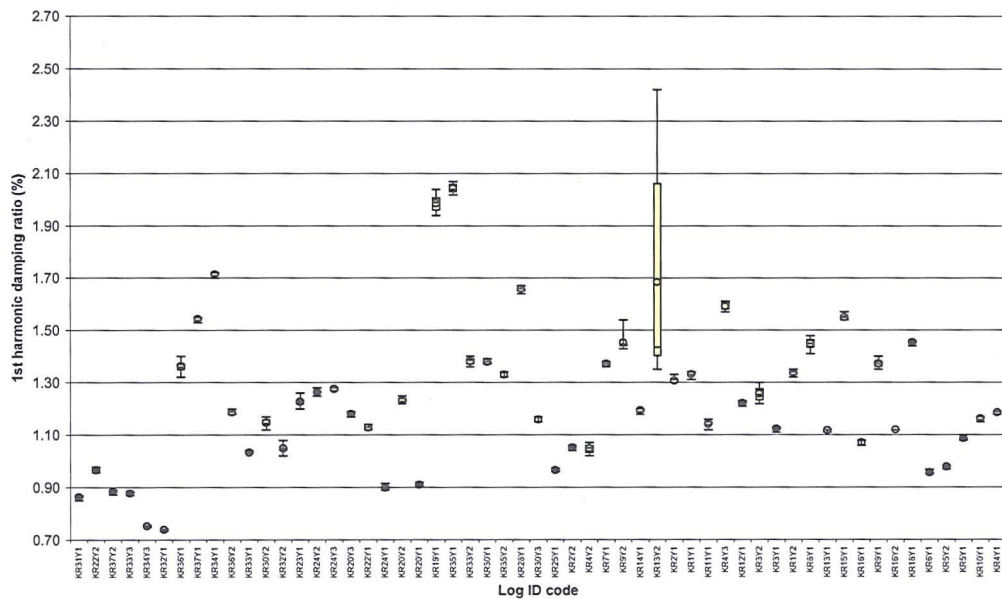


Figure 6.20 Boxplot displaying the 1st harmonic damping ratio variation within each log test for the QCI progeny. Graphs show the maximum, minimum, inter-quartile ranges (yellow boxes), median (black line within boxes) and mean (hollow diamonds) damping ratios of each log. The raw data used in the production of this graph are seen in Appendix B.

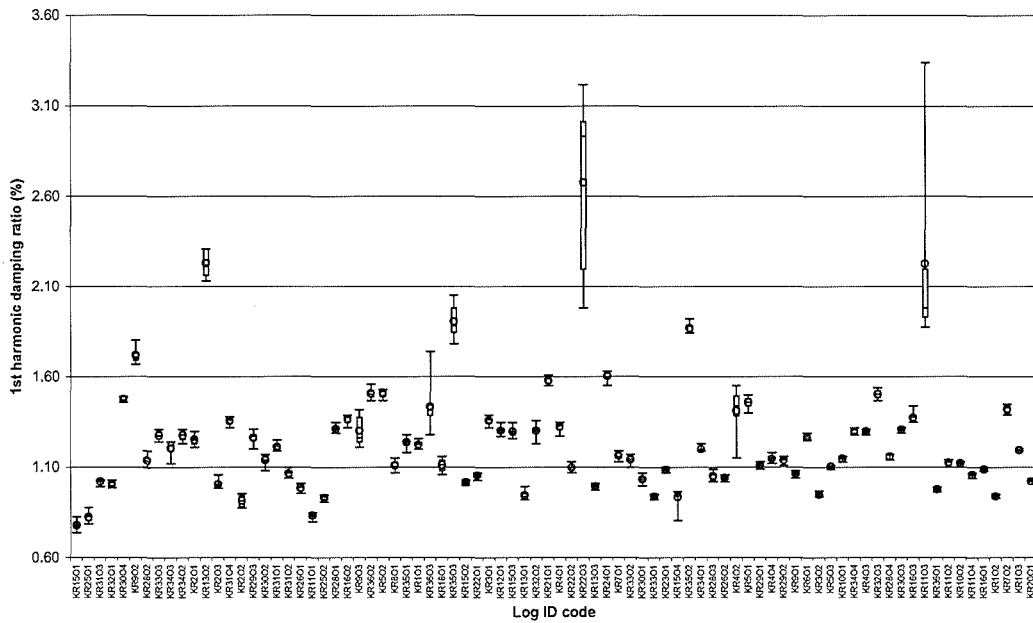


Figure 6.21 Boxplot displaying the 1st harmonic damping ratio variation within each log test for the IN120 progeny. Graphs show the maximum, minimum, inter-quartile ranges (yellow boxes), median (black line within boxes) and mean (hollow diamonds) damping ratios of each log. The raw data used in the production of this graph are seen in Appendix B.

Throughout the R2 tests most logs have a consistent damping ratio however, the reasons for the occurrence of logs with highly variable damping ratios is unclear. No relation to any timber (knot content on logs, taper, or mid-diameter) or acoustic parameter was found.

6.4.4 Acoustic data interrelations

In the following graphs (Figures 6.22 to 6.24) the relative differences between velocity measurements has been assessed for each progeny.

By adding a line between velocity measures for each log, it can be seen that each velocity measurement followed the same general trend of rises and falls in velocity between logs. The TOF P-P velocities were, as expected, always higher than the harmonic velocities, though not to a consistent percentage. The harmonics in turn were, unexpectedly, always higher than the PUNDIT™ TOF velocities. The TOF P-P velocities also had a larger velocity range between logs than the harmonics, which in turn had a larger range than the PUNDIT™ velocities. For example, In

Figure 6.23, QCI progeny, there was a clear drop in all velocities between logs KR9Y2 and KR14Y1. However, the PUNDIT™ velocity only dropped by 428 ms⁻¹, whilst the 1st harmonic velocity dropped by 703 ms⁻¹, and the TOF P-P velocity fell by 820 ms⁻¹. This pattern of amplified increases and decreases in velocity followed the rising mean velocity of each measure across each progeny.

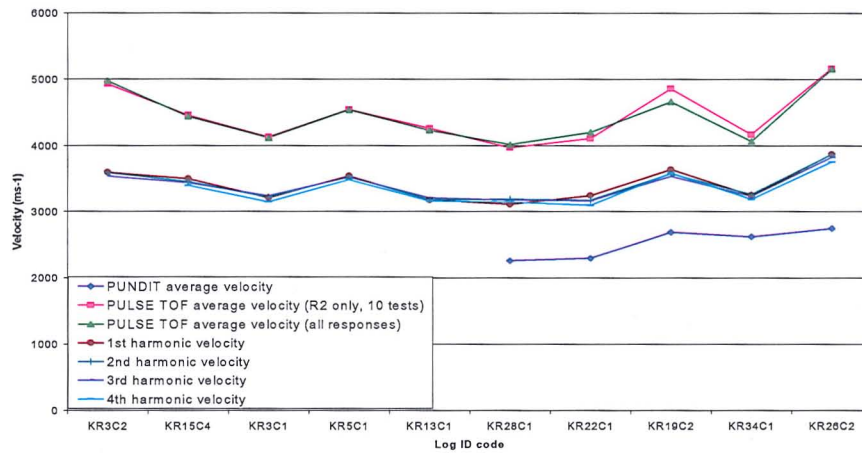


Figure 6.22 Comparison of the various velocity measurements within the IN430 progeny.

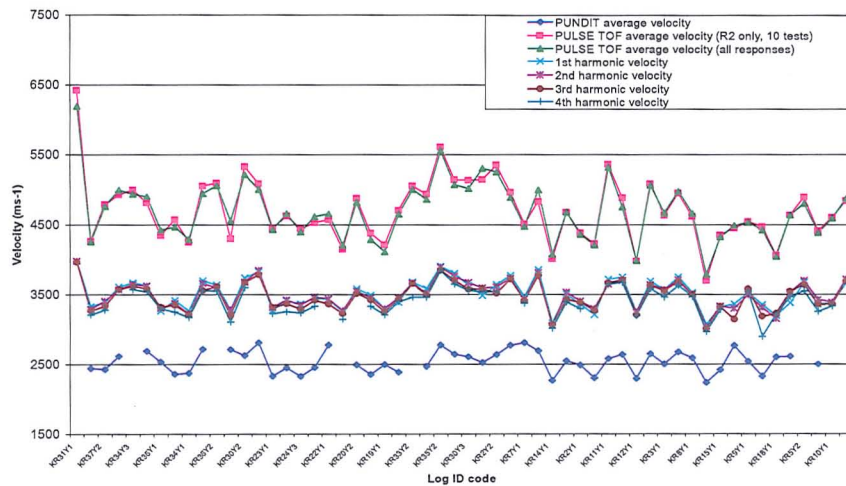


Figure 6.23 Comparison of the various velocity measurements within the QCI progeny.

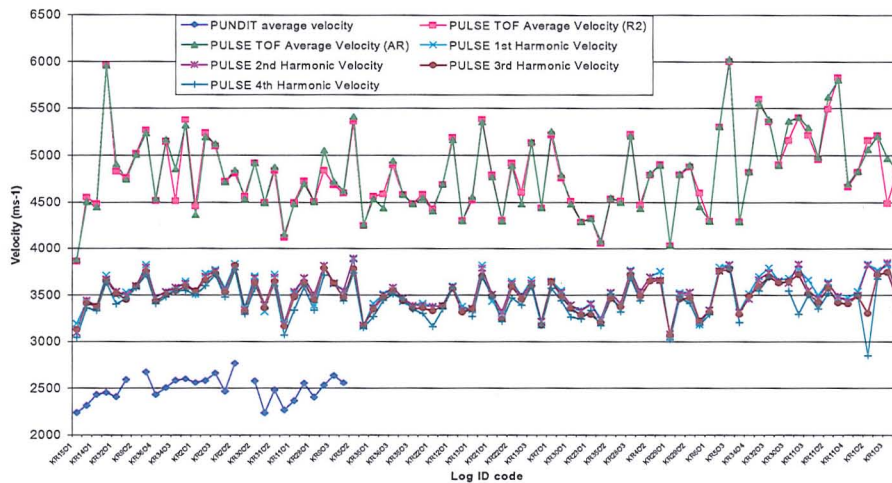


Figure 6.24 Comparison of the various velocity measurements within the IN120 progeny. AR = all 30 responses.

However, the range between velocity measures on each log was not consistent. Indeed it was seen from Figures 6.22 to 6.24 that there are instances, for example QCI log KR19Y1 and KR9Y2 (Figure 6.22), when the PUNDIT™ velocity had risen from the previously charted log, but the TOF P-P and harmonic velocities fell. Similarly, also in Figure 6.23, KR22Y1 velocities for the TOF P-P and PUNDIT™ increased from the previous log, whilst the harmonic velocities decreased. Thus the pattern to this variation was more complex than simply being the result of TOF *versus* resonance methods.

Figure 6.24 shows the percentage of deviation of the TOF velocity measurements from the corresponding 1st harmonic velocity value, which is shown as 0%.

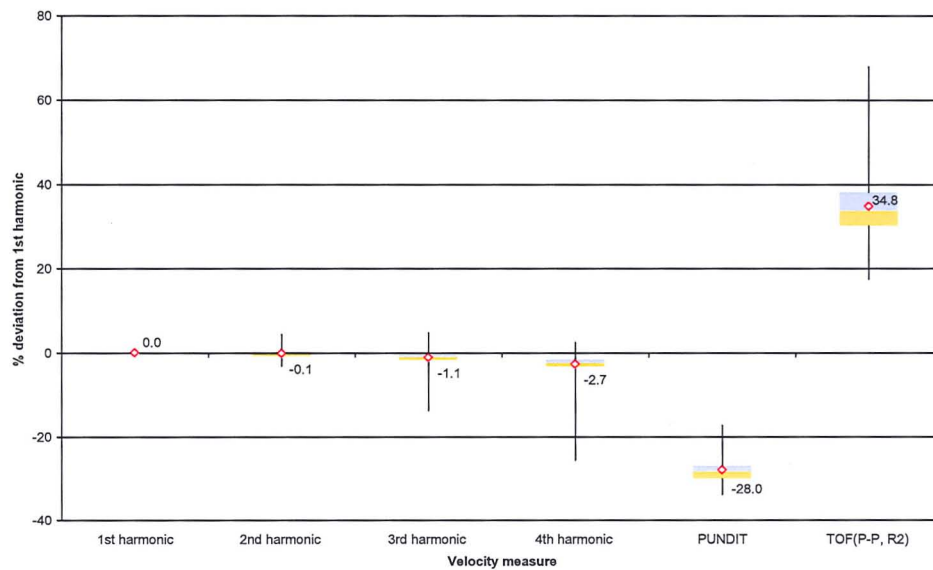


Figure 6.24 Boxplot displaying the percentage deviation (in all tested logs) of harmonics, PUNDIT™, and TOF P-P velocities (mean velocities per log) from the corresponding 1st harmonic log velocity. Graphs show the maximum, minimum, inter-quartile ranges (grey and yellow boxes), median (boundary between quartile-ranges within boxes) and mean (hollow red diamonds) percentage deviation in calculated velocity for all logs tested. The raw data used in the production of this graph are seen in Appendix B.

It can be seen from Figure 6.24 that there was a decrease in the mean velocity calculated by increasing harmonic. The range in overall deviations from the 1st harmonic velocity also increases with increasing harmonic. The average corresponding PUNDIT™ velocity in each log deviated from the 1st harmonic velocity by 28%, whilst the TOF P-P velocity was, on average, 34.8% higher than the 1st harmonic (though this could range between c. 18% to c. 68%).

As previously stated, a review of previous literature^(6.26, 6.31-6.32) would predict that TOF methods will overestimate resonance velocities in logs by 10-30%. The PUNDIT™ results are clearly unexpected underestimates compared to harmonic values based on previous literature, whilst the average TOF P-P values are far greater than would be expected. However, it should be remembered that the method employed in this test series used peak to peak matching for velocity determination, whereas most previous studies used threshold evaluation.

However, as the ranges show, it is not always the case that a higher harmonic produced a lower velocity. Bifurcation (Section 5.7.6) of higher harmonics, with the highest peak of the two occurring at a higher frequency, can result in a higher velocity than is shown by the first harmonic. An example of naturally occurring bifurcation in log resonance tests is shown in Figure 6.25.

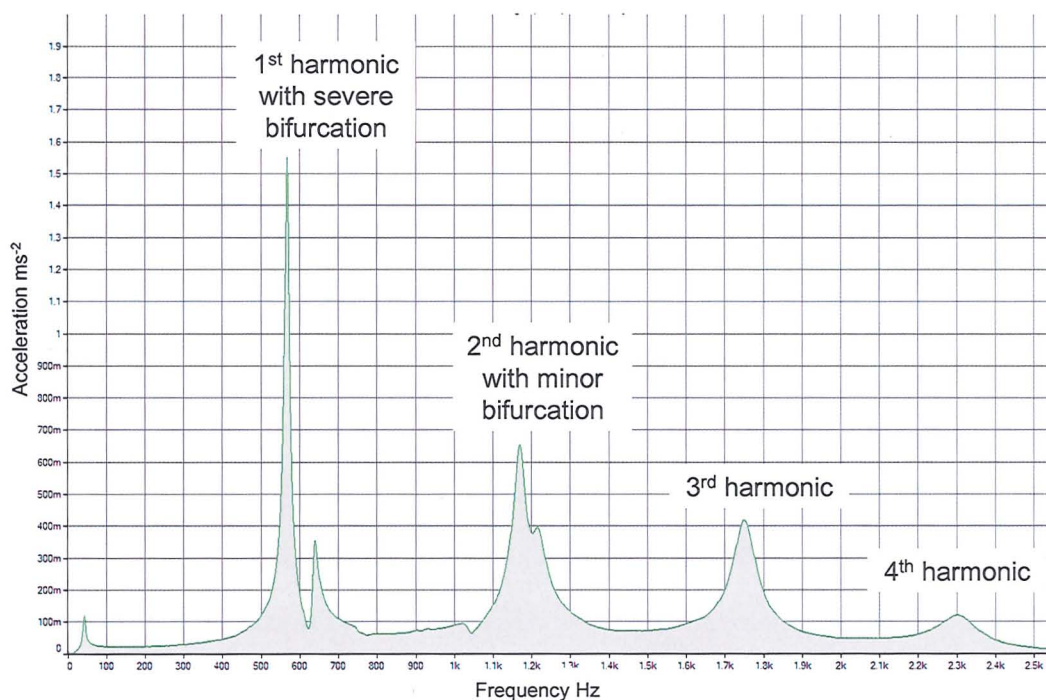


Figure 6.25 Naturally occurring bifurcation in log KR25Y1. Note the decreasing severity of the bifurcation with increasing harmonic mode.

Alternatively, it is possible that the first harmonic may also be bifurcated, and with a lower frequency peak of the bifurcation producing a lower velocity than is produced by unbifurcated 2nd harmonics. Some worst-case deviations may occur during the latter in combination with a bifurcated higher harmonic, which had its greater amplitude peak at the higher frequency peak.

The majority of logs tested were found to have an element of bifurcation on at least one harmonic, though to differing extents and in no instance forming two distinctly separate peaks, rather typically shoulder-like developments as noted in Chapter 5 during the onset of initial bifurcation. However it was found however during this test

series that, in severe cases, bifurcation can be up to c. 100 Hz between peaks involving both logs and battens. It was also noted, anecdotally, that higher harmonics tended to have a frequency separation when bifurcated than lower harmonics. In the case of a 3100 mm batten or log, and using the first harmonic, a potential misidentification of the frequency by, for example, 50 Hz resulted in a 7% error in velocity, or 14% error in MoE_d .

Additionally, it may be the case that the even without bifurcation and using a single peak, the 1st harmonic may produce a resonant peak which is lower than the theoretical value predicted by the division of subsequent harmonics. This can be demonstrated in Figure 6.26. In this, the dashed blue line represents the predicted values of higher harmonics, based on the multiplication of the frequency of the first harmonic. It can be seen that the 2nd, 3rd, and 4th harmonic peaks are of a higher value than in predicted by the theoretical derivation of harmonics, thus returning higher velocities than the 1st harmonic.

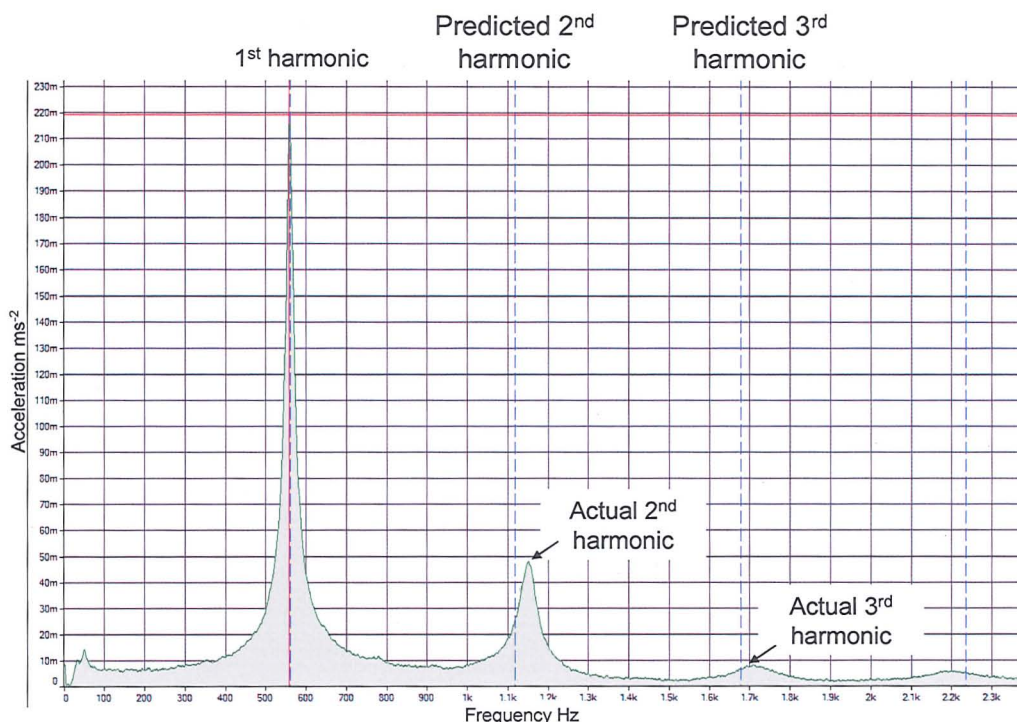


Figure 6.26 A lower 1st harmonic frequency than could be predicted by the division of higher harmonics. The dashed blue indicates the theoretical position of the harmonics based on multiplication of the 1st harmonic. The

higher harmonics can clearly be seen to be above this value, indicating a lower than expected first harmonic.

However the most striking observation from Figure 6.24 is that the PUNDIT™ velocities, a TOF method, are consistently lower than the harmonic velocities for all comparable log samples. Typically, the PUNDIT™ would be expected to overestimate the harmonic resonance velocities due to the PUNDIT™ measuring the fastest pathway of wave transmission rather than an average of the log as a whole, in addition to recording the faster dilatational wave rather than group velocity of a longitudinal rod wave. However, this cannot be occurring in this instance.

As previously noted, not all logs tested by PUNDIT™ returned transit times from which the velocity could be calculated. The PUNDIT™ for each log was placed at the centre of both ends as this was typically the only point at which a transmitted signal would be received. This would indicate that the higher moisture content of the outer wood prevented wave transmission, presumably through increased attenuation. As such, the lower moisture content of the juvenile wood near the pith allowed for some transmission, but with sufficient attenuation to dampen the dilatational wave.

One explanation would be that due to the increased moisture content of wet logs, in comparison to dry beams, the 54 kHz wave was subject to increased attenuation, such that the leading dilatational wave was insufficiently powerful to trigger the stop mechanism of the timer. The removal of the dilatational trigger reduces part of the inherent overestimation of the harmonic method by the US TOF method. Without the energy content in the dilatational wave, the wave velocity will naturally be reduced, following Halmshaw^(6.33) and Craik^(6.34), because whilst for long wavelengths (*i.e.* low frequencies) the group velocity (measured in resonance testing) approximately equals the phase velocity, as the frequency increases the measured longitudinal velocity decreases steadily from the value given by the traditional one-dimensional theory on the basis of the stiffness and density of a specimen, until it ultimately approaches the value of a Rayleigh wave^(6.29). This will

not be the case in dry specimens due to the presence of a dilatational wave of sufficient energy to achieve transmission to the other end of a specimen.

Additionally, if the wave were contained within the typically lower stiffness juvenile zone, it would encounter a higher proportion of defects and compression wood, perhaps increasing the true path length over which the wave has travelled. The potential for containment within the juvenile zone may be increased by less gradational density boundaries between the inner and outer zones of the log, increasing the impedance mismatch and lessening the angle of reflection for the incident wave, potentially accounting for the ten logs which were unable to transmit the 54 kHz wave if these logs had a more gradational change in density. This last point is speculative however.

The question arises, however, of why the PULSE™ TOF P-P wave was significantly higher (and more varied) than the harmonic velocities, as they too were instigated at the centre of the log, yet displayed no variation in velocity across the other end of the log. The general overestimation of TOF P-P in comparison to harmonic results was higher than expected, based on previous log TOF studies, due to the effect of measuring the dilatation wave alone (c. 30% depending on distance^(7.4)). Further, the TOF P-P velocities returned were variable between individual tests within logs, only approaching a stable mean after ten measurements.

The reasons for this latter point are unclear, as no correlations were found between any timber (density, diameter, taper, etc.) or acoustic parameter (frequency, amplitude, harmonic distortion, or damping ratio) and the range or standard deviation of velocities for each log. Another possibility, following the results of Bartholomeu *et al.*^(6.35) on beam specimens, is the conversion of the broadband impulse to flexural surface waves of higher velocity than the bulk longitudinal compressional wave. Their work showed a significant increase in velocity with diameter to wavelength ratios below 1:7, to values greater than 6000 ms⁻¹, as was found in the TOF P-P tests. Thus, unlike longitudinal waves, varying impact force

between tests would affect the dominant frequency of transmission, as bending wave velocity is frequency dependent.

However, this work was theoretical and such high velocities cannot propagate in wet timber, additionally no correlation was found between reception or impact signal amplitude and velocity in each measurement. This may account for the variation observed in other devices, as they typically work by measuring the transit time based on the passing of a threshold value amplitudes in both the wave generation and reception (typically 20%)^(6.36, 6.37). As such, the rise time of the acceleration slope, *i.e.* the gradient, this through differentiation representing the velocity, is dependent on the strength of impact with steeper gradients returning faster transit times. Indeed devices such as TreeTap™ have attempted to compensate for this through the manual rejection of impacts with rise-curves outwith certain specified time lengths^(6.30). This would not however explain the same variation for TOF P-P measurements, which are measuring velocity at a plateau of the acceleration curve.

The phenomenon is not without precedent, in field testing of logs and trees using acoustic TOF tools, for this wide range occurring in current commercial devices (as anecdotal non-published evidence for this has been relayed to the author, separately from FR's Achim, Napier University's Lyon, and The University of Canterbury's Walker and Hensen). Indeed, the Fibre-gen ST300™ requires ten tests to be conducted on live tree specimens measuring the outerwood, most likely to average out this effect. It has been suggested anecdotally by Hensen in personal correspondence that this variation may be related to the impulse delivered upon impact, with more impulsive impacts returning faster transit times.

It can be shown however, that this greater overestimation of velocity is the result of taking the TOF P-P values, rather than impact TOF itself, which indeed is believed to be attributable to the mode conversion to surface waves. In a simple example of this, Figure 6.27 shows the effect of taking threshold values of 10% and 25% of the peak amplitude for use in the transit time calculation for the IN430 progeny. It can be seen that these values reduced the apparent velocity to values closer to the

harmonic velocity. However, the variation, within each log, of the 10% and 25% velocities was not reduced.

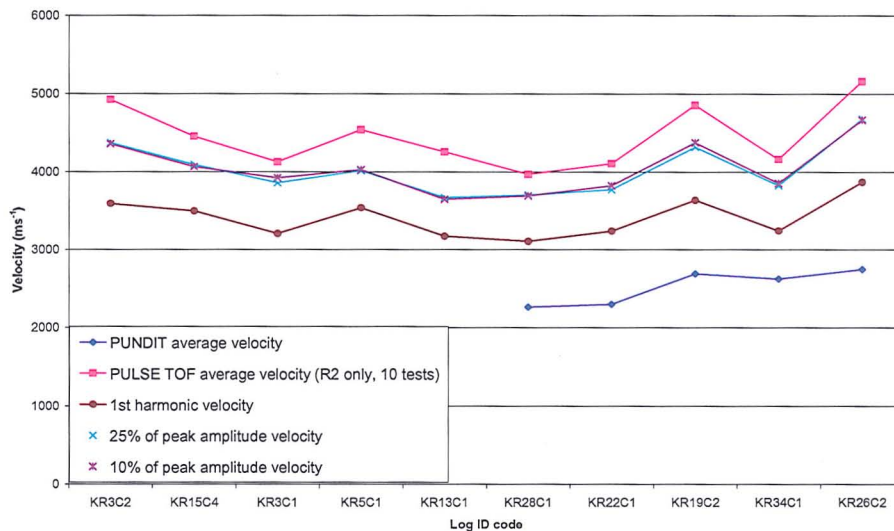


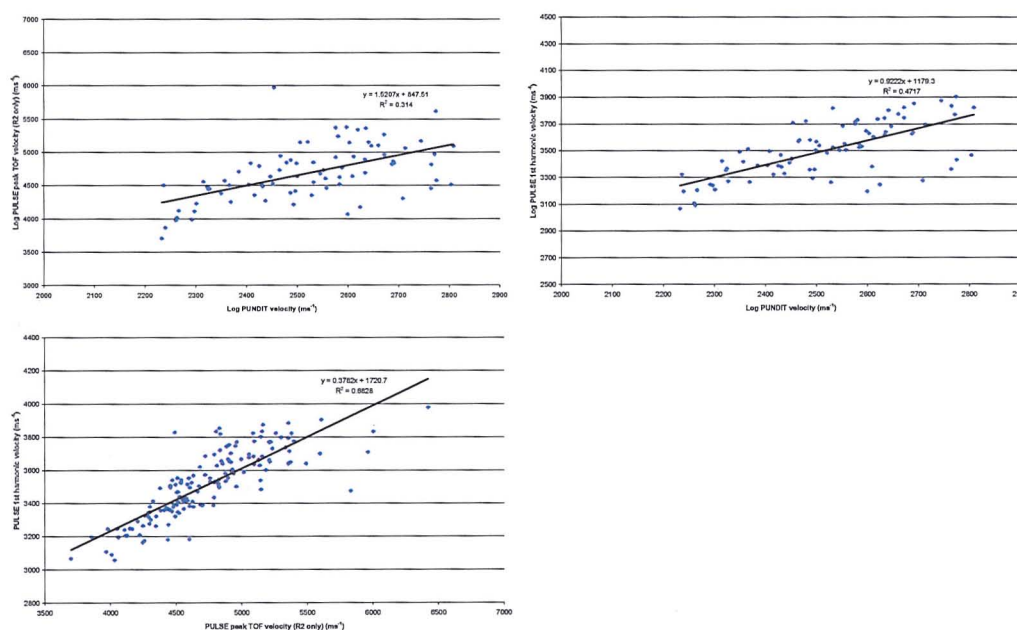
Figure 6.27 10% and 25 % of TOF P-P amplitude velocity values.

From the IN430 progeny alone, the average overestimation of the 1st harmonic velocity by the TOF P-P method is 31% (ranging from 27% to 37%), whilst the 25% and 10% overestimates of the 1st harmonic were, on average, 18% and 19% respectively (with ranges of 13% to 22% and 14% to 22% respectively). The patterns of average velocities between different logs by all methods are again consistent.

This indicates that the harmonic, TOF P-P or TOF percentage methods are sufficient to indicate relative differences between specimens, provided sufficient averages are taken, but should not be used for absolute value calculation due to the variation in percentage overestimation. It may also, should mode conversion to surface waves be the cause of the increased velocity, that TOF surface waves may have timber classification potential. This variable percentage overestimate means that stiffness estimates can not be made on the basis of simply reducing a velocity by a certain percentage, or by applying a weighting equation based on a timber or acoustic parameter value as no relation between the variation and these other variables has been found.

It should also be noted that in conventional theory, after Andrews^(6.26) and Chauchan *et al.*^(6.38), the leading edge of the dilatation wave would be the fastest and first received signal, which should theoretically mean that the 10% of peak value should represent this dilatational wave. As such, this should be of a higher average velocity than the peak value, which should represent the arrival of the higher-energy concentration of the longitudinal wave travelling at the group velocity. This was not the case in the author's results, and as such gives additional weight to the theory that the TOF P-P results are the consequence of surface waves. It is therefore recommended that further investigation into the causes of variation of TOF results, given the lack of correlation to force input, be undertaken.

Figures 6.28a, 6.28b and 6.28c show the linear correlations between the PUNDIT™, 1st harmonic and TOF P-P velocities from all comparable logs tested. The 2nd to 4th velocities show a slightly decreased correlation to the other measures, their correlations can be seen in Table 6.9 at the end of Section 6.4.5. It should be remembered that the number of values available for correlation decreases for the PUNDIT™ tests due to number of logs tested and in the 3rd and 4th harmonic velocities due to an inability in some cases to actively recognise a harmonic peak due to weak amplitude.



Figures 6.28a, 6.28b and 6.28c Linear regression correlations between (clockwise from top left) Log PUNDIT™ velocities and TOF P-P velocities; Log PUNDIT™

velocities and 1st harmonic velocities; and Log TOF P-P velocities and 1st harmonic velocities.

It can be seen from Figure 6.28 that the best correlation between velocities occurred between the 1st harmonic and TOF P-P velocities ($R^2 = 0.68$), whilst the TOF P-P and PUNDIT™ velocities had the weakest correlation ($R^2 = 0.31$).

6.4.5 Log MoE_d interrelations

MoE_d values for the logs were calculated using one-dimensional theory shown in Eq. 3.1 which was also used to calculate the PUNDIT™ MoE_d values. As there is not a physical measure of average density for the logs available, in calculating the MoE_d a value of 1000 kgm⁻³ has been used for fresh, green logs as cited by Andrews^(6.26). Since the density was therefore assumed constant for all logs, the pattern of MoE_d variation in all logs varies in the same manner as the velocity variations shown in Figures 6.13 to 6.15. As can be seen from Figure 6.29, the differences between measurement methods are amplified however due to the squaring of the velocity during conversion to MoE_d. Calculations of the MoE_d were also made during analysis using a predicted density value for the wet logs based on the average of batten dry densities, however this has been removed from the analysis on the basis that this is not a non-destructive measure directly of the logs, and correlations to the average batten properties will be biased on this basis.

Three-dimensional theory (Eqn. 3.4) was not used however, despite being shown to be applicable to PUNDIT™ wave propagation in beam specimens. This was due to the unexpectedly low velocity values found when using the PUNDIT™, which, when used with Eqn. 3.4 (with a consistent density of 1000 kgm⁻³ and Poisson's ratio of 0.3), would reduce the derived MoE_d values by 26%, without changing the relevant correlations, in comparison to those PUNDIT™ MoE_d values calculated from the one-dimensional equation. As such the one-dimensional values are used for a comparison to other acoustic MoE_d values.

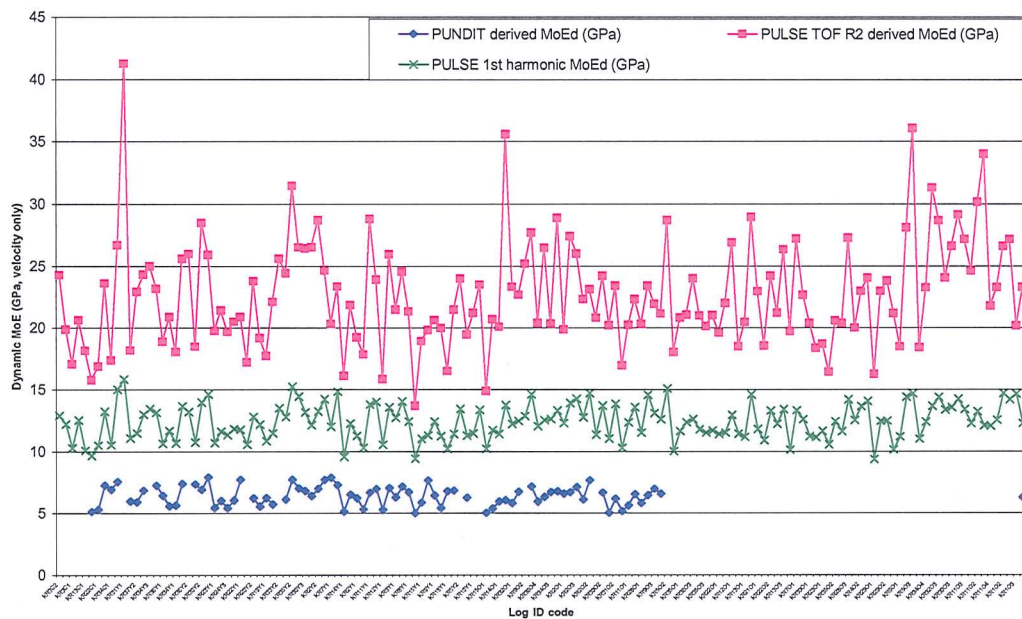


Figure 6.29 Comparison of acoustically derived MoEd measurements for all logs.

Table 6.8 presents the strength classification, C14 to C50, from BS EN 338:2003^(7.17), relating mechanically-graded beam stiffness (GPa) to strength class.

Table 6.8 Strength classification from BS EN 338:2003 for mechanically graded oven-dry beam specimens (12% MC) on the basis of bending stiffness^(7.17).

Strength class	C14	C16	C20	C22	C24	C30	C35	C40	C45	C50
Minimum MoE value (GPa)	7	8	9	10	11	12	13	14	15	16

As can be seen by comparing Table 6.8 with Figure 6.29, all the TOF P-P values of MoE_d predicted a strength classification of C40 or greater. This is clearly a large overestimate of the true stiffness of both the log and the battens which will be cut from the logs. To further illustrate this point, Figure 6.30 shows the MoE_d results of the IN430 plus progeny only. As with the velocity results discussed earlier, it is clear that the pattern of higher and lower dynamic stiffnesses is consistent between all measures of velocity (though as with velocity measures the range increases with increasing mean MoE_d are further amplified due to squaring the velocity).

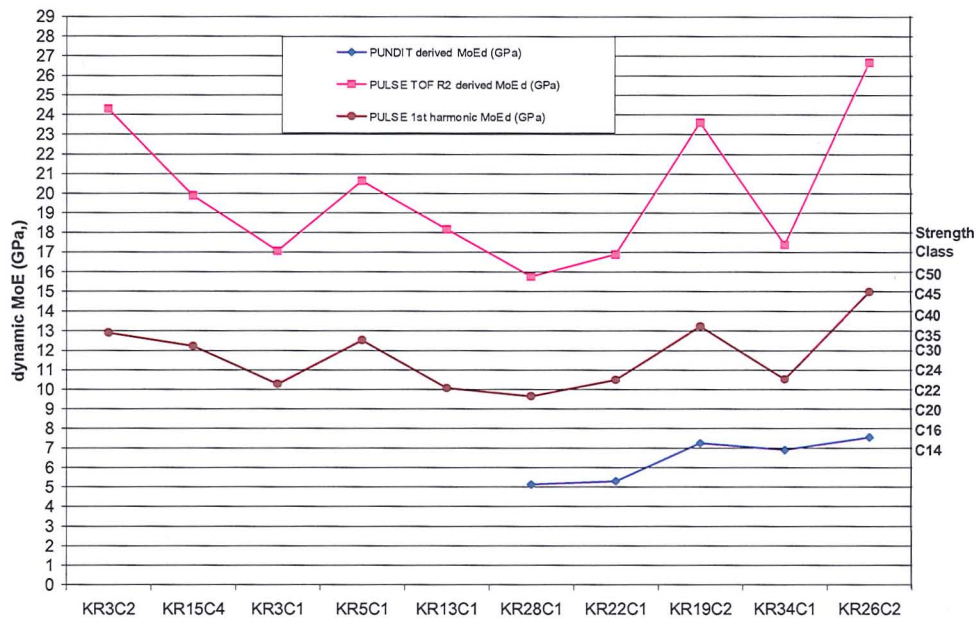


Figure 6.30 Comparison of acoustically derived MoEd measurements for the IN430 progeny. BS EN 338:2003 strength classes are shown on the right side axis^(6.39).

Further discussion on the accuracy of these MoEd predictions is reserved for comparison with the averaged static MoE of the sawn battens, presented in Section 6.6.

However, it is appropriate at this stage to compare the relative MoEd predictions. Figure 6.31 displays the correlations between the PUNDIT™ derived MoEd and other corresponding acoustically-derived MoEd values. Several outliers exist, particularly in the lower right-hand quarter of each graph, as well as in the upper central portion of the TOF MoEd graphs. The highest correlation is found between the PUNDIT™ MoEd and the 4th harmonic MoEd ($R^2 = 0.52$), followed by the 1st harmonic MoEd ($R^2 = 0.46$). The TOF P-P R2 signal graph show a reduced correlation ($R^2 = 0.28$). This was a surprising correlation given previous research, such as Jang^(6.25), who found correlations of $R^2 = 0.46$ between low-frequency TOF measures using a Metriguard 239A and the PUNDIT™ 37 kHz results on 25 year old larch logs.

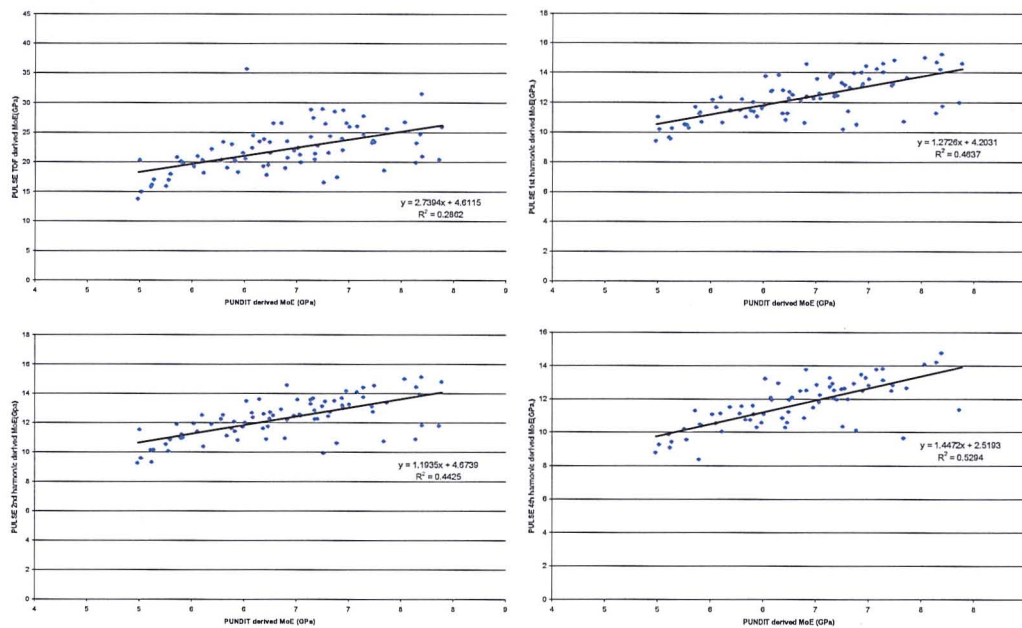


Figure 6.31 PUNDIT™ derived MoEd (x) vs. other acoustically derived MoEd (y) using regressive linear correlations.

Figure 6.32 shows the correlations between the PULSE™ TOF P-P derived MoEd and 1st and 2nd harmonic-derived MoEd values, though not the PUNDIT™ MoEd correlations as this has already been presented in Figure 6.31. It can be seen that both harmonics have a similar positive linear correlation ($R^2 = 0.65$) to the TOF P-P MoEd, however if an exponential regression is used, this correlation would improve to $R^2 = 0.7$ in both cases. No improvement in the correlations in this study was seen when using an exponential regression for the PUNDIT™ correlations.

This compares favourably with the results of Grabianowski *et al.*^(6.31), who found positive linear correlations between FAKOPP™ low-frequency TOF and WoodSpec™ 1st harmonic resonance of $R^2 = 0.64$, on 43 eight to eleven year old green radiata pine logs. Bächle and Walker^(6.40) found a correlation of $R^2 = 0.91$ between Treetap™ low-frequency velocity and WoodSpec™ resonance velocity, but this was on smaller diameter and much younger radiata pine logs. Bächle and Walker^(6.40) also found a slightly lower correlation, on the same logs, to resonance velocities using the US Sylvatest™ 22 kHz device, of $R^2 = 0.86$.

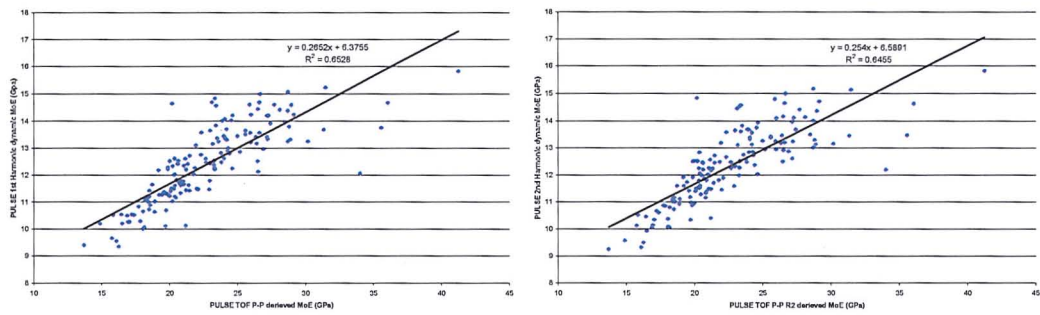


Figure 6.32 PULSE™ TOF peak-to-peak (R2 only) derived MoEd (x) vs. 1st and 2nd harmonically derived MoEd (y) using regressive linear correlations.

Table 6.9 summarises these linear correlations. It can be seen that the different harmonic MoEd values were strongly correlated. The highest correlation was seen between the 1st and 2nd harmonic values ($R^2 = 0.96$), whilst the lowest was seen between both the 1st and 2nd harmonics to the 4th harmonic ($R^2 = 0.76$). The correlations reduce with increasing separation between harmonic mode numbers.

Table 6.9 Summary of correlations (R2) between log velocities (V), MoEd(v), and damping ratios (DR) based on TOF and resonance calculation methods. No velocity to MoEd correlations are made as these are in all cases less than the velocity to velocity or MoEd to MoEd correlations. F1, F2, F3, and F4 are the 1st to 4th harmonic frequencies respectively.

	$V_{(PUNDIT^*)}$	$MoE_{(PUNDIT^*, V)}$	$V_{(TOF, P-P, R2)}$	$MoE_{(TOF, P-P, V, R2)}$	$V_{(F1)}$	$MoE_{(F1, V)}$	$V_{(F2)}$	$MoE_{(F2, V)}$	$V_{(F3)}$	$MoE_{(F3, V)}$	$V_{(F4)}$	$MoE_{(F4, V)}$	mean DR (F1)	mean DR (F2)	mean DR (F3)
$V_{(PUNDIT^*)}$	X	0.98	0.31	0.25	0.47	0.22	0.45	0.28	0.42	0.21	0.54	0.18	0.03	0.00	0.00
$MoE_{(PUNDIT^*, V)}$	X	X	0.22	0.29	0.19	0.46	0.18	0.44	0.18	0.41	0.14	0.53	0.03	0.00	0.01
$V_{(TOF, P-P, R2)}$	X	X	X	0.99	0.68	0.68	0.68	0.67	0.65	0.64	0.60	0.61	0.00	0.04	0.04
$MoE_{(TOF, P-P, V, R2)}$	X	X	X	X	0.85	0.85	0.85	0.65	0.65	0.62	0.59	0.59	0.00	0.03	0.04
$V_{(F1)}$	X	X	X	X	X	0.96	0.96	0.90	0.90	0.74	0.74	0.75	0.00	0.05	0.09
$MoE_{(F1, V)}$	X	X	X	X	X	X	0.96	0.96	0.90	0.90	0.74	0.75	0.00	0.05	0.09
$V_{(F2)}$	X	X	X	X	X	X	X	0.93	0.93	0.93	0.89	0.75	0.00	0.05	0.08
$MoE_{(F2, V)}$	X	X	X	X	X	X	X	X	0.93	0.93	0.89	0.75	0.00	0.05	0.07
$V_{(F3)}$	X	X	X	X	X	X	X	X	X	0.89	0.89	0.90	0.00	0.02	0.04
$MoE_{(F3, V)}$	X	X	X	X	X	X	X	X	X	X	0.90	0.90	0.00	0.02	0.04
$V_{(F4)}$	X	X	X	X	X	X	X	X	X	X	X	0.90	0.02	0.00	0.03
$MoE_{(F4, V)}$	X	X	X	X	X	X	X	X	X	X	X	X	0.01	0.00	0.03
mean DR (F1)	X	X	X	X	X	X	X	X	X	X	X	X	X	0.02	0.04
mean DR (F2)	X	X	X	X	X	X	X	X	X	X	X	X	X	X	0.25
mean DR (F3)	X	X	X	X	X	X	X	X	X	X	X	X	X	X	X

6.4.6 Log non-acoustic characteristics

Measurements of the knot content, top-end and mid-diameters and slope of grain were made on each log prior to sawing, by Napier University colleagues Hapca and Bruechert.

As previously stated, the mean taper value of the logs was 0.94, ranging from 0.8 to 1.28. There was no significant correlation between log taper and any measure of velocity or MoE_d . Due to the generally comparable trend between the various measures of velocity despite their relative percentage differences, and in particular between harmonic velocities, if one measure of velocity or MoE_d failed to show significant correlation then it follows that other velocity measures will also fail to show significant correlation. As such, it was found that there was also no correlation between any MoE_d value and slope of grain measures ($R^2 < 0.1$ in all cases). A very weak linear correlation was observed between harmonic MoE_d and log mid-diameter, which diminished with decreasing harmonic mode ($R^2 = 0.2$ for the 4th harmonic MoE_d , but $R^2 = 0.11$ for the 1st harmonic). It should be remembered however that the number of MoE_d values recovered reduced with increasing harmonic mode.

Knot content was measured by classifying each knot on the log's surface in 5mm diameter bins from 5 mm to 55 mm; the few knots over 55 mm had their diameters measured directly. The knots were also classified by type: live (> 25% of branch circumference intergrown), dead (< 25% intergrown), and unsound (signs of rot visible) as advised by BS EN 844-9:1997^(6.41). The majority (77%) of knots were classified as dead, though this was unsurprising given that the first live branches on the source trees appeared only at 15 m above ground level. Only 2% of knots were classified as live.

An average of 27 branch whorls was counted *per* log, with a maximum of 77 and a minimum of 7. In terms of progeny, IN120 (better straightness) had significantly fewer total branches than other progenies whilst the QCI had significantly more. Despite this, the IN120 was the only progeny to have live branches, whilst having the greatest number of unsound branches. The number of knots in each class was multiplied by their class diameter to produce a total length value for comparative purposes. The total diameter of knots was then summed to give approximate knot content for each log. This value was correlated to the various MoE_d and harmonic damping ratio values. No correlation was observed between the damping ratio and

the knot content or mid-diameter to knot content ratio. No correlation greater than $R^2 = 0.05$ was observed between velocity measures of MoE_d and total knot content.

In comparison to previous research (Such as Xu, 2002^(6.42)), better correlations would have been expected between MoE_d and a measure of knot content, perhaps suggesting a flawed measurement procedure for calculating knot content. Overall 97% of logs were classed by CTE staff as low quality Class C logs under BS EN 1927-1:1999^(6.43), with the remainder in Class B.

6.5 Kershope batten testing

This section evaluates the results from the acoustical and mechanical testing of the battens which were subsequently cut from the logs, including the 358 battens which were taken from the 150 acoustically tested logs. Comparison of these battens' averaged properties with their parent logs takes place in Section 6.6. As seen in Figure 6.33, a total of 645 battens were cut from the 270 logs originally created for the Kershope progeny test series. Of these battens 393 were tested in the first series of experiments, whilst the remaining 252 were tested in the second series.

With regard to acoustic measurements, as noted in Chapter 4, the first series was subject to PUNDIT™ testing, PULSE™ resonance testing, and damping ratio estimation. The second series was only subject to PUNDIT™ testing and PULSE™ resonance testing, though measurements of the second harmonic velocity were also taken using the semi-automated HM200™ log tester^(6.18). Mechanically, the two series also differ.

The first series was subject to static MoE and MoR testing as boards producing $MoE.cen.board$ (local MoE tested as a board), $MoE.glo.board$ (global MoE tested as a board) and $MoR.board$ values. Battens were also measured by CTE colleagues for both KAR and perpendicular KAR.

The second series was tested as boards but also as joists (producing MoE.cen.joist, MoE.glo.joist and MoR.joist values) and spiral grain measurements were also conducted. Volume, density, moisture content, ring parameters (number, average width) and (subjectively estimated) compression wood measurements were made for all battens. The second series were only tested as joists in terms of MoR (MoR.joist).

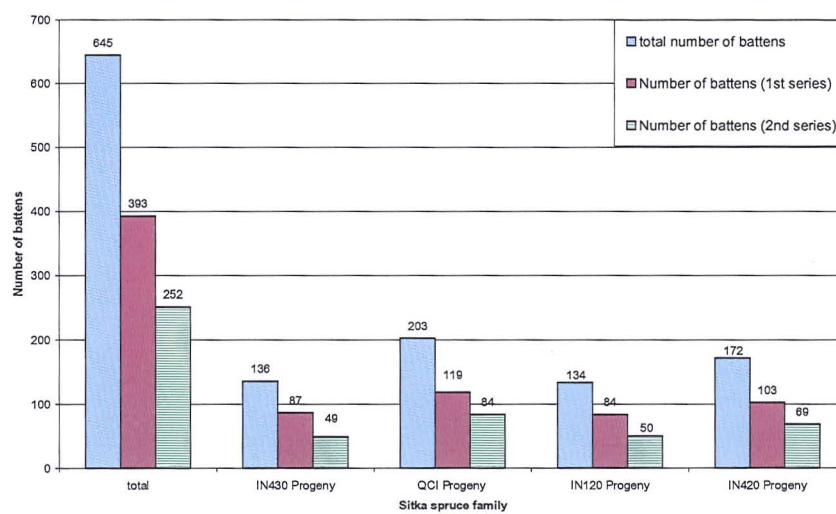
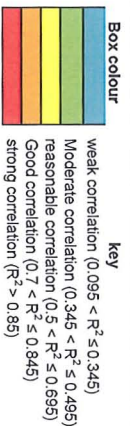


Figure 6.33 Comparison of battens tested in first series, second series and in total.

Table 6.10 also shows a summary of linear correlations (R^2) between all the static and acoustic data collected on battens during this test series.

Table 6.10 Summary of correlations (R2) between battens static MoEs, MoRs, visual data, acoustic velocities and damping ratios.

	(1)	(2)	(3)	(4)	(5)	(6)	(7)	(8)	(9)	(10)	(11)	(12)	(13)	(14)	(15)	(16)	(17)	(18)	(19)	(20)	(21)	(22)	(23)	(24)	(25)	(26)
Basic density (1)	X	0.00	0.04	0.05	0.07	0.12	0.14	0.01	0.03	0.00	0.00	0.05	0.05	0.04	0.04	0.14	0.13	0.13	0.11	0.01	0.22	0.08	0.08	0.00	0.00	0.01
MOE.cen.board (2)	X	X	0.50	0.81	0.53	0.16	0.57	0.06	0.09	0.04	0.02	0.35	0.30	0.33	0.28	0.30	0.27	0.28	0.27	0.26	0.31	0.33	0.31	0.01	0.02	0.00
MOE.glo.board (3)	X	X	X	0.64	0.99	0.39	0.65	0.14	0.19	0.05	0.02	0.55	0.45	0.51	0.47	0.71	0.64	0.66	0.62	0.55	0.66	0.44	0.61	0.16	0.02	0.00
MOE.cen.joist (4)	X	X	X	X	0.65	0.20	Not tested	0.09	0.15	only 5 tests	only 5 tests	0.31	0.27	0.29	0.19	0.30	0.36	0.38	0.33	0.32	0.39	0.26	0.35	Not tested	Not tested	Not tested
MOE.glo.joist (5)	X	X	X	X	X	0.40	Not tested	0.16	0.28	only 5 tests	only 5 tests	0.58	0.51	0.52	0.41	0.70	0.63	0.65	0.63	0.56	0.66	0.48	0.61	Not tested	Not tested	Not tested
MoR.joist (6)	X	X	X	X	X	X	Not tested	0.05	0.15	0.28	0.12	0.16	0.13	0.13	0.08	0.32	0.27	0.28	0.30	0.15	0.30	0.09	0.23	Not tested	Not tested	Not tested
MoR.board (7)	X	X	X	X	X	X	X	0.10	0.13	0.06	0.04	0.27	0.23	0.25	0.20	0.41	0.36	0.39	0.33	Not tested	Not tested	0.22	0.34	0.09	0.01	0.01
Number of rings (8)	X	X	X	X	X	X	X	X	0.64	0.10	0.09	0.08	0.07	0.06	0.06	0.12	0.10	0.10	0.10	0.12	0.13	0.06	0.09	0.02	0.01	0.00
Average ring width (9)	X	X	X	X	X	X	X	X	X	0.12	0.09	0.11	0.09	0.09	0.07	0.18	0.15	0.15	0.14	0.21	0.23	0.08	0.14	0.03	0.00	0.01
Average KAR (all sides) (10)	X	X	X	X	X	X	X	X	X	X	0.77	0.05	0.03	0.03	0.02	0.03	0.02	0.02	0.02	Not tested	Not tested	0.02	0.01	0.01	0.02	0.03
Average perp. KAR (all sides) (11)	X	X	X	X	X	X	X	X	X	X	X	0.02	0.01	0.01	0.01	0.02	0.00	0.01	0.00	Not tested	Not tested	0.00	0.00	0.01	0.00	0.00
1st harmonic Velocity (12)	X	X	X	X	X	X	X	X	X	X	X	X	0.95	0.95	0.76	0.67	0.65	0.65	0.65	0.92	0.60	0.85	0.62	0.19	0.03	0.00
2nd harmonic Velocity (13)	X	X	X	X	X	X	X	X	X	X	X	X	X	0.98	0.93	0.64	0.69	0.67	0.69	0.91	0.59	0.88	0.65	0.20	0.03	0.00
3rd harmonic Velocity (m/s) (14)	X	X	X	X	X	X	X	X	X	X	X	X	X	X	0.94	0.66	0.70	0.70	0.71	0.89	0.59	0.88	0.67	0.18	0.02	0.00
4th harmonic Velocity (15)	X	X	X	X	X	X	X	X	X	X	X	X	X	X	X	0.65	0.66	0.67	0.73	0.84	0.46	0.84	0.63	0.18	0.02	0.00
1st harmonic dynamic MoE (16)	X	X	X	X	X	X	X	X	X	X	X	X	X	X	X	X	0.95	0.96	0.93	0.64	0.93	0.51	0.85	0.15	0.02	0.00
2nd harmonic dynamic MoE (17)	X	X	X	X	X	X	X	X	X	X	X	X	X	X	X	X	X	0.98	0.94	0.64	0.92	0.54	0.88	0.16	0.02	0.00
3rd harmonic dynamic MoE (18)	X	X	X	X	X	X	X	X	X	X	X	X	X	X	X	X	X	X	0.95	0.62	0.90	0.54	0.87	0.14	0.02	0.00
4th harmonic dynamic MoE (19)	X	X	X	X	X	X	X	X	X	X	X	X	X	X	X	X	X	X	X	0.61	0.86	0.58	0.85	0.14	0.02	0.00
Hitman.vel (20)	X	X	X	X	X	X	X	X	X	X	X	X	X	X	X	X	X	X	X	X	0.69	0.88	0.60	Not tested	Not tested	Not tested
HM200™ MoE (21)	X	X	X	X	X	X	X	X	X	X	X	X	X	X	X	X	X	X	X	X	X	0.57	0.89	Not tested	Not tested	Not tested
PUNDIT™ velocity (22)	X	X	X	X	X	X	X	X	X	X	X	X	X	X	X	X	X	X	X	X	X	X	0.70	0.16	0.02	0.00
PUNDIT™ dynamic MoE (23)	X	X	X	X	X	X	X	X	X	X	X	X	X	X	X	X	X	X	X	X	X	X	X	0.12	0.02	0.00
1 st harm. damping ratio mean (24)	X	X	X	X	X	X	X	X	X	X	X	X	X	X	X	X	X	X	X	X	X	X	X	X	0.11	0.04
2 nd harm. damping ratio mean (25)	X	X	X	X	X	X	X	X	X	X	X	X	X	X	X	X	X	X	X	X	X	X	X	X	X	0.05
3 rd harm. damping ratio mean (26)	X	X	X	X	X	X	X	X	X	X	X	X	X	X	X	X	X	X	X	X	X	X	X	X	X	X



6.5.1 Batten TOF results

The use of PUNDIT™ on battens was found to be repeatable between tests and on different battens, as well as much faster than during log testing due to a smaller cross-section available for transmission. No significant difference was observed across the cross-section of the battens.

Figure 6.34 and Figure 6.35 show boxplots representing the overall statistics by progeny for the PUNDIT™ velocity and PUNDIT™ MoE_d respectively, based on results from both the 1st and 2nd test series combined. Regarding the split of batten numbers by progeny, 643 battens in total were tested by PUNDIT™, of these: 137 were IN430 progeny: 133 were QCI progeny: 201 were IN120 progeny: and 172 were IN420 progeny. The IN120 progeny showed the highest mean velocity, though only the IN430 progeny showed a significantly lower mean velocity than the other progenies. The IN420 showed the greatest range in the inter-quartile velocities, whilst the standard deviation across the progenies was consistent at 413 ms⁻¹ (QCI) to 471 ms⁻¹ (IN420).

The mean velocity for all 645 battens tested by PUNDIT™ is 4814 ms⁻¹, and the range between progeny means is 338 ms⁻¹, less than the individual standard deviations and represents 7% of the overall batten mean PUNDIT™ velocity. In comparison to previous research, and particularly with the low PUNDIT™ velocities returned from log tests, the overall mean velocity of 4814 ms⁻¹ is consistent with reported velocities in Chapters 5 and 6 for solid timber, but also that reported by Bucur for ultrasonic longitudinal velocities in juvenile Sitka spruce^(6.44).

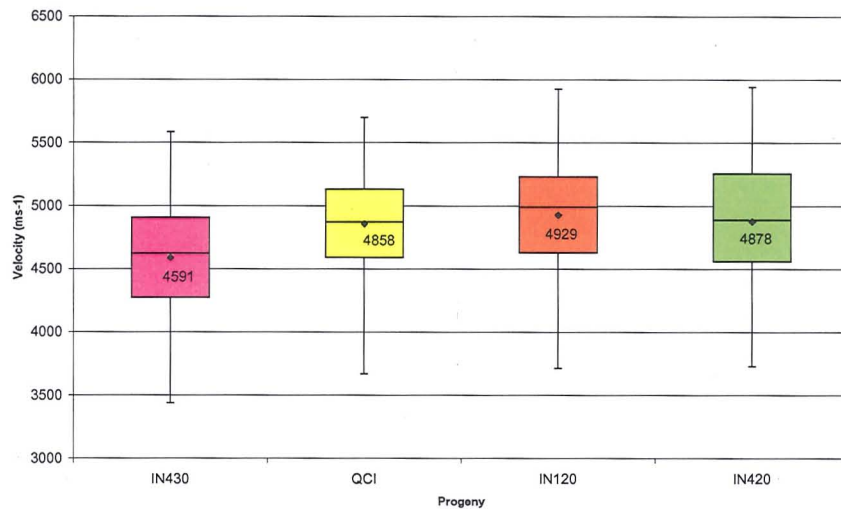


Figure 6.34 Batten PUNDIT™ velocities by progeny. Graphs show the maximum, minimum, inter-quartile ranges (coloured boxes), median (black line within boxes) and mean (black diamonds) velocity values for each progeny. The raw data used in the production of this graph are seen in Appendix B.

On conversion to dynamic MoE values, using the whole batten density values, there was a change in the ranking order. The QCI and IN120 can be seen to have the greatest mean dynamic stiffnesses (9.88 GPa and 9.86 GPa respectively), whilst the high velocity IN420 progeny had a lower mean MoE_d of 9.46 GPa. This change in order was a consequence of similar ultrasonic velocities between the IN120, IN 420 and QCI progenies, meaning the density had a significant influence on the MoE_d values. Hence on this basis it would appear that the IN420 progeny had a lower density than the QCI and IN120 progenies (as is shown in Section 6.5.8). However, as there was a significant drop in mean velocity between these three progenies and the IN430 progeny, the squaring of velocity causes the IN430 to remain the lowest ranking mean MoE_d value.

Noticeably, whilst the velocities of all progenies follow a normal distribution with a slight rightward skew, the MoE_d distributions have a slight leftward skew. Additionally, although for each progeny the ranges were similar, for the MoE_d ranges the IN420 was significantly less widely spread than the other progenies, which could indicate that for this progeny, there was a relationship between density to velocity. Alternatively, the IN120 had a MoE_d range of over 11 GPa. Ultimately, the conclusion could be drawn that there was far more variation between the

battens of the various progenies than between progenies themselves. A discussion of the TOF MoE_d results in terms of other methods and previous studies is presented in Section 6.5.3.

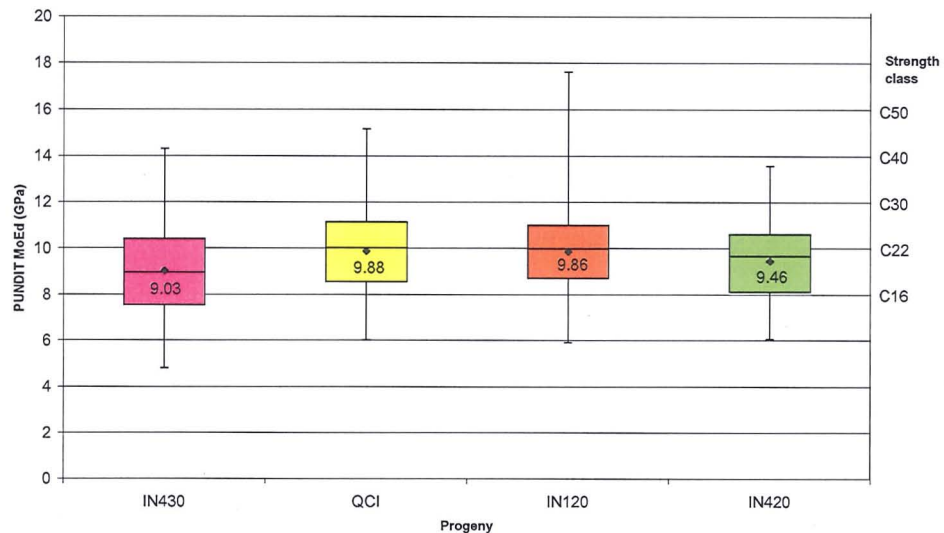


Figure 6.35 Batten PUNDIT™ MoEd by progeny. Graphs show the maximum, minimum, inter-quartile ranges (coloured boxes), median (black line within boxes) and mean (black diamonds) MoE_d values for each progeny. The raw data used in the production of this graph are seen in Appendix B.

6.5.2 Batten resonance results

This section presents the velocities and MoE_d values derived from resonance based testing using the 1st to 4th harmonic frequencies from both test series. The method was as presented in Section 6.2 using the same uniform-windowing and triggering processes. Also presented are the velocities and MoE_d values calculated from velocities returned from the HM200™ log tester. Table 6.11 shows the number of battens tested by each resonance method by progeny and in total.

Table 6.11 Number of battens tested by each method, by progeny and in total.

Acoustic method	IN430	QCI	IN120	IN420	total
1 st harmonic	128	131	190	165	614
2 nd harmonic	128	131	189	164	612
3 rd harmonic	116	115	167	149	547
4 th harmonic	102	98	137	122	459
HM200™	50	50	84	69	253
PUNDIT™	137	133	201	172	643

Figures 6.36 and 6.37 show boxplots representing the 1st harmonic velocity and subsequently derived MoE_d values respectively by progeny. It was found during the analysis that, as expected, all four harmonics produced very similar velocities, though not to the same consistently diminishing velocity pattern (with increasing mode number), which was seen in the log samples. This will be discussed further in relation to TOF velocity measures in Section 6.5.3. Additionally, as expected and seen in the number of battens tested by each harmonic, increasing harmonic modes coincided with decreased acceleration amplitudes of the received signals, meaning the 4th harmonic was indistinguishable from the background vibration in 26% of tests. Since the pattern of velocity and MoE_d variation was consistent between harmonics (with small percentage variations in the actual returned values), it is deemed sufficient to simply present the 1st harmonic results here, whilst the linear correlations of inter-harmonic values can be seen in Table 6.10.

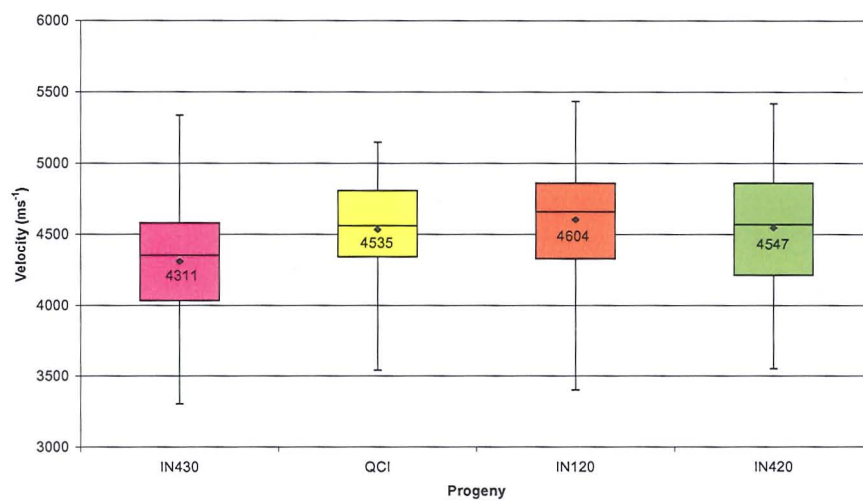


Figure 6.36 Batten 1st harmonic velocity (top) by progeny. Graphs show the maximum, minimum, inter-quartile ranges (coloured boxes), median (black line within boxes) and mean (black diamonds) values for each progeny. The raw data used in the production of this graph is seen in Appendix B.

As in the PUNDIT™ graphs (shown in Figures 6.34 and 6.35), the IN120 progeny shows the highest mean velocity (as well as the greatest range in velocities), though again only the IN430 progeny showed a significantly lower mean velocity than the other progenies. As before, the IN420 showed the greatest range in the inter-quartile velocities, with the QCI progeny showing the lowest variation, whilst

the standard deviation across the progenies is relatively consistent at between c. 330 ms⁻¹ (QCI) to c. 430 ms⁻¹ (IN420), the QCI standard deviation tended to be consistently lower than the other three progenies for all harmonics. Table 6.12 displays the batten harmonic statistical data for all 645 battens tested acoustically.

Table 6.12 Statistical data from both 1st and 2nd batten series acoustic tests.

	1st harmonic vel. (ms ⁻¹)	2nd harmonic vel. (ms ⁻¹)	3rd harmonic vel. (ms ⁻¹)	4th harmonic vel. (ms ⁻¹)	Hitman vel. (ms ⁻¹)	1st harm. MoEd _d	2nd harm. MoEd	3rd harm. MoEd	4th harm. MoEd	HM200 MoEd
Mean	4513	4480	4452	4428	4625	8.35	8.24	8.19	8.23	8.20
Standard deviation	401	408	403	406	405	1.54	1.54	1.54	1.55	1.60
Median	4544	4517	4490	4481	4680	8.41	8.25	8.19	8.26	8.20
Minimum	3306	3288	3284	3252	3700	4.55	4.42	4.31	4.22	5.07
Maximum	5434	5452	5585	5441	5440	14.80	14.83	15.63	14.83	14.83
Range	2128	2164	2301	2189	1740	10.25	10.42	11.32	10.61	9.76
count	614	612	547	459	253	611	609	547	459	252

The 2nd harmonic mean velocity represents a reduction of 0.7% from the 1st harmonic mean velocity, whilst the 3rd and 4th harmonic mean velocities represent reductions of 1.4% and 1.9% respectively from the 1st harmonic mean velocity.

In comparison to the reductions in harmonic velocity from the 1st harmonic of the log results (log 2nd harmonic reduced by 0.1%, 3rd harmonic by 1.1% and 4th harmonic by 2.7%, albeit from lower 1st harmonic velocity due to moisture content and cross-sectional averaging), the pattern of consistent reduction with increasing mode number applies. However, the reduction of the 2nd and 4th harmonics are noticeably greater for dry batten specimens than wet logs, whilst the 3rd harmonic suffers less of a reduction in battens than in wet logs. This was somewhat unexpected given a) taper traditionally induces greater discrepancy between harmonics as indicated by Andrews^(6.26), in this instance the battens had no taper unlike the logs, and b) the greater inherent damping of wet logs in relation to increasing frequency^(6.45).

In much the same way that there was a greater difference in stiffness within progeny logs than between progenies, there was a greater difference across a log's cross-section than between logs. It may be the case that because the 1st harmonic is averaging the stiffness of the cross-section at the longitudinally central

portion of the log, whilst the 2nd harmonic averages the cross-section at quarter-spans, the returned harmonic velocities are less different than in batten specimens which average a far reduced cross-sectional area, producing an increased difference between harmonic results. In this scenario this would also apply to the 3rd harmonic. The greater reduction in the log 4th harmonic compared to the batten 4th harmonic could potentially be explained by a) a significantly less number of samples or more likely b) the influence of increasing attenuation (due to an increased defect to wavelength ratio) in saturated samples in comparison to dry battens.

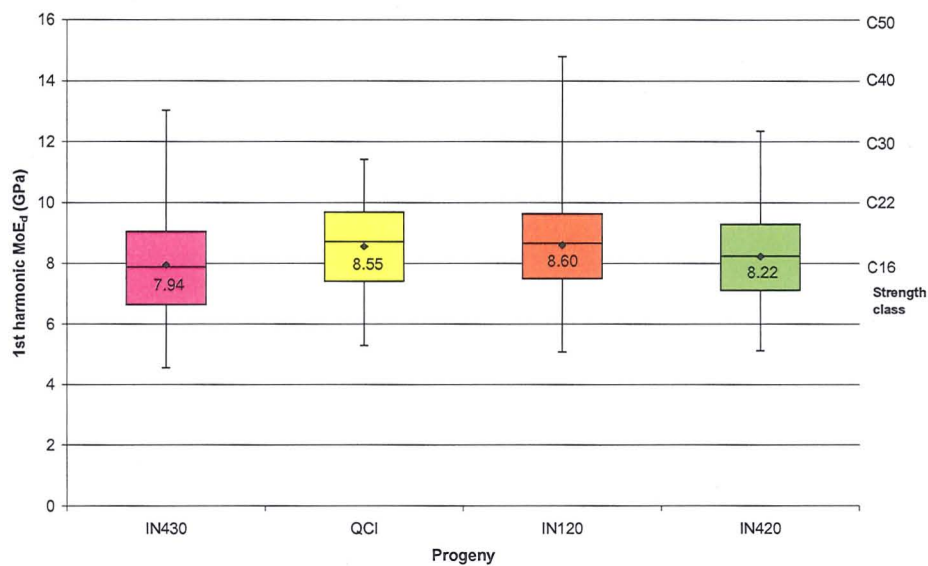


Figure 6.37 Batten 1st harmonic MoE_d (bottom) by progeny. Graphs show the maximum, minimum, inter-quartile ranges (coloured boxes), median (black line within boxes) and mean (black diamonds) values for each progeny. The raw data used in the production of this graph is seen in Appendix B. Strength classes are derived from BS EN 338:2003^(6.39).

The ranking pattern visible in the harmonics' MoE_d values consistent between harmonics, with the QCI progeny having the highest mean MoE_d values (depending on harmonic, as the IN120 is higher in the 3rd harmonic by 0.02 GPa) but only by 0.05 GPa over the IN120 progeny in the 1st harmonic and similarly across all harmonics (see Figure 6.37). The QCI progeny again consistently had the smallest range in MoE_d values. The IN120 progeny became more noticeable than in the velocity graphs for having the largest range in values. As noted previously, the mean values for each progeny were well within the inter-quartile range values of the other progenies, indicating that both sub-species classification

by NDT would be impossible, and that choosing a specific progeny is no guarantee of higher stiffness, better quality timber.

The 1st harmonic velocity and MoE_d values were the highest of the four harmonics. Surprisingly, the 4th harmonic was second highest for the QCI and IN420 progenies and 3rd highest for the IN430 and IN120 progenies. This ranking behaviour was unexpected and appears somewhat erratic (with the exception of the 1st harmonic), however it should be remembered that the 4th harmonic had significantly less samples to average in each progeny to average, which will influence the results.

It can also be seen from Table 6.12 that the HM200™ velocity and MoE_d results are reasonably consistent with those of the harmonic results, despite only being tested on the 253 2nd sub-sample battens. However the mean results are slightly higher whilst the range is lower than the harmonic results, attributed to a reduced sample size. The ranking of progenies, their mean values, standard deviation and ranges were consistent with the harmonic results. The HM200™ MoE_d values by progeny again follows the same trend as with the harmonic estimates despite the reduced sample size, with the QCI battens having the highest mean MoE_d.

6.5.3 Interrelations between acoustic values

In general, the TOF and various resonance measures of MoE_d estimation showed a consistent ranking mean values, ranges and distributions of batten MoE_d within each progeny. As shown in Table 6.10, all velocities showed positive linear correlations to their MoE_d values (calculated from the one-dimensional longitudinal equation, Eqn. 3.1, by $0.68 \leq R^2 \leq 0.73$). As the linear correlation between the velocity and the square of the velocity is effectively a one-to-one relationship, this means that c. 30% of the variation in MoE_d values is attributable to the measured density of the battens.

The PUNDIT™ MoE_d was calculated by both the one- and three-dimensional equations (Eqn. 3.4), using a Poisson's ratio of 0.3, and was found to produce the same correlations in all cases.

Interestingly, It was seen that the 4th harmonic had the highest correlation between the measured velocity and its subsequent MoE_d values ($R^2 = 0.73$). The correlations could be seen to decrease with decreasing harmonic mode, coincident with an increasing number of samples. The PUNDIT™ velocity and 3rd harmonic velocity provided the next highest correlations ($R^2 = 0.7$), followed by the HM200™ and lower PULSE 2nd and 1st harmonics ($R^2 = 0.69$ and 0.67 respectively). This could indicate an increased linkage between density and velocity with increasing harmonic mode (though not to frequency due to the lower PUNDIT™ 54 kHz result). Alternatively, the fact that the whole batten density is used to calculate the MoE_d and that increasing harmonic mode averages a greater longitudinal spatial range (though not area) than lower harmonics may be the driving influence. This would be consistent with the results of Schad *et al.*^(6,46) on SCS which indicated a significant relation ($R^2 = 0.44$) between velocity and density on small clear samples (with little longitudinal density variation).

In terms of velocity interrelations, the 1st harmonic has the second lowest correlation ($R^2 = 0.85$) of the velocity measures to the PUNDIT™ velocity, though there is in general good agreement between all velocity measures ($R^2 \geq 0.84$, except between the 1st and 4th harmonics). As expected, the correlation between harmonics is seen to decrease with increasing range between modes (*i.e.* lowest between the 1st and 4th harmonic, a trend previously seen in the log NDT testing). The 2nd harmonic provides, on average, the best correlations to all other measures of velocity and MoE_d ($R^2 = 0.88$ to 0.95). The 1st harmonic velocity also has a slightly better (1%) positive correlation than the 2nd harmonic to the HM200™, surprising as the HM200™ derives its velocities from the 2nd harmonic. The fact that these do not correlate perfectly may be due to the physical observation of bifurcation phenomena, in which bifurcated peaks separated by tens of hertz may, if close to each other in amplitude, shift small amounts of energy content between each other (possibly dependant on the nature of the hammer impact). The exact analyser specifications of the HM200™ are not disclosed, therefore it is difficult to pass judgement thereon. It should also be remembered that the HM200™ velocity calculations are based on a uniform length of 3100 mm inputted into the device as

required to return a velocity, whereas the PULSE™ harmonic calculations were made using each individual length.

Turning attention to the differences between resonance and US TOF results, Figure 6.38 shows the deviation (as a percentage) of the PUNDIT™ velocity from each harmonic in turn based on all tested battens from both test series. It shows a normal distribution in the range of PUNDIT™ velocity deviations from the harmonic values.

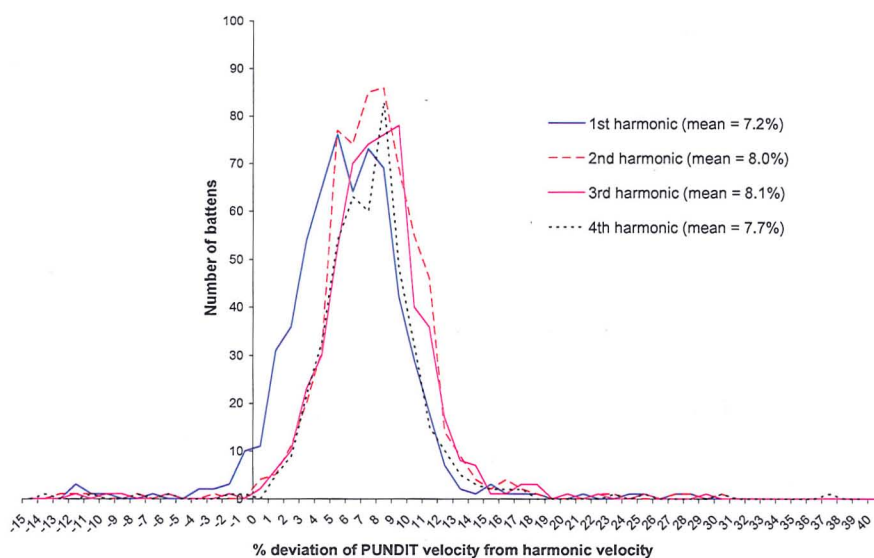


Figure 6.38 Percentage deviations of all tested batten PUNDIT™ velocities from harmonic velocities. Mean percentage increases of PUNDIT™ velocity over harmonic velocity are shown in brackets.

It can be seen that instances do occur where the TOF velocity in a batten can be significantly more (> 30%) or less (< -14%) than the derived harmonic velocity. The reasons for this individual batten variation cannot be fully explained as the percentage deviations show no correlation to any measure of MoE, MoR, KAR or other timber property measured on the battens, or combination of measures using multivariate analysis.

However, certain observations can be drawn. The range of this deviation reduces with increasing harmonic (with 80% of battens having a PUNDIT™ velocity within 3% to 11% higher on the 1st harmonic, to within 6% to 11% on the 4th harmonic). It should be remembered however that the number of battens producing results

decreases with increasing harmonic. It can be seen that the mean velocities of the PUNDIT™ were c. 8% higher than the harmonic velocities, except for the 1st harmonic, which was on average 7.2% lower than the PUNDIT™ velocity. The 1st harmonic also produced velocities greater than or equal to the PUNDIT™ velocities in 11% of the 613 tested battens. In contrast this occurred on less than 1% of battens when using the 2nd, 3rd, or 4th harmonics. The PUNDIT™ velocities tended to be on average 10% higher than the HM200™ velocities; however this was based on the second test sub-series only (248 battens). For the second sub-series battens, the PUNDIT™ velocities were also c. 10% higher across all harmonics.

Using the one-dimensional equation for both measures of velocity in calculating the MoE_d, results in an average 15.1% greater estimation of the MoE_d value by the PUNDIT™ in comparison to the 1st harmonic (averaged from all tested battens). However, if the three-dimensional equation was to be used with a Poisson's ratio of 0.3, this would result in an average 14.5% lower estimation of the 1st harmonic MoE_d by the PUNDIT™ velocity. Taking the average Poisson's ratio value for Sitka spruce (0.37) only serves to increase this underestimation by the PUNDIT™ MoE_d value by a mean of c. 35%. It can therefore be seen that with reducing Poisson's ratio, the one-dimensional and three-dimensional MoE_d estimations tend towards each other (a Poisson's ratio of 0.25 shows a mean 4% difference between the lower PUNDIT™ MoE_d and higher MoE_d values).

To achieve equilibrium between the mean values of MoE_d by both methods, a Poisson's ratio of c. 0.225 would be required, which is unfeasibly low to be an accurate reflection of the true Poisson's ratio of the majority of the timber. However, It can be seen later in Section 7.4, when the acoustic NDT results are discussed in relation to the static MoE results, that the best approximation of the TOF results to the static MoE results occurs when the 3D equation and a Poisson's ratio of between 0.25 and 0.3 is used. Regardless, and as previously noted, the correlation to the individual MoE_d estimations, or static MoE values for that matter, is unaffected.

The overestimation of resonance MoE_d by TOF MoE_d of between 7% and 8% is higher than the overestimation of c. 5% seen in Chapter 5, however the samples used in that study were clear LVL beam specimens as opposed to higher KAR Sitka spruce battens, which has been shown (at modest levels of KAR) to lower the resonance without affecting TOF results.

It would be the author's supposition however that the reasonably consistent level of mean overestimation of the harmonic velocities by the TOF velocities (c. 7% to 8%) was the consequence of measuring the dilatational wave (bulk longitudinal) arrival in the TOF testing whilst measuring dispersive bar velocity by low frequency RF testing, as suggested by Andrews^(6.26) and Chauchan *et al.*^(6.38) Andrews attributed this overestimation of the harmonic velocity by the TOF velocity at 8% to 21%, but this was for low-frequency waves. Low-frequency TOF measures have substantial increases in velocity due to the low diameter-to-wavelength ratio, which is not the case with 54 kHz testing, despite also measuring the dilatational wave. Tests by Chauchan *et al.*^(6.38) suggest a 14% to 26% difference between low-frequency TOF velocity and resonance velocity. Further research by Chauchan *et al.*^(6.47) confirmed 10% difference, again on low frequency TOF.

Interestingly, the PUNDIT™ had noticeably lower mean overestimation of the 1st harmonic, when compared to PUNDIT™ overestimation of the other harmonics despite having the same normal distribution, though with a slightly larger standard deviation. Indeed it had a significant proportion (in comparison to other harmonics) of battens with velocities higher or equal to the TOF velocity (i.e. a negative TOF percentage overestimation in Figure 6.38). As such, the question arises of why either the TOF bulk longitudinal dilatational wave in these instances was not measured (rather the group velocity of the 54 kHz wave was measured) or why the 1st harmonic is so high.

One answer may be that increased energy loss within the battens in these instances mitigates the dilatational wave energy, so as not to trigger the stop function of the PUNDIT™. This would most likely be a function of high compression wood, knot content or particularly high MFA. As such, if this were the case, there

should be a correlation between the percentage deviation and the compression wood content, KAR or MoE generally (reflective of MFA). However, upon further analysis, no such correlation was observed.

Alternatively, as the preferred theory of the author, the knot content between specimens maybe similarly creating enough of a deviated pathway for the TOF wave along the batten as a whole to reduce the transit time, whilst the central portion evaluated by the 1st harmonic may be free of knots and thus appears to be of a higher MoE_d. Additionally it may be the case that there is a relation between the location of the batten with respect to the cross-section of the parent log and the TOF/harmonic velocity.

A further reason for the overestimation may be the increase in strain rate between the low frequency impact and higher frequency TOF, as is typically shown to be the reason for dynamic overestimation of static values (as shown in Chapter 5). However as the deviation between the TOF and resonance velocities generally increases (from the 1st harmonic) with increasing harmonic, this is unlikely to be the primary reason but should still be considered.

6.5.4 Batten damping ratio results

Following the derivation of the resonance and TOF velocities, the damping ratios for the 1st, 2nd and 3rd harmonics (the 4th harmonic having too high a signal to noise ratio to be assessed effectively) were calculated using the auto-damping function. The number of battens tested using the 1st, 2nd and 3rd harmonic damping ratios was the same throughout, *i.e.* of the 393 battens tested in the 1st series, 321 had KAR measurements made on them. It was these battens that were of primary interest concerning damping ratios due to the results presented in the controlled homogeneity test series (Chapter 5). Of this 321, 12 battens had an absent recording due to measurement error and were unavailable for analysis, whilst 82 recording signals failed to excite at the preset trigger level desired for consistent comparison between battens. Of the remaining 227 battens eligible for damping ratio evaluation, 47 were from the IN430 progeny, 49 from the QCI progeny, 72

were from the IN120 progeny, and 59 from the IN420 progeny. Figure 7.29 shows the 1st harmonic damping ratios by progeny.

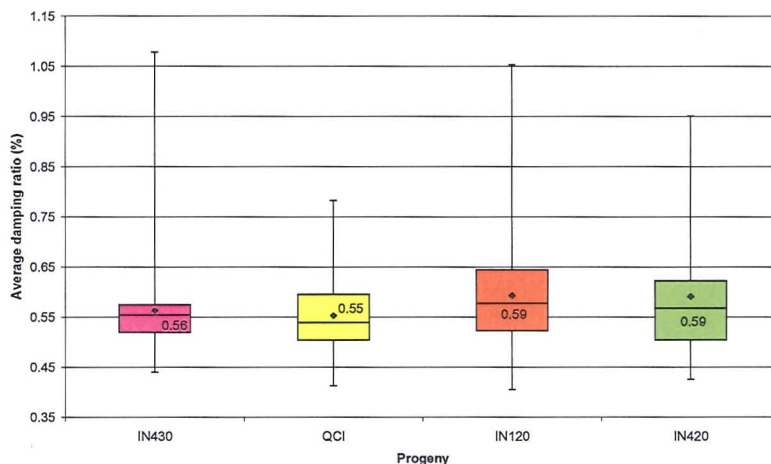


Figure 6.39 Batten 1st harmonic damping ratio by progeny. Graphs show the maximum, minimum, inter-quartile ranges (coloured boxes), median (black line within boxes) and mean (black diamonds) values for each progeny. The raw data used in the production of this graph is seen in Appendix B.

It can be seen that whilst the overall ranges of the various progenies varied, there was little variation in the mean damping ratio (0.03% between the highest and lowest mean). The 2nd and 3rd damping ratios follow the same pattern as has been presented for the 1st harmonic. The 1st harmonic damping ratios returned are higher than the average values predicted for solid timber specimens in Chapter 5 (0.34% to 0.46%), but the samples in this series contain more knots than the Radiata pine samples.

Ultimately it would appear that damping ratio is ineffective at segregating progenies, determining knot content, or improving the prediction to MoR (as seen in Section 6.5.9). It was noted however that the mean damping ratio does increase with increasing harmonic mode, as expected, from which it is taken, with the all batten average damping ratio for the 1st harmonic (0.57%) lower than the 2nd (0.63%) and 3rd (0.72%) harmonic averages. In all harmonics the IN420 progeny is seen to have the highest damping ratio.

As can be seen from Table 6.10, there was no correlation between PUNDIT™ velocity and any of the harmonic damping ratios. A weak correlation was observed to the harmonic velocities. A weak negative correlation was also found between the 1st harmonic damping ratio and the MoE.glo.board values. No other correlations were found to mechanical characteristics, including MoR and KAR measurements. The results of the damping ratio method are somewhat disappointing in their lack of correlation, as previous research by Hori *et al.*^(6.48) calculated the loss tangent in Sitka spruce (though whether this was by the Q-factor or logarithmic decrement was not stated) and found it to have a negative correlation to the velocity-squared ($R^2 = 0.42$). Damping ratios found in the Kershope battens were consistent with the average loss tangents for Sitka spruce of 0.7×10^{-2} reported Hori *et al.*^(6.48), equating to an average damping ratio of 0.63%.

6.5.5 Batten mechanical properties results

The 1st test series (boards) produced 393 density, volume, moisture content, ring parameters, compression wood, MoE.cen.board, MoE.glo.board and MoR.board values for each of the battens. Additionally 321 battens of the 1st series were evaluated for both KAR and perpendicular KAR. The 2nd test series (joists) produced 252 density, volume, ring parameters, compression wood, MoE.cen.board, MoE.glo.board, MoE.cen.joist, MoE.glo.joist and MoR.joist values. Additionally, spiral grain and compression wood measurements were also conducted. The average oven-dry moisture content of the battens was 11.9%, although measurements ranged between 8.8% and 16.8%. Table 6.13 summarises the number of battens tested by both MoE and MoR methods.

Table 6.13 Number of battens tested by each MoE or MoR measure in accordance with BS EN 408:2003^(6.39).

Method	Total Number of battens	IN430 Progeny	QCI Progeny	IN120 Progeny	IN420 Progeny
MoE.cen.board	632	135	134	192	171
MoE.glo.board	646	137	134	203	172
MoE.cen.joist	252	50	49	84	69
MoE.glo.joist	252	50	49	84	69
MoR.board	393	87	84	119	103
MoR.joist	252	50	49	84	69

Battens were tested under the methods described in Section 6.3 and MoE and MoR values calculated using Eqns 6.4 and 6.6 respectively. As can be seen from Table 6.10, there is a significantly linear higher correlation between global MoE measures, and in their relation to dynamic measures, than with the local (MoE.cen.board or MoE.cen.joist) measures. This may in part be attributable to measurement error where the load-deflection transducers not completely free to travel, resulting in apparent overestimation of the local static MoE through an underestimation of the deflection. As such, it was decided that the local measures would be rejected for analysis in favour of the global measures on boards and joist.

However, it is appropriate to note, as seen from Table 6.10, the local and global measurements better have a better correlation when comparing joist measures ($R^2 = 0.64$) with board measures ($R^2 = 0.50$).

Figure 6.40 show an overview of the number of battens in each class of MoE (per 1 GPa increments) as tested by MoE.glo.board and MoE.glo.joist respectively. Classification is based on recommendations given in BS EN 338:2003^(6.39):

A timber population may be assigned to a strength class if its characteristic values of bending strength and density equal or exceed the values for that strength class.... and its characteristic mean modulus of elasticity in bending equals or exceeds 95% of the value for that strength class...(Values were given in accompanying Table 1 in BS EN 338:2003^(6.39)).

The mean MoE value was 7.86 GPa and 7.98 GPa for MoE.glo.board and MoE.glo.joist respectively. This compares well to average MoE values for green Sitka spruce of 7.9 GPa, but significantly lower than the average 9.9 GPa for dry Sitka spruce, as reported by the USDA Wood Handbook^(6.49), though it should be remembered that this is generalised to North America Sitka, and not traditionally lower-quality Scottish Sitka spruce. The values were however consistent with the 7.8 GPa for UK Sitka spruce timber reported by both Gardiner and MacDonald^(6.50) and Reynolds^(6.51). MoE.glo.board values ranged from 4.03 GPa to 12 GPa, whilst MoE.glo.joist values ranged from 4.34 GPa to 12.16 GPa. For the 252 battens tested by both methods, there was a near perfect positive linear correlation of $R^2 = 0.99$. It can be seen that both MoE.glo measures follow the same general pattern.

Figure 6.41 shows the classification of battens (per 10 MPa) in terms of the MoR measurements. The mean MoR value was 44 MPa and 35 MPa for MoR.board and MoR.joist respectively. These values are noticeably higher than the average MoR for both green and dry timber as reported by the USDA Wood Handbook^(6.49).

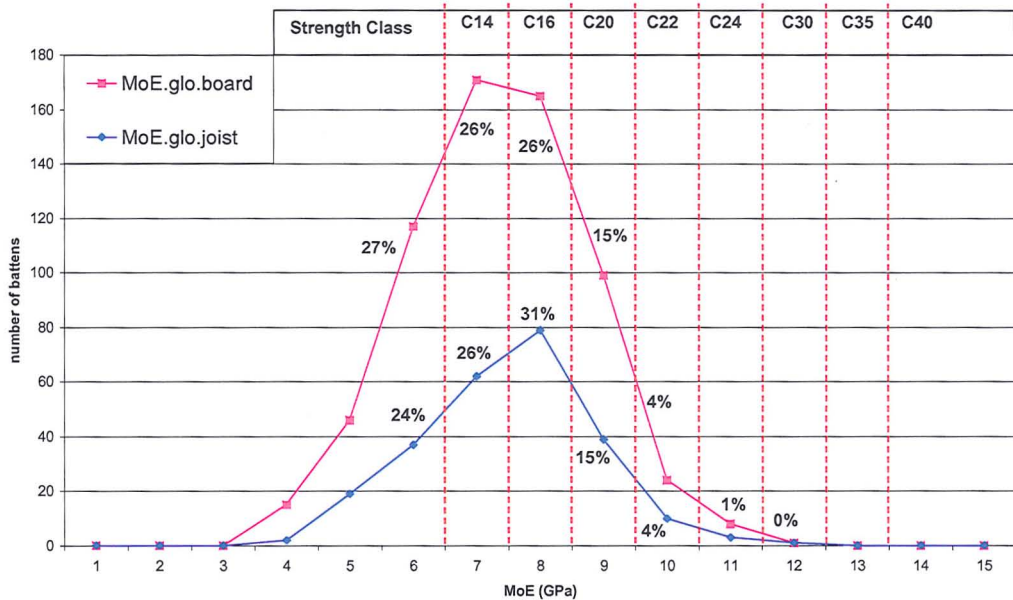


Figure 6.40 Number of battens per each class of MoE.glo.board and MoE.glo.joist (GPa). Total number of battens tested by the two methods was 646 and 252 respectively. Strength classes are taken from BS EN 338:2003^(6.39).

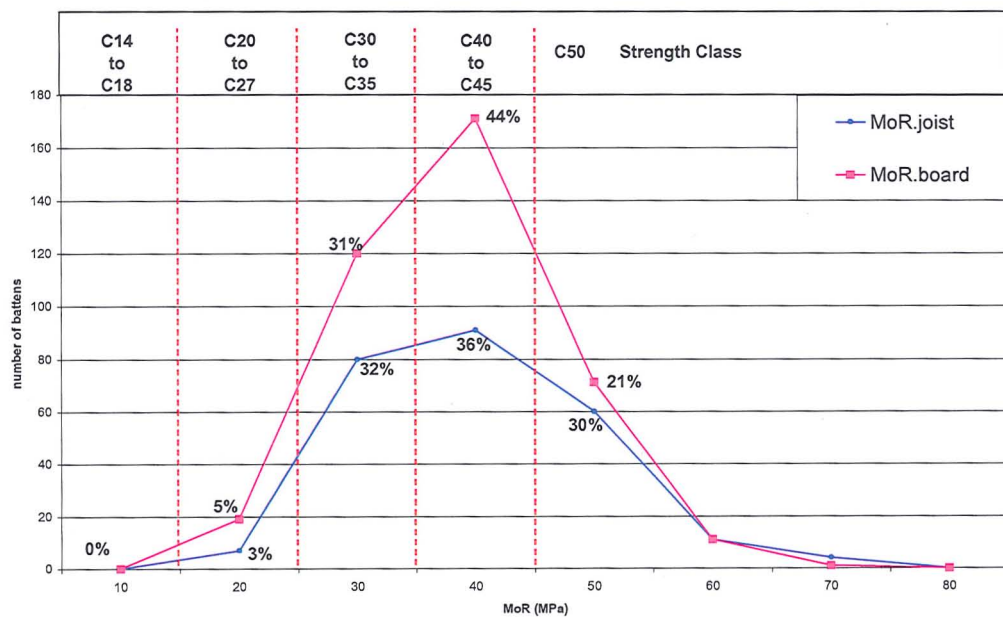


Figure 6.41 Number of battens per each class of MoR.board and MoR.joist (MPa). Total number of battens tested by these two methods was 393 and 252 respectively.

Since the mean MoR values have proved well above the standard for both C16 and C24 grade, and the mean MoE just below C16, it is concluded that the factors controlling stiffness; MFA and density^(6.52) as well as significant drying defects resulting from poor stem straightness, are the cause of the general low grading of Sitka spruce. Hence breeding should be focused on improving these factors. However, as will be seen from the separation of these battens by progeny, selection on this purely basis (although not MFA) does not necessary result in stiffer timber. A key problem seen throughout this section is the high inter-batten variability within progenies, primarily as a result of batten variation within individual logs, and between the trees with a progeny. Hence increasing recovered timber from the more mature outerwood by altering cutting patterns to optimise this recover should yield a higher mean grade of timber.

Since all battens were tested for MoE as boards, Figure 6.42 shows the correlations between the MoE.glo.board values and the corresponding MoR.board (393 battens) and MoR.joist measurements (252 battens). As expected, the correlation between the MoE.glo.board and MoR.board values ($R^2 = 0.65$) was significantly greater than the correlation between MoE.glo.board and MoR.joist values ($R^2 = 0.39$). It can also be seen from Table 6.10 that the MoE.glo.board values has a better linear correlation to its corresponding MoR.board values than between the two joist measures ($R^2 = 0.40$).

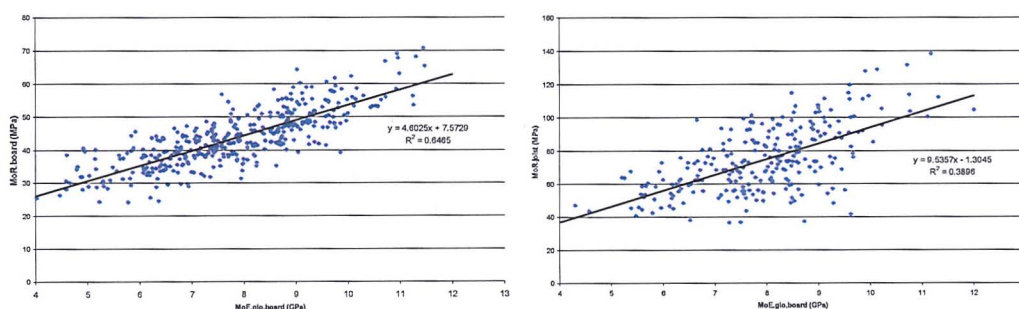


Figure 6.42 MoE.glo.board vs. statically derived MoR measurements.

In comparison to previous research, the correlation between static MoE and MoR are consistent with, though slightly higher than, previous results for Sitka spruce from Brauer *et al.*^(6.53) ($R^2 = 0.56$) and Hanhijärvi *et al.*^(6.54) ($R^2 = 0.57$), whilst slightly less than the results of Johansson and Kliger^(6.55) for Norway spruce ($R^2 =$

0.68). They are however, as expected, with lower as the typical correlations reported for pines ($0.7 \leq R^2 \leq 0.8$).^(6.54, 6.56).

The type of battens tested in both series (by progeny) is presented in Table 6.14, which shows the number of battens in each progeny that are cut from each vertical log position.

Table 6.14 Number of battens within each progeny originating from a specific vertical position from the base within each tree (i.e. log number).

Log number	IN430	QCI	IN120	IN420	Total
1	78	77	88	85	328
2	48	44	59	48	199
3	10	14	40	24	88
4	2	0	16	15	33
5	0	0	0	2	2
Total	138	135	203	174	650

Incidentally and as predicted by the log dynamic MoE experiments and shown in Section 6.5.4, the mean batten static stiffness (as well as the batten dynamic stiffnesses) from the 1st vertical logs in the tree was slightly lower than the mean of the 2nd vertical log. However, such was the variation in values within each log height class, that it is clear there is more variation radially with logs than between height classes. Due to the dependence of MoE on MFA and density^(6.52) and MoR on the MoE and KAR^(6.55) (as discussed in Section 2.2) and due to the significant degree of heritability of the density and MFA in particular, it was expected that the MoE and MoR would vary between progenies. Figures 6.43 and 6.44 show boxplots of the variation in MoE values, by progeny, as tested by MoE.glo.board and MoE.glo.joist respectively. Figure 6.45 shows the same information in terms of the static MoR.board measurements.

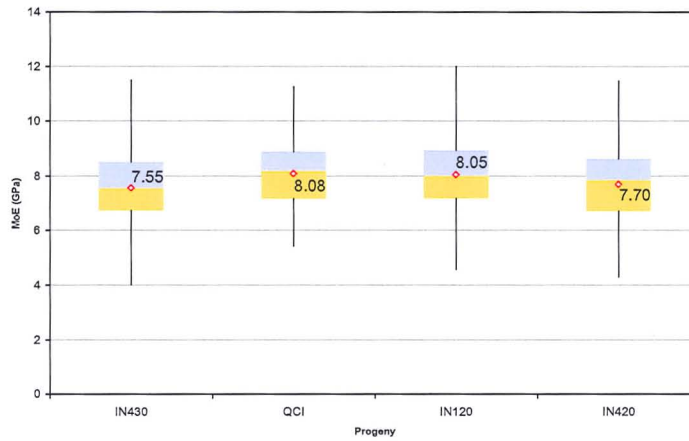


Figure 6.43 Boxplot of MoE.glo.board values by progeny. Graphs show the mean (red diamonds), maximum, minimum, and inter-quartile ranges either side of the median (separation line between grey and yellow boxes) values for each progeny. The raw data used in the production of this graph is seen in Appendix B.

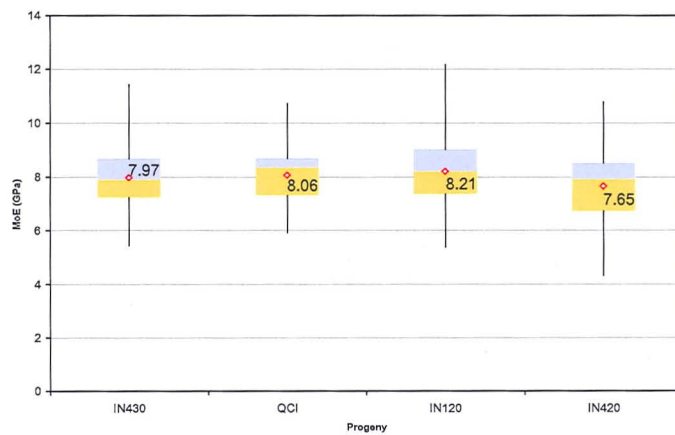


Figure 6.44 Boxplot of MoE.glo.joist values by progeny. Graphs show the mean (red diamonds), maximum, minimum, and inter-quartile ranges either side of the median (separation line between grey and yellow boxes) values for each progeny. The raw data used in the production of this graph is seen in Appendix B.

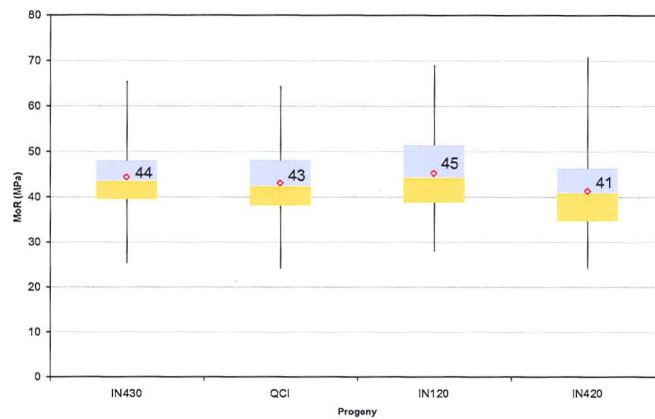


Figure 6.45 Boxplot of MoR.board (left) variation by progeny. Graphs show the mean (red diamonds), maximum, minimum, and inter-quartile ranges either side of the median (separation line between grey and yellow boxes) values for each progeny. The raw data used in the production of this graph is seen in Appendix B.

Due to the near perfect correlation between MoE.glo.board and MoE.glo.joint already mentioned, it follows that the pattern of MoE variation when separated by progeny should be consistent. The standard deviation of each of the progenies is relatively consistent at between 1.25 GPa and 1.40 GPa, whilst the variation between different progeny's mean values is just 0.50 GPa and 0.56 GPa between the highest and lowest ranked progeny. Thus statistically, there is no difference between the specifically selected for improvement progenies and the control progeny in terms of static MoE regardless of the measure. It is clear that inter-tree variation, and subsequent inter-batten variation with each log has a far greater influence on determining the static MoE of a specimen than genetic selection. The same underlying issue can be seen in the MoR results by progeny.

The results presented here confirm the work of Treacy^(6.57), who looked at different Irish progenies of Sitka spruce, in that there is little difference in mechanical properties (MoE, MoR, and density) between progenies of Sitka spruce bred for specific improvements. Indeed it was also found that there were far greater inter-tree variations within stands and inter-batten variations within logs than between progenies.

6.5.6 Comparison of static and dynamic MoE estimations

It can be seen from Table 6.10 that the various measures of MoE_d have a limited range ($R^2 = 0.61$ to 0.71) of positive linear correlations to $MoE.glo.board$. It can also be seen that the MoE_d values across all acoustic measures have improved correlations to the static MoE compared to the velocity alone. The most improved correlation to MoE_d is between the PUNDIT™ velocity ($R^2 = 0.44$) and PUNDIT™ MoE_d ($R^2 = 0.61$). As previously mentioned, the correlation remains the same whether either the one- or three-dimensional dynamic stiffness equation for longitudinal waves is used, due to the use of a constant Poisson's Ratio.

The 1st harmonic MoE_d has the highest correlation ($R^2 = 0.71$) to $MoE.glo.board$, followed by the 3rd, 2nd and 4th harmonics in order of decreasing correlation. The PUNDIT™ is seen to have the lowest correlation ($R^2 = 0.61$). There were no HM200™ measurements on the board specimens. Figure 6.46 displays the best (1st harmonic) and worst (PUNDIT™) correlations to $MoE.glo.board$ in regression plots. It should be noted that the $MoE.glo.board$ also had a weak negative linear correlation ($R^2 = 0.16$) to the 1st harmonic damping ratio.

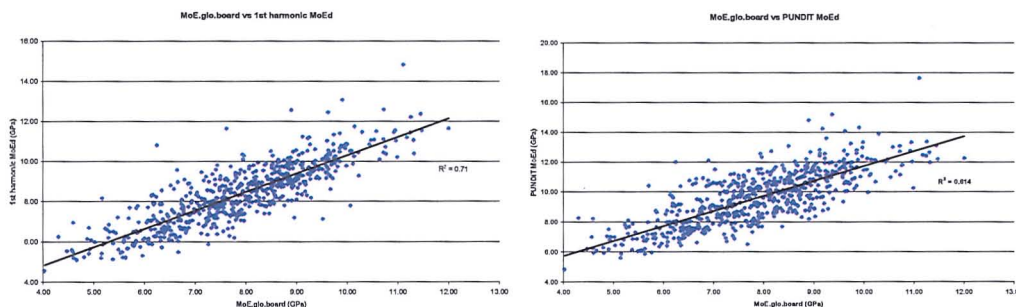


Figure 6.46 $MoE.glo.board$ vs. 1st harmonic (left) and PUNDIT™ (right) MoE_d measurements.

The ranking pattern of highest to lowest correlations was repeated in the other measure of MoE ($MoE.glo.joist$). The 1st harmonic MoE_d again had the highest positive linear correlation to the static value ($R^2 = 0.69$), and the PUNDIT™ lowest at $R^2 = 0.61$. The values for the individual harmonic correlations are also seen in Table 6.10. Their scatter plots are very similar to those shown in Figure 6.46, thus repetition is unnecessary.

In terms of the relation of this research to previous studies, the general conclusion of longitudinal resonance testing have better correlations to static MoE rather than TOF testing, as reviewed in Chapter 3, is confirmed. Higher correlations have been found in previous research^(6.58) between longitudinal resonance MoE_d and static MoE, for example: Cai *et al.*^(6.59) ($R^2 = 0.91$, in southern pine); Castellanos *et al.*^(6.60) ($R^2 = 0.95$, in Japanese sugi); Johansson and Kliger^(6.55) ($R^2 = 0.87$, in Norway spruce); Hanhijärvi *et al.*^(6.54) ($R^2 = 0.95$, in Norway spruce and higher for Scots pine). However these were often for clearer, naturally stiffer timber than U.K. Sitka spruce. In comparable longitudinal resonance tests by Reynolds^(6.51) on U.K. Sitka spruce, the results ($R^2 = 0.71$) are strikingly similar to the Kershope battens' 1st harmonic correlations.

The same is also true of TOF MoE_d studies: De Olivera *et al.*^(6.61) using 22 kHz Sylvatest ($R^2 = 0.8$, in pinus taeda); Castellanos *et al.*^(6.60) using PUNDIT™ 54 kHz ($R^2 = 0.9$, in Japanese sugi); Hanhijärvi *et al.*^(6.54) using 22 kHz Sylvatest ($R^2 = 0.57$, in Norway spruce).

The MoR.board and MoR.joist linear correlations to MoE_d estimations (see Table 6.10) follow the same pattern of ranking order and range of variation (c. 10%) as for the static MoE correlations, however the correlations are reduced by c. 30%. The highest linear correlation to MoR.board is the 1st harmonic MoE_d ($R^2 = 0.41$), though the PUNDIT™ is now higher ($R^2 = 0.34$) than the 4th harmonic ($R^2 = 0.32$). Again there were no HM200™ measurements on the board specimens. The 1st harmonic damping ratio had a weaker negative correlation to MoR.board ($R^2 = 0.09$) than for MoE.glo.board. This was a rebuff to the hypothesis presented at the beginning of this study that the damping ratio would have a stronger correlation with MoR.

The author primarily attributes this to the method of investigation, i.e. using the Q-factor to calculate damping ratio, with the inherent problems resulting from bifurcation as previously discussed. It may also be the case that the damping ratio may be, for example, high due to high knot content without having significant presence at the centre of the beam. However, if this were the case then a

correlation may be expected to the KAR, which there was not. Further, Chapter 5 illustrated that the 1st harmonic damping ratio will remain essentially unchanged unless the significant defect content exists at the centre. Ultimately therefore, either the method is at fault or the correlations observed in Chapter 6 apply to material removal (e.g. rot) but is not significantly affected by semi-continuous defects such as knots.

MoR.joist correlations follow the same pattern as MoR.board although, as with the MoE measurements, the correlations reduced again from board to joist specimens. The 1st harmonic had the highest correlation ($R^2 = 0.31$), followed by the HM200TM ($R^2 = 0.30$). The remaining correlations can be seen in Table 6.10.

Having established the correlations between acoustic MoE_d values, Table 6.215 shows a comparison between the mean MoE.glo.board, MoE.glo.joist, and MoE_d estimations. It should be noted that these are based on all available battens, hence the acoustic battens are typically based on 600+ battens (except for the HM200TM data which was only conducted on the second series), however the MoE.glo.joist values are only based on the 252 2nd series battens.

Table 6.15 Comparison of statistical data returned from static and dynamic MoE measurements.

	MOE. glo. board	MOE. glo. joist	1 st Harm. MoE _d	2 nd Harm. MoE _d	3 rd Harm. MoE _d	4 th Harm. MoE _d	HM200 TM MoE _d	PUNDIT TM MoE _d
Mean (GPa)	7.86	7.98	8.35	8.24	8.19	8.23	8.20	9.58
Standard deviation (GPa)	1.40	1.32	1.54	1.54	1.54	1.55	1.60	1.80
Variance (GPa)	1.97	1.74	2.36	2.37	2.37	2.39	2.56	3.24
Median (GPa)	7.88	8.08	8.41	8.25	8.19	8.26	8.20	9.65
Minimum (GPa)	4.03	4.34	4.55	4.42	4.31	4.22	5.07	4.82
Maximum (GPa)	12.00	12.16	14.80	14.83	15.63	14.83	14.83	17.61
Range (GPa)	7.98	7.83	10.25	10.42	11.32	10.61	9.76	12.79
Number of battens tested	646	252	611	609	547	459	252	634
Deviation from mean MoE.glo. board (%)	-	-	+6.3	+4.8	+4.3	+4.7	+4.3	+21.9
Battens greater or equal to C16 (%)	46%	52%	58%	56%	54%	55%	56%	78%
Battens greater or equal to C24 (%)	1%	1%	5%	2%	3%	3%	3%	21%

The distribution of these static and dynamic measures in terms of strength class in 1 GPa bins are shown in Figure 6.47.

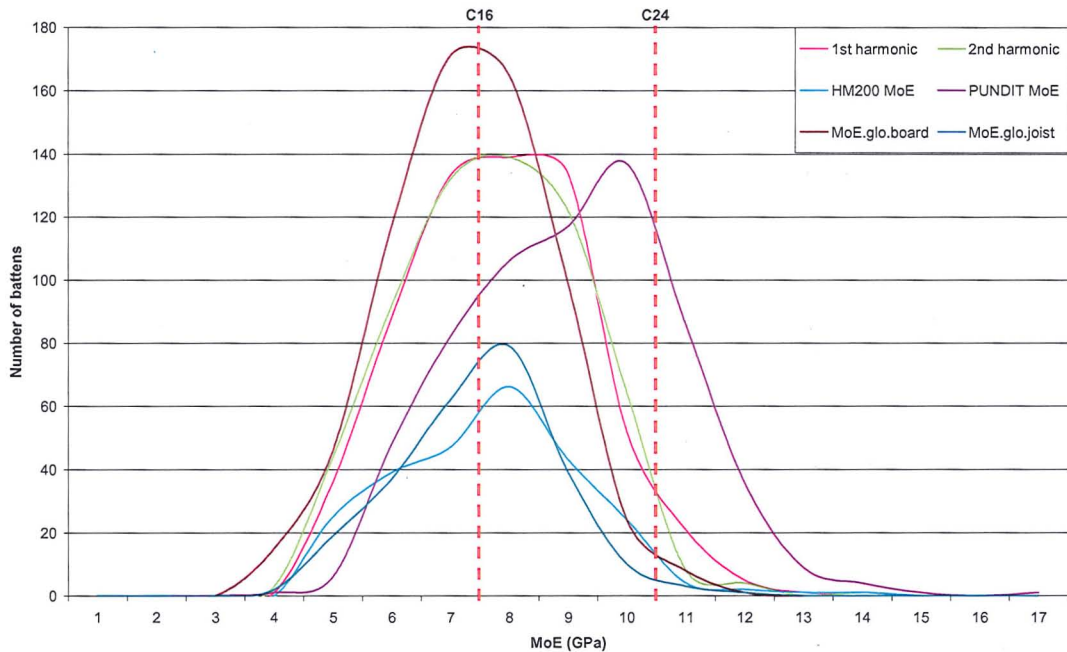


Figure 6.47 Frequency distribution of battens as tested by static and dynamic methods. Note that HM200™ and MoE.glo.joist measures are based on a reduced number of samples.

The static measures had lower mean, standard deviation and range than dynamic measures. The MoE.glo.board measure presented the most normal distribution whilst all other measures had a positive skew to some degree, most noticeably in the TOF results. The TOF results also had the largest range and standard deviation of the NDT methods, whilst presenting a significant over-classification of the stiffness of the battens (32% and 20% more battens classified as C16 and C24, respectively, than MoE.glo.board). However this was based on calculation using the one-dimensional equation, and such issues with the TOF testing shall be discussed shortly.

All harmonic measures reasonably predicted (with up to +6% overestimation) the percentage classification of battens (C16 and C24) based on the MoE.glo.joist measure, however the classifications of MoE.glo.board battens was less accurate. Harmonics typically returned a c.10% overestimate of the MoE.glo.board in terms

of the number of C16 battens or between a 1% and 3% overestimation of the number of C24 battens. The exception was the 1st harmonic, which presented the highest mean overestimation of the static MoE measures, on average 12% greater than the MoE.glo.board and c. 3% overestimate of other harmonic values, whose overestimate of the static MoE varied between them by only 0.5%. It should be noted however that there is not a pattern of diminishing overestimation as the 4th harmonic presents a higher overestimation than the 3rd harmonic.

It is proposed therefore that reference velocities using the 2nd harmonic frequency and an average density for Sitka spruce of 450 kgm^{-3} , whilst adjusting for the inherent 4.8% mean overestimation of the static modulus, would be c. 4040 ms^{-1} and c. 5067 ms^{-1} for C16 and C24 grade respectively.

All harmonic measures had a consistent standard deviation however, the 1st harmonic had a higher positive skew than the other harmonics. The HM200TM had a lower overestimation than the notionally comparable 2nd harmonic; however this was based on a reduced number of samples. In terms of the harmonic results, the 3rd harmonic could be seen to have the closest approximation to the static MoE results; however this benefit is offset by the reduced number of results returned due to the higher SNR (c.10% less battens returning results than the 2nd harmonic). As such, the 3rd harmonic could be deemed to be the most appropriate measure of dynamic MoE, when combined with increased impact strength or more effective SNR filtering. Without this however, the 2nd harmonic is preferable. It should be noted however that Gerhards^(6.69), whilst looking at TOF velocity variation due to cross-grain, noted that the averaging of smaller sections along a specimen produced a closer approximation to the actual MoE of a specimen than measuring the specimen as a whole. Inadvertently, this is proven by the use of higher harmonics, which have been shown in Chapter 6 to sample smaller areas along the specimen length rather than the sample as a whole, or a single area at midspan in the case of the 1st harmonic.

The relative consistency of the MoE_d overestimation of the static MoE is comparable with previous overestimations reported by Machek *et al.*^(6.62) who

quoted general overestimations of static by dynamic MoE by 5% to 15%. Wang *et al.*^(6.63) found that using this one-dimensional equation to calculate a dynamic stiffness overestimated the static MoE by 19 to 37%. Similar ranges of overestimates were reported by De Olivera *et al.*^(6.61) using the 22 kHz Sylvatest, at 20% with no correction for Poisson's ratio.

The most comparable results from this thesis are in Chapter 5, the c. 12% overestimate of static MoE by resonance MoE_d in radiata pine. As shown in Chapter 5, this is a consequence of the strain rate of the relative tests methods, however the range of variation is proposed to be controlled by the defect content and relative stiffness at the point of maximum stress concentration for the harmonic used in resonance testing.

The TOF PUNDIT™'s greater overestimation of the static MoE.glo.board (c.32%) in comparison to resonance testing can be attributed to the use of the one-dimensional equation (Eqn 3.1). This is comparable with low-frequency TOF one-dimensional measures of dilatational velocity (30% overestimation) reported by Andrews^(6.26) However, correction for this overestimation using the three-dimensional equation and an average Poisson's Ratio value for Sitka spruce of 0.37, results in a significant underestimation of the static MoE by c. 32% in terms of mean values, whilst maintaining the same positive linear correlation ($R^2 = 0.61$) between the dynamic and static measure. In contrast, a typical timber Poisson's ratio of 0.3 results in a mean 9.1% underestimation of the MoE.glo.board values. A noticeably low Poisson's ratio of 0.25 has only a 1.6% overestimation of the mean value. However, it should be remembered that the resonance testing resulted in a c. 4.5% overestimation of the MoE.glo.board.

Whilst understanding that the input force into the specimen is far weaker using the ultrasonic TOF method, the rate of the loading is of a comparable order of magnitude. As such, the correct percentage overestimation to achieve using the three-dimensional equation should be c. 4.5%, to make it comparable with resonance testing. This would result however in a Poisson's ratio of less than 0.25 (c. 0.235), which is unfeasibly low for any Sitka timber. This would mean that the

three-dimensional equation is clearly not applicable to estimating the MOE of Sitka spruce. However, if one used the average Poisson's ratio for timber, 0.3, and thus accepted an 8% overestimation, the overestimation could then be attributed not lateral strain but to the measurement of the leading edge of the dilatational wave rather than the group velocity, as proposed by Andrews^(6.26). Further tests are required to validate this theory and observe the shift in US velocities by increasing the sample length so as to remove the occurrence of a dilatational wave.

6.5.7 Frequency shift correlations

Following on from the previous results in Test Series 3 (controlled homogeneity testing; Chapter 5), it was assumed that the 1st harmonic would have a significantly higher relation to MoR than the 2nd harmonic, or that in instances of anomalously large discrepancies in the velocities of the first two harmonics (where the 1st harmonic was significantly lower than the 2nd harmonic), there would be a noticeably low MoR value compared to the sample mean. The reasoning behind this is the dependence on MoR to the location and extent of knots, with knots at midspan providing focal points of rupture occurring at an earlier stage than battens with a similar amount of knots located in other areas.

As shown in Chapter 5, different harmonics evaluate longitudinally separate parts of the batten, with a weighting of the 1st harmonic to the MoE of the midspan and the 2nd harmonic to the MoE of the two quarter-spans due to the focusing of the harmonic on the positions of maximum stress concentration (nodal points of pressure displacement) for that longitudinal wave mode. Any defects at these positions were shown to significantly decrease the relevant harmonic velocity (with pressure displacement anti-nodes at these positions) and hence MoE_d value.

However, in the results of the Kershope battens, only a very minor improvement in terms of linear correlations was seen between the 1st and 2nd harmonic in relation to static MoE. ($R^2 = 0.71$ and 0.64 respectively, see Table 6.10). There was a similar difference between the 1st and 2nd harmonic MoE_d correlations to MoR ($R^2 =$

0.41 and 0.36 respectively, see Table 6.10). However, the higher correlation of the 3rd harmonic MoE_d (compared to the 2nd harmonic) to MoE ($R^2 = 0.66$) and MoR ($R^2 = 0.39$), which has one of three anti-nodes at the midspan of the beams, may indicate, in conjunction with the behaviour of the 1st harmonic, that the weighting of the harmonics to the midspan is significant.

However, there was no correlation or observable pattern between the instances of significant velocity ($> \pm 100 \text{ ms}^{-1}$) and MoE_d differences, between the 1st and 2nd harmonic, and the static MOR, MoE or KAR of the same specimen. No mechanical characteristic appeared to exert an influence over instances of significantly differing 1st and 2nd harmonic velocities.

6.5.8 Batten non-mechanical characteristics

Having discussed MoE and MoR results, we now focus on the same principles involving other mechanical and visual data collected from the 1st and 2nd test series. No incidences of rot, fissures or insect damage were recorded on the battens.

Figure 6.48 shows the boxplot data regarding calculated density for all battens by progeny. The total number of battens in each progeny was presented in Table 6.15. The IN430 progeny shows the highest mean density (425 kgm^{-3}), though the range in mean density is only 26 kgm^{-3} (c. 6% of the overall mean density). This compares to a reported average density (at 12% moisture content) for Sitka spruce of 450 kgm^{-3} ^(7.44). This is as expected given the progeny was specifically selected to produce higher density timber, however in Figure 6.43 the IN430 was seen to have the lowest static and dynamic stiffness, lower than the control QCl. This would concur with the work of Cave and Walker^(6.52), who reported the higher dependence of timber stiffness on MFA over density, as discussed in Chapter 2.

Also as expected, the IN120 and IN420 progenies are, on average, less dense in comparison to the control QCl progeny. The control QCl progeny shows the largest range and inter-quartile range in density, with the IN120 progeny showing the

smallest. The densities show a consistent standard deviation of c. 40 kgm^{-3} across each of the progenies. The range in densities within each progeny can be seen to be far greater than between progenies. Ultimately however it can be seen that there was far greater variation between individual battens than between progenies. As can be seen from Table 6.10, no significant correlations were found between density and other timber properties (including MoE and MoR). It found weak relations to some measures of MoE_d , but this would most likely be due to its use in MoE_d calculation. This was surprising given higher linear correlations between MoE_d and density previously reported by Ilic^(6.66) and Johansson and Kliger^(6.55).

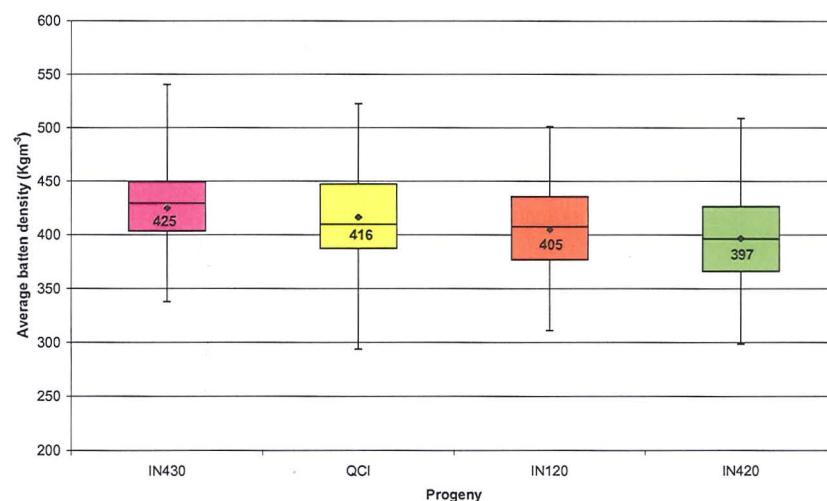


Figure 6.48 Batten densities by progeny.

There was little variation between samples in terms of the mean ring width (potentially related to vigour), with the range between mean values being just c. 0.6 mm. There was no significant correlation between mean ring width and any other mechanical measure or timber property across all comparable battens, as seen from Table 6.10, which is again surprising given some of the correlations between spruce static MoE and ring width shown in Chapter 2 ($-0.2 \leq R^2 \leq -0.4$)^(6.54-6.55). There was similarly no correlation between the measured (by area-percentage grid system on the basis of colour determination) compression wood content or slope of grain and any other parameter. The mean slope of grain angle was 1.9° and there was little difference between progenies' mean values (the IN120 progeny was slightly lower, 1.5° , than the other progenies; IN430 = 1.9° ; IN420 & QCI = 2.1°). The velocity variation of 1% per increase in grain angle proposed by Gerhards^(6.69)

was not observed due to the lack of significant difference in grain angle between mean specimen grain angles.

320 battens from the 1st test series were evaluated for batten surface KAR and the batten KAR measured perpendicularly to the longitudinal axis (perpendicular KAR), the statistical data returned for these boards is shown in Table 6.16.

Table 6.16 Statistical data returned from KAR and perpendicular KAR measurements on all 320 battens in the 1st test series.

	KAR (%)	Perpendicular KAR (%)
Mean	2.1	5.4
SD	0.8	2.3
25 th percentile	1.6	3.8
Median	2.0	5.0
75 th percentile	2.6	6.8
Minimum	0.6	1.3
Maximum	5.6	15.4

On average each batten had 15.4 knots per metre (ranging from 7.4 to 38.5). In direct contrast to the observation of knot content on the logs, the vast majority (81%) of knots were live. This is to be expected as the battens are often sawn from the inner parts of the log and the branches would still have been live during this wood formation. Whilst perpendicular KAR showed a significant increase in the mean and median percentage values, it also shows a higher range and inter-quartile range, as well as a significantly higher standard deviation. This difference between measures is most likely the consequence of knot geometry and orientation with a majority of knots tangentially elongated in an elliptical fashion, so as to have a smaller area when measured by the traditional surface KAR in comparison to the perpendicular KAR.

Whilst there does not appear to be significant difference between the progenies based on the batten surface KAR (%), When looking at the perpendicular KAR the IN430 and IN120 progenies are significantly lower in mean KAR than the control QCI progeny. It can be seen from Table 6.10 that there is no significant correlation between any static mechanical value, or acoustic measure, and KAR or perpendicular KAR. Once again, the lack of correlation to static measures is

surprising given the higher negative correlations shown to MoE ($0.2 \geq R^2 \geq 0.45$)^(6.42, 6.54-6.55) and MoR ($0.3 \leq R^2 \leq 0.6$)^(6.54-6.55, 6.67), from previous literature as described in Chapter 2. Johansson and Kliger^(6.55) had previously reported negative correlations between longitudinal resonance velocity and KAR in Norway spruce of $R^2 = 0.51$.

However, most literature^(6.42, 6.54) correlates MoE and MOR with the BS EN 4978^(6.68) measures Total KAR (TKAR) and/or Margin KAR (MKAR), which are not the same as the KAR measurements taken by CTE researchers in this investigation. KAR takes no account of the proportion of the cross-section occupied by the knots. TKAR is the ratio of all knots intersected by a cross section (typically the worst case in any batten, often in the longitudinal middle of the batten) to the total cross sectional area of the batten, whilst the similar MKAR assesses only the top- and bottom-edged 25th-percentiles of the cross-sectional diameter. However, neither KAR, TKAR, nor MKAR take account of the location of the knots; as such will not be reflective of potential variation in damping ratios or harmonic frequency shifts. Future studies should aim to take account of the location of defects for comparison.

6.5.9 Multi-variance correlations

In the original planning of this investigation it was assumed that the combination of certain acoustic variables could lead, in particular, to an improved correlations with (and thus estimate of) MoE and MoR. Tables 6.17a and 6.17b show the regressive correlation results of combining multiple parameters to try to establish the controls on a dependant variable. It can be seen that, contrary to a previous assumption, a combination of a velocity measure (in this case PUNDIT™ velocity which had the best individual relation to KAR) and 1st harmonic damping ratio does not improve the correlation to KAR and hence cannot be used to predict an individual batten's knot content. Indeed it can be see that in no instances have the combinations of parameters improved the correlation significantly above the correlation of the dominant batten parameter.

Table 6.17a Multivariate correlations between measures of KAR, or static MoE and two acoustical and/or observational predictors in each case.

Dependant variable	Predictors	R	R ²	Adjusted R ²	Std. Error of the Estimate	Predictor	Original linear correlation (R ²) to dependant variable	Std. Error	Significance
Total KAR (%)	Mean 1st harm. Damping ratio (%), PUNDIT™ velocity (ms-1), (Constant)	0.117	0.014	0.005	0.715	(Constant)	X	0.755	0.023
						PUNDIT™ velocity (ms-1)	0.02	0.000	0.869
						Mean 1st harm. Damping ratio (%)	0.014	0.496	0.129
MOE.glo.board (GPa)	Mean 1st harm. Damping ratio (%), 1st Harm. MoEd (GPa), (Constant)	0.856	0.733	0.731	0.771	(Constant)	X	0.520	0.001
						1st Harm. MoEd (GPa)	0.71	0.037	0.000
						Mean 1st harm. Damping ratio (%)	0.159	0.540	0.064
MOE.glo.board (GPa)	Mean 2nd harm. Damping ratio (%), 1st Harm. MoEd (GPa), (Constant)	0.855	0.730	0.728	0.776	(Constant)	X	0.366	0.001
						1st Harm. MoEd (GPa)	0.71	0.035	0.000
						Mean 2nd harm. Damping ratio (%)	0.017	0.293	0.324
MOE.glo.board (GPa)	total KAR (%), 1st Harm. MoEd (GPa), (Constant)	0.854	0.729	0.727	0.772	(Constant)	X	0.305	0.000
						1st Harm. MoEd (GPa)	0.71	0.030	0.000
						total KAR (%)	0.049	0.059	0.004
MOE.glo.board (GPa)	Total KAR perp (%), 1st Harm. MoEd (GPa),(Constant)	0.851	0.725	0.723	0.778	(Constant)	X	0.289	0.000
						1st Harm. MoEd (GPa)	0.71	0.030	0.000
						Total KAR perp (%)	0.018	0.020	0.066

Table 6.17b Multivariate correlations between measures of static MoR and two acoustical and/or observational predictors in each case.

Dependant variable	Predictors	R	R ²	Adjusted R ²	Std. Error of the Estimate	Predictor	Original linear correlation (R ²) to dependant variable	Std. Error	Significance
MoR.board (MPa)	total KAR (%), Density (kgm-3), (Constant)	0.437	0.191	0.186	7.839	(Constant)	X	6.274	0.342
						Density (kgm-3)	0.138	14.541	0.000
						total KAR (%)	0.057	0.578	0.000
MoR.board (MPa)	total KAR (%), MOE.glo.board (GPa), (Constant)	0.806	0.649	0.647	5.152	(Constant)	X	1.977	0.000
						MOE.glo.board (GPa)	0.647	0.205	0.000
						total KAR (%)	0.057	0.388	0.055
MoR.board (MPa)	Total KAR perp (%), MOE.glo.board (GPa), (Constant)	0.809	0.654	0.651	5.120	(Constant)	X	1.837	0.000
						MOE.glo.board (GPa)	0.647	0.201	0.000
						Total KAR perp (%)	0.042	0.130	0.006
MoR.board (MPa)	Mean 1st harm. Damping ratio (%), 1st Harm. MoEd (GPa), (Constant)	0.654	0.428	0.422	6.804	(Constant)	X	4.605	0.000
						1st Harm. MoEd (GPa)	0.413	0.327	0.000
						Mean 1st harm. Damping ratio (%)	0.091	4.770	0.241
MoR.board (MPa)	Mean 2nd harm. Damping ratio (%), 1st Harm. MoEd (GPa), (Constant)	0.654	0.428	0.423	6.800	(Constant)	X	3.223	0.000
						1st Harm. MoEd (GPa)	0.413	0.304	0.000
						Mean 2nd harm. Damping ratio (%)	0.012	2.570	0.198
MoR.board (MPa)	total KAR (%), 1st Harm. MoEd (GPa), (Constant)	0.641	0.411	0.407	6.705	(Constant)	X	2.666	0.000
						1st Harm. MoEd (GPa)	0.413	0.265	0.000
						total KAR (%)	0.057	0.517	0.003

6.6 Kershope log-batten relations

This section presents results from the averaging of the properties of individual battens from the same log, which are then correlated against their corresponding parent log parameters. This analysis could only be performed for the 150 logs which were tested by one or more acoustical methods. Certain assumptions are made in this procedure, inducing potential errors in the correlations; for example not all logs have the same number of battens cut from the log due to cross-

sectional differences. As a result, a greater proportion of the volume of the log may be represented by the averaging of four battens than by averaging only one batten. Similarly, if the one batten is cut from the centre of a thin log then it will be showing the average of the log as juvenile wood as opposed to the average of MoE than one outer wood battens. Of a total of 150 acoustically tested logs, 96% of logs produced 2 or 3 battens for testing and thus averaging: four logs provided just one batten for acoustic testing, 89 logs provided just two battens; 54 logs provided three battens; only one log provided four battens; and two logs provided five battens.

Each batten coming from a log that was acoustically tested had its mechanical properties summed with other battens from that log and then divided by the total number of battens per log to produce an average batten property ($batten_{avg}$). The batten properties under primarily under consideration were the average acoustic velocities, subsequent MoE_d values, harmonic damping ratios, and static bending results. Secondary consideration is given to batten average KAR (used instead of summing the KAR, which would bias larger-diameter logs with more battens) and density. It should be remembered however that not all battens will have results to provide for a $batten_{avg}$. For example, if a log has had two battens cut from it, with one tested as a joist and one as a board, then the $batten_{avg}$ joist stiffness value will be based solely on the one batten with the result. This immediately raises concerns regarding comparisons between the measurements in logs and battens, and upon reflection the comparisons should have been conducted between logs of the same diameter with the same number of battens cut from the same known locations on the parent log. However, as the emphasis of this test series was to assess applicability of log-based field acoustic measures to Sitka spruce and the average returned stiffness grade of recoverable timber, there is validity to the comparison.

A summary of linear correlations between log properties and averaged batten properties is presented in Table 6.18. As the log MoE_d predictions use a constant of 1000 kgm^{-3} only the log MoE_d correlations to average batten parameters are presented here, since adding the velocity only correlations produces the same correlations.

Table 6.18 Summary of correlations (R2) between averaged batten static and acoustic properties and log static and acoustic properties. The colour key is as follows: $0 \leq R^2 \leq 0.09$ (no colour); $0.1 \leq R^2 \leq 0.345$ (blue); $0.35 \leq R^2 \leq 0.495$ (green); $0.5 \leq R^2 \leq 0.695$ (yellow).

	ρ	MOE. glo. board	MOE. glo. joist	MoR joist	MoR board	Avg. KAR	Avg. perp. KAR	1st Harm. Vel.	2nd Harm. Vel.	3rd Harm. Vel.	4th Harm. Vel.	1st Harm. MoEd	2nd Harm. MoEd	3rd Harm. MoEd	4th Harm. MoEd	HM200™ vel.	HM200™ MoEd	PUNDIT™ vel.	PUNDIT™ MoEd	1st harm. DR	2nd harm. DR	3rd harm. DR
MoE _d (PUNDIT™, V)	0.03	0.14	0.11	0.01	0	0.02	0.01	0.08	0.09	0.08	0.07	0.14	0.14	0.13	0.13	0	0	0.05	0.11	0.05	0.03	0
MoE _d (TOF, P-P, V, R2)	0.01	0.16	0.16	0.01	0.02	0.03	0.03	0.33	0.36	0.36	0.2	0.3	0.33	0.34	0.25	0.05	0.15	0.1	0.18	0.06	0.04	0.02
MoE _d (F1, V)	0.02	0.27	0.20	0.02	0.03	0.06	0.03	0.52	0.56	0.54	0.43	0.47	0.51	0.49	0.47	0.1	0.19	0.26	0.33	0.1	0.04	0
MoE _d (F2, V)	0.03	0.31	0.22	0.02	0.02	0.06	0.04	0.5	0.54	0.52	0.41	0.47	0.51	0.49	0.47	0.1	0.19	0.24	0.32	0.08	0.04	0
MoE _d (F3, V)	0.04	0.28	0.22	0.02	0.03	0.08	0.06	0.45	0.48	0.46	0.36	0.46	0.49	0.46	0.45	0.1	0.19	0.21	0.3	0.07	0.03	0
MoE _d (F4, V)	0.02	0.20	0.17	0.05	0.04	0.09	0.06	0.32	0.34	0.34	0.27	0.33	0.36	0.35	0.33	0.12	0.22	0.15	0.19	0.02	0.01	0.03
Log Average dynamic MoE (Gpa, velocity only)	0.03	0.29	0.21	0.02	0.03	0.07	0.05	0.48	0.52	0.5	0.39	0.46	0.5	0.48	0.46	0.11	0.20	0.24	0.31	0.07	0.02	0
1st harm. mean damping ratio	0	0	0	0.06	0.01	0.05	0.05	0.01	0.01	0.01	0	0	0	0	0	0.03	0.01	0.01	0	0	0.01	0
2nd harm. mean damping ratio	0	0.06	0	0	0.01	0	0	0.09	0.09	0.1	0.07	0.07	0.07	0.08	0.06	0.02	0.02	0.1	0.11	0.03	0.01	0
3rd harm. mean damping ratio	0.05	0.01	0.01	0.02	0.02	0.03	0	0.15	0.18	0.16	0.13	0.05	0.07	0.06	0.07	0.02	0.01	0.12	0.09	0.03	0	0.06

There was no significant correlation observed between any measure of log MoE_d and MoR measures of either battens or joists. The log MoE_{d(TOF,P-P)} has the higher correlation to static MoE measures ($R^2 = 0.16$ for both board and joist measures) in terms of the TOF measures of log MoE_d, with the log MoE_{d(TOF,PUNDIT)} having the lowest positive correlation ($R^2 = 0.14$) of all log MoE_d measures (TOF and harmonic). It should be remembered however that the actual values of log TOF P-P MoE_d estimates are significantly higher than the other log acoustic measures, as shown in Figure 6.30.

The harmonic measures of log MoE_d consistently have higher correlations to the static MoE measures. The 2nd harmonic MoE_d can be seen to provide the best correlation to static MoE measures ($R^2 = 0.31$ and 0.22 for board and joist MoE measures respectively). Overall log harmonic MoE_d estimates correlate better to static board measures than joist measures, potentially due to the greater sample number in terms of batten_{avg} boards to average.

In terms of consistency with previous research in this area, this study confirms the work of Andrews^(6.26), in that the 2nd harmonic indeed provides the best correlation to static MoE measures. Recent studies generally showed variable correlations between static and dynamic MoE, dependant on primarily on age and species, to return correlations between $0.4 \leq R^2 \leq 0.7$, as described in more detail in Chapter 3. In particular, Carter *et al.*^(6.70) found excellent correlations between log MoE_d (measured by HM200™) and the average static MoE of both green and air-dried timber beams cut from the log ($R^2 = 0.94$ and 0.89 respectively). Another was Hanhijärvi *et al.*^(6.54), using Norway spruce found the MoE_d of the logs correlated reasonably to the average boards static MoE with a correlation of $R^2 = 0.60$, though weaker for pines. The potential reasons for reduced correlations in this study will be discussed shortly.

There was no significant relation between the batten_{avg} density, batten_{avg} KAR or perpendicular KAR measures and the log MoE_d measures or log damping ratio measures. Also, the theoretical potential for the log harmonic damping ratios to indicate higher KAR values, one of the primary aims of this investigation, was

disproved by the lack of any significant correlation of the log damping ratios to the $batten_{avg}$ KAR values. $Batten_{avg}$ damping ratios show no significant correlation to the log damping ratios, as may have been expected. The very weak correlations of the log 3rd harmonic damping ratio to the $batten_{avg}$ 1st, 2nd and 3rd harmonic velocities and PUNDIT™ velocities (but not acoustic $batten_{avg}$ MoE results) is of some interest, and may simply be a reflection of the log 3rd harmonic's shorter wavelength being subject to greater attenuation by defects, though the lack of correlation of any harmonic damping ratio to the $batten_{avg}$ KAR measures would indicate that knots are certainly not the cause of this.

Regarding $batten_{avg}$ acoustic parameters and log MoE_d estimates, the highest positive linear correlations are found between $batten_{avg}$ 1st, 2nd, and 3rd harmonic velocities and the log harmonic MoE_d values. This was somewhat unexpected, given that generally in recent research (e.g. Grabianowski *et al.*^(6.31)) MoE_d estimates correlate best with other MoE_d estimates; however it should be remembered that the log MoE_d is calculated from the squaring of the velocity only due to effective constant densities. Interestingly, both the $batten_{avg}$ 2nd harmonic velocity and MoE_d show the highest correlations to any Log MoE_d estimates, slightly higher than the $batten_{avg}$ 3rd harmonic velocity and MoE_d values. Conversely to the $batten_{avg}$ harmonic correlations, the $batten_{avg}$ HM200™ MoE_d and PUNDIT™ MoE_d results see a greater correlation between log MoE_d estimates than the $batten_{avg}$ HM200™ and PUNDIT™ velocities. Significantly, the $batten_{avg}$ HM200™ correlations are noticeably less than the $batten_{avg}$ 2nd harmonic correlations to log MoE_d values. That the HM200™ results were calculated from averaging, where possible, a third of the number of battens that the 2nd harmonic results produced (as HM200™ tests were only conducted during the 2nd test sub-series), may be an influencing factor due having to less battens to average per log.

This was not the case for the TOF PUNDIT™ results however, which had the same number of battens as the 2nd harmonic available for averaging. The $batten_{avg}$ PUNDIT™ results provided a weak correlation to the log $MoE_{d(TOF, PUNDIT)}$ results ($R^2 = 0.11$). This could be expected given the particularly weak correlation of $MoE_{d(TOF, PUNDIT)}$ results to static MoE measures, indeed it is noticeable that the

correlations of the $batten_{avg}$ static MoE properties are the same as the $batten_{avg}$ PUNDIT™ results to the $\log MoE_{d(TOF, PUNDIT)}$ values.

Figure 6.49 shows the distribution of each method of MoE determination for batten averaging and $\log MoE_d$ measures in terms of number of logs in each stiffness class (per 1 GPa) relative to threshold values for C16 and C24 timber under BS EN 338:2003^(6.39) guidelines. Note that the \log PUNDIT™ MoE_d results are not adjusted through using the three-dimensional elasticity equation, as any adjustment would only serve to lower the mean value further. Figure 6.50 presents the same graph but without the TOF P-P results for closer analysis of the 0 to 16 GPa range, which encompasses all other MoE_d measures. The $MoE_{glo.board}$ measure has been used to present the batten averaged static elastic modulus distribution for comparison.

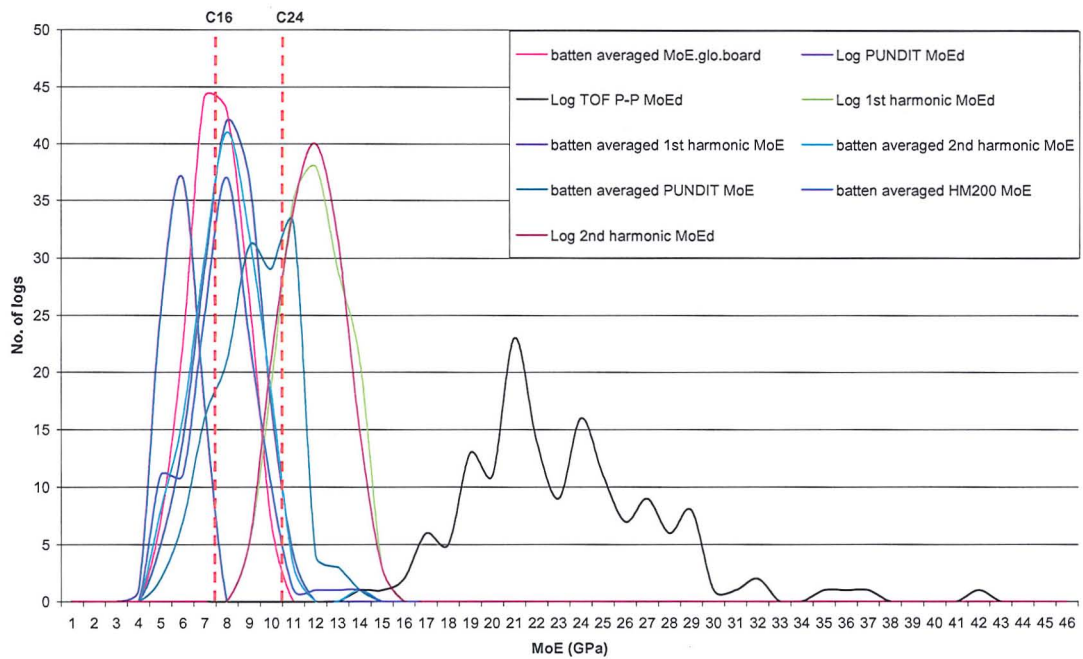


Figure 6.49 Distribution by number of logs per MoE class (per 1 GPa), either by direct measurement on logs or by derived batten averaging where applicable.

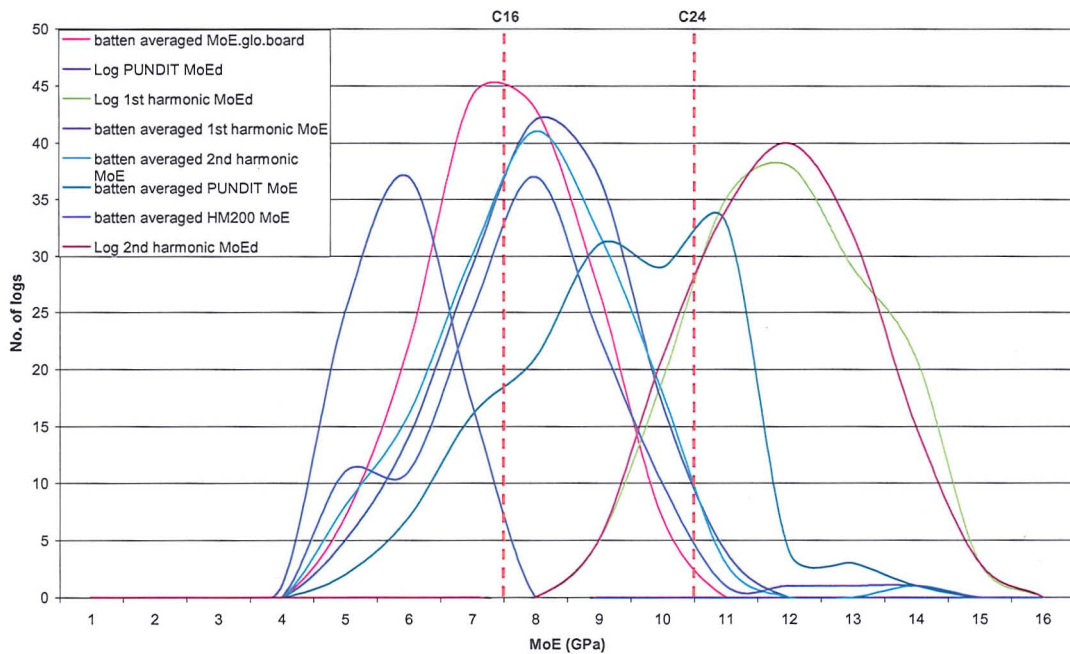


Figure 6.50 Distribution by number of logs per MoE class (per 1 GPa), either by direct measurement on logs or by derived batten averaging where applicable. In this graph the TOF P-P curve has been removed for closer inspection of other measures.

Table 6.19 presents the derived statistical data from the batten averaged data and direct log measurements, to be used in conjunction with Figures 6.49 and 6.50. The equation for skewness is shown in Eqn. 6.7.

$$Skewness = \frac{n}{(n-1)(n-2)} \sum \left(\frac{x_i - \bar{x}}{SD} \right)^3 \quad \text{Eq. 6.7}$$

Where:

n = the total number of data points

x_i = is the i^{th} value

SD = standard deviation of the dataset

Table 6.19 Statistical data derived from the averaging of individual battens per parent log, and MoE_d estimates as shown in Section 6.4.5.

	batten _{avg} MoE.glo. board	batten _{avg} 1 st MoE _d	batten _{avg} 2 nd MoE _d	batten _{avg} HM200™ MoE _d	batten _{avg} PUNDIT™ MoE _d	Log PUNDIT™ MoE _d	Log TOF P-P MoE _d	Log 1 st MoE _d	Log 2 nd MoE _d
Mean (GPa)	8.05	8.61	8.50	8.36	9.77	6.38	22.69	12.39	12.35
% overest- imation of static MoE mean	-	7%	6%	4%	21%	-21%	182%	54%	54%
St. Dev. (GPa)	1.18	1.42	1.47	1.58	1.65	0.77	4.34	1.43	1.37
Var. (GPa)	1.39	2.02	2.16	2.50	2.74	0.60	18.86	2.03	1.88
Max (GPa)	10.64	14.80	14.83	14.83	14.24	7.89	41.27	15.81	15.81
Min (GPa)	5.12	5.20	5.04	5.07	5.77	4.99	13.69	9.34	9.24
Range (GPa)	5.52	9.60	9.79	9.76	8.46	2.90	27.58	6.47	6.57
Skew	-0.21	0.31	0.28	0.57	-0.20	0.02	0.99	0.03	0.01
Logs ≥ C16 (%)	51%	68%	64%	61%	83%	0%	100%	100%	100%
Logs ≥ C24 (%)	0%	2%	3%	3%	28%	0%	100%	84%	83%
Number of logs	150	149	121	147	150	80	150	150	150

From Figure 6.49 it can be seen that, despite the TOF P-P method producing better correlations to the batten_{avg} MoE.glo.board results than the log PUNDIT™ MoE_d results, the distribution of these results are incredibly varied with an oscillating distribution, a heavy positive skew, and an implausible 182% mean overestimation of the MoE.glo.board mean. Thus it could be determined that despite showing the same pattern of high-low stiffnesses between logs as shown in Section 6.4.5, the TOF P-P method is of little use in predicting the static MoE of boards derived from logs. The explanation for this is may be the low diameter to wavelength ratio present when using broadband impact TOF studies, as shown by Bartholomeu *et al.*^(6.35), who observed significantly increasing longitudinal velocity below ratios of 1:7. More likely however it is a cosequence of an flawed measurement technique.

Focusing on Figure 6.50 and regarding the direct log measurements in relation to the batten averaged static MoE of boards, it can be seen that the MoE.glo.board distribution had a slightly negative skew of -0.21 from the mean of 8.05 GPa (standard deviation 1.18 GPa). By comparison the direct log 1st and 2nd harmonic

estimates of $\log MoE_d$ have a normal distribution (the 2nd harmonic slightly more normal than the 1st which had a slight higher MoE_d log increase) around a mean of 12.39 GPa and 12.35 GPa respectively (with a standard deviation of 1.43 and 1.37 respectively). The mean harmonic log measurements overestimate the static average measure by 54%. Conversely, the 80 logs tested by PUNDIT™ also had a normal distribution (and the lowest of all measures' standard deviation at 0.77), but were an average of 21% lower than the static mean log-batten averages, attributed to an inability to measure the dilatational wave. This would indicate that neither NDT method could constructively be used to correctly identify the average static MoE of battens with any particular log of British Sitka spruce.

However, both harmonic and PUNDIT™ measures had similar normal distributions to the average $MoE_{\text{glo.board}}$ (as well as a moderate correlation between log harmonic and average log dynamic stiffness by battens, $R^2 \approx 0.5$ as shown in Table 6.18) and similar distribution to that of the mechanically tested battens. Additionally, as noted by Bucur^(6.32) and Kang and Booker^(6.23), the overestimate will be expected not just on the basis of the change in loading rate, but also due to the high moisture content of logs, which will cause free water to act as a solid, effectively stiffening the specimens as there is no time for moisture to move between the lumen of the cells. This is shown by the results of Carter *et al.*^(6.70), who found reduced correlations between log HM200™ MoE_d tests on green timber boards and the static MoE, and between the boards when dry and the static MoE.

Since the affect of moisture content on stiffness plateaus above FSP^(6.23), the effect could be considered consistent between logs regardless of actual moisture content. This moderate correlation to the average dynamic stiffness is promising given the excellent correlation of dynamic stiffness measured in battens to the static stiffness values ($R^2 \geq 0.85$), as shown in Table 6.10. Thus adjustment of the MoE_d values by the mean percentage overestimation could allow for accurate classification of the static stiffness grade.

The 2nd harmonic would appear to be the favourable harmonic to use for static MoE prediction. If the harmonic values are reduced by 54%, as shown in Figure

6.51, then the distribution of log MoE_d values is similar to that of the batten_{avg} MoE.glo.board distribution. In this instance, the log 2nd harmonic MoE_d results would show 49% of logs failing to achieve an average C16 grade, compared to the static tests also at 49% failure. If the PUNDIT™ results, on 80 logs, were increased by 26%, then 48% of the logs tested by this method would fail to achieve C16 class. Note however that both NDT methods do have a slightly higher standard deviation than the static average.

Thus it can be seen that with adjustments to account for under or overestimation (in the case of PUNDIT™ tests at the pith or resonance testing anywhere across the cross-section), dynamic vibration estimation of stiffness in logs can be used to accurately classify the distribution of the average batten stiffness derived from the logs provided account is made for the higher or lower percentage overestimation.

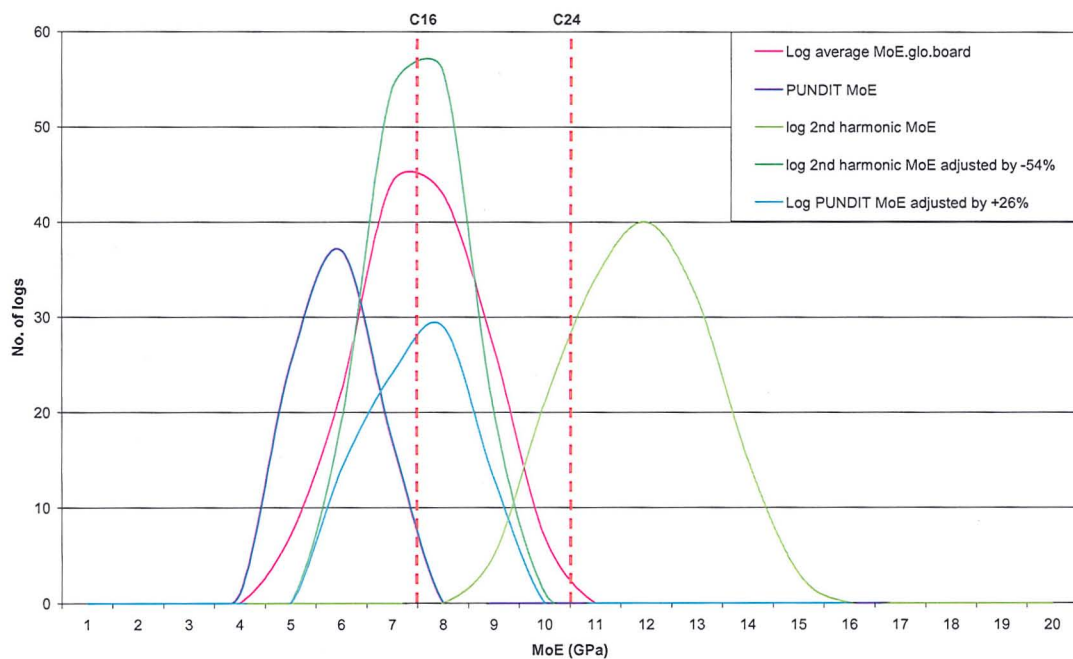


Figure 6.51 Distribution by number of logs per MoE class (per 1 GPa), either by direct measurement on logs or by derived batten averaging where applicable. In this graph the log 2nd harmonic and PUNDIT™ individual values have been adjusted by -54% and +26% respectively and presented as additional curves.

However, this adjustment is only possible due to the knowledge of the average static batten stiffness following milling. This percentage could however be taken as

a reference difference for future studies. As such and accounting for this mean 54% overestimation and assuming a wet density of logs of 1000 kgm^{-3} , a returned velocity of c. 3500 ms^{-1} is proposed for the achievement of C16 grade timber in Scottish Sitka spruce, and thus a reference velocity of c. 4115 ms^{-1} for average achievement of C24 timber. Further study on wet logs should also attempt to establish the validity of the use of 1000 kgm^{-3} for a wet density in logs, as this would significantly affect the outcome of the returned MoE_d .

Based on previous research, the variability of harmonic overestimations, and no prior mention of ultrasonic TOF underestimations, it is clear that the percentage of harmonic overestimation in particular is species specific, but also potentially due to other timber characteristics such as knot content and position. Thus acoustic NDT is only possible for accurate assessment of the Scottish Sitka spruce strength class by a similar set of future testing to determine the influencing factors on the potential overestimation, or to validate the over- or underestimation by the two NDT methods. In this, research such as Lasserre *et al.*^(6.71) were also able to segregate 80% of tested logs to correct strength classes using the HM200™, based on the knowledge of reference velocities.

This difference to previous research correlations could also be explained by the PUNDIT™ device measuring only the central portion (pith region) of the specimens, which is of the lowest stiffness across the cross-section of a log. Thus by not averaging the higher stiffness sections, the prediction of MoE is lower than that averaged from static batten testing. That the PUNDIT™ results maintains a normal distribution is potentially evidence that the stiffness of the juvenile wood, grown early in the tree's life, gradationally changes along the same pattern into mature outerwood. Thus if a tree has a relative low stiffness juvenile wood in comparison to another tree of higher stiffness juvenile wood, this relative difference will continue (given the same silviculture) into the mature outer wood. The lower stiffness of the log due to the significantly higher moisture content would potentially serve to amplify this difference, though it should be remembered that due to the different loading rates the ultrasonic device typically produces an overestimate of the static measure.

This can be seen in the $batten_{avg}$ PUNDIT™ MoE_d results, which coincidentally overestimate the static $MoE_{glo.board}$ distribution by 21%, although the distribution is somewhat bifurcated and has a noticeably negative skew. That the harmonic $batten_{avg}$ results (1st, 2nd and HM200™) have a far lower overestimation of the static MoE average confirms the conclusions of previous sections, which identify the difference between the harmonic averaging of specimens and the TOF methods taking the fastest path, measuring the dilatational wave, and requiring adjustment through the three-dimensional stiffness equation. Interestingly, the $batten_{avg}$ static MoE results have a negative skew of 0.21, whilst the 1st and 2nd harmonic $batten_{avg}$ results have a positive skew of similar proportions. The HM200™ has a less normally distributed pattern with a significant positive skew, but only had roughly two-fifths of the battens to average from to create a parent log value compared to the harmonic and PUNDIT™ $batten_{avg}$ results.

In terms of the log harmonic overestimation, this is more difficult to explain regarding the significantly higher overestimation (54%) of the static mean. Whilst the loading rate should cause an overestimation of the static mean, it would be expected that the moisture content of the log should reduce the apparent stiffness somewhat compared to dry timber. However, it will be the case that the log results will average from significantly more outer wood than the static $batten_{avg}$ measures, due to greater proportions of the battens being cut from the juvenile wood.

Showing precedent, Laserre *et al.*^(6.71) found, using the HM200, that the removal of the bark from a log increased the average value of the MoE_{dyn} , by on average 5.4%, and that the removal of branches from the log resulted in an average 8.3% increase in the MoE_{dyn} . In the case of bark removal, the effect was relatively consistent despite a range in dynamic stiffnesses of samples tested, though in low stiffness logs the removal of branches saw a more pronounced increase in dynamic stiffness. Dickson *et al.*^(6.72) note that there will always be outliers reducing the correlation between average log MoE and the individual board MoE 's simply due to radial stiffness variation within the logs. Similarly, it has been shown by Tsehaye *et al.*^(6.73) that young stems' average log MoE_{dyn} correlate far better to the

MoE_{stat} of the individual boards, due to less variation across the cross-section of the specimen.

A further study is recommended for Scottish Sitka spruce to improve correlations, and predictability by acoustic tools, by sawing, drying, mechanical testing and then averaging of all material in a suitable number of Sitka spruce logs, and correlated to dynamic log measurements. It is hypothesised that the correlation of log dynamic and average batten static measures would improve significantly as a result.

6.7 Summary

The third major test series was effectively split into two parts, Kershope log and batten testing (the latter being further sub-divided into two sections). 150 logs were tested using; three PULSE™ TOF velocity measures; four harmonic velocity measures; a PUNDIT™ velocity measure; and three damping ratio measures. The logs were also assessed for surface knot content, diameter and taper. The logs were then sawn into battens which were subject to further acoustic and static testing (MoE and MoR), as well as quantitative property measurements (KAR, density, compression wood, spiral grain). The battens were mechanically tested in two sub-series: as boards and as joists. In all 651 battens were tested using the same PULSE™ harmonic velocities, PUNDIT™™ TOF velocity, and damping ratio calculations in a repeatable fashion to the log tests. 252 battens tested by the HM200™ device. Descriptive statistics of the averages of each test and correlations were made between variables on both logs and battens and between the averages of the battens and the corresponding logs. This study represented the completion of first known industrial scale NDT of Scottish Sitka spruce's dynamic properties at both the log and batten scale. Additionally, it represented the first use of damping ratios in combination with harmonic MoE_d values to attempt to improve predictions of MoR, the first attempt to find a relationship between the variation in harmonic overtone shift and MoR.

All three methods of log MoE_d determination indicated the same relative variation and ranking pattern between logs, however the actual estimations of stiffness are often impractical. In field usage terms, the PULSE equipment was impractical for extensive measurements. It would also prove excessively expensive, awkward for cabling, and time consuming for accelerometer attachment. Additional need for 230 V power sockets further limit any potential application, the system is purely for laboratory work. However it did allow simultaneous measurement and recording across multiple channels of impacts with far greater frequency resolution than previously possible. However, the time resolution, even when set to maximum, was insufficient to determine variation radially across the end of the samples. Whilst beeswax as a couplant was found unsuitable, due to its unmalleability in the environment, hot glue was found provides adequately repeatable couplant for log testing.

The TOF peak to peak tests, whilst producing a pattern of velocity variation consistent with the more accurate resonance testing, is too unrepeatable to be termed as an adequate measure of MoE_d in logs, with the standard deviations within each progeny representing 10% of the mean velocity. Though a mean overestimation of log resonance velocities by TOF velocities (c. 35%) was similar to the previous studies, when this is converted to MoE_d the spread is unfeasibly large with an undulating distribution, whilst the mean value was c. 23 GPa, an overestimation of the subsequent batten average of 182%. However, TOF P-P may be used as a relative comparison between logs in terms of stiffness ranking, actually showing a better correlation to averaged batten stiffness than PUNDIT™ results and close to the harmonics, but not for accurate average stiffness determination. In contrast, it was noted that taking a 10% or 25% value of the peak amplitude for TOF calculation reduced the TOF overestimation of comparable resonance values, but had the same or greater variation in the spread of velocities as the P-P tests over ten tests on the same log. This was due to a greater dependence, unlike the TOF P-P velocity, on impact strength with generally higher velocities being returned following more forceful impacts. This is consistent with the anecdotal evidence of Walker and Hensen. No variation in velocity was observed radially in either TOF P-P testing or resonance testing, however the former is most

likely the result of inadequate temporal resolution. The PUNDIT™, by contrast, lacks sufficient signal amplitude for transmission through the highest moisture content zones of a 3100 mm long log.

1st to 4th harmonics assessed from the PULSE™ FFT displays were comparatively straightforward to identify from background vibration following impact, and were highly repeatable across ten tests and between three accelerometers. Unexpectedly, there was a greater difference between mean harmonic velocities in dry, untapered battens specimens than between mean harmonic velocities in green, tapered logs. Returned velocities of between 3000 to 3500 ms⁻¹ in wet logs and c. 4500 ms⁻¹ in dry beams were consistent with previous research into green logs though not Scottish Sitka spruce. Variations between harmonics in logs were as expected, with the first harmonic returning the highest mean velocity. However the reduction in velocity with increasing harmonic was less than may have been expected due to the effects of taper as outlined in Andrews^(6.26) and Chapter 3. It was also noted in the batten testing that the reduction in harmonic velocity was more in the rectangular dry samples.

A key feature of the harmonic results was that, contrary to expectations following test series 2, bifurcation of resonant peaks occurs naturally in the majority of log specimens with currently no identifiable pattern. Whilst this is believed to be related in some way to inhomogeneity as indicated by the controlled homogeneity testing of Chapter 6, no conclusive evidence could be found linking the occurrence of bifurcation to defect content or log taper. It was observed however that a bifurcated resonance peak can induce a miscalculation of the harmonic frequency (up to ± 50 Hz), velocity, and MoE_d (up to ± 7%) in comparison to other harmonics. Further research is highly recommended into the causes of resonant peak bifurcation with more controlled conditions (laboratory testing using clear wood samples progressing through to high knot, compression wood and juvenile wood content samples), particularly as the identification of its origins may allow for the determination of material properties upon its occurrence.

Further, the origin of bifurcation may have more beneficial aspects in defect and crack localisation in homogenous material studies where it does not occur naturally, in conjunction with the procedure shown in Chapter 5 for defect localisation. Following on from Chapter 5, it was hypothesised that significant differences between the 1st and 2nd harmonic could indicate knot clusters at the midpoint of the batten specimens. However, no correlation was found between static MoE, MoR and KAR in battens in relation to the percentage deviation between the 1st and 2nd harmonic in either the battens or when these properties were averaged for log comparison. It should be noted however that the measure of KAR in battens has been questioned and future test series should use the more commonly applied TKAR or MKAR. Additionally, no correlations found between log acoustic properties and taper, diameter or combined diameter of knots present on log surface.

Similarly, it was hypothesised that the damping ratios of the logs and battens would reflect the inherent damping between each sample and, with particular focus on the batten samples, provides an assessment technique for defect content. However, whilst Chapter 5 showed the most repeatable and reproducible method of damping ratio calculation was the Q-factor technique, due to the natural occurrence of bifurcation in log and battens solid timber specimens, the returned damping ratios were, despite high repeatability, fatally untrustworthy as a measure of inherent damping. Indeed, no correlation to any measure of KAR, or any parameter other than a weak correlation to harmonic velocity, was found in logs, battens or the average of battens. Further, the incorporation of the 1st harmonic damping ratio with the static MoE or 1st harmonic MoE_d, did not serve to significantly increase the predictability of MoR, as was hypothesised on the basis of high defect content at the batten midspan serving as a focal point for fracture. Indeed this may still be a valid theory, but the Q-factor method is flawed. It is therefore recommended that the Q-factor method is unsuitable for the assessment of timber damping ratios due to natural inhomogeneity.

The method of defect size estimation, based on a comparison to non-defected samples, may still be applicable in more homogeneous material however and its

application should be investigated further. As such, in regards to inherent damping within timber, it is recommended that an efficient method of automatic isolation of resonance frequency be designed and the parameter (frequency centre, taper and shift) be automatically imputed into an impulse response function, which proved more consistent in Chapter 6 than logarithmic decrement.

The PUNDIT™ was also impractical for field measurements despite battery powered portability. Requiring two operators and forceful transducer application, results were primarily surprising as they were significantly lower than the resonance results (c. 28%), which is against conventional theory on TOF overestimation of resonance velocity. This was attributed to an attenuation of the dilatational wave and transmission within the less-stiff core of the logs.

In static testing, out of 646 battens, only 47% achieved greater than C16 grading, with a mean global board static MoE of 7.86 GPa. No battens achieved C24 grade. There were excellent correlations between battens measured as boards and those also measured joists. Static board MoE and MoR measures had a correlation consistent with previous research ($R^2 = 0.57$). In terms of the overarching FR/CTE investigation into progeny performance, it was found that inter-progeny difference between trees and inter-batten variations within logs accounted for a far greater source of variation than between progenies of British Sitka spruce, *i.e.* there is statistically no difference between the progenies. This was reflected in the ranges, means and ranking pattern of progenies in terms of all acoustic and static measures of stiffness, indicating the applicability of NDT testing of timber battens. Without knowing where in a log the batten has come from, there can not be direct comparisons between progenies except on the basis of mean mechanical properties. This should be considered for future investigations. The exception is that the progeny bred for specifically higher density, IN430, was indeed ranked highest in terms of density, yet this bore no indication of increased stiffness, as all dynamic measures on logs, battens and static MoE ranked this progeny lowest in terms of stiffness.

The dynamic testing of the logs firstly confirms the results of previous studies. (that the 2nd vertical log in a tree is the stiffest comparative to the 1st and 3rd) but rather for Scottish Sitka spruce.

All dynamic batten measures had correlations to each other $R^2 \geq 0.85$. Interestingly, the HM200™ and PULSE 2nd harmonic correlation was only $R^2 = 0.92$, despite measuring the same frequency, suggesting issues with the measurement nature of one or other device, potentially related to automatic recognition of the second harmonic. Despite the normal distribution of results in terms of mean overestimation of TOF results compared to resonance results (-15% to +40%, mean c. 8%), further research recommended in to the underlying reasons for the variation, as these could not be attributed to the influence of any specific characteristic as was predicted (in relation to knots or other defects) at the beginning of the investigation. The mean overestimation is attributable to the response of the ultrasonic longitudinal waves to the presence of lateral constraint not seen by the low-frequency waves.

However, it should be noted that to totally account for an 8% overestimation requires a calculation involving an unfeasibly low Poisson's ratio (0.255). This requires further investigation. Once this is taken into account, It is hypothesized that the variation above and below the influence of lateral strain is a combination of defect size and location affecting the transmission path of the ultrasonic wave (or potentially the clarity, or lack of, of the area measured by the harmonics), and as such, if this were the case, the difference could prove useful in defect location and more accurate MOE determination.

In terms of static-dynamic correlations, the 1st harmonic had highest correlation to static global MoE ($R^2 = 0.71$), whilst PUNDIT™ has worst ($R^2 = 0.61$). These values are consistent with previous research on spruces of the same age. In terms of MoR, the 1st harmonic again had the best correlation to MoR ($R^2 = 0.41$). Harmonic MoE_d values for boards overestimated the static MoE values by c. 4.5%, except for the 1st harmonic which had a greater overestimation of 6.3%. The 3rd harmonic had the closest mean values to the static values (4.3%), though a

reduced number of samples due to higher SNR means the 2nd harmonic is potentially the most appropriate. The TOF, in contrast, overestimated by c. 22%, unless it was adjusted for lateral strain influence, which even then requires a particularly low Poisson's ratio. It is therefore surmised that the TOF measures the dilatational wave as proposed by Andrews^(6.26).

No evidence was found of a correlation between the relative percentage variations between harmonic velocities and static measures or KAR measures. Lack of correlations to KAR may be a consequence of not measuring TKAR or MKAR. Additionally, no correlation was found to slope of grain, though there was a minor correlation to ring width. The 1st harmonic's correlation to MoR was not significantly higher than the 2nd harmonic as was surmised at the outset.

In terms of the relation of log dynamic measurements to the average properties of battens cut from the logs, no correlation was found between the log MoE_d and the average MoR of the subsequent battens. However weak yet significant correlations between MoE.glo.board and log MoE_d measures were found, the best being the 2nd harmonic at $R^2 = 0.31$. Note that even better correlations were found to the averaged batten dynamic properties. No correlation was found between any other averaged batten property and any of the dynamic measures on logs. In terms of overestimation of the average static MoE of logs (as created from their subsequent battens), on average the log PUNDIT™ tended to underestimate the batten static average MoE by 21%, the log TOF overestimate by 182%, and the harmonics overestimate by 54%. It is presumed that the averaging of the battens neglected to measure a significant part of the outer wood which was averaged by the log measurements, due to the cutting process of the battens. The higher moisture content may even serve to stiffen the apparent dynamic MoE of the harmonics somewhat as the rapid rate of loading dictates that the moisture will not have time to move between cells, effectively stiffening the material when dynamically measured.

Ultimately it is a conclusion of this series that 2nd harmonic resonance testing of logs gives the most accurate and repeatable measure of NDT for dynamic stiffness

when correlated to static properties. However when reviewing NDT testing of battens, the PUNDIT™, with modification to account for the effects of lateral strain (albeit with a questionable mean poisson's ratio) and loading rate, gives the most correct classification of the static MoE results in terms of C16 and C24 grade timber.

6.8 References

- 6.1 Satellite Images from Google Earth™ - <http://earth.google.com>
- 6.2 Bruechert F., Hapca A., Moore J., Mackenzie R., *Comparison of wood properties and timber quality between the progeny of improved Sitka spruce from the Kershope study: Summary of protocols used by Napier University*, SIRT, CTE internal document, July 2006
- 6.3 DD ENV 1927-1:1999 – *Qualitative classification of softwood round timber, Spruces and firs* – 1999, BSI, U.K.
- 6.4 Brüel & Kjær literature, *PULSE™ knowledge library*, 2005, B & K, Noerum, Denmark.
- 6.5 Andrews M., *Which Acoustic Speed?*, In: Proc. 13th Int. Symp. NDT wood, Berkley, California, USA, August 19-21 2002, Ed. F. C. Beall, Forest Products Society, Madison, Wisconsin, USA.
- 6.6 BS EN 518:1995 – *Structural Timber – Grading – Requirements for visual strength grading standards* – 1995, BSI, U.K.
- 6.7 prEN 14081-1 - *Timber structures – Strength graded structural timber with rectangular cross section – Part 1: General requirements* – 2001, BSI, U.K.
- 6.8 BS EN 4978:1996 – *Specification for visual grading of softwood* – 1996, BSI, U.K.
- 6.9 Grindosonic operations manual, J.W. LEMMENS N.V. Geldenaaksebaan 456, B3001 Leuven
- 6.10 Brüel & Kjær, PULSE 12 Product data sheet no. BU-0229-27, 2007-09, www.bskv.com B & K, Noerum, Denmark.
- 6.11 Dell™ Latitude™ D600 Systems User's Guide, Nov. 2004, P/N 6T524, www.dell.com
- 6.12 Brüel & Kjær, Accelerometers and conditioning: Product catalogue February 2005, pp. 51-54 www.bskv.com, B & K, Noerum, Denmark.

- 6.13 Brüel & Kjær, Type 3508-B accelerometer Product data sheet no. BP-1841-14, 04/06, www.bskv.com, B & K, Noerum, Denmark.
- 6.14 Brüel & Kjær, Type 4294 calibrator Product data sheet no. BP-2101-11, 05/06, www.bskv.com, B & K, Noerum, Denmark.
- 6.15 Brüel & Kjær, Endevco Model 8202 Modal hammer Product data sheet, 0805, www.bskv.com, B & K, Noerum, Denmark.
- 6.16 PUNDIT 6, 54 kHz concrete tester instruction manual, CNS Farnell Ltd, Borehamwood, Herts.
- 6.17 A Proctor Group UK, *Proctor dynamic batten performance sheet*, 2006 Blairgowrie, UK,
- 6.18 HM200™, Manufacture's Website: <http://www.fibre-gen.com/hm200.html>
- 6.19 Zwick Z050 stress-grading machine operations manual, Zwick Testing Machines Ltd, Leominster, Herefordshire, UK
- 6.20 McKenzie W.M.C., *'Design of Structural Elements'*, Palgrave Mcmillan, 2004
- 6.21 Brancheriau L. Bailleres H., Guitard D., *Comparison between modulus of elasticity values calculated using 3 and 4 point bending tests on wooden samples*, 2002, Wood Science and Technology, 36, pp. 367-383
- 6.22 BS EN 408:2003 – *Timber structures – Structural timber and glued laminated timber. Determination of some physical and mechanical properties* –2003, BSI, U.K.
- 6.23 Kang H., Booker R.E., *Variation of stress-wave velocity with MC and temperature*, Wood Sci. Tech., v.36, 2002, pp. 41-54.
- 6.24 Wang X., Ross R.J., McCellan M., Barbour R.J., Erickson J.R., Forsman J.W., McGinnis G.D., *Strength and stiffness assessment of standing trees using a non-destructive stress wave technique*, Res. Paper, FPL-RP-585, 2001, FPL, USDA Forest Service
- 6.25 Jang S.S., *Evaluation of Lumber Properties by applying stress waves to larch logs grown in Korea*, For. Prod. J., v.50, n.3, 2000, pp. 44-48.
- 6.26 Andrews M., *Which Acoustic Speed?*, 2002, Proc. 13th Int. Symp. NDT wood, University of California, Berkeley Campus, California, USA, Forest Products Society, Madison, Wisconsin.
- 6.27 Xu P., Walker J.C.F., *Stiffness gradients in radiata pine trees*, Wood Sci. and Tech., v.38, n.1, 2004, pp.1-9.

- 6.28 McLean, J.P. *Wood properties of four genotypes of Sitka spruce*. PhD Thesis, 2008, Department of Analytical and Environmental Chemistry, University of Glasgow, Glasgow, United Kingdom. 269 p.
- 6.29 Timoshenko S.P., Goodier J.N., *Theory of Elasticity: 3rd edition*, 1970, McGraw-Hill Publishing Co., New York, USA.
- 6.30 Personal communication with John Walker, March 2006.
- 6.31 Grabianowski M., Manley B., Walker J.C.F., *Acoustic measurements on standing trees, logs and green lumber*, Wood Sci. and Tech., v.40, 2006, pp. 205–216.
- 6.32 Bucur V., *Acoustics of Wood*, 2nd Ed., 2005, CRC Press, London, U.K.
- 6.33 Halmshaw R., *Non-Destructive Testing; 2nd Edition*, 1991, Edward Arnold publishing, London, U.K.
- 6.34 Craik, R.J., *Sound Transmission Through Buildings: Using Statistical Energy Analysis*, 1996, Gower Publishing Company, Aldershot, U.K.
- 6.35 Bartholomeu A., Gonclaves R., Bucur V., *Dispersion of ultrasonic waves in Eucalyptus lumber as a function of the geometry of boards*, Scientia Forestalis, v.63, 2003, pp. 235-240.
- 6.36 Berndt H., Johnson G.C., Schiewind A.P., using phase slope for arrival time determination, In *Proc. 14th Int. Symp. NDT wood, Hanover, Germany, May 2-4 2005*, Ed. F-W Broker, Shaker Verlag, Germany.
- 6.37 Carter P., Wang X., Ross R.J., Briggs D., *NDE of logs and standing trees using new acoustic tools. Technical application and results*, In *Proc. 14th Int. Symp. NDT wood, Hanover, Germany, May 2-4 2005*, Ed. F-W Broker, Shaker Verlag, Germany.
- 6.38 Chauchan S.S., Entwistle K.M., Walker J.C.F., 2005, *Differences in acoustic velocity by resonance and transit-time methods in an anisotropic laminated wood medium*, *Holzforschung*, 59, 2005, pp. 428-434.
- 6.39 BS EN 338:2003 - *structural timber – strength classes*, 2003, BSI, U.K.
- 6.40 Bächle H. & Walker J.C.F., *The influence of temperature on the velocity of sound in green pine wood*, *Holz als Roh und Werkstoff*, v.64, n.5, 2006, pp 429-430.
- 6.41 BS EN 844-9:1997 - *Round and sawn timber. Terminology. Terms relating to features of sawn timber – 1997*, VSI, U.K.
- 6.42 Xu P., *Estimating the influence of knots on the local longitudinal stiffness in radiata pine structural timber*, *Wood Sci. Tech.*, v.36, 2002, pp. 501-509.

- 6.43 BS EN 1927-1, *Qualitative classification of softwood round timber — Part 1: Spruces and firs* – 1999, BSI, U.K.
- 6.44 Bucur V., *Acoustics as a tool for the non-destructive testing of wood*, Proc. Int. Symp. NDT contribution to Infrastructure safety systems, Nov 22-26, 1999.
- 6.45 Ouis D., *On the frequency dependence of the modulus of elasticity of wood*, Wood Sci. Tech., 36, 2002, pp. 335-346.
- 6.46 Schad K.C., Kretschmann D.E., McDonald K.A., Ross R.J., Green D. W., *Stress wave techniques for determining quality of dimensional lumber from switch ties*, Research Note, FPL-RN-0265, 1995, USDA Forest Service.
- 6.47 Chauchan S.S., Walker J.C.F., *Variations in acoustic velocity and density with age, and their interrelationship in radiata pine*, For. and Eco. Man., 229, 2006, pp. 388-394.
- 6.48 Hori R., Muller M., Watanabe U., Lichtenegger H.C., Fratzi P., Sugiyama J., *The importance of seasonal differences in the cellulose microfibril angle in softwood in determining acoustic properties*, J. Mat. Sci., 37, 2002, pp. 4279-4284.
- 6.49 *Wood Handbook: Wood as an engineering material*, General technical report, FPL-GTR-113, 1999, FPL, USDA Forest Service.
- 6.50 Gardiner, B., Macdonald, E, *Compression wood in conifers - The characterisation of its formation and its relevance to timber quality*. EU FP5 Project QLRT-2000-00177, 2005, Forest Research, Roslin, UK.
- 6.51 Reynolds T.N., *Compression wood project – Final Report*, BRE Client Report No., 218-309, 2004, Building Research Establishment Ltd.
- 6.52 Cave I.D., Walker J.C.F., *Stiffness of wood in fast-grown Plantation softwoods: the influence of microfibril angle*, For. Prod. J., v. 44, n.5, 1994, pp. 43-45.
- 6.53 Brauner L, Hoffmeyer P., Poulsson L., *Mechanical properties of Picea sitchensis*, Scand. J. of For. Res., v.15, n.1, 2000
- 6.54 Hanhijärvi A., Ranta-Maunus Alpo., Turk, G., *Potential of strength grading of timber with combined measurement techniques*. Rep. of the Combigrade-project: phase 1, 2005, VTT Publications 568. 81 pgs. + app. 6 pgs.
- 6.55 Johansson M., Kliger R., *Variability in strength and stiffness of structural Norway spruce timber – influence of raw material parameters*, Proc. World Conf. Timber Eng. 2000, Whistler, Canada, 2000.

- 6.56 Deresse T., Shepard R.K., Shaler S.M., *Microfibril angle variation in red pine (Pinus resinosa Ait.) and its relation to the strength and stiffness of early juvenile wood*, For. Prod. J., v.53, n.7/8, 2003, pp. 34-40
- 6.57 Treacy M., *A comparison of mechanical and physical wood properties of a range of Sitka spruce provenances*, 2000, COFORD, p.35
- 6.58 Bodig J., *The process of NDE research for wood and wood composites*, In: Proc. 12th Int. Symp. NDT wood, University of West Hungary, Sopron, Hungary, September 13-15 2000, Ed. Divos F.
- 6.59 Cai Z., Hunt M.O., Fridley K.J., Rosowky D.V., *New technique for evaluating damping of longitudinal free vibration in wood based materials*, J. Testing and Ev., 25, 4, 1997, pp.456-460.
- 6.60 Castellanos J.R.S., Nagao H., Ido H., Kato H., Onishi Y., *NDE methods applied to the study of a wood beam's discontinuity*, In: Proc. 13th Int. Symp. NDT wood, Hanover, Germany, May 2-4 2005, Ed. Broker F.W, Shaker Verlag, Germany.
- 6.61 de Olivera, F.G.R., de Campos J.A.O., Pletz E., Sales A., *Assessment of mechanical properties of wood using an ultrasonic technique*, In: Proc. 13th Int. Symp. NDT wood, Berkley, California, USA, August 19-21 2002, Ed. F. C. Beall, Forest Products Society, Madison, Wisconsin, USA.
- 6.62 Machek L., Militz H., Sierra-Alvarez R., *The influence of wood moisture content on dynamic modulus of elasticity measurements in durability testing*, Forschung Verwertung, 5, 2001, pp. 97-100.
- 6.63 Wang X., Ross R.J., Mattson J.A., Erickson J.R., Forsman J.W., Geske E.A., Wehr M.A., *Non-destructive evaluation techniques for assessing modulus of elasticity and stiffness of small diameter logs*. For. Prod. J., v.52. n.2, 2002, pp. 79-85.
- 6.64 Petersen, E.B., Petersen N.M., Weetman G.F., Martin P.J., Stanek. W. *Ecology and Management of Sitka Spruce*, 1997, Univ. of BC Press, Vancouver, BC. 240 pgs.
- 6.65 Verkasalo E., Leban J-M., *Predicting modulus of elasticity and modulus of rupture of the major softwoods from Finland and France for the comparison of wood quality*, In: Proc. 13th Int. Symp. NDT wood, Berkley, California, USA, August 19-21 2002, Ed. F. C. Beall, Forest Products Society, Madison, Wisconsin, USA.
- 6.66 Ilic J. *Variation of the dynamic elastic modulus and wave velocity in the fiber direction with other properties during the drying of Eucalyptus regnans Muell F.*, Wood Sci. Tech., 35, 2001, pp. 157-166.

- 6.67 Gaunt D., Van Wyk L., *Literature review of machine stress grading accuracy check methods*, Project No. PN02.1905, 2003, Australian Government, Forest and Wood Products Development Corporation.
- 6.68 BS 4978:2007 – *Visual strength grading of timber: specification*, 2007, BSI, UK
- 6.69 Gerhards C.C., *Effect of cross grain on stress waves in lumber*, Res. paper, FPL 368, May 1980, USDA Forest Service.
- 6.70 Carter P., Chauchan S., Walker J., *Sorting logs and lumber for stiffness using Director HM200*, *Wood and Fibre Sci.*, 38, 1, 2006, pp. 49-54.
- 6.71 Lasserre J.P., Mason E.G., Watt M.S., *Assessing corewood acoustic velocity and modulus of elasticity with two impact based instruments in 11-year-old trees from a clonal-spacing experiment of Pinus radiata Don D*, *For. and Eco. Man.*, 239, 2007, pp. 217–221.
- 6.72 Dickson R.L., Matheson A.C., Joe B., Ilic J., Owen J.V., *Acoustic segregation of Pinus radiata logs for sawmilling*, *NZ J. of For. Sci.*, 34, 2, 2004, pp. 175-189.
- 6.73 Tsehaye A., Buchanan A.H., Walker J.C.F., *Sorting of logs using acoustics*, *Wood Sci. Tech.*, 34, 2000, pp. 337-344.

Chapter 7 Conclusions and future recommendations

7.1 Introduction

This thesis has examined the applicability of acoustic NDT as a means of assessing the quality of British Sitka spruce. It has further analysed the variation in the behaviour of acoustic and ultrasonic waves due to the mechanical characteristics of British Sitka spruce and timber inhomogeneities in general. The variations between longitudinal velocities have been investigated both in terms of method used and material properties. Chapters 2 and 3 have provided a critical review of recent literature and background theory of wood NDT research.

Influences on the propagation velocity of compression waves in Sitka spruce have been examined, in addition to the variability of the relation between this propagation velocity and the stiffness of the material. The differing behaviour of resonance-based and TOF-based velocities in response to changing inhomogeneity in wood and to macro defects has been examined. Reference velocities for accurate dynamic stiffnesses, based on strength grade, in green and oven-dry Sitka spruce and estimations on the ability of acoustic tools to segregate specimens have been examined.

7.2 Specific conclusions

In Chapter 4 the repeatability and reproducibility of TOF low-frequency stress-wave NDT within a dry C16 grade Sitka spruce sample has been examined. It has been found that derived velocities from low-frequency transient TOF NDT are highly dependent on the distance between the transducers. Small separations (< 400 mm) have been found to induce an unacceptable error range in returned low-frequency longitudinal velocities from broadband impact testing, requiring over 20 tests to obtain a repeatable mean velocity. Returned velocities ($4000 \text{ ms}^{-1} \leq V \leq 5000 \text{ ms}^{-1}$) above this separation have been found to be consistent with TOF velocities from previous research and it was noted that five repeatable TOF tests on dry samples were sufficient to achieve an accurate velocity. As the side of the

beam tested (and thus local defects) became less significant with increased transducer separation, it was clear that the error range in lower-separation samples was induced by a failure to achieve a planar wave front due to interaction between longitudinal and surface wave types and variable energy content within the leading edge of the dilatational wave. It is therefore recommended that surface NDT probe placement be repeated on at least two sides in tests with transducer separations below 800 mm. Ultrasonic testing at 54 kHz, due to the smaller wavelength, has been found to be repeatable with the smallest transducer separations (200 mm).

It has also been observed that, upon achieving a repeatable measure of the transient TOF velocity, measured ultrasonic velocities in dry Sitka spruce were consistently be c. 5% higher. It was shown that this was attributable to the influence of lateral strain when using smaller wavelengths. It is proposed that the difference between the two velocities may have the potential for establishing the longitudinal Poisson's ratio of a specimen.

An examination of the relationships between density, KAR, slope of grain, heartwood content, annual ring width and acoustic velocity have also been presented in Chapter 5. Density, heartwood content, slope of grain and annual ring width variation within a single sample have been found to have no significant correlation with longitudinal velocity across different sizes of tested areas. However, the range of longitudinal variation in these properties between the separate areas was small in the 2200 mm long Sitka spruce beam sample. Therefore it was proposed that further investigation using more significant variations in these properties may have different results. Greater longitudinal variation was observed in KAR, which was reflected in a variation in velocity, which was found to have a moderate negative linear correlation to KAR ($0.51 \leq R^2 \leq 0.35$ for US and impact testing respectively). It was therefore concluded that whilst parameters such as density and slope of grain may still control the clearwood stiffness of the timber and hence the velocity, the knot content had a significant influence on reducing the returned velocity when present.

Reference values of low-frequency resonance and ultrasonic TOF velocities and damping ratios (using a Brüel and Kjær PULSE™ acoustic analyser) have been established and reported in Chapter 5. Static MoEs, for varying scales of timber inhomogeneity in glue-laminated and solid radiata pine beams were also established. It has also been confirmed that TOF MoE_d predictions overestimate harmonic resonance MoE_d values, being attributed (following Andrews^(7.1)) to the TOF measurement of the dilatational wave as opposed to the group velocity. Acoustic MoE_d measures in turn have been found to overestimate the static MoE and have been shown, following minor modification of the research of Divos and Tanaka^(7.2), to be a result of increasing orders of magnitude of the strain rate between static and dynamic testing. Further to the research of Sandoz *et al.*^(7.3), and Divos^(7.4), in conjunction with the theories of Andrews^(9.1), it has been shown that the TOF velocity does not alter with varying cross-sectional inhomogeneity whilst the majority of the cross-section remains a viable transmission path.

Optimum conditions for laboratory transient and continuous excitation of specimens have been established. It was observed that support conditions and placement, provided sufficient specimen isolation is achieved, were of no consequence in terms of returned velocities. Hot glue was found to be the most appropriate method of transducer couplant.

Four separate methods of damping ratio calculation (logarithmic decrement, Q-factor, impulse response, and reverberation time) have been evaluated in terms of repeatability, in which the Q-factor was the most accurate and logarithmic decrement the most variable in solid beam specimens. Advice on the suitable application of each measure has been presented.

Artificial defects were inserted at specific locations to increase the longitudinal inhomogeneity of the specimens. Although these were initially intended to simulate dead knots in wood, the lack of induced grain deviation in the remaining cross-section meant that their effects were generally similar to that of rot.

A principal finding of this test series was that individual harmonics would only detect the presence of these defects should they coincide with the positions of maximum compressional stress-concentration for the particular harmonic wave, *i.e.* the anti-nodal positions of the standing wave. It has been shown that a single defect, at a specific location, accounting for 80% of the cross-sectional area of a beam will have a significant effect on a particular harmonic, but minimal influence on another harmonic. This test was extrapolated to show that the longitudinal location of single or multiple defects can be established through the relative variation of the harmonics. Again, this may have more potential application for homogenous specimens where reference velocities have already been established. Further investigation of this method and its potential applications is recommended. The additional implication of this is that a beam may have a clear section at mid-span (or quarter spans) yet have a high knot content which was missed by a single-harmonic MoE_d device. It has been proposed that this may explain the reduced correlations ($0.6 \leq R^2 \leq 0.7$) seen in previous research between static and dynamic stiffness measures in more knotty wood, yet high correlations were ($R^2 > 0.9$) seen in small specimens and clear wood. It also explains differences in harmonic correlations.

In relation to previous research, it has been suggested that this dismisses the commonly held theory that a defect must be of comparable size to a wavelength to be observed, at least for resonance testing, as the effects of 6 mm diameter defects were observable by harmonics, provided that they coincided with anti-nodal positions.

It has also been proposed that measures be taken to limit the potential for resonance NDT devices, operating on a single harmonic, to miss significant defects due to coincidence with harmonic anti-nodes. In contrast to the previous common preconception of resonance methods averaging the whole specimen stiffness, it has been proposed that whilst this is not debated in terms of the cross-section, values returned from harmonics are significantly weighted towards the position of maximum stress concentration for that harmonic. As such, it has been suggested that higher harmonics will return a more longitudinally-averaged result

than the first harmonic, for example, which is heavily and solely weighted towards the centre of a specimen. It is therefore recommended that an average of at least one even and one odd harmonic velocity be used in MoE_d determination.

However, it has also been shown that resonant peaks used to derive harmonic velocities in both solid wood and laminated wood samples were highly susceptible to bifurcation of the peaks with increased transverse inhomogeneity in specimens, inducing subsequent errors in dynamic MoE and Q-factor damping ratio calculation. Additionally, bifurcation was an observed coincident phenomenon when manually increasing the longitudinal inhomogeneity. Further investigation into the effects and causes of resonant peak bifurcation is required, particularly the reasons for its natural occurrences (as seen in Chapter 6). It has been suggested that this is a consequence of the flexural wave modes occurring at the same frequency as longitudinal wave modes, albeit of a different harmonic order.

In addition to the problems stated above and in confirmation of the work of Ouis^(7.5), it has been found that there is the potential for longitudinal timber rot quantification (and potentially other stiffness reducing defects) based on increased damping ratio from established reference values for timber. The first harmonic damping ratio was found to have an excellent negative correlation to defect volume ($R^2 = -0.98$). To this end, there was significant potential application to more homogenous material defect investigations, given their more repeatable reference values. It is recommended that this method (damping ratio *versus* defect content) be further investigated.

An attempt, as described in Chapter 6, has been made to recreate, during full scale log and sawn-batten NDT, the conditions for observation of the previous results in terms of the variation in harmonic velocity and damping ratio. It is believed to be the first attempt to use harmonic damping ratios in combination with harmonic MoE_d values to improve predictions of MoR_d , as well as the first attempt to find a relationship between the variation in harmonic overtone shift (the difference between the first and second harmonics) and MoR on the basis of defect

identification. This was the first industrial scale investigation into the application of acoustic NDT to Scottish Sitka spruce.

A total of 150 logs have been tested using: three PULSE™ TOF velocity measures, four harmonic velocity measures, a PUNDIT™ velocity measure, and three damping ratio measures. Testing has been undertaken on 651 battens using the same PULSE™ harmonic velocities, PUNDIT™ TOF velocity, and damping ratio calculations in a repeatable fashion to the log tests. A further 252 battens have been tested using the Fiber-gen HM200™ device. Measurements have been made on both logs and battens to assess density, taper, spiral grain, ring width, ring count, and knot content. The battens were subject to static MoE and MoR testing. The properties of the battens were then averaged (using all available battens cut from the same log) for comparison with the acoustic tests on the logs.

The PULSE™ and PUNDIT™ systems were found to be impractical and inefficient for extensive field testing of logs. All NDT methods used on the logs were found to produce the same pattern of variation in terms of log dynamic stiffnesses, following normal distributions except for the low frequency TOF testing. The mean MoE_d ranking was correct in terms of the mean stiffness of the four Sitka spruce progenies investigated. No variation in radial TOF velocity was found, which can be attributed to poor temporal resolution and the longitudinal wave approaching a plane wave, rather than a lack of radial stiffness variation. However, low-frequency TOF investigation was found to produce highly variable results, overestimating the averaged batten MoE by an average of 182%. The PUNDIT™ results, by contrast, have significantly underestimated (by 22%) the batten averaged MoE, which can be attributed to the attenuation of the dilatational wave energy due to high moisture content. The wave was also hypothesised to travelled solely within the central pith region, which due to a lower moisture content, provided the only measurable part of the cross-section by ultrasonic testing.

Calculated low frequency TOF velocities were also found to vary significantly between tests on the same log, in comparison with highly repeatable harmonic velocities, and PUNDIT™ values where available.

The log harmonic MoE_d values were found to overestimate the average batten stiffness from logs by 54%. By adjustment of the timber logs' PUNDIT™ and harmonic MoE_d values by +22% and -54% respectively, both NDT methods were found to correctly classify the percentages of C16 and C24 grade timber recovered from each log. As such, reference mean velocities of c. 3500 ms^{-1} and c. 4115 ms^{-1} are proposed to equate to an average batten grade of C16 and C24 respectively in Scottish Sitka spruce timber. However, there was a very weak correlation between batten averaged static MoE and logs' PUNDIT™ MoE ($R^2 = 0.14$), with a more significant, yet still weak correlation, to second harmonic MoE ($R^2 = 0.31$).

In terms of Sitka spruce progeny, acoustic methods on logs correctly ranked the mean values of average MoE_d to match the ranking of the mean values of static MoE tested on battens by progeny. It was noted however, that the actual log static MoE values may well be lower on the basis of the sawn timber being disproportionately sourced from the lower-stiffness juvenile region of the logs. In addition the number of battens available for averaging varied between samples, potentially reducing the effective correlations. It is recommended that further studies statically measuring and averaging all of a number of green logs and subsequent battens in conjunction with harmonic NDT be conducted.

It has been found that, in general, the second harmonic was the best measure of dynamic stiffness, consistent with the work of Andrews^(7.1) and Carter *et al*^(7.6). For battens however, the first harmonic gave the highest correlation to static MoE ($R^2 = 0.71$), but provided a higher overestimation (by 6.3%, and with a x% greater standard deviation) than the second harmonic (4.8%), which may therefore be preferable. Results were consistent with the correlation in radiata pine specimens, described in Chapter 6, between first harmonic MoE_d and static MoE ($R^2 = 0.57$). Interestingly, the third harmonic MoE_d had both a lower overestimate of the static MoE (4.3%) and better correlation to static MoE ($R^2 = 0.66$), but was discounted as a recommendation due to 10% fewer battens being measurable. An average 8% overestimate of the harmonic MoE_d by the TOF PUNDIT™ confirmed the results given in Chapter 5, in that this was attributable to the effects of lateral strain.

However, in both test series this required the use of a lower average Poisson's ratio than may have been expected (0.25), particularly for Sitka spruce. A large variation (-15% to +30%) in terms of the difference between harmonic and TOF results could not be attributable to any single timber characteristic, such as KAR, as was predicted. As such, further research is recommended into the underlying reasons for the variation, perhaps through finite element analysis of wave propagation around defects of varying size and orientation.

No relationship was found between damping ratio in either log or batten measurements and any timber parameter (including MoR and KAR) measured at each scale. However, the process of damping ratio measurement was effectively compromised due to naturally occurring bifurcation of resonance peaks. It is therefore recommended that the Q-factor not be used as a measure of damping ratio in naturally inhomogeneous specimens, although its relation to defect content and size in more homogenous material may still be applicable however. As such, no improvement in the ability to predict static MoR, or improvement in the harmonic correlation to static MoE, has been found by the incorporation of the first harmonic damping ratio with the harmonic MoE_d measures. The incorporation of the KAR with a dynamic MoE measure also failed to improve correlations to static MoR.

With regard to inherent damping within timber, it is recommended that an efficient method of automatic isolation of resonance frequency be designed and the parameter (frequency centre, taper and shift) be automatically calculated and entered into an impulse response function's parameter limits, which proved more consistent (Chapter 5) than logarithmic decrement. This would significantly reduce the impulse response method's main flaw; the trial and error calculation of the parameter limits.

Bifurcation of resonant peaks appears to occur naturally in the majority of log and batten specimens with no identifiable pattern, as was described in Chapter 6, where it was shown that it could be attributed in part to increasing inhomogeneity. It may be the case that this was an interaction between zones of different density, stiffness or moisture content and further research is required. No evidence has

been found linking the occurrence of bifurcation to either KAR, taper, diameter, or any mechanical parameter such as MoE, MoR or KAR in battens. It was observed however that a bifurcated resonance peak can induce a miscalculation of the harmonic frequency (up to ± 50 Hz), velocity, and MoE_d (up to $\pm 7\%$) in comparison to other harmonics. It is recommended that acoustic tools for dynamic stiffness from harmonics using automated peak detection have a system incorporated to identify bifurcated peaks. It is proposed, on the basis of observations, that the central point of these peaks will represent the true harmonic frequency. Further research is recommended into the causes of resonant peak bifurcation with more controlled conditions (laboratory testing using clear wood samples progressing through to high KAR, compression wood and juvenile wood content samples), particularly as the identification of its origins may allow for the determination of material properties upon its occurrence.

It has been hypothesised that significant differences between the 1st and 2nd harmonics could indicate knot clusters at the midpoint of the batten specimens. However, no correlation was found between static MoE, MoR and KAR in battens in relation to the percentage deviation between the first and second harmonics in either the battens or when these properties were averaged for log comparison. The 1st and 2nd harmonic velocities in battens had a positive linear correlation of $R^2 = 0.95$, indicating some potential for variance due to internal factors. It should be noted that the measure of KAR used in battens has been questioned and future test series should use the more commonly applied TKAR or MKAR. As such, a further more controlled study on solid battens is recommended to address the issue of the potential 1st and 2nd harmonic variance.

In terms of the overarching FR/Napier University investigation into progeny performance, it has been found that inter-progeny difference between trees and inter-batten variations within logs accounts for a far greater source of variation than between progenies of Scottish Sitka spruce, *i.e.* there was statistically no difference between the progenies. As such, the previously stated reference values were valid for the classification of Scottish Sitka spruce logs regardless of progeny. A more detailed study along the lines of this investigation, specifically evaluating

where in a log any particular batten comes from and comparing with other battens of the same physical location, but from different progenies, is more likely to be of value and would be a recommendation for future research.

7.3 Conclusions balanced against objectives

Following the review of the principal findings of this thesis, the success or failure in meeting the objectives listed in Chapter 1 (repeated in this section in italics) are discussed:

1. *The derivation and comparison of multiple dynamic stiffness estimates for a representative sample of felled timber with the subsequent dynamic, static stiffness and strength measures on battens. In this, establishing the applicability and the best method, if it exists, for the acoustic NDT of generally low stiffness, high knot content, high compression wood Scottish Sitka spruce.*

150 Sitka spruce logs from four separate progenies were subject to acoustic NDT using sonic resonance and both sonic and ultrasonic TOF techniques. 645 battens sawn from these logs were tested for dynamic stiffness by the same methods, as well as being tested for static MoE and MoR. It was clear from the test series in Chapter 6 that, for both logs and battens, the use of the 2nd harmonic frequency to calculate MoE_d represents the best method of acoustic NDT for stiffness in Scottish Sitka spruce. It had an excellent repeatability between tests and produced the most reliable results of the acoustic methods used with correlations between batten MoE_d to static MoE ($R^2 = 0.69$) consistent with previous research on similar defect prone species. Correlations of 2nd harmonic MoE_d on logs to averaged static log were low ($R^2 = 0.31$). However with appropriate adjustment, based on the mean overestimation by dynamic methods, correct classification of average log stiffness could be achieved. US TOF was ineffective for field classification of timber due to its low transmission rate. Low frequency TOF provided highly variable

velocities for MoE_d calculation, often detecting flexural velocities rather than longitudinal, and its use should be avoided where possible.

- 2. Reference values of velocity for both wet and dry Sitka spruce progenies should be recorded for future research comparisons, provided the applicability in terms of accurate strength classification can be achieved.*

For green timber logs, reference 2nd harmonic velocities of 3500 ms⁻¹ and 4115 ms⁻¹ are proposed to represent an average batten achievement of C16 and C24 grade respectively. A caveat is that these values may reduce if more efficient cutting methods are developed to increase the amount of higher stiffness mature wood recovered from logs. For dry timber beams, reference velocities were c. 4040 ms⁻¹ and c. 5067 ms⁻¹ for C16 and C24 grade respectively.

- 3. To address current inconsistencies regarding the use of acoustic NDT in timber.*

As discussed in Chapter 3, the inconsistencies with the current commercial methods of NDT have been identified as primarily the variance within TOF and RF parameters. In particular regarding TOF transit time inconsistency, most devices appear to take their start time from different points of the arrival signal that has been shown in Chapter 7 to be a cause of derived velocity variation. This has also been seen in Chapter 8 regarding the use of standing tree basement tools. In resonance tools the inconstancy seen between the Hm200 and PULSE 2nd harmonic, and the Woodspec and Pulse 1st harmonic, appears to be related to the method of automated frequency detection, which does not take account of the effects of bifurcation as discussed in Chapters 5 and 6.

- 4. To evaluate factors influencing both TOF and resonance velocity.*

It was found that TOF velocities are dependant on the distance travelled (due to the influence of the dilatational wave outwith the Fresnel region) and to an extent the presence of defects. However whilst a pathway around these defects still exists

then it may not unduly influence the velocity. TOF velocities, due to the low-frequency impact used, also have a tendency to variably overestimate the resonance-based velocities due to the longitudinal wave suffering mode-conversion to faster surface bending waves, which even uniaxial accelerometers can be influenced by. For resonance based velocities, the MoE of a specimen at specific nodal points of the harmonic wave is the primary control on the returned velocity.

5. *To compare TOF and resonance velocities under controlled and field conditions, to observe whether differences can be attributable to mechanical properties, thus potentially providing new methods of timber property quantification.*
6. *To conduct a similar comparison between harmonics in both controlled conditions and field conditions.*
7. *To investigate the possibility of using an acoustic measure of the inherent damping of the timber to quantify specific timber characteristics.*

These comparisons were conducted and discussed during Chapters 5 (controlled) and 6 (field). It was found that the defect content artificially simulated in controlled beams significantly affected the relations between different harmonic velocities and damping ratios depending on the location of the defect. However, the same was not observed in field testing of logs and battens. This inconstancy was attributed to the in material composition during the control series, hence more akin to rot rather than knots. Inherent damping was not found to be related to any timber properties during the field testing, and was variable when derived by the Q-factor method.

8. *To improve correlations between dynamic stiffness estimates and static stiffness through the addition of more acoustic information than simply that of velocity alone.*

Attempts were made during Chapter 6 to using multi-parameter analysis to improve the correlation between dynamic MoE and static MoE and MoR. No attempt to produce significant improvements in the correlation was found.

9.4 Summary of future recommendations

To summarise, further research has been recommended in the following areas:

- The investigation in timber, or indeed other, homogenous materials, of the ability to locate defects due to the difference between longitudinal harmonic velocities. This may be coupled with investigations into the ability of damping ratio estimates to quantify the extent of defects. Reference values of damping ratios should be established using impulse response or logarithmic decrement for the specimens investigated for potential application as commercial damage or defect investigation tools.
- Further investigation into the reasons for the natural occurrence of resonant peak bifurcation is recommended. A priority for such research should be its generation in homogenous samples, followed by more detailed observation of its behaviour in relation to potential application as a defect identification method in uniform samples. In relation to subsequent NDT for timber research, the causes, the full extent of its natural occurrence, variation between clear and high-defect species, and the potential for velocity error inducement should be quantified to benefit manufacturers of commercial devices.
- It is recommended that future study of the comparisons between dynamic stiffness estimates on logs and their subsequent battens take full account of the wasted material during the sawing process. Without this, the average batten stiffness predicted by log harmonic NDT testing will tend to overestimate due to measurement of unusable, yet significant quantities, of mature wood. Reference values for the percentage overestimation by harmonic NDT of logs may well be related to the age and average diameter of specimens, which varies between stands. A clear understanding of the wastage and more consistent cutting patterns would allow more accurate testing. Hence a study involving multiple log specimens of varying diameters, followed by sawing of all material within a log and static testing, should allow for the improvement of log to average batten correlations.

- Additionally, when future comparisons of different progenies are conducted, and a suggested repetition of the Kershope timber quality study is recommended, comparison between battens from the same area of a log should be compared as mean comparisons are redundant based on the inter-tree, and more importantly inter-batten, variations within a log. The creation of a simple location grid-pattern on one end of the log should be sufficient for batten location within a log.
- Whilst mean overestimates of static and harmonic dynamic stiffness by TOF methods have been established, further research is recommended into the underlying causes of variation in this overestimation (which can range from -15% to +35%). It is recommended that this take the form of repeatability experiments on homogenous specimens, followed by clear wood, followed by more defective timber. It is hypothesised that it is the result of MFA, defect content, input force, or a combination of these factors and each should be controlled (as far as possible) during experiments. Small sample testing may provide a more appropriate starting point. Finite element analysis of wood with a varying knot content and knot position may also be of benefit.

7.5 References

- 7.1 Andrews M., *Which Acoustic Speed?*, 2002, Proc. 13th Int. Symp. NDT wood, University of California, Berkeley Campus, California, USA, Forest Products Society, Madison, Wisconsin.
- 7.2 Divos F., Tanaka T., *Effect of creep on modulus of elasticity determination of wood*, J. Vib. and Acous., 2000, V.122, 1, pp.90-92
- 7.3 Sandoz J.L., Benoit Y., Demay L., *Wood testing using Acousto-ultrasonic*, In: Proc. 12th Int. Symp. NDT wood, University of West Hungary, Sopron, Hungary, September 13-15, 2000, Ed. Divos F.
- 7.4 Divos F., Daniel I., Bejo L., *Defect detection in timber by stress wave time and amplitude*, E-J. of NDT, Vol. 6 no.3, 2001.
- 7.5 Ouis D., *Frequency dependence of strength and damping properties of wood and their influence by structural defects and rot*, In: Proc. 14th Int. Symp. NDT
415

wood, May 2-4 2005, Hanover, Germany, May 2-4 2005, Ed. F-W Broker, Shaker Verlag, Germany.

- 7.6 Carter P., Wang X., Ross R.J., Briggs D., *NDE of logs and standing trees using new acoustic tools. Technical application and results*, In Proc. 14th Int. Symp. NDT wood, Hanover, Germany, May 2-4 2005, Ed. F-W Broker, Shaker Verlag, Germany.

Appendix C – Tables showing previous correlations as referred to in Chapter 2

Appendix C1

Correlations between MoE and MoR and individual wood parameters

Parameter	Specimen type	species	sample size	Method of Measurement	R ² vs. MoE	R ² vs. MoR	R ² vs. axial compressional strength	Reference
Grain angle	beams	Norway Spruce	207	static bending	-0.22	-0.4		Johansson and Kliger ^(2.7)
Grain angle				x-ray diffraction and Polarized light microscopy				Saren <i>et al.</i> ^(2.104)
Grain angle	beams	spruce	100	Finnograder (gamma rays, microwaves, IR thermography)	-0.02	-0.07		Hanhijärvi <i>et al.</i> ^(2.29)
Grain angle (at given knot location)	beams	pine	100	Finnograder	-0.14	-0.2		Hanhijärvi <i>et al.</i> ^(2.29)
Grain angle (at given knot location)	beams	spruce	100	Finnograder	-0.07	-0.11		Hanhijärvi <i>et al.</i> ^(2.29)
Spiral grain	increment cores		44	image analysis			-0.42	Lindstrom <i>et al.</i> ^(2.42)
Density	SCS		200 specimens		0.88		0.9	Dinwoodie ^(2.23)
Density	SCS		47				0.84	Gindl and Teischinger ^(2.57)
Density	SCS	Red pine	5		0.41	0.56		Deresse <i>et al.</i> ^(2.3)
Density	SCS	Radiata pine	104	Silviscan®	0.7			Evans and Ilic ^(2.58)
Density	SCS	Radiata pine	29	Silviscan®	0.44			Ball <i>et al.</i> ^(2.76)
Density	SCS	pine (Finland)	181	static bending	0.8	0.7		Verkasalo and Leban ^(2.34)
Density	SCS	pine (France)	119	static bending	0.29	0.39		Verkasalo and Leban ^(2.34)
Density	SCS	fir (France only)	115	static bending	0.34	0.2		Verkasalo and Leban ^(2.34)
Density	SCS	spruce (Finland)	181	static bending	0.43	0.34		Verkasalo and Leban ^(2.34)
Density	SCS	spruce (Finland)	181	static bending	0.43	0.34		Verkasalo and Leban ^(2.34)
Density	SCS	spruce (France)	119	static bending	0.55	0.67		Verkasalo and Leban ^(2.34)
Density	increment cores	Radiata pine	44	Silviscan®			0.31	Lindstrom <i>et al.</i> ^(2.42)
Density	beams					0.2-0.4		Denzler ^(2.45)
Density	beams	Eucalyptus	32	static bending	0.81	0.77		Ilic ^(2.310)

Density	beams	Norway Spruce	207	static bending	0.75	0.43		Johansson and Kliger ^(2,7)
Density	beams	Eucalyptus	255	gravimetric method		0.46		Piter <i>et al.</i> ^(2,46)
Density	beams	spruce	100	gravimetric method	0.58	0.37		Hanhijärvi <i>et al.</i> ^(2,29)
Density	beams	pine	100	gravimetric method	0.72	0.58		Hanhijärvi <i>et al.</i> ^(2,29)
Parameter	Specimen type	species	sample size	Method of Measurement	R² vs. MoE	R² vs. MoR	R² vs. axial compressional strength	Reference
Density	beams	spruce	100	Goldeneye x-ray	0.59	0.37		Hanhijärvi <i>et al.</i> ^(2,29)
Density	beams	pine	100	Goldeneye x-ray	0.76	0.56		Hanhijärvi <i>et al.</i> ^(2,29)
Density	beams	spruce	100	Finnograder (gamma rays, microwaves, IR thermography)	0.54	0.35		Hanhijärvi <i>et al.</i> ^(2,29)
Density	beams	pine	100	Finnograder (gamma rays, microwaves, IR thermography)				Hanhijärvi <i>et al.</i> ^(2,29)
Density	beams	various species				0.15-0.40		Gaunt and van Wyk ^(2,9)
S ₂ MFA	thin sections		47	iodine staining and microscopy			0.1	Gindl and Teischinger ^(2,57)
S ₂ MFA	thin sections	Red pine	5	iodine staining and microscopy	-0.68	-0.53		Deresse <i>et al.</i> ^(2,3)
S ₂ MFA	thin sections	Norway spruce		iodine staining and microscopy	-0.95			Gindl ^(2,47)
S ₂ MFA	SCS	Radiata pine	29	Silviscan®	-0.81			Ball <i>et al.</i> ^(2,78)
S ₂ MFA	SCS		104	Silviscan®	0.85			Evans and Ilic ^(2,38)
S ₂ MFA	increment cores	Radiata pine	44				-0.87	Lindstrom <i>et al.</i> ^(2,42)
Cell wall thickness	SCS	Radiata pine	29	Silviscan®	0.7			Ball <i>et al.</i> ^(2,78)
Annual ring width	beams	various species				0.2-0.4		Gaunt and van Wyk ^(2,9)
Annual ring width	beams	Norway Spruce	404	static bending	-0.43	-0.52		Johansson and Kliger ^(2,7)
Annual ring width	logs	pine	100	Bintec Log X-ray device	-0.23	-0.19		Hanhijärvi <i>et al.</i> ^(2,29)
lignin content	ground samples	Norway spruce		UV spectroscopy	-0.94			Gindl ^(2,47)
knots (KAR)	beams	various species				0.15-0.3		Gaunt and van Wyk ^(2,9)
knots (KAR)	beams	Norway spruce	404	static bending	-0.4	-0.58		Johansson and Kliger ^(2,7)

Knots (KAR)	beams	Eucalyptus	349	Visual observation			-0.32	Piter <i>et al.</i> ^(2.46)
Knots (KAR)	beams	Radiata pine	150	Visual observation	-0.38 to -0.46			Xu ^(2.42)
Knot content	beams	spruce	100	Goldeneye x-ray	0.34	0.38		Hanhijärvi <i>et al.</i> ^(2.29)
Parameter	Specimen type	species	sample size	Method of Measurement	R² vs. MoE	R² vs. MoR	R² vs. axial compressional strength	Reference
Knot content	beams	pine	100	Goldeneye x-ray	0.46	0.68		Hanhijärvi <i>et al.</i> ^(2.29)
Knot content	beams	spruce	100	Finnograder	0.2	0.31		Hanhijärvi <i>et al.</i> ^(2.29)
Knot content	beams	pine	100	Finnograder	0.34	0.61		Hanhijärvi <i>et al.</i> ^(2.29)
Knot content	logs	spruce	100	Bintec Log X-ray device	0.14	0.2		Hanhijärvi <i>et al.</i> ^(2.29)
Knot content	logs	pine	100	Bintec Log X-ray device	0.43	0.67		Hanhijärvi <i>et al.</i> ^(2.29)
Maximum stress concentration (based on knot parameters)	beams	not specified	1080	X-ray machine (not specified)		0.41		Saravi <i>et al.</i> ^(2.34)
compression wood	increment cores	Radiata pine	44	Silviscan®			-0.13	Lindstrom <i>et al.</i> ^(2.42)

Appendix C2

Relationships of combined parameters to MoE and MoR (DEN = density, RW = ring width, AGE = radial position from pith, MFA = microfibril angle, KAR = knot area ratio, KVR = knot volume ratio, GA = grain angle, MC = moisture content, MoE = modulus of elasticity, DD = drying defects)

Combined parameter	Type	Species	Sample size	Method of Measurement	R ² vs. MoE	R ² vs. MoR	Reference
DEN, RW, AGE	SCS	pine (Finland)	181	static bending	0.83	0.72	Verkasalo and Leban ^(2.34)
DEN, RW, AGE	SCS	pine (France)	119	static bending	0.42	0.52	Verkasalo and Leban ^(2.34)
DEN, RW, AGE	SCS	spruce (Finland)	181	static bending	0.5	0.38	Verkasalo and Leban ^(2.34)
DEN, RW, AGE	SCS	spruce (France)	119	static bending	0.6	0.68	Verkasalo and Leban ^(2.34)
DEN, RW, AGE	SCS	fir (France only)	115	static bending	0.16	0.41	Verkasalo and Leban ^(2.34)
DEN, MFA	SCS	Radiata pine	29	Silviscan®			Ball <i>et al.</i> ^(2.76)
DEN, MFA	SCS		104	Silviscan®	0.96		Evans and Ilic ^(2.38)
DEN, MFA	SCS			Silviscan®	0.87		Yang and Evans ^(2.4)
DEN, KAR						0.40-0.60	Denzler ^(2.45)
DEN, KAR				X-ray densitometry		0.42	Diebold <i>et al.</i> ^(2.50)
DEN, KAR						0.35-0.60	Gaunt and van Wyk ^(2.6)
DEN, KVR	beams	spruce	100	Goldeneye x-ray	0.7	0.57	Hanhijärvi <i>et al.</i> ^(2.29)
DEN, KVR	beams	pine	100	Goldeneye x-ray	0.79	0.78	Hanhijärvi <i>et al.</i> ^(2.29)
DEN, KAR, GA	beams	spruce	100	Finnograder (gamma rays, microwaves, IR thermography)	0.38	0.35	Hanhijärvi <i>et al.</i> ^(2.29)

DEN, KAR, GA	beams	pine	100	Finnograder	0.49	0.65	Hanhijärvi <i>et al.</i> ^(2.29)
DEN, KAR, RW, GA, DD	beams	Norway Spruce	255	combined parameters	0.7		Johansson and Kliger ^(2.7)
DEN, KAR, RW	beams	Sitka Spruce	513			0.35-0.52	Brauer <i>et al.</i> ^(2.38)
DEN, MC	beams			Radio-frequency waves		0.58	Steele ^(2.51)
KAR, RW	beams	Sitka Spruce	513	static bending		0.26-0.31	Brauer <i>et al.</i> ^(2.38)
KAR, GA	beams	Norway Spruce	255	static bending	0.62		Johansson and Kliger ^(2.7)
KAR, RW	beams	various species				0.35-0.50	Gaunt and van Wyk ^(2.6)
MoE, DEN, KAR	beams	Eucalyptus	255	combined parameters		0.82	Piter <i>et al.</i> ^(2.46)
MoE, DEN, KAR	beams					0.55-0.80	Denzler ^(2.45)
MoE, KAR	beams	various species				0.35-0.80	Gaunt and van Wyk ^(2.35)
MoE, KAR	beams					0.55-0.75	Denzler ^(2.45)
MoE, KAR	beams					0.8	Green <i>et al.</i> ⁽⁵⁾
MoE, DEN, KAR	beams			X-ray densitometry and static bending		0.55	Diebold <i>et al.</i> ^(2.50)

Appendix C3

Recent examples of the use of NDT methods to evaluate wood properties and the correlation of these results to either other parameters or traditional methods of evaluating the same parameter:

NDT method	parameter measured	direct or indirect measurement	Commercial device?	correlated against 2nd parameter =	2nd parameter derived by:	sample size	R ²	Reference
X-ray diffraction	MFA	Indirect	Silviscan®	MoE	Transverse vibration	104	0.86	Evans and Illic ^(2.38)
X-ray diffraction	MFA	Indirect	Silviscan®	MoE	static bending	130	0.87	Yang and Evans ^(2.4)
X-ray diffraction	MFA	Indirect	x-ray diffractometer (Shimadzu, XD-w1)	MFA	iodine method (microscopy)	5 to 10	0.71	Abasolo <i>et al.</i> ^(2.57)
X-ray diffraction	MFA	Indirect	Silviscan®	MoR	static bending	130	0.82	Yang and Evans ^(2.4)
X-ray diffraction	MFA	Indirect	Silviscan®	Density	X-ray densitometry (Silviscan®)	130	0.35	Yang and Evans ^(2.4)
X-ray diffraction and X-ray densitometry	MoE	indirect (via density/MFA)	Silviscan®	MoE	Transverse vibration	104	0.96	Evans and Illic ^(2.38)
X-ray diffraction and X-ray densitometry	MoE	indirect (via density/MFA)	Silviscan®	MoE	static bending	130	0.92	Yang and Evans ^(2.4)
X-ray diffraction and X-ray densitometry	MoE	indirect (via density/MFA)	Silviscan®	MoR	static bending	130	0.92	Yang and Evans ^(2.4)
X-ray densitometry	Density	Direct	Silviscan®	Density	Gravimetric immersion method	104	0.97	Evans and Illic ^(2.38)
X-ray densitometry	density	Direct	Goldeneye	density	Gravimetric method	100	0.94	Hanhijärvi <i>et al.</i> ^(2.29)

X-ray densitometry	density	Direct	Finnograder (Gamma-ray, microwave and IR lasers)	density	Gravimetric method	200	0.87-0.90	Hanhijärvi <i>et al.</i> (2.29)
X-ray densitometry	density, KVR, RW	Direct	Bintec X-ray Log grader	MoE	static bending	200	0.46-0.58	Hanhijärvi <i>et al.</i> (2.29)
X-ray densitometry	density, KVR, RW	Direct	Bintec X-ray Log grader	MoR	static bending	200	0.47-0.69	Hanhijärvi <i>et al.</i> (2.29)
X-ray densitometry	density, KVR, RW	Direct	Bintec X-ray Log grader	density	Gravimetric method	200	0.51-0.58	Hanhijärvi <i>et al.</i> (2.29)
X-ray densitometry	Density	Direct	Silviscan®	MoE	Static bending	104	0.7	Evans and Ilic (2.38)
X-ray densitometry	Density	Direct	Silviscan®	MoE	static bending	130	0.81	Yang and Evans (2.4)
X-ray densitometry	density	Direct	Silviscan®	MoR	static bending	130	0.8	Yang and Evans (2.4)
X-ray densitometry	density	Direct	Silviscan®	basic density (bolts)	Gravimetric method	22	0.96	Lindstrom <i>et al.</i> (2.42)
X-ray densitometry	density	Direct	Silviscan®	basic density (disks)	Gravimetric method	22	0.93	Lindstrom <i>et al.</i> (2.42)
X-ray densitometry	density	Direct	Silviscan®	MFA	x-ray diffractometry (Silviscan®)	22	0	Lindstrom <i>et al.</i> (2.42)

NDT method	parameter measured	direct or indirect measurement	Commercial device?	correlated against 2nd parameter =	2nd parameter derived by:	sample size	R ²	Reference
X-ray densitometry	density	direct	Goldeneye	density	gravimetric method	200	0.94	Hanhijärvi <i>et al.</i> (2.29)
X-ray densitometry	density and knot content	direct		MOR	Static bending	800	0.68-0.78	Schajer (2.58)
X-ray densitometry	density and knot content	direct		MOR	Static bending	30	0.53	Steele (2.51)
X-ray densitometry	density and knot content	direct		MoE	Static bending	800	0.5-0.6	Schajer (2.58)
X-ray densitometry	green heartwood density and knot content	indirect (via density and knots)	Remalog X-ray	MoE (beams)	cook-bolinder MSG		0.44	Oja <i>et al.</i> (2.26)
X-ray densitometry	knot content	indirect (via density variations)	Somatom AR.T (medical CT scanner)	knot content	visual inspection		0.81	Oja (2.59)
X-ray densitometry	MoE	indirect (via density and knot variations)	Somatom AR.T (medical CT scanner)	MoE	cook-bolinder MSG	29	0.56-0.65	Oja (2.60)
X-ray densitometry	Density	indirect (CT numbers)	Somatom Plus (medical CT scanner)	Density (dry)	gravimetric method	2	0.29-0.69	Hou (2.61)
X-ray densitometry	density (heartwood)	direct	Remalog X-ray	density	gravimetric method	29	0.94	Oja (2.60)
X-ray densitometry	density (sapwood)	direct	Remalog X-ray	density	gravimetric method	29	0.73	Oja (2.60)
X-ray densitometry	knot diameters	indirect (via density variations)	Somatom AR.T (medical CT scanner)	knot diameters	measured on boards cut from logs	5	0.52 (heart wood) to 0.72 (sap wood)	Nordmark (2.62)
X-ray densitometry	knot content (number)	indirect (via density variations)	Somatom AR.T (medical CT scanner)	knot content (number)	measured on boards cut from logs	5	0.9	Nordmark (2.62)
Grey scale image analysis	Compression wood content (%)	direct	CCD camera	MFA	Silviscan®	22	0.33	Lindstrom <i>et al.</i> (2.42)
Grey scale image analysis	Compression wood content (%)	direct	CCD camera	Density	Silviscan®	22	0.36	Lindstrom <i>et al.</i> (2.42)
Grey scale image analysis	Compression wood content (%)	indirect (end grain observation)					NA	Donaldson and Turner (2.96)

Polarized light microscopy	MFA	direct					NA	Xu ^(2.42) , Donaldson and Turner ^(2.96)
laser reflectance	Spiral grain (under bark)	direct	CMOS camera	spiral grain (on sawn surface)	scribe method	7881	0.82	Nystrom and Grunberg ^(2.64)
MW scanning	Density	indirect	Satimo 9.4GHz MW camera	Density	gravimetric method	8	0.98 (above FSP) 0.95 (below FSP)	Johansson <i>et al.</i> ^(2.83)
MW scanning	Moisture content	indirect	Satimo 9.4GHz MW camera	MC	electrical resistivity	8	0.99 (above FSP) 0.97 (below FSP)	Johansson <i>et al.</i> ^(2.83)
NIR spectroscopy	MoE	indirect		MoE	static bending		0.54-0.57	Thumm <i>et al.</i> ^(2.66)
NIR spectroscopy	MFA (green)	direct	NIRSystems inc. model 5000 scanning spectrometer	MFA (dry)	Silviscan®	32	0.68	Schimleck <i>et al.</i> ^(2.62)
NDT method	parameter measured	direct or indirect measurement	Commercial device?	correlated against 2nd parameter =	2nd parameter derived by:	sample size	R²	Reference
NIR spectroscopy	MFA (dry)	direct	NIRSystems inc. model 5000 scanning spectrometer	MFA (dry)	Silviscan®	15	0.93	Schimleck <i>et al.</i> ^(2.62)
NIR spectroscopy	density (green)	direct	NIRSystems inc. model 5000 scanning spectrometer	Density (dry)	Silviscan®	32	0.74	Schimleck <i>et al.</i> ^(2.62)
NIR spectroscopy	density (dry)	direct	NIRSystems inc. model 5000 scanning spectrometer	Density (dry)	Silviscan®	15	0.9	Schimleck <i>et al.</i> ^(2.62)
NIR spectroscopy	MoE (green)	indirect (via density and MFA)	NIRSystems inc. model 5000 scanning spectrometer	MoE (dry)	Silviscan®	32	0.81	Schimleck <i>et al.</i> ^(2.62)
NIR spectroscopy	MoE (dry)	indirect (via density and MFA)	NIRSystems inc. model 5000 scanning spectrometer	MoE (dry)	Silviscan®	15	0.95	Schimleck <i>et al.</i> ^(2.62)
NIR [®] spectroscopy	MFA	direct	NIRSystems inc. model 5000 scanning spectrometer	MoE	Silviscan®	120	0.9	Jones <i>et al.</i> ^(2.63)
NIR spectroscopy	Density	direct	NIRSystems inc. model 5000 scanning spectrometer	MoE	Silviscan®	120	0.83	Jones <i>et al.</i> ^(2.63)
NIR spectroscopy	MoE	indirect (via density and MFA)	NIRSystems inc. model 5000 scanning spectrometer	MoE	Silviscan®	120	0.93	Jones <i>et al.</i> ^(2.63)
NIR spectroscopy	Density	direct	NIRSystems inc. model 5000 scanning spectrometer	density	gravimetric method	70	0.93	Schimleck <i>et al.</i> ^(2.69)
NIR spectroscopy	MFA	direct	NIRSystems inc. model 5000 scanning spectrometer	MFA	Silviscan®	70	0.83	Schimleck <i>et al.</i> ^(2.69)
NIR spectroscopy	MoE	indirect (via density and MFA)	NIRSystems inc. model 5000 scanning spectrometer	MoE	Silviscan®	70	0.88	Schimleck <i>et al.</i> ^(2.69)

NIR spectroscopy	MoE	indirect (via density and MFA)	NIRSystems inc. model 5000 scanning spectrometer	MoE	Silviscan®	2	0.90-0.93	Schimleck <i>et al.</i> (2.64)
NIR spectroscopy	MoE	indirect (via density and MFA)	NIRSystems inc. model 5000 scanning spectrometer	MoE	Silviscan®		0.87	Schimleck <i>et al.</i> (2.64)
NIR spectroscopy	lignin content	direct	NIRSystems inc. model 6500 scanning spectrometer	lignin content	chemically measured	34	0.98	Yamada (2.71)
NIR spectroscopy	Cellulose content	direct	NIRSystems inc. model 6500 scanning spectrometer	cellulose content	chemically measured	34	0.96	Yamada (2.71)
NIR spectroscopy	Cellular density	direct		cellular density	gravimetric method		0.98	Pongracic (2.58)
NIR spectroscopy	Various parameters	both		MoE	Silviscan®		0.23-0.67	McKinley <i>et al.</i> (2.56)
Thermography	Heartwood content	indirect (heat variations)	Thermovision camera	heartwood content	manual estimation	180	0.72	Gjerdrum and Hoibo (2.74)

NDT method	parameter measured	direct or indirect measurement	Commercial device?	correlated against 2nd parameter =	2nd parameter derived by:	sample size	R ²	Reference
resistance drilling (2-20 mm)	drill resistance (N)	direct	Drill resistance measurement system	compressive strength	static compression testing	30	0.43	Machado <i>et al.</i> (2.36)
resistance drilling (2-20 mm)	drill resistance (N)	direct	Drill resistance measurement system	density	gravimetric method	30	0.31	Machado <i>et al.</i> (2.36)
Pilodyn	penetration depth	direct	pilodyn	MoE	static bending (4pt test)	16	0.38-0.56	Jacques <i>et al.</i> (2.93)
Ring width measurement	Ring width	direct		Density	Gravimetric method	513	0.17-0.24	Brauer <i>et al.</i> (2.38)

Appendix D – Dispersion curves for a wet wooden log

Included in this appendix are dispersion curves showing longitudinal rod wave (blue lines) and flexural wave (green lines) modes. Graphs were constructed using a MATLAB routine, called PCDISP, to model dispersive behaviour within a wet wooden log, as investigated in Chapter 6. The initial parameters of the rod model were (as shown in Figures D1 and D2): An initial rod speed (C_0) of 3000 ms^{-1} ; Poisson's ratio = 0.37, density = 450 kgm^{-3} ; radius of the rod 0.125 m and cut-off frequency tolerance of 0.1 Hz. Dashed horizontal lines C_L , C_T , and C_R represent bulk longitudinal, bulk transverse and Rayleigh wavespeeds respectively. The mode names displayed in graphs represent the type of wave; (L) Longitudinal (rod wave) and (F) Flexural, whilst the numbers in brackets (n, m) denotes; (n) the order of symmetry around the longitudinal axis (NOTE: $n = 0$ denotes symmetrical modes), whilst (m) denotes the number of the wave of a particular family in ascending order of wavespeed.

The parameters were then varied to observe the effect of changing these parameters, and the variations has been further analysed in Chapter 6.

Table D1 Parametric study of variables presented in this thesis. Changes from the initial state (D1 and D2) are shown in **bold**.

Figure	Dispersion curve type	C_0 (ms ⁻¹)	ρ (kgm ⁻³)	μ	Radius of rod specimen (m)	Frequency range (Hz)
D1	Phase	3000	450	0.37	0.125	> 10,000
D2	Group	3000	450	0.37	0.125	> 10,000
D3	Phase	4000	450	0.37	0.125	> 10,000
D4	Group	4000	450	0.37	0.125	> 10,000
D5	Phase	5000	450	0.37	0.125	> 10,000
D6	Group	5000	450	0.37	0.125	> 10,000
D7	Phase	3000	400	0.37	0.125	> 10,000
D8	Group	3000	400	0.37	0.125	> 10,000
D9	Phase	3000	500	0.37	0.125	> 10,000
D10	Group	3000	500	0.37	0.125	> 10,000
D11	Phase	3000	450	0.3	0.125	> 10,000
D12	Group	3000	450	0.3	0.125	> 10,000
D13	Phase	3000	450	0.4	0.125	> 10,000
D14	Group	3000	450	0.4	0.125	> 10,000
D15	Phase	3000	450	0.37	0.2	> 10,000
D16	Group	3000	450	0.37	0.2	> 10,000
D17	Phase	3000	450	0.37	0.075	> 10,000
D18	Group	3000	450	0.37	0.075	> 10,000
D19	Phase	3000	850	0.37	0.125	> 10,000
D20	Group	3000	850	0.37	0.125	> 10,000
D21	Phase	3000	1000	0.37	0.125	> 10,000
D22	Group	3000	1000	0.37	0.125	> 10,000
D23	Phase	3000	450	0.37	0.125	>50,000
D24	Group	3000	450	0.37	0.125	>50,000

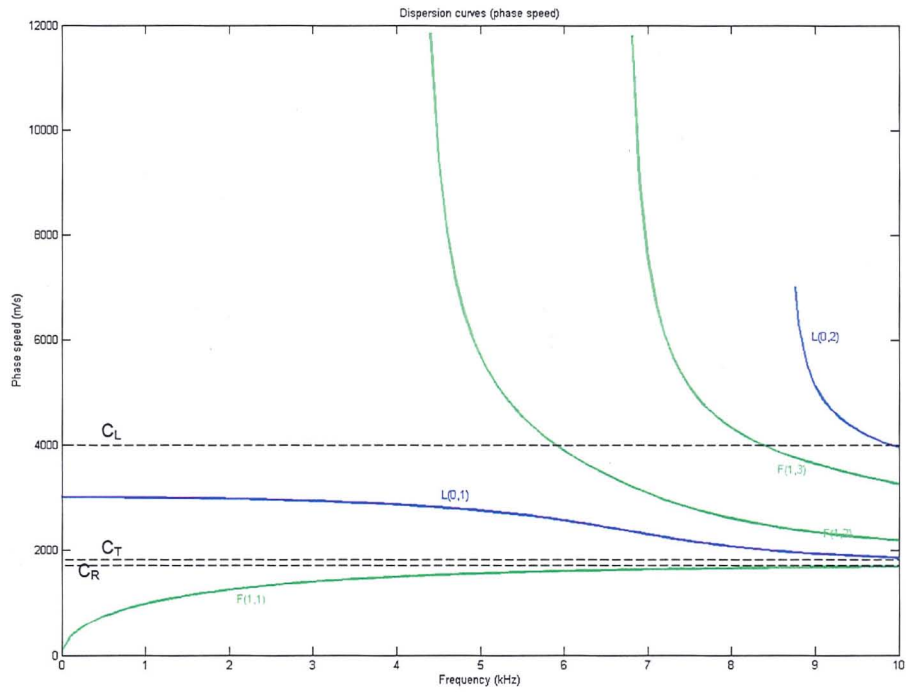


Figure D1 Phase velocity dispersion curves for benchmark case

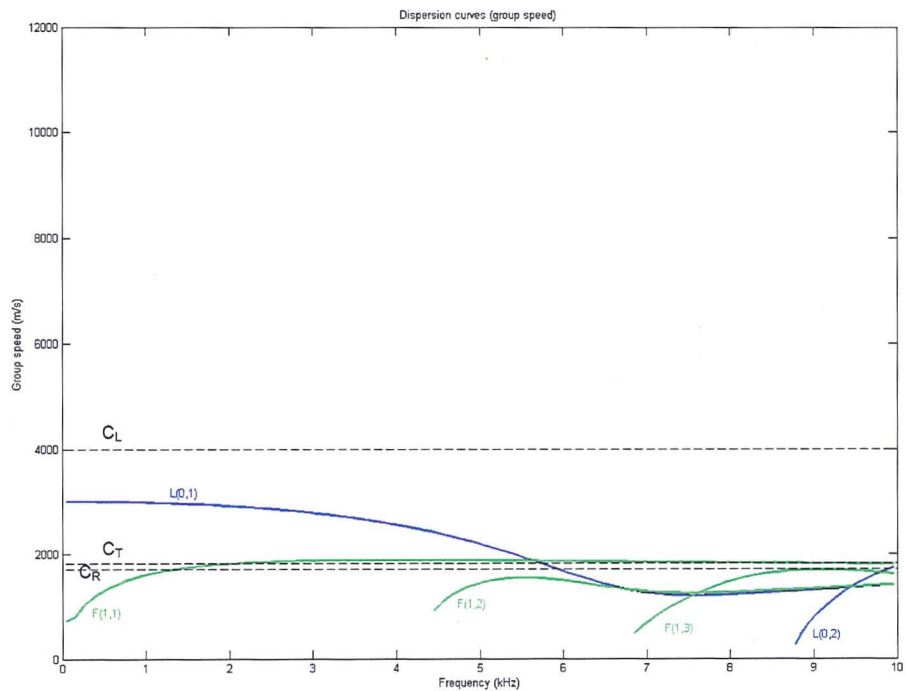


Figure D2 Group velocity dispersion curves for benchmark case

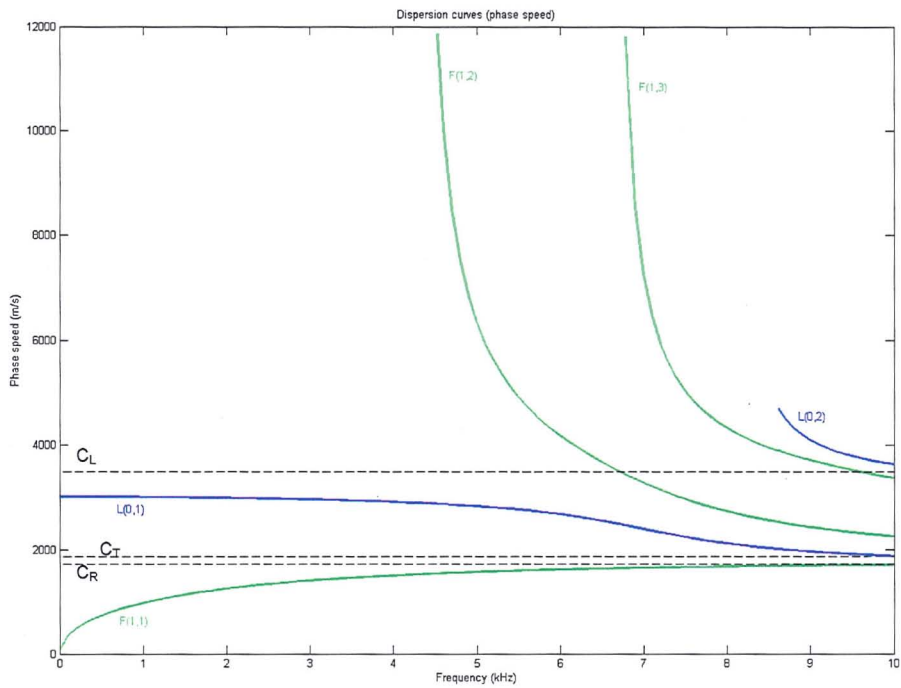


Figure D3 Phase velocity dispersion curves: increased C_0 to 4000 ms^{-1}

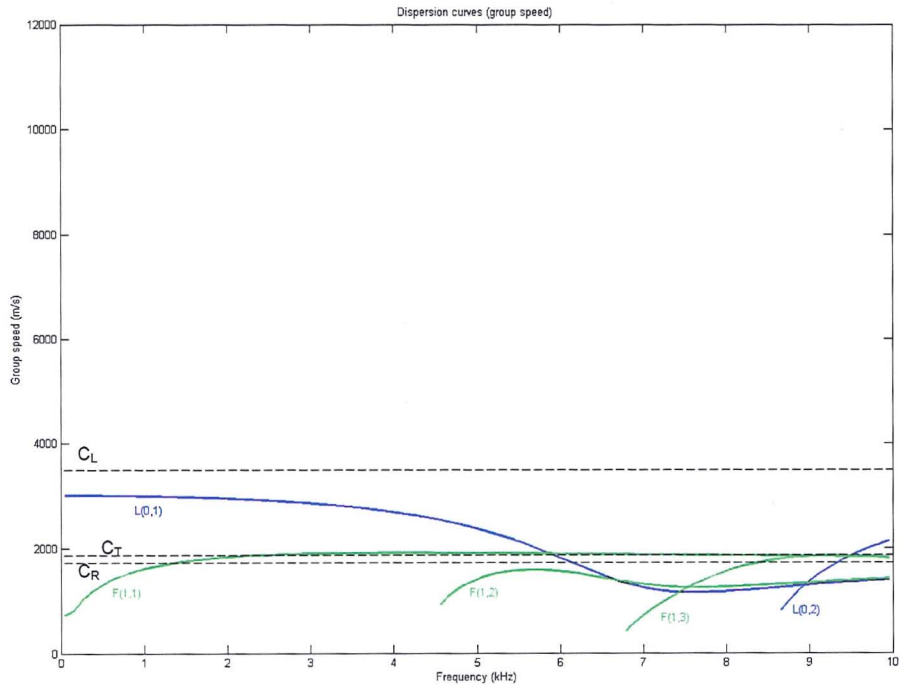


Figure D4 Group velocity dispersion curves: increased C_0 to 4000 ms^{-1}

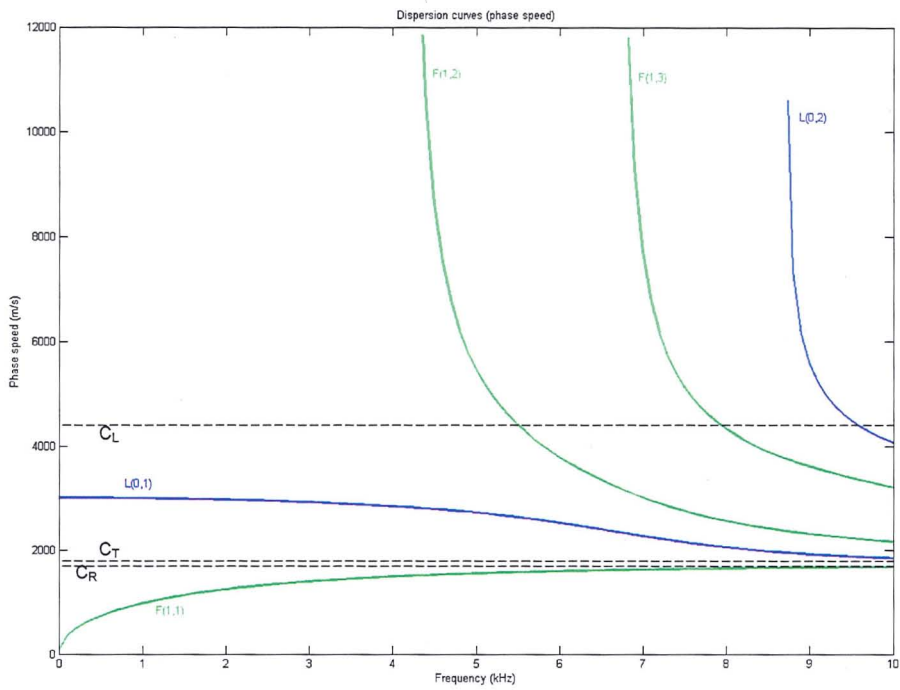


Figure D5 Phase velocity dispersion curves: increased C_0 to 5000 ms^{-1}

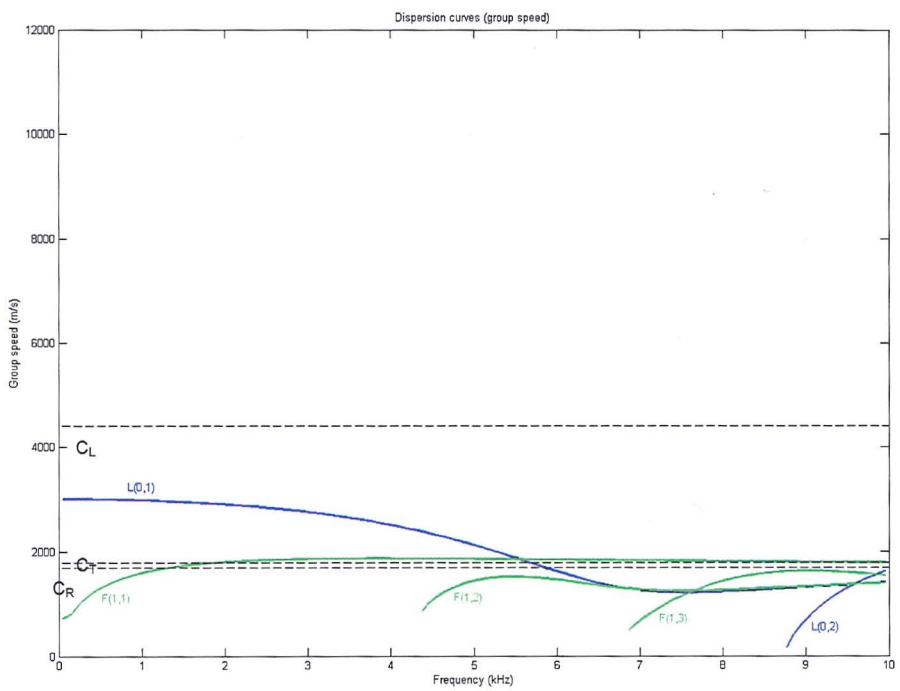


Figure D6 Group velocity dispersion curves: increased C_0 to 5000 ms^{-1}

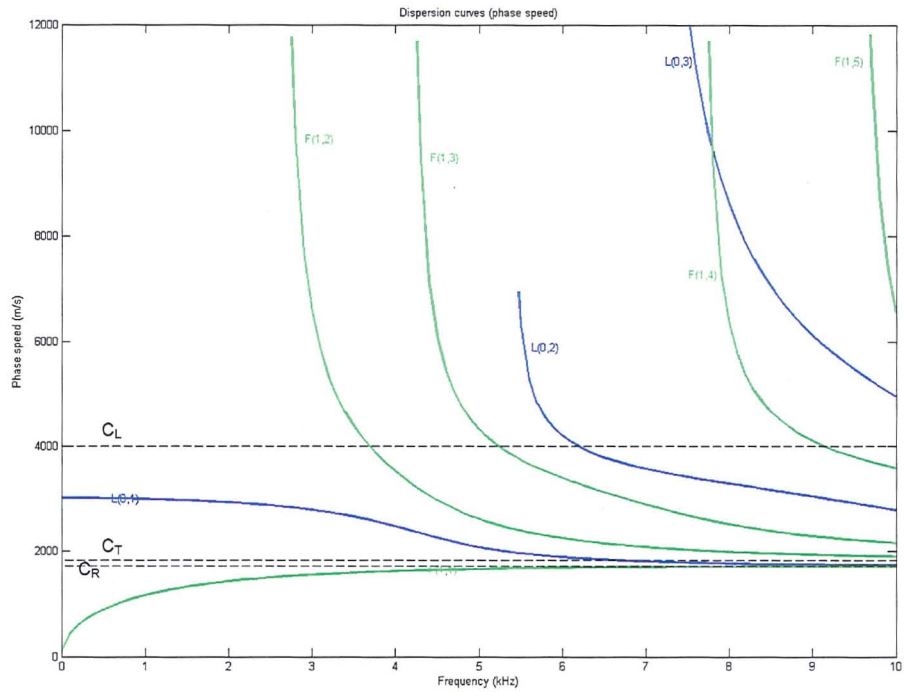


Figure D7 Phase velocity dispersion curves: decreased ρ to 400 kgm^{-3}

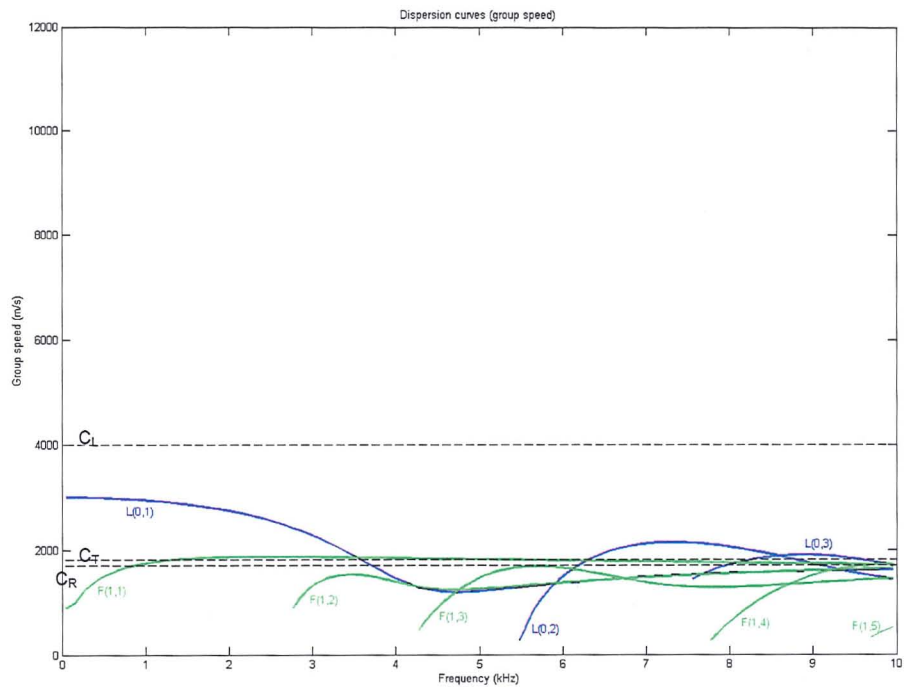


Figure D8 Group velocity dispersion curves: decreased ρ to 400 kgm^{-3}

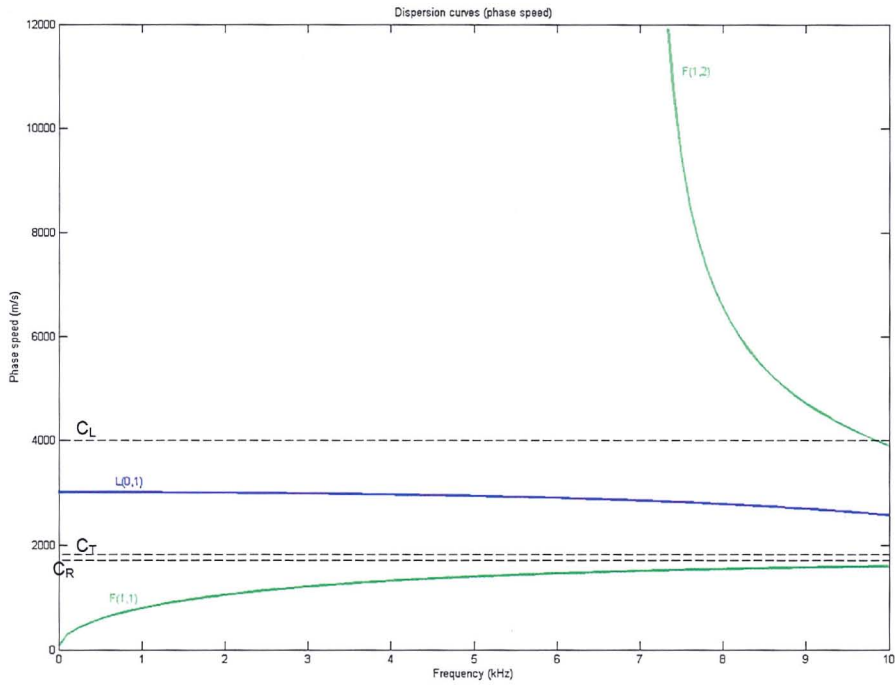


Figure D9 Phase velocity dispersion curves: increased ρ to 500 kgm^{-3}

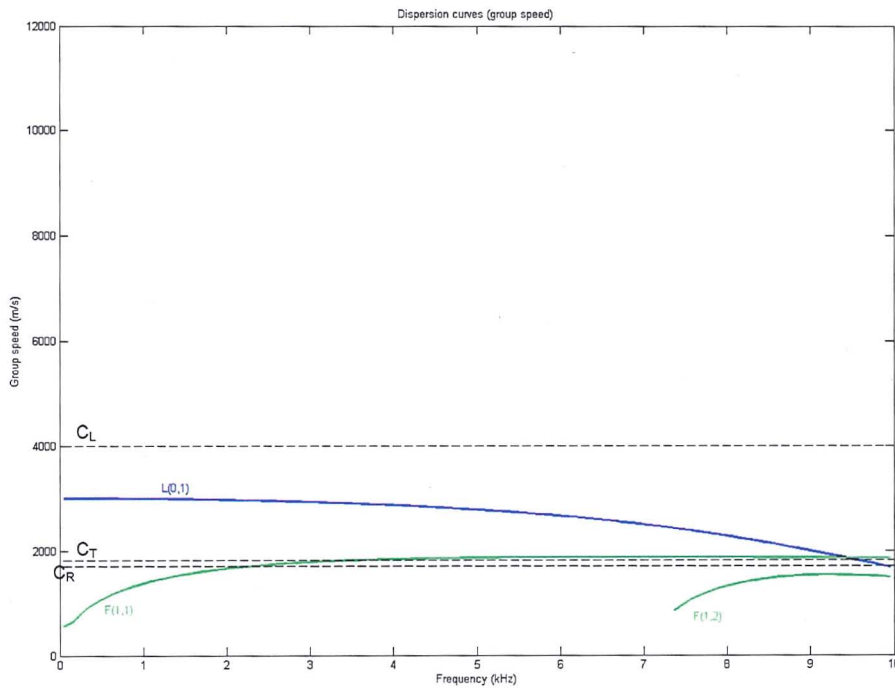


Figure D10 Group velocity dispersion curves: increased ρ to 500 kgm^{-3}

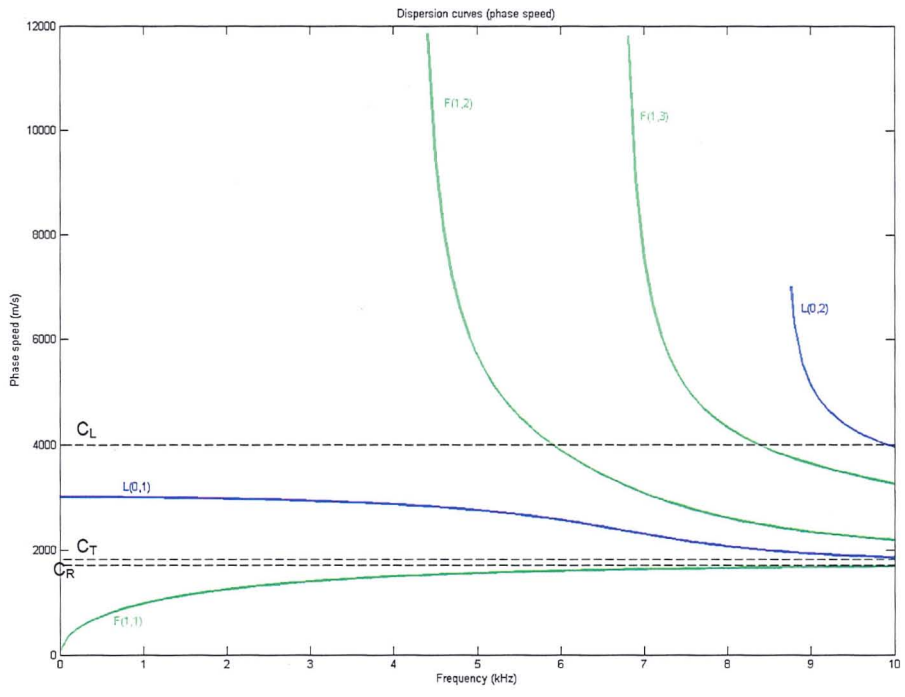


Figure D11 Phase velocity dispersion curves: decreased μ to 0.3

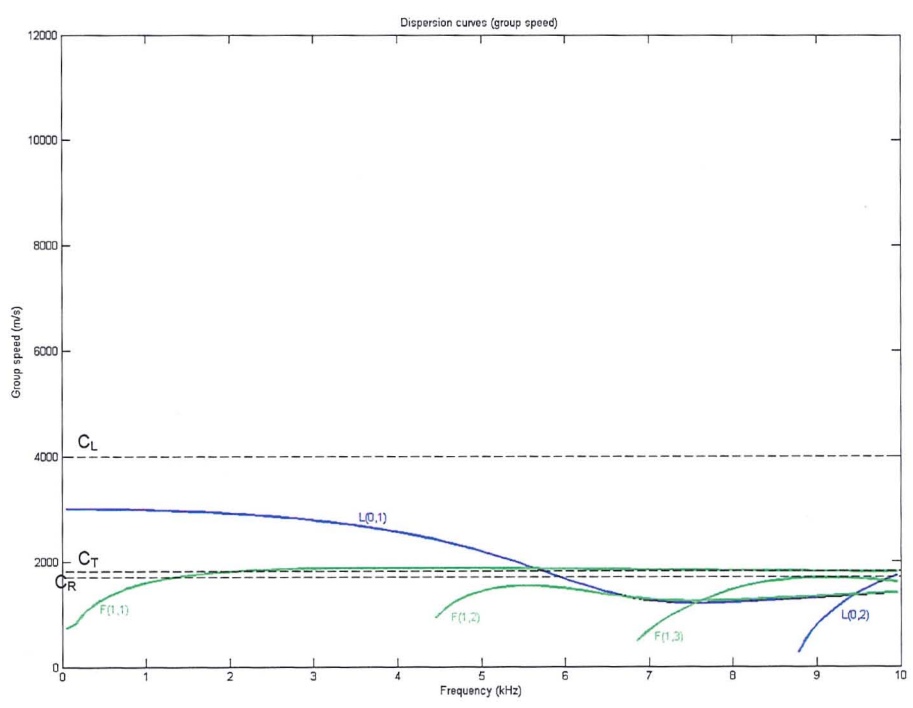


Figure D12 Group velocity dispersion curves: decreased μ to 0.3

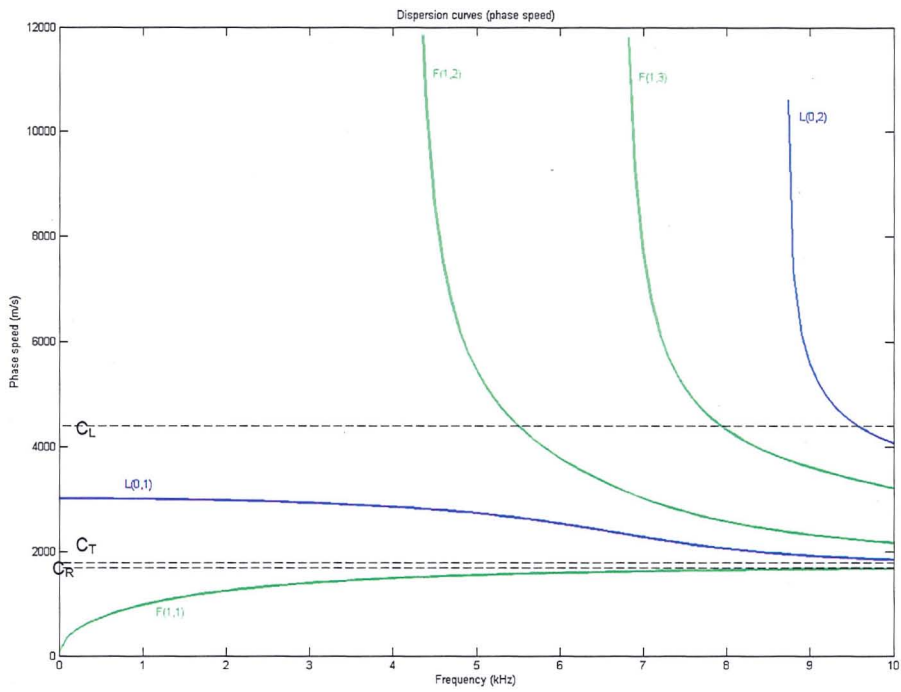


Figure D13 Phase velocity dispersion curves: increased μ to 0.4

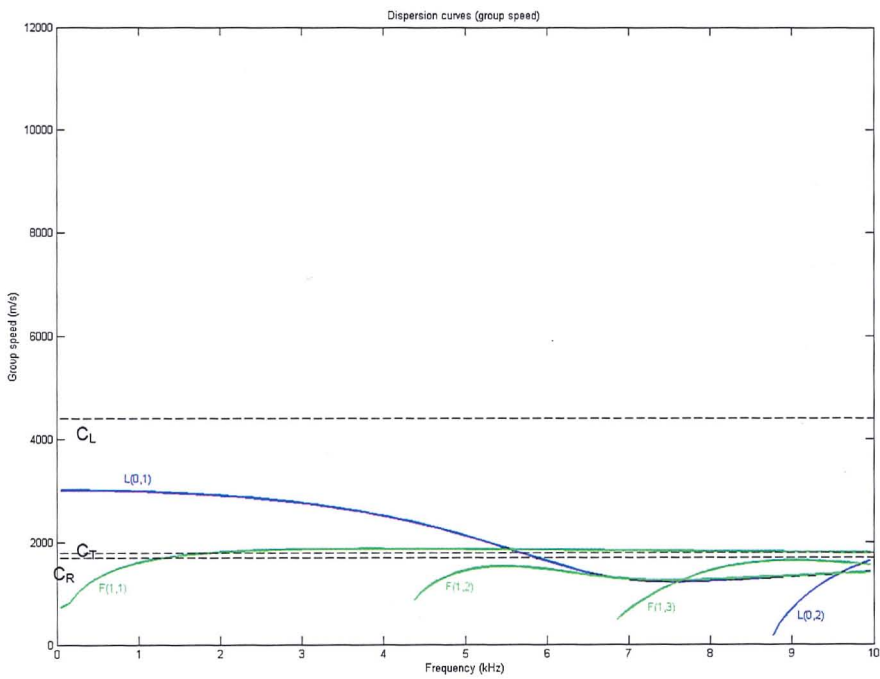


Figure D14 Group velocity dispersion curves: increased μ to 0.4

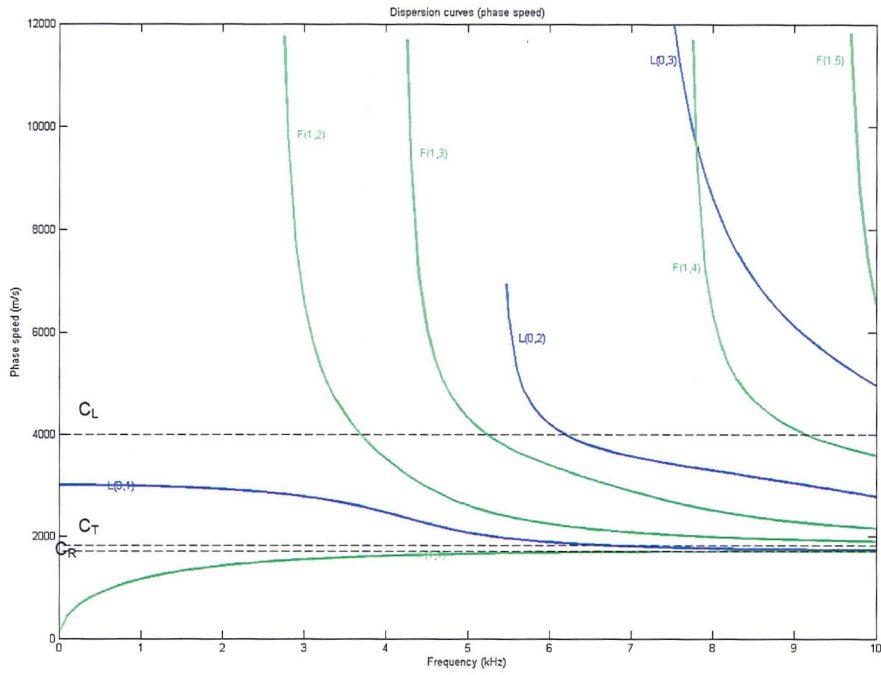


Figure D15 Phase velocity dispersion curves: increased radius to 0.2 m

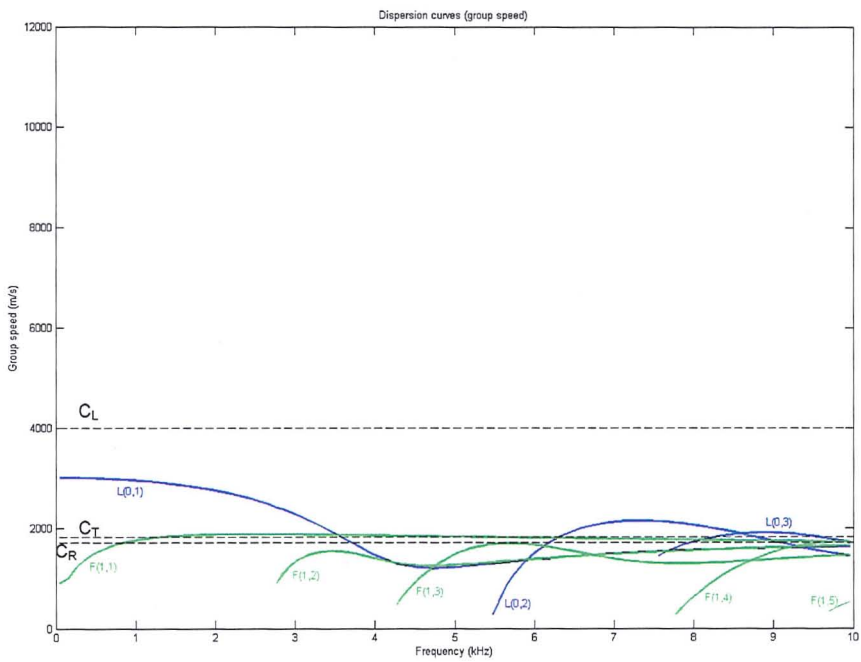


Figure D16 Group velocity dispersion curves: increased radius to 0.2 m

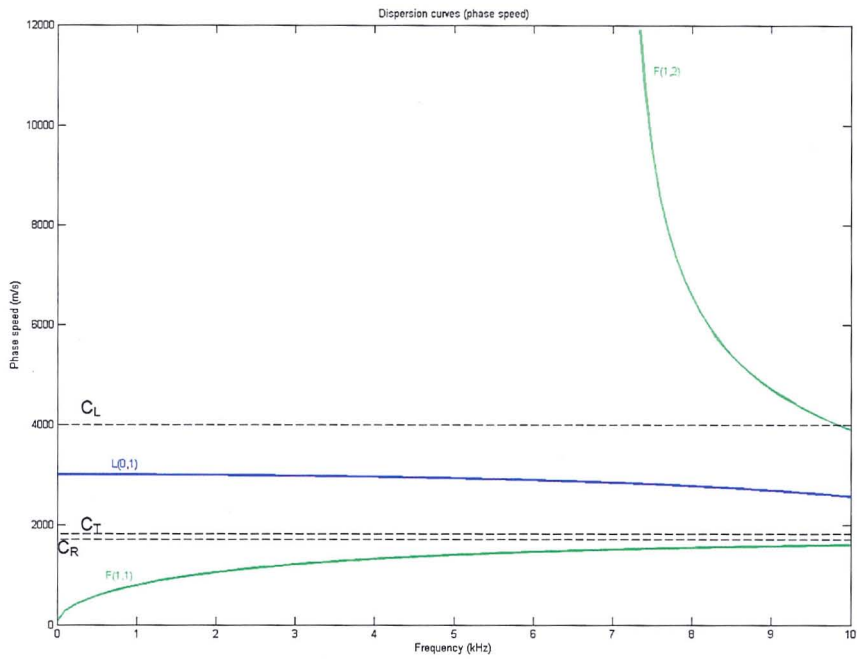


Figure D17 Phase velocity dispersion curves: decreased radius to 0.075 m

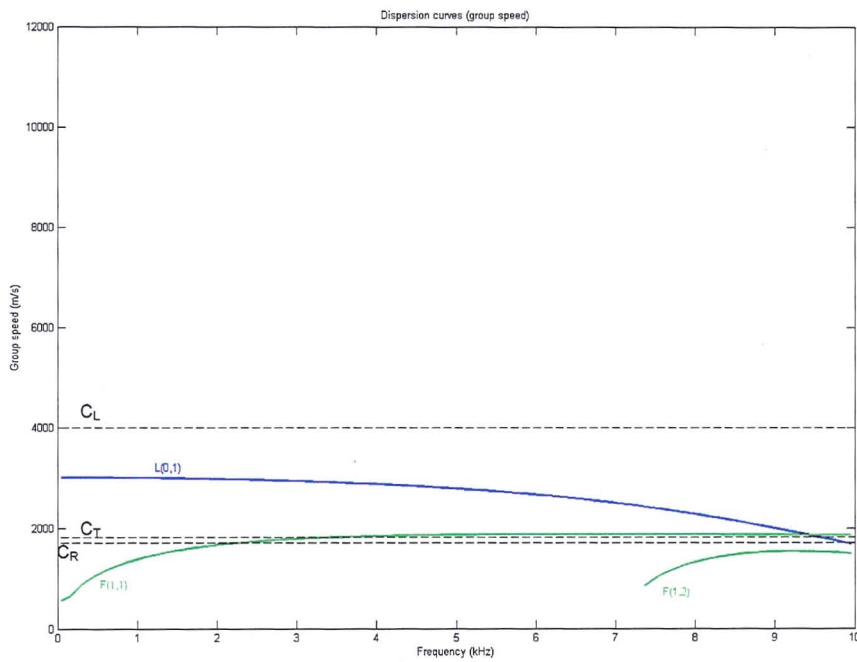


Figure D18 Group velocity dispersion curves: decreased radius to 0.075 m

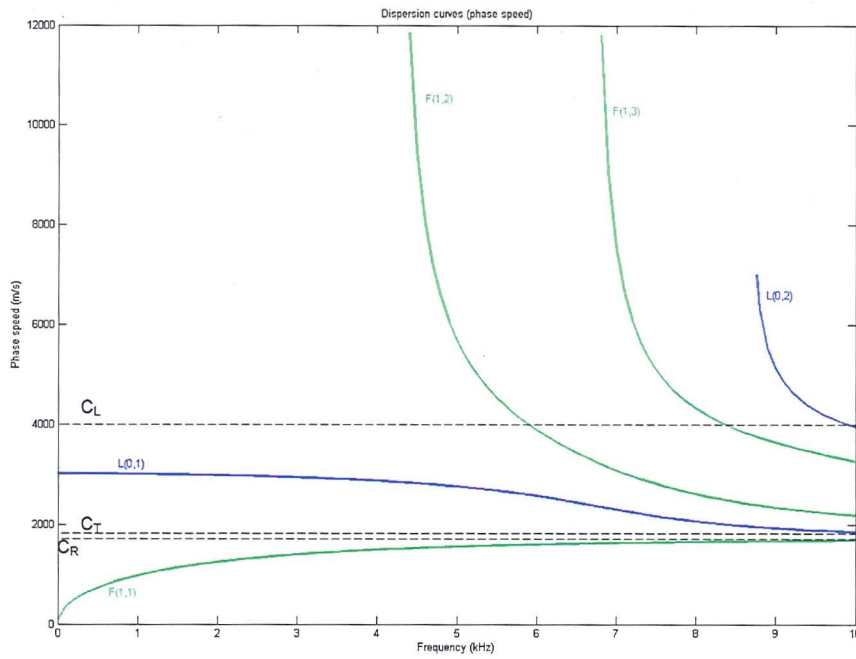


Figure D19 Phase velocity dispersion curves: increased ρ to 850 kgm^{-3}

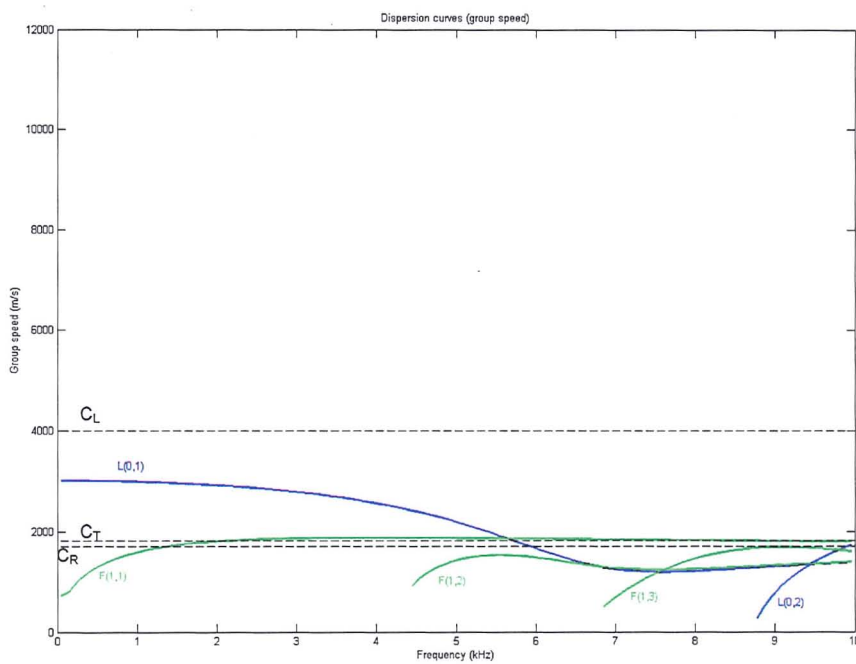


Figure D20 Group velocity dispersion curves: increased ρ to 850 kgm^{-3}

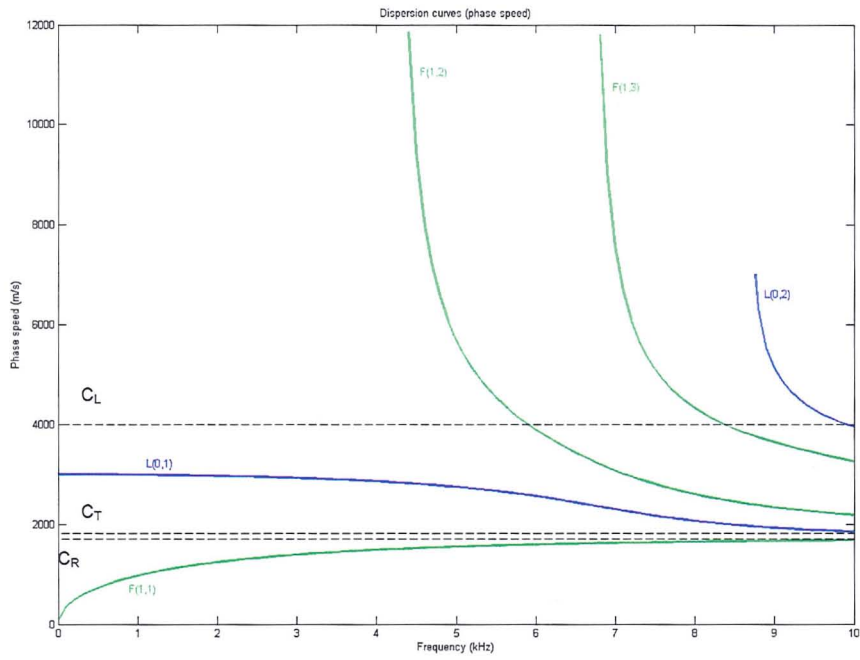


Figure D21 Phase velocity dispersion curves: increased ρ to 1000 kgm^{-3}

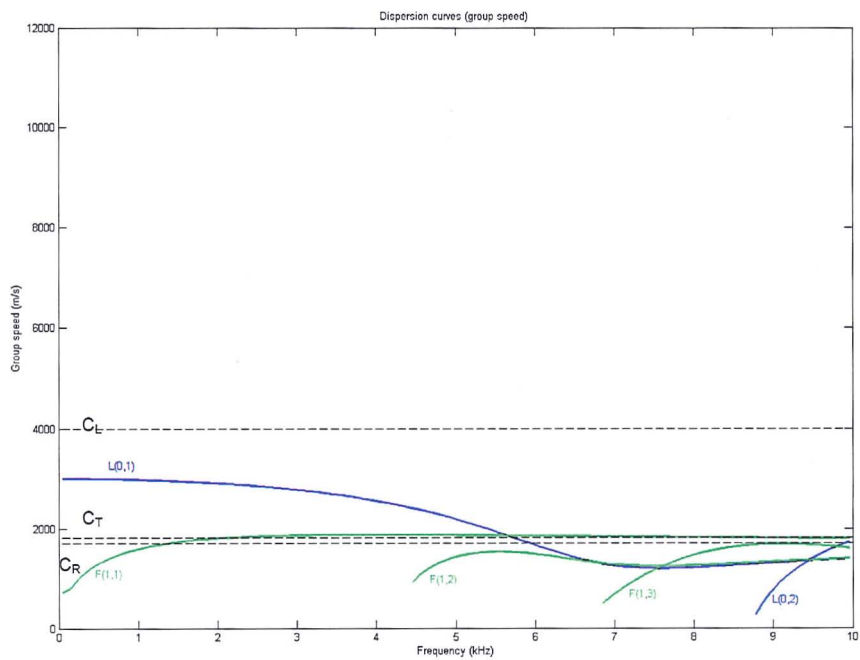


Figure D22 Group velocity dispersion curves: increased ρ to 1000 kgm^{-3}

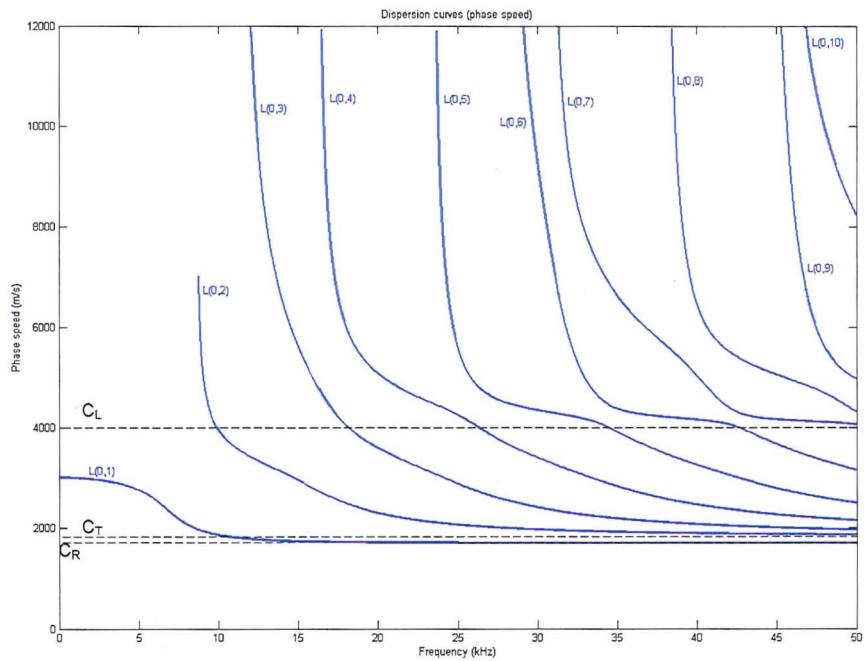


Figure D23 Phase velocity dispersion curves for benchmark case (Longitudinal modes only, > 50 kHz)

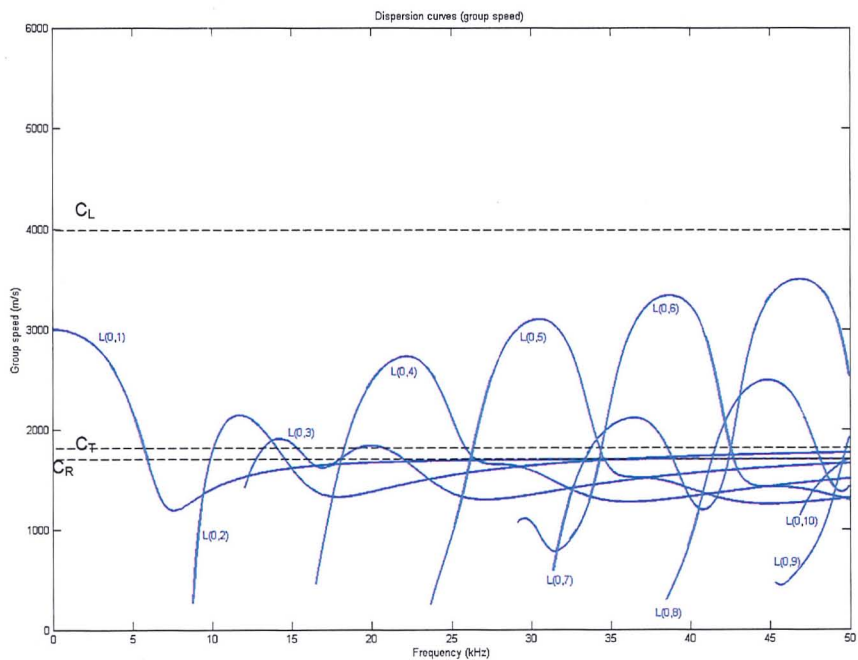


Figure D24 Group velocity dispersion curves for benchmark case (Longitudinal modes only, > 50 kHz)

**PAGE
MISSING
IN
ORIGINAL**